MIA25 · LISBOA

XI SIMPÓSIO SOBRE A MARGEM IBÉRICA ATLÂNTICA
XI SIMPOSIO SOBRE EL MARGEN IBÉRICO ATLÁNTICO

29-31 OUTUBRO | OCTUBRE

hidrográfico
marinha · portugal

ATAS

Actas
Proceedings

Lisboa

Título – Atas do XI Simpósio sobre a Margem Ibérica Atlântica/ XI Simposio sobre el Margen Ibérico Atlántico (MIA2025)
Autor – Instituto Hidrográfico
Editores – Aurora Rodrigues, Anabela Oliveira, Mónica Ribeiro, Sandra Moreira
Edição e execução gráfica – Luis Gonçalves/Joana Gomes
Logotipo MIA2025 - Joana Gomes
Capa – Joana Gomes
ISBN – 978-989-705-185-2

ÍNDICE GERAL
Índice general
General index

I.

COMISSÕES
Comités
Committees

Comissão Permanente
Comité Permanente
Permanent Commitee

João M. Alveirinho Dias *(Univ. Algarve)*
F. Javier Hernández-Molina *(Univ. London)*
Federico Vilas Martín *(Univ. Vigo)*
Fernando Rocha *(Univ. Aveiro)*
Germán Flor Rodríguez *(Univ. Oviedo)*
Maria da Conceição Freitas *(Univ. Lisboa/IDL)*
Víctor Díaz del Río *(IEO)*
Pedro Cunha *(Univ. Coimbra)*
Alejandro Cearreta *(Univ. País Vasco)*

Comissão Científica
Comité Científico
Scientific Committee

Ana Brito *(Univ. Lisboa/MARE)*
Anabela Oliveira *(IH/IDL)*
Antonio Manuel Bode Riestra *(Centro Ocean. A Coruña/IEO)*
Aurora Bizarro *(IH/IDL)*
Carla Candeias *(Univ. Aveiro/Geobiotec)*
Carla Palma *(IH)*
Carlos Marques da Silva *(Univ. Lisboa/IDL)*
César González-Pola Muñiz *(Univ. Vigo/IEO)*
Cristina Bernardes *(Univ. Aveiro/CESAM)*
Davide Gamboa *(Univ. Aveiro/CESAM)*
Eduard Puig Montella *(IEO)*
Eugenio Fraile Nuez *(Centro Ocean. Canarias)*
Felipe Cerezo Andreo *(Univ. Cádiz)*
Francisco Fatela *(Univ. Lisboa/IDL)*
Guillermo Francés *(Univ. Vigo)*
Javier Benavente González *(Univ. Cádiz)*
João Duarte *(Univ. Lisboa/IDL)*
Joaquim Pombo *(IH)*
Jorge Macías Sánchez *(Univ. Málaga)*
José Luis Granja Bruña *(Univ. Complutense de Madrid)*
José Paulo Pinto *(IH)*
Juan Santos Echeandía *(Centro Ocean. Vigo/IEO)*
Luís Menezes Pinheiro *(Univ. Aveiro/CESAM)*
Luis Miguel Fernández Salas *(Centro Ocean. Cádiz/IEO)*
Manuel Ruiz Villareal *(Centro Ocean. A Coruña/IEO)*
Margarita García García *(Centro Ocean. Cádiz/IEO)*
María Carmen Fernández Puga *(Univ. Cádis)*
Maria da Conceição Freitas *(Univ. Lisboa/IDL)*
Maria Virgínia Martins *(Univ. Aveiro/CESAM)*
Mário Cachão *(Univ. Lisboa/IDL)*
Marta Álvarez *(IEO-CSIC)*
Mónica Ribeiro *(IH)*
Montserrat Pérez Rodríguez *(Centro Ocean. Vigo/IEO)*
Nieves López González *(Centro Ocean. Málaga/IEO)*
Óscar Ferreira *(Univ. Algarve)*
Paula Freire *(LNEC)*
Paulo Baganha Baptista *(Univ. Aveiro/CESAM)*
Pedro Costa *(Univ. Coimbra/IDL)*
Pilar Ríos *(Centro Ocean. Gijón/IEO)*
Ricardo Sánchez Leal *(Univ. Cádiz)*
Rui Quartau *(IH/IDL)*

Rui Taborda *(Univ. Lisboa/IDL)*
Sandra Moreira *(IH/IDL)*
Soledad García Gil *(Univ. Vigo)*
Susana Costas *(Univ. Algarve)*
Teresa Drago *(IPMA/IDL)*
Victoria Besada Montenegro *(Centro Ocean. Vigo/IEO)*

Comissão Organizadora (IH)
Comité organizador (IH)
Organising Comitee (IH)

João Delgado Vicente
Aurora Bizarro
Anabela Oliveira
Sandra Moreira
Mónica Ribeiro
Sérgio Leitão
Joana Gomes
Telmo Dias
Nuno Costa

Entidades Associadas
Entidades Asociadas
Associated Entities

Faculdade de Ciências da Universidade de Lisboa – FCUL

II.

PATROCINADORES E APOIOS

Patrocinadores y apoyos
Sponsors and supporters

Casco Antiguo

VÓRTICE

QUALITAS INSTRUMENTS

EXAIL

KONGSBERG

Casco Antiguo

DIVING - OCEANOGRAPHY - RESCUE

exail

KONGSBERG

vórtice

Equipamentos Científicos, Lda.

qualitas instruments

III.

NOTA INTRODUTÓRIA

Nota introductoria
Introductory note

O Simpósio sobre a Margem Ibérica Atlântica (MIA) constitui um fórum de debate aberto em torno da margem ibérica (Península Ibérica, Açores, Madeira, Canárias), cuja primeira edição teve lugar em Lisboa, em 1994. Este evento, realizado trienalmente, tem proporcionado uma discussão dos processos e da evolução da MIA, ao mesmo tempo que reforça os laços de cooperação e interligação entre os investigadores.

O Instituto Hidrográfico (IH), é o herdeiro das mais antigas instituições portuguesas dedicadas à investigação marinha, com origem nos Descobrimentos Marítimos, durante o período do Renascimento, quando a cartografia e a navegação se desenvolveram com base em metodologias científicas sistemáticas. Fundado em 1960, o IH é uma unidade da Marinha Portuguesa e, desde 1992, Laboratório do Estado para as ciências do mar. A atividade abrange a realização de levantamentos hidrográficos, cartografia náutica, oceanografia, apoio a operações militares, segurança da navegação, infraestruturas de dados marítimos, geologia e geofísica marinhas e química e poluição do meio marinho que alia a vertente de investigação científica aplicada à disponibilização de serviços a uma vasta comunidade de utilizadores do mar.

Com presença assídua desde a primeira edição destes simpósios ibéricos, o IH foi convidado a organizar a XI edição do MIA na sede, localizada na Rua das Trinas, em Lisboa. Esta edição decorre no período de 29 a 31 de outubro de 2025, com o apoio do Departamento de Geologia da Faculdade de Ciências da Universidade de Lisboa. Os resumos alargados, apresentados neste livro de atas, correspondem a 78 contribuições submetidas, das quais 54 são apresentações orais e 24 são pósteres, cobrindo as várias áreas temáticas do Simpósio. Os resumos refletem o empenho e a dedicação dos autores e ilustram as apresentações e discussões técnicas, de desenvolvimento científico no reforço da importância do conhecimento do mar ibérico atlântico para a gestão sustentada dos recursos marinhos vivos e não vivos.

Destaco o relevante contributo das empresas patrocinadoras, cujo apoio pode ser interpretado como um incentivo e factor de motivação para prosseguir os objetivos deste Simpósio com maior determinação, também para os investigadores, em particular para os mais jovens, que se dedicam ao estudo dos processos e dinâmicas que afetam a MIA.

Expresso um reconhecido agradecimento aos membros da Comissão Científica, e a todos os envolvidos na organização e realização do MIA2025, em particular à Comissão Organizadora, pela disponibilidade e empenho demonstrados. Igualmente devido um reconhecimento aos participantes, nas diversas modalidades, expressando o desejo de que este evento promova uma frutífera partilha de ideias e experiências.

O DIRETOR-GERAL

João Paulo Ramalho Marreiros
Contra-almirante

A tectónica da Margem Sudoeste Ibérica: uma breve revisão da evolução do conhecimento

João C. Duarte

Instituto Dom Luiz (IDL) e Departamento de Ciências da Terra e Energia, Faculdade de Ciências, Universidade de Lisboa, Lisboa

UNIARQ, Centro de Arqueologia da Universidade de Lisboa, Lisboa

Na manhã do dia 1 de novembro de 1755, um grande terramoto (magnitude ~8,7) atingiu a Margem Sudoeste Ibérica. Este foi o terramoto mais forte alguma vez sentido na Europa Ocidental. Este evento teve um impacto profundo nos pensadores da época, em particular nos filósofos do Iluminismo, como Voltaire, Rousseau e Kant. O Grande Terramoto de Lisboa é considerado por muitos um momento crucial no nascimento das Ciências da Terra. Após o terramoto de 1755, Kant e outros autores escreveram vários textos acerca das causas dos terramotos e estiveram perto de identificar alguns elementos do que hoje chamamos de tectónica de placas. Mais de duzentos anos mais tarde, em 1969, a região voltou a ser atingida por um grande terramoto (magnitude ~7,9). Este aconteceu precisamente durante o período em que a teoria da tectónica de placas estava a ser desenvolvida. Geocientistas como Fukao, Purdy e Mackenzie focaram a sua atenção nesta área, sugerindo que se podia estar a gerar aqui uma nova zona de subducção. Na sequência destes trabalhos, António Ribeiro sugeriu que a margem (passiva) oeste ibérica poderia estar a ser reativada, um processo que, com o tempo, poderia levar à formação de uma nova zona de subducção ao longo desta margem. Nos anos subsequentes, houve um grande investimento em estudos de geologia e geofísica marinha que vieram apoiar esta ideia. Nesta apresentação, irei destacar os marcos mais importantes na evolução do conhecimento tectónico da Margem Sudoeste Ibérica, acabando com a exploração dos dados, ideias e modelos mais recentes. Estes mostram que poderá estar a ocorrer nesta região um processo raro e pouco conhecido: a delaminação de uma placa oceânica.

Sistemas de observación e infraestructuras de datos en el Margen Ibérico Atlántico: una herramienta para comprender la dinámica oceánica y apoyar a usuarios finales

Manuel R. Villarreal

Centro Oceanográfico de A Coruña, Instituto Español de Oceanografía, IEO-CSIC, A Coruña, Spain

Las observaciones oceánicas se obtienen a partir de una gran variedad de plataformas a diferentes escalas espaciales y temporales. Además, es necesario medir un gran número de variables físicas, químicas, geológicas y biológicas para caracterizar y comprender la dinámica oceánica y el ecosistema marino. En esta contribución, presentaré una revisión de cómo los sistemas de observación existentes en el margen ibérico atlántico contribuyen a aumentar nuestro conocimiento sobre la variabilidad oceanográfica de la zona y su impacto en el ecosistema marino. Proporcionaré ejemplos de los sistemas de observación sostenidos en la zona, desde sistemas regionales hasta sistemas más locales, con especial referencia a los operados por el Instituto Español de Oceanografía, mostrando cómo nos permiten caracterizar la variabilidad de los diferentes fenómenos oceanográficos en el Margen Ibérico Atlántico a diferentes escalas espaciales y temporales. También mostraré cómo estas observaciones, junto con los esfuerzos de modelización, apoyan el desarrollo de servicios marinos para los usuarios finales en áreas como la acuicultura, el ocio, la protección costera o la contaminación marina. Por último, presentaré avances recientes en infraestructuras de datos en el área ilustrando cómo facilitan la búsqueda y el acceso a diversos datos oceanográfico y permiten un uso eficiente de las observaciones oceánicas y los resultados de los modelos para aumentar nuestro conocimiento de la dinámica oceánica y del ecosistema oceánico, así como para producir información, servicios y productos que apoyen a la gran diversidad de partes interesadas en el ámbito marino.

V.

RESUMOS ALARGADOS

Resúmenes extendidos

Extended abstracts

Natureza e estrutura da Margem Continental Ibérica e da Macaronésia

Naturaleza y estructura del Margen Continental Ibérico y Macaronésico

Nature and structure of the Macaronesian and Iberian Continental Margin

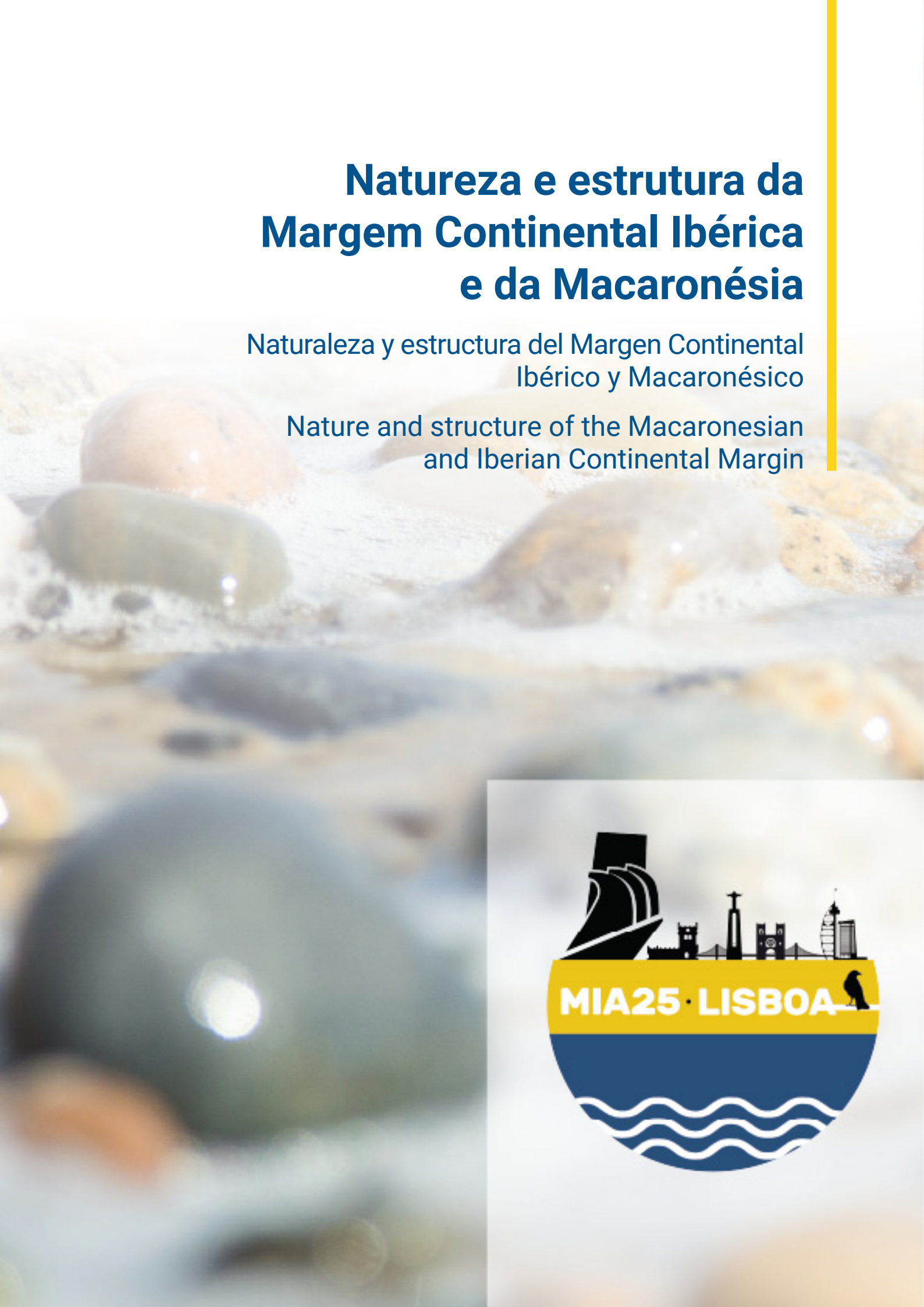

Insights into the deepwater Nazaré Canyon submarine fan, offshore Western Portugal

D. Gamboa (1,2), D. Leite (1) and C. Roque (3,4)

(1) Departamento de Geociências, Universidade de Aveiro, Aveiro, Portugal. dgamboa@ua.pt
(2) CESAM, Universidade de Aveiro, Aveiro, Portugal
(3) EMEPC, Estrutura de Missão para a Extensão da Plataforma Continental, Paço de Arcos, Portugal
(4) IDL, Instituto Dom Luiz, Faculdade de Ciências da Universidade de Lisboa, Campo Grande, Lisbon, Portugal

Abstract: Submarine canyons and associated deepwater submarine fans are major morphological features on continental margins. Located on the West Iberian Margin, the Nazaré Canyon has major control on sediment distribution from the shelf to deepwater domains. Yet, its distal features are poorly known. This study combines bathymetric and seismic data to provide insights into the characteristics of the deepwater Nazaré fan. Overall, channel morphometry shows an increase of size across the canyon, channel and distal fan domains, and transitions can be sharp when lateral confinement suddenly drops. Seismic analysis suggests that an initial deepwater fan developed towards the central domain of the Iberia Abyssal Plain. Sea-level and/or sedimentary dynamics of the margins later forced a southward shift of 15-20 km of the deep-sea channel and fan system to its modern location.

Keywords: *submarine canyon, submarine fan, submarine morphology, submarine channels, Nazaré Canyon*

1. INTRODUCTION

Submarine canyons consist of very large slope incisions, occurring in a variety of dimensional ranges and morphologies (Shepard, 1972). The paths vary between straight to highly sinuous and tend to be fed by a drainage network composed of tributaries, subsidiary channels and/or numerous upslope gullies. Submarine canyons are enhanced by submarine erosion, where recurrent turbidite flow and mass-wasting events are main processes (Bührig *et al*., 2022; Fisher *et al*., 2021).

As the turbidite flows exit the canyon and their confinement is largely decreased, sediment laterally disperses and leads to the deposition of deepwater fans (Wahab *et al*., 2022). Submarine channel systems develop on the deepwater fans, with the main channel aligning with the canyon mouth. Submarine channels are commonly bordered by levees that gradualy decrease in thickness away from the channel axis. Most deepwater channels tend to present symmetric levees on both flanks, but asymmetric channels with only one levee also occur, particularly on slope with marked topographic barriers or confining structures. Submarine channels are characterized by lateral and vertical migration paths, and the overall patterns are a function of the basin accommodation space and topographic confinement.

Located on the West Iberian Margin (WIM), the Nazaré Canyon is a major feature incising the shelf and slope (Figure 1) and plays an important role in the transport of sediment to the deepwater system (Masson *et al*., 2011). Despite this, knowledge of its distal domains and how they spread on the Iberia Abyssal Plain are still lacking. Here we present early results on a combined morphological and seismic analysis of the Nazaré deepwater channel and fan system.

2. GEOLOGICAL SETTING

The West Iberia Margin origin is linked to Late Triassic to the latest Jurassic-Early Cretaceous rifting episodes related to the opening of the North Atlantic. During rifting, the Variscan basement was segmented in several extensional basins separated by ~ENE-WSW strike-slip transfer faults (Pereira and Alves, 2011). One of these faults was the Nazaré Transform Fault (NTF), which represented a major structural boundary separating two different sectors of the Peniche basin, (Alves *et al*., 2003). The oblique convergence of Africa and Eurasia plates since the Late Cretaceous and collision through the Eocene-Oligocene and Miocene was responsible for tectonic inversion of the Mesozoic sedimentary basins. The NNW-SSE Miocene compression generated a transpressional regime that reactivated the Mesozoic faults, including the NTF that bounds the north of the Estremadura Spur and extends westwards to the Tore seamount (e.g., Terrinha *et al*., 2009; Zitellini *et al*., 2009). The origin of the Nazaré Canyon was controlled by the NTF and surrounding deformation network, with early incision paths dating from the middle Miocene, subsequently

evolving to the present-day morphology (Vanney and Mougenout, 1990).

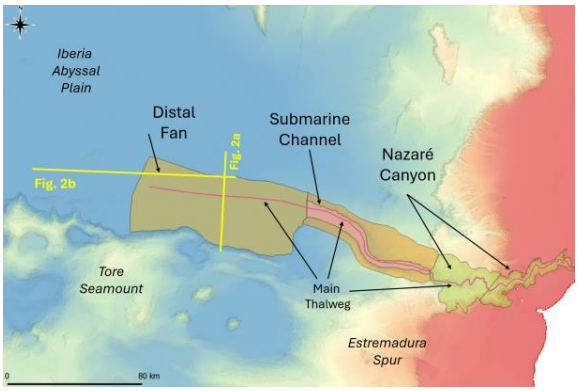

Figure 1. Map of the study area showing the Nazaré canyon and deepwater channel and fan.

3. DATA AND METHODS

This work integrates seismic reflection data and bathymetric data to analyze the submarine channel morphologies. Seismic analysis was made using multichannel seismic lines running E-W and N-S on the Iberia Abyssal Plain. These lines were acquired in 2006 onboard the R/V *Akademik Shatskiy* using a 5720 in^3 bolt gun array, a streamer of 7950 m length with 636 channels and a shooting distance of 50 m. Bathymetric data made available by EMODNet was used for the seafloor morphometric analysis, namely panel F3, Version 2022 (EMODnet Bathymetry Consortium, 2022). At the latitude of Iberia, the lateral resolution of the bathymetry raster is estimated to be circa 100 m.

Integration of the datasets was made by converting the bathymetry raster to time domain using a sound velocity in water of 1500 m/s. Vertical adjustments of the seismic data were made for the best approximation of the seafloor reflection to bathymetric bottom. No other time-depth conversions were made. Morphometric analysis of the canyon and fan systems were made on GIS environment and based on the bathymetric raster, with all measurements and analysis made in the depth domain.

4. RESULTS

4.1. Seafloor morphology

The Nazaré submarine canyon and deepwater fan show morphological continuity, with expected marked changes across the different erosional and depositional settings. Three main morphological domains were established, namely the canyon, submarine channel and distal fan (Figure 1).

The canyon is defined as a predominantly incisional feature bordered by steep walls. The domain is subdivided into two sections: the shelf incision, with circa 78,5 km, and the slope incision with circa 53 km. The canyon width steadily increases to the shelf edge where the broader erosion envelope can reach up to 10 km. While the broader drainage network can reach over 15 km, the deep incision width ranges between 3 to 5 km, increasing to 9 km at the transition to the channel system.

The channel-levee morphological domain reaches up to 20 km at its wider limits, from crest to crest of the broad levee. This feature is markedly asymmetric, with a steep southern flank dipping up to 25 degrees, and the wide northern flank up to 5 degrees. The submarine channel has a bent morphology with a southwest-directed convex flank. The steeper SW flank is interpreted as being actively eroded.

The transition of the distal fan is represented by a marked drop in relief. This domain is about 50 km in width and about 100 km in length. The southern limit is imposed by the steep topography of the volcanic Tore seamount. The northern limit is defined by the gradual decrease in height, with a 300 m high levee that loses expression until mingles with the background morphology of the Iberia Abyssal Plain. Erosional morphologies are less evident on the fan, but a trail of scours aligned with the estimated path of turbidite flows and canyon outflows is well evident on the seafloor, indicating relevant deepwater current activity likely associated to the canyon flow.

4.2. Seismic Interpretation

The Narazé submarine fan overlays stratigraphic units deformed by the Miocene margin tectonic reactivation events (Figure 2). On the slope canyon and channel domains, erosion of the older deformed units occurred within locations near the modern incision path, and it is possible that the morphological features created by structures may have limited the shift of the canyon with time. Levees on the slope and channel domain only developed significantly on the unconfined northern flanks. Seismic facies of levees are generally of low or moderate amplitude, indicating generally fine sediment.

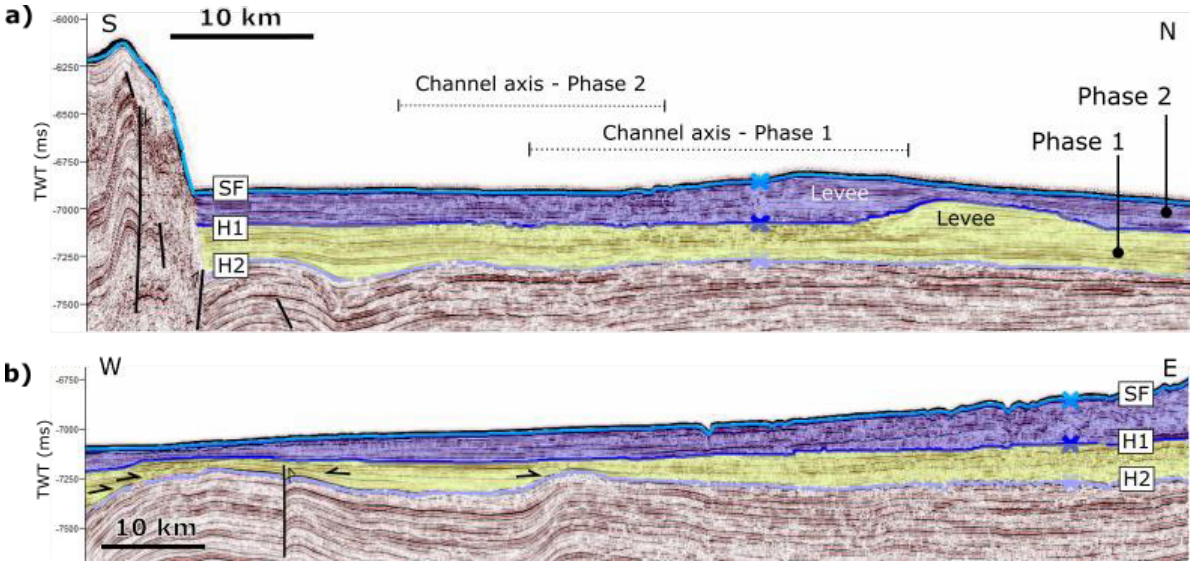

Figure 2. a) Seismic profile perpendicular to the distal channel and fan, highlighting the sequences of the interpreted Phase 1 and Phase 2. The limits of the channel axis for each phase are shown, indicating a southward shift of the system. b) seismic section along the length of the fan, showing Phase 1 sequences infilling paleoreliefs and onlapping onto folds. Phase 2 deposits as a west-thinning wedge.

On the distal domains, the deepwater fan system is defined by where the proximal abyssal plain acquires a flatter, low gradient morphology. We consider a broad Pliocene to Holocene interval for these stratigraphic sequences. We here interpret two general development stages, Phase 1 and 2. The earlier Phase 1 fan system, limited by H2 and H1 (Figure 2), presents an asymmetric channel with a developed levee on the northern flank and is limited to the south by the Tore seamount (Figure 2a). Early deposition of Phase 1 fan sediments was constrained by pre-existing deformation, with the first sequences infilling depressions and terminating toward the crest anticlines with paleo-topographic expression on the paleo-seafloor (Figure 2). Compared to the modern system, the channel axis and levee of the older Phase 1 is located between 15 to 20 km northward (Figure 2a). The recent Phase 2 fan, between H1 and the seafloor (SF) shows generally higher seismic amplitudes. The seismic facies shift between high amplitude continuous reflections with slightly disturbed reflections. Towards the deepwater distal regions, the earlier sediments of the Phase 2 fan still pinch-out towards subtle paleo-reliefs, but as the fan evolved this was overcome and the sediment deposition spread without frontal confinement (Figure 2b).

The onset of the youngest submarine channel and fan systems is estimated to have initiated around the Pliocene and shows at least two major phases. The first is interpreted to have been northward of the modern system, and its submarine channels possibly directed to the NW towards the central area of the Iberia Abyssal Plain. This system presents an asymmetric morphology, with only a northern levee. If similar to the younger system, the south flank could have been limited just by the Tore Mountain. However, there may be the possibility that a southern levee developed and was later eroded during Phase 2. A southward shift of 15 to 20 km occurred, changing the depositional locus to the present. The timing of this shift is unknown, but the depositional architecture suggests a rapid lateral migration. Causes for this are speculative, but maybe sea-level influence and/or increased sediment input to the Iberia Abyssal Plain from northeastern sources could have played a role.

5. FINAL CONSIDERATIONS

The work presents preliminary results of the overall trends of the deepwater channel-fan system adjacent to the Nazaré Canyon. We here focused on the fan sequences of estimated Pliocene to Holocene age. The first phase of development it interpreted to have been directed towards the NW of the Nazaré canyon, followed by lateral migration of the fan and formation of the modern fan. A major limitation to understand this fan system is the lack of wide-reaching data coverage, and further campaigns would be vital to understand the deepwater sedimentary dynamics associated to one of the major sediment sinks of the margin.

Acknowledgements

D. Gamboa thanks funding to CESAM by national funds through FCT – Fundação para a Ciência e a Tecnologia I.P., under the project/grant UID/50006 + LA/P/0094/2020. C. Roque´s work is also supported by the Portuguese Fundação para a Ciência e Tecnologia, FCT, I.P./MCTES through national funds

(PIDDAC): UID/50019/2025 and LA/P/0068/2020 https://doi.org/10.54499/LA/P/0068/2020).

REFERENCES

Alves, T.M., Gawthorpe, R.L., Hunt, D.W. and Monteiro, J.H. (2003). Post-Jurassic tectono-sedimentary evolution of the Northern Lusitanian Basin (Western Iberia Margin). *Basin Research*, 15, 227-249.

Bührig, L. H., Colombera, L., Patacci, M., Mountney, N. P., and McCaffrey, W. D. (2022). A global analysis of controls on submarine-canyon geomorphology. *Earth-Science Reviews*, 233, 104150.

EMODnet Bathymetry Consortium (2022). EMODnet Digital Bathymetry (DTM 2022). EMODnet Bathymetry Consortium. https://doi.org/10.12770/ff3aff8a-cff1-44a3-a2c8-1910bf109f85

Fisher, W. L., Galloway, W. E., Steel, R. J., Olariu, C., Kerans, C., and Mohrig, D. (2021). Deep-water depositional systems supplied by shelf-incising submarine canyons: Recognition and significance in the geologic record. *Earth-Science Reviews*, 214, 103531.

Masson, D. G., Huvenne, V. A. I., De Stigter, H. C., Arzola, R. G., and LeBas, T. P. (2011). Sedimentary processes in the middle Nazaré Canyon. *Deep Sea Research Part II: Topical Studies in Oceanography*, 58(23-24), 2369-2387.

Pereira, R. and Alves, T.M. (2011). Margin segmentation prior to continental break-up: A seismic-stratigraphic record of multiphased rifting in the North Atlantic (Southwest Iberia). *Tectonophysics*, 506, 17-34.

Terrinha, P., Matias, L., Vicente, J., Duarte, J., Luís, J., Pinheiro, L., Lourenço, N., Diez, S., Rosas, F., Magalhães, V., Valadares, V., Zitellini, N., Roque, C. and Víctor, L.M. (2009). Morphotectonics and strain partitioning at the Iberia–Africa plate boundary from multibeam and seismic reflection data. *Marine Geology*, 267, 156–174.

Shepard, F. P. (1972). Submarine canyons. *Earth-Science Reviews*, 8(1), 1-12.

Vanney, J. R., and Mougenot, D. (1990). A Gouf-type canyon, the Canhão-da-Nazaré (Portugal). *Oceanologica Acta*, 13(1), 1.

Wahab, A., Hoyal, D. C., Shringarpure, M., and Straub, K. M. (2022). A dimensionless framework for predicting submarine fan morphology. *Nature Communications*, 13(1), 7563.

Zitellini, N., Gràcia, E., Matias, L., Terrinha, P., Abreu, M.A., DeAlteriis, G., Henriet, J.P., Dañobeitia, J.J., Masson, D.G., Mulder, T., Ramella, R., Somoza and L., Diez, S. (2009). The quest for the Africa–Eurasia plate boundary west of the Strait of Gibraltar. *Earth and Planetary Science Letters*, 280, 13–50.

Exploring Holocene marine depositional system off Sado river (Portugal)

A. Oliveira (1,2), J. Pombo (1), N. Lapa (1), J. Duarte (1,2), A. Vinhas (1), S. Moreira (1,2) and A. Rodrigues (1,2)

(1) Instituto Hidrográfico, Lisboa, Portugal. anabela.oliveira@hidrografico.pt
(2) Instituto D. Luiz, Faculdade de Ciências, Universidade de Lisboa, Portugal.

Abstract: During the IH SEDMAR expedition (2021), three vibrocores were collected to identify significant changes in marine depositional environments off Sado River (Portugal). With a detrital nature, the analysed sedimentary column show, from bottom to top, four major mineralogical units. All the cores show a siltation process (increase of clay minerals and silt) in the top layer, reflecting a notorious decrease in local hydrodynamic energy confirming the reduction of sandy sediments exported by the river to the shelf, in the last century (anthropogenic effect).This paper present new radiocarbon dating to further explore the middle-shelf depositional systems.

Keywords: *sediments, marine deposits, Sado river, Holocene*

1. INTRODUCTION

Sedimentological chart (Instituto Hidrográfico, 2010) indicates the presence of coarse sandy sediments on the inner shelf along the Arrábida chain and finer sandy sediments in the submarine delta of the Sado River. However, in the middle-shelf region, at depths greater than the 70 m, an elongated sandy muddy and muddy deposit develops parallel to the coastline (Figure 1).

During the SEDMAR campaign, conducted by the Instituto Hidrográfico aboard the NRP Gago Coutinho in April 2021, three vibrocores (VC) were collected from the middle-shelf muddy deposits at depths ranging from 71 to 82 m. The purpose of this study is to analyse and describe significant past changes in marine depositional environments (Figure 1).

2. METHODS

The three VC's were retrieved, using a P-3C Vibrocorer Rossfelder system and exhibited varying lengths: 5.05 m (VC2), 3.65 m (VC1) and 2.13 m (VC3). Grain-size analyses were performed using two complementary methods, laser diffraction (<500 µm) and sieving (>500 µm). The sediments grain-size classification followed the simplified Folk (seven classes). The multi-mineral analysis semi-quantification were carried out on the fraction <500µm, by X-ray diffraction (XRD), using an AERIS Panalytical benchtop system, with Kα Cu (λ=1.5406) radiation. Terrigenous/biogenic and fine/coarse mineralogical ratios, were constructed.

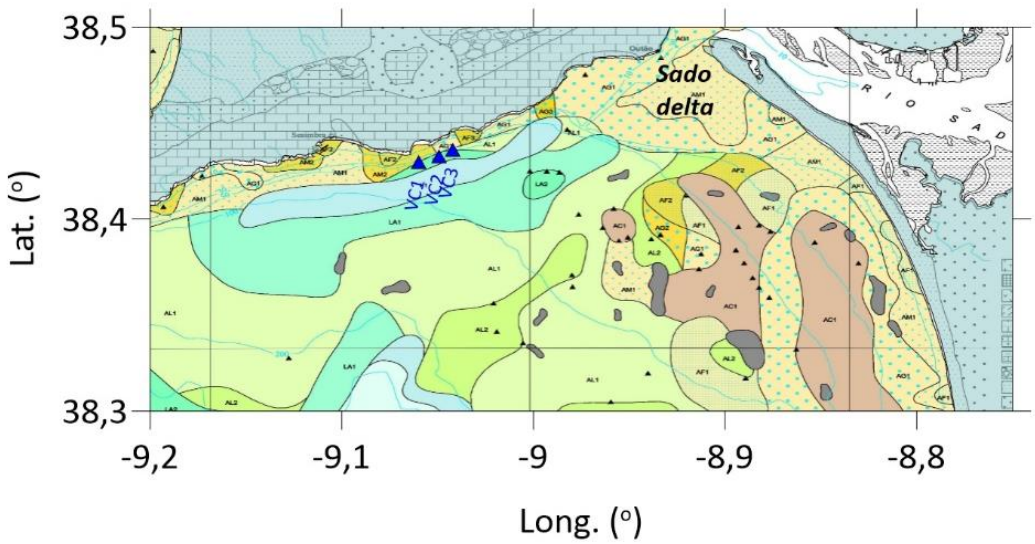

Figure 1. Vibrocores sampling position map, superimposed on an extract of IH-SED5 chart. In the chart, yellow-brown colour represent gravel-sandy sediments, green—blue colours indicate muddy sediments, and grey areas correspond to rocky outcrops.

Five radiocarbon dating of intact bivalves shells from VC2, were performed by standard AMS ^{14}C at Beta Analytic Radiocarbon Dating Laboratory (USA). The five dates will be used to construct an age-depth model, which is essential for establishing a reliable chronological framework. This framework enables accurate temporal correlation of sedimentary events and environmental changes recorded in the cores.

3. RESULTS

With a typical detrital signature the mineral assemblages of the studied vibrocores include quartz (73-30%), calcite (25-2%), dolomite (20-1%), aragonite (25-1%), microcline (13-1%), albite (9-2%), and vestigial minerals - muscovite, kaolinite, chlorite, augite and orthoclase (<5%).

In all vibrocores, four major textural and mineralogical units were identified. In VC3, only the two upper units (U3 and U4) were sampled.

Units from VC2 (Figure 2): U1 (~500-284 cm) – muddy sands sediments, where quartz (43-62%) and feldspars prevails; U2 (~284-216 cm) – sandy sediments, corresponds to a quartz increasing interval (50-73%); U3 (~216-56 cm) – muddy sands to mixed sediments, consistent to a quartz decreasing sequence with increment of biogenic carbonated content; U4 (~56-0 cm) – sandy muds sediments, consistent with an increase of clay mineral namely muscovite (7-23%), kaolinite (1-10%) and fine/coarse ratio. This last unit can be divided in two sub-units (U4a and U4b) related with an increase of silt and clay minerals to the top (~15-30 cm).

Dating of VC02, at the base (481-482 cm), provided a 95.4 % probability calibrated range of 8381-8032 cal BP ; and at the top layer limit (61-62 cm) an age of 485-142 cal BP. The two other dates (331-332 cm and 189-191 cm) permitted to delimit the U2 unit (sandy layer) given an age of 5454-5019 cal BP, at the base, and 3537-3142 cal BP, at the top (Figure 2).

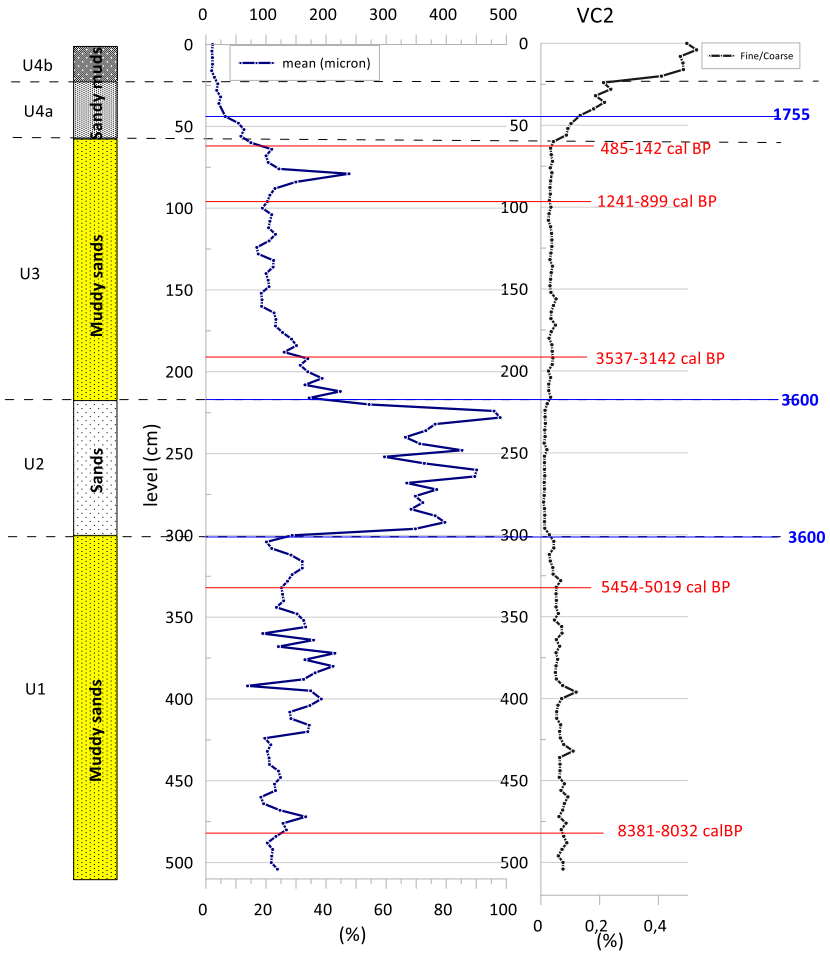

Figure 2. Along cores variability of mean grain size and mineralogical ratio (fine/coarse). Red lines represents the radiocarbon dating layers; and blue lines represents possible layers of 1755 and 3.6 cal BP tsunamis.

4. FINAL CONSIDERATIONS

The sedimentary and multi-mineral description of the three vertical samples, was previously presented by Oliveira *et al*. (2024) and Pombo *et al*. (2024), and are coherent with major changes in the marine environmental depositional system, namely (Figure 2):

a) in all VC, the upper layer (thickness ranging between 55 to 60 cm) show an increase in clay minerals and silt fraction percentage, reflecting a notable decrease in local hydrodynamic energy to the top;

b) an exotic clean sandy level was detected interbedded between muddy sand sediments, with a thickness of 52 cm (in VC01) and 68 cm (in VC2); this layer was not found in VC3.

Dating confirms the reduction of sandy sediments exported by the river to the shelf, over the last centuries, and raises the possibility that extreme high-energy events have affected this sector of the Portuguese Margin, inducing tsunami waves such as the 1755 and the 3.6 cal BP episodes.

Acknowledgements

This work is a contribution to the SEDMAR programme, an internal IH program addressed to the study and mapping of the Portuguese Marine Sedimentary Deposits. The authors wish to thanks the crew of the navy ship NRP "Gago Coutinho" and laboratory staff of the Marine Geology Division.

REFERENCES

Instituto Hidrográfico (2010). *Sedimentos superficiais da plataforma continental*. Folha SED5 (Do Cabo da Roca ao Cabo de Sines), esc. 1:150 000, 1ª Edição.

Oliveira, A., Pombo, J., Lapa, N., Duarte, J., Vinhas, A., Moreira, S., and Rodrigues, A. (2024). Multi-mineral approach to detect hydrodynamic changes in the recent sedimentary layer off Sado continental shelf (Portugal). *Actas das 3as Jornadas Luso Españolas de Hidrografia*. 9 a 11 de outubro, Cádis, Espanha, pp.158-161.

Pombo, J., Oliveira, A., Duarte, J., Moreira, S., Vinhas, A., Lapa, N., and Rodrigues, A. (2024). Mid-shelf depository associated with Sado River and Arrábida Ridge – Portugal. *Actas das 3as Jornadas Luso Españolas de Hidrografia*. 9 a 11 de outubro, Cádis, Espanha, pp.198-201.

Cross-Shore Sediment Transport and Depositional Patterns of a Clinoform on the Northeastern Madeira Shelf: From Siliciclastic to Mixed Siliciclastic-Carbonate Deposition

S. Moreira (1,2), R. Quartau (1,2), A. Oliveira (1,2), J. Pombo (1), A. Rodrigues (1,2), N. Lapa (1), M. Ribeiro (1) and A. Vinhas (1)

(1) Instituto Hidrográfico, Lisboa, Portugal. sandra.moreira@hidrografico.pt
(2) Instituto Dom Luiz, Lisboa, Portugal

Abstract: The spatial distribution of surface sediments along a cross-shore transect of a clinoform structure on the northeastern shelf of Madeira Island reveals a distinct shift in both textural and compositional characteristics. This pattern reflects the influence of hydrodynamic forcing, with sediment distribution controlled by grain size and density-dependent sorting processes. Additionally, the offshore increase in biogenic particles is interpreted as resulting from reduced terrigenous input with increasing distance from the coast, combined with enhanced carbonate marine productivity. These results highlight the dynamic relationship between sediment provenance, transport processes, and depositional conditions, illustrating how these factors collectively control the structure and sedimentary characteristics of a clinoform on a wave-dominated volcanic island shelf.

Keywords: *subaqueous clinoforms, volcanic island, wave-dominated shelf, sediment transport, hydraulic sorting*

1. INTRODUCTION AND OBJETIVES

Subaqueous clinoforms are progradational sedimentary features commonly developed on the shelves of volcanic islands, which reflect the interplay between sediment supply, hydrodynamics, and shelf morphology. These sedimentary forms play a key role in understanding sediment transport pathways, depositional processes, and the long-term evolution of insular shelves.

On Madeira Island (Portugal), located in the North Atlantic Ocean, the shelf reflects its volcanic origin and is subjected to contrasting oceanographic conditions. The southern shelf, sheltered from the prevailing wave regime from the northern quadrant, has been the focus of previous studies that identified several types of clinoforms (Belvisi, 2024). In contrast, the northern shelf, where the hydrodynamic regime is more energetic due to the direct influence of wave action (Rusu and Soares, 2012), remains poorly studied regarding its sedimentary architecture and nature.

This study focuses on the northeastern shelf of Madeira Island, aiming to characterise the surface sediments in relation to seabed morphology. Specifically, it seeks to investigate sediment textural and compositional variability along a cross-shore transect; establish potential relationships between sediment properties and seabed morphological features; and provide insights into to sediment sources, transport processes, and depositional dynamics in an exposed insular shelf setting.

2. DATA ACQUISITION

In May 2017, within the framework of the Marine Sediments Mapping Program (SEDMAR), a survey was conducted aboard the Portuguese research vessel NRP *Almirante Gago Coutinho* on the northeastern shelf of Madeira Island (Figure 1). The survey aimed to collect acoustic and geological data through high-resolution multibeam bathymetry, sub-bottom seismic profiling, and surface sediment sampling using grabs along a cross-shore transect.

3. METHODOLOGY

A total of 10 surface sediment samples were collected along the transect and analysed at the facilities of Instituto Hidrográfico for textural and compositional characterization.

Textural analysis was performed using a combined approach. After subsampling, the sediments were subjected to a stepwise treatment with hydrogen peroxide to remove organic matter and then wet-sieved using a 500 µm mesh sieve. The fraction coarser than 500 µm was analysed by dry sieving, while the fraction finer than 500 µm was analysed by laser diffraction using a Malvern Mastersizer 2000. Grain size statistics were calculated following the Folk and Ward (1957) method, using the software *Gradistat* (version 9.1).

The mineralogical composition was assessed by X-ray diffraction (XRD) on bulk powdered samples to identify and semi-quantify the main minerals.

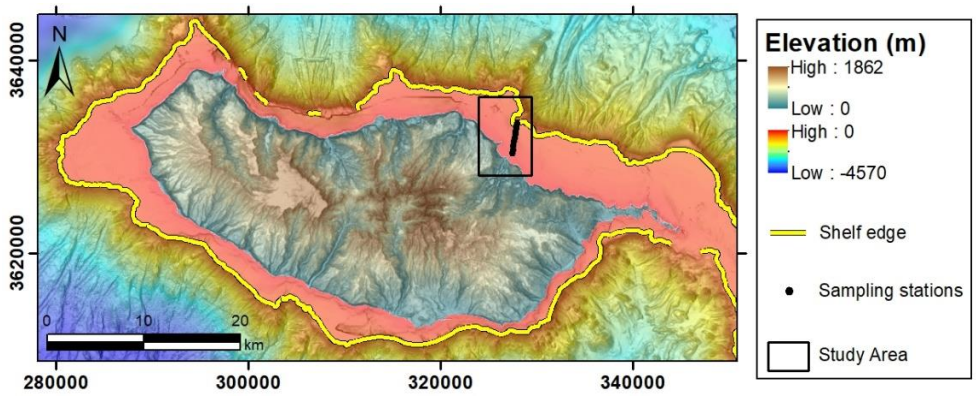

Figure 1. Location of the study area and sediment sampling stations on the northeastern shelf of Madeira Island.

The survey aimed to collect geological and acoustic data, including grab sediment samples, multibeam bathymetry, and seismic profiles. In this study, the results from the analysis of surface samples from the sedimentary cover, collected along a shelf cross-shore transect (Figures 1 and 2),

4. RESULTS AND DISCUSSION

The morphological data analysis revealed the presence of a clinoform structure with a rollover point at a depth of *ca*. 45 m (Figure 2) on the studied sector.

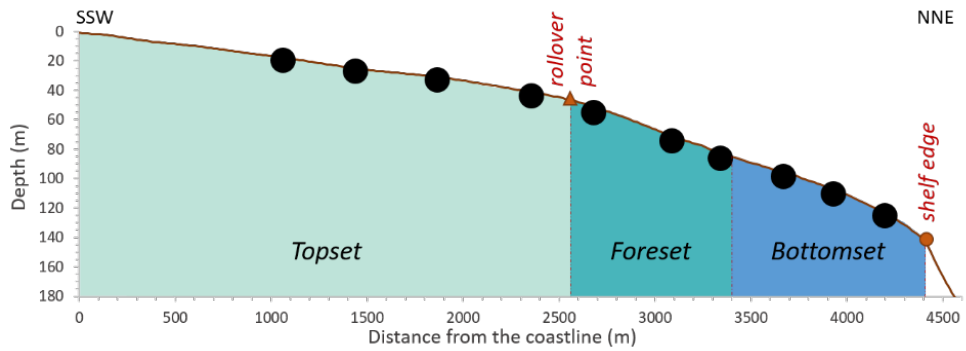

Figure 2. Cross-shore bathymetric profile of the northeastern shelf of Madeira Island, with the location of sediment sampling stations and the identified clinoform geometry.

The sediments are composed predominantly of sand-sized particles (>70%), with negligible gravel content (<1%) (Figure 3). A progressive increase in the muddy fraction is observed with increasing depth, not exceeding 25%, resulting in a seawards-fining trend. This is expressed by a gradual sedimentary facies transition across the clinoform, from sand on the topset to sandy mud on the foreset and bottomset, reflected in both mean grain size (Figure 3) and modal class. All samples exhibit unimodal grain size distributions, but sediments become increasingly poorly sorted with increasing distance from the coastline. Grain size curves broaden, become more peaked, and show greater asymmetry, reflecting differential depositional processes along the transect.

Silicates such olivine, pyroxene, and plagioclase represent more than 75% of the sediment mineralogical composition, occurring in variable proportions, whereas oxide minerals, although ubiquitous across the insular shelf, occur in very low concentrations (Figure 4). However, this siliciclastic signature is progressively diluted offshore by bioclastic carbonate material. Although Ca-bearing carbonates are scarce in the inner shelf near the coast (depths shallower than 50 m), their contribution becomes more pronounced beyond the rollover point, with concentrations increasing from 4 to 22% (Figure 4).

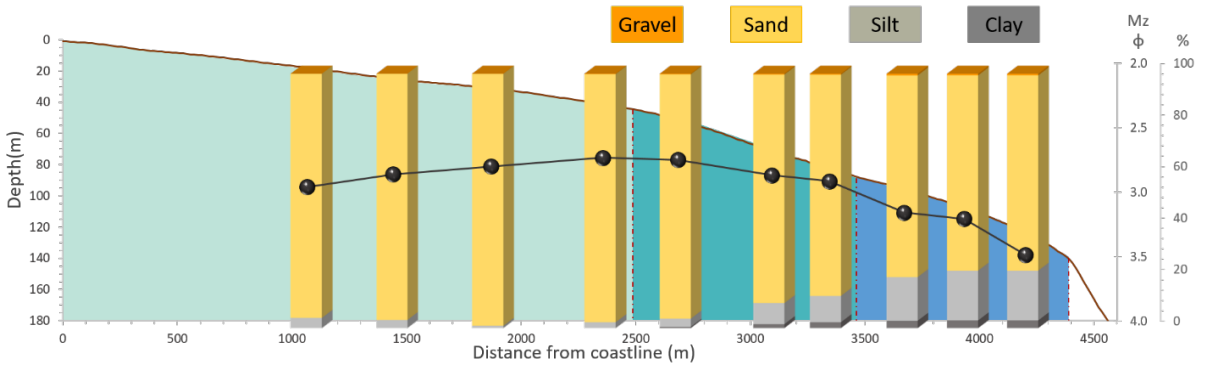

Figure 3. Spatial variation of the main textural classes and the mean grain size (Mz) of surface sediments along the cross-shore bathymetric profile.

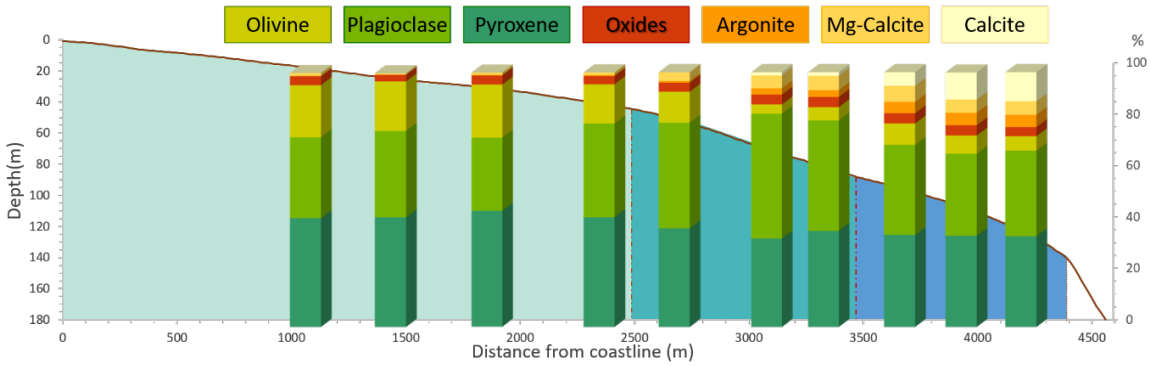

Figure 4. Spatial variation in the mineralogical composition of surface sediments along the cross-shore bathymetric profile.

The mineralogical pattern along the profile highlights a relative increase in plagioclase abundance along the topset and foreset down to 75 m depth, accompanied by a decrease in other silicates, reflecting density-dependent selective transport. Similarly, in the topset and foreset, Mg-calcite dominates over aragonite and, where present, calcite, while in the bottomset, calcite becomes the dominant carbonate mineral type.

The spatial distribution of textural and compositional sediment parameters along the clinoform reflects a clear zonation, with coarser siliciclastic sedimentation on the topset, whereas a mixed siliciclastic-carbonate assemblage prevails offshore. This pattern reflects the increasing distance to terrigenous particle sources and the progressive decrease in hydrodynamic energy, both influencing the nature of the sediments along the offshore gradient. Along the study transect, grain size is influenced by the winnowing of finer particles that subsequently settle by gravitational settling as hydrodynamic energy decreases, while mineralogical composition is controlled by density-based segregation of minerals during transport and deposition.

The offshore increase in bioclastic content likely results from a reduced terrigenous sediment input, which raises their relative proportion, possibly combined with a moderate increase in local biogenic productivity. The transition from Mg-calcite dominance to calcite dominance further supports a decline in energy levels, as calcite's crystal structure is more prone to mechanical breakage than that of Mg-calcite and aragonite.

5. CONCLUSIONS

These findings highlight the combined influence of terrigenous input and hydraulic sorting in controlling both sediment texture and mineralogical composition along the clinoform. The change from fine sands nearshore to very fine sands offshore reflects the combined action of winnowing and gravitational settling in response to the prevailing hydrodynamic conditions, which lead to an offshore increase in the muddy fraction. Regarding mineralogical composition, the spatial distribution is controlled by density-based sorting of the lithoclastic component and a progressive decline in terrigenous input, which enhances the relative abundance of biogenic particles. This reveals the complex interactions that govern sediment distribution along a volcanic island shelf, providing new insights into the sedimentary dynamics of Madeira Island shelf. Understanding these processes is

critical for interpreting sedimentary environments and for supporting informed policy decision-making aimed at the protection and sustainable exploration of these natural systems.

Acknowledgments

This is a SEDMAR Program Contribution. The authors thank all IH staff involved in the oceanographic survey, the crew of the N.R.P. "Gago Coutinho", the Portuguese Navy Hydrographic Brigade and the laboratory staff of the Division of Marine Geology for their support.

REFERENCES

Belvisi, V. (2024). *Sedimentary dynamics on the southern insular shelf of Madeira Island: insights from geophysical and sediment sampling data*. PhD Thesis, Universidade de Lisboa, 194 p.

Folk, R.L. and Ward, W.C. (1957). Brazos River bar: a study in the significance of grain size parameters. *Journal of Sedimentary Petrology*, 27, 3-26.

Rusu, E. and Soares, C.G. (2012). Wave energy pattern around the Madeira Islands. *Energy*, 45(1), 771-785.

Morpho-stratigraphic characterization and seafloor sediment distribution on the shelf of Corvo Island (Azores Archipelago)

S. Innocentini (1,2), R. Quartau (3,4), J. Madeira (4), D. Casalbore (1,2), P. Brito (5) and A. Rodrigues (3,4)

(1) Istituto di Geologia Ambientale e Geoingegneria, Consiglio Nazionale delle Ricerche, Rome, Italy
(2) Dipartimento Scienze della Terra, Sapienza Università di Roma, Rome, Italy
(3) Divisão de Geologia Marinha, Instituto Hidrográfico, Lisboa, Portugal. rui.quartau@hidrografico.pt
(4) Instituto Dom Luiz, Faculdade de Ciências, Universidade de Lisboa, Portugal
(5) Divisão de Geologia Marinha e Georecursos, Instituto Português do Mar e da Atmosfera, Lisboa, Portugal

Abstract: This study presents a morpho-stratigraphic and sedimentary characterization of Corvo Island's shelf (Azores Archipelago), based on the interpretation of multibeam data, seismic reflection profiles, and sediment samples. The shelf, shaped by volcanic construction and marine reworking, exhibits marked asymmetry and variable sediment cover with thickness and architecture controlled by shelf morphology and wave exposure. Seismic data reveal an erosional volcanic basement, mostly overlain by the recent sedimentary cover and locally outcropping as remains of lava flows. Sediment sampling and textural analysis indicate a dominance of moderately sorted volcaniclastic sands and gravels, with low carbonate content. Grain size distribution correlates with backscatter intensity, allowing classification into three main sediment types, with coarser material on the more exposed side of the island and finer material concentrated in more sheltered sectors.

Keywords: *morpho-bathymetry, sediment distribution, volcanic basement, insular shelf, Corvo Island*

1. INTRODUCTION

Corvo, part of the Azores' western group and located on the North American plate, has a geological history tied to the Mid-Atlantic Ridge. Its exposed position, lacking natural barriers, makes it one of the archipelago's most wave-impacted islands. Waves mainly approach from the west and northwest (55% of cases; 2.6–2.7 m), followed by the north (22%; 2.1–2.3 m), southwest (9%; 2.4–2.6 m), and eastern sectors (14%; 2.0–2.3 m) (Quartau *et al*., this volume).

Unlike larger and geologically more complex volcanic islands, Corvo's small size and relatively simple structure provide a clearer framework for investigating the processes that shape its insular shelf, including both constructional and erosional dynamics. This study combines morpho-bathymetric mapping, sub-bottom seismic interpretation, and sediment analysis to examine the seafloor and underlying sedimentary architecture.

2. DATA AND METHODS

Corvo's submarine environment was newly mapped through targeted oceanographic campaigns within the framework of the HAZARDOUS project.

2.1. Geophysical dataset

Multibeam bathymetry and backscatter strength data (Figures 1A and 1B, respectively) were collected during two DGNSS-positioned surveys conducted in the summers of 2018 and 2019 (Instituto Hidrográfico, 2018, 2019). The first survey focused on deeper waters (approx. -40 to -2000 m), using KONGSBERG EM710 and EM120 multibeam echo sounder (MBES), operating at 12 kHz and 70–100 kHz, respectively, with 120° angular coverage. The second survey targeted shallower areas (approx. -2 to -70 m), employing a KONGSBERG 2040C MBES, at 300 kHz, with 100° angular coverage. Data was processed with CARIS HIPS software (v10.4.15), to produce high-resolution bathymetric surfaces and backscatter mosaics. The 2018 backscatter data was processed at an 8 m resolution, while the 2019 dataset achieved a finer 2 m resolution.

A seismic reflection survey was carried out in the summer of 2022 onboard the "Senhora dos Milagres" launch. Data was collected with an Applied Acoustics Engineering equipment (boomer system) using Delph Seismic Acquisition software. The positioning of the seismic survey was ensured by an onboard DGPS (average horizontal positioning error of less than 1 m). Survey lines were spaced up to 250 m apart, forming orthogonal grids in the western and southern shelf sectors, with a sparser network across the remaining shelf (see Figure 1A, Quartau, 2022). Since seismic data (Figure 1C) exhibited significant environmental noise and artifacts, 75 representative profiles were selected for processing from the initial dataset. Seismic data processing was carried out using RadExPro 2019.2, at Instituto Português do Mar e da Atmosfera (IPMA) to enhance the signal-to-noise ratio.

The processing employed a velocity model assuming a constant speed of 1500 m/s for the water column, increasing linearly at 35 s^{-1} with depth below the sea bottom. Subsequent seismic interpretation and sediment thickness estimation was carried out using DELPH RoadMap 4.0.

2.2. Sediment samples

In 2022, nine seafloor sediment samples were collected using a Van Veen grab (Quartau, 2022). A subsequent 2023 campaign aboard the catamaran Physeter yielded 42 additional samples using a Smith-McIntyre grab (Quartau, 2024), significantly expanding the dataset (Figure 1B). Sample locations were recorded via DGPS, with horizontal uncertainty of several tens of metres—negligible at map scale.

Laboratory analysis at IH included organic matter removal, grain-size analysis (wet/dry sieving, Dynamic Image Analysis, and Laser Diffraction) , and statistical processing with Gradistat 8.0 (Blott and Pye, 2001) using the Udden-Wentworth scale. Total Inorganic Carbon (TIC) was measured via non-dispersive infrared spectroscopy, and $CaCO_3$ content was estimated using a conversion factor of 8.33 (Verardo *et al.*, 1990).

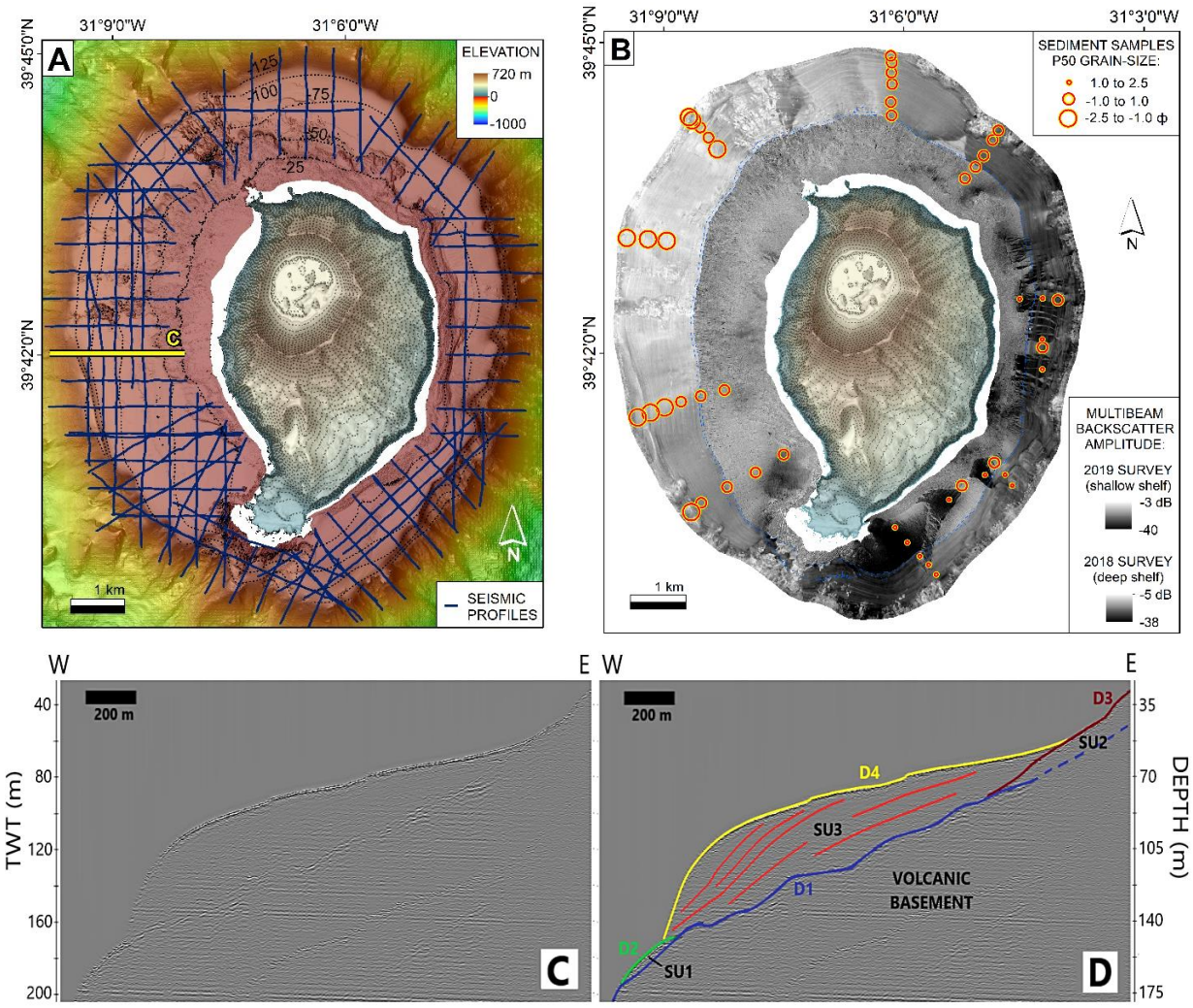

Figure 1. (A) Uninterpreted hillshade bathymetry and seismic profiles (blue lines) acquired at the insular shelf of Corvo. Yellow line locates seismic profile in (C) and (D). Thin dashed black contour lines are spaced every 25 m. (B) Multibeam backscatter mosaics of 2018 and 2019 on the same area. Lighter tones represent high backscatter values (in dB), while darker tones lower values (in dB). Orange circles mark sediment sample locations: circle size reflects median grain-size (D50 in ϕ). (C) Uninterpreted and (D) interpreted example of the E-W seismic profile, highlighted at (A). "TWT" = two-way times (in ms).

3. RESULTS AND DISCUSSION

3.1. Morpho-bathymetry of the shelf

The insular shelf of Corvo Island has a total area of ~45 km^2. The shelf is asymmetric, strongly reflecting the wave regime: its western sector reaches a maximum width of ~3.2 km, the northern sector up to 2.5 km, and the eastern sector only up to 1.7 km (Figure 2A). The morphology of the southern shelf reflects the submarine extension of the Vila Nova do Corvo lava delta, characterized by distinct, prominent convex ridges or digitated crests that rise up to 15 m above

the surrounding seafloor. Similar remains of lava flows are locally present on the western and northwestern shelves, featuring about 6% of the shelf area (~3 km^2).

The inner shelf exhibits relatively rugged morphologies, with wide extensions and lobate fronts in the west and north (Figure 1A and 2B), while the eastern side forms a narrower, shore-parallel ridge, interpreted as debris deposits accumulated from cliff failures, which cover 32% of the shelf (~14 km^2). The remaining seafloor (62%; ~28 km^2), is characterized by smooth surfaces typical of sandy sedimentary cover, with depositional rollovers extending to the outer shelf.

3.2. Shelf seismic stratigraphy

Seismic data reveal an acoustic basement marked by a continuous, high amplitude reflector (D1) on top and internal out-of-plane scattering (Figure 1D). This feature is interpreted as volcanic basement (Figure 2A), exhibiting an erosive surface that generally dips seaward at 2.5–3°, steepening up to 20° beyond the shelf break. In the eastern sector, the basement is steeper (~5°), though the shelf edge is less clearly defined. The basement depth below the sandy sediments varies, typically between 100-140 m, reaching 170 m in the southwest and shallowing to ~75 m near the Southern lava delta (Figure 2A).

Above the basement, three seismic units are identified: SU1 – a thin, stratified unit with low-amplitude reflections, forming a local clinoform body in the Western outer shelf (rollover at 150-160 m). SU2 – a chaotic unit linked to inner shelf debris deposits. Its boundary with the basement (D1) is often indistinct due to low acoustic contrast. SU3 – a more extensive, stratified unit from mid- to outer shelf, showing sigmoidal progradational bodies onlapping SU2. It culminates in a distinct rollover at the sea bottom (D4), with slope changes from <3° to ~23°, at depths from 110 m (West) to 45 m (East).

The spatial distribution of debris (SU2) and sediment cover (SU3) on the insular shelf is uneven. SU3 accumulates mainly in two areas (Figure 2B): a southwestern depocenter (up to ~70 m thick) and a continuous depocenter along the eastern shelf (up to 50 m thick). The western shelf holds the largest sediment volume (~0.23 km^3), the northern shelf the least (~0.06 km^3) and the eastern shelf is intermediate (~0.19 km^3). However, when normalized for area, the eastern shelf has the highest sediment volume per unit area (~0.20 km^3/km^2).

3.3. Seafloor sediment texture and distribution

Seafloor sediment samples are predominantly composed of moderately sorted coarse sand or fine gravel, typically exhibiting a unimodal grain-size distribution. The sediments are mainly volcaniclastic in origin (Figure 3A), with small accumulations of bioclasts, including skeletal fragments of recent organisms and in some cases red algae-encrusted volcanic cobbles (Figure 3B). The $CaCO_3$ content is generally very low, not exceeding 6%, although three samples show concentrations between 6% and 12%, and one sample has a $CaCO_3$ content up to 32%. No consistent correlation was identified between grain size, $CaCO_3$ concentration, and water depth.

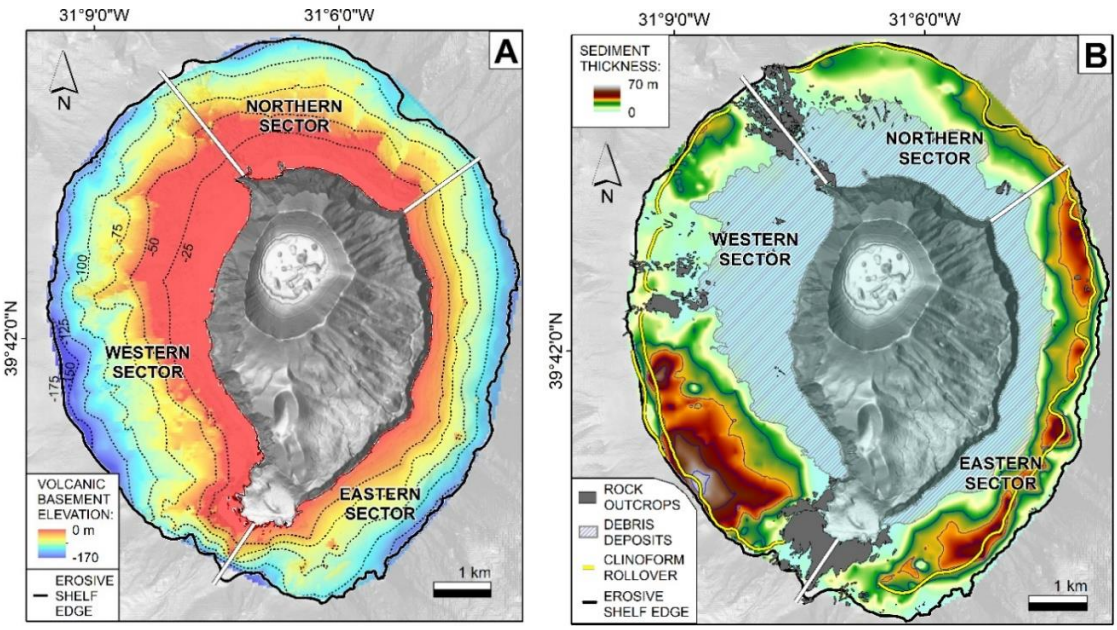

Figure 2. (A) Volcanic basement across the insular shelf. Thin dashed black contour lines are spaced every 25 m. (B) Sedimentary cover thickness (in m) of the insular shelf. Thin dashed blue isopaches are spaced every 10 m. The white lines delineate the boundaries between the shelf's sectors. Data in both maps are represented with cells size of 50 m^2.

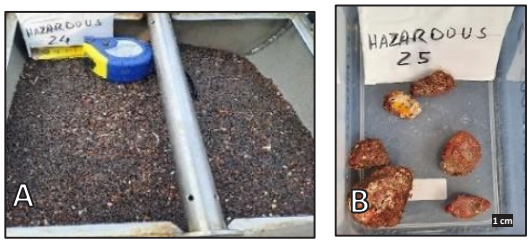

Figure 3. (A) Volcaniclastic sand with very low content of bioclasts and (B) red-algae encrustations on cobbles.

The integration of sediment texture data with corresponding acoustic backscatter intensity from multibeam data from the 2018 mosaic enabled a detailed classification of the sedimentary cover on Corvo insular shelf into three main textural categories (Figure 4):

I. Fine to very fine gravel, characterized by D50 values between -2.5 and -1.0 ϕ and backscatter strengths ranging from -5 to -15 dB. This sediment type covers approximately 20% of the shelf (~9 km²) and is predominantly present in the north, northwestern and western sectors of the shelf, as well as locally along the upper slopes surrounding the island.

II. Very coarse to coarse sand, with D50 values between -1.0 and 1.0 ϕ and backscatter strengths from -15 to -24 dB. It is the most widespread sediment class, covering around 28% of the shelf (~13 km²) and, is especially prevalent across the southwestern, northeastern, and much of the eastern sectors.

III. Medium to fine sand, defined by D50 values ranging from 1.0 to 2.5 ϕ and backscatter strengths between -24 and -38 dB. This class covers about 14% of the shelf (~6 km²), primarily concentrated along the eastern shelf, where it forms elongated cross-shore ridges. Additional significant deposits occur on the southeastern shelf, next to the lava delta.

4. CONCLUSIONS

The submerged portion of Corvo Island was studied through the integration of multibeam bathymetric data and acoustic backscatter intensity, seismic stratigraphy, and sediment textural analysis, employing a remote sensing-based approach to characterize the shelf.

The inner shelf is primarily covered by coarse heteromorphic debris deposits, originating from cliff erosion and collapse driven by marine processes. In contrast, the remainder of the shelf is generally mantled by sandy sediments, locally interrupted by remnants of ancient lava flows.

Sediment thickness and distribution varies unevenly across the insular shelf, displaying a clear pattern of textural sorting likely shaped by wave dynamics. Sediment accumulates forming depocenters, with coarser sand concentrated on the most exposed northwestern shelf, while finer sediment retained along the eastern and more sheltered side.

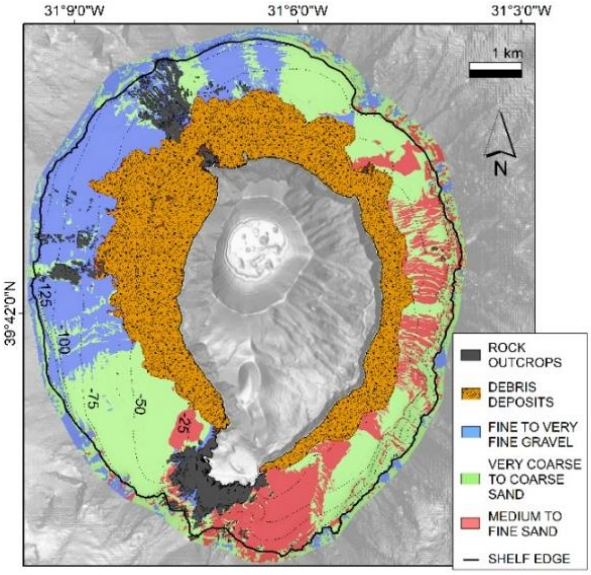

Figure 4. Seafloor characterization of Corvo's insular shelf.

Acknowledgements

This work was supported by the project HAZARDOUS (https://doi.org/10.54499/PTDC/CTA-GEO/0798/2020) funded by the Portuguese Fundação para a Ciência e a Tecnologia (FCT) I.P./MCTES.

REFERENCES

Blott, S.J. and Pye, K. (2001) GRADISTAT: a grain size distribution and statistics package for the analysis of unconsolidated sediments. *Earth Surf. Process. Landf.*, 26, 1237–1248.

Instituto Hidrográfico (2018). REL TF HI 10/18, NRP Almirante Gago Coutinho, elemento dt21mp01. Levantamento Hidrográfico Oceânico no Arquipélago dos Açores, RELATÓRIO TÉCNICO FINAL, 2018-05-04 A 2018-08-02.

Instituto Hidrográfico (2019). REL TF HI 13A/19, Brigada Hidrográfica, elemento Dt21mp01. Levantamento Topo-Hidrográfico no Arquipélago dos Açores, RELATÓRIO TÉCNICO FINAL, Vol. I, 2019-07-18 A 2019-08-2.

Quartau, R. (2022). MISSÃO HAZARDOUS 1/2022: RELATÓRIO DE CAMPO. REL PT GM 11/22. Instituto Hidrográfico, Lisboa, Portugal. pp. 21.

Quartau, R. (2024). MISSÃO HAZARDOUS 2/2023: RELATÓRIO DE CAMPO. REL PT GM 1/24. Instituto Hidrográfico, Lisboa, Portugal. pp. 28.

Quartau, R., Innocentini, S., Zhao, Z. and Rodrigues, A. (2025). Submarine landslide on the shelf of Corvo Island triggered during the winter of 2018. *XI Simpósio sobre a Margem Ibérica Atlântica*, 29-31 outubro 2025. Lisboa. Portugal.

Verardo, D.J., Froelich, P.N., and McIntyre, A. (1990). Determination of organic carbon and nitrogen in marine sediments using the Carlo Erba NA-1500 Analyzer. *Deep Sea Research Part A. Oceanographic Research Papers*, 37, 157–165.

Soft sediments from northern MAR – Azores plateau: preliminary mineralogical and geochemical results

A. Oliveira (1,2), S. Moreira (1,2), J. Pombo (1), N. Lapa (1), J. Duarte (1,2), A. Rodrigues (1,2), G. Taranto (3) and T. Morato (3)

(1) Instituto Hidrográfico, Lisboa, Portugal. anabela.oliveira@hidrografico.pt
(2) Instituto Dom Luiz, Lisboa, Portugal
(3) Instituto de Investigação em Ciências do Mar Okeanos, Universidade dos Açores, Portugal

Abstract: This paper presents preliminary results from the sedimentological analysis of eight box-cores collected in the northern Mid-Atlantic Ridge (MAR) - Azores Plateau. The data include grain-size distribution, organic and inorganic carbon content, mineralogy and elemental concentrations. Notably, intra- and inter-core compositional variability was observed, primarily due to the type of predominant biogenic remains and the presence of gravel-sized bioclasts in certain layers, some of which likely exhibit Fe-Mn oxide incrustations. The sediments are predominantly composed of planktonic organisms ($CaCO_3$ >70 %), characteristic of calcareous ooze, except in the southernmost sample, where the sediment source exhibits a plagioclase basaltic rock signature.

Keywords: *sediments, Azores, Mid Atlantic Ridge, mineralogy, elemental composition*

1. INTRODUCTION

In this paper, sediment samples collected aboard the RV "Pelagia", during the Eurofleets+ iMAR (*Integrated assessment of the distribution of vulnerable marine ecosystem along the Mid-Atlantic Ridge in the Azores region*) cruise, are analysed within the scope of the SEAMAP 2030 (*Mapping the Portuguese Sea*) program of the Instituto Hidrográfico (IH).

The iMAR cruise sought to assess the Mid-Atlantic Ridge's (MAR) influence on deep-sea biogeography, connectivity, and the spatial distribution of deep-sea benthic megafauna. It explored lesser-visited areas of the northern MAR in the Azores region, including associated ridges and seamounts at depths ranging from 300 to 1,200 meters (Morato *et al*., 2021). The acquisition of sediment samples with a box-corer also enabled, for the first time, to carry out additional sedimentological, compositional and geochemical studies along this portion of the MAR.

The Azores is a volcanic archipelago that lies at the triple junction between the North American, African and Eurasian plates, with nine islands spreading across the MAR and the Terceira Ridge (TR). The region's unique geological setting, influenced by the MAR and the Azores plateau, results in a complex depositional environment. Deep-sea sediments are primarily composed by biogenic material, such as the remains of planktonic organisms. However, volcanic activity – including hydrothermal vents, volcanic ash and other pyroclastic materials-can also contributes with authigenic particles to the sediment composition (Huneke and Mulder, 2011). Near islands and seamounts, volcanic epiclastic contribution through canyons and mass wasting events can also reach the deep-sea.

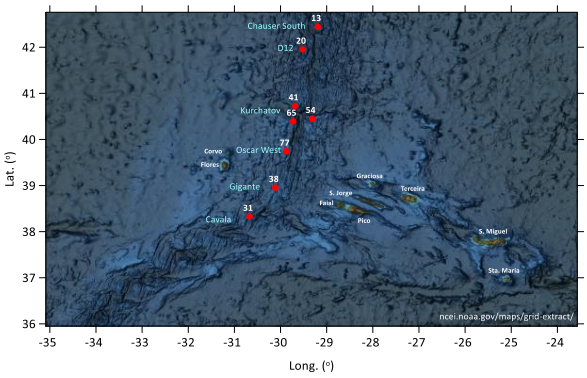

Figure 1. Study area and box-core sampling locations (red dots). Basemap extracted from ncei.noaa.gov/maps/grid-extract/.

2. METHODS

2.1. Sampling

Eight box-cores (BC) were collected between May 18 and June 2, 2021, from soft sediments overlying seamounts and ridge complexes (Figure 1) along a latitudinal gradient of the MAR. Core lengths ranged from 11 cm (BC13) to 33 cm (BC38). The cores were stored at -20°C until processing at the IH laboratory. After opening, a visual and magnetic susceptibility description was performed and subsamples were taken from selected layers. Each sample was analysed following international standards for grain size, mineralogy, total inorganic and organic carbon contents, and element concentrations.

Ancient-looking bivalve remains (>25 mm) with black spots incrustations, mainly found in the sediment

samples BC13 (3-10 cm) and BC38 (10-15 cm), after being washed and dried at 40ºC, were separated from the bulk sediment for identification and mineralogical and elemental analysis.

2.2. Analytical methods

2.2.1. Grain-size, carbonates and organic carbon

Grain size analyses were performed by combining two complementary methods, laser diffraction (<63µm) and dynamic image analysis (>63µm), according to ISO 13320:2020 and ISO 13322-2:2021. The total inorganic carbon content [converted to $CaCO_3$ % = (TIC) x 8.333] and the total organic carbon content (TOC) was determined according to IH internal accredited methods, based on EN 15936:2022.

2.2.2. Mineralogy and elemental composition

Semi-quantitative multi-mineral analyses were performed on the <500 µm fraction using X-ray diffraction (XRD) with an AERIS Panalytical benchtop system equipped with Cu Kα radiation (λ = 1.5406 Å). After sieving, the samples were ground to obtain a fine, homogeneous powder (5–10 µm) and placed in random-oriented holders. XRD patterns were collected continuously over a 2θ range of 4° to 65°, with a step size of 0.02° and a scan step time of 149 seconds. Semi-quantification of crystalline phases was determined using HighScore Plus software and Rietveld refinement.

The elemental composition of seven major and minor elements – aluminium (Al), silicon (Si), potassium (K), titanium (Ti), calcium (Ca), manganese (Mn) and iron (Fe) – was determined by X-ray fluorescence spectrometry (XRF) on bulk ground sediment, after oven-drying at 105ºC. Samples were prepared by manually pressing the powdered sediment into high-density polyethylene (HDPE) sample cups covered with an ultra-thin Mylar film. Analyses were performed using an Oxford X-MET 7500 handheld XRF spectrometer, employing two distinct factory-embedded analytical methods based on fundamental parameters calibrations. Quality control included duplicate sample analyses and repeated measurements of reference materials and internal standards.

3. RESULTS AND DISCUSSION

The lab analysis allows to present the following sedimentological results:

- All BCs mainly consist of coarse-grained sediments, with sands representing the dominant textural class, with very low TOC content (< 1.1 %).
- The highest contents of gravel-sized particles occur in the uppermost 10 cm of BC13 and BC38, reaching maxima of 47% at 3-10 cm and 42% at 5-10 cm, respectively.
- With exception of the southernmost box-core (BC31), all BCs display high TIC contents (≥ 9%), corresponding to an estimated $CaCO_3$ content of at least 70%.
- BC31 presents the highest sand content (>94%) and the lowest TIC content, not exceeding 1%.
- Although variable in content, the muddy fraction (<63µm) occurs in higher proportions in BC20 (mean 43%), BC38 (mean 19%), BC41 (mean 42%), BC54 (mean 42%), BC65 (mean 28%), and BC77 (mean 18%).

The XRD mineralogy reflects the observed grain-size variability and TIC content. In all BC samples, carbonate minerals (calcite, aragonite and Mg-calcite) predominate (Figure 2) as it is shown by the Ca concentration (30-37 %, at least an order of magnitude higher than other analysed elements) except in BC31:

- In BC13, carbonates values are around 97 %, with quartz (<3%) present in trace amounts. The elemental abundance follows the order: Ca > Si and Al > Fe > K > Mn > Ti
- In the BC31 sample, a strong basaltic rock signal was detected (Figure 3), with elemental concentrations occurring in the following order of abundance: Si > Ca > Al > Fe > Ti > K > Mn. The Ca-Na plagioclase (bytownite), pyroxene (diopside) and olivine predominate, with carbonated minerals comprising less than 20%, being dominated by calcite (aragonite and Mg calcite were absent). The Ca content in these sediments (9.9% –10.4%) is 3 to 4 times lower than in the other BCs.
- In BC77, a slight basaltic signal was detected with only Ca-Na plagioclase present (2-16%), while carbonate minerals accounts for more than 92%. The relative abundance of elements decreases in the following sequence: Ca > Si > Al >Fe > K > Ti > Mn.
- In BC20, BC38, BC41, BC54, and BC65, carbonate minerals dominate, representing over 99% of the mineral content (Figure 2). Quartz and biotite were also detected in trace amounts (<1%). For BC20 and BC41, the order of elemental abundance is Ca > Si > Al > Fe > K > Mn > Ti, while in BC54 and BC65 a shift is observed in the order of abundance between Mn and Ti. In BC38, two sectors can be identified based on the elemental order of abundance: in the uppermost 10 cm, the order is Ca > Si ~ Fe > Al > Mn > K > Ti, whereas in the remaining BC the dominant abundance sequence is Ca > Si >Al > Fe > K > Ti > Mn.

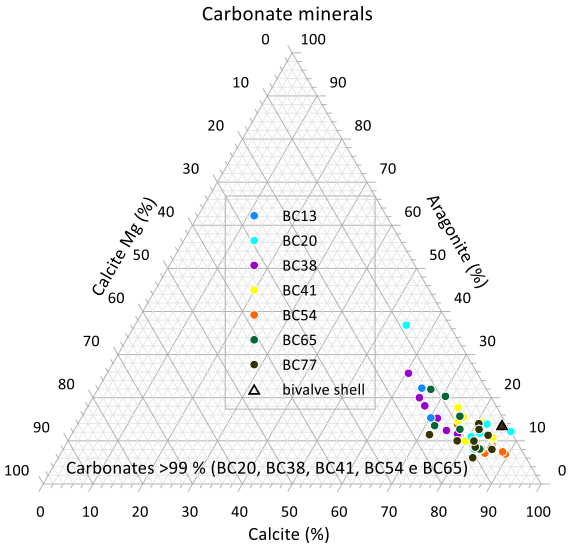

Figure 2. Ternary diagram showing the carbonate minerals of the analysed sediments, compared with XRD data from a bivalve shell. Intra and inter-BC variability can be observed.

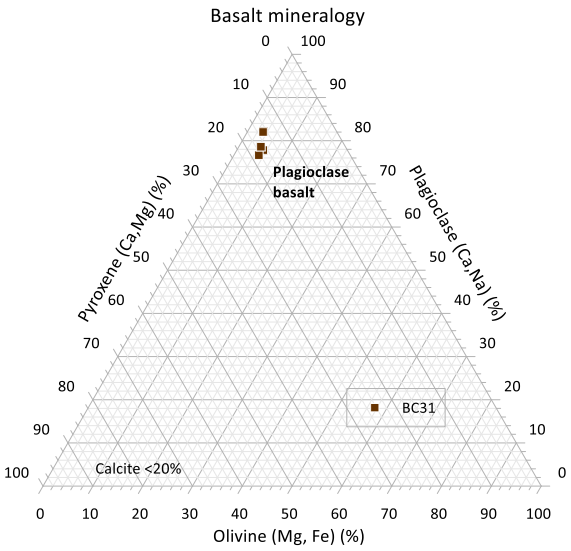

Figure 3. Ternary diagram of the basaltic mineralogy of BC31 sample. Internal variability can be observed.

As expected, the sediments are predominantly formed by carbonates mainly due to remains of biogenic planktonic organisms. A visual inspection by binocular magnifying glass of the fraction <500 µm allowed the identification of abundant planktonic foraminifera, isolated valves of ostracods and sponge spikes (*triactinas*, typical of *Calcarea class* - formed by calcite and aragonite). In the fraction 0.5-30 mm remains of old broken grey bivalve shells (not identified) with black incrustations, ancient coral rubble (probably *Scleractinia*) and modern pelagic gastropods - *pteropods* with aragonitic shells - were found. Coral rubble has been extensively documented in imagery collected from these sites (Morato *et al.*, 2021). XRD analysis performed on the ground grey bivalve shell showed a composition of 85 % calcite, 14 % aragonite, and 1 % Mg-calcite.

An example of compositional variability can be observed in BC38 (Figure 4). The general downcore variation in elemental concentrations shows a broadly concomitant behaviour between Ca and Mn, indicating that Mn is associated with carbonate minerals, whose abundance increases towards the surface. In contrast, the other elements exhibit an opposite trend. Two distinct sequences can be identified along the BC38 sample:

a) a lower section, from the bottom up to 15 cm below the surface, where Ca concentrations range from 34% to 35% and Mn contents remain low (0.1% – 0.2%); and

b) the uppermost 10 cm, where both Ca (~36%) and Mn (0.4% – 0.5%) concentrations are higher (Figure 4) and the gravel content ranges from 28% to 42%.

This variation was attributed to high content of reworked bioclastic fragments with blackish incrustations, observed in the uppermost sequence. Elemental analysis conducted directly on the surface of two distinct fragments revealed Ca concentrations of 17% and 26%, and Mn concentrations of 5.7% and 4.95%. These Mn values are approximately ten times higher than those observed in the bulk sediment, indicating a strong association of this element with the bioclastic fraction (probably as Fe-Mn oxides precipitates). The dilution of Mn in the bulk sediment likely reflects the contribution of other modern carbonate sources.

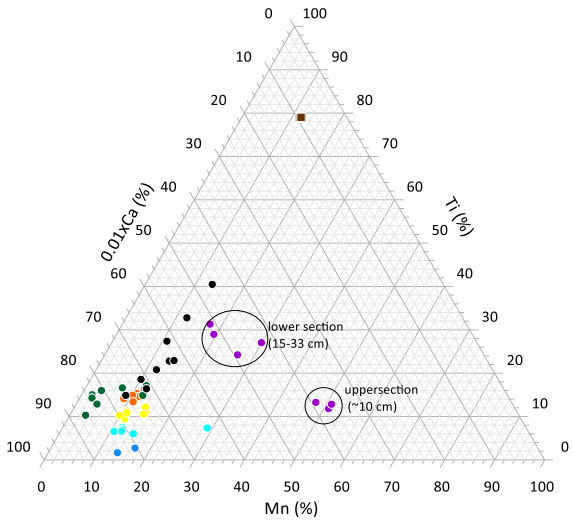

Figure 4. Ternary diagram showing the Ca-Ti-Mn interrelationships for BC samples. Calcium (Ca) content was divided by 100, for graphical representation. The two layers of BC38 are delimited by open circles.

Figure 4, represents the relation between Ca, Ti and Mn contents to assess the variability of terrigenous sources (represented by Ti) versus the biogenic component (represented by Ca) and Mn (a probable hydrothermal element).

4. FINAL CONSIDERATIONS

Preliminary results of the sedimentology, mineralogy, and major elements of eight box-cores collected in the MAR Azores region show that:

1) all BCs mainly consist of coarse-grained sediments, with sands as the dominant textural class;
2) the carbonate signal (calcite, aragonite and Mg-calcite minerals) prevails, with $CaCO_3 > 70$ %, compatible to a calcareous ooze. Exception was observed in BC31, where the sediment shows a plagioclase basic rock (basalt) signature;
3) the observed intra- and inter-BC compositional variability is mainly due to the type of predominant biogenic remains, as well as the presence of gravel-sized bioclasts, likely in the form of Fe-Mn oxide incrustations observed in some layers.

The presence of gravel-sized bioclasts with Fe-Mn oxide incrustations raises several questions: Could this characteristic indicate continuous and/or ancient hydrothermal activity and plume dispersion driven by deep-sea currents? Do local conditions favour the precipitation of Mn, a hydrothermal chemical element transported in suspension, onto shells, away from the venting area? Could the biogenic remains (broken shells) found in gravel bioclastic layers be the result of transport by turbidity currents or submarine landslides?

Acknowledgements

This paper is a contribution to the SEAMAP 2030 (Mapping the Portuguese Sea) program of the Portuguese Hydrographic Institute (IH).

RV “Pelagia” ship-time was provided free of charge as part of the iMAR project which received funding from the European Union's H2020 Research & Innovation Programme under grant agreement No. 824077 EUROFLEETS+. Additional funding was provided by the European Union’s Horizon 2020 research project iAtlantic (No 818123), and the project M1.1. A/REEQ. CIENTÍFICO UI&D/2021/010, and FCT - Foundation for Science and Technology, I.P., under the project OKEANOS UIDB/05634/2020 and UIDP/05634/2020. The authors would like to thank Lieutenant Laura Neves de Sousa for sediment sampling aboard RV “Pelagia”.

REFERENCES

Huneke, H. and Mulder, T. ed. (2011). Deep-Sea Sediments, Volume 63, Elsevier, 849 p. ISBN: 9780444530004.

Morato, T., Dominguez-Carrió, C., Evans, S., Taranto, G., Neves de Sousa, L., Mohn, C. and Carreiro-Sillva, M. (2021). R/V Pelagia, cruise nº 64PE487, Eurofleets+iMar cruise report, Horta, Portugal, 66p.

Morato, T., Dominguez-Carrió, C., Evans, S., Taranto, G. H., Neves de Sousa, L., Mohn, C. and Carreiro-Silva, M. (2021). iMAR: Integrated assessment of the distribution of Vulnerable Marine Ecosystem along the Mid-Atlantic Ridge in the Azores region. *Zenodo*. https://doi.org/10.5281/zenodo.6556837

EN 15936:2022. Soil, waste, treated biowaste and sludge. Determination of total organic carbon (TOC) by dry combustion, 24p.

ISO 13320:2020. Particle size analysis – Laser diffraction methods, Ed.2, 2020-01, 59p.

ISO 13322-2:2021. Particle size analysis – Image analysis methods - Part 2: Dynamic image analysis methods, Ed.2, 2021-12, 53p.

Compositional Diversity of Seafloor Sediments at the Gigante Seamount Complex (GSC; Azores Plateau): Tracing Biogenic, Volcanic, and Hydrothermal Sources

P. Costa (1), Á. A. Dias (1,2,3), R. Quartau (4,3), S. Moreira (4,3), R. Santos (4,3), J. F. Duarte (4,3) and A. Rodrigues (4,3)

(1) Institute of Science and Environment (ISE), University of Saint Joseph (USJ), Macao SAR. 201800459@usj.edu.mo
(2) Departamento de Geologia da Faculdade de Ciências (FCUL), Universidade de Lisboa, Portugal. ascdias@fc.ul.pt
(3) Instituto Dom Luiz (IDL), Faculty of Sciences of the University of Lisbon, Portugal.
(4) Instituto Hidrográfico (IH), Divisão de Geologia Marinha, Lisboa, Portugal

Abstract: The Gigante Seamount on the Azores Plateau (North Atlantic) hosts the Luso hydrothermal field, characterized by low-temperature venting. We analyzed eight surface sediment samples via X-ray diffraction and bulk geochemical techniques (ICP-MS, INAA, FUS-ICP). Mineralogical and geochemical variability defines three sediment facies: carbonate-rich pelagic deposits, volcaniclastic sediments, and mixed volcanic–biogenic sands. Carbonate-rich samples are dominated by biogenic calcite and display high Ca and Sr but low trace metal content, reflecting dilution of volcanic and hydrothermal signals. In contrast, volcaniclastic and mixed facies show elevated Fe, Mn, and trace metals (e.g., Cu, Zn, Ni, Co), as well as basalt-like rare earth element (REE) profiles with slight positive Eu anomalies, indicating scavenging by hydrothermal Fe–Mn oxyhydroxides. Spatially, hydrothermal influence is strongest near Luso, evidenced by Fe-rich clays and metal enrichments, and diminishes in distal carbonate-rich sediments.

Keywords: *Gigante Seamount Complex (GSC), seafloor sediment composition, Fe-Mn oxyhydroxides deposits, seafloor hydrothermal signatures*

1. INTRODUCTION

The Gigante Seamount Complex (GSC), located between Flores and Faial islands on the Mid-Atlantic Ridge, is situated near the Azores triple junction, where the North American, Eurasian, and Nubian plates meet. Rising sharply from abyssal depths (~2400 m) to shallow summits (~150 m), the GSC hosts the Luso hydrothermal field on its eastern flank, discovered during the 2018 Blue Azores expedition. This site comprises active and inactive vent structures aligned along ENE-WSW faults at ~570 m depth. Chimneys emit a translucent, low-temperature fluids (max. 63 °C), forming unusual ochre-colored Fe-rich chimneys composed primarily of ferrihydrite, amorphous silica (opal-A), and Fe-rich smectite clays (nontronite), consistent with low-temperature hydrothermal circulation in basaltic lithologies associated to oceanic seamount settings.

2. SAMPLES AND METHODS

This study investigated the mineralogy and geochemical composition of eight surface samples collected by ROV across different morphological sectors of the GSC (Figure 1).

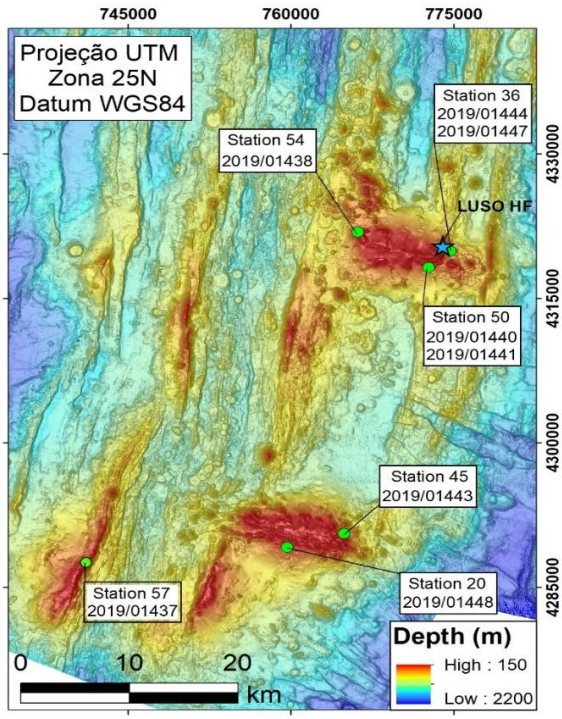

Figure 1. High-resolution bathymetric map of the SGSC area showing the location of sampling stations and corresponding sample references collected during the 2019 campaign. The Luso hydrothermal field (Luso HF) is marked with a star.

The main objectives where to determine the sediment provenance, spatial distribution and evaluate the hydrothermal influence. Samples were analyzed for mineralogy by X-ray diffraction (XRD) and for whole geochemical composition (ICP-MS, INAA, and FUS-ICP).

3. RESULTS AND DISCUSSION

Three different compositional groups were identified: (1) carbonate-rich pelagic sediments, dominated by biogenic calcite and aragonite, with high Ca and Sr and low trace metal and REE concentrations, showing negative Ce and Eu anomalies; (2) volcaniclastic-rich sediments with abundant basaltic debris and Fe–Mn oxides, enriched in metals such as Co, Ni, Cu, Zn, V and ΣREE, and exhibiting basalt-like REE patterns with slight positive Eu anomalies; and (3) transitional volcanic–biogenic sediments with intermediate compositions. Geochemical proxies, including (e.g., Fe/Mn and Fe/Ti ratios), trace metal enrichments (e.g., Cu, Zn, Co, Ni), ΣREE concentrations, the occurrence of nontronitic clays, and PCA compositional clusters confirmed that hydrothermal influence is more evident close the areas adjacent to the Luso HF. However, similar signatures were also observed in distal settings, including associated to the seamount at south indicating that hydrothermal activity extends across a wider area than previously recognized. This is further supported by Fe/Ti vs. Al/(Al+Fe+Mn) and Fe-Mn-(Co-Cu-Ni) discriminatory diagrams, which show diluted hydrothermal signatures in the dominant volcanic and biogenic components.

4. CONCLUSIONS

The GSC sediments record a complex mixture of biogenic, volcanic, and hydrothermal sources. While pelagic carbonates dominate distal areas, volcaniclastic sediments with variable hydrothermally influenced are concentrated near seamounts. These findings provide new evidence that low-temperature hydrothermal systems, characterized by Si–Fe–Mn oxyhydroxide deposition associated with seamount magmatism, are more widespread across the Azores Plateau than previously documented.

Acknowledgments

This work was supported by the Macao FDCT (SeaMin project 0041/2021/A1) and by the Portuguese FCT, I.P./MCTES through national funds (PIDDAC): UID/50019/2025 and LA/P/0068/2020. We acknowledge the Blue Azores project (Fundação Oceano Azul) and the University of the Azores, as the data collected for this work were obtained during the Oceano Azul Scientific Expedition to the Azores in 2018, promoted and organized by the Oceano Azul Foundation, the Waitt Institute, the Regional Government of the Azores and National Geographic Pristine Seas, with the collaboration of the Hydrographic Institute of the Portuguese Navy, the University of the Azores/IMAR and the Portuguese Task Group for the Extension of the Continental Shelf.

Volcanic and erosional morphologies on the insular slope of La Palma (Canary Islands): A geomorphological approach to edifice evolution

R. Jiménez-Romero (1), M. Sayago-Gil (1), O. Sánchez-Guillamón (2), I. Villar-Menéndez (3), J. T. Vázquez (2) and L. M. Fernández-Salas (1)

(1) Spanish Institute of Oceanography (IEO-CSIC), Cádiz Oceanographic Centre, Spain. raul.jimenez@ieo.csic.es
(2) Spanish Institute of Oceanography (IEO, CSIC), Málaga Oceanographic Centre, Spain
(3) Spanish Institute of Oceanography (IEO, CSIC), Gijón Oceanographic Centre, Spain

Abstract: This study analyzes the submarine morphology of La Palma (Canary Islands) using high-resolution bathymetric mosaics and semi-automated mapping techniques, including Bathymetric Position Index (BPI) analysis and hydrological tools (Hydrology and ArcHydro9 in ArcGIS). 537 volcanic edifices were identified between 230 and 4030 m depth, mainly aligned along northern, northwestern, and southern rift zones, indicating subaerial-submarine structural continuity. In contrast, landslide-affected areas show lower edifice density. Twenty-one drainage basins and nine well-defined submarine canyons—up to 4000 m deep—were mapped, mainly along the eastern and western slopes, corresponding to subaerial valleys and mass-wasting pathways. These findings highlight the interplay between constructive volcanic activity and destructive processes such as erosion and gravitational collapse. The integration of bathymetric data with spatial analysis provides insights into the island's geomorphological evolution and offers a methodological framework applicable to other oceanic volcanic islands.

Keywords: *Submarine volcanism, submarine canyons, geomorphological evolution, La Palma, Canary Islands*

1. INTRODUCTION

Oceanic volcanic islands represent the emergent summits of large volcanic edifices that rise abruptly from the seafloor. While subaerial geological analyses of these islands provide valuable insights into their evolution, they offer only a partial perspective on the complex geodynamic history involved. Therefore, examining the oceanic islands, in conjunction with observations from their emergent parts, can yield a more comprehensive and detailed understanding of their development and evolution Quartau *et al*., 2018).

The geomorphological structure of reflects the interplay between constructive volcanic processes - responsible for the formation of cones and lava flows- and destructive mechanisms such as gravitational collapse, erosion, and depositional (Santos *et al*., 2019). These opposing forces generate a wide variety of morphological features, including landslide scars, submarine channels and canyons, sediment waves, and scour depressions. Recent studies have identified potentially unstable flanks in several oceanic islands, such as the western sector of La Palma (Rollwage *et al*., 2024), highlighting the relevance of these destructive processes.

In this study, recently acquired high-resolution multibeam bathymetric mosaics of La Palma Island, part of the Canary Archipelago, were used to analyze both the spatial distribution and origin of volcanic edifices and submarine drainage features. This geomorphological approach aims to clarify the evolutionary processes shaping the island's submarine flanks and to contribute to broader interpretations of oceanic island development.

2. REGIONAL SETTING

The Canary Archipelago, located on the central-eastern margin of the Atlantic Ocean, northwest of the African continent (Figure 1A) is an active volcanic region. Two main models explain its geodynamic origin: a multifocal hotspot hypothesis (Hoernle and Schmincke, 1993), and a tectonically controlled model that emphasizes the influence of regional structures on volcanic activity (Anguita *et al*., 2025).

La Palma is among the youngest islands of the archipelago and is currently in a dynamic stage of shield growth (Carracedo *et al*., 1999). The island rises from approximately 4,000 m below sea level to 2,400 m above, forming a steep, complex volcanic edifice.

Its geological evolution comprises three main phases (Figure 1A): (1) Construction of the northern shield volcanoes (Taburiente-Garafía complex) between 4.0 and 0.44 Ma, including multiple collapse events (Masson *et al*., 2002); (2) formation and collapse of the Cumbre Nueva ridge along a N-S rift between 0.7 and 0.53 Ma (Ancochea *et al*., 1994); and (3)

development of the currently active Cumbre Vieja volcanic complex, since ~0.13 Ma (Guillou *et al*., 1998) forming the current southern rift with the same direction. These episodes have produced prominent subaerial and submarine morphological features, including avalanche deposits and scarps that influence the present submarine landscape.

3. DATASET AND METHODOLOGY

This study is based on multibeam bathymetric data acquired between 2021 and 2023 using an EM710 echosounder aboard the R/V Ramón Margalef and Ángeles Alvariño, during several research cruises (VULCANA_0921, VULCANA_1021, CANZEC_2022, and CIRCAN_2023). Data processing with Caris HIPS & SIPS 11.4 yielded high-resolution bathymetric mosaics (1-10 m grid) from 40 m to 1,600 m depth. For deeper zones, coarser-resolution mosaics (60-80 m) completed the full coverage of La Palma insular slope, down to 4,200 m (Krastel and Cruise Participants, 2024; Instituto Hidrográfico de la Marina, 2023) (Figure 1A).

Volcanic edifices were identified through a semi-automated approach based on the Bathymetric Position Index (BPI), computed at a 2,000 meters of scale factor using ArcGIS Pro 3.5. (Mena and Fernandez-Salas, 2023) Spatial density of volcanic edifices (Figure 1B) was calculated using the Kernel Density algorithm implemented in ArcGIS Pro 3.5.

The submarine drainage network was mapped through a semi-automated hydrology analysis using ArcGIS tools (Hydrology toolbox, ArcHydro9). The workflow included delineation of drainage basins, hierarchical classification of channels, and identification of main flow paths. Final outputs were reviewed and refined through expert validation (Figure 1C).

4. RESULTS

A total of 537 volcanic edifices were identified along the insular slope of La Palma. These structures are located at depths ranging from 230 to 4030 meters below sea level (Figure 1B). These structures exhibit a wide variety of morphologies, including conical, sub-conical, composite, and complex forms. Their spatial distribution highlights three areas of maximum density: the southern, northern, and northeastern areas (> 0.24 edifices/km^2; Figure 1B) with known subaerial volcanic axes. Notably, the edifices in these three areas are consistently aligned in a N–S direction. In contrast, regions affected by large-scale landslides, such as Santa Cruz, Playa de la Veta and Cumbre Nueva (Figure 1B), show markedly lower edifice density (0 – 0.24 edifices/km^2), likely due to morphological modification of burial.

The insular slope of La Palma Island are characterized by a complex network of channels grouped into 21 drainage basins, with areas ranging from 115 to 554 km^2 (Figure 1C). These channels vary in length from 37 to 65 km and extend from the shelf edge to the base of the insular edifice, reaching depths of up to 2820 m in the southeastern sector and 4000 m along the western, eastern and northern flanks. The average channel gradients range between 7° and 11°.

Among these, seven major channels are deeply incised into the seafloor, forming well-defined submarine canyons. Four are located along the western margin and three along the eastern margin, coinciding with prominet subaerial valleys and mass-wasting pathways.

5. DISCUSSION

The insular slope of La Palma exhibit a complex morphology shaped by the interplay of constructive volcanic processes and destructive gravitational and sedimentary processes, a duality also observed in other volcanic island systems (Quartau *et al*., 2018; Santos *et al*., 2019).

The identification of 537 volcanic edifices, predominantly aligned along the northern, northwestern, and southern areas, reflects the intense submarine volcanic activity and structural continuity with subaerial emission zones. This distribution highligths the tectonic control over the location of eruptive centers, as observed in other oceanic island settings (Santos *et al*., 2019).

In contrast, areas with lower densities of volcanic edifices coincide with regions affected by major gravitational landslides, such as Santa Cruz, Playa de la Veta, and Cumbre Nueva. These events, extensively documented in the geological evolution of La Palma (Masson *et al*., 2002), have significantly altered the seafloor morphology by erosion or burying pre-existing volcanic structures and generating avalanche deposits that reshape the local topography.

Erosional and sedimentary processes play a key role in reshaping the submarine landscape. The incision of channels and canyons, sediment remobilization by marine currents, and debris flow deposition are fundamental mechanisms in this dynamic. Subaerial fluvial system likely contribute to canyon development as flows reach the steep submarine slopes, they accelerate and incise the substrate, initiating erosion of the seafloor (Mazuel *et al*., 2016).

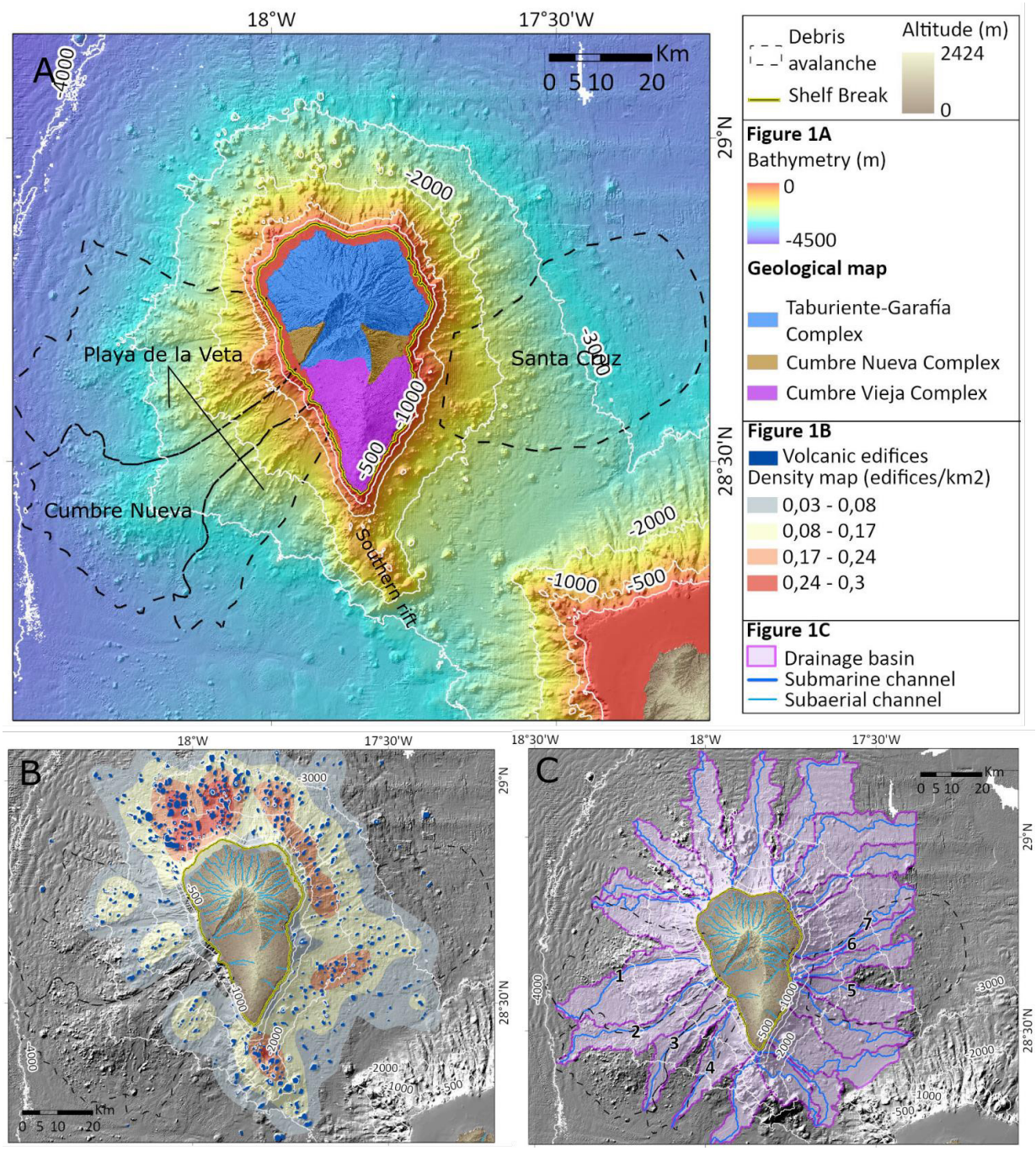

Figure 1. A) Bathymetric and simplified geological map of La Palma. The black dashed line indicates mass transport deposits (Masson et al., 2002) .; B) Density map of volcanic edifices surrounding the island of La Palma; C) Drainage basins boundaries and main drainage channels of La Palma. The well-defined canyons are numbered from 1 to 7.

The seven well-defined submarine canyons (Figure 1C), mainly located along the western and eastern could be closely related to the areas of mass transport deposits, as they appear to coincide spatially. These deposits are more susceptible to erosion than volcanic rocks, and the headscarps associated with them might trigger new, smaller collapses that promote canyon development (Mazuel *et al*., 2016). Similar canyon systems have been widely documented in other volcanic archipelagos, such as Madeira and the Azores (Quartau *et al*., 2018; Santos *et al*., 2019), where submarine canyons act as sediment pathways from the shelf to the basin.

This mechanism is particularly relevant in the older regions of the island where volcanic activity has ceased or diminished — such as the eastern and western areas — allowing erosional processes to dominate slope evolution. In contrast, in younger regions with recent or ongoing volcanic activity, such as the southern rift of La Palma, constructive processes tend to counterbalance or obscure erosive

effects. This explains both the absence of incised submarine canyons and the higher density of volcanic edifices in these areas. Nevertheless, there are also older regions, such as the northern and northeastern parts of the island, where slope have been rejuvenated by volcanic activity, altering their original morphology and limiting the development of deep erosional features.

6. CONCLUSIONS

The results of this study provides an integrated interpretation of the morphological evolution of La Palma's insular slope, highlighting the importance of volcanic, gravitational, and sedimentary processes in shaping the insular relief. The combination of high-resolution bathymetric data with spatial analysis techniques enables not only the characterization of terrain features but also the inference of past and present geodynamic processes that have shaped the island's submarine environment. These techniques enhances our understanding of the island's geomorphological evolution and provides a methodology applicable to other oceanic volcanic settings.

Acknowledgements

We would like to express our gratitude to the crews of the research vessels Ramón Margalef and Ángeles Alvariño, as well as to the VULCANA project team, for their valuable contribution to the data acquisition for this study. We also extend our sincere thanks to Dr. Sebastián Krastel from the University of Kiel and the "Instituto Hidrográfico de la Marina" for providing access to the deep-water bathymetric data collected during MSM-113 and ZEE Spanish cartography programs, respectively. This work was carried out within the ESMARES2 and ESMARES3 projects of the Spanish Institute of Oceanography (IEO-CSIC), under assignments from the Spanish Ministry for the Ecological Transition and the Demographic Challenge (MITERD) as part of the implementation of the Marine Strategy Framework Directive (MSFD) in Spanish waters.

REFERENCES

Ancochea, E., Hernán, F., Cendrero, A., Cantagrel, J. M., Fúster, J., Ibarrola, E. and Coello, J. (1994). Constructive and destructive episodes in the building of a young Oceanic Island, La Palma, Canary Islands, and genesis of the Caldera de Taburiente. *Journal of Volcanology and Geothermal Research*, *60*(3–4), 243–262. https://doi.org/10.1016/0377-0273(94)90054-X

Anguita F., Fernández C., Márquez Á., León R. and Casillas R. (2025) The Canary hotspot revisited: Refutation of the Hawaii paradigm and an alternative, plate-based hypothesis. *Earth-Science Reviews*, 261, art. no. 105038. DOI: 10.1016/j.earscirev.2024.105038

Carracedo, J. C., Day, S. J., Guillou, H. and Gravestock, P. (1999). Later stages of volcanic evolution of La Palma, Canary Islands: Rift evolution, giant landslides, and the genesis of the Caldera de Taburiente. *Bulletin of the Geological Society of America*, *111*(5), 755–768. https://doi.org/10.1130/0016-7606(1999)111<0755:LSOVEO>2.3.CO;2

Guillou, H., Carracedo, J. C. and Day, S. J. (1998). Dating of the Upper Pleistocene–Holocene volcanic activity of La Palma using the unspiked K–Ar technique. *Journal of Volcanology and Geothermal Research*, *86*(1–4), 137–149. https://doi.org/10.1016/S0377-0273(98)00074-2

Hoernle, K. and Schmincke, H. U. (1993). The Role of Partial Melting in the 15-Ma Geochemical Evolution of Gran Canaria: A Blob Model for the Canary Hotspot. *Journal of Petrology*, *34*(3), 599–626. https://doi.org/10.1093/PETROLOGY/34.3.599

Instituto Hidrográfico de la Marina. (2023). Mosaico batimétrico 80 m. Isalas Canarias.

Krastel, S., Cruise Participants, 2024. R/V Maria S. Merian Cruise Report MSM 113, Las Palmas (Spain) – Las Palmas – Las Palmas (Spain), 09.12. – 12.01.23.

Masson, D. G., Watts, A. B., Gee, M. J. R., Urgeles, R., Mitchell, N. C., Le Bas, T. P. and Canals, M. (2002). Slope failures on the flanks of the western Canary Islands. *Earth-Science Reviews*, *57*(1–2), 1–35. https://doi.org/10.1016/S0012-8252(01)00069-1

Mazuel, A., Sisavath, E., Babonneau, N., Jorry, S. J., Bachèlery, P. and Delacourt, C. (2016). Turbidity current activity along the flanks of a volcanic edifice: The Mafate volcaniclastic complex, La Réunion Island, Indian Ocean. *Sedimentary Geology*, *335*, 34–50. https://doi.org/10.1016/J.SEDGEO.2016.01.020

Mena, A and Fernández-Salas, L.M. (2024). Optimizing bathymetric position index (BPI) calculation: An analysis of parameters and recommendations for the selection of their optimal values. *Applied Computing and Geosciences*, 23, 100168. https://doi.org/10.1016/j.acags.2024.100168

Quartau, R., Ramalho, R. S., Madeira, J., Santos, R., Rodrigues, A., Roque, C., Carrara, G. and Brum da Silveira, A. (2018). Gravitational, erosional and depositional processes on volcanic ocean islands: Insights from the submarine morphology of Madeira Archipelago. *Earth and Planetary Science Letters*, *482*, 288–299. https://doi.org/10.1016/j.epsl.2017.11.003

Rollwage, L., Sánchez-Guillamón, O., Sippl, C., León, R., Vázquez, J. T., Urlaub, M., Gross, F., Böttner, C., Krastel, S. and Geersen, J. (2024). Geomorphological evidence for volcano-tectonic deformation along the unstable western flank of Cumbre Vieja Volcano (La Palma). *Geomorphology*, 465, 109401. https://doi.org/10.1016/j.geomorph.2024.109401

Santos, R., Quartau, R., Brum da Silveira, A., Ramalho, R. and Rodrigues, A. (2019). Gravitational, erosional, sedimentary and volcanic processes on the submarine environment of Selvagens Islands (Madeira Archipelago, Portugal). *Marine Geology*, *415*, 105945. https://doi.org/10.1016/j.margeo.2019.05.004

Preliminar sedimentological and magnetic susceptibility characterization of box-corers from the Mid-Atlantic Ridge

J. Pombo (1), A. Oliveira (1,2), A. Rodrigues (1,2), J. Duarte (1,2), S. Moreira (1,2), N. Lapa (1), G. Taranto (3) and T. Morato (3)

(1) Instituto Hidrográfico, Lisboa, Portugal. Joaquim.pombo@hidrografico.pt
(2) Instituto Dom Luiz, Lisboa, Portugal
(3) Universidade dos Açores, Portugal

Abstract: This study analyzes marine sediments from the Mid-Atlantic Ridge, focusing on grain size, magnetic susceptibility, and geochemical composition ($CaCO_3$). Most sediments are sands and gravelly muddy-sands, typically very poorly sorted and strongly fine-skewed. In contrast, some samples of poorly sorted medium sands indicate selective sediment process instead. Magnetic susceptibility varied significantly, with certain samples showing peak values up to 87.4×10^{-5} SI, while others displayed stable or decreasing trends, likely reflecting variations in sedimentary processes. Calcium carbonate content was consistently high (around 91.6%) in most cores, especially those rich in bioclasts observed on macroscopic analysis, whereas lower values in some samples suggest the influence of lithoclastic material or reduced carbonate productivity. Overall, the results reflect a combination of carbonate-dominated and lithoclast-influenced sedimentary settings, offering insights into depositional dynamics and providing a valuable baseline for future paleoenvironmental studies.

Keywords: *Sediments, Grain-size, Carbonate content, Magnetic susceptibility, Mid Atlantic Ridge*

1. INTRODUCTION

The study area lies within the Azores domain, a geologically complex region located in the Mid-Atlantic Ridge (MAR), where geological settings are affected by the triple junction of the Eurasian, North American, and African plates (Le Pichon, 1968).

The Azores Platform is characterized by elevated topography with an overall triangular configuration (Gente *et al.*, 2003). It includes the Azores Archipelago, (east of the MAR) and the conjugate Faial and Corvo-Flores ridges (Vogt, 1976; Cannat *et al.*, 1999; Escartin *et al.*, 2001). Unlike the surrounding seafloor, which displays the pronounced ruggedness typical of a slow-spreading ridge, the shallow features present relatively smooth bathymetry (Gente *et al.*, 2003). The presence of recent sediments is discreet, with only a very thin and irregular layer in small depressed basins.

The main objective of this study is to analyze and characterize eight sediment samples collected during the iMAR cruise (Integrated assessment of the distribution of vulnerable marine ecosystems along the Mid-Atlantic Ridge in the Azores region), distributed along the Mid-Atlantic Ridge (Figure 1). This analysis was carried out within the framework of the SEDMAR program (Mapping Marine Sediments), led by the Portuguese Hydrographic Institute (IH).

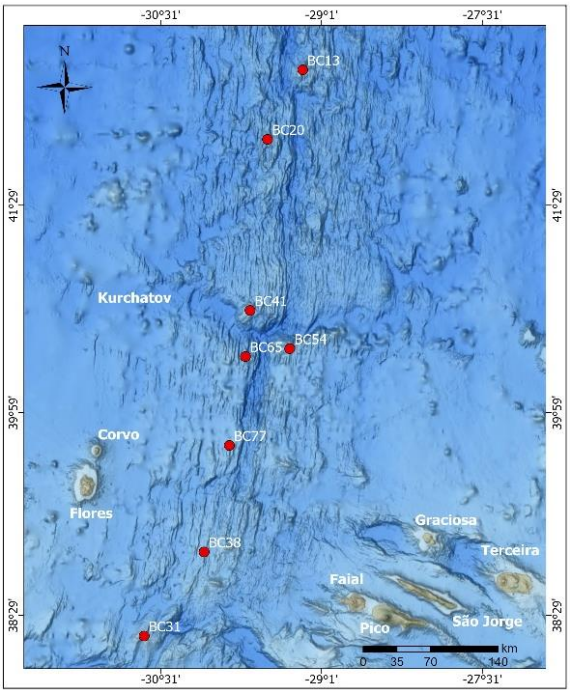

Figure 1. Study area and box-corer sampling locations (red dots). Basemap: Esri, HERE, Garmin, FAO, USGS; General bathymetric chart of the oceans (GEBCO); NOAA National Centers for Environmental Information (NCEI).

2. METHODS

2.1. Sampling

Eight corers (Figure 1) were collected between May 18 and June 2, 2021, using a box corer system aboard the RV Pelagia, during the iMAR cruise. Samples, ranging from 11 cm (BC13) to 33 cm (BC38) long, were stored at -20°C until processed.

2.2. Laboratory analysis

The characterization of sediments on the collected samples focused on their physical properties (grain size and magnetic susceptibility) and carbon content (total inorganic carbon – TIC, and calcium carbonate percentage – $CaCO_3$).

The along corer magnetic susceptibility was measured at the very beginning of the laboratory work, in accordance with ODP Technical Note 26 (Blum, 1997).

Following corer splitting, sub-samples were collected based on visually and magnetically identified stratigraphic layers. Lab analyses followed standard protocols and internationally recognized methods.

Grain size distribution was assessed using a combination of laser diffraction for particles <63 µm and image analysis for particles > 63 µm, in compliance with ISO 13320:2020 and ISO 13322-2:2021.

Total inorganic carbon (TIC) was quantified and converted to calcium carbonate content using the factor $CaCO_3$ (%) = TIC × 8.333. Measurements were performed using IH's accredited internal methods, based on EN 15936:2022.

3. RESULTS

According to Folk's (1954) sediment classification, based on the relative proportions of gravel, sand, and mud, grain size analysis indicates that the sedimentary deposits at the sampling sites are predominantly composed of muddy sand and gravelly muddy-sand (Figure 2).

The representative polimodal grain-size distribution curves (Figure 3) generally indicates the presence of four particles populations, ranging from extremely poorly sorted to poorly sorted (Figure 4). In terms of skewness (Figure 5), samples exhibit considerable variability, ranging from strongly coarse-skewed (observed in a single medium sand sample) to strongly fine-skewed distributions. The latter indicates a significant enrichment in fine particles.

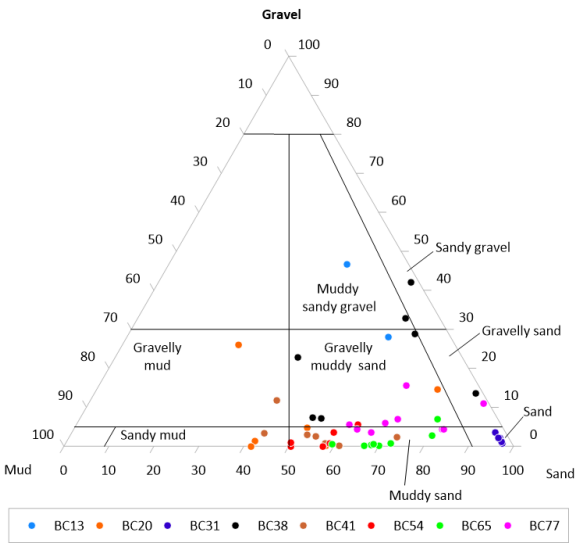

Figure 2. Sediments classification on the Folk ternary diagram.

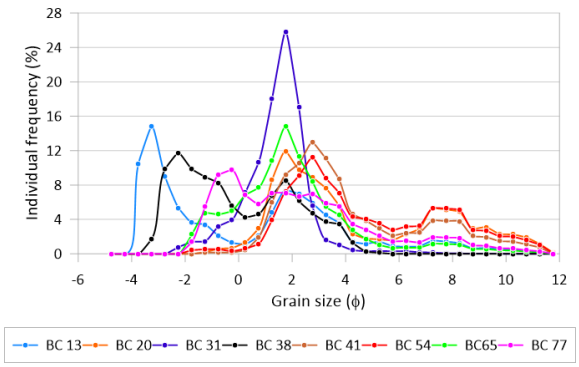

Figure 3. Grain size distribution.

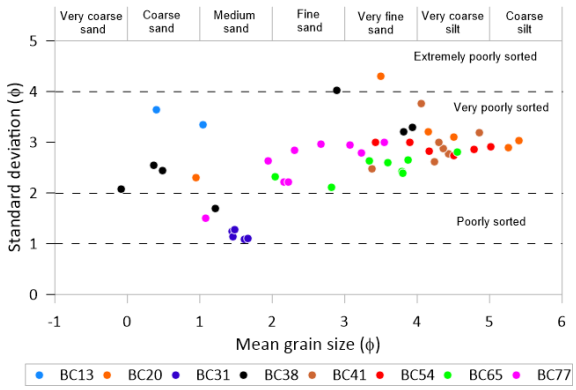

Figure 4. Relationship between the mean grain size and standard deviation.

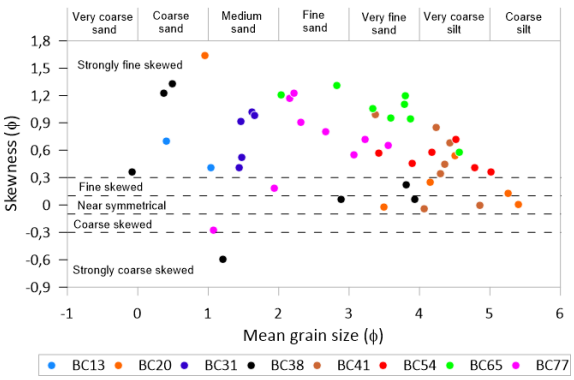

Figure 5. Relationship between the mean grain size and skewness.

Box-corer 13 (length: 10 cm). The magnetic susceptibility of the sedimentary column, ranged from –0.8 to –0.17 × 10^{-5} SI. At the top of the corer (0–1 cm), the sediments are composed of gravelly muddy sand, grading into muddy sandy gravel between 3 and 10 cm. The mud fraction throughout the corer is approximately 13%. The sediments are very poorly sorted and strongly fine-skewed. The carbonate ($CaCO_3$) content was high, reaching 91.6%.

Box-corer 20 (length: 31.5 cm). Magnetic susceptibility values were not valid. At the surface (0–3 cm), the sediments are formed by gravelly muddy-sand with a mud content of approximately 9%. These sediments are very poorly sorted and very fine-skewed. From 3 cm to the base (31.5 cm), we observe a transition to muddy sand/sandy mud sediments, also very poorly sorted and fine-skewed. An exception is observed between 10 and 20 cm, where the composition includes 26% gravel, 26% sand, and 48% silty-clayey sediments. The carbonate ($CaCO_3$) content was high, reaching 91.6%.

Box-corer 31 (length: 20.5 cm). Magnetic susceptibility values ranged from 12.2 × 10^{-5} to 29.4 × 10^{-5} SI, with the highest value recorded at 13 cm, matching with a slight decrease in grain size. The sediments are unimodal and primarily composed of medium sands (>95%), with minor gravel and fine fractions (both reaching up to ~3%). These sediments are poorly sorted and strongly fine-skewed. $CaCO_3$ content was very lower, ranging from 6.5% to 8.3%.

Box-corer 38 (length: 33 cm). Magnetic susceptibility, based on 17 measurements, ranged from 5.9 × 10^{-5} to 47.7 × 10^{-5} SI, with relatively constant values from the surface to 12 cm, followed by an increasing trend. The upper 15 cm consist of gravelly sand / sandy gravel, mainly shell fragments, very poorly sorted with variable skewness. $CaCO_3$ content was high than 91.6%. From 15 to 33 cm, the sediments are gravelly muddy sand, also very poorly sorted, near-symmetrical, and fine-skewed. $CaCO_3$ content decreased to 81.6% between 15 and 25 cm, increasing again to 91.6% toward the base.

Box-corer 41 (length: 30 cm). Magnetic susceptibility, based on 16 measurements, ranged from 5.6 × 10^{-5} to 18.2 × 10^{-5} SI units, with generally stable values throughout the corer and a slight decrease near the base. The corer is composed mainly of muddy sand, with gravel virtually absent except in the basal sample, where it reaches 12%. The sediments are very poorly sorted and exhibit variable skewness, ranging from near-symmetrical to strongly fine-skewed. $CaCO_3$ content was consistently higher than 91.6%

Box-corer 54 (length: 23 cm). Magnetic susceptibility showed a slight decrease from the surface (21.7 × 10^{-5} SI) to 8 cm (14.1 × 10^{-5} SI), followed by a progressive increase to a maximum of 40.3 × 10^{-5} SI at 14 cm, then declining and stabilizing around 14 × 10^{-5} SI towards the base. As with Box-corer 41, sediments are muddy sand, very poorly sorted and strongly fine-skewed, with minimal gravel. $CaCO_3$ content remained very high (91.6%).

Box-corer 65 (length: 24 cm). Magnetic susceptibility showed a clear decreasing trend from top to base, ranging from 2.4 × 10^{-5} to 18.2 × 10^{-5} SI. The sediments are muddy sands, very poorly sorted, and strongly fine-skewed, with negligible gravel content. Carbonates were the dominant component, with $CaCO_3$ content consistently at 91.6% throughout the corer.

Box-corer 77 (length: 29 cm). The sample displayed the highest magnetic susceptibility values among all samples. A maximum of 87.4 × 10^{-5} SI was recorded at 6 cm, followed by a decline to approximately 45 × 10^{-5} SI between 6 and 14 cm, and a further decrease to ~12 × 10^{-5} SI towards the base. The upper 15 cm consist of slightly gravelly muddy sands, transitioning to gravelly sands below this level. Sediments throughout the corer are very poorly sorted and generally strongly fine-skewed, except in two measurements. $CaCO_3$ content was also high, starting at 91.6% (0–4 cm), decreasing to 70.4% (4–6 cm), 60.8% (6–8 cm), and 83.3% (8–10 cm), then increasing again to 91.6% toward the base.

4. FINAL CONSIDERATIONS

The analysis of sedimentological and magnetic properties across the studied box-corers reveals significant spatial variability in sediment composition, sorting, skewness, and magnetic susceptibility, reflecting differences in depositional environments.

Sediments from Box-corer 20, 41, 54, 65, and 77 are generally characterized by very poor sorting and strong fine skewness, indicating low-energy depositional settings dominated by fine-grained material and limited hydrodynamic sorting. Similarly, Box-corers 13 and 38 also exhibit very poor sorting and strong fine skewness; however, they contain a

significant gravel fraction. In contrast, Box-corer 31 stands out for its poorly sorted medium sands.

High calcium carbonate content (91.6%) was consistently observed in most corers, particularly in those dominated by shell fragments or bioclastic material, such as corers 13, 38, and 41. This indicates a strong biogenic influence in sediment composition, possibly linked to nearby carbonate-producing organisms or reworking of older carbonate-rich layers. Lower carbonate values in Box-corer 31 and layers of Box-corer 77 may indicate reduced productivity.

Magnetic susceptibility results varied widely across corers, with Box-corer 77 exhibiting the highest values (up to 87.4×10^{-5} SI), suggesting increased magnetic mineral concentration or input from lithoclastic sources at specific depths. Trends such as the increasing susceptibility with depth in corers 38 and 54, or the clear decreasing profile in corer 65, may reflect distinct sedimentary dynamic processes (particle sources, transport patterns).

Overall, the data suggest the coexistence of multiple sedimentary regimes within the study area, ranging from carbonate - dominated, bioclast-rich environments to more lithoclastic-influenced muddy settings. These results provide a basis for future studies aimed at describing, mapping and understanding the dynamic processes that occur on the mid-Atlantic ridge in remote areas of the Azores islands.

Acknowledgements

This paper is a contribution to the SEDMAR (Mapping Marine Sediments) program of the Portuguese Hydrographic Institute (IH).

RV “Pelagia” ship-time was provided free of charge as part of the iMAR project which received funding from the European Union's H2020 Research & Innovation Programme under grant agreement Nº 824077 EUROFLEETS+. Additional funding was provided by the European Union’s Horizon 2020 research project iAtlantic (No 818123), and the project M1.1. A/REEQ. CIENTÍFICO UI&D/2021/010, and FCT - Foundation for Science and Technology, I.P., under the project OKEANOS UIDB/05634/2020 and UIDP/05634/2020. The authors would like to thank Lieutenant Laura Neves de Sousa for sediment sampling, aboard RV “Pelagia”.

REFERENCES

Blum, P. (1997). Physical properties handbook. ODP Tech. Note, 26. doi:10.2973/odp.tn.26.1997

Cannat, M., Briais, A., Deplus, C., Escartín, J., Georgen, J., Lin, J., Mercouriev, S., Meyzen, C., Muller, M., Pouliquem, G., Rabain, A. and Da Silva, P. (1999). Mid-Atlantic Ridge—Azores hot spot interactions: Along-axis migration of a hot spot-derived magmatic pulse 14 to 4 myrs ago. *Earth and Planetary Science Letters*, 173(3), 257-269. https://doi.org/10.1016/S0012-821X(99)00234-4

EN 15936 (2022). Soil, waste, treated biowaste and sludge - Determination of total organic carbon (TOC) by dry combustion. European Standards.

Escartin, J., Cannat, M., Pouliquen, G., Rabain, A. and Lin, L. (2001). Crustal thickness of V-shaped ridges south of the Azores: Interaction of the Mid-Atlantic Ridge (36°–39°N) and the Azores hot spot. *Journal of Geophysical Research*, 106(B10), 21719–21735.

Folk, R.L. (1954). The distinction between grain size and mineral composition in sedimentary-rock nomenclature. *Journal of Geology*, 62(4), 344-359.

ISO 13322-2 (2021). Particle size analysis — Image analysis methods - Part 2: Dynamic image analysis methods. ISO 2021. Switzerland.

ISO 13320 (2020). Particle size analysis – Laser diffraction methods. ISO 2020. Switzerland.

ISO 17892-1 (2014). Geotechnical investigation and testing - Laboratory testing of soil - Part 1: Determination of water content. ISO 2014. Switzerland.

Gente, P., Dyment, J., Maia, M. and Goslin, J. (2003). Interaction between the Mid-Atlantic Ridge and the Azores hot spot during the last 85 Myr: Emplacement and rifting of the hot spot-derived plateaus. *Geochemistry, Geophysics, Geosystems*, 4(10), 8514. doi:10.1029/2003GC000527.

Le Pichon, X. (1968). Seafloor spreading and continental drift. *Journal of Geophysical Research*, 73, 3661–3697.

Vogt, P. R. (1976). Plumes, Subaxial pipe flow and topography along the mid-oceanic ridge. *Earth and Planetary Science Letters*, 29, 309–325.

Dinâmica, sedimentação e evolução ambiental da zona costeira

Dinámica, sedimentación y evolución ambiental de la zona costera

Dynamics, sedimentation and environmental evolution of the coastal zone

Cyclic behavior of bulge attachment updrift of a natural ebb-tidal delta

V. Kümmerer (1), S. Costas (1), V. Fanti (1) and J. Santos (1)

(1) Centro de Investigação Marinha e Ambiental, Universidade do Algarve, Faro, Portugal.
vkuemmerer@ualg.pt

Abstract: Ebb-tidal deltas are dynamic coastal systems shaped by tides and waves, with morphological evolution influenced by changes in tidal prism. This study examines the long-term evolution of the Culatra-Armona ebb-tidal delta, where artificial stabilization of the Faro-Olhão inlet significantly reduced the tidal prism of the adjacent Armona inlet. Using satellite-derived shorelines from Landsat imagery (1984–2024), three cycles of swash bar attachment driving barrier elongation through updrift welding were observed. Shoreline heatmaps reveal cyclic bulge formation and alongshore migration, with storm events triggering dilution and shoreline realignment. The barrier island length increased from ~3 km to ~7 km, with growth rates peaking post-stabilization and declining in the last decade, indicating a potential approach to equilibrium. Results highlight the interplay between hydrodynamic forcing, ebb-delta morphology, and sediment transport in shaping barrier evolution, offering insight into coastal response to anthropogenic interventions and climate-driven storm variability.

Keywords: *Ebb-tidal delta, Shoreline evolution, Remote Sensing, Barrier Islands, Inlet dynamics*

1. INTRODUCTION

Ebb-tidal deltas are complex and dynamic morphological features shaped by the interaction of tidal and wave-generated currents (Fitzgerald, 1984). Both natural processes and human interventions that alter the tidal prism can significantly influence the evolution of adjacent barrier systems. The stabilization of the Faro-Olhão inlet through jetty construction led to a reduction in the tidal prism of the Armona inlet, subsequently driving the elongation of Culatra (Kombiadou *et al*., 2019; Pacheco *et al*., 2010; Figure 1). The island's length increased from approximately 3 km in 1873 to about 7 km in 2014, with growth rates accelerating from 17.5 m/year prior to the inlet stabilization to 40.8 m/year thereafter (Kombiadou *et al*., 2019). Concurrently, the inlet width narrowed from nearly 4 km in 1915 to around 700 m in 2010, indicating two distinct trends before and after the inlet stabilization (Pacheco *et al*., 2010). This elongation has been driven by the updrift attachment of the ebb-tidal shoals in the form of bulges—convex sand accumulation at the shoreline, Garel *et al*., 2014—which exhibit recurring cycles of growth and alongshore dilution. In this study, satellite-derived shorelines from Landsat 5, 7, and 8 were used to analyse and characterize the behavior of these bulges at the Culatra-Armona ebb-tidal delta over the past 40 years, as well as to identify the potential drivers initiating and terminating the observed cycles.

2. STUDY SITE

The Armona inlet served as the primary inlet of the Ria Formosa in Portugal until the opening (1929) and subsequent stabilization (completed in 1955) of the updrift Faro-Olhão inlet, which altered the tidal prism and led to a reduction in the size of the Armona ebb-tidal delta. In 1985, the Armona inlet accounted for approximately 48% of the Ria Formosa's total spring tidal prism, but this contribution had declined to an estimated 28% by 2010 (Pacheco *et al*., 2010). The inlet is ebb-dominated and characterized by semi-diurnal tides, with a spring tidal range of 2.8 m, a neap range of 1.3 m, and a maximum tidal range of 3.5 m. The offshore mean significant wave height (H_s) is about 1 m with an average wave peak period (T_p) of 8.2 s. Wave energy is predominantly from the west/southwest (over 70%), with approximately 20% coming from the east/southeast.

Figure 1. Aerial image of the study site from ESRI World imagery layer. Transects 1 to 72 in Culatra island are spaced at 100 m.

3. METHODOLOGY

3.1. Satellite-derived shorelines

Satellite-derived shorelines from April 1984 to February 2024 were extracted using Landsat 5, 7, and 8 imagery processed with the open-source Python toolbox CoastSat (Vos *et al.*, 2019). Shorelines were delineated as the sand/water contour using the Modified Normalized Water-Index. Shoreline positions were obtained by intersecting this contour with equally spaced (~100m) cross-shore transects (Figure 1) and then vertically corrected using beach slope and tidal levels at the satellite fly-over time, obtained from the FES22 model. To improve temporal consistency, the tidally corrected shoreline positions were averaged monthly. Shoreline change was assessed by calculating the deviation from the mean shoreline position at each transect, allowing the identification of relative patterns of erosion and accretion (Figure 2a). A ±10 m uncertainty band (i.e., error in Figure 2a) was applied to account for potential errors in shoreline detection. The bulge area was estimated by identifying the zero-crossing of the monthly averaged shoreline positions between each consecutive month and within transects 40 to 58, where bulge attachment consistently occurs.

3.2. Hydrodynamic forcing

The wave forcing offshore of the Armona inlet was characterised using data from the Faro Costeira buoy, supplemented with the ERA5 wave reanalysis extracted at the nearest grid point to fill data gaps and missing periods. A storm de-clustering algorithm was applied following Kümmerer *et al*. (2024) to identify independent storm events exceeding the 95th percentile of H_s. For each identified storm, storm power was estimated using Hs and peak period (Tp), and annual cumulative storm power was calculated. This metric was used to assess the relationship between storm activity and the growth of the barrier through bulge attachment.

4. RESULTS

The results indicate that barrier elongation occurs through a stepwise mechanism involving the updrift attachment of swash bars from the ebb-tidal delta, forming shoreline bulges (Figure 2a and 2b, around profile 50 in 1987, 2001 and 2012). Three distinct welding cycles were identified: 1985–1999, 1999–2011, and 2011–2020. These phases are separated by years of elevated cumulative storm power (1996, 2010, Figure 2c), which appear to drive bulge dilution and subsequent shoreline straightening.

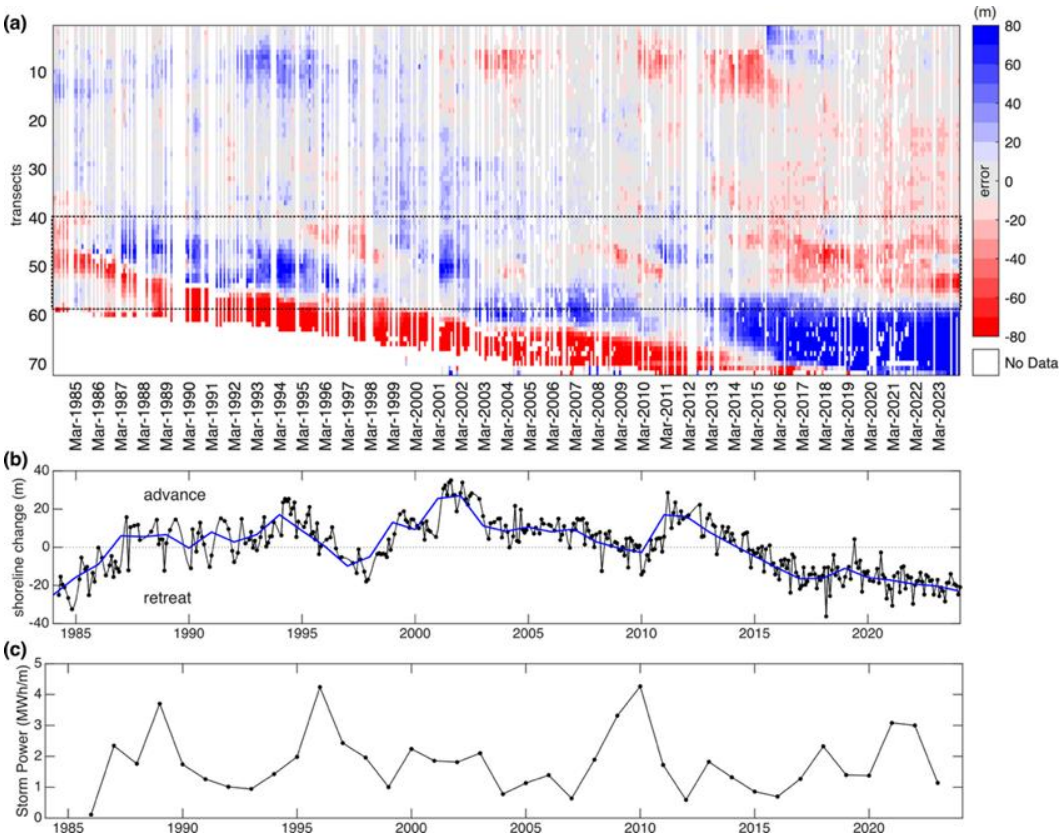

Figure 2. a) Heatmap of monthly averaged satellite-derived shoreline position (in meters) relative to the mean position at each transect (red for erosion, blue for accretion). b) Shoreline change between profiles 40 and 58 (black line) with yearly average (blue line). c) Cumulative yearly storm power in MWh/m.

Localized erosion was observed in the lee of the bulges, likely due to wave shadowing effects.

The cumulative bulge area—estimated from the zero-crossing of tidally corrected, satellite-derived shorelines between consecutive months and averaged annually—showed a moderate positive correlation with annual wave power (Pearson's R = 0.4, p-value < 0.5). This suggests that both storm events and prevailing wave energy play key roles in controlling swash bar evolution.

In the last decade, continued spit accretion has been observed (Figure 2a), likely resulting from the alongshore migration of previously welded bulges, aligned with the dominant west/southwest-directed sediment transport driven by the prevailing wave regime.

5. DISCUSSION

Previous models describe the downdrift welding of swash bars to the barrier shoreline as being primarily controlled by the morphology and size of the ebb-tidal delta, along with wave and tidal energy (Fitzgerald *et al*., 2000). However, satellite imagery at Culatra reveals a contrasting pattern, where swash bars weld in an updrift position, driving the barrier island's elongation over the past four decades. Multiple swash bar attachment sites have been identified, influenced by variations in delta configuration and typically aligning with the delta's visible outer edges. Despite an overall trend of sustained elongation, the bulge formations exhibit recurring cycles of development and alongshore dilution (Figure 2a).

Although elongation has persisted, the rate has declined over the last decade, suggesting the system may be approaching a new dynamic equilibrium between the reduced tidal prism and prevailing wave energy. Nonetheless, the future behavior of the system—particularly in response to storm events and the pathways and origins of swash bars—remains uncertain and requires further investigation.

6. CONCLUSION

This study highlights the critical role of ebb-tidal delta dynamics and swash bar welding in the long-term morphological evolution of the Culatra barrier island. The observed updrift attachment of bulges—a departure from typical downdrift patterns—has driven sustained barrier elongation over the past four decades. However, this growth exhibits a stepwise pattern governed by cycles of bulge formation and dilution, modulated by storm activity. The reduction in elongation rate over the last decade suggests the system may be approaching a new dynamic equilibrium. These findings underscore the importance of understanding the feedback between anthropogenic modifications, hydrodynamic forcing, and sediment transport pathways at ebb-tidal deltas. As coastal systems face increasing pressure from climate-driven changes and human interventions, long-term satellite-derived shoreline analysis offers a valuable tool for anticipating future behavior and informing sustainable coastal management strategies.

Acknowledgments

FCT projects: 2022.05392.PTDC, LA/P/0069/2020 and UID/00350/2020.

REFERENCES

Fitzgerald, D. M. (1984). Interactions between the ebb-tidal delta and landward shoreline: Price Inlet, South Carolina. *Journal of Sedimentary Research*, 54(4), 1303-1318.

Fitzgerald, D. M., Penland, S., and Nummedal, D. A. G. (1984). Control of barrier island shape by inlet sediment bypassing: East Frisian Islands, West Germany. *Marine Geology*, 60(1-4), 355-376.

FitzGerald, D. M., Kraus, N. C., and Hands, E. B. (2000). Natural mechanisms of sediment bypassing at tidal inlets.

Garel, E., Sousa, C., Ferreira, Ó., and Morales, J. A. (2014). Decadal morphological response of an ebb-tidal delta and down-drift beach to artificial breaching and inlet stabilisation. *Geomorphology*, 216, 13-25.

Kombiadou, K., Matias, A., Ferreira, Ó., Carrasco, A. R., Costas, S., and Plomaritis, T. (2019). Impacts of human interventions on the evolution of the Ria Formosa barrier island system (S. Portugal). *Geomorphology*, 343, 129-144.

Kümmerer, V., Ferreira, Ó., Fanti, V., and Loureiro, C. (2024). Storm identification for high-energy wave climates as a tool to improve long-term analysis. *Climate Dynamics*, 62(3), 2207-2226.

Pacheco, A., Ferreira, Ó., Williams, J. J., Garel, E., Vila-Concejo, A., and Dias, J. A. (2010). Hydrodynamics and equilibrium of a multiple-inlet system. *Marine Geology*, 274(1-4), 32-42.

Vos, K., Splinter, K. D., Harley, M. D., Simmons, J. A. and Turner, I. L. (2019). CoastSat: A Google Earth Engine-enabled Python toolkit to extract shorelines from publicly available satellite imagery. *Environmental Modelling & Software,* 122, 104528.

Challenges in assessing longshore transport along the Eastern Algarve coast: insights from analysis of different wave data sources

J. Santos (1,2,3), S. Costas (2) R. Taborda (1), J. Garzon (2) and T. Drago (1,3)

(1) Instituto Dom Luiz, FCUL, Universidade de Lisboa, Portugal. jacsantos@ualg.pt
(2) Centro de Investigação Marinha e Ambiental / ARNET, Universidade do Algarve, Faro, Portugal
(3) Instituto Português do Mar e da Atmosfera, Tavira, Portugal

Abstract: Estimating coastal sediment budgets can be a challenging due to complex nearshore morphology and temporal variability of wave directional spectra. This study examines longshore sediment transport (LST) in the eastern Algarve coast estimated from different wave data sources. Nearshore wave conditions were simulated with the SWAN model, forced by ERA5 and Faro buoy data. LST was estimated using a wave energy flux approach based on deep water conditions. Results highlight the importance of selecting appropriate wave inputs for accurate simulation of nearshore dynamics and sediment transport, emphasizing the need for high-resolution models that account for both local and regional wave processes.

Keywords: *Longshore sediment transport, Wave data sources, Wave modelling, Eastern Algarve*

1. INTRODUCTION

Accurate estimation of longshore sediment transport (LST) is critical for understanding coastal dynamics and developing effective shoreline management strategies. As LST is predominantly governed by wave parameters such as direction, height, and period, the choice of wave data source can substantially influence transport estimates. This study investigates the sensitivity of LST calculations to variations in wave input, highlighting the implications for coastal modeling and erosion mitigation efforts.

The Algarve coast in southern Portugal is exposed to a bimodal wave climate, predominantly influenced by W-SW swell generated in the Eastern Atlantic, with secondary contributions from "Levante" conditions—short-period waves driven by southeasterly Mediterranean winds (Ramos *et al*., 2021; Plomaritis *et al*., 2015). This coastline has undergone considerable anthropogenic alterations in recent decades, which disrupted natural sediment transport processes (Kombiadou *et al*., 2019). As a result, the region exhibits complex longitudinal patterns of shoreline changes, characterized by altering trends of erosion and accretion.

These dynamics reflect the combined influence of human interventions and natural processes, with shoreline change rates averaging 8.96 ± 0.2 m/year (Lira *et al*., 2016).

This study investigates longshore sediment transport along the Algarve eastern coast, a highly complex coast with contrasting degrees of wave exposure and a bimodal wave regime by exploring estimating potential longshore sediment transport (LST) from different wave data sources. The focus is on evaluating the sensitivity of LST estimates to these sources and assessing the resulting impact on model accuracy.

2. METHODS

2.1. Bathymetry, wave datasets and propagation

The nearshore wave regime was simulated using the SWAN wave model in non-stationary mode (Booij *et al*., 1999). First, an unstructured grid was built in MATLAB OceanMesh2D tool (Roberts *et al*., 2019) with available bathymetric data from two different sources: (i) INGMAR ("Investigação em Geología Marinha"), produced by the National Laboratory of Energy and Geology (LNEG), and (ii) REDIAM ("Rede de Información Ambiental de Andalucía"). The mesh has a spatial resolution ranging from 20 km in the deep ocean to 20 m nearshore (Figure 1).

The wave spectral domain was discretized into 31 frequency bins and a direction spreading of 36 (10º). Offshore boundary conditions were driven by two different wave data sources: (i) ERA5 hindcast (36.5°N, -9.0°W) and the Faro buoy (36.39°N, -8.06°W) (Figure 1). Wind-wave processes were disabled, and the model was validated against ADCP wave data from two different locations moored 9 and 20 m depth (Figure 1). The SWAN model was run for the time interval with observational data available and the wave parameters were extracted at validation sites (Figure 1, ADCP dots). Wave data from the ADCP measurements and from SWAN simulations, extracted at ADCP locations, were backpropagated offshore using Snell's law. The wave parameters obtained in deeper water through this procedure were then used to estimate longshore sediment transport.

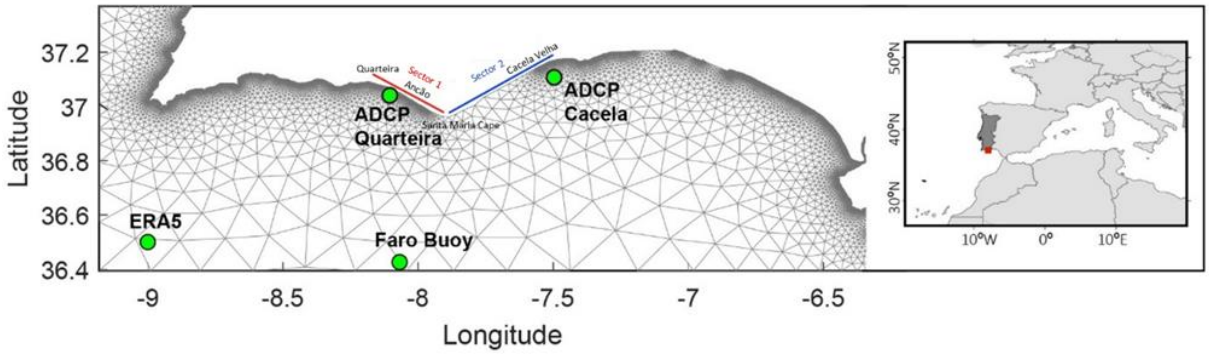

Figure 1. Location of the two sectors, offshore buoy and wave data point from the ERA5 hindcast model used as boundary conditions (in green), and location of two ADCP moorings used for validation.

2.2. Potential longshore sediment transport

Longshore sediment transport calculations were conducted using the CERC formula (Eq.1) (Asthon and Murray, 2006) to determine the net and gross longshore sediment transport, extracting the corresponding main components of sediment transport (W-E and E-W), with net transport direction defined as positive towards the east and negative towards west.

$$Qs = K_2\, H_{S0}^{\frac{12}{5}} T^{\frac{1}{5}} cos^{\frac{6}{5}}(\theta_{loc}) \sin(\theta_{loc}) \qquad \text{(Eq.1)}$$

where, the value used for K_2 was 0.497 (calibrated with the ADCP data and assuming an average sediment transport of 1.1x10^5 m³/year in the sector Quarteira to Garrão (Santos *et al.*, 2014). H_{S0} is the significant wave height offshore (m), T is the peak wave period (s), θ_{loc} is the relative angle of wave incidence for waves offshore.

The calculation was performed for 2 coastal sectors with different exposure of waves and representative shoreline orientation (Figure 1). Sector 1, extending from Quarteira to Ancão, has a representative shoreline orientation of 125°, while Sector 2, spanning from Santa Maria Cape to Cacela Velha, exhibits a representative shoreline orientation of 55°.

3. RESULTS AND DISCUSSION

3.1. Validation of wave propagation scheme

Wave modelling strategy was assessed by comparing simulated wave parameters (Hs, Tp, and Dir) against observational data from ADCPs (Table I) suggesting better overall agreement with observational data.

Results indicate that the model driven with the Faro Buoy dataset generally outperformed the ERA5-driven model approach, particularly in terms of wave height (Hs). Using Faro Buoy data as boundary condition produced lower biases and RMSE values, along with higher correlation coefficients for Hs and Tp.

Results indicate that the model driven by the Faro Buoy dataset generally outperformed the ERA5-driven model, particularly in terms of wave height (Hs). Using Faro Buoy data as boundary condition produced lower biases and RMSE values, along with higher correlation coefficients for Hs and Tp, suggesting better overall agreement with observational data.

3.2. Potential longshore sediment transport

The analysis of longshore sediment transport (LST) across the two sectors reveals distinct trends influenced by both wave data sources (Table II).

Table I. Summary of SWAN model performance compared with ADCP wave data. OBS-Observation data.

		Bias			RMSE			r		
OBS Data	**Boundary conditions**	**Hs**	**Tp**	**Dir**	**Hs**	**Tm**	**Dir**	**Hs**	**Tp**	**Dir**
ADCP Quarteira	ERA5	0.21	2.00	-22.68	0.33	4.08	44.96	0.72	0.49	0.29
	Faro Buoy	-0.01	0.90	-4.86	0.24	3.75	33.91	0.78	0.48	0.53
ADCP Cacela	ERA5	0.33	-0.24	-36.60	0.42	3.48	55.76	-0.02	0.33	0.17
	Faro Buoy	0.20	-0.45	-16.58	0.29	3.59	42.48	0.51	0.29	0.44

Table II. Longitudinal sediment transport for the sectors (1- Quarteira - Ancão, 2- Santa Maria Cape - Cacela Velha) and boundary conditions, including net transport and west-east, east-west components (x $10^5 m^3$/year). OBS-observational data. Code is the approach and coastal sector (1: Sector 1; 2: Sector 2).

Approach	Boundary condition	Code	W-E	E-W	Net
SWAN	Buoy	sBUOY-1	15.21	14.87	0.33
SWAN	ERA5	sERA5 -1	15.24	1.54	13.69
OBS	-	OBS-1	16.52	15.42	1.10
SWAN	Buoy	sBUOY-2	0.007	0.09	-0.08
SWAN	ERA5	sERA5-2	0.0	0.0	-
OBS	-	OBS-2	5.23	3.04	2.18

In the southwest-facing Sector 1, simulations based on sBUOY-1 and OBS-1 yield nearly equivalent transport magnitudes in both directions, although the net transport remains directed to the east. In contrast, sERA5-1, the west-to-east transport component clearly exceeds the east-to-west component. Sector 2 exhibits overall lower net LST magnitudes. This sector is relatively sheltered from high-energy wave conditions arriving from the west but remains exposed to easterly waves, and the period simulated was during the summer, resulting in lower and more variable transport rates. Both sectors exhibit broadly consistent LST trends, with the west-to-east transport component generally exceeding the east-to-west.

4. FINAL REMARKS

The analysis of longshore sediment transport (LST) estimates vary depending on the wave data source defined in the boundary conditions. These findings underscore the critical importance of selecting appropriate wave forcing inputs when applying numerical models to simulate the nearshore wave climate and to estimate sediment transport with accuracy. The inherent complexity of the study area, characterized by the coastal configuration and the influence of a bimodal wave climate—comprising Atlantic swell and locally generated Levante waves—demands a robust and detailed modeling approach.

Acknowledgements

This work was funded by FCT -Portuguese Foundation for Science and Technology, Ref. 2023.03101, and is a contribution of Coastal Resilience Remote Sensing Monitoring Project funded by FCT - Portuguese Foundation for Science and Technology Reference 2022.05392.PTDC, doi: https://doi.org/10.54499/2022.05392.PTDC. Associate Laboratory ARNET under the project LA/P/0069/2020 and CIMA through the grant UIDP/00350/2020 (https://doi.org/10.54499/UIDP/00350/2020). The authors would also like to thank Prof. Paulo Relvas (CCMAR) and Dr. Erwan Garel (CIMA) for providing the ADCP data for validation.

REFERENCES

Ashton, A.D. and Murray, A.B. (2006). High-angle wave instability and emergent shoreline shapes: 1. Modeling of sand waves, flying spits, and capes. *Journal of Geophysical Research: Earth Surface*, 111, 1–19.

Booij, N., Ris, R.C. and Holthuijsen, L.H. (1999). A third-generation wave model for coastal regions: 1. Model description and validation. *Journal of Geophysical Research: Oceans*, 104(C4), 7649–7666.

Kombiadou, K., Matias, M., Ferreira, O., Carrasco, A.R., Costas, S. and Plomaritis, T. (2019). Impacts of human interventions on the evolution of the Ria Formosa barrier island system (S. Portugal). *Geomorphology* 343, 129–144.

Lira, P.C., Nobre, S.A., Taborda, R. and Andrade, C. (2016). Coastline evolution of Portuguese low-lying sandy coast in the last 50 years: an integrated approach. *Earth System Science Data*, 8(1), 265–278.

Plomaritis, T.A., Benavente, J., Laiz, I. and Del Río, L. (2015). Variability in storm climate along the Gulf of Cadiz: the role of large scale atmospheric forcing and implications to coastal hazards. *Climate Dynamics,* 45, 2499–2514.

Ramos, J., Gomiz-Pascual, J.J. and Bruno, M. (2021). Analysis of wave and wind energy in the Cádiz Gulf coast. *Proceedings of the 14th European Wave and Tidal Energy Conference*, pp. 1–13.

Roberts, K.J., Pringle, W.J. and Westerink, J.J. (2019). OceanMesh2D 1.0: MATLAB-based software for two-dimensional unstructured mesh generation in coastal ocean modeling. *Geoscientific Model Development,* 12(5), 1847–1868.

Santos, F., Lopes, A., Moniz, G., Taborda, R. and Ramos, L. (2014). *Gestão da Zona Costeira: O Desafio da Mudança*. Portuguese Littoral Working Group Report, 237 pp. (in Portuguese).

Tomografia computorizada como suporte para a interpretação paleoambiental do estuário do Rio Lima, Portugal

A. Alberto (1,2), A. Shchepetkina (3), T. Drago (1,4), M. C. Freitas (1,2), V. Magalhães (1,4) e V. Lopes (1,2)

(1) Instituto Dom Luiz (IDL), Faculdade de Ciências da Universidade de Lisboa, Lisboa, Portugal. aidalberto@ciencias.ulisboa.pt
(2) Departamento de Geologia, Faculdade de Ciências da Universidade de Lisboa, Lisboa, Portugal
(3) Department of Earth Sciences, University of Western Ontario, London (ON), Canada
(4) Instituto Português do Mar e da Atmosfera, Tavira, Portugal

Abstract: Estuaries are dynamic transitional environments influenced by fluvial, marine, climatic, and anthropogenic factors, resulting in complex sedimentation patterns. This study integrates high-resolution computed tomography (CT) and grain size data to analyse three sediment cores retrieved from the Lima River estuary (NW Portugal). CT scans were acquired using the Geotek MSCL-XCT system, and grayscale values were extracted using FIJI (ImageJ) to infer relative material density variations. The results reveal heterogeneous successions dominated by sandy deposits, interbedded with gravel, mud, and shell-rich layers. Fine-grained intervals with planar lamination indicate low-energy deposition, while bioclastic layers are likely linked episodic marine incursions. Grayscale profiles correlate well with textural changes. CT imaging proved crucial for identifying internal structures and variations in density and composition along core depth, providing better insight into the Lima Estuary as a depositional environment over the past 15000 years.

Keywords: *Computed tomography, grain size, sedimentary structure, Lima River estuary.*

1. INTRODUÇÃO

O Rio Lima é um curso de água transfronteiriço que tem origem na Serra de Talariño, na província espanhola de Ourense. Com uma extensão total de aproximadamente 135 km, cerca de 67 km percorrem o noroeste de Portugal antes de desaguar no oceano Atlântico, nas proximidades da cidade de Viana do Castelo. O estuário do rio Lima apresenta uma morfologia em funil e estende-se por cerca de 20 km para o interior. Durante marés vivas e em períodos de reduzida descarga fluvial, os processos de circulação e mistura estuarina são predominantemente condicionados pela ação das marés oceânica, sob um regime semi-diurno e mesotidal, com uma amplitude média de cerca de 3,7 m. Em contraste, no inverno, particularmente durante eventos de cheia, a dinâmica estuarina é principalmente controlada por processos fluviais (Alves, 1996).

Enquanto zonas de transição de ambientes fluviais e marinhos, os estuários são fortemente influenciados por fatores hidrodinâmicos, climáticos e antrópicos, dando origem a variações nos padrões de sedimentação ao longo do espaço e do tempo (Leeder, 2011). A identificação e caracterização dessas variações são essenciais para compreender os processos de transporte, deposição e, eventualmente, as alterações ambientais a que estes ambientes estão sujeitos.

Entre os métodos disponíveis para o estudo de sedimentos, a tomografia computorizada (TC) é frequentemente usada como uma técnica não destrutiva e de alta resolução para a análise estrutural interna de sondagens, permitindo a visualização de heterogeneidades não evidentes à observação macroscópica (Ashi, 1997; Dann *et al*., 2010; Mitra *et al*., 2024). O processo de aquisição das imagens envolve a realização de múltiplas radiografias com raio-X ao longo da sondagem, a partir de diferentes ângulos, que são posteriormente processados por algoritmos computacionais para gerar imagens tridimensionais ou cortes transversais bidimensionais, com base nas diferenças de densidade e composição dos materiais que compõem o sedimento.

Com base em imagens de TC e dados de distribuição granulométrica, o presente trabalho teve como objetivo identificar padrões que possam refletir variações nos processos deposicionais em três zonas distintas do estuário do Rio Lima (Figura 1), situado no noroeste de Portugal.

2. METODOLOGIA

Neste estudo foram analisadas 3 sondagens realizadas no estuário do Rio Lima, em 2005, pela empresa Teixeira Duarte, através de perfuração rotativa (*rotary drilling*). A sondagem designada por Furo1 (com 6,4 m) foi colhida na margem norte do estuário, enquanto as

sondagens Furo2 (com 17,5 m) e Furo3 (com 6,3 m) foram colhidas na margem sul (Figura 1).

Figura 1. Localização das sondagens (Furo1, Furo2 e Furo3) no estuário do Rio Lima.

Foram adquiridas imagens de TC das três sondagens utilizando o equipamento MSCL-XCT da Geotek, instalado no laboratório de sedimentologia da Estação de Tavira do Instituto Português do Mar e da Atmosfera, I.P. (IPMA). A extração de valores de cinzento a partir das imagens de TC foi realizada utilizando o software FIJI (ImageJ). Posteriormente, as sondagens foram divididas em duas metades, e da metade de trabalho foram colhidas amostras para análise de granulometria por difração a laser na fração fina, e peneiração na fração grosseira. Adicionalmente, foram colhidas amostras para datação por radiocarbono (^{14}C), as quais foram realizadas nos laboratórios A. E. Lalonde AMS Laboratory (Canada) e Vilnius Radiocarbon (Lituânia).

3. RESULTADOS E CONCLUSÕES

As imagens de tomografia computorizada (TC) obtidas nas três sondagens evidenciam elevado contraste e resolução, permitindo identificar com clareza os limites entre camadas sedimentares com diferentes características.

A análise integrada das imagens de TC, das texturas sedimentares e dos valores de cinzento revela sucessões heterogéneas, dominadas por depósitos arenosos ao longo das sondagens, intercalados com níveis cascalhentos, lodosos e fragmentos de conchas (e.g., Furo2, secções 2, 12, 22 e 25). A presença de estruturas laminadas (e.g., Figura 2, secção 2 – 1,05 a 1,17 m) e de níveis lodosos (e.g., Figura 2, secção 12 – 7,97 a 8,07 m) indicam episódios de menor energia. Em contraste, os níveis bioclásticos, constituídos por fragmentos de conhas, como os registados na secção 22 (15,09 a 15,96 m e 15,18 a 17,27 m, Figura 2), poderão refletir eventos de maior energia, com provável influência marinha. Os valores de cinzento acompanham consistentemente a variação textural, com maiores densidades associadas aos níveis cascalhentos e bioclásticos, reforçando a sua utilidade como indicador indireto de composição e textura.

Os dados obtidos sugerem uma alternância entre fases deposicionais de baixa e elevada energia, possivelmente refletindo a transição entre os domínios fluvial e marinho. As datações disponíveis sugerem que o registo sedimentar documentado nas três sondagens reflete variações paleoambientais e eustáticas ocorridas ao longo dos últimos 15 mil anos. Numa fase subsequente do trabalho, os resultados obtidos serão integrados com outros indicadores paleoambientais, nomeadamente o teor em carbonato de cálcio, o conteúdo em matéria orgânica, parâmetros geoquímicos e a suscetibilidade magnética.

O recurso à tomografia computorizada (TC) revelou-se uma ferramenta fundamental para a caracterização detalhada dos sedimentos, permitindo a identificação de heterogeneidades internas que não são evidentes à observação macroscópica, melhorando significativamente a resolução interpretativa do registo estratigráfico.

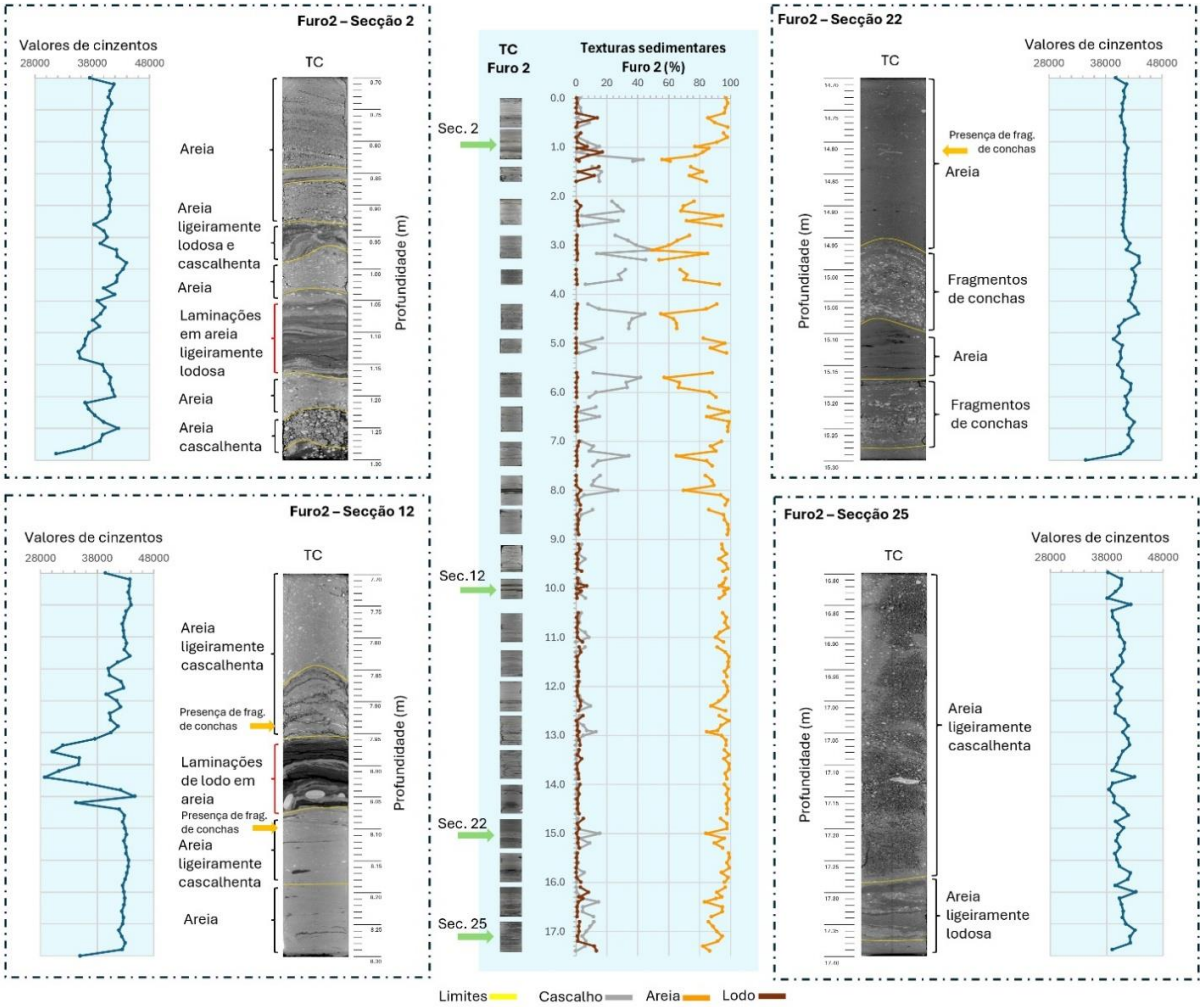

Figura 2. O painel central apresenta as imagens de tomografia computorizada (TC) e as percentagens das texturas sedimentares ao longo da profundidade da sondagem Furo2 (% de cascalho a cinzento; % de areia a amarelo; e % de lodo a castanho). À esquerda e à direita do painel central são mostradas, com maior detalhe, as TC de quatro secções selecionadas (Sec. 2, 15, 22 e 25), onde são visíveis as estruturas sedimentares preservadas e os seus limites (a amarelo). Estão igualmente representados os respetivos perfis de densidade ao longo da profundidade, expressos em valores de cinzentos (adimensionais).

Agradecimentos

Este estudo recebeu fundos nacionais portugueses da FCT (Fundação para a Ciência e Tecnologia) através dos fundos nacionais UIDP/50019/2020-IDL e PINFRA/22157/2016–EMSO-PT. As sondagens foram colhidas no âmbito do projeto ENVI-CHANGES (FCT/PLE/12/00). Ana Alberto recebeu apoio financeiro através da bolsa de doutoramento UIBD/151497/2021 (IDL). Ana Alberto agradece ao Instituto Português do Mar e da Atmosfera (IPMA) pela cedência das suas instalações e equipamentos, que foram fundamentais para a realização do presente trabalho.

REFERÊNCIAS

Alves, A. (1996). *Causas e processos da dinâmica sedimentar na evolução actual do litoral do alto Minho.* Dissertação de Mestrado, Universidade do Minho, Braga, 442 p.

Ashi, J. (1997). Computed Tomography Scan Image Analysis of Sediments1. In: Shipley, T.H., Ogawa, Y., Blum, P., e Bahr, J.M. (eds.), *Proceedings of the Ocean Drill Program, Scientific Results*, 156. College Station, TX (Ocean Drilling Program), pp. 151-158.

Dann, R., Turner, M., Close, M., e Knackstedt, M. (2010). Multi-scale characterization of coastal sand aquifer media for contaminant transport using X-ray computed tomogaphy. *Environmental Earth Sciences*, 63, pp. 1125-1137.

Leeder, M. R. (2011). *Sedimentology and sedimentary basins: From turbulance to tectonics* (2nd ed.). Wiley-Blackweel, 784 p.

Mitra, S., Paris, R., Bernard, L., Abbal, R., Charrier, P., Falvard, S., Costa, P. e Andrade, A. (2024). X-ray tomography applied to tsunami deposits: Optimized image processing and quantitative analysis of particle size, particle shape, and sedimentary fabric in 3D. *Marine Geology*, 470, 107247.

Monitoring beach nourishment performance with satellite-based analysis: the case of the Forte Novo - Garrão coastal stretch (Portugal)

M. Neves Silva (1), R. Taborda (1), A. Nobre Silva (1-2), A. Vaz (1), C. Aleixo Pinto (2), J. Santos (3), S. Teixeira (4) and S. Costas (3)

(1) Instituto Dom Luiz, Faculdade de Ciências, Universidade de Lisboa, Lisboa, Portugal. marianasilva2@edu.ulisboa.pt
(2) Agência Portuguesa do Ambiente, Amadora, Portugal
(3) Centre for Marine and Environmental Research (CIMA), Universidade do Algarve, Faro, Portugal
(4) Agência Portuguesa do Ambiente (ARH Algarve), Faro, Portugal

Abstract: Artificial beach nourishment is a recognized coastal management measure used to combat coastal erosion and coastline retreat. Remote sensing has proven to be an advantageous process for providing the information needed to analyse earth's surface. Open-source satellite imagery provides data that enable long-term coastal monitoring and the assessment of various site-specific processes. This study evaluates the evolution, behaviour and performance of artificial beach nourishment in the Forte Novo - Garrão coastal stretch (Algarve, Portugal), based on an analysis of the spatiotemporal variation in shoreline position and beach volume between 2000 and 2024, derived from the Earth Observation (EO) programs. The results were compared and validated with observations. This study demonstrates that indicators extracted from satellite imagery effectively reproduces both the volumes of artificial beach nourishment and their spatiotemporal evolutions and gradual volume losses, showing strong agreement with the observations.

Keywords: *beach nourishment, remote sensing, coastal monitoring, shoreline change*

1. INTRODUCTION

Beaches are dynamical environments, where morphological variations can occur at a wide range of spatial and temporal scales (Carapuço *et al*., 2016). Natural and human factors, such as storms, sea-level rise and human occupation, influence coastal dynamics (Vitousek *et al*., 2023). Human interventions in such dynamic systems can aggravate impacts, such as the retreat of the coastline and the reduction of beach area, especially in areas with fixed artificial structures.

Artificial beach nourishment is a measure considered environmentally acceptable and increasingly adopted as a solution, aimed at protecting and defending the coast and contributing to beach regeneration (Pinto *et al*., 2018). In mainland Portugal, beach nourishment interventions began in 1950 (Pinto *et al.*, 2020). In general, the added sediments to the beach help minimize erosion caused by infrastructures that interrupt the littoral drift, capturing sand updrift of a jetty or groin. Monitoring the redistribution of sand after artificial nourishment is essential not only to assess the performance, impact and longevity of the intervention, but also to understand the associated coastal dynamics (Pinto *et al*., 2022). However, there are few studies in Portugal aimed at assessing the performance of artificial nourishment, especially when it comes to quantifying the area and volume of beaches and assessing trends in littoral drift (Pinto *et al*., 2020).

Remote sensing (RS) techniques and Earth Observation (EO) programs like Sentinel and Landsat, have contributed to a significant increase in the spatial extent of monitored areas. The combination of satellite images and machine learning models has contributed to this increase in monitored beaches and to alleviating the lack of data (Vitousek *et al*., 2023). Satellite-derived shorelines have been increasingly used for coastal monitoring, but verification of the results and their suitability for studying the evolution of nourishment and the fate of nourishment sands are still scarce. Continuous analysis of these data makes it possible to identify patterns of evolution that describe long-term trends or cyclical changes in the behaviour of the coastline.

It is necessary and advantageous to continue investigating aspects related to coastal dynamics and to invest in monitoring to deepen knowledge to understand processes, predict evolution and support interventions in terms of planning and coastal defence (Gomes, 2007). In addition, understanding the processes and timescales of beach recovery contributes to assessing coastal resilience in a changing climate (Dodet *et al*., 2019). The main objective of this work is to assess the capacity of indicators extracted from satellite imagery to monitor

the performance of artificial beach nourishment works.

2. STUDY AREA

The study focused along the Vale do Lobo coastline (the coastal stretch between the beaches of Forte Novo and Garrão). It is located in the municipality of Loulé, in the district of Faro (Algarve, Portugal). It is a practically straight stretch of coastline ≈ 4.5 km long, located to the east of the Quarteira groin field and to the west of the Ancão Peninsula, with an approximate NW to SE orientation. This seems to reflect the dominant sea waves that induce a longshore sediment transport of the order of 1 x 10^5 m^3/yr (Pinto and Teixeira, 2022; Santos *et al*., 2014).

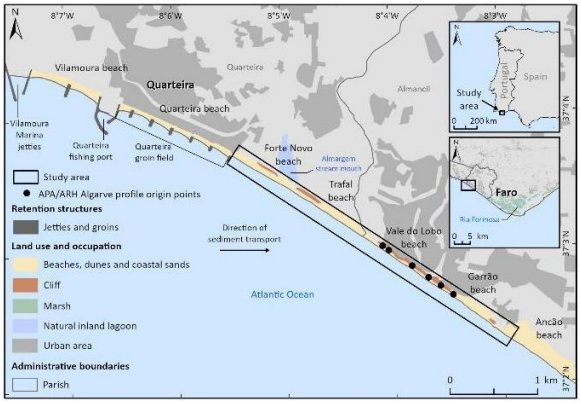

Figure 1. Geographical setting of the study area.

Between 2000 and 2024, the evolution of the beach was marked by a sudden increase because of the 2006 and 2010 nourishments, followed by a gradual decrease due to the sediment deficit caused by drift retention in updrift coastal structures and due to the fact that the sediment has moved out of the intervened cell as a result of the predominant drift from W to E.

3. METHODS

Using the Python toolkit CoastSat (Vos *et al*., 2019), images from Landsat 5 to 9 and Sentinel-2 Level 1C constellations were classified to extract shorelines for all images available with low cloud coverage. In the satellite data, the shoreline indicator corresponds to the instantaneous waterline, whereas in the field data it is represented by the beach width at mean sea level (MSL). Beach width (distance between the base of the cliff and the shoreline) values were obtained using the USGS DSAS software (Himmelstoss *et al*., 2024) for six APA/ARH Algarve profiles (Figure 1). Average beach widths and evolution rates were calculated and validated with field data from Pinto and Teixeira (2022) and Teixeira (2019). A matrix was also created with the average annual beach width every 10 m, allowing the spatiotemporal dynamics to be visualized, namely erosion and accretion trends, over the 24 years of study (2000 – 2024).

The beach volume was estimated by the product of beach area with the beach height, estimated by the difference between berm height (Zberm = 5.5 m, MSL) and the beach toe (BT = -3.5 m, MSL).

4. RESULTS AND DISCUSSION

4.1. Beach width

Figure 2 shows the beach width variation along the studied coastal sector during the study period. The longshore extension of the two nourishments is also represented. The 2006 nourishment has a shorter extent, concentrating on the Vale do Lobo beach area. The 2010 nourishment extends over the entire study area. At the beginning of the study period, in 2000 and 2001, there was still a greater width, also on Vale do Lobo beach, because of the 1998 nourishment. After this period, roughly from 2003 until the 2006 nourishment, there was already a gradual decrease in the width of the beach during the subsequent years. After the 2010 nourishment, there was an increase in beach width, whose trend reverted from 2014 onwards, showing signs of gradual beach width decrease, especially at the updrift section, Forte Novo.

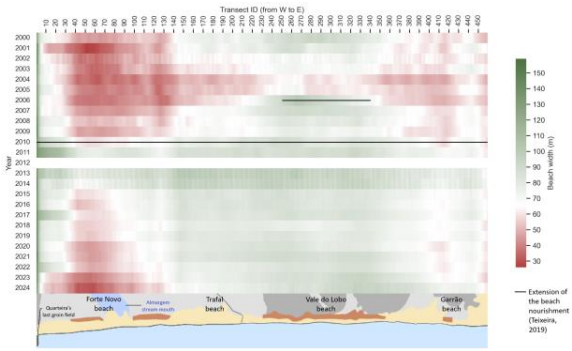

Figure 2. Evolution of the average annual width (m) of the study area, from 2000 to 2024, along the transects drawn every 10 m. The black lines indicate the extent of the beach area that was artificially nourished.

Figure 3 shows the evolution of the average beach width after artificial nourishment on the beaches of Forte Novo, Vale do Lobo and Garrão, between 2000 and 2024.

At Forte Novo beach (Figure 3a), there was a relatively stable trend until 2010, around 40 m, when the trend shifted and with larger average beach widths. However, a gradual decrease was soon identified.

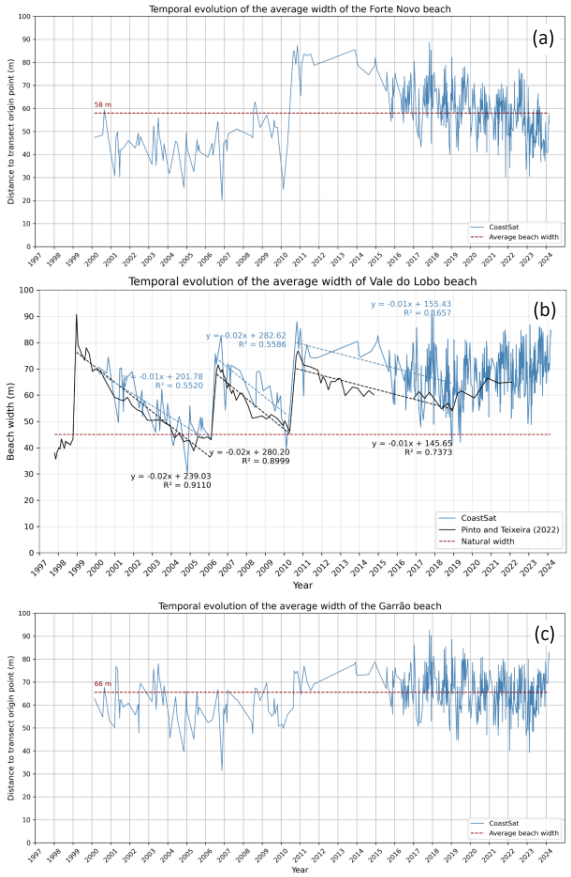

Figure 3. Evolution of the three sectors under analysis: (a) Forte Novo beach; (b) Vale do Lobo beach; (c) Garrão beach.

The evolution of the Vale do Lobo beach (Figure 3b) is mainly controlled by the littoral drift, which is directed eastwards (Teixeira, 2019; Pinto *et al*., 2020). The results based on the average of six profiles and obtained from satellite images and data collected in the field are quite similar, despite the differences in spatial resolution and the shoreline indicators used. The temporal resolution of the images made it possible to reduce uncertainties, resulting in average values close to those recorded on in situ (Pinto and Teixeira, 2022). After the 2006 and 2010 nourishments, observations document that the shoreline advanced 29 m, with similar results from the satellite images (33 m and 28 m, respectively), showing minimal differences between both approaches. The interventions were followed by a period of gradual reduction in beach width, with rates following 2006 intervention of 5.8 m/year (5.7 m/year for RS) and 1.8 m/year (1.9 m/year for RS) for the 2010 intervention. The comparison between the data obtained showed the congruence between the field observations and RS results, proving that RS techniques and semi-automatic methods can be an asset for monitoring the evolution of beach nourishments. Despite differences in shoreline indicators, results are generally concordant. In fact, for the period of analysis of the artificial nourishments in Vale do Lobo, the beach width seems to increase based on the six cross-sectional profiles. The third trend line shows a systematic difference, i.e. although we see a bias, the trend is similar (Figure 3b).

Conversely, the shoreline at Garrão beach (Figure 3c) displays greater temporal stability, fluctuating around its mean position. The fact that Garrão beach remains stable indicates the absence of a gradient in longshore drift and that the magnitude of sediment that enters the westward boundary is equal to the outflux at the eastern boundary.

4.2. Beach volume

Results from the evolution of beach volume are displayed in Figure 4.

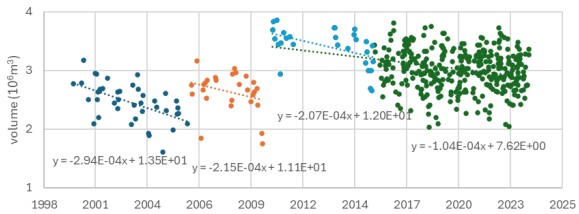

Figure 4. Evolution of beach volume (violet - 2/2000 to 2/2006; orange - 5/2006 to 2/2010; blue - 8/2010 to 12/2015; green - 12/2015 to 12/2024) and best fit lines (slope in $10^6 m^3$/day).

The slopes of the three trend lines indicate an overall decrease in beach volume across the study site during the intervals between nourishment events, with rates ranging from 1.1×10^5 m³/year to 0.7×10^5 m³/year (Table I).

Table I. Estimated reduction in beach volume between nourishment events, based on the slopes of the best-fit lines shown in Figure 4.

Period	Start	End	Slope ($10^6 m^3$/day)	Slope (m³/year)
after first nourishment	Feb-2000	Feb-2006	2.94E-04	107310
after second nourishment	May-2006	Feb-2010	2.15E-04	78475
about five years after third nourishment	Aug-2010	Dec-2015	2.07E-04	75555
entire period after third nourishment	Aug-2010	Dez-2024	1.04E-04	37960

When considering the entire period following the third nourishment, the trend line shows an average decrease of approximately 0.4×10^5 m³/year.

To assess the nourishment volume, the difference between the trend line values immediately before and after each nourishment event was calculated (Table II).

Table II. Estimates of beach volume variation at each nourishment event (in 106m3). vbn – beach volume before nourishment; vaf – beach volume after nourishment, env – estimated nourished volume (vaf – vbn).

Nourishment	vbn	vaf	env
2006	2.11	2.75	0.64
2010	2.45	3.64	1.18

Despite the noise inherent in the derived satellite shoreline data, which were not corrected for tidal or wave effects, nor filtered in any way, and the uncertainties in both beach toe estimates and the beach profile model used, the results nonetheless demonstrate the viability of this method for monitoring the evolution of nourished beaches. The findings are consistent with previous estimates of longshore drift at the site and show reasonable agreement with the reported values by Teixeira (2019).

5. CONCLUSIONS

Comparison between field data and satellite derived shoreline demonstrated strong agreement, validating the use of semi-automatic shoreline extraction methods as effective tools for monitoring beach nourishment evolution. The proposed methodology yielded promising results for estimating longshore sediment transport and provided evidence that it can be used to estimate nourishment volumes. Nevertheless, field data and satellite derived shorelines should be complementary, with each enhancing the strengths of the other. When integrated, they offer a more comprehensive monitoring framework by combining the high precision of field data with the broad spatial and temporal coverage of remote sensing.

Acknowledgements

This work is supported by the Portuguese Fundação para a Ciência e Tecnologia, FCT, I.P./MCTES through national funds (PIDDAC): (https://doi.org/10.54499/UIDB/50019/2020) UID/50019/2025, and UIDB/50019/2020 LA/P/0068/2020 (https://doi.org/10.54499/LA/P/0068/2020). The work is a contribution to the CREST project, funded by FCT through Grant 2022.05392.PTDC (doi:10.54499/2022.05392.PTDC). Authors also recognize the support of national funds through FCT, under the project LA/P/0069/2020 (doi:10.54499/LA/P/0069/2020), granted to the Associate Laboratory ARNET, and UID/00350/2020 (doi:10.54499/UIDB/00350/2020) granted to CIMA.

REFERENCES

Carapuço, M. M., Taborda, R., Silveira, T. M., Psuty, N. P., Andrade, C. and Freitas, M. C. (2016). Coastal geoindicators: Towards the establishment of a common framework for sandy coastal environments. *Earth-Science Reviews*, 154, 183-190. https://doi.org/10.1016/j.earscirev.2016.01.002

Dodet, G., Castelle, B., Masselink, G., Scott, T., Davidson, M., Floc'h, F., Jackson, D. and Suanez, S. (2019). Beach recovery from extreme storm activity during the 2013–14 winter along the Atlantic coast of Europe. *Earth Surface Processes and Landforms*, 44, 393–401. https://doi.org/10.1002/esp.4500

Gomes, F. V. (2007). A gestão da zona costeira portuguesa. *Revista de Gestão Costeira Integrada/Journal of Integrated Coastal Zone Management*, 7(2), 83-95.

Himmelstoss, E. A., Henderson, R. E., Farris, A. S., Kratzmann, M. G., Bartlett, M. K., Ergul, A., McAndrews, J., Cibaj, R., Zichichi, J. L. and Thieler, E. R. (2024). Digital Shoreline Analysis System version 6.0: U.S. Geological Survey software release. https://doi.org/10.5066/P13WIZ8M

Pinto, C. A. and Teixeira, S. B. (2022). Evolução e Comportamento das Alimentações Artificiais de Praia em Vale do Lobo (Algarve – Portugal). *6ª Conferência Morfodinâmica Estuarina e Costeira*, Lisboa, pp. 23-24.

Pinto, C. A., Silveira, T. M. and Teixeira, S. B. (2018). Alimentação artificial de praias na faixa costeira de Portugal Continental: Enquadramento e retrospetiva das intervenções realizadas (1950 - 2017). Relatório Técnico. Agência Portuguesa do Ambiente, 60p. https://doi.org/10.13140/RG.2.2.24446.48969

Pinto, C. A., Silveira, T. M. and Teixeira, S. B. (2020). Beach nourishment practice in mainland Portugal (1950–2017): Overview and retrospective. *Ocean & coastal management*, 192, 105211. https://doi.org/10.3390/jmse10020146

Santos, F., Lopes, A., Moniz, G., Taborda, R., and Ramos, L. (2014). Gestão da Zona Costeira: O Desafio da Mudança. Portuguese Littoral Working Group Report, 237 pp. (in Portuguese).

Teixeira, S. B. (2019). Beach nourishment as a coastal management solution to mitigate soft cliff erosion on Quarteira coast (Algarve-Portugal). *Proceedings of the 5ª Conferência sobre Morfodinâmica Estuarina e Costeira* (MEC2019), Lisbon, Portugal, pp. 33-34.

Vitousek, S., Buscombe, D., Vos, K., Barnard, P. L., Ritchie, A. C. and Warrick, J. A. (2023). The future of coastal monitoring through satellite remote sensing. Cambridge Prisms: Coastal Futures, 1, e10, 1–18. https://doi.org/10.1017/cft.2022.4

Vos, K., Splinter, K. D., Harley, M. D., Simmons, J. A. and Turner, I. L. (2019). CoastSat: A Google Earth Engine-enabled Python toolkit to extract shorelines from publicly available satellite imagery. *Environmental Modelling & Software*, 122, 104528. https://doi.org/10.1016/j.envsoft.2019.104528

Tavira marsh evolution assessment in a sea-level rise context

M. Inácio (1) and M. C. Freitas (1)

(1) IDL, Faculty of Sciences of University of Lisbon, Lisbon, Portugal. mfinacio@fc.ul.pt

Abstract: Salt marshes are highly recognized for their ecological services. However, these environments are vulnerable to the impact of climate change, particularly sea-level rise (SLR). In this study, the evolution of a small marsh in Tavira (Faro, Portugal) was projected considering three SLR scenarios ranging from 60 to 214 cm by 2100. In addition, it was assessed whether an IPMA facility would be located in a flood-prone area. The study was carried out using a two-dimensional rule-based model of reduced complexity. The results indicate that the marsh is resilient to SLR, compensating for considerable area losses by expanding inland. In addition, the IPMA facility is located in a flood zone for intermediate and severe SLR scenarios.

Keywords: *climate change, modelling, accretion rates, remote sensing, reduced-complexity models*

1. INTRODUCTION

Salt marshes are vegetated intertidal areas widely recognized for their ecological services, such as coastline protection, biodiversity, water filtration, and blue carbon storage, and their preservation is crucial. They are highly vulnerable to the impacts of climate change, particularly to sea-level rise (SLR). To project the evolution of salt marshes in this context, a reduced complexity two-dimensional rule-based model was developed, the Simplified Marsh Response Model (SMRM), which was first applied to marshes of the Sado estuary (Inácio *et al.*, 2022a). This work presents the first results of applying the model to an area other than the one that served as a pilot for its development. The new area is in Ria Formosa, near Tavira (Portugal) – Figure 1.

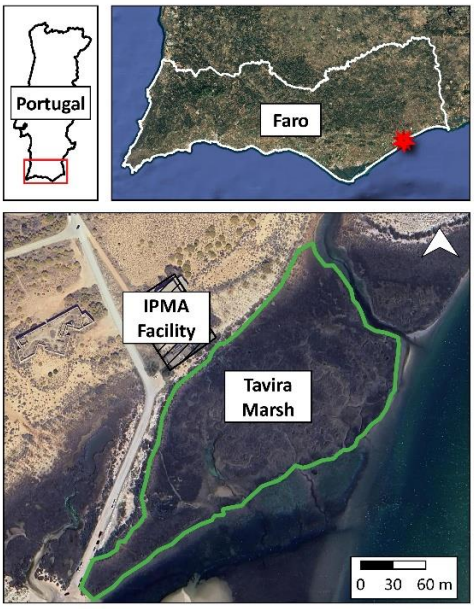

Figure 1. Tavira marsh and the IPMA facility location in the Faro district of Portugal.

The studied salt marsh is located on the lagoon terrestrial margin, protected by Cacela barrier island, and has an area of 3.4 ha.

This work aims to estimate the impact of the SLR on marsh evolution and comprehend whether the IPMA Facility (a Portuguese public institution) is in the inundation area for marsh growth until the end of the century.

2. MATERIALS AND METHODS

The considered model requires the input of four parameters: (1) a high-resolution digital terrain model (DTM) representing the studied environments and the surrounding area, to simulate their possible future expansion and inundation; (2) transition heights among sub-environments (tidal flat – TF; low marsh – LM; high marsh – HM; dune – D). These levels are usually associated with local tidal levels (Davis and Fitzgerald, 2004): mean high water neaps to the transition from TF to LM, mean high water to the transition between LM and HM, and mean high water springs to the upper limit of HM; (3) at least one SLR scenario, which must include an initial rate and optionally a constant acceleration value; (4) accretion rates for different sub-environments (TF, LM, and HM) and, optionally, an acceleration value for these rates.

The script for this model was written in Python, and the code is open for use and editing (Inácio *et al.*, 2022b).

The DTM was obtained from the 2011 LiDAR survey conducted through a partnership between Agência Portuguesa do Ambiente (APA) and Direção-Geral do Território (DGT) (Silva *et al.*, 2012), two Portuguese public institutions. It has a 2 m horizontal resolution and a precision between 8 and 24 cm. The DTM was compared with DGPS data obtained in the field.

Local tidal levels were consulted from the annual tidal tables available on the Instituto Hidrográfico (Hydrographic Institute) website. However, comparing the published values with the DTM (previously validated with field data) led to the conclusion that the published levels do not match the theoretical height distribution of the studied marsh. Therefore, an empirical selection of elevations was conducted to find the heights that would satisfactorily define the transition between sub-environments. The defined areas were validated by comparison with satellite images from Google Earth. The elevations used were: TF/LM = 0.40 m; LM/HM = 0.50 m; HM/D = 1.40 m (values regarding Portuguese Cascais datum, 1938) and the 2025 morphological map is shown in Figure 2.

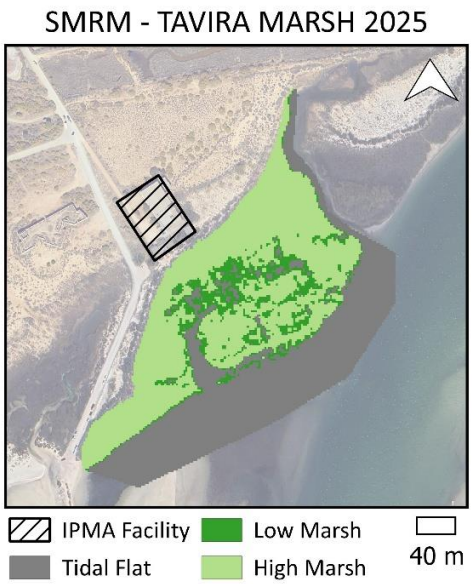

Figure 2. 2025 Tavira marsh morphological map, considering the defined transition heights.

The evolution of the marsh areas was modeled using three different SLR scenarios: conservative scenario – IPCC SSP1-2.6 (IPCC, 2021): 35 cm until 2050 and 60 cm until 2100; intermediate scenario – Mod.FC_2b (Antunes, 2019): 43 cm until 2050 and 111 cm until 2100; severe scenario – NOAA High (Sweet *et al.*, 2017): 65 cm until 2050 and 214 cm until 2100.

Local accretion rates should be obtained directly from field data (short cores), using dating methods suitable for recent sedimentation periods, such as the analysis of ^{137}Cs and ^{210}Pb isotope activity. However, in its absence, values from literature were considered. Accretion rates between 1.51 mm/year and 3.62 mm/year were determined for the Ria Formosa marshes near Faro (Martins *et al.*, 2022). In this specific exercise, an average value of 2.57 mm/year was incorporated in the modeling process with similar for all the sub-environments.

3. RESULTS

The results are presented in order of severity of SLR.

The most conservative scenario (IPCC SSP1-2.6) does not produce very significant variations in the global area by the end of the century (Figure 3). A 10% growth in marshland is projected by 2050 due to flooding that will occur landwards (Figure 4A). By 2100, the expansion will continue, but it will not be enough to offset seaward losses (Figure 4B), resulting in a global area loss of around 4%. It is worth mentioning that the changes in the sub-environments by the end of the century are not the same, with high marsh losing 8% of their area and low marsh growing by 14%.

The intermediate scenario (Mod.FC_2b) produces significant modifications in the second half of the century, although these are offset (Figure 5). No significant variations are projected until 2050, with losses of only 2%, where losses on the lagoon side are offset by the landward expansion of the marsh (Figure 4C). By 2100, there are no variations in the overall area, a situation that is only possible due to very significant flooding of the present-day supratidal area, which compensates for the losses on the lagoon side (Figure 4D). With this scenario, flooding is expected in the area where the IPMA Facility is located.

Finally, the NOAA High scenario is the one that produces the most significant changes in the study area (Figure 6). A loss of 28% is projected by 2050, and although there will be significant flooding landwards, this will not compensate for the heavy losses' lagoon wards (Figure 4E). By 2100, a loss of 73% is expected, with most of the area currently occupied by marsh becoming tidal flat (Figure 4F). The area loss is not uniform among sub-environments, with the high marsh losing 80% of its current area and the low marsh only 42%. It is also worth noting that the IPMA Facility area will be essentially occupied by tidal flat, as will the surrounding area.

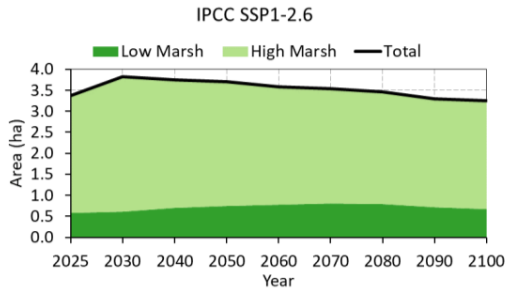

Figure 3. Tavira marsh decennial evolution considering the IPCC SSP1-2.6 SLR scenario.

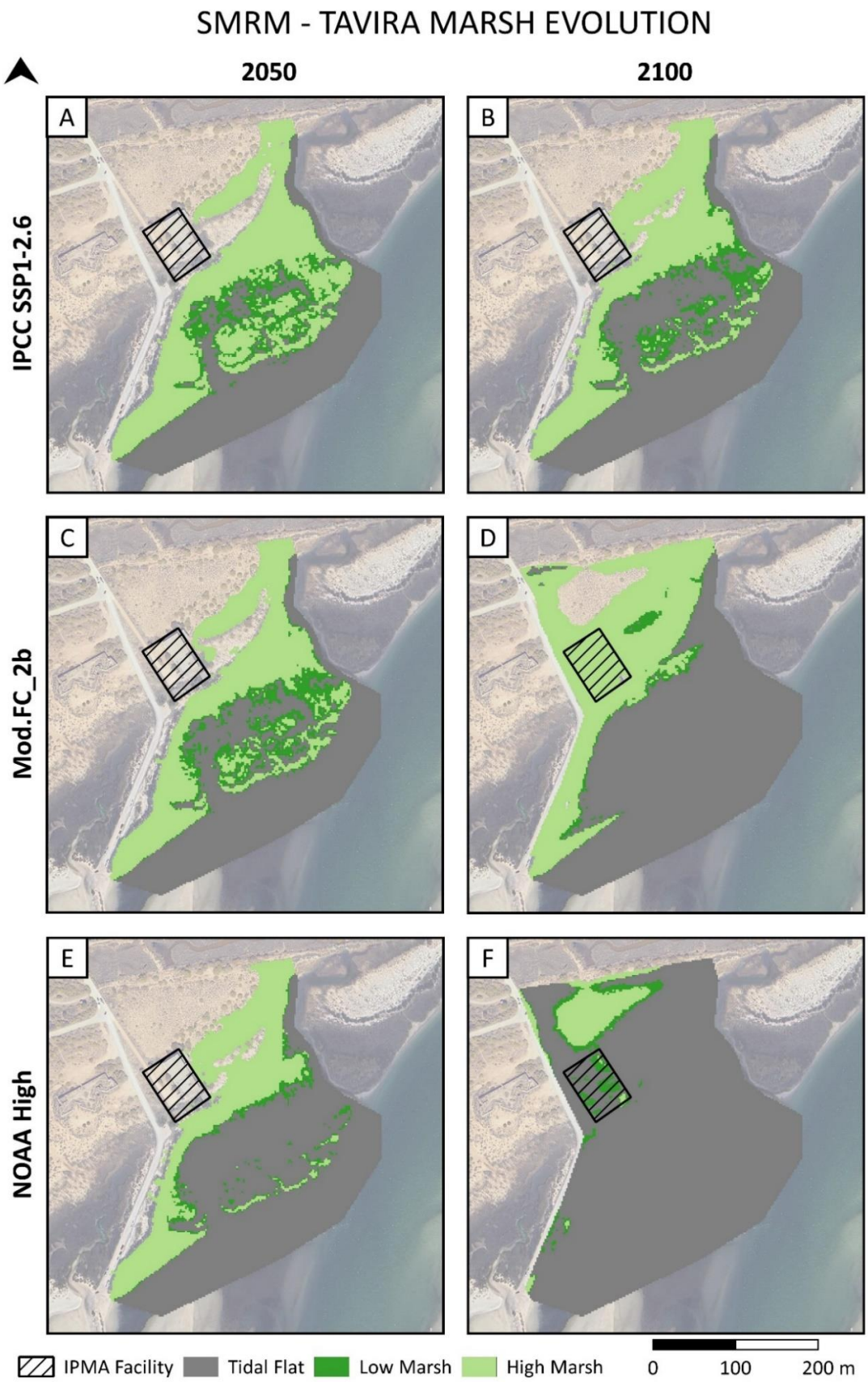

Figure 4. Tavira marsh morphological maps considering IPCC SSP1-2.6 (A: 2050; B: 2100), Mod.FC_2b (C: 2050; D: 2100) and NOAA High (E: 2050; F: 2100) SLR scenarios.

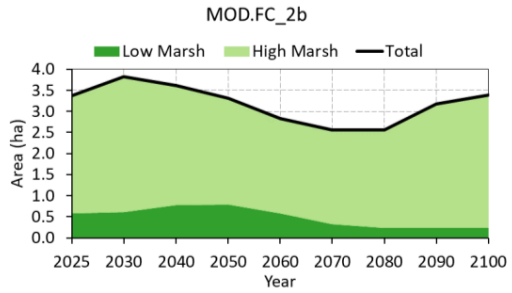

Figure 5. Tavira marsh decennial evolution considering Mod.FC_2b SLR scenario.

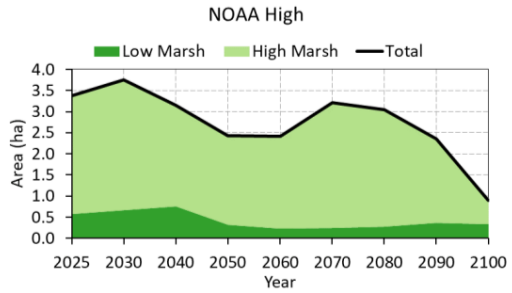

Figure 6. Tavira marsh decennial evolution considering NOAA High SLR scenario.

4. CONCLUSION

The studied marsh's response depends essentially on the chosen SLR scenario and on the availability of land for its expansion.

The most conservative scenario predicts a negligible area loss, with losses on the lagoon ward side partially offset by the inundation of the marsh landwards. Under this projection, the IPMA facility is not located in an area occupied by the expansion of the marsh.

In the intermediate scenario, by 2070, the loss of area on the lagoon side is expected to be more significant than flooding landwards. However, between 2070 and 2100, flooding landwards becomes more significant than losses on the lagoon side, with a partial recovery of area. In this situation, the IPMA facility will not be at risk in 2050, but by the end of the century, it will be in an area potentially flooded and that could be colonized by plants of high marsh.

Finally, in the most severe scenario, the behavior is the same as in the previous one, but the stages of evolution occur more quickly. In addition, from 2070 onwards, the rate of SLR becomes so significant that flooding inland cannot compensate for the loss of area, resulting in a significant reduction in the marsh area. The IPMA facility will be at high risk of flooding in this scenario, as most of its area will be at levels compatible with tidal flat by the end of the century.

These simulations consider the evolution of the marsh based on the topography provided by the DTM without considering artificial physical barriers such as buildings like the IPMA Facility. Thus, the simulations represent the expansion of the marsh if the surroundings were natural. These results also allow us to conclude that the studied marsh shows high resilience to SLR and can adapt and respond by moving landwards when no barriers are imposed.

Acknowledgements

This work was funded by the Portuguese Fundação para a Ciência e a Tecnologia (FCT) I.P./MCTES through national funds (PIDDAC) – UIDB/50019/2020 (https://doi.org/10.54499/UIDB/50019/2020), UIDP/50019/2020 (https://doi.org/10.54499/UIDP/50019/2020) and LA/P/0068/2020 (https://doi.org/10.54499/LA/P/0068/2020). The authors would like to thank Marcos Rosa, who helped to obtain DGPS field data.

REFERENCES

Antunes, C. (2019). Assessment of Sea Level Rise at West Coast of Portugal Mainland and Its Projection for the 21st Century. *Journal of Marine Science and Engineering*, 7(3), 61.

Davis, R.A., and FitzGerald, D.M. (2004). Beaches and Coasts. *Blackwell Publishing Company*.

Inácio, M., Freitas, M. C., Cunha, A. G., Antunes, C., Leira, M., Lopes, V., Andrade, C., and Silva, T. A. (2022a). Simplified Marsh Response Model (SMRM): A Methodological Approach to Quantify the Evolution of Salt Marshes in a Sea-Level Rise Context. *Remote Sensing*, 14(14), 3400.

Inácio, M., Freitas, M.C., Cunha, A.G., Antunes, C., Leira, M., Lopes, V. and Andrade, C. (2022b). SMRM. *Figshare*, https://doi.org/10.6084/m9.figshare.20237409.v2

IPCC. (2021). Climate Change 2021: The Physical Science Basis. Contribution of Working Group I to the Sixth Assessment Report of the Intergovernmental Panel on Climate Change (V. Masson-Delmotte, P. Zhai, A. Pirani, S. L. Connors, C. Péan, S. Berger, N. Caud, Y. Chen, L. Goldfarb, M. I. Gomis, M. Huang, K. Leitzell, E. Lonnoy, J. B. R. Matthews, T. K. Maycock, T. Waterfield, O. Yelekçi, R. Yu, and B. Zhou, Eds.). *Cambridge University Press*.

Martins, M., los Santos, C. B.; Masque, P.; Carrasco, A. R., Veiga-Pires, C. and Santos, R. (2022). Carbon and Nitrogen Stocks and Burial Rates in Intertidal Vegetated Habitats of a Mesotidal Coastal Lagoon. *Ecosystems,* 25, 372–386.

Silva, M., Patrício, P., Mariano, A., Morais, M., and Valério, M. (2012). Obtenção de Dados LiDAR para as Zonas Costeiras de Portugal Continental. *Segundas Jornadas de Engenharia Geográfica*, 107(1), 19–22.

Sweet, V. W., Kopp, R. E., Weaver, P. C., Obeysekera, J., Horton, M. H., Thiele, E. R., and Zervas, C. (2017). Global and Regional Sea Level Rise Scenarios for the United States. *National Oceanic and Atmospheric Administration.*

Assessing tidal wetland ecosystem services in the future through remote sensing and modelling

A. R. Carrasco (1), J. Duarte (1), I. Carneiro (1), M. Silva (1) and K. Kombiadou (1)

(1) CIMA/ARNET – Centre for Marine and Environmental Research/Aquatic Research Network, Universidade do Algarve, Campus de Gambelas, 8005-139 Faro, Portugal. azarcos@ualg.pt

Abstract: This study develops a framework to assess current and future blue carbon in the Ria Formosa wetlands, combining satellite image classification and simplified modeling. Using Random Forest Regression on Sentinel-2 images, the fractional cover of marsh species across various wetland categories was accurately mapped for 2015, delineating vegetation limits and ecological zonation. Future projections up to 2100, based on land cover change simulations from the SLAMM model, explore how the system may naturally adapt under sea-level rise scenarios. Under the IPCC SSP5-8.5 scenario projections, significant transitions of high to low marshes, low marshes to tidal flats, and tidal flats to subtidal bare sediment occur, leading to a decline in organic carbon within the lagoon. This integrated approach provides valuable insights into ecosystem dynamics and resilience, supporting informed management and conservation strategies for wetlands facing environmental changes.

Keywords: *wetlands, remote sensing, zonation, ecosystem services, monitoring*

1. INTRODUCTION

As interest in natural climate solutions grows, coastal and ocean ecosystems, known as "blue carbon," are increasingly recognized as vital (e.g., Macreadie *et al*., 2019). To meet climate targets, protecting and restoring blue carbon sinks must be grounded in solid scientific understanding and include effective methods to assess future trajectories influenced by both natural and human factors. Projecting the future spatial and temporal dynamics of blue carbon sinks, such as coastal wetlands, is a complex challenge, complicated even further by changing climate conditions (e.g., Campbell *et al*., 2019; Blount *et al*., 2022).

Satellite imagery has shown a strong potential for acquiring comprehensive and long-term observations over extensive areas, enabling the characterization of wetland habitat change on various spatial scales (e.g., Lopes *et al*., 2019). When combined with modelling approaches, satellite imagery appears to be an excellent tool for supporting projections of future evolution of salt marsh zones in the medium and long term (e.g., Yang *et al.*, 2025). This study employs a predictive approach that combines satellite image remote sensing with simplified modeling techniques to assess the current and future status of wetland zonation in Ria Formosa coastal lagoon, considering the impacts of sea-level rise. Wetland zonation is further translated into estimates of future blue ecosystem services (i.e., organic carbon stock).

2. METHODS

2.1. Satellite-derive data

The research was conducted in the Ria Formosa system, one of the main coastal lagoons of Portugal. The Random Forest Regression algorithm (RFR; Yang *et al.*, 2020) was used to estimate the fractional cover of wetland zonation classes in the Ria Formosa lagoon from Sentinel-2 Level 2A images from 2015. A separate RFR was trained for each class, allowing the estimated class fractional cover at a subpixel level. As the predictions come from different RFRs, their values need to be rescaled, so that their sum equals 1 in each pixel. Data from high-resolution UAV and Worldview-3 imagery were used as ground-truth information for estimating class fractional cover from the Sentinel-2 imagery. The selected tidal wetland classes include the high and low marsh and vegetated tidal flat, while the RFR algorithm is written in Python, using the open Scikit-learn package (Pedregosa *et al*., 2011). To estimate model performance, the root-mean-square error (RMSE) and the coefficient of determination (R2), between predicted and observed fractional cover, were calculated for each class for both training and testing populations.

2.2. Long-term land cover change and blue carbon estimates

The long-term adaptation of wetlands to sea-level rise (shifts in habitats) over approximately 90 years (until 2100) was estimated using the Sea Level Affecting Marshes Model approach, SLAMM (e.g., Glick *et al*., 2013), a landscape-based model that simulates changes in land cover (i.e., shifts in the ecological

zonation). Future sea-level rise (SLR) projections were based on the Shared Socioeconomic Pathway 8.5 (SSP-8.5) SLR scenario from the IPCC (IPCC, 2021). This scenario depicts a high emission pathway, representing a worst-case scenario with continued rise in emissions and minimal mitigation (IPCC, 2021). Land cover type conversions in the model occur when SLR exceeds accretion rates and when the cell elevation falls below the lower limit of its category (i.e., the elevation where one category transitions to another). Initial conditions for SLAMM wetland categories (non-vegetated and vegetated tidal flat, low marsh, and high marsh) were based on the fractional cover derived from the 2015 Sentinel-2 RFR results. Model simulations were conducted over a uniform grid with 10 m spacing, considering the elevations in marsh and tidal flat areas from available LiDAR data (2011). Current and projected aboveground biomass and organic carbon stocks (Corg; up to 2100) were estimated from values reported in literature, with 2023 used as the reference condition for spatial variation (Santos *et al*. (2023), and Mazarrasa *et al*. (2023) and Martins *et al*. (2022), respectively).

3. RESULTS AND DISCUSSION

3.1. Regression accuracy

The application of the RFR algorithm to Sentinel-2 data achieved high accuracy in predicting the fractional cover of marsh and seagrass vegetation over different zones (RMSE<0.11 and R2>0.73), allowing for reliable estimates for the wetland categories considered. The RFR model accuracy was variable between categories, showing higher values for the non-vegetated tidal flats (R2>0.95), vegetated tidal flats (R2>0.93), and high marshes (R2>0.81). The results are very positive, but face limitations mainly related to the resolution of Sentinel-2 itself, as also noted by Yang *et al*. (2025).

Figure 1 displays the fractional abundance for each zonation, calculated based on the RFR results. In 2015, the non-vegetated tidal flats and low marshes represented the largest areas among the wetland environments (Figure 1). Similar to the methods developed by Lanceman *et al*. (2022), this study proposes a user-friendly workflow for classifying Sentinel-2 imagery, providing valuable insights to enhance blue carbon restoration and monitoring efforts.

Figure 1. Ecological zonation of the Ria Formosa wetlands for 2015, based on the Sentinel-2 imagery.

3.2. Habitat change and blue carbon in the future

The results of the SLAMM simulation for the SSP5-8.5 scenario are given in Figure 2 and indicate that rising sea-levels are expected to cause high salt marshes to turn into low salt marshes, low salt marshes to become tidal flats, and tidal flats to turn into open water. By 2100, the areas of low and high salt marshes in the Ria Formosa wetlands are likely to decrease, while the areas of tidal flats, both vegetated and non-vegetated, are expected to increase (Figure 2). This indicates that a critical challenge related to spatial accommodation will arise, consistent with the predictions made by Carrasco *et al*. (2021).

Based on these habitat shifts, a decrease in organic carbon stock is expected for the lagoon system of the Ria Formosa wetlands, particularly in the low and high salt marsh environments (Figure 3). Conversely, an increase in organic carbon is anticipated in the shallow vegetated and non-vegetated tidal areas.

Figure 2. Spatial variation of environments in the wetland zonation of the Ria Formosa coastal lagoon between 2015 and 2100, considering the sea-level rise scenario SSP5-8.5 (IPCC, 2021).

Figure 3. Spatial variation of the organic carbon stock in the wetland zonation of the Ria Formosa coastal lagoon between 2023 and 2100, considering the sea-level rise scenario SSP5-8.5 (IPCC, 2021).

By 2100, the potential for organic carbon storage in the non-vegetated tidal flats is unlikely to offset the losses in the low and high salt marshes (Table I). Despite uncertainties in carbon sequestration related to landward migration, observed in other case studies (e.g., Kirwan and Mudd, 2012), our results suggest an overall reduction in the carbon sequestration potential, primarily due to the loss of vegetated areas situated in higher elevations due to coastal squeeze. Advancing the future potential of blue carbon requires protecting and restoring ecosystems, while also supporting adaptive shifts in ecosystem distribution in response to climate change, actions that will also provide important adaptation benefits (Lovelock and Reef, 2020).

Table I. Temporal variation of the organic carbon stock (in gigagrams) in the wetland zones of the Ria Formosa (TF: tidal flat; VTF: vegetated tidal flat; LM: low marsh; HM: high marsh) between 2015 and 2100, considering sea-level rise scenario SSP5-8.5 (IPCC, 2021).

Stock Corg (Gg)						
Habitat	2015	2025	2040	2060	2080	2100
TF	219.5	207.2	208.2	211.9	220.3	234.1
VTF	49.1	69.6	69.9	71.2	74.0	78.6
LM	188.6	188.2	186.9	181.8	170.2	148.8
HM	4.0	4.0	3.9	3.8	3.4	2.5

4. FINAL REMARKS

This study demonstrated that the RFR method can accurately classify marsh species using Sentinel-2 data. It also highlights that Sentinel-2 is a cost-effective and efficient tool for obtaining detailed ground data necessary for vegetation analysis across various sensors. SLAMM proved to be a simplified yet reliable approach for predicting environmental changes in wetland habitats.

When considered within the context of the dominant natural influences, the outcomes and the applied methodology substantially advance scientific understanding of vegetation succession and associated ecosystem services in mesotidal systems. More importantly, these findings might work as crucial tools for regional coastal decision-makers, allowing them to identify conservation priorities, develop strategic landscape management plans, and enhance the sustainability of vital ecological functions, such as carbon sequestration, within these ecosystems.

Acknowledgments

The work contributes to project C-Land (CEXC/4647/2024) funded by the Plano Recuperação e Resiliência and the Fundação para a Ciência e Tecnologia (FCT). A. R. Carrasco and K. Kombiadou were supported by the individual contracts https://doi.org/10.54499/CEECINST/00052/2021/CP2792/CT0007 and https://doi.org/10.54499/CEECINST/00146/2018/CP1493/CT0011, respectively, funded by FCT. All authors had the support of the funding attributed to CIMA (https://doi.org/10.54499/UIDB/00350/2020) and the Associate Laboratory ARNET (https://doi.org/10.54499/LA/P/0069/2020), while the WV-3 imagery used was provided by the DEVISE project (http://doi.org/10.54499/2022.06615.PTDC), all funded by FCT. The authors would also like to thank Zhicheng Yang and Sonia Silvestri for their guidance on remote sensing techniques and Lara Talavera Madrigal for conducting and processing UAV flights in Culatra island, used as part of the training.

REFERENCES

Blount T., Carrasco, A.R., Cristina S. and Silvestri S. (2022). Exploring open-source multispectral satellite remote sensing as a tool to map long-term evolution of salt marsh shorelines. *Estuarine Coastal and Shelf Science*, 266.

Campbell A. and Wang Y. (2019). High spatial resolution remote sensing for salt marsh mapping and change analysis at fire Island national seashore. *Remote Sensing*, 11.

Carrasco, A.R., Kombiadou, K., Amado, M. and Matias, A. (2021). Past and future marsh adaptation: lessons learned from the Ria Formosa lagoon. *Science of the Total Environment*, 790.

Glick, P., Clough, J., Polaczyk, A., Couvillion, B. and Nunley, B. (2013). Potential effects of sea-level rise on coastal wetlands in southeastern Louisiana. Journal of Coastal Research SI 63, 211–233.

Intergovernmental Panel on Climate Change (IPCC) (2021). Climate Change 2021 – The Physical Science Basis: Working Group I Contribution to the Sixth Assessment Report of the Intergovernmental Panel on Climate Change. Cambridge University Press; 2023.

Kirwan, M. and Mudd, S. (2012). Response of salt-marsh carbon accumulation to climate change. *Nature*, 489, 550–553.

Lanceman, D., Sadat-Noori, M., Gaston, T., Drummond, C. and Glamore, W. (2022). Blue carbon ecosystem monitoring using remote sensing reveals wetland restoration pathways. *Frontiers in Environmental Science*, 16 p.

Lopes, C.L., Mendes, R., Caçador, I. and Dias, J.M. (2019). Evaluation of long-term estuarine vegetation changes through Landsat imagery. *Science of the Total Environment*, 653:512–22.

Lovelock, C. and Reef, R. (2020). Variable Impacts of Climate Change on Blue Carbon. *One Earth*, 3.

Macreadie, P.I., Anton, A., Raven, J.A. *et al.* (2019). The Future of Blue Carbon Science. *Nature Communications* 10.1 (2019): 1–13

Martins, M., de los Santos, C. B., Masqué, P., Carrasco, A. R., Veiga-Pires, C., Santos, R. (2022). Carbon and nitrogen stocks and burial rates in intertidal vegetated habitats of a mesotidal coastal lagoon. *Ecosystems, 25*(2), 372–386. https://doi.org/10.1007/s10021-021-00660-6

Mazarrasa, I., Neto, J. M., Bouma, T. J., Grandjean, T., García Orellana, J., Masqué, P., Recio Espinosa, M., Serrano, Ó., Puente Trueba, M. A., Juanes de la Peña, J. A. (2023). Soil Corg stocks and burial rates decreased from inner to outer estuarine sections in most estuaries: Evidence from Europe's unexplored regions. *Science of the Total Environment*, 886, 163957.

Pedregosa, F., Varoquaux, G., Gramfort, A., Michel, V., Thirion, B. Grisel, O., Blondel, M., Prettenhofer, P., Weiss, R., Dubourg, V., Vanderplas, J., Passos, A., Cournapeau, D., Brucher, M., Perrot, M. and Duchesnay (2011). Scikit-learn: Machine Learning in Python, *Journal of Machine Learning Research*, 12, 2825-2830.

Santos, R., Ito, P., de los Santos, C.B. (2023). Relatório Científico II: Os 10 principais ecossistemas de carbono azul em Portugal continental. Projeto Gulbenkian Carbono Azul. Relatório científico. Centro de Ciências do Mar. Faro, 140pp.

Yang, Z., D'Alpaos, A., Marani, M. and Silvestri, S. (2020). Assessing the fractional abundance of highly mixed salt-marsh vegetation using random forest soft classification. *Remote Sensing*, 12:1–25.

Yang, Z., Bount, T., Lester, C., Blackford, N., D'Alpaos, A., Marani, M., Murray, B. and Silvestri, S. (2025). Unmixing marsh vegetation species across multiple sensors and spatial scales. *Geoscience & Remote Sensing*, 62, 1, 2481689.

How resilient are Portuguese beaches? A decade later: Impacts and recovery of sandy beaches after the 2014 *Christina* storm on the central-western Portuguese coast

R. Taborda (1), A. P. Bastos (1), A. N. Silva (1,2), C. Andrade (1), C. Ponte Lira (1,3), D. Mendes (4), M. Carapuço (1,5), M. Ribeiro (6) and T. Silveira (1,3)

(1) Instituto Dom Luiz, FCUL, Faculdade de Ciências, Universidade de Lisboa, Portugal. rtaborda@fc.ul.pt
(2) Agência Portuguesa do Ambiente, I.P., Lisboa, Portugal
(3) Instituto Português do Mar e da Atmosfera, Lisboa, Portugal
(4) CERIS – Civil Engineering Research and Innovation for Sustainability, Instituto Superior Técnico, Lisbon, Portugal
(5) Atlantic International Research Centre, Lisbon, Portugal
(6) Instituto Hidrográfico, Portugal

Abstract: This study aims to analyse the recovery of beaches along the central-west coast of Portugal over a decadal time scale, following the impact of the 2013/14 winter storm cluster, which was dominated by the extreme event *Christina*. The analysis focuses on morphological changes and long-term recovery trends, contextualised within oceanographic forcing and geological controls. Results show that, over ten years, most beaches regained their pre-*Christina* profile configuration and beach volume. However, recovery was spatially heterogeneous, and in some cases, full recovery was not achieved. These findings highlight the critical role of local geomorphological and geological settings, sediment availability, and boundary conditions in modulating beach resilience. The results underscore the importance of site-specific analyses for understanding post-storm beach dynamics and recovery time scales, which are essential for informing effective coastal management strategies — particularly under future climate change scenarios that may lead to increased storm intensity and frequency.

Keywords*: Extreme storm events; Beach morphology; Coastal erosion; Field observations*

1. INTRODUCTION

Sandy beaches are inherently dynamic systems, with their shape and volume continuously adjusting to changes in wave energy. During extreme storm events, they can experience significant morphological changes, often marked by substantial sediment loss from the subaerial portion of the beach profile, and in severe cases, they may be entirely eroded. Storm-driven reduction in subaerial beach volume significantly increases the risk of damage to coastal infrastructure. It also threatens nearby communities and land, and raises the chance of wave overtopping and foredune erosion. When the beach-land interface consists of an active cliff, mass movements may be triggered. Once the storm wanes the beach starts recovery, though the rate and extent of recovery are highly variable. While significant recovery can occur within days, more often it takes several months. In cases of severe storms, full beach recovery may require up to a decade, or it may not occur at all, especially when sediment is permanently lost from the beach system to offshore, alongshore, or landward sinks.

Global concern is increasing over the future of beaches, as climate change is expected to accelerate sea level rise and potentially intensify both the frequency and severity of storm events (Pilkey and Cooper, 2020). While large-scale analyses with low spatial resolution warn of future widespread beach and dune erosion, with some projections suggesting that over half of the world's sandy beaches could disappear by the end of this century (Vousdoukas *et al*., 2020), other studies recommend caution when adopting such forecasts, as they may overlook critical geological, regional, and local-scale factors influencing coastal vulnerability (Cooper *et al*., 2020).

In light of this debate, there is an urgent need to improve our understanding of the dynamics of beach systems, and particularly on the timescales and processes governing beach recovery, providing a robust baseline for projections of future behavior and informing effective coastal management strategies. This understanding has to be framed by local/regional beach configuration and particularities.

The main objective of this study is to describe patterns and time-scale of beach recovery after extreme storm events in a wide range of coastal geological and morphological settings sharing similar tidal and deep-water wave regimes. Beach topographic data and photographic records, coupled with tidal data and nearshore wave observations were used to explore

the drivers of beach and foredune change imposed by the *Christina* storm, and place those changes within the context of subsequent recovery, aiming at understanding beach resilience. We used a mesoscale spatial approach to address the pre- and post-storm states of a number of sand beaches and understand their recovery a decade after the 2013/14 winter storm cluster, which included multiple storms in close succession, and was dominated by the *Christina* extreme event.

2. METHODS

This study presents new data and observations on beach–foredune changes monitored at the coastal stretch extending between Pedras Negras and Lagoa de Albufeira (Figure 1), in the western coast of Portugal. This is a high-energy and mesotidal coast featuring a broad range of geomorphic and coastal hydrodynamic settings. The morphological data on both the supra- and intertidal domains of the twelve beach sites addressed in this study were collected via the Instituto Dom Luiz (IDL) Coastal Processes Group during multiple field surveys of a monitoring program aiming at assessing morphological changes using topographic and Global Navigation Satellite System (GNSS) surveying equipment (Diogo *et al*., 2014). Computed changes in the sediment volume observed at all surveyed beaches represent changes in the dune, backshore and intertidal beach domains, but exclude the subtidal region of the beach profile.

To characterize and understand post-*Christina* recovery over a ten-year period, a comprehensive survey of all twelve beaches in the study area was conducted on October 17 and 18, 2024. Although this survey was not preceded by systematic field monitoring at most sites, precluding the examination of recovery processes and respective time scales, it provided a synoptic snapshot of beach conditions a decade after the storm events of the 2013/14 winter.

3. RESULTS

3.1. The 2014 *Christina* storm and impacts on the beaches

During the winter of 2013/2014, the European Atlantic coastal fringe, including the western Portuguese coast, was impacted by an unusually intense sequence of Atlantic storms (Masselink *et al*., 2016). This winter was marked by a series of intense extratropical cyclones in the North Atlantic, which generated strong winds, high waves, and heavy rainfall. Matthews *et al*. (2014) marked this winter as the stormiest since at least 1948 over the North Atlantic, with large expansions of the European coast having been impacted.

These storms caused significant damage to coastal structures, flooding, and widespread beach erosion along the study area. The data revealed pronounced dune retreat, beach profile lowering, and destruction of coastal infrastructure at several locations. Maximum run-up levels recorded during the *Christina* storm were assessed against setback lines based on end of 21st century projections for flood and erosion risk scenarios, established in coastal management instruments in force. This comparison highlighted the high exposure of these coastal areas to extreme meteorological events. In most cases, beach erosion driven by *Christina* involved a decrease in the sand volume over the subaerial beach. Waves removed sand from the foreshore, determining retreat of the beach face, and also from the berm, turning pre-storm convex profiles into concave and lower sloping profiles. Notwithstanding the above, the magnitude and nature of the impacts were highly variable, with some beaches experiencing abrupt morphological changes (particularly in rock-bounded platform beaches, cf. Bastos *et al*., 2022), while others even experienced accretion (Figure 1 and Figure 2, Diogo *et al*., 2014).

3.2. Post storm recovery – 10 years after

Ten years after *Christina* most beaches exhibit profile shapes and volumes similar to pre-storm conditions. Nevertheless, the degree of beach recovery displayed considerable inter-site and intra-site variations. Example of a typical beach behavior over the study area is displayed in the top panel of Figure 2. Rainha beach (PRA1) represents the most common beach behavior under storm and post-storm conditions, characterized by strong storm-induced erosion (which corresponds to a minimum in beach volume), and evolving subsequently to a configuration that cannot be distinguished from pre-storm conditions. Examples of atypical behaviours are represented by the beaches of Baleal - Peniche (PBP4) (i) and Coxos (PCX1) (ii):

(i) The profile located at the southern end of the Baleal - Peniche embayment reacted to *Christina* storm by accreting to the highest beach volume recorded during the monitoring program, but after a second storm event (February 7) the beach showed a configuration indistinguishable from the pre-storm conditions.

(ii) The only case that did not show shape and volumetric recovery after being impacted by the 2013/14 winter storm cluster was Coxos beach, a small pocket beach deeply encased in an otherwise rocky coast and backed by a cliff. Here, *Christina* storm waves enabled abrupt and massive erosion of the whole subaerial beach that was triggered by wave reflection at the landward hard boundary of the beach.

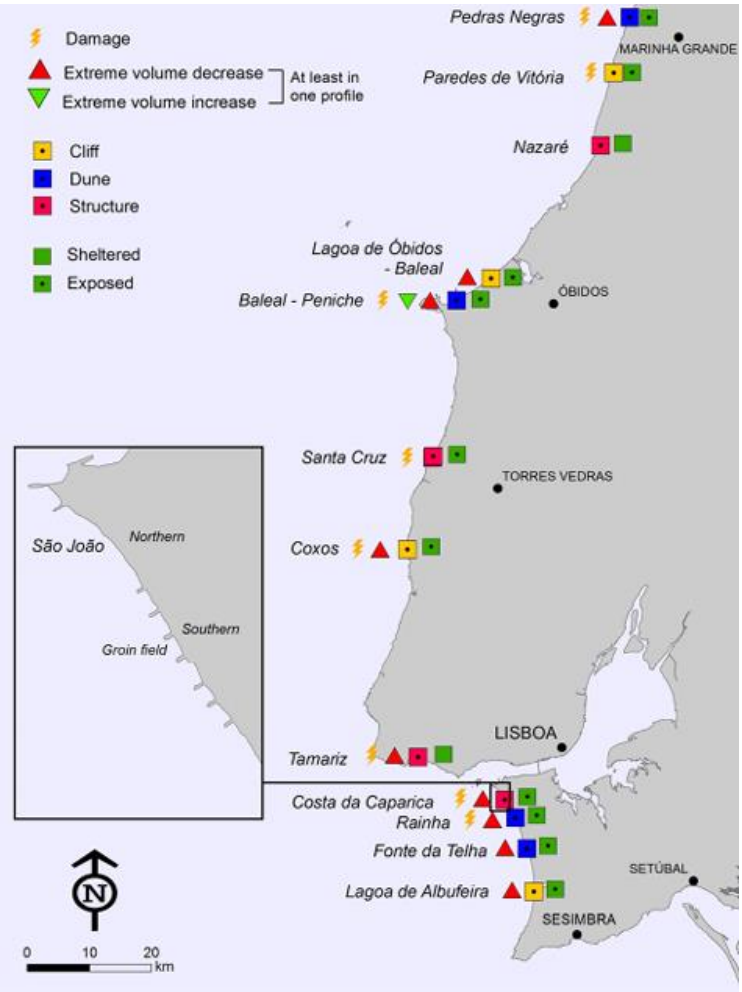

Figure 1. Coastal stretch under study. Location of the 12 selected beach sites and main features: landward beach boundary, presence of reports of damage to coastal structures (e.g. damages to waterfront promenades, beach accesses, restaurants), and type of beach volume change (increase vs. decrease) in response to the Christina 2014 storm, as observed in at least one beach profile. Reproduced from Diogo et al., (2014).

Also, long-term beach recovery, which is proceeding at an extremely low rate, is highly dependent on the geological framework, which controls sediment exchanges with adjacent sediment cells (Bastos *et al*., 2022).

At some sites, elevated water levels and wave action led to foredune erosion. While the beach profile recovered relatively quickly, full profile recovery was delayed due to the slower pace of natural dune regeneration. A clear example is Foz do Lizandro beach, where the dune toe still lies landward of its pre-storm position.

4. DISCUSSION AND CONCLUSIONS

Analysis of post-storm recovery along the central-western Portuguese coast following the 2013/14 winter storms reveals that most beaches exhibited a notable capacity for recovery, with profiles and sediment volumes returning to pre-storm conditions over a decadal time scale. However, recovery was not uniform: certain sites, such as Coxos (a small, cliff-backed beach) experienced limited recovery, while at locations like Foz do Lizandro, the dune foot remained landward of its pre-storm position, indicating slow or incomplete recovery of the system. These results show that beach resilience is not solely determined by storm frequency and intensity, but is strongly influenced by site-specific geological factors, sediment availability, and the presence of hard boundaries. The study highlights the need for a deeper understanding of the rates and mechanisms of beach recovery, which should be assessed at appropriate time and spatial scales to effectively inform targeted adaptation and management strategies in the context of climate change and increasing storm activity.

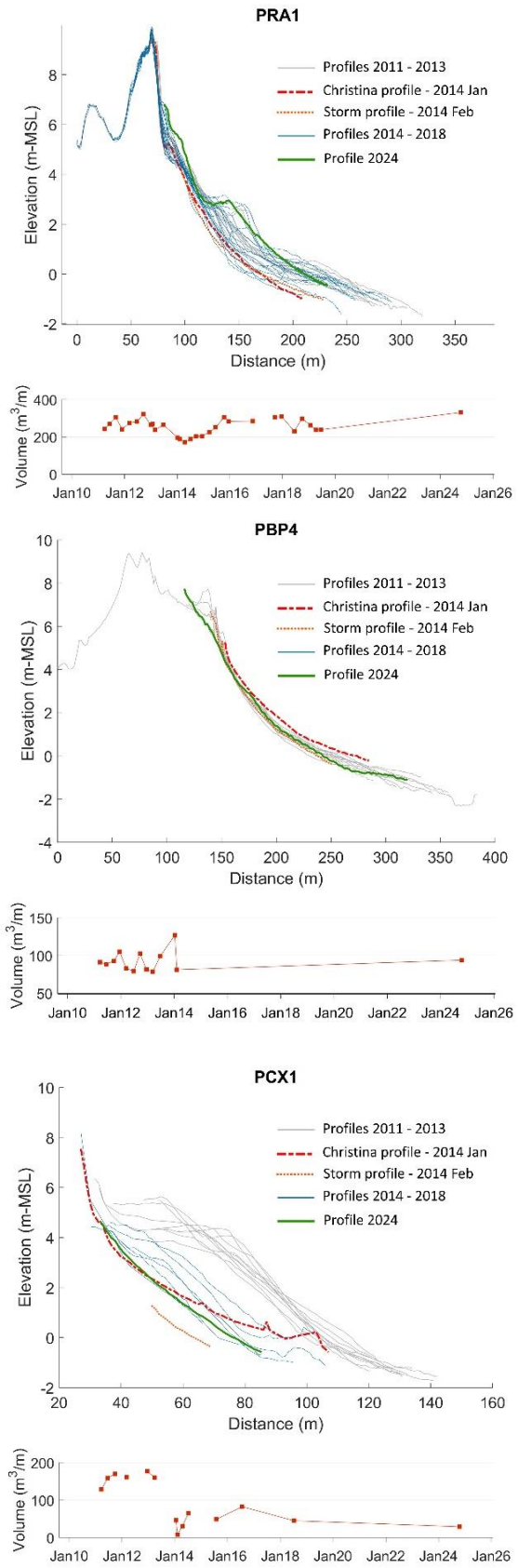

Figure 2. Beach profiles (Rainha beach - top panel; Baleal - Peniche sector – middle panel; Coxos beach – bottom panel) and variation in volumetric sediment retention: pre-Christina; aftermath of Christina, post-Christina recovery.

Acknowledgements

This work is supported by the Portuguese Fundação para a Ciência e Tecnologia, FCT, I.P./MCTES through national funds (PIDDAC): UID/50019/2025, LA/P/0068/2020 and UIDB/04625/2020. (https://doi.org/10.54499/LA/P/0068/2020). The work is also a contribution to the CREST project, funded by FCT through Grant 2022.05392.PTDC (doi:10.54499/2022.05392.PTDC).

REFERENCES

Bastos, A.P., Taborda, R., Silva, A.N., Ponte Lira, C., Andrade, C. and Calvão, J.M. (2022). A punctuated equilibrium model for storm response of geologically controlled beaches: application to western Portuguese beaches. *Geomorphology*, 404: 108184. https://doi.org/10.1016/j.geomorph.2022.108184

Diogo, Z., Bastos, A., Lira, C., Taborda, R., Freire de Andrade, C., Silveira, T., Ribeiro, M., Silva, A., Carapuço, M., Pinto, C. and Freitas, M. (2014). Morphological impacts of Christina storm on the beaches of the central western Portuguese coast. *Comunicações Geológicas*, 101 (III), Laboratório Nacional de Energia e Geologia, Lisboa, pp. 1445-1448. URL: https://www.lneg.pt/wp-content/uploads/2020/03/75_3127_ART_CG14_ESPECIAL_III.pdf

Cooper, J.A.G., Masselink, G., Coco, G., Short, A., Castelle, B., Rogers, K., Anthony, E., Green, A., Kelly, J., Pilkey, O. and Jackson, D. (2020). Sandy beaches can survive sea-level rise. *Nature Climate Change,* 10:993–995. https://doi.org/10.1038/s41558-020-00934-2.

Masselink, G., Scott, T., Poate, T., Russell, P., Davidson, M. and Conley, D. (2016). The extreme 2013/2014 winter storms: hydrodynamic forcing and coastal response along the southwest coast of England. *Earth Surface Processes and Landforms*, 41(3):378-391. https://doi.org/10.1002/esp.3836

Matthews, T., Murphy, C., Wilby, R. and Harrigan, S. (2014). Stormiest winter on record for Ireland and UK. *Nature Climate Change*, 4(9):738-740. https://doi.org/10.1038/nclimate2336

Pilkey, O. H. and Cooper, J. A. G. (2020). *The last beach*. Duke University Press, Durham, North Carolina, USA, 256 p.

Vousdoukas, M. I., Ranasinghe, R., Mentaschi, L., Plomaritis, T., Athanasiou, P., Luijendijk, A. and Feyen, L. (2020). Sandy coastlines under threat of erosion. *Nature Climate Change*, 10(3):260-263. https://doi.org/10.1038/s41558-020-0697-0

Shoreface sedimentary dynamics revealed by a fluorescent tracer experiment

J. Cascalho (1), R. Taborda (1) T. Drago (1,2) and M. Rosa (2)

(1) Instituto Dom Luiz, FCUL, Lisboa, Portugal. jpcascalho@ciencias.ulisboa.pt
(2) Instituto Português do Mar e da Atmosfera, Tavira, Portugal.

Abstract: This study investigates sediment transport in a shoreface environment near a shelf borrow site used for beach nourishment. A fluorescent sand tracer experiment was conducted, deploying 600 kg of coated sand at a depth of 11 meters (mean sea level) on August 17, 2020. Sediment samples were collected during 7 sea missions which extended over 437 days, from August 24, 2020, to October 27, 2021. Oceanographic data, including waves and currents, were simultaneously recorded using an Acoustic Doppler Current Profiler (ADCP). The research analyzed the successive positions of the tracer's center of mass, diffusion coefficients, and transport rate values. Results indicate relatively high sediment mobility but very low net sediment transport rates.

Keywords: *fluorescent tracer, shoreface, oceanographic data, maximum shear stress, critical shear stress*

1. INTRODUCTION AND OBJECTIVES

The shoreface is a coastal environment that remains relatively understudied in terms of sedimentary processes compared to subaerial environments. One reason for this disparity is the difficulty in collecting shoreface data, as opposed to the relative ease of data collection on subaerial beaches. The primary goal of this research is to evaluate sedimentary dynamics at a shoreface borrow site used for nourishing Belharucas Beach. This beach is located at the updrift boundary of a sedimentary cell, defined between the far northwest portion of Belharucas Beach and the Vilamoura entrance jetty along the Algarve's southern coast of Portugal (Figure 1).

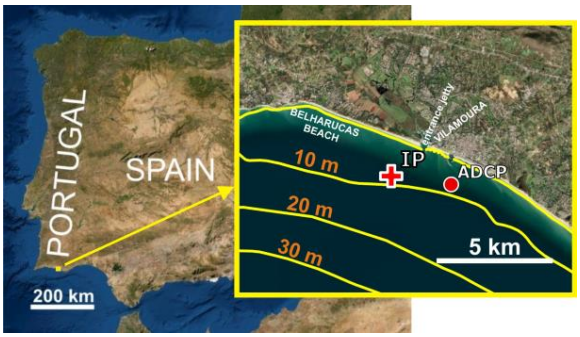

Figure 1. Location of the tracer injection point (IP) and the Acoustic Doppler Current Profiler position (ADCP). Depth contour lines on the right map are referred to hydrographic zero.

2. METHODS

This study is supported by a sand tracer experiment in which approximately 600 kg of sand coated with fluorescent orange ink was placed by divers at a depth of 11 meters (relative to mean sea level) on August 17, 2020. Sediment sampling—totaling 223 samples—was conducted between August 24, 2020, and October 27, 2021, using a Van Veen grab and an adaptive sampling grid that accounted for tracer dispersion over time. During sediment collection, simultaneous oceanographic data (waves and currents) were recorded using an Acoustic Doppler Current Profiler (ADCP) deployed near the tracer release site at the same depth (Figure 1). Sediment data were analyzed for both native sediment and injected tracer particles. Processing followed these steps:

a) Laboratory analysis of tracer particle concentrations in each sample via image analysis.

b) Determination of the textural characteristics of the native sediment via classical sieve analysis.

c) Determination of successive tracer center-of-mass positions.

d) Calculation of tracer diffusion coefficients.

e) Computation of tracer transport rate values.

Native sediment and tracer data were obtained using methodologies from Silva *et al.* (2007) and Bosnic *et al.* (2017), with sampling intervals consistent with this experimental study (Figure 2).

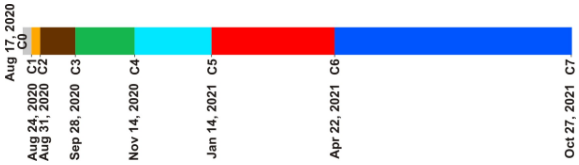

Figure 2. Timeline representing at scale the various sea campaigns from the injection of the tracer (C0) to the last sediment collection campaign (C7). A total of 437 days is counted between C0 and C7, corresponding to seven observational periods. During this period during oceanographic data (waves and currents) were acquired by the ADCP deployed at the location shown in Figure 1.

Additionally, for the native sediment, the critical shear stress (τ_{cr}) was determined using the formulations of Soulsby (1997). The diffusion coefficient of tracer particles was calculated separately for along-shelf and cross-shelf directions, incorporating the dimensionless calibrated tracer mass for different time periods between successive sampling campaigns. Oceanographic data (waves and currents) were acquired using an upward-looking ADCP, with analysis focusing on the first measurement bin at 2.75 m from the sea bed. The data were processed through Python routines specifically developed to determine key hydrodynamic parameters:

a) Current-induced shear stress (τ_c).

b) Wave-induced shear stress (τ_w).

And the combined effects (waves and currents) represented by:

a) Cycle-mean bed shear stress (τ_m).

b) Maximum bed shear stress (τ_{max}).

These calculations were based on established formulations from Soulsby and Smallman (1986), Soulsby and Clark (2005), and van Rijn (2013), assuming the friction factor for rough turbulent flows from Soulby (1997) .

3. RESULTS

3.1. Currents

The along-shelf velocity component showed shows great variability, with extreme values in the fall and winter months, with velocities reaching 0.23 m/s (ESE-directed) and -0.30 m/s (WNW-directed). Cross-shelf currents exhibited a similar seasonal pattern but with reduced magnitude. The onshore (positive) velocities peaked at 0.13 m/s, while maximum offshore (negative) flow reached -0.12 m/s, demonstrating a narrower range of variation compared to along-shelf currents (Figure 3).

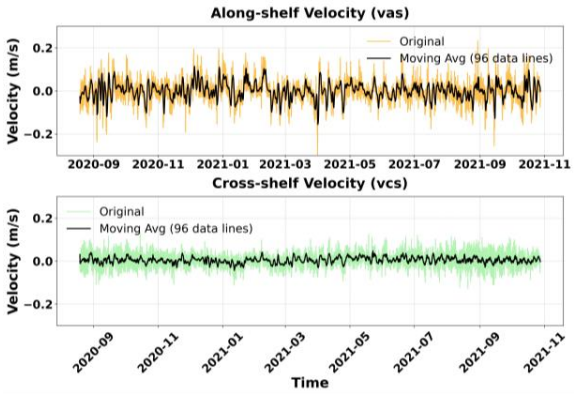

Figure 3. Time-series of along-shelf (top) and cross-shelf current velocity components for the entire measurement period (from August of 2020 to October of 2021) at 2.75 m from the bottom. The above bar represents the timeline according to the time between the successive sampling campaigns. The colored lines in both plots represent the original measured values while the black lines represent the moving average with a window equal to 96 data lines (corresponding to one day of measurements).

3.3. Waves

Wave analysis revealed distinct seasonal patterns. The predominant wave direction ranged between WSW and SW, particularly during fall and winter months. However, a notable difference is observed in fall of 2020 (C2-C3 interval), with significant wave frequency from S-SSE to SE-SSE directions. Significant wave height (Hs) showed clear seasonal variation:

a) Spring/summer periods (C0-C2, C6-C7): Heights rarely exceeded 0.8 m (0 % in C0-C2, and less than 10 % in C6-C7).

b) Fall/winter periods (C3-C4, C4-C5, C5-C6): Frequent occurrences exceeding 1.0 m (> 25 %).

3.3. Native sediment

The native sand is essentially composed of coarse sand moderately sorted (Figure 4).

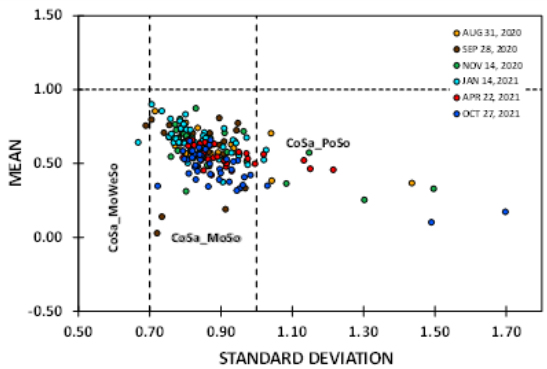

Figure 4. Mean versus standard deviation of native sediment collected in the various sampling campaigns (moments method).

3.4. Tracer

The first evidence of fluorescent tracer dispersion appeared just two weeks after deployment, with the center of mass (CM2) positioned approximately 2 m north-northeast (NNE) of the injection point (no tracer particles were detected in the initial sampling campaign C1). Subsequent sampling campaigns (through C4) revealed successive mass centers remaining within 2 m of the origin, though exhibiting directional variability: shifting south (S) from CM2 to CM3, then north-northwest (NNW) from CM3 to CM4. During campaigns C5 and C6, the centers of mass migrated more than 5 m from the injection point, first moving east-southeast (ESE) from CM4 to CM5, then north-northwest (NNW) from CM5 to CM6. The final campaign (C7) showed the center of mass approximately 2 m from the injection point, indicating a south-southwest (SSW) displacement from CM6 to CM7 (Figure 5). Diffusion analysis (calculated by adapting the formula of Miller and Komar, 1979) revealed significantly lower coefficients during the first two observational periods, particularly in the along-shelf direction (Table I). Transport rates showed peak values during the three middle sampling intervals (C3-C4, C4-C5, and C5-C6), with comparatively lower rates during other periods (C0-C2, C2-C3, and C6-C7) (Table II).

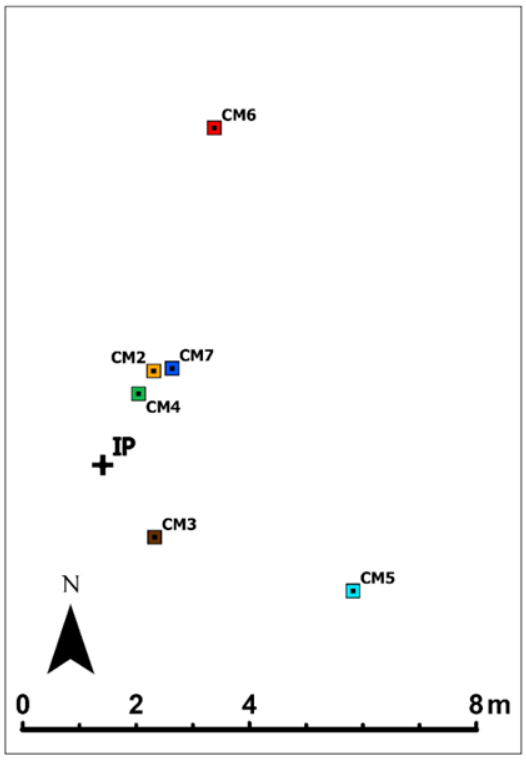

Figure 5. Positions occupied by the successive centers of mass of the tracer (CM2 to CM7). Note: the center of mass for the first sampling campaign (CM1) is not represented because no tracer particles were detected. IP – Injection point. Each color represents a different sampling interval being correspondent to the colors used in Figure 1.

Table I. Tracer diffusion coefficients for along-shelf (Das) and cross-shelf (Dcs) directions according to the different observational periods. Dr represents the resultant diffusion considering these two directions.

Observational period	Das ($x10^{-8}$) m^2/s	Dcs ($x10^{-8}$) m^2/s	Dr ($x10^{-8}$) m^2/s
C0-C2	3.4	294.0	294.0
C2-C3	32.4	329.8	331.4
C3-C4	521.5	270.7	587.6
C4-C5	657.7	319.0	731.0
C5-C6	510.3	572.9	767.2
C6-C7	102.3	210.9	234.4

Table II. Tracer net transport rates for along-shelf (Qas) and cross-shelf (Qcs) directions during to the different observational periods.

Observational period	Qas ($x10^{-8}$) $m^3/m/s$	Qcs ($x10^{-8}$) $m^3/m/s$
C0 – C2	0.07	0.58
C2 – C3	3.39	-8.27
C3 – C4	-3.87	7.18
C4 – C5	3.83	-1.44
C5 – C6	-6.67	8.34
C6 – C7	0.26	-1.23

4. DISCUSSION

The measured sediment transport rates exhibited very low net values (Table II), consistent with previous findings for similar environments (Patterson and Nielsen, 2016; Bosnic *et al.*, 2017; Romão *et al.*, 2024). The theoretical threshold for particle motion initiation occurs when τ_{max} exceeds τ_{cr} (0.294 N/m² in this study). Notable temporal variations emerged in the percentage of time that τ_{max} exceeded τ_{cr}:

a) Initial (C0-C2) and final (C6-C7) periods showed minimal exceedance durations.

b) These periods corresponded with the lowest observed transport rates (Tables II and III).

Table III. Percentage of time (in each observational period) when there are conditions for the remobilization of tracer particles.

Observational period	% time when: $\tau_{max}>\tau_{cr}$
C0 – C2	0.1
C2 – C3	13
C3 – C4	22
C4 – C5	26
C5 – C6	41
C6 – C7	5

Our data indicate that during the most energetic periods (C3–C4, C4–C5, and C5–C6), τ_{max} frequently exceeded τ_{cr} (Table III), consistent with the observed increase in tracer net transport and diffusion during these intervals (Table II). However, the position of CM7

relative to CM6 (C6–C7 period) presents an anomalous pattern, showing offshore displacement of the tracer's center of mass (Figure 3) despite prevailing onshore wave propagation. This discrepancy could be due to four factors:

a) The sporadic exceedance of τ_{max} over τ_{cr} during this period (Table III).

b) The dominant influence of intense diffusion masking net tracer transport (Table I).

c) Due to the ripple-induced phase differences between the peak concentrations and peak velocities.

d) Asymmetry and irregularity in the sampling mesh combined with the very long-time interval (approximately six months).

5. CONCLUSIONS

This study presents over one year of monitoring data tracking the dispersion of a 600 kg fluorescent tracer, establishing clear connections between hydrodynamic forcing and sediment transport patterns. Our results demonstrate that while sediment mobilization occurs relatively frequently, net transport rates remain characteristically low for a lower shoreface environment - consistent with previous studies of this depositional setting. The analysis reveals significant temporal variations in sediment dynamics. During initial (C0-C2) and final (C6-C7) periods, τ_{max} exceeded τ_{cr} only briefly (≤ 5% of the time), corresponding to minimal sediment transport rates. The most energetic intervals (C3-C4 through C5-C6) showed:

a) Frequent threshold exceedance ($\tau_{max} > \tau_{cr}$ in average for > 25% of observations).

b) Markedly relative higher transport rates.

c) Maximum observed displacement of tracer mass centers.

Notably, these energetic periods accounted for nearly 80% of the total tracer displacement recorded during the study, despite representing just 45% of the monitoring duration.

Acknowledgements

This work was supported by ECOEXA project (MAR-01.04.02-FEAMP-0016) and by the Portuguese Fundação para a Ciência e Tecnologia, FCT, I.P./MCTES through national funds (PIDDAC): UID/50019/2025 and LA/P/0068/2020: https://doi.org/10.54499/LA/P/0068/2020). It is also supported by the project "Reduced complexity modelling of barrier island adaptation to sea level rise (MOBILE)", with the "Balcão dos Fundos code": ALGARVE-FEDER-00742700, and reference: c4165555-7168-496f-9d50-1fdc6d46b71d, co-funded by ALGARVE 2030. Lisboa 2030, Portugal. The authors wish also to thank Erwan Garel (CIMA/UALG) and Paulo Relvas (CCMAR/UALG) for the ADCP data acquisition and, in particular, to Erwan Garel for data compilation. The authors wish also to thank Erwan Garel for the ADCP data compilation, and to CCMAR team for the availability of the PARGUS vessel.

REFERENCES

Bosnic, I., Cascalho, J., Taborda, R., Drago, T., Hermínio, J., Rosa, M., Dias, J. and Garel, E. (2017). Nearshore sediment transport: Coupling sand tracer dynamics with oceanographic forcing. *Marine Geology*, 385: 293-303.

Miller, M. C. and Komar, P. D. (1979). Measurements of sand spreading rates under near-bottom wave orbital motions. *The Journal of Geology*, 87(6): 593-608.

Patterson, D. C. and Nielsen, P. (2016). Depth, bed slope and wave climate dependence of long-term average sand transport across the lower shoreface. *Coastal Engineering*, 117: 113-125.

Silva, A., Taborda, R., Rodrigues, A., Duarte, J. and Cascalho, J. (2007). Longshore drift estimation using fluorescent tracers: New insights from an experiment at Comporta Beach, Portugal. *Marine Geology*, 240(1-4): 137-150.

Soulsby, R. L. (1997). Dynamics of Marine Sands: A manual for Pratical Applications. ThomasTelford, London, 272 p.

Soulsby, R. L. and Clarke, S. (2005). Bed shear-stress under combined waves and currents on smooth and rough beds (TR 137). Technical Report. HR Wallingford, Wallingford, 137 p. https://eprints.hrwallingford.com/558/1/TR137.pdf

Soulsby, R. L. and Smallman, J. V. (1986). A direct method of calculating bottom orbital velocity under waves. Report No SR 76, February 1986. https://eprints.hrwallingford.com/112/1/SR76-method-calculating-orbital-velocity-waves.pdf

Romão, S., Silva, P. A., Taborda, R., Cascalho, J., Silva, A. N. and Baptista, P. (2024). Assessing shoreface sediment transport at Costinha beach, Aveiro, Portuguese Northwest coast. *Marine Geology*, 467: 107200.

Van Rijn, L. C. (2013). Simple general formulae for sand transport in rivers, estuaries and coastal waters. Retrieved from www.leovanrijn-sediment.com, Technical Report, 20 p.

A field-based approach to the aerodynamic and equivalent roughness at a sand beach: first results

C. Andrade (1), A. P. Bastos (1), A. N. Silva (1,2) and R. Taborda (1)

(1) Instituto Dom Luiz, Faculdade de Ciências da Universidade de Lisboa, Lisboa, Portugal. candrade@fc.ul.pt
(2) Agência Portuguesa do Ambiente, I.P., Lisboa, Portugal.

Abstract: The aerodynamic roughness length (z_0) at a subaerial beach surface under non-transport conditions was evaluated resourcing to a field experiment. Three wind sensors installed at different heights recorded 10-minute interval wind data over 25 hours. No aeolian sand transport was observed, as wind shear velocities remained below the threshold for moist sand. Analysis of wind speed profiles allowed for z_0 estimation, which ranged from 2 to 17 mm (mean 8.8 mm), and are much higher than expected based on grain size alone. Results suggest that shadow micro-dunes significantly contributed to surface roughness, with secondary contributions from ripples and footprints.

Keywords: *aerodynamic roughness length, wind profile, beach, micro-topography*

1. INTRODUCTION AND OBJECTIVES

Sand entrainment and transport by wind are governed by interaction mechanisms between airflow and the surface, those mechanisms being influenced by bed roughness, which affects near-surface shear stress, the threshold for sediment motion, and transport rates. The aerodynamic roughness length (z_0, the notional height above ground where wind speed theoretically vanishes) has been widely used as a proxy for the surface physical roughness (Dong *et al.*, 2001). Since Bagnold's (1941) pioneering work, numerous wind tunnel studies have explored these parameters using high-resolution measurements of near-bed wind profiles. In contrast, relatively few field studies addressed natural surface morphologies, relying on lower-resolution wind data collected at greater heights above the ground.

The objective of this work is to investigate the aerodynamic roughness length (z_0) of a subaerial beach surface under natural, non-transport (fixed bed) conditions, using wind profiles of low vertical resolution obtained during a field experiment carried out on the beach of Porto Santo under the scope of the EU LIFE Dunas project (LIFE 19 CCA/PT/001178).

2. METHODS

2.1. Study area – location, morphology, sediments

The study area is located in the southwestern sector of the NE–SW beach–dune's system along the southern coast of Porto Santo, a volcanic island in the Madeira archipelago (Portugal) (Figure 1). The coast is mesotidal (mean annual tidal range of 1.5 m and mean spring tidal range of 2.1 m), and low-energy wave regime (mean annual significant wave height < 1 m; mean annual wave period ≈ 8 s).

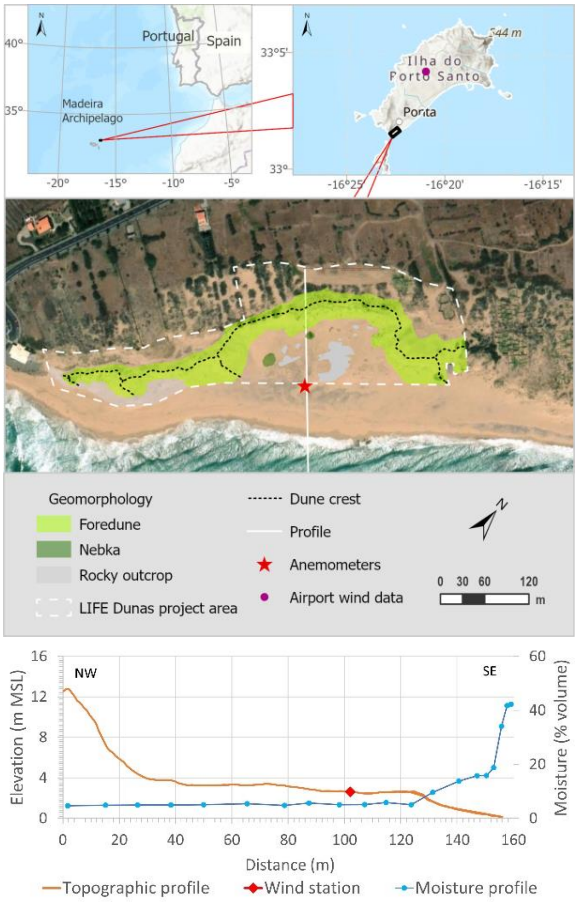

Figure 1. Top panel: Location of the study area and airport wind station (purple dot). Middle panel: Geomorphology of the study area; location of the anemometer station (red mark), cross-shore profile and boundaries of LIFE Dunas project. Bottom panel: cross-shore (orange line) and moisture (blue line) profiles.

The coastline trends ca. N50° in the study area, and the beach is intermediate–reflective (Bastos *et al.*, 2024). During the field experiment, the beach had a near-horizontal berm approximately 30 m wide, located at

ca. 2.60 m above mean sea level (MSL). The berm crest merged with a concave beach face, which terminated at an intertidal rocky platform (not shown in Figure 1) extending seaward below MSL. Landward, the berm transitioned diffusely into an aeolian deflation surface ca. 60 m wide and situated at 3.3 m MSL, which extended inland to the toe of the foredune. The extent of the deflation surface has increased over recent decades, in association with the landward retreat of the central dune sector (Bastos *et al*., 2024). Several aeolianite outcrops (protruding up to ca. 0.5 m above the sand surface) and few active nebkas are scattered across that surface, and vegetation restricts to the foredune and nebkas. Beach and dune mostly consist of moderately well sorted carbonate-rich and light-toned medium sand (mean grain size of 1.82 ϕ [0.28 mm]; sorting: 0.54 ϕ).

2.2. The experiment – instruments and surface conditions

The field experiment took place on 15–16 April 2024 during spring tide and fair weather: partly cloudy skies, low wind, no rainfall, and small NE spilling breakers (Hs ≈ 0.5 m) arriving obliquely. The beach face was smooth, composed of carbonate medium sand with no coarse debris. The berm exhibited a more complex surface, consisting of a mosaic of patches of coarser greyish sand, composed of oblate and plated basalt particles (lag deposits), interspersed with lighter-toned carbonate medium sand. Both sediment types showed inactive aeolian ripples. Footprints were scattered across the berm and deflation surface. Numerous shadow micro-dunes (SMD) populated the berm, having formed through wind interaction with algae remains left behind by previous tides. SMD extended up to ca. 20 m inland from the berm crest, with decreasing spatial density toward the backshore. SMD remained inactive throughout the experiment.

Three ultrasonic METOS (Pessl Instruments) wind sensors were mounted on a tripod at 1.98 m (S1), 0.97 m (S2), and 0.26 m (S3) above the bed, recording 10-minute average wind speed and direction over 25 hours at the berm - deflation surface boundary (Figure 1). This scheme represents a compromise between meeting the experiment's objectives and minimizing interference of the sensors with the airflow, which would be more likely at smaller spacings. Wind data from the airport station (10 m height) were also analyzed (Figure 1). Volumetric soil moisture was measured using a DELTA-T ML3 Theta Probe, both near the sensors (four readings) and along a cross-shore profile. One horizontal and one vertical (75 cm) Leatherman-type sand trap were placed near the sensors and monitored for aeolian transport.

2.3. Wind data processing

Assuming conditions of rough airflow and fully developed turbulence the vertical profile of the wind speed follows the so-called "Law of the Wall" (eq.1),

$$u_z = {}^{u_*}/_{\kappa}\ ln({}^{z}/_{z_0}) \qquad \text{[eq. 1]}$$

where, u_z (m/s) is the wind speed at a distance z (m) from the ground, u_* (m/s) is the shear velocity, z_0 (m) is the aerodynamic roughness length, and κ is the von Karman constant (0.4). Eq. 1 is equivalent to eq. 2:

$$u_z = {}^{u_*}/_{\kappa}\ ln(z) - {}^{u_*}/_{\kappa}\ ln(z_0) \qquad \text{[eq. 2]}$$

which describes a straight line in its standard form Y = mX + B, with m = ${}^{u_*}/_{\kappa}$ and B = $-\ {}^{u_*}/_{\kappa}\ ln(z_0)$.

Following Wiggs *et al*. (1996) and Dong *et al*. (2001), a least squares method was used to determine the parameters m and B of the line that best fits each 10-minute data set yielded by the wind sensors, in turn allowing estimation of u* and z_0. The quality of the fit of the straight line to the data was assessed by the coefficient of determination (R^2).

3. RESULTS AND DISCUSSION

3.1. Moisture, sediment texture and micro-morphological elements

Volumetric water content was ca. 5 % in the dune, deflation surface, and berm, and rose to 7 % near the wind equipment at dawn due to dew. Moisture increased to 10 – 15 % on the upper beach face and peaked to 35 – 40 % in the swash zone after wave backwash. According to Cornelis and Gabriels (2003), the threshold shear velocity (u^*_{th}) on a beach berm is 0.2–0.3 m/s for dry sand but exceeds 0.5 m/s under the moisture levels observed in the field. Wind direction inferred from aeolian ripples and SMD was consistent, aligned with N60° ± 20°. Ripples averaged 6 cm in length and 0.4 cm in height. SMD dimensions averaged 53 cm in length, 19 cm in width, and 4.4 cm in height. Textural analysis of lag deposit samples revealed bimodal grain size distributions due to unavoidable mixing with underlying finer sand during sampling, with the coarser mode consisting of coarse sand (mean grain size of –0.24 ϕ [1.18 mm]).

3.2. Sand transport by wind

No sand transport occurred throughout the experiment, as confirmed by visual observations and absence of sand grains in both sand traps.

3.3. Wind speed and direction

Average wind speed at S1 (~2 m above ground) ranged from 1.8 to 4.8 m/s, remaining between 3 and 4 m/s for 57% of the time (Figure 2).

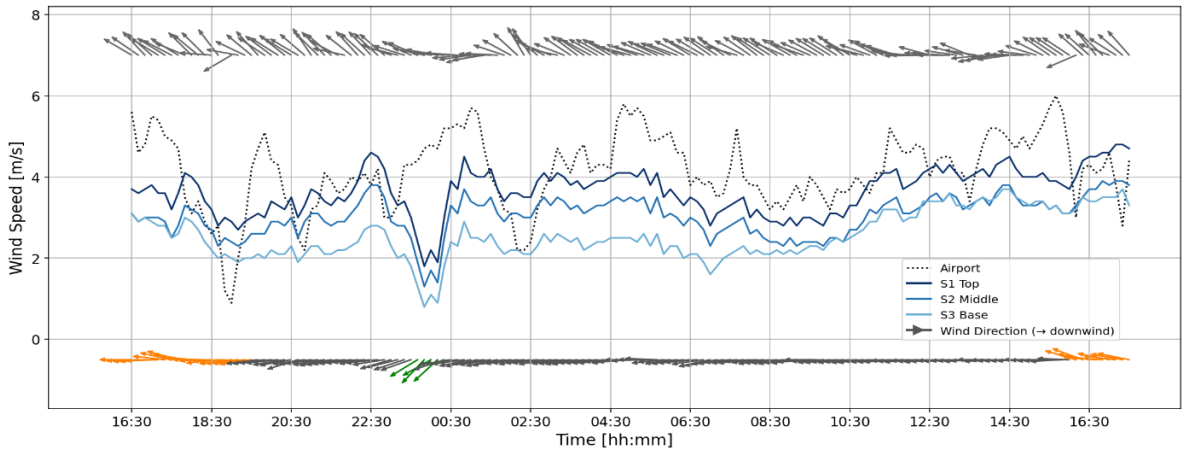

Figure 2. Top: time variation in airport wind direction. Middle: time variation of wind speed in airport, S1 to S3. Bottom: time variation in S1 direction.

A brief drop occurred between 23:40 [Apr 15] and 00:50 [Apr 16]. Sensors S2 and S3 showed similar patterns, though the speed gap between them varied, especially during mid-experiment. In contrast, the S1–S2 difference remained steady, suggesting boundary layer adjustments during early and late periods. Wind speed at the airport was generally higher and rotated toward the SE. While both datasets show similar temporal variation, the airport series had higher fluctuations in speed and direction.

This contrast likely results from wind steering by the beach-foredune ridge NE of the field site, which becomes more influential when wind aligns with it. Notably, the airport data did not record the midnight wind drop —instead, it showed a steady speed increase from 23:00 to 01:10, along with a consistent counterclockwise shift from ca. 105° to 80° (Figure 2). At the field site, wind direction was mostly stable, with a gradual clockwise rotation (ca. 0.5°/hr). Over two-thirds of readings deviated less than ±5° from the mean vector direction (N85°, 35° to coastline). This trend was disrupted during: (i) the early hours until 19:30 [Apr 15], when wind was 5° more clockwise; (ii) a midnight event, when wind rotated counterclockwise to near-parallel with the coastline, becoming erratic (± 12° swings); and (iii) the final phase (after 16:10 [Apr 16]), when a second clockwise shift increased wind obliquity by 15°.

3.4. Wind profile, shear velocity, aerodynamic roughness and equivalent grain roughness

The R^2 values from logarithmic fits to wind speed data (S1–S3, every 10 min) were consistently high ($R^2 \geq 0.95$; mean = 0.993) between 18:30 [Apr 15] and 08:10 [Apr 16] (Figure 3). Outside this interval, R^2 dropped below 0.95 (means of 0.785 and 0.712), affecting about half the dataset and indicating wind profiles deviated from the logarithmic law, making derived z_0 and u_* estimates unreliable. A discussion of the causes of these deviations is beyond the scope of this extended abstract. Thus, only data from the high-fit period are considered in the analysis presented below. During that period, z_0 ranged between 2.0 and 17.0 mm (mean = 8.8 mm, median = 9.1 mm), excluding four outliers associated with low wind speed and wind direction aligned with the coastline, where z_0 peaked at 24–52 mm despite good fits. Shear velocity (u_*) varied between 0.20–0.33 m/s and tracked z_0 trends, except during the outlier episode, when they diverged. The observed range in u_* is close to the 0.25 m/s threshold for dry sand transport (Bagnold, 1941) but remains below the > 0.5 m/s required for moist sand under the conditions observed - hence, aeolian transport was inhibited.

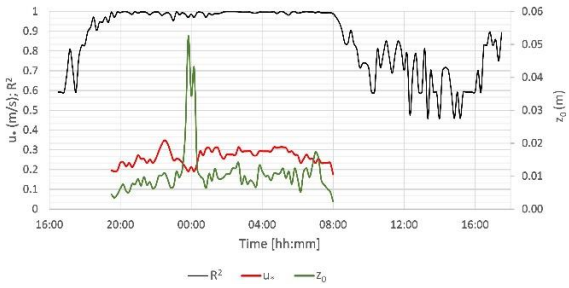

Figure 3. Time variation of R^2 (all data, grey line), z_0 (green line) and u^*(red line).

The "1/30 law" (eq. 3) relates aerodynamic roughness to bed roughness (k_s), with k_s approximated by the mean grain diameter in idealized surfaces (Bagnold, 1941), (cf. Dong *et al.*, 2001 for a summary of work leading to this relation):

$$z_0 = {}^{1}/_{30} \cdot k_s \qquad \text{[eq. 3]}$$

where k_s is the equivalent, or effective bed roughness as defined by Nikuradse (1933), a single parameter dependent on, and describing the physical length of the irregularities of a surface actuated by a flow. k_s is the grain roughness (for densely packed hypothetical sand grains of uniform size and shape) that would

produce the same wind profile as the irregular surface. van Rijn and Strypsteen (2020) found that the grains in the coarser tail of a grain size distribution provide more reliable estimates of k_s and proposed:

$$k_s = 3d_{90} \quad \text{[eq. 4]}$$

$$k_s = d_{90} \quad \text{[eq. 5]}$$

to evaluate k_s of sand with mean diameter < 0.5 mm (eq. 4) and coarser (eq. 5). Use of equations 3 to 5 combined with textural data of berm sand and of lag deposits in the studied beach led to k_s and z_0 estimates in Table I.

Table I. Equivalent grain roughness (ks) and aerodynamic roughness (z_0) inferred from beach textural data.

Roughness parameter (mm)	Berm sand		Lag deposits	
	k_s	z_0	k_s	z_0
van Rijn and Strypsteen (2020)	1.87	0.06	2.83	0.09
Bagnold (1941)	0.28	0.009	1.18	0.04

Rippled beds increase roughness, though no fixed relation with z_0 exists. Field and Pelletier (2018) reported k_s between 0.5 - 5 mm ($z_0 \approx 0.017 – 0.17$ mm) under sub-threshold wind, with ripple dimensions and grain size similar to those in Porto Santo. Lancaster and Baas (1998) found $k_s \approx 27$ mm ($z_0 \approx 0.9$ mm) for coarser and taller ripples. Footprint geometry was not measured in the field and we rely on the exploratory findings of Smits *et al*. (2024) for comparison. They reported that barefoot imprints generated z_0 values between 0.08–0.16 mm, over static surfaces and noted that these bedforms significantly impact the deflation threshold. z_0 correspondent to larger, non-erodible elements, can be assessed using Lettau's (1969) equation:

$$z_0 = 0.5 \cdot \bar{h} \cdot \frac{\overline{A_s}}{S} \quad \text{[eq. 6]}$$

where $\bar{h}$ (m) is the mean height of the elements, $\overline{A_s}$ is the frontal area of the mean element, and S the elements' lot area, computed by the ratio between the total area of a horizontal surface of known dimensions and the number of elements it contains. Applying eq 6 to Porto Santo's SMD, which remained inactive throughout the experiment, yields z_0 up to 5.6 mm ($k_s \approx 168$ mm) for densely distributed elements (spacing ≈ 0.25 m) and cross-shore wind. Although this is broadly consistent with wind-derived roughness, discrepancies remain: while eq. 6 predicts lower z_0 with more oblique wind directions over the study area, field data suggest the opposite—an issue warranting further investigation.

4. CONCLUSIONS

In general terms, the estimates of both aerodynamic and equivalent roughness length calculated from fits to logarithmic wind speed profiles obtained in this experiment, agree with values inferred from the geometric characteristics of shadow micro-dunes populating the beach berm. These estimates exceed those derived from grain size, ripple height and footprint size. However, further research is required to fully understand the impact of changing wind angles on both the structure of the boundary layer and surface roughness.

Acknowledgements

Airport wind data was kindly provided by Dr Victor Prior (IPMA, I.P.) This paper is a contribution of EU LIFE Dunas project (LIFE 19 CCA/PT/001178) and was supported by the Portuguese Fundação para a Ciência e Tecnologia, FCT, I.P./MCTES through national funds (PIDDAC): UID/50019/2025 and LA/P/0068/2020 https://doi.org/10.54499/LA/P/0068/2020).

REFERENCES

Bagnold, R. A. (1941). *The physics of blown sand and desert dunes*. Methuen, New York, 265 p.

Bastos, A. P., Taborda, R., Andrade, C., Ponte Lira, C., and Nobre Silva, A. (2024). Short-term foredune dynamics in response to invasive vegetation control actions. *Remote Sensing*, 16(9): 1487.

Cornelis, W. and Gabriels, D. (2003). The effect of surface moisture on the entrainment of dune sand by wind: an evaluation of selected models. *Sedimentology*, 50(4): 771-790.

Dong, Z., Wang, X., Zhao, A., Liu, L., and Liu, X. (2001). Aerodynamic roughness of fixed sandy beds. *Journal of Geophysical Research: Solid Earth*, 106(B6): 11001-11011.

Fiels, J. and Pelletier, J. (2018). Controls on the aerodynamic roughness length and the grain-size dependence of aeolian sediment transport. *Earth Surface Processes and Landforms,* 43(12): 2616-2626. DOI: 10.1002/esp.4420.

Lancaster, N. and Baas, A. (1998). Influence of vegetation cover on sand transport by wind: field studies at Owens Lake, California. *Earth Surface Processes and Landforms*, 23: 69-82.

Lettau, H. (1969). Note on aerodynamic roughness-parameter estimation on the basis of roughness-element description. *Journal of Applied Meteorology, 8*: 828-832.

Nikuradse, J. (1933). Laws of flow in rough pipes. *Technical Memorandum 1292*, National Advisory Committee for Aeronautics. Washington D. C., 1950, 62 p.

Smits, N., Goossens, D. and Riksen, M. (2024). Effect of pedestrian trampling on aeolian sand dynamics on beach surfaces: an experimental study. *Geomorphology,* 455:109181.

Wiggs, G., Livingstone, I., Thomas, D. and Bullard, J. (1996). Airflow and roughness characteristics over partially vegetated linear dunes in the southwest Kalahari Desert. *Earth Surface Processes and Landforms*, 21(1): 19-34.

Van Rijn, L. and Strypsteen, G. (2020). A fully predictive model for aeolian sand transport. *Coastal Engineering*, 156, 103600.

Coupling/decoupling of surface and deep ocean processes during the upper Pleistocene and Holocene off the NW Iberian Margin

M.V. Alves Martins (1, 2), J.M. Alveirinho Dias (3), J.C.J. Moreno (4), D. Terroso (2), E. Salgueiro (5) and F. Rocha (2)

(1) Universidade do Estado do Rio de Janeiro, UERJ, 20550-013 Rio de Janeiro, RJ, Brazil. virginia.martin@ua.pt
(2) Universidade de Aveiro, GeoBioTec, Departamento de Geociências, Campus de Santiago, 3810-193 Aveiro, Portugal.
(3) Universidade do Algarve, FCMA, Campus de Gambelas, 8000 Faro, Portugal.
(4) Faculdade de Ciências, Universidade de Lisboa, 1749-016 Lisboa, Portugal.
(5) Instituto Português do Mar e da Atmosfera

Abstract: This study aims to assess changes in the water column and sedimentary environment on the NW Iberian Continental Margin related to climate change and sea level variations during the last ≈40 Ka BP. Isotopic data, textural (microparticle size), mineralogical (by X-ray diffraction on oriented and non-oriented powders), and micropaleontological (benthic and planktonic foraminifera) data were studied along a core (5 m long) collected at 2000 m depth off Galicia. The analysed core records significant changes in grain size and sediment composition. The planktonic foraminifera data enabled the observation of episodic high abundance of species associated with Arctic-Subarctic environmental conditions, suggesting a record of climatic events related to ice-rafted debris (IRD), specifically Heinrich Events. The $\delta^{18}O$ and $\delta^{13}C$ values revealed a higher frequency variation in planktonic than in benthic foraminifera, indicating higher variability in surface ocean conditions. The textural data, together with the compositional data, provided evidence suggesting a variation between two primary environments: one dominated by a carbonate context and a second one, associated with detrital input, related to a period when sea level was lower and the coastline was closer to the study area. This study should be improved to better characterize the changes and evolution of the different scenarios over this interval.

Keywords: *Sediments, foraminifera, stable isotopes, textural data, mineralogy, compositional analysis*

1. INTRODUCTION

Paleoclimate studies are crucial for predicting future climate change, as they provide possible scenarios based on the analysis of paleoclimatic, paleoecological, and paleoenvironmental multiproxies. During the Quaternary period, critical climatic changes manifested as alternating periods of glacial and interglacial conditions. The North Atlantic played a crucial role in this cycle of glacier advance and retreat during the Quaternary period (Dansgaard *et al*., 1993). Changes in (surface and deep) ocean circulation affected temperature and heat distribution, directly influencing the formation and melting of glaciers. During the glacial maximum phases, when glaciers reached their maximum extent, large volumes of water were stored in the ice sheets, resulting in a significant reduction of sea levels (Lambeck *et al*. 2002). In the last glacial period, climate instability caused massive iceberg discharges in the North Atlantic (Heinrich events). These events resulted in changes in water temperature and salinity (Voelker and Abreu, 2011).

Heinrich events are episodes of debris discharge associated with melting icebergs in the North Atlantic Ocean (Heinrich, 1988). These events are characterized by a decrease in seawater temperature, which generates a drop in salinity and productivity in the marine environment (Salgueiro *et al*., 2014).

This work aims to distinguish the coupling/decoupling of surface and deep ocean processes off the NW Iberian Continental Margin during the last ≈37 Ka BP (thousand years before the present).

2. REGIONAL SETTING

The study area is located in the North Atlantic, on the western continental margin off the coast of Galicia (NW Spain). This area is crucial for understanding the interactions between polar climate systems and the complex ocean circulation of the North Atlantic. It also exhibits seasonal climate variability, which is controlled by the Azores anticyclone during the summer and the Westerlies during the winter (Fiúza *et al*., 1982).

The system of ocean currents present in the Iberian Peninsula is highly complex, as the region serves as a point of convergence for various water masses from the Mediterranean Sea and the Atlantic Ocean (Fiúza *et al*., 1982).

In the surface zone, at a distance of 70 to 80 km from the coast and between 0 and 100 meters deep, the ocean currents are strongly affected by the water inflow from the continent. The surface current known as the Iberian Poleward Current (IPC; Maestro *et al*., 2013) occurs in this region. As it is a surface current, the IPC is also strongly influenced by ocean-atmosphere interactions, which is why it exhibits seasonal variations. When the southerly winds are most intense, the IPC typically settles on the continental shelf, generally between October and March, and heads north along the Iberian coast, inducing downwelling phenomena. During the spring and summer months (usually from May to September), the northerly winds become more vigorous, leading to upwelling events (Fiúza *et al*., 1998) and bringing cold, low-salinity waters to the coast (Fiúza *et al*., 1998).

As a result of upwelling events, the Northwest Atlantic Central Water (ENACW) rises from average depths of 100 - 400/600 meters (Fiúza, 1983). Its temperature is lower than the IPC due to the contributions of subpolar and subtropical water masses to its formation. The ENACW is rich in nutrients, inducing a significant increase in ocean productivity (Castro *et al*., 2006).

3. MATERIALS AND METHODS

This work presents and analyses the results obtained from core OMEX PE 109-13, collected on the continental slope of Galicia, at latitude 42º 34.32', longitude 9º 41.4' and a depth of 2000 m, during the cruise Pelagia, RV PELAGIA - Mission PE 64/109 (15/07/1997 to 6/08/1997). The core, measuring 540 cm in length, was sampled at 10 cm intervals (55 samples), with each sample taken to a thickness of 1 cm.

The results of this work comprise: textural data obtained either with a laser microgranulometer and by dry screening the sand fraction (>63 µm); mineralogical data obtained by X-ray diffraction (XRD) methods in the fine (<63 µm) and clay (<2 µm) fractions; data of the sand fraction (>63 µm) composition by counting the main types of particles under the microscope; benthic foraminifera; and stable isotopes, $\delta^{13}C$ and $\delta^{18}O$, in *Lobatula wuellerstorfi*. These data were compared with some results obtained by Martins *et al*. (2015).

3.1. Textural and compositional analyses

Grain size analyses were carried out using a laser microgranulometer (Mastersizer 2000 from Malvern Panalytical) after removing organic matter with hydrogen peroxide at a 1:120 volume ratio and removing calcium carbonate from the sediment samples with acetic acid. Textural parameters were estimated according to the method of Folk and Ward (1957).

3.2. Mineralogical analyses

The mineralogical study of the fine and clay fraction was carried out by X-ray diffraction (XRD) on the fine fraction (<63 µm) and the fraction <2 µm of the sediments in oriented and non-oriented aggregates. The semiquantification of the identified principal minerals followed the method described by Martins *et al*. (2007).

3.3. Foraminiferal analyses

The micropaleontological study of benthic foraminifera was based on sorting and recording the number of individuals/species/sample in more than 300 specimens/sample in the sedimentary fraction >63 µm.

For the identification of foraminifera species, the Ellis and Messina Catalogue of Foraminifera (1995, with subsequent updates) was used. For suprageneric systematic determination, the taxonomy of Loeblich and Tappan (1988) and other specialized publications were consulted.

3.4. $\delta^{13}C$ and $\delta^{18}O$ in foraminifera tests

Stable isotopes, $\delta^{13}C$ and $\delta^{18}O$, were analyzed on (10 to 15) specimens of *Lobatula wuellerstorfi* collected in the sedimentary fraction 300 to 350 µm.

4. RESULTS AND DISCUSSION

4.1. Age model and sedimentological data

The age model established by Martins *et al*. (2015) enabled us to infer that core PE109-13 comprises a sedimentary record from the studied site dating back to approximately the last 38 Ka BP. This core consists of alternating layers of silt and clayey silt, distinguished by their distinct grain sizes and compositions.

The sediments in the sand fraction are essentially composed of biogenic (bioclasts and foraminifera), authigenic, and lithogenic components (mica, quartz, other minerals, and sediment agglomerates). The lithogenic component showed patterns opposite to those of the biogenic ones. Among the lithogenic components, mica was identified as the most abundant detrital component in most samples, with percentages reaching ≈80% of the grains in some samples, followed by quartz.

In the middle portion of the core, between 190 and 130 cm depths, there was a higher proportion of lithogenic and authigenic/diagenetic components, and a lower proportion of biogenic components. The sand fraction is predominantly siliciclastic between 530-510

cm, 440-430 cm, 410-380 cm, 250-240 cm, 200-100 cm, and also at 340 cm and 270 cm.

4.2. Mineralogy of fine fraction

The main mineralogical components present in the fine fraction are: quartz ($\bar{x}$ = 50.6 %); calcite ($\bar{x}$ = 21.2 %), K-feldspar ($\bar{x}$ = 3.3 %), mica/illite ($\bar{x}$ = 6.9 %); dolomite ($\bar{x}$ = 3.7 %); plagioclase ($\bar{x}$ = 5.1 %), and kaolinite ($\bar{x}$ = 3.8 %). The following minerals were also found with relative abundance reaching 2-5 %: opal CT ($\bar{x}$ = 0.9 %), pyrite ($\bar{x}$ = 0.5 %), siderite ($\bar{x}$ = 0.9 %), anatase ($\bar{x}$ = 0.8 %), anhydrite ($\bar{x}$ = 1.0 %) and chlorite ($\bar{x}$ = 0.9 %). The presence of zeolites, magnesite and hematite was also identified in some levels (with a percentage ≤2%).

4.3. Benthic foraminifera

Foraminifera density (number per gram of bulk sediment) varied between 216 and 3296 n°/g. The foraminifera's highest density was reached between approximately 30-35 Ka BP, but mostly between approximately 0.9-15.3 Ka BP. Two hundred and fifty-one species/taxa of benthic foraminifera were identified. The Shannon index (H'), indicating species diversity, ranged between 2.3-3.5. The lowest H' values, <2.5, were found in the interval between 540-200 cm, corresponding to an age of around ≈37.6 Ka BP and ≈16.9 Ka BP, i.e., during the isotopic stages 3 and 2.

The species that reached the highest relative abundance (up to 41.5 %) along the core were *Cassidulina teretis* ($\bar{x}$ = 12.4 %) and *Eilohedra vitrea* ($\bar{x}$ = 12.8 %). With a relatively high percentage (between 10.5-25.7 %) were found *Nonionella iridea, Cassidulina laevigata/Paracassidulina neocarinata, Bulimina striata, Paracassidulina minuta, Stainforthia fusiformis, Stainforthia feylingi, Trifarina angulosa, Gavelinopsis praegeri* and *Epistominella exigua.*

Cassidulina teretis reached the highest relative abundance between ≈36.7-16.9 Ka BP; *Eilohedra vitrea* and *Bulimina striata* rose mainly between 36.9-21.1 Ka BP; *Nonionella iridea* mainly scored the Heinrich stadials (HS) HS1 and HS2a; *Cassidulina laevigata/Paracassidulina neocarinata, Paracassidulina minuta* and *Gavelinopsis praegeri* have reached higher relative abundances in general since ≈16.1 Ka BP.

4.4. Stable isotopes, SST and Exported productivity

The $\delta^{18}O$ and $\delta^{13}C$ values in *Lobatula wuellerstorfi* ranged from 4.37 to 2.26 ‰ ($\bar{x}$ = 3.55 ‰) and from 1.18 to 0.66 ‰ ($\bar{x}$ = 0.66 ‰), respectively. The $\delta^{18}O$ and $\delta^{13}C$ in *Globigerina bulloides* ranged from 0.16‰ and 3.31‰ ($\bar{x}$ = 2.17 ‰) and from 0.03 to -1.18 ‰ ($\bar{x}$ = -0.58 ‰), respectively.

Sea surface temperatures (SST) for July-September, estimated based on the planktonic foraminifera (data from Martins *et al*., 2015), ranged between 4.8-23.8 ºC ($\bar{x}$=15.8 ºC) and exported productivity varied between 50.7-212.6 gC/m^2 ($\bar{x}$=91.3 gC/m^2).

The benthic foraminifera high oxygen proxy (BFOI) ranged from 10.0-77.5 ($\bar{x}$ = 44.3 %) and showed generally below average values in the period between ≈24-6 Ka BP. The percentage of the indicator species of swifter currents ($\bar{x}$ = 10.6%) decreased significantly between ≈approximately 29.3-21.8 Ka BP, ≈approximately 17.6-14.6 Ka BP, and around 19.8 Ka BP.

Significant changes in the percentage of deep infauna (31.4-78.8 %; $\bar{x}$ = 47.6 %) were also observed along core PE 109-13. The most significant reductions in deep infauna were observed between ≈31.1-24.5 Ka BP, ≈23.1-18.3 Ka BP, and in the last ≈7 Ka BP. The epifaunal individuals ranged from 7.1-45.8 % ($\bar{x}$ = 24.2 %) and showed a general pattern opposite to that of the deep infauna.

4.5. Statistical results

The plot of factor 1 versus factor 2 of the PCA, explains most of the data variability (64%); factor 1 accounts for 40%, and Factor 2 accounts for 24%. Factor 1 is positively correlated with $\delta^{13}C_{.Lw,}$ benthic foraminifera indicator of swifter currents (BFSC), foraminifera density (FD), species richness (SR), H' (Shannon Index), J' (equitability), anatase, sediment mean grain size (SMGS), sand (namely very fine and fine sand fractions) and coarse silt fractions, calcite and anatase. Factor 1 is negatively correlated with $\delta^{18}O_{.Gb}$, $\delta^{18}O_{.Lw}$, fine sediment fractions (namely clay, very fine and fine silt), fine/coarse detrital minerals, detrital minerals (namely kaolinite, mica/illite, chlorite, smectite, and quartz). Factor 2 is positively correlated with fine fraction, namely clay, very fine and fine silt, calcite, BFOI (benthic foraminifera oxygen index) and opportunistic epifaunal species. Factor 2 is negatively correlated with SMGS, coarse silt, very fine sand, and fine sand fractions, sortable silt, quartz, dolomite, detrital minerals and deep infauna foraminifera species.

The results for $\delta^{18}O_{.Gb}$ and $\delta^{18}O_{.L.w}$ show a similar general pattern, as well as $\delta^{13}C_{.Gb}$ and $\delta^{13}C_{.Lw}$, marking the coldest period of the last glaciation with higher (benthic and planktonic) $\delta^{18}O$ values and lower (benthic and planktonic) $\delta^{13}C$ values. However, the reduction in $\delta^{18}O$ values occurred earlier on the ocean bottom than on the sea surface and with smaller oscillations.

The variation in sediment grain size may be related to the type of sediment supplied and accumulated, as well as to variations in the velocity of the bottom

currents. The progressive increase in benthic foraminifera species that indicate active currents suggests that bottom hydrodynamics may have increased since the end of the last glaciation.

The sediment lithogenic component was generally higher during the last glaciation. There was a trend towards a reduction in this component and an increase in the biogenic carbonate constituent since ≈17 ka BP. The lithogenic component of the sediments increased significantly during the Heinrich events, characterized by an increase in the density of lithic grains >350 µm in size related to ice-rafted detritus. During these events, there was a significant increase in the relative abundance of the species *N. pachyderma* and an abrupt decrease in SST, indicative of a rapid decline in ocean surface temperatures caused by icebergs and glaciers melting.

These changes are typically marked on the ocean bottom by a reduction in BFOI and BFSC benthic foraminifera species, indicating a sharp decline in sediment oxygen content and sluggish current activity. These changes generally occurred during phases in which exported productivity decreased. This suggests that the decrease in oxygenation conditions at the bottom was not caused by changes in productivity at the ocean surface, but rather by other factors, likely related to the aging of the water masses on the ocean floor.

It can be observed that since approximately 17 Ka BP, carbonates have increased, accompanied by a decline in detrital minerals. During the Holocene, the lower contribution from lithogenic particles resulted in a higher density of foraminifera. The reduction in the lithogenic component may have resulted from the coastline's migration towards the continent as the sea level rose.

5. CONCLUSIONS

The results obtained from the studied core indicate significant changes in both the surface ocean and the ocean bottom since the last glaciation. They reveal high variability in surface ocean conditions and also show how these changes have influenced the ocean floor. However, the data also corroborate that the conditions on the ocean floor have been an expression of the influence of climate change on deep ocean circulation and the characteristics of water masses.

REFERENCES

Castro, M., Dale, A.W., Gómez-Gesteira, M., Prego, R. and Alvarez, I. (2006). Hydrographic and atmospheric analysis of an autumnal upwelling event in the Ria of Vigo (NW Iberian Peninsula). *Estuarine, Coastal and Shelf Science,* 68:529-537.

Dansgaard, W., Johnsen, S.J., Clausen, H.B., Dhal-Jensen, D. Gundestrup, N.S., Hammer, C.U., Hvidberg, C.S., Steffensen, J.P., Sveinbjörnsdottir, A.E., Jouzel, J. and Bomnd, G. (1993). Evidence for general instability of past climate from a 250-kyr ice-core record. *Nature,* 364:218-220.

Ellis, B.F. and Messina, A.R. (1995, and subsequent updates) – Catalogue of Foraminifera. The American Museum of Natural History, New York. Sp. Public.

Fiúza, A., Hamann, M., Ambar, I., Díaz Del Río, G., González, N. and Cabanas, J. M. (1998). Water masses and their circulation off western Iberia during May 1993. *Deep-Sea Research I,* 45:1127-1160.

Fiúza, A. (1983). Upwelling patterns off Portugal. In*:* Suess, E. and Thiede, J. (Eds.), Coastal upwelling - Its sediment record, part A, Plenum Press, pp. 85-98.

Fiúza, A., Macedo, M., Guerreiro, R. (1982). Climatological space and time variation of the Portuguese coastal upwelling. *Oceanologica Acta*, 5:31-40.

Heinrich, H. (1988). Origin and consequences of cyclic ice rafting in the Northeast Atlantic Ocean during the past 130000 years. *Quaternary Research,* 29:142-152.

Lambeck, K., Esat, T.M. and Potter, E.K. (2002). Links between climate and sea levels for the past three million years. *Nature*, 419:199-206.

Loeblich, A.R. and Tappan, H. (1988). Foraminiferal genera and their classification. Van Nostrand Reinhold, New York, 970 pp.

Maestro, A., López-Martínez, J., Llave, E., Bohoyo, F., Acosta, J., Hernández-Molina, F.J., Muñoz, A. and Jané, G. (2013). Geomorphology of the Iberian Continental Margin. *Geomorphology*, 196:13-35.

Martins, M.V.A., Perretti, A.R., Salgueiro, E., Frontalini, F., Moreno, J., Soares, A.M., Mahiques, M., Silva, S., Carlos A. de Azevedo, C.A. and Alveirinho Dias, J. (2015). Atlantic sea surface temperatures estimated from planktonic foraminifera off the Iberian Margin over the last 40 ka BP. *Marine Geology*, 367:191-201.

Martins, V., Dubert, J., Jouanneau, J.-M., Weber, O., Silva, E. F., Patinha, C., Alveirinho Dias, J.M. and Rocha, F. (2007). A multiproxy approach of the Holocene evolution of shelf–slope circulation on the NW Iberian Continental Shelf. *Marine Geology*, 239:1–18.

Salgueiro, E., Naughton, F., Voelker, A.H.L., Abreu, L., Alberto, A., Rossignol, L., Duprat, J., Magalhães, V.H., Vaqueiro, S., Turon, J.-L. and Abrantes, F. (2014). Past circulation along the western Iberian margin: a time slice vision from the Last Glacial to the Holocene. *Quaternary Science Reviews,* 106: pp. 316-329.

Voelker, A.H.L. and Abreu, L. (2011). A review of abrupt climate change events in the northeastern Atlantic Ocean (Iberian margin): latitudinal, longitudinal and vertical gradients. In: Rashid, H., Polyak, L., Mosley-Thompson, E. (Eds.), Abrupt Climate Change: Mechanisms, Patterns, and Impacts. AGU, Washington D.C, pp. 15-37.

Vinhas, A. and Rodrigues, A. (2023). A cobertura sedimentar da plataforma continental do barlavento algarvio: análise sismo-estratigráfica e evolução recente. *Livro de resumos do XI Congresso Nacional de Geologia*, Coimbra, pp. 173-174.

Foraminifera and Ostracoda assemblages in the Tavira salt marsh (SE Portugal) under autumnal conditions – preliminary results

M. Gonçalves (1), F. Fatela (1, 2), M. C. Cabral (1, 2), and T. Drago (2, 3)

(1) Departamento de Geologia, Faculdade de Ciências, Universidade de Lisboa, 1749-016 Lisboa, Portugal. fc56499@alunos.ciencias.ulisboa.pt
(2) Instituto Dom Luiz (IDL), Faculdade de Ciências, Universidade de Lisboa, 1749-016 Lisboa, Portugal
(3) Instituto Português do Mar e da Atmosfera, I.P. (IPMA), 8800-737, Tavira, Portugal

Abstract: Ten samples were collected in October 2024 across a NNW-SSE transect in the Tavira salt marsh. The samples included sediment from the tidal flat, low marsh and high marsh to characterise the recent foraminiferal and ostracod assemblages. In this work 13 species of foraminifera and 11 species of ostracods were considered. Living foraminiferal assemblages appear to be closely related to altitude (submersion time), where species typical of inner continental shelf dominate in the tidal flat (Asterigerinata mamilla and Reophax communis), being replaced by Quinqueloculina spp., Entzia macrescens and Trochammmina inflata towards the high marsh. Living ostracods are rare but even so, the identified assemblages allow us to distinguish the three zones of the salt marsh, with the presence of at least one typical species in each one.

Keywords: *Foraminifera, Ostracoda, sediment grain size, Tavira salt marsh, Portugal*

1. INTRODUCTION

Benthic foraminifera and ostracods are widely used as proxies for palaeoenvironmental parameters such as salinity, temperature, bottom-water oxygenation and organic fluxes (e.g. Jorissen *et al*., 2007; Rodriguez-Lazaro and Ruiz-Muñoz, 2012). For this reason, it is necessary to study the recent foraminiferal and ostracod assemblages and correlate them with the environmental parameters which constrain their distribution. This approach is essential to ensure a high degree of confidence in palaeoenvironmental reconstructions.

Although many studies have been conducted over the past decades to characterise the tidal marsh assemblages of Foraminifera (e.g. Andrade *et al*., 2004; Fatela *et al*., 2009; Camacho *et al*., 2015; Schönfeld and Mendes, 2022) and Ostracoda (e.g. Ruíz-Muñoz *et al.*, 1996; Loureiro *et al*., 2009; Cabral and Loureiro, 2013; Cabral *et al*., 2017; Horne *et al.,* 2022) along the Portuguese coast, the Tavira salt marsh has yet to be studied in detail. Salt marshes are important depositional environments within the marginal-marine domain, where high sedimentation rates allow a good resolution of palaeoenvironmental reconstructions (Gehrels and Woodworth, 2013).

2. REGIONAL SETTING

The Tavira salt marsh lies to the east of the Gilão River, near the Tavira inlet, in an area commonly known as "Quatro Águas" (Figure 1). It is part of Ria Formosa, a coastal lagoon system that extends from Ancão on the west to Cacela Velha on the east (Newton and Mudge, 2003). With a mesotidal regime, this lagoon has a tidal range that varies between 0,60 m on low tide up to 3,90 m during high tide (e.g. Antunes, 2025).

The Gilão is an important river in eastern Algarve. Its watershed has a surface about 221 km^2 (Isidoro *et al*., 2010), draining an area with a Csa climate type (mediterranean with hot and dry summers alternating with mild and wet winters). According to the official available data, the average annual air temperature is 18 °C, ranging from 19 °C to 30 °C in August and 7 °C to 16 °C in January; the annual precipitation averages are 516 mm (e.g. IPMA, APA websites).

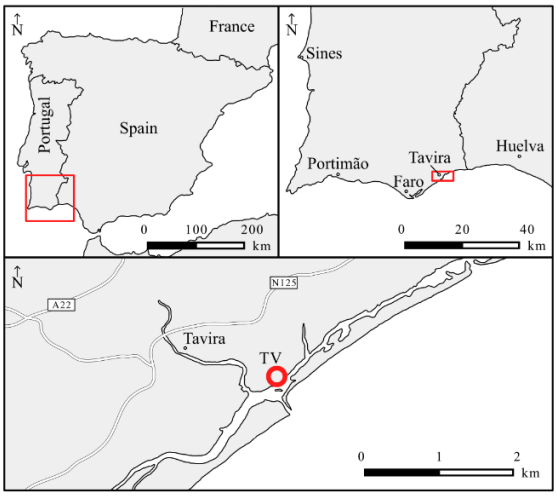

Figure 1. Regional setting and Tavira (TV) sampling profile location.

3. MATERIAL AND METHODS

Ten surface sediment samples were collected in October 2024 along a NNW-SSE transect that extended across the tidal flat (P1, P2), low marsh (P3, P4) and high marsh (P5, PJ5', P6, P7, P8 and P9). Each sample consists of 30 cm^3 (3x10 cm^3) of the 1 cm topmost sediment layer, which was stored in alcohol. Ten concomitant samples were collected for sedimentological analysis. At each sampling point, the temperature, salinity, pH, conductivity and dissolved oxygen of the interstitial water were measured using WTW probes. The same measurements were conducted on the estuarine water, close to the profile, at low tide slack.

In the laboratory, the samples were washed through 63 µm and 500 µm sieves. The residue was immersed in a Rose Bengal solution [1 g/L] overnight and then washed again to remove excess stain. Foraminifera and ostracods were separated from the sediment by a dry picking process. Whenever possible, a minimum of 300 foraminifera *per* sample were counted to ensure statistical representativeness (Fatela and Taborda, 2002). For ostracods, less abundant, a preliminary picking was done in 1/16th of the total sample, to get a rough estimate of the number of specimens. For samples with at least 10 individuals, half of the sample was analysed. Taxonomy followed Loeblich and Tappan (1988) for foraminifera and Horne *et al*. (2002) for ostracods, among other specialized publications.

Grain size analyses were performed using laser diffractometry (Malvern Mastersizer 3000) after the organic matter had been destroyed using a hydrogen peroxide (H_2O_2) treatment. The resulting data was processed via GRADISTAT software (Blott and Pye, 2001).

4. RESULTS AND DISCUSSION

4.1 Foraminiferal assemblages

Only the 13 species of foraminifera with abundances over 2% in one sample and presence in at least two samples were considered. Figures 2 and 3 summarise canonical correspondence analysis (CCA) results of the dead and living assemblages. Species and samples are grouped into three main clusters corresponding to the tidal flat (TF), the low marsh (LM) and the high marsh (HM). In the dead assemblages, the eigenvalues of axis 1= 0,633 and axis 2= 0,074 explaining 90,1% of the species-environment relationship. In the living assemblages they explain 84,1% (eigenvalues of axis 1= 0,644 and axis 2= 0,159).

The results show that both dead and living assemblages are mostly explained by the first axis, which is strongly related to the altitude. This should be interpreted not as an environmental driver *per se*, but as a *proxy* for the submersion times of the sampling points. The limited variation of the other parameters and the euryparametric behaviour of the main species attenuates their influence on the assemblages' distribution.

In the tidal flat the species *Reophax communis* and *Asterigerinata mamilla* are dominant in the biocenosis, followed by *Quinqueloculina* spp., *Bolivina ordinaria*, *Ammonia* gr. *tepida, Ammonia gr. parkinsoniana, Globigerinoides ruber* and *Lepidodeuterammina ochracea*. In both low marsh samples *Quinqueloculina* spp. is the dominant species. *Asterigerinata mamilla, Ammonia* gr. *tepida, Ammonia* gr. *parkinsonianana, Trochammina inflata, Entzia macrescens, Bolivina ordinaria* and *Ammotium salsum* are all secondary species. In the high marsh (P5, P6, P7, P8) *Quinqueloculina* spp. and *E. macrescens* are dominant, but *T. inflata* and *Tricohyalus aguayoi* are also widely present. In the highest high marsh (P8) *T. aguayoi* is the second most abundant species.

PJ5' is located between P5 and P6 on a patch of isolated *Juncus* sp. within a high marsh dominated by *Salicornia* sp. This peculiar occurrence is partially mirrored in the foraminiferal assemblages, which include many low marsh species. Such deviation is more pronounced in the dead assemblage (Figure 2), where CCA groups PJ5' with P3 and P4 low marsh samples. Further research is required to determine the underlying causes of such occurrence.

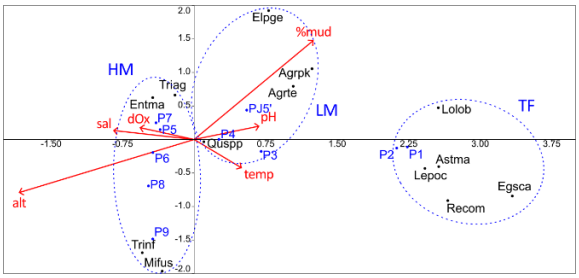

Figure 2. CCA plot of the dead foraminiferal assemblages and environmental factors altitude (alt), salinity (sal), dissolved oxygen (dOx), temperature (temp), pore waters pH, mud content (%mud). TF - tidal flat; LM - low marsh; HM - high marsh. Triag - T. aguayoi; Entma - E. macrescens; Trinf - T. inflata; Mifus - M. fusca; Elpge - E. gerthi; Agrpk - A. gr. parkinsoniana; Agrte - A. gr. tepida; Quspp - Quinqueloculina spp.; Lolob - L. lobatula; Astma - A. mamilla; Lepoc - L. ochracea; Egsca - E. scabrum; Recom - R. communis.

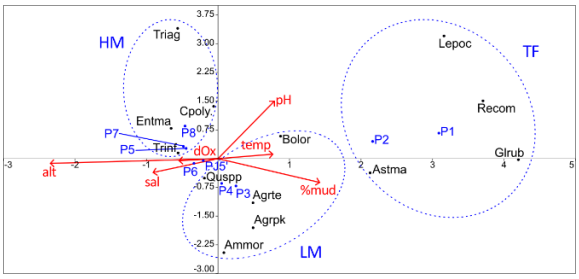

Figure 3. CCA plot of the living foraminiferal assemblages and alt, sal, dOx, temp, pH and %mud. Cpoly - C. polygyra; Bolor - B. ordinaria; Ammor - A. morenoi; Glrub - G. ruber.

4.2 Ostracod assemblages

Only the 11 species of ostracods with abundances over 2% in one sample and presence in at least two samples were considered. Due to the reduced number of specimens, no statistical analysis was carried out for ostracods. Figure 4 summarises the distribution of ostracods along the profile. All living species are brackish, tolerating different salinity ranges.

In the tidal flat over a dozen marine species were recorded, often represented by a few valves, except for *Urocythereis britannica*. Within the living assemblage, *Cytherois fischeri* is dominant and *Leptocythere fabaeformis* is a significant secondary species. In the low marsh, only sample P3 yielded a significant number of specimens. *Leptocythere lacertosa* dominates in this environment while species such as *C. fischeri* and *Loxoconcha malcomsoni* are also present. In the high marsh, sample PJ5' was the only one with a considerable number of specimens. The living assemblage comprises only one species, *Leptocythere ciliata*, typical of the high marsh

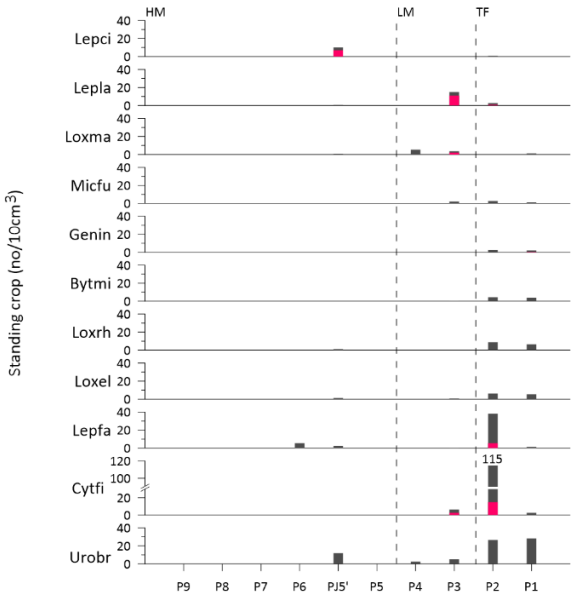

Figure 4. Distribution of the living (red) and dead (dark grey) ostracods along TV transect. HM - high marsh, LM - low marsh, TF - tidal flat. Lepci - L. ciliata; Lepla - L. lacertosa; Loxma - L. malcomsoni; Micfu - M. fulva; Genin - Gen. ind.; Bytmi - "Bytocythere" minima; Loxrh - L. rhomboidea; Loxel - L. elliptica; Lepfa - L. fabaeformis; Cytfi - C. fischeri; Urobr - U. britannica.

4.3 Sediment grain size

The average particle size increases gradually from the tidal flat (55 µm) to the high marsh (435 µm) except for P7 which appears markedly finer.

Figure 5 summarises the percentages of the textural types of the samples collected. Samples P1 to P4 (tidal flat and low marsh) show a high percentage of mud (81,9 % to 59,9 %) while samples P5 and P6 (lower high marsh) show almost the same percentage of sand and mud (51,8 % to 41,5 %); P7 is the only high marsh sample with a higher percentage of mud (73,8 %). High marsh samples P8 and P9 consist essentially of sandy sediment, with 15,7 % and 8,8 % of mud.

Samples P1 to PJ5' and P7 are classified as sandy silts and P6, P8 and P9 as silty sands. In all samples, the sediment is poorly to very poorly sorted.

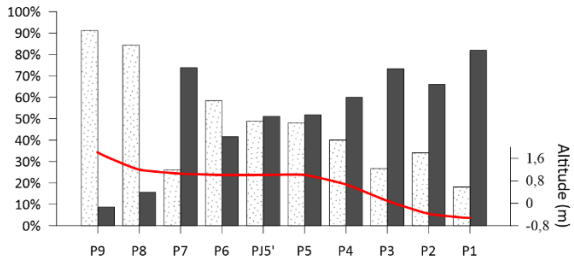

Figure 5. Percentage of sand (dots) and mud (dark grey) in sampling points (red line; topographic profile obtained with GSSN – datum Cascais).

5. CONCLUSIONS

Foraminiferal assemblages from the Tavira tidal marsh show a distribution strongly related to the marsh zonation. In the tidal flat the most abundant species are those typically found in the inner continental shelf, with *A. mamilla* and *R. communis* being dominant. Towards the high marsh, those are replaced by euryhaline species, namely *E. macrescens* and *T. inflata,* reflecting the general pattern of Iberian salt marshes. Considering the present data, the foraminiferal assemblages distribution seems to be almost independent of sediment granulometry. Although living ostracods are rare, three assemblages can be defined. In the tidal flat *C. fischeri* and *L. fabaeformis* are the most common species. In the low marsh *L. lacertosa* and *L. malcomsoni* become dominant and are replaced by *L. ciliata* in the high marsh. The foraminiferal and ostracod assemblages record the strong marine influence in this segment of Ria Formosa.

Acknowledgements

Authors acknowledge Marcos Rosa for the altimetric survey and Telmo Nunes for taking the SEM images. This work was supported from FCT I.P./MCTES through national funds (PIDDAC) – UIDB/50019/2020 (https://doi.org/10.54499/UIDB/50019/2020), UIDP/50019/2020 (https://doi.org/10.54499/UIDP/50019/2020), and LA/P/0068/2020 (https://doi.org/10.54499/LA/P/0068/2020).

REFERENCES

Andrade, C., Freitas, M.C., Moreno, J. and Craveiro, S.C. (2004). Stratigraphical evidence of Late Holocene barrier breaching and extreme storms in lagoonal sediments of

Ria Formosa, Algarve, Portugal. *Marine Geology*, 210:339-362.

Antunes, C. (2025). Previsão de Marés dos Portos Principais de Portugal. IDL/FCUL. https://webpages.ciencias.ulisboa.pt/~cmantunes/hidrografia/hidro_mares.html

Blott, S.J. and Pye, K. (2001). GRADISTAT: a grain size distribution and statistics package for the analysis of unconsolidated sediments. *Earth Surface Processes and Landforms*, 26:1237-1248.

Cabral, M.C. and Loureiro, I.M. (2013). Overview of Recent and Holocene ostracods (Crustacea) from brackish and marine environments of Portugal. *Journal of Micropalaeontology*, 32:135-159.

Cabral, M.C., Fatela, F., Lopes, V., Freitas, M.C. and Andrade, C. (2017). Cyprideis torosa (Jones, 1850) in mainland Portugal: what do we know? *Journal of Micropalaeontology*, 36:94-112.

Camacho, S., Moura, D., Connor, S., Scott, D. and Boski, T. (2015). Ecological zonation of benthic foraminifera in the lower Guadiana Estuary (southeastern Portugal). *Marine Micropaleontology*, 114:1-18.

Fatela, F. and Taborda, R. (2002). Confidence limits of species proportions in microfossil assemblages. *Marine Micropaleontology*, 45:169-174.

Fatela, F., Moreno, J., Moreno, F., Araújo, M.F., Valente, T., Antunes, C., Taborda, Andrade, C. and Drago, T. (2009). Environmental constraints of foraminiferal assemblages distribution across a brackish tidal marsh (Caminha, NW Portugal. *Marine Micropaleontology*, 70:70-88.

Gehrels, W. and Woodworth, P. (2012). When did modern rates of sea-level rise start? *Global and Planetary Change*, 100:263-277.

Horne, D.J., Cohen, A. and Martens, K. (2002). Taxonomy, Morphology and Biology of Quaternary and Living Ostracoda. In: Holmes, J.A., Chivas, A.R. (eds.), *The Ostracoda: Applications in Quaternary Research*. American Geophysical Union, Geophysical Monograph, pp. 5-36.

Horne, D.J., Cabral, M.C., Fatela, F. and Radl, M. (2022). Salt marsh ostracods on European Atlantic and North Sea coasts: Aspects of macroecology, palaeoecology, biogeography, macroevolution and conservation. *Marine Micropaleontology*, 174:101975.

Isidoro, J.M., Rocheta, V.L. and Lança, R. (2010). Delimitação de áreas inundáveis por acção fluvial - Aplicação ao Rio Séqua/Gilão na área urbana de Tavira. *10º Congresso da Água - Marcas d'Água*, Algarve.

Jorissen, F., Fontanier, C. and Thomas, E., (2007). Paleoceanographical Proxies Based on Deep-Sea Benthic Foraminiferal Assemblage Characteristics. In: Stein, R. (ed.), *Developments in Marine Geology*. pp. 327-358.

Loeblich, A.R., and Tappan, H. (1988). Foraminiferal Genera and their Classification. Van Nostrand Reinhold Company, 970 p.

Loureiro, I.M., Cabral, M.C. and Fatela, F. (2009). Marine influence in Ostracod assemblages of the Mira River estuary: comparison between lower and mid estuary tidal marsh transects. *Journal of Coastal Research*, 56:1365-1369.

Newton, A. and Mudge, S. (2003). Temperature and salinity regimes in a shallow, mesotidal lagoon, the Ria Formosa, Portugal. *Estuarine, Coastal and Shelf Science,* 57:73-85.

Rodriguez-Lazaro, J. and Ruiz-Muñoz, F. (2012). A General Introduction to Ostracods: Morphology, Distribution, Fossil Record and Applications. In: Horne, D.J., Holmes, J., Rodriguez-Lazaro, J., Viehberg, F.A. (eds.), *Ostracoda as Proxies for Quaternary Climate Change*. Developments in Quaternary Science, Elsevier, 17:1-14.

Ruiz-Muñoz, F., González-Regalado, M.L. and Gonzáles, J. (1996). Distribución y ecología de los foraminíferos y ostrácodos actuales del estuario mesomareal del río Guadiana (SO España). *Geobios,* 29:513-528.

Schönfeld, J. and Mendes, I. (2022). Benthic foraminifera and pore water carbonate chemistry on a tidal flat and salt marsh at Ria Formosa, Algarve, Portugal. *Estuarine, Coastal and Shelf Science,* 276:108003.

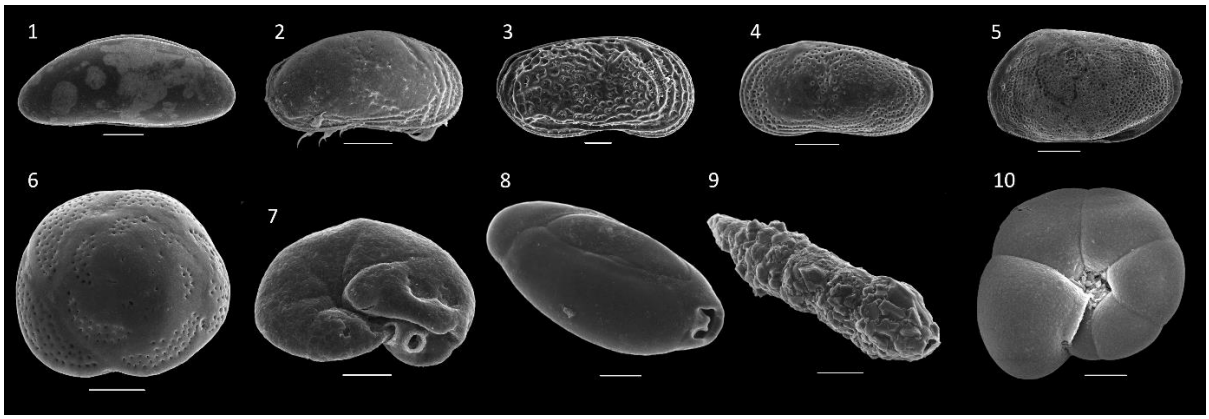

Plate 1. Some of the most representative species of Ostracoda (top row) and Foraminifera (bottom row) in the Tavira salt marsh. C, carapace; f, female; m, male. Scale bar 100 µm. 1: Cytherois fischeri (Sars, 1866), C, left view. 2: Leptocythere ciliata Hartmann, 1957, C, right view, f. 3: Leptocythere fabaeformis (Müller, 1894), C, right view, f. 4: Leptocythere lacertosa (Hirschmann, 1912), C, left view, m. 5: Loxoconcha malcomsoni Horne & Robinson, 1985, left valve, external view, f. 6: Asterigerinata mamilla (Williamson 1858), dorsal side. 7: Entzia macrescens (Brady, 1870), ventral side. 8: Quinqueloculina sp. 9: Reophax communis Lacroix, 1930. 10: Trochammina inflata (Montagu, 1808), ventral side.

Evolução recente do sistema praia-arriba de Forte Novo

P. Lourenço (1), B. Rodrigues (2) e C. Loureiro (3)

(1) Faculdade de Ciências e Tecnologia, Universidade do Algarve, Faro, Portugal; a79878@ualg.pt
(2) Agência Portuguesa do Ambiente, Faro, Portugal.
(3) CIMA-ARNET, Faculdade de Ciências e Tecnologia, Universidade do Algarve, Faro, Portugal.

Abstract: Entre Outubro de 2018 e Março de 2025, foram quantificadas as taxas de erosão da arriba e praia de Forte Novo com recurso a ortofotografia obtida com drones e levantamentos topográficos da praia. A evolução durante o Inverno de 2024/25 foi analisada em detalhe, para caracterizar a dinâmica do sistema praia-arriba em resposta a tempestades. Este período foi marcado por um recuo acentuado da arriba, com variação significativa ao longo do litoral de Forte Novo. A variação da resistência ao longo da arriba e da topografia da praia são pouco significativas e não permitem, de forma clara, justificar a variabilidade longilitoral no recuo da arriba. A aceleração no recuo da arriba coincidiu com o período estimado para a perda de efeito da realimentação realizada em 2010, verificando-se uma correspondência entre o recuo acelerado da arriba e a ocorrência de grupos de tempestades, destacando a vulnerabilidade do sistema praia-arriba face à agitação marítima.

Keywords: *erosão costeira, arriba, tempestades, drones, realimentação de praia*

1. INTRODUÇÃO

Litorais rochosos compostos por arribas e plataformas rochosas encontram-se presentes em cerca de 50% das zonas costeiras mundiais (Alessio e Keller, 2020), o que indica a prevalência deste tipo de litoral. Contudo, em muitos casos os litorais rochosos ocorrem em conjunto com litorais arenosos (Gallop *et al*., 2020), resultando em ambientes costeiros compostos por sistemas de praia e arriba. Nestes sistemas, tem-se verificado que aumentos episódicos na erosão das arribas estão relacionados com a redução da largura e elevação das praias, verificando-se que nos setores em que a praia se encontra em erosão o recuo da arriba é também mais rápido e intenso (Sallenger *et al*., 2002; Nunes *et al*., 2011).

A erosão de sistemas praia-arriba está fortemente relacionada com a intensidade da agitação marítima, uma vez que as ondas são o principal agente erosivo em litorais expostos. A capacidade erosiva da ondulação está naturalmente dependente das características e energia das ondas, mas também das caraterísticas litológicas das arribas que determinam a resistência dos materiais à erosão (Bezerra *et al*., 2011), bem como os mecanismos de instabilidade e queda das arribas. Assim, é fundamental compreender os processos e padrões de erosão em litorais rochosos, de forma a proteger pessoas, bens e infraestruturas de eventuais movimentos de massa devido à instabilidade em arribas (Alessio e Keller, 2020). Em zonas costeiras densamente ocupadas e com elevada atividade turística ao longo de praias e arribas, como acontece no litoral algarvio, é fundamental uma melhor compreensão sobre os processos costeiros nos sistemas rochosos (Nunes *et al*., 2009), uma vez que existe uma crescente exposição de turistas e residentes aos perigos causados por movimentos de massa em arribas (Teixeira, 2021).

Grande parte dos estudos sobre a dinâmica de sistemas de praia-arriba baseia-se na caracterização das taxas de erosão de praias e arribas ao longo de períodos longos, da ordem dos anos a décadas. Para isso, são normalmente integradas imagens aéreas ou de satélite e levantamentos de campo. Hoje em dia, com a crescente disponibilidade de equipamentos para monitorização de zonas costeiras, como drones equipados com câmaras de alta resolução, em conjunto com novas técnicas de fotogrametria digital, é possível fazer uma monitorização temporalmente e espacialmente mais detalhada. Os dados obtidos com estes novos equipamentos e técnicas podem ser integrados através de Sistemas de Informação Geográfica (SIG), permitindo uma melhor análise e visualização das tendências e processos de erosão em litorais rochosos. Esta integração de informação é crucial para os gestores costeiros (Nunes *et al*., 2009), permitindo que se explorem diferentes medidas de gestão e minimização do risco em sistemas de praia-arriba (Teixeira, 2021).

O presente trabalho tem como objetivo principal apresentar os resultados de um programa de monitorização detalhada do sistema praia-arriba em Forte Novo, incluindo a quantificação das taxas de erosão da arriba entre Outubro de 2018 e Março de 2025, bem como a relação entre a evolução da praia e erosão diferencial da arriba em resposta à agitação marítima durante o inverno de 2024/25.

2. ÁREA DE ESTUDO E MÉTODOS

O sistema praia-arriba de Forte Novo está situado na freguesia de Quarteira, concelho de Loulé, Algarve. As arribas neste sector do litoral algarvio são compostas por sedimentos areno-argilosos vermelhos, pouco consolidados e com reduzida resistência à erosão (Teixeira, 2004), e a praia, realimentada artificialmente em 2010, apresenta largura variável sendo composta maioritariamente por areia média a grosseira (Nunes *et al*., 2011). O litoral de Quarteira é densamente ocupado, e imediatamente a oeste de Forte Novo encontra-se o campo de esporões e molhes da marina de Vilamoura e porto de pesca de Quarteira. Estas estruturas interrompem o transporte sedimentar longilitoral, que no litoral algarvio apresenta uma direção predominante de oeste para este, resultante de um clima de agitação marítima dominado por ondas moderadas de W-SW, mas com ondulação de tempestade de SW bastante energética (Ferreira *et al*., 2016).

Figura 1. Localização do sistema praia-arriba de Forte Novo (retângulo branco) enquadrado pelas estruturas de proteção costeiras de Vilamoura e Quarteira a oeste (Imagem de base: OrtoSat 2023 – Direção Geral do Território).

A arriba e praia de Forte Novo têm vindo a ser monitorizadas pela Agência Portuguesa do Ambiente com recurso a drones desde 2018. Os levantamentos foram realizados com diversos equipamentos, mas em todos os casos foi obtida uma cobertura densa de fotografias aéreas, a partir das quais foram gerados ortofotografias e modelos digitais do terreno obtidos por fotogrametria digital através do método SfM (Structure from Motion). A precisão posicional e altimétrica foi assegurada por pontos de controlo (GCPs) ou drones com posicionamento RTK-GNSS (Real-Time Kinematic Global Navigation Satellite System). Entre Outubro de 2018 e Março de 2025 foram realizados 11 levantamentos com drone, sendo que 5 dos quais se realizaram entre Setembro de 2024 e Março de 2025 de forma a caracterizar a evolução do sistema praia-arriba durante o Inverno de 2024/25. Nestes 5 levantamentos foi também monitorizado o perfil de praia em 4 setores com recurso a um recetor RTK-GNSS, bem como determinada a dureza da arriba em 14 locais ao longo da face da arriba com recurso a um martelo de Schmidt.

As ortofotografias obtidas a partir dos 11 levantamentos com drone foram importadas para o programa QGIS, no qual foram vetorizadas manualmente a linha da crista e base da arriba para cada levantamento. A determinação de diferentes métricas para caracterização da evolução da crista da arriba, incluindo o envelope de variação da linha de costa (SCE – Shoreline Change Envelope) e a taxa de regressão linear (LRR – Linear Regression Rate), foi realizada com recurso ao programa Digital Shoreline Analysis System (DSAS) versão 6.0, desenvolvido por Himmelstoss *et al*. (2024). Para aplicação do DSAS estabeleceram-se transeptos perpendiculares à linha da crista da arriba com um espaçamento de 1 m. De forma a analisar especificamente a contribuição das tempestades e agitação marítima para a erosão da praia e da arriba de Forte Novo durante o inverno de 2024/25, a análise da variação da linha de costa foi feita separadamente para o período entre Outubro de 2018 a Agosto de 2024 e entre Setembro de 2024 e Março de 2025.

3. RESULTADOS E DISCUSSÃO

Com base na métrica SCE, a crista da arriba de Forte Novo recuou em média 1.09 m durante o período entre 10/2018 e 08/2024, tendo o valor médio de recuo aumentado para 3.96 m durante o Inverno de 2024/25. Para estes dois períodos o recuo máximo (mínimo) foi de 6.22 (0.08) m e 13.21 (0.47) m, respetivamente, evidenciando uma variação significativa ao longo da arriba de Forte Novo. Durante o primeiro período a erosão da crista da arriba concentrou-se nos extremos da área de estudo, onde a arriba era mais proeminente (Figura 2), enquanto que durante o Inverno de 2024/25 o recuo da arriba é mais generalizado, apesar de mais evidente na metade ocidental da área de estudo (Figura 3).

No que diz respeito às taxas de erosão obtidas com recurso à métrica LRR para a crista da arriba de Forte Novo, o primeiro período apresenta uma taxa média de 0.01 m/ano. Este valor encontra-se dentro da margem de erro da análise e não é estatisticamente significativo. Durante o período de Inverno de 2024/25, a crista da arriba apresentou uma taxa média de erosão de 4.24 m/ano. É importante notar que no primeiro período de análise a erosão da crista da arriba foi registada em 39% dos transeptos, enquanto que no segundo período esse valor foi de 93%. Contudo, considerando a incerteza posicional da crista da arriba, em apenas 3% e 15% dos transeptos essa erosão foi estatisticamente significativa para o primeiro e segundo período, respetivamente.

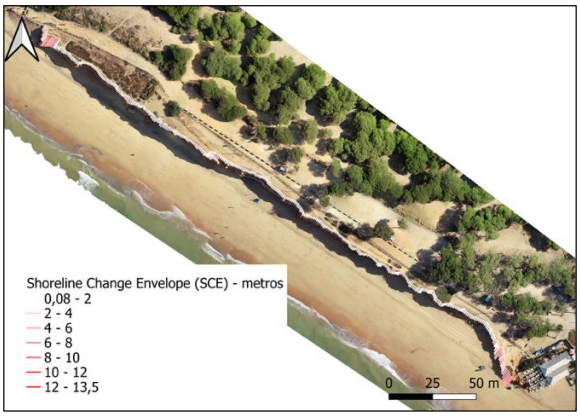

Figura 2. Erosão da crista da arriba de Forte Novo entre Outubro de 2018 e Agosto de 2024.

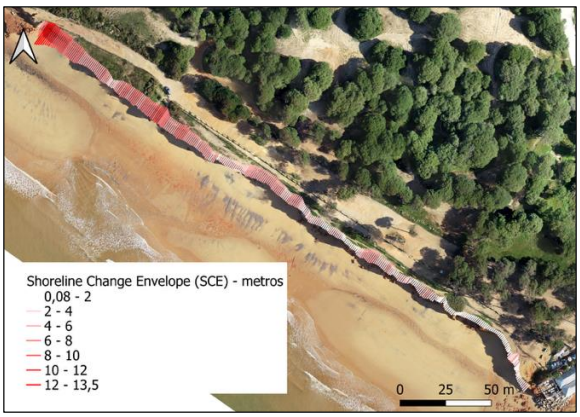

Figura 3. Erosão da crista da arriba de Forte Novo entre Agosto de 2024 e Março de 2025.

Face à variabilidade longilitoral do recuo da arriba de Forte Novo, foi analisada a variação da topografia da praia nos 4 perfis topográficos monitorizados, bem como a variação na dureza da face da arriba. Para ambas a variáveis não se verificaram variações relevantes ao longo da arriba, quer no que diz respeito à largura e altura da praia, quer no que se refere à resistência da arriba, uma vez que os valores de dureza média não apresentam diferenças estatisticamente significativas (Figura 4).

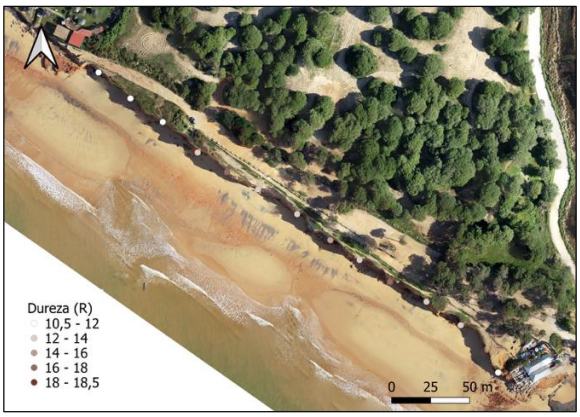

Figura 4. Variação dos valores de dureza da face da arriba medidos com o martelo de Schmidt.

As diferenças entre os valores médios e variabilidade longilitoral no recuo da crista da arriba de Forte Novo entre os dois períodos de análise refletem diferentes processos que caracterizam a dinâmica conjunta de sistemas praia-arriba. O aumento considerável da erosão da arriba no inverno de 2024/25 resulta, em primeiro lugar da erosão cumulativa da praia, que foi perdendo o seu papel de proteção face à agitação marinha. Após a realimentação artificial realizada em 2010, a praia foi progressivamente reduzindo o seu volume sedimentar, tendo sido estimado por Teixeira (2019) que a longevidade da realimentação atingisse o seu limite em Março de 2024. Assim, existe uma correspondência clara entre o período estimado para a perda de efeito da realimentação de 2010 e o início do recuo acelerado da arriba. Cumulativamente, o Inverno de 2024/25 caracterizou-se por sequências ou grupos de tempestades de elevada intensidade, particularmente entre Janeiro e Março de 2025, que em vários casos coincidiram com períodos de marés vivas. Durante o Inverno de 2024/25, a frequência de condições de ondulação com altura significativa acima dos 3 m foi superior em pelo menos 150% em relação aos invernos anteriores desde 2018/19 (Figura 5).

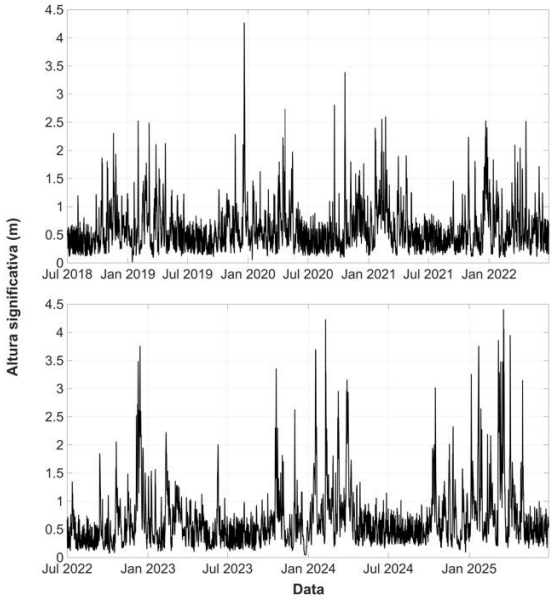

Figura 5. Variação da altura significativa da ondulação ao largo de Forte Novo entre Julho de 2018 e Junho de 2025. Dados obtidos a partir do modelo numérico MFWAM desenvolvido para a região Iberia-Biscay-Ireland e disponibilizado pelo Copernicus Marine Service (https://marine.copernicus.eu).

Tal como observado por Nunes *et al*. (2011), na ausência de uma praia larga e alta a proteger a arriba de Forte Novo, a erosão da arriba acelera de forma considerável sob a ação de grupos de tempestades, com maiores recuos observados no setor ocidental de Forte Novo.

Apesar de ser ainda necessário avaliar em maior detalhe a evolução conjunta do sistema praia-arriba de Forte Novo, este trabalho fornece elementos fundamentais para caracterizar a variabilidade temporal e espacial no recuo de arriba, quer em termos da sua relação com a evolução da praia pós realimentação, quer em resposta a sequências de tempestades.

Agradecimentos

Os autores agradecem ao Programa COSMO da Agência Portuguesa para o Ambiente pela disponibilização de dados para o litoral de Forte Novo.

REFERÊNCIAS

Alessio, P., e Keller, E. A. (2020). Short-term patterns and processes of coastal cliff erosion in Santa Barbara, California. *Geomorphology*, *353*, 106994.

Bezerra, M. M., Moura, D., Ferreira, Ó., e Taborda, R. (2011). Influence of wave action and lithology on sea cliff mass movements in Central Algarve Coast, Portugal. *Journal of Coastal Research*, 27, 162-171.

Ferreira, Ó., Matias, A. e Pacheco, A. (2016). The East coast of Algarve: a barrier island dominated coast. *Thalassas*, 32, 75-85.

Gallop, S.L., Kennedy, D.M., Loureiro, C., Naylor, L.A., Muñoz-Pérez, J.J., Jackson, D.W.T. e Fellowes, T.E. (2020). Geologically controlled sandy beaches: their geomorphology, morphodynamics and classification. *Science of the Total Environment*, 731, 139123.

Himmelstoss, E.A., Henderson, R.E., Farris, A.S., Kratzmann, M.G., Bartlett, M.K., Ergul, A., McAndrews, J., Cibaj, R., Zichichi, J.L., e Thieler, E.R. (2024). *Digital Shoreline Analysis System version 6.0*: U.S. Geological Survey software release. https://doi.org/10.5066/P13WIZ8M

Nunes, M., Ferreira, Ó., Schaefer, M., Clifton, J., Baily, B., Moura, D., e Loureiro, C. (2009). Hazard assessment in rock cliffs at Central Algarve (Portugal): A tool for coastal management. *Ocean and Coastal Management*, 52, 506-515.

Nunes, M., Ferreira, Ó., Loureiro, C. e Baily, B. (2011). Beach and Cliff Retreat Induced by Storm Groups at Forte Novo, Algarve (Portugal). *Journal of Coastal Research*, SI64, 795-799.

Sallenger, A.H., Krabil, W., Brock, J., Swift, R., Manizade, S. e Stockdon, H. (2002). Sea cliff erosion as a function of beach changes and extreme wave run-up during the 1997-1998 El Niño. *Marine Geology*, 187, 279-97.

Teixeira, S. B. (2004). Evolução do litoral de Quarteira (Portugal). *Actas do Seminário de Valorização Turística do Património Arqueológico Submerso de Quarteira,* 22-57.

Teixeira, S. B. (2019). Beach nourishment as a coastal management solution to mitigate soft cliff erosion on Quarteira coast (Algarve-Portugal). *Livro de resumos da 5a Conferência sobre Morfodinâmica Estuarina e Costeira - MEC2019,* Lisboa, Portugal, pp. 33-34.

Teixeira, S. B. (2021). Reducing sea cliffs hazard in pocket beaches through beach nourishment. *Journal of Integrated Coastal Zone Management*, 21, 215-226.

Caracterização da sedimentação recente da Baía de São Paio e da Praia do Cabedelo (Douro, Portugal).

A. Alberto (1,2), T. Drago (1,3) e M. C. Freitas (1,2)

(1) Instituto Dom Luiz (IDL), Faculdade de Ciências da Universidade de Lisboa, Lisboa, Portugal. aidalberto@ciencias.ulisboa.pt
(2) Departamento de Geologia, Faculdade de Ciências da Universidade de Lisboa, Lisboa, Portugal
(3) Instituto Português do Mar e da Atmosfera, Tavira, Portugal

Abstract: This study characterizes the modern sedimentary dynamics of São Paio Bay and Cabedelo Beach, located in the Douro River estuary (NW Portugal), to assess the influence of local forcing conditions on sediment deposition. A total of 16 surface sediment samples were collected and analysed for grain size distribution, organic matter, and calcium carbonate content. Results reveal a predominance of quatz-rich sandy sediments at both sites, with textural variations reflecting the action of distinct transport agents: tidal and wave energy in the intertidal zone, and aeolian processes in the supratidal zone. In São Paio Bay, low fine fraction and organic matter contents suggest accelerated silting following hydrodynamic changes induced by breakwater construction. At Cabedelo, a stable energy gradient is observed, with localized high-energy deposits. These findings provide a valuable modern analogue for supporting paleoenvironmental interpretations in studies on the sedimentary evolution of the Douro estuary.

Keywords: *Douro River estuary, Sedimentary dynamics, São Paio Bay, Cabedelo Beach, Grain size distribution.*

1. INTRODUÇÃO

Os estuários desempenham um papel fundamental na acumulação de sedimentos e no ciclo de nutrientes, configurando-se como ambientes bastante dinâmicos, e de elevada relevância ecológica e social. A sua evolução morfodinâmica e sedimentar é condicionada por fatores globais, nomeadamente variações eustáticas e alterações climáticas, mas também por fatores locais, como marés, tempestades, descarga fluvial e intervenções humanas.

O estuário do Rio Douro, localizado na costa noroeste de Portugal entre as cidades do Porto e Vila Nova de Gaia, desagua no Oceano Atlântico e caracteriza-se por uma elevada dinâmica hidrológica. O regime fluvial do Douro é fortemente influenciado pelo ciclo anual da precipitação, com caudais intensos no inverno e substancialmente reduzidos no verão (Gómez-Gesteira *et al*., 2011). Este comportamento reflete um regime torrencial, frequentemente associado a episódios de cheias significativos, em que a velocidade da corrente pode atingir os 8m/s. A montante, o estuário é limitado pela barragem de Crestuma-Lever, que regula o escoamento fluvial. Do ponto de vista morfológico, trata-se de um estuário em funil, característico de sistemas mesotidais estreitos, com elevada variabilidade interanual no escoamento fluvial, o que contribui para a complexidade hidrodinâmica e sedimentar da zona. Durante períodos de baixo escoamento fluvial, as correntes são dominadas por processos de maré, com velocidades máximas de vazante da ordem de 1.2 m/s (Costa *et al*., 2001). As alturas médias da maré variam entre 0,7 m (baixa-mar de maré viva) e 3,3 m (preia-mar de maré viva), com valores intermédios de 1,3 m e 2,6 m durante maré morta (Portela, 2008). A ondulação no litoral oceânico tem direção predominantemente de noroeste, com média da altura significativa de 2 a 3 m, e períodos de 8 a 12s. Em alturas de tempestade, frequentes no inverno e com origem no Atlântico Norte, a altura significativa das ondas pode atingir os 8 m (Costa *et al*., 2001).

Na margem sul da foz do estuário desenvolve-se uma restinga arenosa - o Cabedelo - orientada perpendicularmente ao eixo do estuário, com aproximadamente 700 m de comprimento e uma largura que varia entre os 300 m e os 700 m (medições em 8 de maio de 2020; Fernandes *et al*., 2021). Formado pela deposição de sedimentos provenientes da deriva litoral e do transporte fluvial, o Cabedelo começou a estabilizar e a crescer mais rapidamente depois da construção dos quebra-mares, concluída em 2007-2008 (Bastos *et al*., 2012). Numa área abrigada da ação direta das ondas e correntes de maré, entre o flanco interno do Cabedelo e a margem do estuário, desenvolveu-se a Baía de São Paio. O efeito da barreira natural, favoreceu o estabelecimento de uma zona de sapal, caracterizada por substratos arenosos e lodosos, e por vegetação típica de ambientes dunares e de sapal.

Este trabalho tem como principal objetivo a caracterização da sedimentação atual da Baía de São Paio e da Praia do Cabedelo, com base nas características granulométricas de amostras de sedimento. Os resultados irão contribuir, como análogos atuais, para apoiar a interpretação paleoambiental do estudo multidisciplinar de sondagens colhidas no estuário do Douro.

2. MEDODOLOGIA

A 11 de agosto de 2022, foram recolhidas oito amostras de sedimento na Baía de São Paio, durante a maré baixa. Em cada ponto de amostragem foi colhida uma amostra de 500g dos primeiros 2 cm de sedimento superficial, seguindo maioritariamente um perfil com orientação NNE-SSO, do baixo intertidal até à duna secundária. Foram também colhidas oito amostras na Praia do Cabedelo (utilizando a mesma metodologia), mas num perfil com a orientação E-O, da face de praia até às paliçadas de contenção sedimentar (Figura 1).

Figura 1. Localização das amostras (pontos vermelhos) na Baía de São Paio (BSP1 a BSP8) e na Praia do Cabedelo (Cab1 a Cab8), situadas no estuário do Rio Douro.

No laboratório, a fração fina (<63 µm) foi separada da fração grosseira (>63 µm), sendo esta última posteriormente submetida ao método de peneiração convencional. Os parâmetros estatísticos (i.e., média, desvio padrão, assimetria, curtose) das distribuições granulométricas de todas as amostras foram determinados através do software GRADISTAT (Blott e Pye, 2001), e foram classificadas quanto à distribuição do tamanho das suas partículas (Blott e Pye, 2012). A fração de 0.5 mm de cada amostra foi analisada de forma semi-qualitativa quanto à sua composição e características morfoscópicas utilizando a lupa binocular. Adicionalmente, as amostras foram analisadas quanto ao conteúdo em matéria orgânica (por queima na mufla – LOI) e de carbonato de cálcio (por volumetria, com recurso a um calcímetro de Eijkelkamp).

3. RESULTADOS E DISCUSSÃO

Os resultados da análise às amostras colhidas na Baía de São Paio (Figura 2) indicam que estas são maioritariamente constituídas por areia (91,5%–99,7%) com predominância de quartzo e conteúdos em cascalho baixos (<7%). O teor de silte e argila são geralmente residuais (<1%), com exceção do terraço de maré (BSP2, 2,5%) e na depressão interdunar (BSP7, 5,1%). A fração arenosa apresenta relativa uniformidade granulométrica, com diâmetros médios entre 0,4 mm (BSP8 - duna secundária) e 1 mm (BSP4 - canal interno). O canal interno (BSP4) revela sedimentos ligeiramente mais grosseiros que o banco de areia (BSP1), sendo ambas as amostras classificadas como areias ligeiramente cascalhentas. Estes dados sugerem que, apesar de ambos os depósitos se encontrarem sujeitos a condições ambientais semelhantes, o canal está sujeito a uma energia deposicional ligeiramente mais elevada. As amostras do terraço de maré (BSP2) e da face de praia (BPS3) refletem a ação de correntes de maré, com sedimentos com média de 0,8 mm a 0,7 mm, mal calibrados, compostos por quartzo hialino brilhante, sub-anguloso a rolados. Na transição para as dunas embrionária (BSP5) e primária (BSP6), dominam as areias de 0,5 mm de diâmetro e moderadamente bem calibradas, enquanto na duna secundária (BSP8) dominam as areias de 0,8 mm, moderadamente calibradas. Estas amostras são todas compostas por grãos de quartzo hialino baço, angulosos a sub-rolados. Estes resultados sugerem a ação do vento como principal agente de transporte nestas três zonas. A depressão interdunar (BSP7), de areia muito ligeiramente cascalhenta e ligeiramente lodosa mal calibrada, poderá refletir deposição episódica relacionada com cheias fluviais e/ou correntes de maré. Os teores de matéria orgânica são baixos, atingindo no máximo 2,8% (BSP7), onde se observou pouca abundância de restos vegetais.

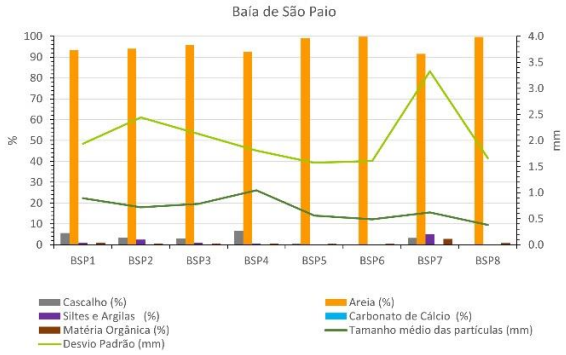

Figura 2. Resultados da análise textural (percentagens em cascalho, areia, e siltes e argilas), dos teores em carbonato de cálcio e matéria orgânica, e dos parâmetros estatísticos (média e desvio padrão), das amostras da Baía de São Paio.

A ausência de carbonato de cálcio nas amostras resulta da inexistência de componentes biogénicos na sua composição.

Os resultados da análise às amostras do perfil da praia do Cabedelo (Figura 3) também apresentam uma forte dominância da fração arenosa, com teores de areia entre 29,1% e 100%, composta por quartzo hialino brilhante, sub-rolado a rolado. O cascalho tem proporções variáveis, desde valores residuais até 70,9% (Cab8). As frações de silte e argila são inexistentes, o que reflete um ambiente de elevada energia, pouco propício à deposição de partículas finas. A acumulação de carbonato de cálcio (de origem biogénica) e matéria orgânica é geralmente baixa, atingindo no máximo 3,5% e 0,5%, respetivamente (Cab7 – face de praia). Ao longo do perfil intertidal–supratidal, observa-se uma tendência de correlação entre o diâmetro médio das partículas e o desvio padrão. A amostra colhida na face de praia (Cab7) é puramente composta por areia (100%) com diâmetro médio de 0,4 mm e moderadamente bem calibrada, e apresenta o valor em carbonato de cálcio mais elevado, 3,5%. Esta homogeneidade sedimentar reflete um ambiente de elevada energia, exposto à ação seletiva da agitação marítima. Na primeira berma, a amostra Cab6 revela uma areia com características semelhantes às da face de praia, indicando deposição associada a processos de rebentação regular. Contudo, também na berma foi identificada uma mancha com propriedades sedimentares distintas, da qual se recolheu a amostra Cab8. Esta é classificada como cascalho arenoso (com 70,9% de cascalho), mal calibrado, com diâmetro médio de 3,5 mm e sem teor em carbonato de cálcio. Este depósito poderá corresponder a um evento deposicional de alta energia (ex. tempestades), evidenciando variabilidade lateral associada a eventos episódicos e dinâmica sazonal.

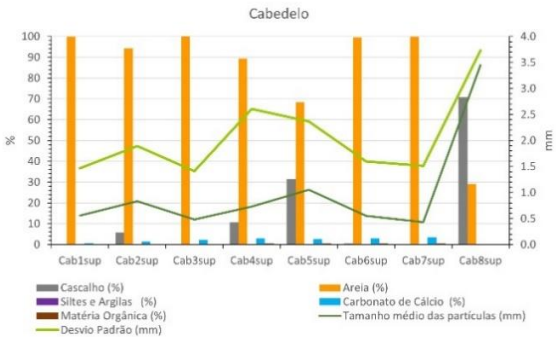

Figura 3. Resultados da análise textural (percentagens em cascalho, areia, e siltes e argilas), dos teores em carbonato de cálcio e matéria orgânica, e dos parâmetros estatísticos (média e desvio padrão), das amostras do Cabedelo.

A segunda berma (Cab5) apresenta uma areia cascalhenta (31,6% de cascalho) mal calibrada, média granulométrica de 1,1 mm, e é identificada como berma de tempestade. Na base da berma (Cab4), a areia ligeiramente cascalhenta (89,3% de areia), com alguma presença de carbonato de cálcio (2,6%), refle uma zona de transição entre os domínios marinhos e subaéreos, sujeita a remobilização. Nas zonas mais interiores, observa-se uma crescente homogeneidade e diminuição da granulometria. A duna primária (Cab3) e a paliçada (Cab1) são compostas por 100% de areia, sem cascalho, com granulometria média entre 0,5 e 0,6 mm, e baixos teores de matéria orgânica e carbonato de cálcio. Estas características são compatíveis com transporte eólico dominante e fraca influência hidrodinâmica. A depressão interdunar (Cab2) apresenta ligeiro aumento de cascalho (5,7%) e é moderadamente calibrada, sugerindo acumulação local de sedimentos transportados tanto por vento como por escoamento superficial.

4. CONCLUSÕES

Os resultados obtidos na Baía de São Paio e na Praia do Cabedelo indicam uma predominância de sedimentos arenosos em ambos os sistemas. Na Baía de São Paio, a sedimentação local é fortemente influenciada pela dinâmica das águas estuarinas, cuja intrusão gradual na zona, modulada pelo regime de marés, estabelece condições hidrodinâmicas propícias à deposição de sedimentos grosseiros (Jesus, 2003). A predominância de sedimentos arenosos em detrimento de finos, associada aos baixos teores de matéria orgânica, corrobora a interpretação de Bastos *et al*. (2012), segundo a qual as alterações nos padrões de circulação na baía, resultantes da construção dos quebra-mares, têm favorecido um processo contínuo de assoreamento e a descaracterização progressiva das suas feições típicas de sapal. O perfil sedimentar do Cabedelo reflete um gradiente de energia variável, consistente com a dinâmica típica da estação de verão, caracterizando-se por uma zona intertidal dominada pela ação das marés e da ondulação marítima, e uma zona supratidal onde predomina o transporte eólico de sedimentos.

Os resultados obtidos fornecem suporte, com base em análogos modernos, para interpretações paleoambientais em estudos sedimentológicos.

Agradecimentos

Este estudo recebeu fundos nacionais portugueses da Fundação para a Ciência e Tecnologia (FCT) I.P./MCTES através de fundos nacionais UIDP/50019/2020-IDL. Ana Alberto recebeu apoio financeiro através da bolsa de doutoramento UIBD/151497/2021 (IDL). Ana Alberto agradece ao Instituto Português do Mar e da Atmosfera (IPMA) pela cedência das suas instalações e equipamentos, que foram fundamentais para a realização do presente trabalho.

REFERÊNCIAS

Bastos, L., Bio, A., Pinho, J. L. S., Granja, H., e Silva, A. J. (2012). Dynamics of the Douro estuary barrier sand spit before and after breakwater construction. *Estuarine, Coastal and Shelf Science*, 109, 53–69.

Blott, S. J., e Pye, K. (2001). Gradistat: A grain size distribution and statistics package for the analysis of unconsolidated sediments. *Earth Surface Processes and Landforms*, 26 (11), 1237–1248.

Blott, S. J., e Pye, K. (2012). Particle size scales and classification of sediment types based on particle size distributions: Review and recommended procedures. *Sedimentology*, 59 (7), 2071-2096.

Costa, M., Silva, R., e Vitorino, J. (2001). Contribuição para o estudo do clima de agitação marítima na costa portuguesa. In *Actas das 2ªs Jornadas de Engenharia Costeira e Portuária*. Associação Internacional de Navegação, Sines, Portugal, 17-19 de outubro.

Fernandes, R. M., Gomes, A. A., e Teixeira, J. (2021). Quantificação das mudanças recentes na forma e volume da restinga do Cabedelo, foz do rio Douro. In *Geografia, riscos e proteção civil: Homenagem ao Professor Doutor Luciano Lourenço*, Vol. 1, pp. 205–216

Gómez-Gesteira, M., Gimeno, L., DeCastro, M., Lorenzo, M. N., Alvarez, I., Nieto, R., Taboada, J. J., Crespo, A. J. C., Ramos, A. M., Iglesias, I., Gómez-Gesteira, J. L., Santo, F. E., Barriopedro, D., e Trigo, I. F. (2011). The state of climate in NW Iberia. *Climate Research*, 48(2–3), 109–144.

Jesus, M. E. R. V. de (2003). Morfodinâmica do Cabedelo da Foz do Rio Douro: Perspectiva histórica e monitorização por GPS para o conhecimento da sua evolução actual. Aplicabilidade pedagógica numa vertente CTSA. Dissertação de mestrado, Universidade do Porto. Repositório Aberto da Universidade do Porto, pp. 211

Portela, L.I., 2008. Sediment transport and morphodynamics of the Douro River estuary. *Geo-Marine Letters*, 28, 77–86.

Application of Micro-Raman spectroscopy as a tool for the identification of sediment mineralogy

T. Drago (1,2), A. Alberto (2) and J. Cascalho (2,3)

(1) Portuguese Institute for Sea and Atmosphere, Tavira, Portugal. tdrago@ipma.pt
(2) Instituto Dom Luiz, FCUL, Lisboa, Portugal
(3) Faculdade de Ciências, Universidade Lisboa, Lisboa, Portugal

Abstract: Identifying the mineralogical composition of a sediment sample is an important step in determining its origin. This information is essential for reconstructing palaeoenvironments and understanding sediment transport patterns, among other things. However, this identification can be sometimes difficult to achieve using a binocular or optical microscope. In this study, we present an accurate methodology for mineralogical identification based on micro-Raman spectroscopy.

Keywords: *mineralogy, micro-raman, coastal and continental shelf sediments*

1. INTRODUCTION

Understanding the mineralogical composition of costal and continental shelf sediments is essential for identifying sediment sources and transport pathways. This knowledge helps with paleoenvironmental reconstructions, clarifies sediment transport patterns, and supports modern coastal management, among other applications.

This analysis can be done using traditional methods, such as identification with a binocular or optical microscope, or more precisely, with a confocal micro-Raman microscope. This instrument employs vibrational spectroscopy, analyzing the inelastic (Raman) scattering of laser light as it interacts with a mineral's atomic vibrations. Since each mineral has a unique Raman spectrum—like a fingerprint—this method allows for highly accurate identification.

Raman systems have a common setup, consisting of 1) source of the incident beam of light, 2) optical components used to illuminate the sample and collect the Raman scattered light, 3) components for the spectral analysis of the light, and 4) a device for the light detection (Nasdala *et al*., 2004) (Figure 1).

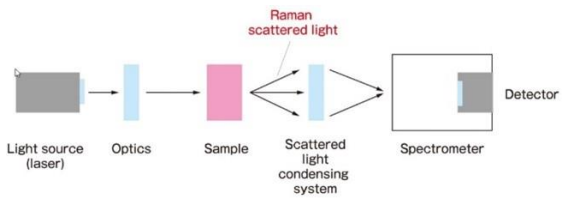

Figure 1. Common setup of Raman systems (www.hamamatsu.com).

In this study, we present an application of this methodology to sediment grains collected from very different environments (Algarve coast and continental shelf; Estremadura Spur).

2. METHODOLOGY

The equipment used was a confocal Raman microscope WITec®Alpha300R system (Figure 2) installed at Tavira station of the Portuguese Institute for Sea and Atmosphere. The system is equipped with an Ultrahigh-throughput UHTS300 Spectrometer and a DV401 laser detector. The excitation source is a diode laser operated at 532 nm wavelength, with 38 mW maximum power output. The spectral resolution of the spectrometer is 4-5 cm^{-1}. Zeiss® microscope objectives of 10X, 50X and 100X magnifications were used, attaining a sub-micron spatial resolution (Figure 2).

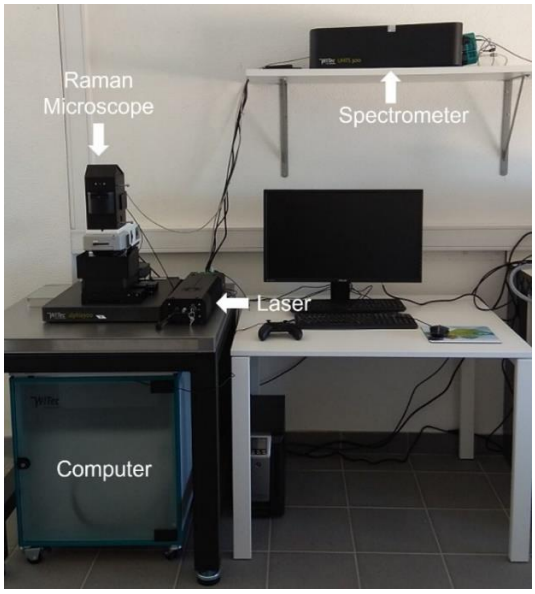

Figure 2. Confocal Raman microscope WITec® alpha300 R system at EEMT, IPMA Tavira.

The spectral calibration of the equipment was performed using Raman measurements of a pure silicon reference sample. The reference sample was

used to calibrate the Raman shift to the known position of the crystalline Si Raman band (520.7 cm-1). In order to obtain optimal spectra, in which the signal-to-noise ratio was sufficient to identify characteristic Raman peaks of the minerals.

After the calibration, the sample (microscopy slide with sand particles) was placed on the controlled piezo-driven scanning stage. A 10×/0.25 magnification lens was implemented to search for target particles, after which 50×/0.75, and 100×/0.9 lenses were used for observation and detection according to practical needs (Figure 3).

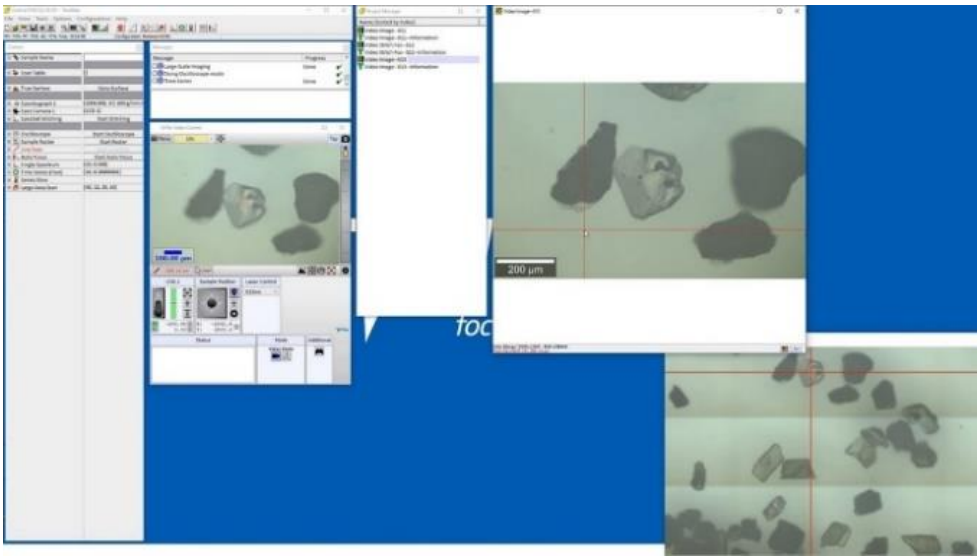

Figure 3. Search for sand target particles with the 10x/0,25 magnification lens of the confocal Raman microscope WITec® alpha300 R system.

The WITec® Control Five software, was then used for image processing and spectroscopic data export. Prior to the interpretation of the spectroscopic data, the spikes originating from the cosmic radiation were removed, a baseline correction was applied to the spectra and the positions of the Raman lines peaks were determined using standard fitting procedures.

The final step involved, obtained spectra for specific minerals were compared to an existing inorganic spectra database. For this search the WITec® TrueMatch software was used.

Extensive databases of Raman spectra for various minerals are available to compare against the unknown sample's spectrum. Some of these reference databases require a subscription or payment, such as the ST Japan database, while others are freely accessible, like the RRUFF Project.

3. RESULTS

During this experimental phase, grains from different environments were analysed. Representative examples included a sample from Tavira beach (Figure 4A) and sediments from Algarve and Estremadura Spur continental shelf. For example, quartz grains were identified in the Tavira beach sample, while yellow-colored lizardite grain (mineral belonging to the serpentine group) were found in the Estremadura Spur samples (Figure 4B), based on a comparison of the Raman spectra of the constituent minerals with the reference data from the ST Japan database.

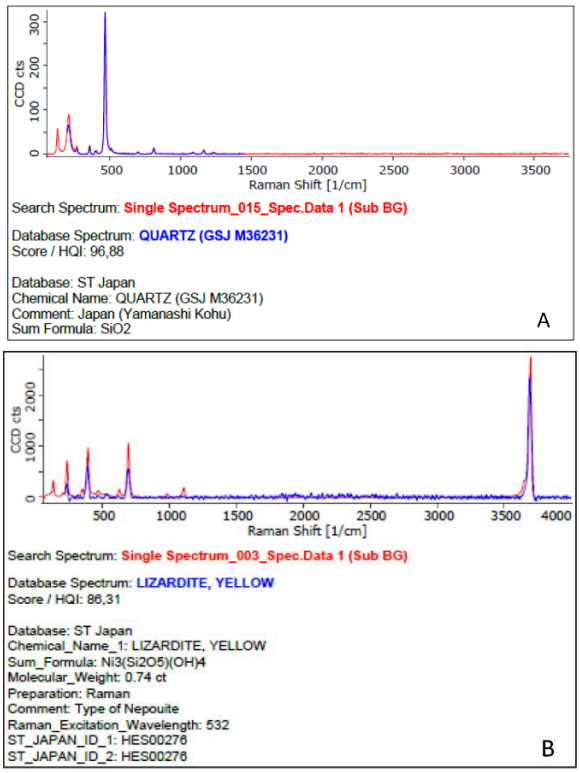

Figure 4. Two examples of the spectra obtained by micro-Raman analysis: A – grain from Tavira beach (Algarve); B - grain from the Estremadura Spur.

Future work will include the use of Witec's ParticleScout software, which will provide a significant enhance in speed and efficiency of particle detection, classification, mineralogical identification and quantification within a sample.

Overall, the Confocal Raman Imaging Microscope has proven to be a powerful instrument for the analysis and identification of mineral species in sediment samples. It also provides a quick and reliable way of determining the chemical composition of sediments without the need for sample preparation.

Acknowledgements

This study received funding from National Roadmap of Research Infrastructures (RNIE) through the project EMSO-PT project - PINFRA/22157/2016. Ana Alberto received financial support through the doctoral scholarship UIBD/151497/2021 (IDL).

REFERENCES

Nasdala, L., Smith, D. C., Kaindl, R. and Ziemann, M. A. (2004). Raman spectroscopy: analytical perspectives in mineralogical research. EMU *Notes in Mineralogy*, 6(May 2014), pp. 1–63.

Determinação da profundidade na região costeira de baixa profundidade através de imagens multiespectrais de satélite

R. Santos (1), C. Monteiro (1), M. Miranda (1) e C. R. Marques (1)

(1) Divisão de Hidrografia – Instituto Hidrográfico. ruben.santos@hidrografico.pt

Abstract: Since 2004, Portugal has been committed to acquiring high-resolution bathymetric data across its entire seafloor jurisdiction, achieving coverage of more than 65%, predominantly in deeper offshore regions. This research addresses the mapping of shallow coastal areas, specifically focusing on accurately estimating seafloor depth along the Portuguese coast using multispectral satellite imagery. Such mapping is particularly challenging due to spatial and temporal variations in seafloor characteristics and variability in the inherent optical properties (IOPs) of water, both of which significantly affect light propagation to optical sensors. To overcome these challenges, we compared classical (Stumpf algorithm) and advanced (Neural Networks – NN) methodologies applied to the Setúbal–Tróia region. This study aims to outline clearly the advantages and limitations of each methodological approach.

Keywords: *Bathymetry, Multispectral, Stumpf, Neural Network, Coastal*

1. INTRODUÇÃO

Desde 2004, Portugal está comprometido com a sondagem batimétrica de alta resolução de toda a área sob jurisdição nacional, tendo já alcançado mais de 65% da cobertura pretendida. No entanto, grande parte desta cobertura incide sobre regiões de maior profundidade, e para garantir a cobertura completa do fundo marinho, incluindo as zonas costeiras de baixa profundidade, o Instituto Hidrográfico (IH) tem vindo a desenvolver diversos estudos no âmbito da Batimetria Derivada por Satélite (SDB), recorrendo a metodologias que visam permitir uma cartografia mais rápida, eficaz e adaptada às especificidades destas áreas mais dinâmicas e desafiadoras. Inicialmente, o IH implementou e estudou amplamente o algoritmo de Stumpf *et al.* (2003), baseado numa regressão linear entre os rácios dos logaritmos de duas bandas espectrais e a profundidade obtida por dados *in-situ* (Guerreiro e Moura, 2015; Guerreiro e Moura, 2016; Vilar *et al.*, 2018). Mais recentemente, têm sido aplicados algoritmos avançados de inteligência artificial capazes de identificar padrões não-lineares (Santos *et al.*, 2025; Santos e Quartau, 2024; Santos e Quartau, 2023a; Santos e Quartau, 2023b), com o objetivo de melhorar a estimativa da batimetria em zonas costeiras de baixa profundidade ao longo do litoral português, recorrendo a dados multiespectrais.

O estudo que se apresenta tem como objetivo comparar resultados obtidos pelos algoritmos de Stumpf *et al.* (2003) e por redes neuronais (NN), aplicando-os à mesma região de Setúbal-Tróia (Figura 1).

2. DADOS E MÉTODOS

2.1. Dados

Neste estudo foram utilizados dados batimétricos adquiridos em 6 levantamentos hidrográficos (LHs), realizados pela brigada hidrográfica do IH, no interior e exterior do estuário do rio Sado, obtendo superfícies batimétricas com uma resolução espacial de 0.5 e 1.0 m. Estes dados foram adquiridos com sondadores multifeixe (MBES) durante o mês de abril de 2021, onde as profundidades, referidas ao Zero Hidrográfico (ZH), se encontram entre os -4 m e -40 m.

Adicionalmente, a este estudo, juntou-se uma fiada adquirida pelo projeto COSMO da Agência Portuguesa do Ambiente (APA) e dados LIDAR do satélite ICESAT-2 da Agência Espacial Americana (NASA). A fiada da APA foi obtida com sondador de feixe simples no dia 05/05/2021 e os dados do satélite ICESAT-2 foram registados a 17/04/2021, segundo o track 367 (Figura 1).

As imagens utilizadas foram adquiridas pelo satélite Sentinel-2, com nível de processamento L2A. Para o processo de calibração e treino dos algoritmos, foram selecionadas três imagens obtidas em datas próximas à aquisição dos dados batimétricos de referência: 15 de março, 4 de abril e 4 de maio de 2021. Para a validação do modelo de NN, foram utilizadas outras seis imagens do mesmo satélite, adquiridas em 13, 23 e 28 de junho, e em 13, 18 e 23 de julho de 2021. O objetivo desta etapa é avaliar a capacidade de generalização temporal do modelo treinado, testando o seu desempenho em novas datas sem necessidade de reconfiguração ou novo treino com imagens adicionais.

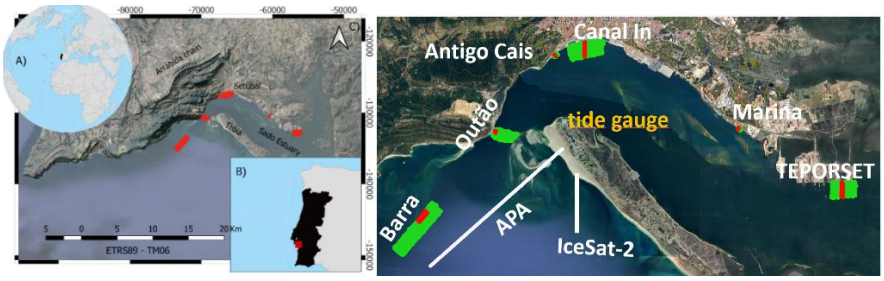

Figura 1. A), B) e C) Localização da área de estudo. As áreas cobertas pelos LHs estão representadas pelos polígonos vermelhos, na imagem do lado esquerdo. Na imagem do lado direito, estão representados os dados dos LHs utilizados na calibração do modelo (vermelho), no controlo (verde) e as fiadas de feixe simples adquiridos pela APA e LIDAR ICESAT-2 (branco). A localização do marégrafo está representada por "tide gauge".

Os dados de maré, obtidos pelos marégrafos de Setúbal-Tróia do IH, foram utilizados na determinação da altura de maré para cada aquisição das imagens de satélite, de forma a corrigir as profundidades à referência vertical do ZH.

2.2. Processamento dos dados

Os dados batimétricos e os dados de satélite necessitam de um processamento prévio para serem utilizados na derivação da batimetria.

A resolução espacial dos dados batimétricos foi reduzida para 10 m, de modo a coincidir com a resolução das imagens de satélite. O método de interpolação bilinear foi utilizado neste processo de reamostragem das profundidades. Estes dados foram divididos em 2 subconjuntos, um para calibração/treino do modelo e outro para validação.

Em cada imagem, a área de estudo foi delimitada com base em coordenadas elipsoidais no sistema WGS84, compreendidas entre 38.57°, -9.00° e 38.34°, -8.60°. Foram utilizadas as seguintes bandas espectrais do Sentinel-2: Coastal (B1), Blue (B2), Green (B3), Red (B4) e Near Infrared (B8). A banda B1, originalmente com resolução espacial de 60 metros, foi reamostrada para 10 metros, a fim de igualar a resolução das demais bandas e garantir uniformidade no processamento.

O efeito do brilho solar na superfície da água foi reduzido/removido através da análise da banda B8 com o algoritmo de Hedley *et al.* (2005).

As reflectâncias das bandas espectrais foram normalizadas através do método *Pseudo-Invariant Feature* (PIF), implementado na ferramenta Sen2Coral. A imagem utilizada como referência foi a adquirida a 04/04/2021. De seguida, aplicou-se um filtro passa-baixo com uma janela 3x3 a todas as bandas, de forma a reduzir o ruído entre pixéis.

A remoção das áreas de terra, nuvens e espuma branca foi efetuada com recurso a uma máscara gerada pelo Sen2Coral, utilizando a banda B8 e aplicando um valor limiar apropriado para discriminar essas áreas. Esta etapa visou garantir que apenas os píxeis da superfície de água fossem considerados no processamento.

Com estes resultados, foi criada uma tabela com a informação (batimetria e reflectâncias) utilizada na calibração do modelo de regressão linear (Stumpf *et al.*, 2003). Para o treino do modelo de rede neural, foram ainda incorporadas as coordenadas geográficas e a data de aquisição das imagens. O processo de treino encontra-se detalhado em Santos *et al.* (2025).

Para testar diferentes configurações da regressão linear em distintos ambientes, os dados dos LHs foram agrupados por regiões (Tabela I), por intervalos de profundidade e por combinações das bandas espectrais. Esta abordagem permitiu otimizar os modelos e selecionar os parâmetros que apresentaram os melhores resultados (Tabela II).

Tabela I. Regiões definidas na determinação dos parâmetros da regressão linear do modelo de Stumpf.

Regiões	LHs
Porto	Antigo Cais + Canal In
Inlet	Marina + TEPORSET
Barra	Barra + Outão

Os parâmetros das regressões lineares deram origem a 9 superfícies SDB. O modelo NN deu origem a mais 9 SDBs.

Estes SDBs foram validados com os dados batimétricos (MBES, feixe simples e ICESAT-2). Permitindo um panorama geral da qualidade dos resultados através da análise aos coeficientes de correlação (R^2) e aos resíduos obtidos. A fiada de feixe simples da APA e os dados do ICESAT-2 permitiram visualizar a dispersão dos resultados.

Quanto ao processamento dos dados do ICESAT-2, concentrou-se nos feixes fortes (GT2L), que garantem maior número de retornos de fotões e melhor qualidade do sinal. A correção da refração foi aplicada, com base na Lei de Snell, para compensar os desvios provocados na interface ar-água. A referência altimétrica foi ajustada ao geoide EGM08, assegurando medições de profundidade consistentes e precisas (Santos *et al.*, 2025).

Tabela II. Definição das parametrizações A, B e C para cada imagem: o rácio das duas bandas espectrais, a profundidade máxima dos dados de calibração em metros (Prof), a região dos dadas utilizados na calibração.

	04/05/2021			04/04/2021			15/03/2021		
	Rácio	Prof.	Regiões	Rácio	Prof.	Regiões	Rácio	Prof.	Regiões
A	B3/B2	8	Porto + inlet	B3/B2	20	Barra	B3/B4	10	Todas
B	B3/B2	20	Barra	B3/B1	20	Barra	B3/B2	10	Barra
C	B3/B4	20	Barra	B3/B4	20	Barra	B3/B2	10	Barra

3. RESULTADOS

Os melhores resultados foram obtidos com as parametrizações A e B (Tabela II) para a imagem de 04/05/2021, utilizando o rácio entre as bandas B3/B2, com dados de calibração provenientes das regiões Porto+Inlet e Barra, até às profundidades de -8 m e -20 m, respetivamente. A parametrização C destacou-se para a imagem de 04/04/2021, com o rácio B3/B4 e calibração baseada exclusivamente na região da Barra até aos -20 m. Já para a imagem de 15/03/2021, as parametrizações B e A, ambas com o rácio B3/B2, apresentaram os melhores desempenhos quando calibradas com dados da região da Barra e, no caso da parametrização A, incluindo todas as regiões até às profundidades de -10 m e -16 m. A análise revelou que as melhores correlações entre os resultados SDB e os dados acústicos foram obtidas quando se utilizaram dados da região da Barra, em particular com o rácio entre as bandas espectrais B3/B2.

Para a imagem de 04/05/2021, os resíduos foram analisados por intervalos de profundidade de 1 m. Na região da Barra, a média e o desvio padrão dos resíduos revelam que as parametrizações B e C apresentam desempenhos semelhantes. Verifica-se um aumento gradual dos resíduos médios até à profundidade de -8,5 m, com os resíduos a variar entre -1 e -2 m. A partir dessa profundidade, o gradiente aumenta, com os resíduos a tornarem-se progressivamente mais significativos, atingindo valores entre -2 e -8 m até à profundidade máxima de -20 m. Este comportamento está associado com a perda de correlação entre os resultados SDB e os dados observados (Esta é a definição da profundidade de corte, onde o sensor multiespectral do satélite deixa de ser capaz de registar a radiação solar refletida pelo fundo marinho). Por outro lado, para a parametrização A, os resíduos mantêm-se próximos de zero até cerca dos -10 m de profundidade.

No que concerne, aos R^2, estes variaram entre 0.51 e 0.95, considerando todas as parametrizações.

Os resultados obtidos pelo modelo de NN revelam consistência nas estimativas ao longo das profundidades de validação. A análise da correlação e dos resíduos médios, agrupados em intervalos de profundidade de 1 m, evidencia variações significativas no desempenho do modelo entre as diferentes regiões estudadas. Essas diferenças resultam principalmente da variação da turbidez da água, sendo esta mais acentuada no interior do estuário, onde a profundidade máxima detetável pelo sensor do satélite é de aproximadamente -4 m, enquanto na região da Barra esta profundidade atinge cerca de -7 m.

A região da Barra apresentou os melhores resultados, com R^2 elevados, entre 0.81 e 0.95, e resíduos médios próximos de zero ao longo de toda a gama de profundidades analisada. Nas regiões estuarinas interiores, observou-se uma redução acentuada no desempenho do modelo. Os valores de R^2 nestas zonas foram baixos a moderados, não ultrapassando 0.58, e os resíduos médios revelaram um padrão de subestimação sistemática.

3.1. Comparação com os dados da APA

De uma forma simples e independente dos dados de calibração e treino dos modelos, pode-se observar as diferenças entre os resultados do modelo de *Stumpf* e NN com os dados batimétricos da APA e ICESAT-2 na região de Tróia (Figura 1). Na Figura 2 (na imagem superior) é notória a coerência dos resultados do modelo NN ao longo do tempo.

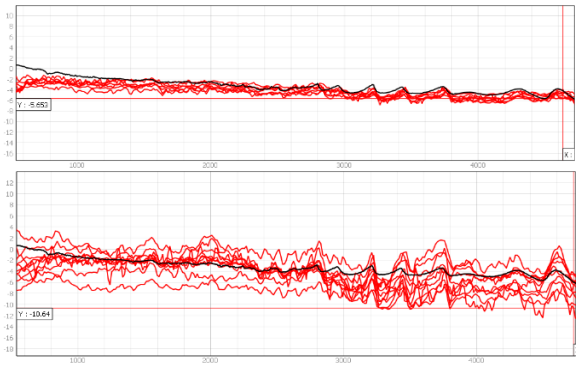

Figura 2. Na imagem em cima, estão representados a preto o perfil de feixe simples da APA, e a vermelho os perfis obtidos com o modelo NN. Em baixo, as linhas de cor vermelha representam os dados do modelo de Stumpf, ao longo do mesmo perfil da APA (a preto). Nas duas imagens, o eixo dos xx representa a distância ao longo do perfil (m) e eixo dos yy representa a profundidade (m).

Os resultados do modelo de Stumpf apresentam uma variação vertical superior, no entanto, algumas parametrizações foram otimizadas para outras regiões.

3.2. Comparação com os dados do ICESAT-2

Na Figura 3, estão os resultados de ambos os modelos NN e Stumpf, respetivamente, representados pelas linhas a vermelho, confrontados com a profundidade obtida com os dados do satélite ICESAT-2 (linha a preto). Os resultados do modelo NN apresentam mais ruído em comparação com a Figura 2, mas os resultados representam bem a forma do fundo e na sua generalidade são coerentes entre si. Quanto aos resultados do modelo de Stumpf, mais uma vez apresentam uma maior variação vertical, mas também representam bem a forma do fundo, apesar do desvio sistemático muito acentuado em algumas situações.

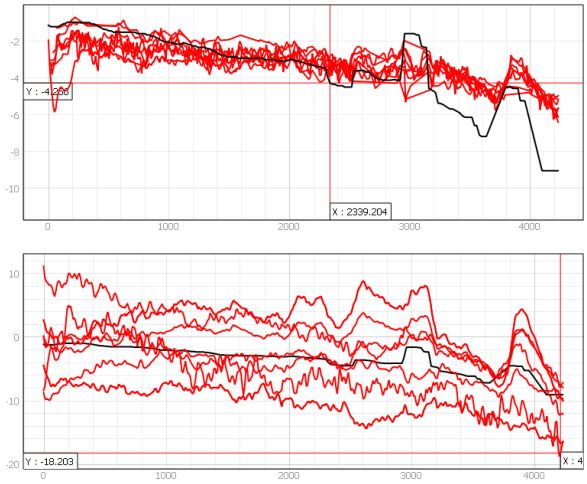

Figura 3. Na imagem do topo está a comparação entre os dados do ICESAT-2 (linha preta) e os resultados do modelo NN (linhas vermelhas). Em baixo, as linhas de cor vermelha representam os perfis do modelo de Stumpf em comparação com o mesmo perfil ICESAT-2. Nas duas imagens, o eixo dos xx representa a distância ao longo do perfil (m) e eixo dos yy representa a profundidade (m).

4. CONCLUSÃO

Os resultados obtidos evidenciam a dificuldade em estimar com precisão as profundidades em toda a área de estudo, devido às diferentes características físicas na coluna de água e à variabilidade da natureza do fundo marinho.

A combinação das bandas B3 e B2, no modelo de Stumpf, revelou-se ser a mais eficaz, mostrando bom desempenho tanto em áreas costeiras abertas como no interior do estuário, confirmando a sua robustez em contextos distintos.

A região da Barra destacou-se com os melhores resultados, possivelmente devido à menor turbidez e à maior qualidade ótica da coluna de água, tal como a maior densidade de dados nas maiores profundidades.

O modelo NN demonstrou um comportamento estável ao longo do tempo, com capacidade para fornecer estimativas de profundidade mais precisas, mesmo face à variação espacial e temporal de parâmetros como a turbidez. Mesmo quando foram obtidos SDBs com imagens fora do conjunto de dados de treino, o modelo foi coerente com os dados batimétricos de referência.

A validação com dados do satélite ICESAT-2 reforça o potencial da abordagem SDB, sobretudo em zonas onde não existem medições batimétricas *in-situ*, representando uma mais-valia em áreas remotas ou de difícil acesso.

Agradecimentos

Os autores agradecem, a disponibilidade dos dados Sentinel-2A e do *software* (SNAP – ESA, QGIS, Anaconda - Python), incluindo as diversas bibliotecas gratuitas utilizadas neste trabalho.

REFERÊNCIAS

Guerreiro, R. e Moura, A. (2016). A utilização de imagens de satélite multiespectrais de elevada resolução espacial para a derivação de batimetria. *Actas das 4ªs Jornada de Engenharia Hidrográfica,* pp.41-44.

Guerreiro, R. e Moura A. (2015) Aplicação de uma Metodologia de Derivação de Batimetria a partir de Imagens de Satélite. *VIII Conferência Nacional de Cartografia e Geodesia*, Lisboa.

Hedley, J. D., Harborne, A. R. e Mumby, P. J. (2005). Simple and robust removal of sun glint for mapping shallow-water benthos. *International Journal of Remote Sensing*, 26(10), 2107-2112.

Santos, R. e Quartau, R. (2023a). Capacidade de determinação da profundidade na região costeira através de modelo de Machine Learning e de série temporal de imagens PlanetScope. *X Conferência Nacional de Cartografia e Geodesia*.

Santos, R. e Quartau, R. (2023b). Impacto da parametrização do algoritmo Random Forest na determinação da profundidade na região costeira através de imagens PlanetScope. *X Conferência Nacional de Cartografia e Geodesia*.

Santos, R. e Quartau, R. (2024). Predicting bathymetry in shallow regions using a machine learning model and a time series of PlanetScope images. *EGU General Assembly 2024,* Vienna, Austria, EGU24-22165.

Santos, R., Quartau, R., Lamas, L., Cândido, R. e Pinto, J. P. Application of Neural Networks for Bathymetric Estimation Using a Short Time-Series of Sentinel-2. A Case Study: Setúbal-Troia, Portugal. Development and Training of the Neural Network Model. DOI: 10.2139/ssrn.5180220

Stumpf, R.P., Holderied, K. e Sinclair, M. (2003). Determination of water depth with high-resolution satellite imagery over variable bottom types. *Limnology and Oceanography*,48.

Vilar, P., Moura, A., Lamas, L., Guerreiro, R., e Pinto, J. P. (2018). Coastal water bathymetry retrieval using high-resolution remote sensing data. In: Remote Sensing of the Ocean, Sea Ice, Coastal Waters, and Large Water Regions 2018, vol. 10784. SPIE, pp. 46–63.

Reconstructing Environmental Quality in the Sado Estuary (Portugal): A Palaeoecological Record Based on Benthic Foraminifera

J. Moreno (1), F. Fatela (1,2), F. Moreno (1), E. Leorri (3), M. Leira (4), M. C. Freitas (1,2) and P. Masqué (5)

(1) Instituto Dom Luiz (IDL), Faculdade de Ciências, Universidade de Lisboa, 1749-016 Lisboa, Portugal. jcmoreno@fc.ul.pt
(2) Departamento de Geologia, Faculdade de Ciências, Universidade de Lisboa, 1749-016 Lisboa, Portugal
(3) Department of Geological Sciences, East Carolina University, Greenville, NC, 27858-4353, USA
(4) Departamento de Bioloxía, Universidade da Coruña, Campus da Zapateira, 15071 A Coruña, Spain
(5) School of Science and Centre for Marine Ecosystems Research, Edith Cowan University, Joondalup, Western Australia 6027, Australia

Abstract: The Sado estuary, a major Portuguese port and industrial hub, has experienced important ecological changes in recent decades from human activity. This study adopts a palaeoecological approach, using benthic foraminiferal assemblages and three associated indices – Exp(H'_{bc}), EQR, and the A–E index – to reconstruct past ecological quality status (Palaeo-EcoQS) from a dated sediment core. Results reveal a consistent pattern: periods of economic recession (e.g., 1973–78, 1983–84, 1992–93, 2002–03) aligned with temporary improvements in ecological quality, while economic growth (e.g., 1985, 1994, 2007–08) corresponded to "Moderate" to "Poor" Palaeo-EcoQS. Port expansion and dredging, namely in 1985 and 1994, increased sediment resuspension and metal remobilization/contamination, favouring stress-tolerant species (e.g., *Ammonia tepida* morphogroup and *Haynesina germanica*). Despite the inherent challenges of assessing EcoQS in transitional waters, these findings underscore the value of bioindicator-based metrics applied to sedimentary archives in revealing long-term ecosystem responses and supporting sustainable estuarine management.

Keywords: *Palaeoecological reconstruction, Benthic foraminifera, Foraminiferal-based indices, Socio-economic cycles, Estuarine ecosystems*

1. INTRODUCTION

The Sado estuary, located in southwest Portugal (Figure 1), is a key socio-ecological system that is subject to multiple anthropogenic pressures (e.g., Caeiro *et al*., 2005; Freitas *et al*., 2008). A wide range of industrial, agricultural, and port-related (Port of Setúbal) activities – including fertilizer and pesticide manufacturing, metalworking, ship repair, intensive rice cultivation, aquaculture, and routine dredging – have contributed significantly to contaminant and pollutant inputs, as well as to alterations in the estuary's hydrodynamic conditions. Understanding the long-term ecological consequences of these pressures is essential for informing effective management and conservation strategies.

A major challenge in assessing ecological conditions in transitional waters (TWs), such as estuaries, is the difficulty of distinguishing anthropogenically induced ecological changes from those driven by natural environmental variability – a phenomenon referred to as the *Estuarine Quality Paradox* (Dauvin, 2007; Elliott and Quintino, 2007). In this context, the present study reconstructs the Palaeo-ecological quality status (Palaeo-EcoQS) of the Sado estuary over the past five decades, based on analyses of total benthic foraminiferal assemblages. It further investigates how changes in ecological quality parallel historical trends in Portuguese economic activity, characterized by alternating phases of economic expansion (growth or boom) and contraction (recession or downturn), reflecting the broader business cycle.

Figure 1. Location of the Sado estuary in the SW coast of Portugal and the CLIM_A2 core.

2. MATERIALS AND METHODS

An 86 cm sediment core (CLIM_A2; Figure 1) was collected from the Sado estuary in June 2019 and examined for benthic foraminiferal species

composition. To reconstruct the Palaeo-EcoQS, three indices were applied: (i) the Exp(H'$_{bc}$) index, based on benthic foraminiferal diversity (Hill, 1973; Chao and Shen, 2003); (ii) the Ecological Quality Ratio (EQR), which quantifies deviation from reference conditions; and (iii) the *Ammonia–Elphidium* (A–E) index, a well-established indicator of palaeo-hypoxia in water depths shallower than 30 m (Platon and Sen Gupta, 2001).

The A–E index was calculated according to Sen Gupta *et al*. (1996) and Sen Gupta and Platon (2006) using the following formula:

A–E index = [NA / (NA + NE)] × 100

where NA is the relative abundance (%) of the *Ammonia tepida* morphogroup, and NE is the relative abundance (%) of *Cribroelphidium* species (*C. gunteri*, *C. excavatum*, and *C. williamsoni*) in each sample.

The EQR is defined as the ratio between the observed value of a biological parameter for a given water body and its expected value under reference conditions (Van de Bund and Solimini, 2007). This ratio ranges from 0 to 1, with values close to 1 indicating high ecological status, and values near 0 reflecting bad ecological conditions. In this study, the EQR was calculated as follows:

$$EQR = Exp(H'_{bc})_{observed\ value} / Exp(H'_{bc})_{reference\ value}$$

Since the CLIM_A2 sediment core does not extend back to the pre-industrial period, the highest Exp(H'$_{bc}$) value recorded within the core (16.36, corresponding to "High" ecological status) was used to establish local reference conditions. Palaeo-EcoQS was then classified according to the Exp(H'$_{bc}$)-based thresholds proposed by Bouchet *et al*. (2018), with EQR class boundaries adapted from de Jesus *et al*. (2020) (Table I).

Table I. Criteria adopted to define the Palaeo-EcoQS based on Exp(H'$_{bc}$) and EQR values.

Indices/Palaeo-EcoQS	High	Good	Moderate	Poor	Bad
Exp(H'$_{bc}$)	> 15	11–15	7–11	3–7	< 3
EQR	> 0.9	0.7–0.9	0.5–0.7	0.25–0.5	< 0.25

To explore the relationship between ecological trends and human influence, reconstructed Palaeo-EcoQS patterns were compared with phases of Portuguese economic activity documented by Aguiar-Conraria *et al*. (2024), as well as with major industrial and infrastructural developments in the Sado estuary.

Additionally, sediment grain size and total organic matter (TOM) content were analysed to provide further insight into prevailing environmental conditions and depositional settings (Moreno *et al*., 2025, and references therein).

The core was dated using ^{137}Cs gamma spectrometry and ^{210}Pb (via ^{210}Po alpha spectrometry; Sanchez-Cabeza *et al*., 1998). A CF-CS model based on changes of activity concentrations of unsupported Pb or in excess (^{210}Pbex) was employed (e.g., Krishnaswamy *et al*., 1971).

3. RESULTS AND DISCUSSION

A total of 114 benthic foraminiferal species and genera were identified along the CLIM_A2 core (Moreno *et al*., 2025). The assemblages were dominated by the *A. tepida* morphogroup (29–62%), accompanied by *Haynesina germanica* (4–27%), *C. gunteri* (2–17%), *Ammonia parkinsoniana* (2–26%), *Porosononion granosum* (1–16%), and *Ammonia beccarii* (0–13%).

Grain-size analysis revealed that 94% of the CLIM_A2 samples consisted of silt and clay, while the sand content at the base ranged from 100% to 40% (early to mid-1970s and mid-1980s). The core samples presented high TOM contents, ranging from 7% to 11%. Overall, TOM generally increased from the base to the top of the core, with the highest value recorded around AD 2017. The main peaks in TOM, which is recognized as a common stressor in TWs, occurred in AD 2006, AD 2009/10, and AD 2016/17, coinciding with periods classified as having a "Poor" Palaeo-EcoQS.

Palaeo-EcoQS indices derived from the foraminiferal assemblages show Exp(H'$_{bc}$) values ranging from 5.24 to 16.36, and EQR values from 0.32 to 1. These span four ecological status classes, from "Poor" to "High" (Table I). The co-occurrence of the *A. tepida* morphogroup, *H. germanica*, *C. gunteri*, *J. macrescens*, and increased abundances of *Quinqueloculina* spp. and *Bolivina* spp. between AD 1972 ± 6.4 and AD 1983 ± 5.4 suggests less brackish conditions at the base of the core. This interval also showed slightly lower TOM and reduced oxygen stress (A–E index), marking the best ecological quality based on both Exp(H'$_{bc}$) and EQR, with "Good" to "High" Palaeo-EcoQS. A peak "High" status was recorded around AD 1981–1983, declining to "Moderate" by AD 1986. A recovery to "Good" occurred in AD 1989, and the last "High" status was observed in AD 2002 ± 4.4.

Between AD 1994 ± 4.6 and AD 1999 ± 4.4, both indices consistently indicated a "Poor" ecological status, marking the most degraded conditions in the record. This period was characterized by a higher abundance of brackish foraminifera and increased palaeo-hypoxia. Post-2003, ecological conditions fluctuated between "Moderate" and "Poor", with multiple "Poor" episodes (e.g., AD 2004–2005, 2006–2008, 2010, 2013, and 2015–2017) corresponding with peaks in brackish species dominance and lower levels of oxygen. Despite occasional classifications as

"Moderate", the upper core indicates a long-term decline in ecological quality, with EQR results showing a transition from "Good"/"High" in the early 1980s to predominantly "Moderate"/"Poor" conditions in recent decades.

Fluctuations in Portuguese economic cycles closely correlate with changes in the foraminifera-based Palaeo-EcoQS of the Sado Estuary. Recession periods – specifically 1973–1978, 1983–84, 1992–93, and 2002–03 – generally coincide with "Good" to "High" Palaeo-EcoQS in the CLIM_A2 core. These downturns, triggered by events such as the 1973 oil crisis, the 1974–75 political transition, the 1976–78 balance of payments crisis, International Monetary Fund (IMF) interventions, and international financial instability (e.g., the Gulf War and European Exchange Rate Mechanism (ERM) disruptions, often led to reduced industrial output (Aguiar-Conraria *et al*., 2024), aligning with periods of ecological improvement (Table II).

Table II. Summary of periods of economic growth and downturn, as defined by Aguiar-Conraria et al. (2024), alongside the corresponding Palaeo-EcoQS observed in the CLIM_A2 sediment core from the Sado estuary, based on the Exp(H'$_{bc}$) and EQR indices.

Period	Economic Phase	Key Economic/Industrial Events	Palaeo-EcoQS
2016	Economic growth	Continued industrial activity, port dredging	Poor
2013	Economic recovery		Poor
2010–2013	Economic downturn	Sovereign debt crisis, longest recession since 1980	Moderate
2010	Short economic recovery		Poor
2008–2009	Economic downturn	Great financial crisis	Moderate
2005, 2007–2008	Economic growth	Industrial production increase	Poor
2002–2003	Economic downturn	Public deficit adjustment, decreased investments	High
1994	Economic recovery	Autoeuropa plant established, increased port activity, Port deepening and dredging	Poor
1992–1993	Economic downturn	Gulf War, German reunification, European Exchange Rate Mechanism (ERM) instability	Good
1985	Economic growth	Port deepening and dredging, Multiuse Platform built	Moderate
1983–1984	Economic downturn	Delayed adjustment to 1979 oil price crisis, International Monetary Fund (IMF) intervention	High
1973–1979	Economic downturn	Oil crisis (1973), Political crisis (1974–75), Balance of payments crisis (1976–78), Global recession oil crisis (1979)	Good

In contrast, periods of economic expansion and peak activity – such as in 1985, 1994, 2005, 2007–08, 2010, 2013, and 2016 – correspond to "Moderate" to "Poor" ecological status (Table II). These declines appear to be linked to intensified industrial activity as well as major dredging campaigns (in 1985, 1994), which, despite improving water circulation, likely exacerbated environmental stress. Dredging led to the resuspension of fine sediments rich in TOM and metal(loid)s, facilitating their remobilization and increasing their bioavailability (e.g., Moreira *et al*., 2009), which in turn contributed to ecological degradation.

Although metal(loid) data from the core are absent, the incidence of stress-tolerant species (e.g., *H. germanica*, *C. gunteri*, the *A. tepida* morphogroup, and *C. excavatum*) – taxa known to be associated with metal(loid) contamination in the Sado estuary (Moreno *et al*., 2025) and in other contaminated or polluted environments worldwide (e.g., Coccioni, 2000; Armynot du Châtelet *et al*., 2004; Ferraro *et al*., 2006; Frontalini *et al*., 2009; Francescangeli *et al*., 2016; Dimiza *et al*., 2022; El-Kahawy and Mabrouk, 2023) – supports this interpretation.

Recognizing inherent limitations, including the lack of pre-industrial baseline data, the application of Exp(H'$_{bc}$) and EQR indices calculated from foraminiferal assemblages successfully correlated with historical ecological variations. The Palaeo-EcoQS record reflects fifty years of economic activity and industrial development in the Setúbal region, emphasizing the vulnerability of estuarine ecosystems to human-related disturbances. These findings demonstrate that foraminifera-based indices can be very useful tools for reconstructing long-term environmental changes in transitional settings.

4. CONCLUSION

This study highlights the effectiveness of benthic foraminiferal assemblages and resulting biotic indices in reconstructing the ecological quality of TWs, exemplified by the Sado estuary over the past five decades. The reconstructed Palaeo-EcoQS reveals a clear correspondence with socio-economic cycles, where periods of economic recession tend to coincide with improved ecological status, whereas phases of economic expansion overlap with increased environmental degradation driven by industrial and infrastructural activities. Although distinguishing naturally induced stress from anthropogenic impacts remains challenging in TWs, this palaeoecological approach offers valuable insights for the sustainable management and preservation of the estuarine system, while also advancing interdisciplinary research for evaluating environmental health. Future work should focus on integrating contaminant data, such as metal(loid)s, polychlorinated biphenyls (PCBs), and polycyclic aromatic hydrocarbons (PAHs), and expanding temporal coverage to refine local reference conditions and enhance ecological assessments.

Acknowledgments

This research was supported by the CLIMARES (PTDC/CTA-GEO/28412/2017) and WestLog (PTDC/CTE/105370/2008) project. Funding was granted by the Fundação para a Ciência e a Tecnologia (FCT), I.P./MCTES through national funds (PIDDAC) under grants UID/50019/2025 and LA/P/0068/2020 (https://doi.org/10.54499/LA/P/0068/2020).

REFERENCES

Aguiar-Conraria, L., Bação, P., Horta Correia, I., Ferreira, J.A., Reis, R., Tavares, J., Valério, N. and Varejão, J. (2024). *Crises in the Portuguese Economy: From 1910 to 2022*. Fundação Francisco Manuel dos Santos, Lisboa, 231 p.

Armynot du Châtelet, E., Debenay, J.P. and Soulard, R. (2004). Foraminiferal proxies for pollution monitoring in moderately polluted harbours. *Environmental Pollution*, 127, 27–40.

Bouchet, V.M., Goberville, E. and Frontalini, F. (2018). Benthic foraminifera to assess Ecological Quality Statuses in Italian transitional waters. *Ecological Indicators*, 84, 130–139.

Caeiro, S., Costa, M.H., Ramos, T.B., Fernandes, F., Silveira, N., Coimbra, A., Medeiros, G. and Painho, M. (2005). Assessing heavy metal contamination in Sado Estuary sediment: An index analysis approach. *Ecological Indicators*, 5, 151–169.

Chao, A. and Shen, T.-J. (2003). Nonparametric estimation of Shannon's index of diversity when there are unseen species in sample. *Environmental and Ecological Statistics*, 10, 429–443.

Coccioni, R. (2000). Benthic foraminifera as bioindicators of heavy metal pollution – a case study from the Goro Lagoon (Italy). In: Martin, R.E. (ed.), *Environmental Micropaleontology: The Application of Microfossils to Environmental Geology*. Kluwer Academic/Plenum Publishers, New York, pp. 71–103.

Dauvin, J.C. (2007). Paradox of estuarine quality: benthic indicators and indices, consensus or debate for the future. *Marine Pollution Bulletin*, 55, 271–281.

de Jesus, M.S.S., Frontalini, F., Bouchet, V.M.P., Yamashita, C., Sartoretto, J.R.,Figueira, R.C.L. and de Mello e Sousa, S.H. (2020). Reconstruction of the palaeo-ecological quality status in an impacted estuary using benthic foraminifera: the Santos Estuary (São Paulo state, SE Brazil). *Marine Environmental Research*, 162, 105121.

Dimiza, M.D., Triantaphyllou, M.V., Portela, M., Koukousioura, O. and Karageorgis, A.P. (2022). Response of living benthic foraminifera to anthropogenic pollution and metal concentrations in Saronikos Gulf (Greece, Eastern Mediterranean). *Minerals*, 12, 591.

El-Kahawy, R.M. and Mabrouk, M.S. (2023). Benthic foraminifera as bioindicators for the heavy metals in the severely polluted Hurghada Bay, Red Sea coast, Egypt. *Environmental Science and Pollution Research*, 30, 70437–70457.

Elliott, M. and Quintino, V. (2007). The estuarine quality paradox, environmental homeostasis and the difficulty of detecting anthropogenic stress in naturally stressed areas. *Marine Pollution Bulletin*, 54, 640–645.

Ferraro, L., Sprovieri, M., Alberico, I., Lirer, F., Prevedello, L. and Marsella, E. (2006). Benthic foraminifera and heavy metals distribution: a case study from the Naples Harbour (Tyrrhenian Sea, Southern Italy). *Environmental Pollution*, 142, 274–287.

Francescangeli, F., Du Châtelet, E.A., Billon, G., Trentesaux, A. and Bouchet, V.M.P. (2016). Palaeo-ecological quality status based on foraminifera of Boulogne-sur-Mer harbour (Pas-de-Calais, Northeastern France) over the last 200 years. *Marine Environmental Research*, 117, 32–43.

Freitas, M.C., Andrade, C., Cruces, A., Munhá, J., Sousa, M.J., Moreira, S., Jouanneau, J.M. and Martins, L. (2008). Anthropogenic influence in the Sado estuary (Portugal): a geochemical approach. *Journal of Iberian Geology*, 34, 271–286.

Frontalini, F., Buosi, C., Da Pelo, S., Coccioni, R., Cherchi, A. and Bucci, C. (2009). Benthic foraminifera as bio-indicators of trace element pollution in the heavily contaminated Santa Gilla lagoon (Cagliari, Italy). *Marine Pollution Bulletin*, 58, 858–877.

Hill, M.O. (1973). Diversity and evenness: a unifying notation and its consequences. *Ecology*, 54, 427–432.

Krishnaswamy, S., Lal, D., Martin, J. M. and Meybeck, M. (1971). Geochronology of lake sediments. *Earth and Planetary Science Letters*, 11, 407–414.

Moreira, S., Freitas, F.C., Araújo, M.F., Andrade, C., Munhá, J., Fatela. F. and Cruces, A. (2009). Contamination of intertidal sediments – The case of Sado estuary (Portugal). *Journal of Coastal Research*, SI56, 1380–1384.

Moreno, J., Moreno, F., Fatela, F., Leorri, E., Leira, M., Masqué, P. and Freitas, M.C. (2025). Patterns of ecological quality in Portuguese transitional waters over the last five decades: a framework based on benthic foraminifera for the Sado estuary. *Marine Pollution Bulletin*, 218, 118215.

Platon, E. and Sen Gupta, B.K. (2001). Foraminiferal Communities of Oxygen-Stressed Environments on the Louisiana Continental Shelf. In: Rabalais Gupta, N.N., Turner, R.E., (eds.), *Coastal Hypoxia: Consequences for Living Resources and Ecosystems*. American Geophysical Union Coastal and Estuarine Studies, 58. American Geophysical Union, Washington, pp. 147–163.

Sanchez-Cabeza, J.A., Masqué, P. and Ani-Ragolta, I. (1998). ^{210}Pb and ^{210}Po analysis in sediments and soils by microwave acid digestion. *Journal of Radioanalytical and Nuclear Chemistry*, 227, 19–22.

Sen Gupta, B.K., Turner, R.E. and Rabalais, N.N. (1996). Seasonal oxygen depletion in continental-shelf waters of Louisiana: historical record of benthic foraminifers. *Geology*, 24, 227–230.

Sen Gupta, B.K. and Platon, E. (2006). Tracking past sedimentary records of oxygen depletion in coastal waters: use of the *Ammonia-Elphidium* foraminiferal index. *Journal of Coastal Research*, SI39, 1351–1355.

Van de Bund, W. and Solimini, A. (2007). *Ecological Quality Ratios for Ecological Quality Assessment in Inland and Marine Waters*. European Commission Reports, 23 p.

Beyond the Label: Do Coastal NbS Fulfill the Scope of EC and IUCN Definitions?

P. Pires da Rocha (1), T. Plomaritis (2) and S. Costas (1)

(1) Centre for Marine and Environmental Research (CIMA), University of Algarve, Campus de Gambelas, 8005-139 Faro, Portugal. pfrocha@ualg.pt

(2) Instituto Universitario de Investigación Marina, (INMAR), Campus Rio San Pedro (CASEM), Puerto Real 11510, Cádiz, Spain.

Abstract: Sandy coastal systems are increasingly threatened by erosion, driven by both local human activities and global climate change. While traditional grey infrastructure has been used for coastal protection, it often leads to negative long-term impacts. Nature-Based Solutions (NbS) have emerged as an alternative, promising ecological, social, and economic benefits. However, inconsistent definitions and misuse of the term raise concerns about the effectiveness and authenticity of many NbS implementations. This study conducted a literature review of 60 peer-reviewed manuscripts (2015–2025) to evaluate how well proposed NbS align with core principles outlined by the International Union for Conservation of Nature and the European Commission. Results show that while most projects target hazards like flooding and erosion, fewer address sustainability, cost-effectiveness, or resilience in measurable ways. We highlight the need for a clear evaluative framework and emphasize the importance of involving local communities in the development and implementation of NbS for truly sustainable coastal management.

Keywords: *Nature-Based Solutions, Literature Review, Erosion, Sea-level rise, Flooding*

1. INTRODUCTION

Coastal systems are currently under significant threat due to a combination of local and global pressures (Bozzeda *et al*., 2023). Locally, human activities such as beach sediment removal, beach grooming, and removal and constructions on dune play a major role. Additionally, inland activities like, dam construction and mining may also disrupt sediment supply to coastal zones (Defeo *et al*., 2009; Mclachlan *et al*., 2013). On a global scale, climate change exacerbates these issues, primarily through drought, sea-level rise and increased storm surges (Bozzeda *et al*., 2023; Leatherman *et al*., 2000).

Traditionally, coastal protection has relied on grey infrastructure solutions such as groynes, seawalls, sloping structures, and offshore barriers (Morris *et al*., 2024; Zanin *et al*., 2024). However, these conventional defenses often have negative long-term impacts, including disruption of sediment transport, ecosystem damage, alterations to local hydrodynamics, aesthetic degradation, and high implementation and maintenance costs (Morris *et al*., 2024).

To address coastal protection challenges, the concept of Nature-Based Solutions (NbS) has emerged over the past decade as a promising alternative. NbSs are proposed to offer not only protection but also a range of co-benefits for both society and the environment (Mortensen *et al.*, 2024). NbSs are often described as cost-effective, adaptive and long-term strategies that enhance resilience in coastal systems, for instance in the face of sea-level rise (Nehren *et al*., 2023).

Despite their potential, confusion and inconsistency remains regarding what qualifies as an NbS. Differing definitions can lead to misinterpretations and flawed implementations (Cohen-Shacham *et al*., 2019). The definitional differences (e.g. IUCN (International Union for Conservation of Nature) tending for environmental conservation and EC (European Commission) for development and infrastructure planning), can result in misguided project planning and implementation—an issue that motivates the current study.

To identify how coastal NbSs are understood, an in-depth analysis of the IUCN and EC definitions was performed based on an extensive literature review.

2. APPROACH

The review was based on a search conducted using the Scopus search engine to identify peer-reviewed manuscripts. The search utilized the TITLE-ABS-KEY (title, abstract, keywords) and "All" search mechanisms, with the query: "Nature Based Solutions and Coastal and Dunes." This search was completed on the 26th of February 2025, retrieving a total of 198 manuscripts published between 2015 and 2025. After excluding non-English documents (to avoid misinterpretation and mistranslation), review papers, editorials, conference abstracts, and errata, 156 manuscripts remained for full analysis. Preliminary results are presented here based on the analysis of the

first 60 manuscripts, sorted in alphabetically by author.

The analysis was structured around two sets of questions (Table I)—hereafter referred to as criteria — derived from the definitions provided by the IUCN and the EC. The exercise consisted of evaluating if the selected manuscripts were aligned or answering the defined criteria. For that, we first quantified how many of the criteria were addressed by each manuscript by converting the qualitative responses identified from the manuscripts into a binary matrix, where a value of 1 indicated the criteria were addressed and 0 indicated the opposite. Then, qualitative manuscript answers were examined in detail through a coding analysis. In this phase, one or more keywords were identified for each answered question and grouped into codes. For example, keywords such as “flood”, “flooding”, “inundation”, and “overtopping” were consolidated under the code “flooding”. It is important to note that some manuscripts propose solutions that address more than one hazard, including multiple codes; for example, wave energy, erosion and flooding.

Table I. Questions addressed based on the IUCN and EC NbS definitions.

Definitions	Questions								
IUCN	What kind of protection the NbS provides?	Is there a sustainable environmental managing?	Is for restoration or modification of the environment?	Which societal challenges are addressed?	Which are the biodiversity benefits?	Which are the human well-being benefits?			
EC	How does NbS helps society?	How does NbS helps the environment?	Which are the challenges addressed? (economic, societal environmental)	How is sustainability approached?	How is measured if it is sustainable/cost-effective?	What nature aspect does NbS mimic?	Does the NbS uses the nature? (yes/no)	What is understood by resilience?	Are they new or already existent solutions?

3. RESULTS AND DISCUSSION

Regarding the IUCN definition, none of the criteria were answered by all the manuscripts. From the six criteria, four were addressed by more than 70% of the manuscripts, while two were addressed by fewer than 45%.

The EC definition-based criteria were also not answered by all manuscripts. Five criteria were answered by more than 80% of the manuscripts, two by less than 40%, and one by 65%. Notably, aspects related to sustainability, resilience, and cost-effectiveness were among the least addressed in both sets of criteria. This raises concerns about whether the proposed NbS in these studies truly align with the core principles outlined in the definitions of NbS, suggesting a potential mismatch between theoretical definitions and practical implementations.

Regarding the coding analysis based on the IUCN definition, most of the analysed manuscripts proposed solutions aimed at addressing flooding, erosion, and general coastal protection (Figure 1A). It is important to note that the coastal protection code—used for both the IUCN and EC criteria—encompasses a broad range of undefined or loosely defined protection types. These often involve vague terms such as "mitigating natural hazards" or "addressing climate change-induced hazards." When examining the criterion related to sustainable management, only a small portion of manuscripts (31.6%) addressed this aspect. Among those, the most frequently identified codes were collaborative approaches and monitoring (Figure 1B), which were interpreted as key elements of sustainable management. However, 8.3% manuscripts described sustainable management merely as a stakeholder perception, lacking clear implementation or evidence.

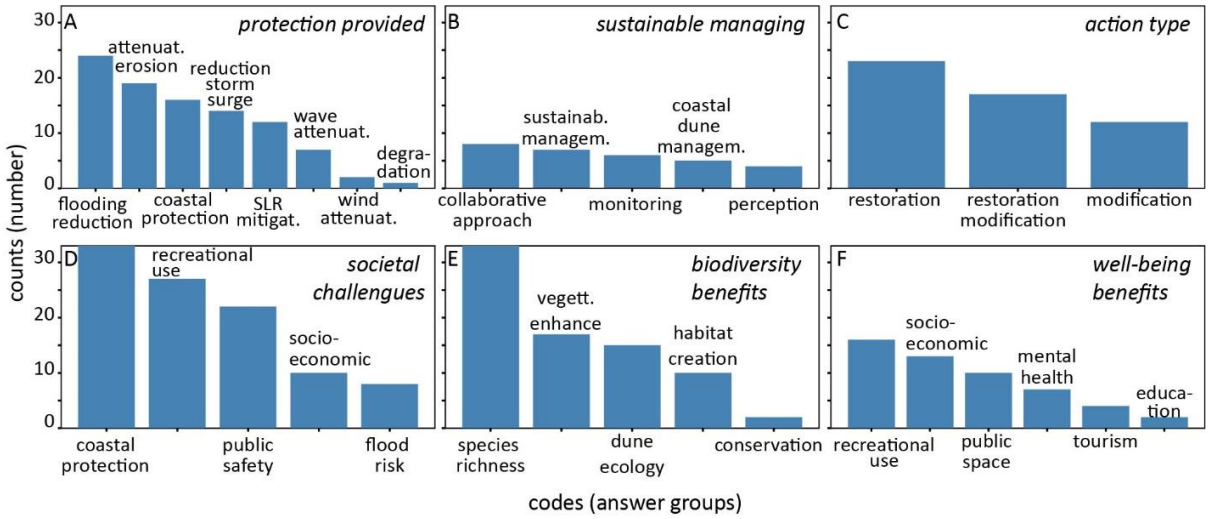

Figure 1. IUCN codes addressed by the analysed manuscripts.

In terms of the nature of interventions (Figure 1C), most manuscripts classified their solutions as environmental restoration or a hybrid approach, combining restoration and modification.

The most addressed societal challenges were related to the safety of coastal communities and the protection of coastal assets (Figure 1D). As for human well-being, most proposed solutions emphasized recreational use and socioeconomic benefits, such as the development of local economies and the preservation of traditional cultural and economic practices. Some manuscripts also highlighted mental health benefits, citing aesthetic improvements and the creation of spaces for activities such as meditation and relaxation (Figure 1F).

Biodiversity benefits were frequently mentioned, typically described as increases in species richness, re-vegetation efforts and the construction or restoration of coastal dune systems (Figure 1E).

The coding of the manuscripts based on the European Commission (EC) definition produced results that were broadly similar to under the IUCN criteria, particularly in terms of how the proposed NbS aims to benefit society (Figure 2A). Most solutions focused on protecting coastal areas from climate change-induced hazards, flooding and erosion. Environmental benefits were most frequently described in terms of increased biodiversity and the preservation of natural systems (Figure 2B). Regarding the societal challenges addressed, many manuscripts tackled economic, social, and environmental issues. However, when specifically examining how sustainability and cost-effectiveness were approached, only 6.6% manuscripts provided clear responses.

Sustainable management (Figure 2 D) was mentioned in 21.6% of the manuscripts often in reference to solutions implemented under the Natura 2000 network in Europe. In contrast, 13.3% of the manuscripts proposed a more holistic approach to sustainability, emphasizing the importance of collaborative implementation strategies. These included involving communities in the decision-making process and prioritizing bottom-up approaches for greater success and legitimacy.

Most of the analysed manuscripts described their proposed solutions as mimicking natural processes (Figure 2F); especially dunes and sediment transport mechanisms, whether driven by wind or currents. While many claimed to use nature in their solutions, in some cases, "nature" was interpreted loosely. For example, natural materials like cobbles were used to construct artificial beaches, or sand was used to build entirely new dunes, suggesting a hybrid or engineered interpretation of nature-based practices.

In terms of resilience, most manuscripts referred to it in general terms, either by defining what resilience means or by claiming that the proposed solutions were adaptable to climate change or capable of recovering from storm events (Figure 2E). However, among the 40% of the manuscripts that addressed the concept, none offered concrete methods or metrics to assess how resilience would be achieved or evaluated in practice. An important consideration is the adaptability of dunes, frequently cited as resilient systems. While manuscripts in the present analysis claimed that dunes can adapt to climate change, it is known that due to limited accommodation space caused by coastal development, dunes often lose the ability to adapt effectively (Feagin *et al*., 2015; Cooper *et al*., 2020; Davidson-Arnott and Bauer, 2021). Despite being labelled as NbS, that is a term recently applied, most of the proposed solutions were described as existent and not novel in general. Only seven manuscripts presented their solutions as novel. Some "existent" approaches included long-established

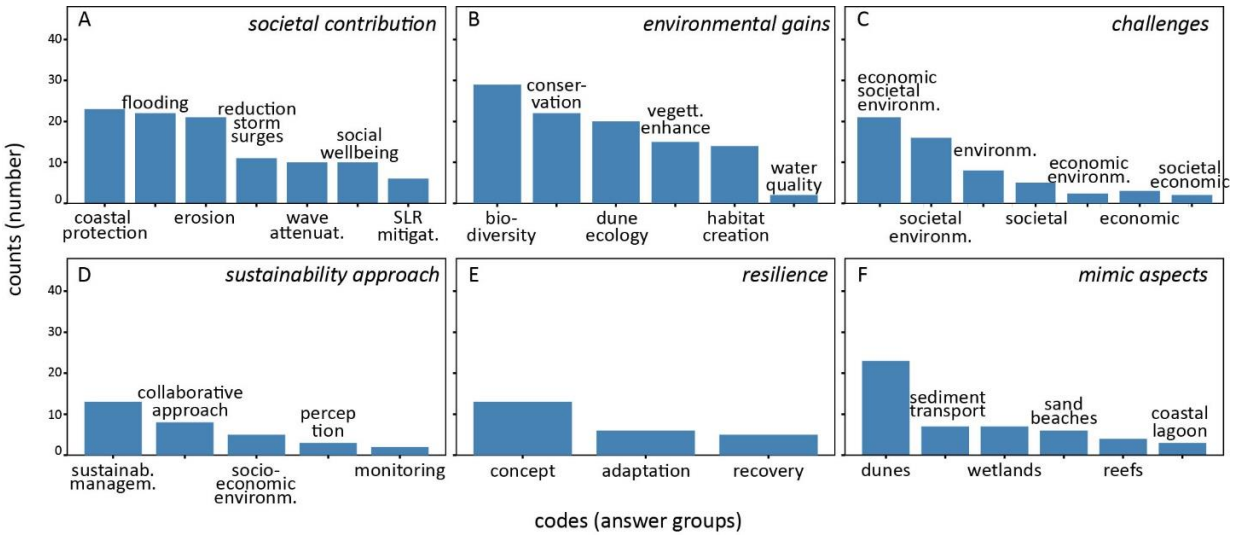

Figure 2. EC codes addressed by the analysed manuscripts.

practices like wetland restoration, which has been implemented, for instance, in Germany since the 18th century (Hofstede, 2024). Genuinely novel examples were either new modelling approaches to predict NbS performance (Kumar and Leonardi, 2024) or locally innovative applications, such as the use of Melaleuca in Vietnam to trap fine sediments and promote mangrove development (Nguyen, 2018).

4. CONCLUSIONS

Nature-Based Solutions (NbS) are increasingly being implemented for coastal protection, with a marked rise in the use of the term in coastal contexts since 2015. While this trend reflects a growing interest in alternatives to traditional grey infrastructure, it also highlights a persistent misunderstanding of what NbSs are fundamentally intended to achieve. This confusion could be from the lack of specific criteria for projects implementation and loose definitions across institutions or from the term becoming a buzzword, leading to inconsistent or superficial applications.

Our findings emphasize the need for a more critical and in-depth analysis of the true aims and principles of NbS. We recommend the development of a robust evaluative framework to assess all core aspects of NbS—ecological, social, economic, and technical—prior to project implementation. Additionally, it is worth of notice that some manuscripts recommend involving local coastal communities throughout the planning and implementation process using a bottom-up approach. Such approach is pinpointed as essential to ensure that NbS are context-specific, socially accepted, and aligned with local needs.

Acknowledgements

We would like to thank the Ph.D. Grant GA 101089757 SEA-EU 2.0, and the FCT funding UID/00350/2020 CIMA and LA/P/00069/2020.

REFERENCES

Bozzeda, F., Ortega, L., Costa, L. L., Fanini, L., Barboza, C. A., McLachlan, A., and Defeo, O. (2023). Global patterns in sandy beach erosion: unraveling the roles of anthropogenic, climatic and morphodynamic factors. *Frontiers in Marine Science*, 10, 1270490.

Cohen-Shacham, E., Andrade, A., Dalton, J., Dudley, N., Jones, M., Kumar, C., Maginnis, S., Maynard, S., Nelson, C, R., Renaud, F, G., Welling, R. and Walters, G. (2019). Core principles for successfully implementing and upscaling Nature-based Solutions. *Environmental Science & Policy*, 98, 20-29.

Cooper, J.A.G., Masselink, G., Coco, G., Short, A.D., Castelle, B., Rogers, K., Anthony, E., Green, A.N., Kelley, J.T., Pilkey, O.H. and Jackson, D. W. (2020). Sandy beaches can survive sea-level rise. *Nature Climate Change, 10*(11), 993-995.

Davidson-Arnott, R.G. and Bauer, B. O. (2021). Controls on the geomorphic response of beach-dune systems to water level rise. *Journal of Great Lakes Research, 47*(6), 1594-1612.

Defeo, O., McLachlan, A., Schoeman, D.S., Schlacher, T.A., Dugan, J., Jones, A., Lastra, M., Scapini, F. (2009). Threats to sandy beach ecosystems: a review. *Estuarine, Coastal and Shelf Science*, *8* (1), 1–12. https://doi.org/10.1016/j.ecss.2008.09.022

European Commission: European Research Executive Agency, Nature-based solutions – EU-funded NBS research projects tackle the climate and biodiversity crisis. (2024). *Publications Office of the European Union*. https://data.europa.eu/doi/10.2848/8542246

Feagin, R. A., Figlus, J., Zinnert, J. C., Sigren, J., Martínez, M. L., Silva, R., ... and Carter, G. (2015). Going with the flow or against the grain? The promise of vegetation for protecting beaches, dunes, and barrier islands from erosion. *Frontiers in Ecology and the Environment*, *13*(4), 203-210.

Hofstede, J. L. (2024). Status and prospects of nature-based solutions for coastal flood and erosion risk management in the Federal State of Schleswig–Holstein, Germany. *Journal of Coastal Conservation*, *28*(2), 40.

Kumar, P., and Leonardi, N. (2024). Exploring mega-nourishment interventions using Long Short-Term Memory (LSTM) models and the sand engine surface MATLAB framework. *Geophysical Research Letters*, *51*(4), e2023GL106042.

Leatherman, S. P., Zhang, K., and Douglas, B. C. (2000). Sea level rise shown to drive coastal erosion. *Eos, Transactions American Geophysical Union, 81*(6), 55-57.

McLachlan, A., Defeo, O., Jaramillo, E., and Short, A. D. (2013). Sandy beach conservation and recreation: guidelines for optimising management strategies for multi-purpose use. *Ocean & Coastal Management*, *71*, 256-268.

Morris, R. L., Campbell-Hooper, E., Waters, E., Bishop, M. J., Lovelock, C. E., Lowe, R. J., ... and Swearer, S. E. (2024). Current extent and future opportunities for living shorelines in Australia. *Science of the Total Environment*, *917*, 170363.

Mortensen, E., Tiggeloven, T., Kiesel, J., and Ward, P. J. (2024). For resilient rural shorelines: reviewing Nature-based Solutions for flood risk reduction in small coastal communities. *Nature-Based Solutions*, *6*, 100189.

Nehren, U., Arce-Mojica, T., Barrett, A. C., Cueto, J., Doswald, N., Janzen, S., ... and Walz, Y. (2023). Towards a typology of nature-based solutions for disaster risk reduction. *Nature-Based Solutions*, *3*, 100057.

Nguyen, T. P. (2018). Melaleuca entrapping microsites as a nature based solution to coastal erosion: A pilot study in Kien Giang, Vietnam. *Ocean & Coastal* Management, 155, 98-103.

Zanin, G. M., Muwafu, S. P., and Costa, M. M. (2024). Nature-based solutions for coastal risk management in the Mediterranean basin: A literature review. *Journal of Environmental Management*, 356, 120667.

Therapeutic potential of saline materials from the Portuguese Atlantic Coast

L. Almeida (1), F. Rocha (1) and C. Candeias (1)

(1) GeoBioTec, Department of Geosciences. University of Aveiro, Santiago Campus, 3810-193, Aveiro, Portugal. larasralmeida@ua.pt

Abstract: Natural materials, such as saline sediments and marine peloids, have been traditionally used for therapeutic purposes due to their mineral-rich composition and thermal properties. Electropelotherapy, an innovative technique combining pelotherapy with electrical stimulation, offers promising advances in physical rehabilitation and dermatological treatments by enhancing skin permeability and active substance delivery. The Portuguese Atlantic Coast, particularly the Ria de Aveiro and Ria Formosa regions, hosts diverse natural materials with significant but underexplored therapeutic potential. Recent studies demonstrated the safety, rheological properties, and clinical applicability of saline sediments and hypersaline waters from these areas. This review synthesizes current knowledge on pelotherapy, thalassotherapy, and electrotherapy, highlighting the integration of these methods in electropelotherapy. Emphasis is placed on the development of specialized devices and the need for further clinical research to optimize protocols. The unique geological settings of the Portuguese coast represent a valuable resource for advancing natural and electrotherapeutic treatments in modern healthcare.

Keywords: *Portuguese coast, saline materials, therapeutic potential, thalassotherapy, electrotherapy*

1. INTRODUCTION

Natural materials have long been employed in healthcare and well-being practices throughout human history (Gomes and Silva, 2007). Recent advances have brought renewed scientific interest to these resources, especially in the development of innovative approaches such as electropelotherapy, a technique that combines the application of peloids with electrical stimulation for use in physical rehabilitation and skin treatments (Bastos *et al*., 2022; Almeida *et al*., 2025b). This emerging strategy builds upon the well-established principles of pelotherapy and thalassotherapy, which utilize the mineral-rich properties of clays, muds, and mineral waters to promote healing, regeneration, and anti-inflammatory responses (Almeida *et al*., 2025b).

Portuguese Atlantic margin offers a particularly promising setting for the advancement of electropelotherapy. Its diverse coastal and geological environments (e.g., estuarine sediments, thermal springs, and marine-derived peloids), which possess unique mineral compositions and physicochemical properties that may enhance therapeutic efficacy. Despite this potential, the region remains underexplored. Recent studies in the Ria de Aveiro have demonstrated that both saline phases, sediments (Almeida *et al*., 2023a; 2023b) and waters (Almeida *et al*., 2025a) can contribute meaningfully to health and well-being outcomes, highlighting the opportunity for integrating these natural materials into clinical and rehabilitative practices. By bridging traditional therapy using georesources with modern electrotherapeutic techniques, electropelotherapy opens new avenues for clinical innovation. This work aims to synthesize current knowledge while emphasizing the untapped therapeutic value of the Portuguese Atlantic Coast.

2. PELOTHERAPY AND THALASSOTHERAPY

Since ancient times, peloids (Figure 1) have been applied as therapeutic agents for their thermal properties (Maraver *et al*., 2021).

Pelotherapy, which involves the topical application of peloids (usually clay-based) (Bastos *et al*., 2022), remains a fundamental component of health resort medicine and is commonly practiced through balneotherapy and thalassotherapy modalities (Maraver *et al*., 2021). Gomes *et al*. (2013) proposed a most recent definition of peloids as “a mature mud or mud suspension or dispersion with curative or cosmetic properties, consisting of a complex mixture of fine-grained materials of geological and/or biological origin, mineral or sea water, and organic compounds commonly arising from some biological metabolic activity”. This mixture of natural materials with healing properties with therapeutic and cosmetic purposes, have been studied by numerous scientists over the years, in particular for dermatological (Bergamaschi *et al*., 2020; Katona *et al*., 2020) and rheumatological conditions (Fioravanti *et al*., 2007; Fraioli *et al*., 2011). Thalassotherapy, derives from the Greek word *thálassa* (sea), related to sea or ocean, a

therapeutic technique that includes seawater-based treatments (Munteanu and Munteanu, 2019). Kazandjieva *et al*. (2008) described it as "a modality of therapeutic and prophylactic application of sea water, mud, algae, sand and climate". Several studies have proved the efficacy of thalassotherapy in different fields, e.g., skin diseases, including psoriasis (Kazandjieva *et al*., 2008), muscle damage and sports rehabilitation (Kim *et al*., 2020), and oncology-related skin repair and well-being improvement after cancer therapies (Mourelle *et al*., 2023). Together, pelotherapy and thalassotherapy form the foundation of many marine and mud-based clinical applications, offering safe, natural, and effective alternatives or complements to conventional treatments.

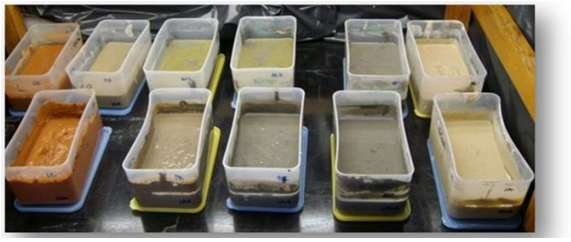

Figure 1. Peloids.

3. ELECTROPELOTHERAPY

Electrotherapy, the use of electrical energy to the body for medical and rehabilitative purposes, is widely recognized as a clinical treatment modality (Tiktinsky *et al*., 2010). To address the inherent challenge of transdermal drug delivery, iontophoresis has emerged as a promising non-invasive electrotherapy method. Commonly applied in physical medicine and rehabilitation, it employs a low-intensity electric current to facilitate the movement of charged molecules across the skin barrier (Roustit *et al*., 2014).

Bastos *et al*. (2022) conducted the first pilot study exploring the combination of pelotherapy and iontophoresis as a single, integrated therapeutic approach within the field of physical medicine and rehabilitation. The study emphasizes the complementary effects of each modality: pelotherapy provides pain relief and anti-inflammatory benefits, while iontophoresis facilitates the transdermal delivery of ionized substances using a low-intensity electric current. The integration of these techniques may enhance therapeutic outcomes by increasing skin permeability through the heat generated by pelotherapy, thereby facilitating the penetration of active substances driven by electrotherapy. However, the study highlights key challenges, including barrier function of the skin and the lack of regulatory standards for peloid quality compared to pharmaceuticals. Preliminary results are promising, particularly for rheumatic and dermatological conditions, but further clinical research is needed to optimize protocols and evaluate efficacy. The study also identifies critical variables such as current density (0.5 mA/cm^2), temperature (40-45 °C), treatment duration (15-20 minutes), and electrode composition. A specialized device was developed for this application (Figure 2), using matured peloids while excluding saline phases (Bastos *et al*., 2022).

Figure 2. Electropelotherapy device Edersensae® (Bastos et al., 2022).

4. THERAPEUTIC POTENTIAL OF PORTUGUESE COAST NATURAL MATERIALS

The Portuguese Atlantic coast is home to a wide variety of natural materials with untapped therapeutic potential. These include marine and estuarine sediments, saline muds and waters, thermal springs, and naturally occurring peloids, all characterized by unique properties that may enhance clinical efficacy. This section focuses on the properties, recent research findings, and potential clinical applications of natural materials sourced from two key Portuguese coastal environments: Ria de Aveiro and Ria Formosa (Figure 3), emphasizing their prospective suitability for dermatological, rheumatological, and rehabilitative purposes.

Figure 3. Location of Ria de Aveiro and Ria Formosa in Portugal.

4.1 Ria de Aveiro

Recent studies (Figure 4) have confirmed the suitability of Portuguese saline sediments for therapeutic applications, specifically for skin treatments (Almeida *et al*., 2023a, 2023b), demonstrating low toxicity, high thermal retention, and favorable rheological behavior (Almeida *et al*., 2023a; 2023b). Likewise, hypersaline waters from this environment have shown potential to be used as a liquid phase for dermatological therapies (Almeida *et al*., 2025a).

Figure 4. Ria de Aveiro study area location (Almeida et al., 2023a, 2023b, 2025a).

4.2 Ria Formosa

Ongoing research is currently being conducted within the scope of a PhD project to evaluate the therapeutic potential of saline materials sourced from various saltpans in the Ria Formosa region. These investigations focus on characterizing these materials and assessing their safety and clinical applicability, aiming to advance their use in innovative treatment modalities such as electropelotherapy.

5. FINAL CONSIDERATIONS

The integration of natural materials, especially saline phases, from the Portuguese Atlantic Coast into clinical practice, particularly through electropelotherapy, represents a promising frontier in physical rehabilitation and dermatological care. This approach leverages the unique mineralogical and physicochemical properties of these saline materials, especially those from the Ria de Aveiro and Ria Formosa. Preliminary studies confirm their safety, therapeutic potential, and compatibility with electrotherapy-based applications. Despite the encouraging results, further interdisciplinary research is needed to standardize treatment protocols, evaluate long-term efficacy, and ensure regulatory quality control of natural materials. The development of specialized devices, such as Edersensae®, demonstrates the feasibility of bridging traditional therapeutic methods with modern technological solutions. Ultimately, harnessing the therapeutic potential of portuguese coastal resources not only contributes to scientific innovation but also offers sustainable and locally sourced alternatives for integrative medicine, potentially benefiting both patients and regional economies.

Acknowledgements

L.A. is thankful for the FCT PhD funding (2023.01752.BDANA; https://doi.org/10.54499/2023.01752.BDANA). All authors are grateful for the financial support to Research Unit GeoBioTec (UIDB/04035) financed by national funds through the FCT/MCTES.

REFERENCES

Almeida, L., Rocha, F. and Candeias, C. (2023a). Geochemical and mineralogical characterization of Ria de Aveiro (Portugal) saltpan sediments for pelotherapy application. *Environmental Geochemistry and Health*, 45:3199-3214.

Almeida, L., Rocha, F. and Candeias, C. (2023b). Portuguese Lagoon Clay Sediments for Pelotherapy Applications: The Study of Technological Properties. *Journal of Applied Sciences*, 23:185-193.

Almeida, L., Rocha, F. and Candeias, C. (2025a). Characterization of saline waters from Ria de Aveiro (Portugal) for potential use in SPA treatments. *Comunicações Geológicas*, 112, Especial I:243-246.

Almeida, L., Rocha, F. and Candeias, C. (2025b). Pelotherapy, thalassotherapy, and electrotherapy for skin treatment: current insights and future perspectives on electropelotherapy. *International Journal of Biometeorology*.

Bastos, C.M., Rocha, F., Gomes, N. and Marinho-Reis, P. (2022). The challenge in combining pelotherapy and electrotherapy (Iontophoresis) in one single therapeutic modality. *Applied Sciences*, 12(3):1509.

Bergamaschi, B., Marzola, L., Radice, M., Manfredini, S., Baldini, E., Vicentini, C.B., Marrocchino, E., Molesini, S., Ziosi, P., Vaccaro, C. and Vertuani, S. (2020). Comparative study of SPA mud from bacino idrominerario Omogeneo dei Colli Euganei (B.I.O.C.E.)-Italy and industrially optimized mud for skin applications. *Life*, 10(6):78.

Fioravanti, A., Perpignano, G., Tirri, G., Cardinale, G., Gianniti, C., Lanza, C.E., Loi, A., Tirri, E., Sfriso, P. and Cozzi, F. (2007). Effects of mud-bath treatment on fibromyalgia patients: a randomized clinical trial. *Rheumatology International*, 27:1157-1161.

Fraioli, A., Serio, A., Mennuni, G., Ceccarelli, F., Petraccia, L., Fontana, M., Grassi, M. and Valesini, G. (2011). A study on the efficacy of treatment with mud packs and baths with sillene mineral water (Chianciano spa, Italy) in patients suffering from knee osteoarthritis. *Rheumatology International*, 31:1333-1340.

Gomes, C., Carretero, M.I., Pozo, M., Maraver, F., Cantista, P., Armijo, F., Legido. J.L., Teixeira, F., Rautureau, M. and Delgado, R. (2013). Peloids and pelotherapy: historical evolution, classification and glossary. *Applied Clay Science*, 75-76:28-38.

Gomes, C. and Silva, J.B.P. (2007). Minerals and clay minerals in medical geology. *Applied Clay Science*, 36:4-21.

Katona, G., Vojvodić, S., Kalic, M., Sarač, M.S., Klimó, A. and Lješković, N.J. (2020). The effect of Kanjiža peloid on skin hydration and skin barrier function. *Macedonian Pharmaceutical Bulletin*, 66(Suppl 1):105-106.

Kazandjieva, J., Grozdev, I., Darlenski, R. and Tsankov, N. (2008) Climatotherapy of psoriasis. *Clinics in Dermatology*, 26(5):477–485.

Kim, N.I., Kim, S.J., Jang, J.H., Shin, W.S., Eum, H.J., Kim, B., Choi, A. and Lee, S.S. (2020). Changes in Fatigue Recovery and Muscle Damage Enzymes after Deep-Sea Water Thalassotherapy. *Applied Science*, 10(23):8383.

Maraver, F., Armijo, F., Fernandez-Toran, M.A., Armijo, O., Ejeda, J.M., Vazquez, I., Corvillo, I. and Torres-Piles, S. (2021). Peloids as Thermotherapeutic Agents. *International Journal of Environmental Research and Public Health*, 18:1965.

Mourelle, M.L., Gómez, C.P. and Legido, J.L. (2023). Cosmeceuticals and Thalassotherapy: Recovering the Skin and Well-Being after Cancer Therapies. *Applied Sciences*, 13(2):850.

Munteanu, C. and Munteanu, D. (2019). Thalassotherapy today. *Balneo Research Journal*, 10(4):440-444.

Roustit, M., Blaise, S. and Cracowski, J.L. (2014). Trials and tribulations of skin iontophoresis in therapeutics. *British Journal of Clinical Pharmacology*, 77(1):63-71.

Tiktinsky, R., Chen, L. and Narayan, P. (2010). Electrotherapy: yesterday, today and tomorrow. *Haemophilia*, 16(s5):126-131.

Biologia e ecossistemas marinhos

Biología marina y ecosistemas

Marine biology and ecosystems

Checklist of Marine and Estuarine Non-Indigenous Species in the Bay of Biscay

M. Díez-Muñoz (1), R. López-Alonso (1), E. Shorter-Rodríguez (1), P. Pereda-Bezanilla (1), E. Pascual-Parra (1), V. Soto-López (2), D. Menéndez-Teleña (2), C. González-Toral (3), E. Cires (1), A. Arias (1) and J. M. Rico (1)

(1) Department of Organisms and Systems Biology, University of Oviedo, Oviedo, Spain. mariadiezmunoz3@gmail.com
(2) Department of Nautical Science and Technology, University of Oviedo, Gijón, Spain
(3) Royal Botanic Gardens, Kew, Richmond, TW9 3AE, UK

Abstract: The spread of invasive species has intensified in recent decades, promoting the need for robust databases to monitor their status and pathways. This study presents an updated inventory of 359 non-indigenous species (NIS)—including exotic, invasive, cryptogenic, and tropicalization-related taxa—recorded in the Bay of Biscay. The database includes first records in the Bay and Europe, introduction pathways, and detection dates. Of the 321 NIS identified from literature, 76.13% are exotic and 23.87% invasive, comprising 83 algae and 238 animal species. Arthropoda (68 species) was the most represented phylum, followed by Rhodophyta (66), Mollusca (50), and Annelida (49). Initial introductions are largely linked to *Magallana gigas* oyster transport in the 1960s–70s, while maritime activities account for their secondary spread. The phylum Chordata was particularly notable in the context of species tropicalization.

Keywords: *Checklist, Non-Indigenous, Invasive, Bay of Biscay, Exotic*

1. INTRODUCTION

Monitoring and management of Non-Indigenous Species (NIS) - defined as species introduced outside of their native distribution range and outside of their natural dispersal potential by intentional or unintentional human activities (Zenetos *et al*., 2005; Zorita *et al*., 2009)) - in a context of increasing environmental alterations and globalization is among the most urgent issues to address (Cinar *et al*., 2021). The introduction of NIS represents a significant global threat to biodiversity, with well-documented ecological, economic and health consequences (Sylvester *et al*., 2011). Some NIS become invasive, displacing native species and reducing overall biodiversity. These invasions can alter community composition, disrupt food webs, and modify both the physical properties of habitats and key ecosystem functions (Galanidi *et al*., 2023; López and Ritcher, 2017). In severe cases, biological invasions may result in substantial economic losses, such as declines in fisheries (López and Ritcher, 2017; Zenetos *et al*., 2005).

Management efforts for NIS are most effective when focused on preventing new entries through the control of potential introduction pathways, since eradication of already established population is rarely successful (López and Richter, 2017; Sylvester *et al*., 2011). Therefore, the development of inventories of NIS remains a key scientific priority, as they enable early detection of new introductions – crucial for preventing their establishment and potential transformation into invasive species (Sylvester *et al*., 2011). Maintaining an up-to-date checklist not only facilitates rapid detection and impact assessment, but also helps authorities prioritize control, mitigation or eradication measures and use resources efficiently (Pergl *et al.,* 2020). These checklists also allow researchers to correlate the occurrence of NIS with climate change factors. Moreover, they serve as tools for science communication and public awareness, informing society and policymakers about the risks these species pose and promoting stronger regulation and preventive action.

Located in Northwestern Europe, the Bay of Biscay (BoB) is bordered by the northern coast of Spain and the western coast of France. It is part of the eastern Atlantic Ocean and serves as a transitional zone between the more boreal regions to the north and the subtropical regions of the North Atlantic (Arias *et al*., 2022; López-Alonso *et al*., 2023). It hosts several protected areas such as El Cachucho Marine Protected Area or the Arcachon Bay Marine Natural Park (Figure 1). It is also a highly biodiverse region, with estimation of over 2000 different animals' species (Arias *et al*., 2022). On the other hand, it is also the marine gateway to Europe, serving several key ports such as Bilbao and Santander, in Spain, and Nantes and Saint-Nazaire, in France. Because of these wide-ranging effects, is it crucial to have an understatement of the number of NIS since it is a key area that posses a high risk of invasions.

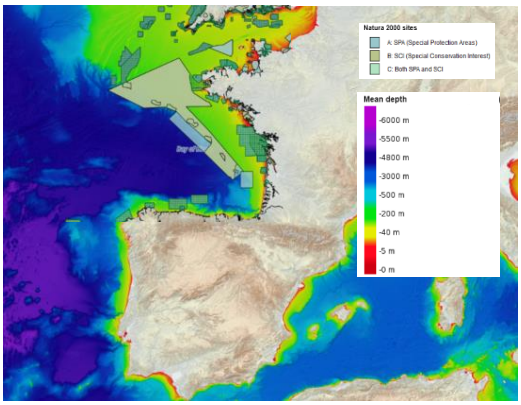

Figure 1. Natura sites, mean oceanic depth and geomorphology or the Bay of Biscay. Modified from EMODnet, (2025).

The NIS of the BoB have been previously documented in several regional studies. These include the list of NIS algae and invertebrates in the marine and brackish coastal waters of Normandy by Pezy *et al*. (2021); a species list from the Le Havre area by Breton (2014); records of introduced marine species in Brittany by Blanchard *et al*. (2010); a checklist for the Arois-Picardie Bay by Dewarumez *et al*. (2011); and reports on exotic marine species along the Basque Country coast by Zorita *et al*. (2009) and Martinez and Adarraga (2006). However, each of these works focused on specific, smaller coastal regions rather than the broader Bay of Biscay. Additional resources include Goulletquer, (2016) book on exotic species in France and the checklist by Png-Gonzalez *et al*. (2023), both of which include information on the Bay of Biscay, although their scopes were either broader or taxonomically limited.

Despite these contributions, there remains a gap in the literature: no comprehensive inventory exists that specifically focuses on marine and estuarine NIS of animals and algae exclusively within the BoB. The aim of this study is to fill that gap by providing the first dedicated inventory of NIS in this region. In addition to species records, we include key information relevant to NIS management—such as larval type, introduction pathways, first record location, date, and authorship—covering both the BoB and the broader Atlantic coast of Europe. This dataset also enables an analysis of regional trends in introduction pathways and biogeographic origins of NIS in the area.

2. METHODOLOGY

In order to compile this inventory, the literature was thoroughly reviewed in search of animals and algae NIS all around the continental coast of the BoB. Following the quality criteria only peer-review publications were considered. Synonymized names for each species were checked. For nomenclatural purposes, names were updated according to the World Register of Marine Species (WorMs, 2025) and Algabase (2025). The native distribution of all NIS was assigned to broad oceanic regions according to the classification proposed by Briggs (1974), with one modification: in this work the Mediterranean is considered a different biogeographic region different from the East Boreal Atlantic (Figure 2).

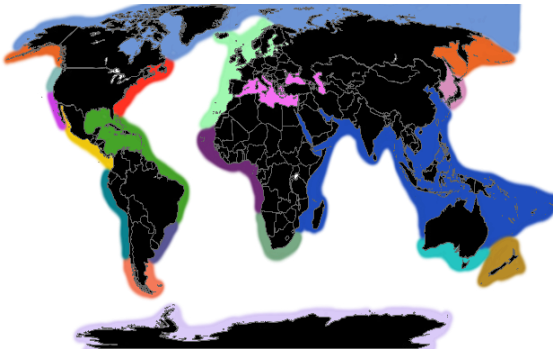

Figure 2. Biogeographic regions considered for Natural Distributions of Non-Indigenous Species. Modified from Briggs (1974).

Species were classified into the following categories: Cryptogenic — species whose native or introduced status cannot be confidently determined, often because their introduction may have occurred long ago and was undocumented (Carlton, 1996; Zenetos *et al*., 2005); Exotic — species with a geographically expanded natural range as a result of human-mediated introductions (Carlton, 1996); Invasive — exotic species that pose a threat to ecosystems, economic activities, and/or human health (IUCN, 2020); and Tropicalized — species whose natural range has expanded by their own means but facilitated by climate change (Vergés *et al*., 2014).

The introduction pathway for each species was addressed, identified and categorized according to the framework proposed by Pergl *et al*. (2020). The categories are as follows: Release in nature — intentional introductions, including those for recreational purposes, unwanted pets, and other deliberate releases; Escape from confinement — unintentional escapes from facilities such as aquaculture farms, aquaria, or zoos; Transport-contaminant — species introduced accidentally through association with other species (e.g., parasites or hitchhikers); Transport-stowaway — species introduced via biofouling on vessels or in ballast water; and Corridor — species that spread through artificial or natural connections between water bodies, such as canals or modified river basins.

3. RESULTS

A total of 321 NIS were addressed in the study area. Of these, a significant majority—76.13%—were

classified as exotic species, while the remaining 23.87% were recognized as invasive, indicating their capacity to cause ecological or economic harm. Taxonomically, the NIS consisted of 83 algal species and 238 animal species. Among the different phyla, *Arthropoda* was the most represented group, accounting for 68 species, followed closely by *Rhodophyta* with 66 species, *Mollusca* with 50 species, and *Annelida* with 49 species.

Historical records suggest that the initial introduction of many of these species is closely tied to the translocation of the cultured oyster *Magallana gigas* Thunberg, 1793 during the 1960s and 1970s. This activity played a key role in the primary dispersal of several exotic organisms. Subsequently, maritime transport has been identified as the main vector facilitating the secondary spread of these species into new environments. In the context of the topicalization phenomenon—the process by which certain taxa become central to ecological discussions—the phylum *Chordata* emerged as the most prominently featured group, highlighting its relevance in current NIS dynamics.

4. CONCLUSIONS

This comprehensive assessment of non-indigenous species in the BoB highlights the considerable taxonomic diversity and growing ecological influence of both exotic and invasive taxa in the region. Moving forward, the findings reinforce the urgent need for continuous monitoring and coordinated regional strategies to mitigate the introduction and spread of NIS. Future research should aim to better understand the ecological consequences of these species and develop predictive tools to assess potential invasions under changing climatic and anthropogenic pressures.

Acknowledgments

This work was funded by project PA-24-BIODIVERSIDAD-008 from the Complementary Biodiversity Programme, within the framework of the Recovery, Transformation and Resilience Plan, funded by the European Union (Next Generation EU).

REFERENCES

Arias, A., Ríos, P., Cristobo, J. and Paxton, H. (2022). The Bay of Biscay: Almost two centuries inspiring global oceanography. *Estuarine, Coastal and Shelf Science*, 281. https://doi.org/10.1016/j.ecss.2022.108196

Blanchard, M., Goulletquer, P., Hamon, D., Le Mao, P., Nezan, E., Gentil, F., Simon, N., Viard, F., Ar Gall, E., Grall, J., Hily, C., Le Duff, M., Stiger-Pouvreau, V., Acou, A., Derrien-Courtel, S., Feunteun, E., D'Hondt, J., Canard, A., Ysnel, F. and Perrin, B. (2010). Liste des espèces marines introduites dans les eaux bretonnes et des espèces introduites envahissantes des eaux périphériques. https://archimer.ifremer.fr/doc/00026/13737/

Breton, G. (2014). Espèces introduites ou invasives des ports du Havre, d'Antifer et de Rouen (Normandie, France). *Hydroécol. Appl.*, 18, 23-65. https://doi.org/10.1051/hydro/2014003

Briggs, J. C. (1974). *Marine Zoogeography*. McGraw-Hill Book Company, New York, 475 p.

Carlton, J. T. (1996). Biological Invasions and Cryptogenic Species. *Ecology*, *77*(6), 1653-1655. https://doi.org/10.2307/2265767

Çinar, M. E., Bilecenoğlu, M., Yokeş, M. B., Öztürk, B., Taşkin, E., Bakir, K., Doğan, A. and Açik, Ş. (2021). Current status (as of end of 2020) of marine alien species in Turkey. *PLoS One* *16*(5). https://doi.org/10.1371/journal.pone.0251086

Dewarumez, J. M., Gevaert, F., Masse, C., Foveau, A., Desroy, N., and Grulois, D. (2011). Les espèces marines animales et végétales introduites dans le bassin Artois-Picardie. https://archimer.ifremer.fr/doc/00158/26894/

Galanidi, M., Aissi, M., Ali, M., Bakalem, A., Bariche, M., Bartolo, A. G., Bazairi, H., Beqiraj, S., Bilecenoglu, M., Bitar, G., Bugeja, M., Carbonell, A., Castriota, L., Chalabi, A., Çinar, M. E., Dragičević, B., Dulčić, J., Ahmed, A. E., Farrag, M. M., … and Zenetos, A. (2023). Validated Inventories of Non-Indigenous Species (NIS) for the Mediterranean Sea as Tools for Regional Policy and Patterns of NIS Spread. *Diversity*, *15*(9), 962. https://doi.org/10.3390/d15090962

Goulletquer, P. (2016). Guide des organismes exotiques marins. Editions Belin, France, 306.

Guiry, M. D., and Guiry, G. M. (2025). *AlgaeBase*. National University of Ireland, Galway. https://www.algaebase.org

IUCN (International Union for Conservation of Nature). (2000). *Guidelines for the Prevention of Biodiversity Loss Caused by Alien Invasive Species.*

López, E. and Richter, A. (2017). Non-indigenous species (NIS) of polychaetes (Annelida: Polychaeta) from the Atlantic and Mediterranean coasts of the Iberian Peninsula: an annotated checklist. *Helgol. Mar. Res.*, 71, 19. https://doi.org/10.1186/s10152-017-0499-6

López-Alonso, R., Sánchez, O., Pascual-Parra, E., Borrel, Y. J., Matínez-Pérez, J. and Arias, A. (2023). *Plicopurpura patula* and *Monoplex parthenopeus* (Gastropoda: Caenogastropoda): New evidence of the tropicalization of the Bay of Biscay (NE Atlantic). *Journal of Sea Research*, 194. https://doi.org/10.1016/j.seares.2023.102412

Martínez, J. and Adarraga, I. (2006). Programa de Vigilancia y Control de la Introducción de Especies Invasoras en los Ecosistemas Litorales de la Costa Vasca. Sociedad Cultural de Investigación Submarina.

Pergl, J., Brundu, G., Harrower, C. A., Cardoso, A. C., Genovesi, P., Katsanevakis, S., Lozano, V., Perglová, I., Rabitsh, W., Richards, G., Roques, A., Rorke, S. L., Scalera, R., Schönrogge, K., Stewart, A., Tricarico, e., Tsiamis, K., Vannini, A., Vilà, M., Zenetos, A. and Roy, H.

E. (2020). Applying the Convention on Biological Diversity Pathway Classification to alien species in Europe. *NeoBiota, 62*, 333-363. https://doi.org/10.3897/neobiota.62.53796

Pezy, J. P., Baffreau, A., Raoux, A., Rusig, A. M., Mussio, I. and Dauvin, J. C. (2021). Non-indigenous species in marine and brackish waters along the Normandy coast. *BioInvasions Records, 10*(4), 755-774. https://doi.org/10.3391/bir.2021.10.4.01

Png-Gonzalez, L., Comas-González, R., Calvo-Manazza, M., Follana-Berná, G., Ballesteros, E., Díaz-Tapia, P., Falcón, J. M., García Raso, J. E., Gofas, S., González-Porto, M., López, E., Ramos-Esplá, A. A., Velasco, E., and Carbonell, A. (2023). Updating the National Baseline of Non-Indigenous Species in Spanish Marine Waters. *Diversity*, *15*(5), 630. https://doi.org/10.3390/d15050630

Sylvester, F., Kalaci, O., Leung, B., Lacoursière-Roussel, A., Murray, C. C., Choi, F. M., Bravo, M. A., Therriault, T. W., and MacIsaac, H. J. (2011). Hull fouling as an invasion vector: Can simple models explain a complex problem? *Journal of Applied Ecology*, *48*(2), 415-423. https://doi.org/10.1111/j.1365-2664.2011.01957.x

Vergés, A., Steinberg, P. D., Hay, M. E., Poore, A. G. B., Campbell, A. H., Ballesteros, E., Heck, K. L., Booth, D. J., Coleman, M. A., Feary, D. A., Figueira, W., Langlois, T., Marzinelli, E. M., Mizerek, T., Mumby, P. J., Nakamura, Y., Roughan, M., van Sebille, E., Sen Gupta, A., Smale, D. A., Tomas, F. Wernberg, T. and Wilson, S. K. (2014). The tropicalization of temperate marine ecosystems: climate-mediated changes in herbivory and community phase shifts. *Proceedings of the Royal Society B: Biological Sciences*, *281*(1789). https://doi.org/10.1098/rspb.2014.0846

WoRMS Editorial Board. (2025). *World Register of Marine Species*. https://www.marinespecies.org

Zenetos, A., Cinar, M., Pancucci-Papadopoulou, M., Harmelin, J., Furnari, G., Andaloro, F., Bellou, N., Streftaris, N., and Zibrowius, H. (2005). Annotated list of marine alien species in the Mediterranean with records of the worst invasive species. *Mediterranean Marine Science*, *6*(2), 63–118. https://doi.org/10.12681/mms.186

Zorita, I., Solaun, O., Galparsoro, I. and Borja, A. (2009). Especies exóticas en el medio marino del País Vasco, en relación con el cambio global. Informe para Dirección de Biodiversidad de la Viceconsejería de Medio Ambiente. Gobierno Vasco. 60.

Ejemplos de casos de uso para la Plataforma Integrada de datos del Plan Complementario de Ciencias Marinas de Galicia

D. Abal (1), M. Ruiz-Villarreal (1), G. Gonzalez-Nuevo (1), J. Valeiras (1), M. Barreiro (1), E. Abad (1), P. Prieto (2), T. Rodríguez (1), C. Grela (2) y J. Cacheiro (2)

(1) Instituto Español de Oceanografía (IEO, CSIC), España. daniel.abal@ieo.csic.es
(2) Centro de Supercomputación de Galicia (CESGA), Santiago de Compostela, España

Abstract: The Complementary Plan for Marine Sciences in Galicia aims to build an integrated platform to make marine research data more accessible and reusable. This work focuses on testing the platform's ability to manage and process multimedia data, specifically images of phytoplankton collected using FlowCam. Several use cases were developed: (1) standardization of taxonomic data using the World Register of Marine Species (WoRMS), (2) linking multimedia content with tabular data to improve data exploration, and (3) extracting new information from images using edge detection algorithms such as Canny. These examples demonstrate the platform's potential to handle complex and diverse datasets while providing tools for large-scale analysis. Python and Jupyter Notebooks were used for all developments. The results suggest that the integration of multimedia content into scientific data platforms can significantly enhance marine research workflows and data quality.

Keywords: *phytoplankton, data integration, FlowCam, WoRMS, image analysis, Python*

1. INTRODUCCIÓN

El presente documento expone una serie de casos de uso desarrollados en el marco del Plan Complementario de Ciencias Marinas, en particular en relación con su infraestructura de datos. Se contextualiza primero el programa y sus objetivos, con especial atención al paquete de trabajo 4, para posteriormente mostrar cómo se han aplicado herramientas de análisis y visualización a conjuntos de datos multimedia.

1.1. Planes complementarios y Programa de Ciencias Marinas de Galicia

Los Planes Complementarios son un instrumento creado por el Ministerio de Ciencia, Innovación y Universidades en colaboración con las comunidades autónomas, enmarcado en el componente 17 del Plan de Recuperación, Transformación y Resiliencia dirigido a establecer colaboraciones en acciones de I+D+I que tengan objetivos comunes (Gobierno de España, 2025, 19 de marzo).

El Plan Complementario de Ciencias Marinas tiene por objetivo el despliegue de una estrategia conjunta de investigación e innovación para abordar de forma sostenible los nuevos desafíos en monitorización y observación marina, el cambio climático, la acuicultura y otros sectores de la economía azul.

Los ámbitos de colaboración se establecen como:

- Observación y monitorización del medio marino y litoral.
- Acuicultura sostenible, inteligente y de precisión.
- Economía azul: innovación y oportunidades.

Para ello se divide en once paquetes de trabajo como vemos en la Figura 1 de los que vamos a prestar especial atención al paquete de trabajo 4 de infraestructura de datos (ThinkinAzul Galicia, 2025).

1.2. Paquete de trabajo 4: Datamare

El paquete de trabajo 4 del Plan Complementario de Ciencias Marinas de Galicia está orientado a construir una infraestructura que facilite el acceso y la reutilización de datos relevantes para la investigación marina. En este ámbito, no siempre resulta sencillo encontrar datos que sean accesibles, comprensibles o reutilizables, bien por la falta de estandarización, por la variedad de formatos o por la ausencia de metadatos que permitan entender su origen y calidad. Esta iniciativa busca precisamente dar respuesta a esos problemas, ofreciendo una plataforma pensada para integrar y poner a disposición de la comunidad científica datos de diversas fuentes. Como punto de partida, se han seleccionado conjuntos de datos que ya presentan un cierto grado de estandarización — incluyendo información física, biogeoquímica, biológica, socioeconómica y humana — y que cuentan con metadatos mínimos. Estos datos se han integrado en una plataforma común mediante un modelo estructurado y federado, que permite su conexión sin necesidad de centralizarlos en un único sistema. Tras esta primera fase, se han comenzado a explorar nuevos tipos de información, entre ellos los datos multime-

dia, con el fin de ampliar las capacidades de la plataforma. El sistema está diseñado para ser interoperable, es decir, para poder comunicarse fácilmente con otras herramientas y entornos.

El acceso a la plataforma se plantea, en esta primera fase, a través de entornos técnicos como Python y Jupyter Notebooks, que permiten a los usuarios consultar y trabajar con los datos de forma flexible y reproducible. Esta versión inicial se ha desarrollado como un Producto Mínimo Viable, con la idea de ir ampliando progresivamente su alcance, incorporando en el futuro conjuntos de datos menos estructurados o que procedan de otros paquetes de trabajo del mismo plan.

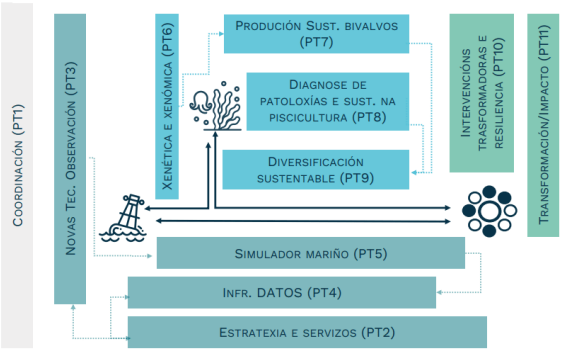

Figura 1. Organización de los paquetes de trabajo. Modificado de ThinkinAzul Galicia (2025).

Además, la plataforma incorpora herramientas básicas de control de calidad, que permiten comparar parámetros similares provenientes de distintas fuentes y ámbitos, ayudando así a detectar posibles inconsistencias o errores. A medio plazo, esta infraestructura servirá también como base para construir productos y servicios climáticos, que podrán acceder a los datos a través de APIs y utilizarse en aplicaciones o desarrollos propios.

2. CASOS DE USO

El presente trabajo se centra en la la generación de casos de uso de la Plataforma Integrada de datos del Plan Complementario de Ciencias Marinas para poner a prueba el potencial de contener los conjuntos de información multimedia que se están volcando actualmente desde la herramienta Jupyter notebook, con el lenguaje de programación Python.

Los casos de uso desarrollados se centran en la estandarización de datos taxonómicos, la conexión del material multimedia con sus datos y la obtención de nueva información a partir del material multimedia.

Vamos a empezar utilizando como ejemplo los datos e imágenes de fitoplancton obtenidas mediante la herramienta Flowcam (Fluid Imaging Technologies, 2025). Esta es una herramienta de microscopía que permite fotografiar partículas suspendidas en un fluido, permitiendo identificar, contar y clasificar dichas partículas. Como salida de este procesado, obtenemos una serie de fotografías y un archivo de datos en el que tenemos una tabla con una linea de datos para cada fotografía. En esta línea encontramos información como las dimensiones de la partícula en cuestión.

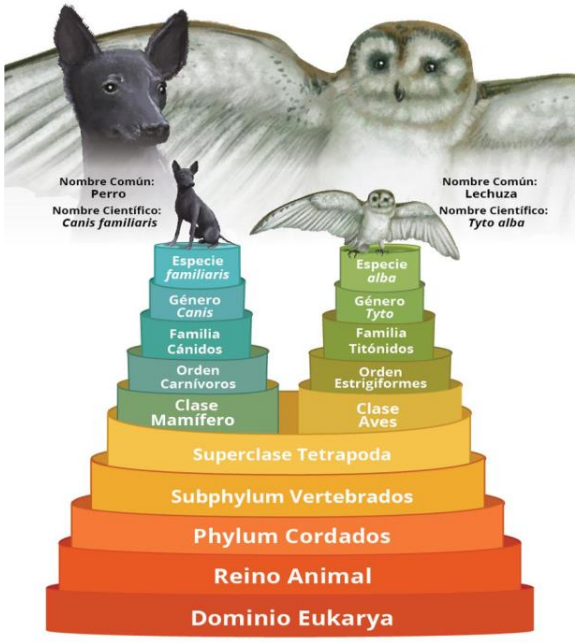

Figura 2. Ejemplo de clasificación taxonómica donde podemos ver, a través de las distintas categorías taxonómcas, los diferentes taxones para dos especies de vertebrados. Tomado de Colegio de Ciencias y Humanidades, UNAM (2025).

2.1. Estandarización de datos taxonómicos

Para estandarizar los datos taxonómicos, los referenciaremos al Registro Mundial de Especies Marinas (WoRMS Editorial Board, 2025). En este registro tenemos una entrada para cada taxón, referenciado a un identificador único. La información se mantiene actualizada y los taxones obsoletos están enlazados con el correspondiente valor actualizado. Además, cada taxón se mantiene conectado con su taxón superior, manteniendo una ontología por la que se puede navegar fácilmente. En la Figura 2 podemos ver un ejemplo de clasificación taxonómica para ilustrar mejor como se estructura este tipo de datos.

Accediendo a datos de muestras de fitoplancton analizadas con flowcam, tenemos una clasificación taxonómica que se presenta como una cadena de texto. Mediante la librería PyWoRMS podemos utilizar esta cadena de texto para acceder a la información extendida de este taxón, así como los taxones superiores en los que se clasifica.

Esto nos permite agrupar la información a un determinado nivel taxonómico para realizar distintos estudios estadísticos. En el ejemplo de la Figura 3 pode-

mos ver un ejemplo sencillo en el que se agruparon los organismos identificados a nivel de clase y orden.

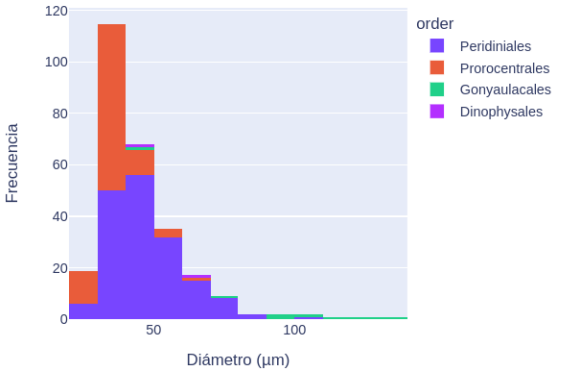

Figura 3. Distribución de frecuencias de tamaños en muestra de dinoflagelados. Los colores representan los distintos órdenes de los individuos encontrados en la muestra, mostrando así a la vez los niveles taxonómicos clase y orden

2.2. Conexión entre datos y material multimedia

Las fotografías y la tabla de datos que nos devuelve Flowcam son datos que se entienden mejor cuando estos se visualizan en conjunto. Por ello, buscar un modo de poder unirlos puede ser una herramienta potente especialmente cuando hablamos de datos masivos. Para ello podemos usar la propia estructura de directorios para localizar la imagen a la que hace referencia cada línea. Esto nos permite acceder a las imágenes que nos interesen directamente desde la referencia en la tabla.

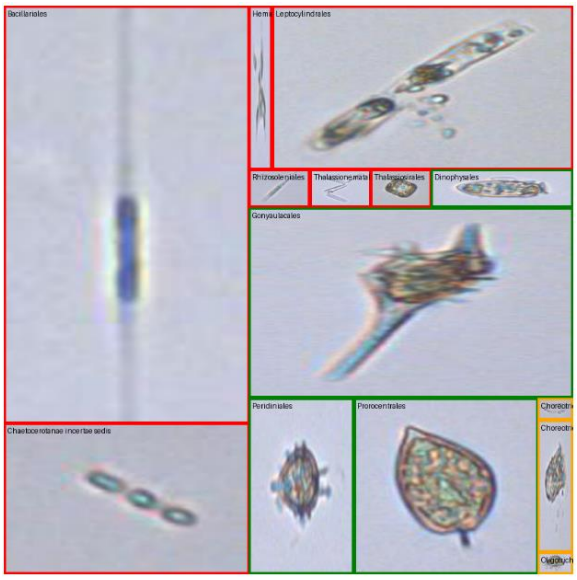

Figura 4. Tremap de abundancias de distintos grupos taxonómicos. Los colores de los bordes agrupan distintas clases y las fotografías representan el orden correspondiente. Rojo: Bacillariophyceae, Verde, Dinophyceae, Naranja: Oligotrichea.

Por ejemplo, podemos formatear estas imágenes y mostrarlas dentro de una tabla de datos de la librería pandas como se muestra en la Figura 4. Esto nos permite unir a la visualización toda la potencia de pandas para filtrar o unir datos, capacidades cruciales en un contexto de datos masivos.

Con esta capacidad, un taxónomo puede, por ejemplo, filtrar las líneas que le interesen y comprobar cómodamente y de forma armonizada si sus datos contienen algún tipo de error.

Por otro lado, una vez que la tabla hace referencia a las imágenes, se pueden usar estas imágenes para representar los datos de la tabla. En la Figura 4 podemos ver un ejemplo en el cual el área de las fotografías es proporcional a la abundancia de cada uno de los grupos taxonómicos.

2.3. Obtención de nueva información a partir del material multimedia

Una vez que las imágenes están vinculadas a los datos, es posible aplicar técnicas de procesamiento digital para obtener información adicional no disponible directamente en los metadatos originales.

	taxa	datetime	geometry	image
388	Dinophysis acuta	2024-10-04 09:46:00	POINT (-8.286390000000001 43.3992)	
69	Dinophysis acuta	2024-10-04 09:46:00	POINT (-8.286390000000001 43.3992)	
716	Dinophysis acuminata	2024-10-10 11:03:00	POINT (-8.23889 43.3622)	
355	Dinophysis acuminata	2024-10-04 09:46:00	POINT (-8.286390000000001 43.3992)	

Figura 5. Submuestra de tabla de datos filtrada para mostrar el género Dinophysis en la que se ha añadido una columna con las imágenes a las que se hace referencia.

En este caso, se ha empleado un método sencillo basado en la detección de bordes, con el objetivo de estimar el número de células u otras estructuras presentes en cada imagen para distintos casos en los que Flowcam detectó una colonia como un único individuo.

El algoritmo utilizado es Canny una técnica clásica ampliamente utilizada en análisis de imágenes. Este método permite identificar los contornos de los objetos resaltando los cambios bruscos de intensidad en la imagen, lo que facilita la localización de los límites de las células u organismos capturados por el sistema FlowCam.

A partir de la imagen procesada, se pueden aplicar diferentes criterios para aproximar un recuento de objetos, como la identificación de regiones cerradas o puntos clave dentro de los bordes detectados. Aunque este enfoque tiene limitaciones — por ejemplo, en casos de solapamiento entre organismos o de estructuras mal definidas —, resulta útil como estimación inicial en estudios que manejan grandes volúmenes de datos, o como herramienta de apoyo al análisis visual.

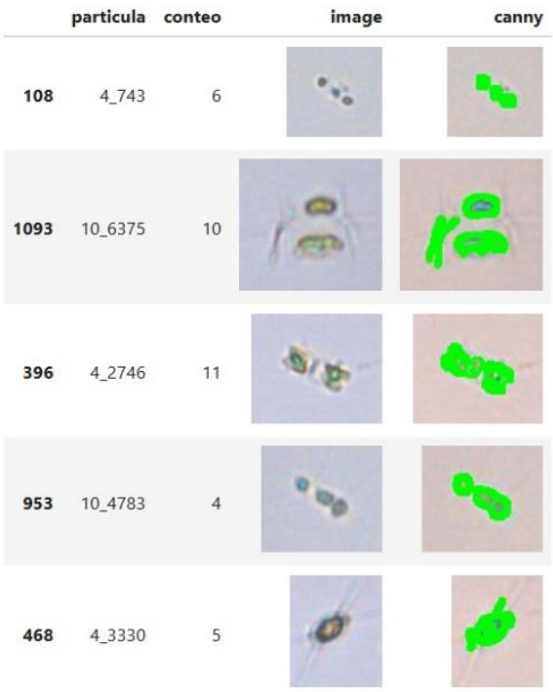

	particula	conteo	image	canny
108	4_743	6		
1093	10_6375	10		
396	4_2746	11		
953	10_4783	4		
468	4_3330	5		

Figura 6. Resultado de aplicar el algoritmo Canny Para detección de bordes en un intento de lograr un conteo de células. Se puede observar que los bordes se localizan correctamente aunque estos se contabilizan múltiples veces.

En la Figura 6 podemos observar el resultado de aplicar este algoritmo. Aunque el resultado del conteo no es satisfactorio, esto es probablemente debido a la falta de experiencia en análisis de imagen, pero podemos observar que los bordes son correctamente detectados. Es necesario dedicar más esfuerzos a optimizar este análisis, pero se podría obtener una herramienta capaz de mejorar los cálculos de abundancias de fitoplancton y aplicarlo de manera eficiente en grandes cantidades de fotografías pertenecientes a conjuntos de datos publicados en la Plataforma Integrada de datos del Plan Complementario de Ciencias Marinas.

3. CONCLUSIÓN

La Plataforma Integrada de datos del Plan Complementario de Ciencias Marinas de Galicia representa una oportunidad para avanzar en el estudio de los ecosistemas marinos. Ofrece acceso a conjuntos de datos diversos y capacidades de cómputo adecuadas para su procesamiento masivo.

El uso de Python como lenguaje aporta gran versatilidad, permitiendo trabajar con datos tabulados, imágenes, audio, vídeo y otros formatos. Además, la posibilidad de integrar datos procedentes de diferentes proyectos y de naturaleza heterogénea (multimedia, biológica, física, etc.) abre nuevas vías para el análisis interdisciplinar.

Los casos de uso presentados muestran cómo esta plataforma puede facilitar tanto la estandarización como la exploración y reutilización de datos científicos, mejorando la eficiencia en tareas de validación, análisis y generación de nuevo conocimiento.

Agradecimientos

El Programa de Ciencias Mariñas de Galicia que forma parte de los Planes Complementarios de Ciencia del Ministerio de Ciencia, Innovación y Universidades incluidos en el Plan de Recuperación Transformación y Resiliencia (PRTR-C17.I1). Financiado a través de la Xunta de Galicia con fondos Next-GenerationEU y Fondo Europeo Marítimo, de la Pesca y de la Acuicultura de la Unión Europea.

REFERENCIAS

Colegio de Ciencias y Humanidades, UNAM (2025). Características generales, dominios y reinos. Categorías taxonómicas. Recuperado el 30 de junio de 2025, de https://portalacademico.cch.unam.mx/biologia2/caracteristicas-generales-dominios-y-reinos/categorias-taxonomicas. Accessed 2025-07-22.

Fluid Imaging Technologies (2025). Fluid Imaging Technologies: Flow Imaging Microscopy. Recuperado de https://www.fluidimaging.com. Accessed 2025-07-22.

Gobierno de España (2025, 19 de marzo). Conoce el Plan Complementario de I+D+i en ciencias marinas – PRTR. Recuperado de https://planderecuperacion.gob.es/noticias/conoce-el-plan-complementario-de-idi-en-ciencias-marinas-prtr. Accessed 2025-07-22.

Ministerio de Ciencia, Innovación y Universidades (2021). Planes complementarios de I+D+I: Documento marco. Recuperado de https://www.ciencia.gob.es. Accessed 2025-07-22.

PyWoRMS (2024). Python interface to WoRMS API. Recuperado de https://pypi.org/project/pyworms/. Accessed 2025-07-22.

ThinkinAzul Galicia (2025). Programa de Ciencias Mariñas de Galicia. Recuperado de https://galicia.thinkinazul.es. Accessed 2025-07-22.

WoRMS Editorial Board (2025). World Register of Marine Species. Available from https://www.marinespecies.org/ at VLIZ. Accessed 2025-07-22. DOI:10.14284/170

Trophic niches of zooplankton and planktivorous fish in NW Iberia characterized by stable isotopes in bulk samples and amino acids

N. Mondéjar (1), I. G. Viana (1), R. García-Seoane (1), J. Otero (1) and A. Bode (1)

(1) Instituto Español de Oceanografía (IEO-CSIC), Centro Oceanográfico de A Coruña, A Coruña, Spain. nuria.mondejar@ieo.csic.es

Abstract: Understanding marine food web dynamics requires accurate characterization of trophic niches, particularly in mid-trophic level omnivores. Here, we analysed the trophic niche of mesozooplankton, and four small pelagic fish species, i.e., Atlantic mackerel (*Scomber scombrus*), Atlantic chub mackerel (*Scomber colias)*, European sardine (*Sardina pilchardus),* and European anchovy (*Engraulis encrasicolus)* between two different regions in northern Spain (northeast Atlantic) using stable isotopes ($\delta^{13}C$ and $\delta^{15}N$) in bulk tissue and $\delta^{15}N$ in amino acids. Zooplankton exhibited spatial segregation and broader niches in Galicia, consistent with higher productivity and variable carbon sources. Fish showed greater isotopic overlap across regions, especially for bulk $\delta^{15}N$, suggesting potential competition for resources. European sardine and chub mackerel are the only species exhibiting evidence of localized populations. The identification of both migratory and resident fish populations highlights the contribution of behavioral diversity of these species to the structure of the food web, which is crucial for the management of fisheries and ecosystem conservation. Additionally, our work shows the utility of compound-specific isotope analysis to improve niche differentiation in complex food webs.

Keywords: *isotopic niche, plankton, small pelagic fish, food web, mid-trophic level omnivores*

1. INTRODUCTION

Understanding food web functioning and the ecological roles of species requires accurately quantifying the trophic niche of populations (Layman *et al*., 2012). Stable isotope analysis allows for the estimation of trophic niche width (Newsome *et al*., 2007), with carbon and nitrogen isotopes indicating dietary sources and trophic position, respectively (Peterson and Fry, 1987). Compound-specific isotope analysis enhances the differentiation between sources (i.e., the type and origin of nutrient inputs to the food web) and trophic effects (McMahon and McCarthy, 2016). However, dietary plasticity and variations in the trophic position related to the ecosystem productivity for omnivores, such as mid trophic level fishes, complicate niche characterization.

The aim of this study is to analyse the trophic niche of mesozooplankton and various planktivorous fish species in Galicia and the southern Bay of Biscay (northwestern Iberian Peninsula) to assess spatial variability in relation to the upwelling dynamics. Furthermore, we aim to compare the use of bulk stable isotope analysis and compound-specific isotope analysis of amino acids to understand trophic relationships in these organisms.

2. MATERIAL AND METHODS

2.1. Sample collection

Sampling sites were distributed across two areas, the northwestern Iberian shelf (Galicia) and southern Bay of Biscay (mar Cantábrico) (Figure 1).

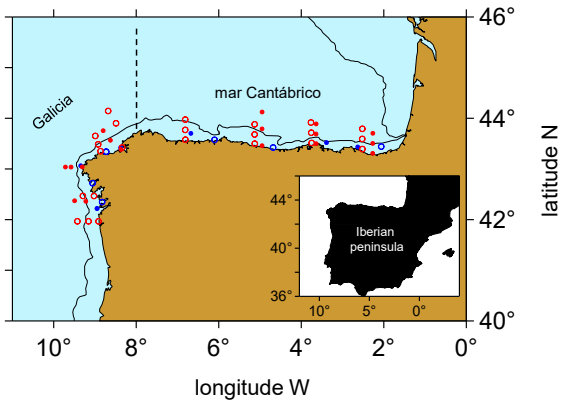

Figure 1. Location of sampling stations and study areas (Galicia, mar Cantábrico, separated by the dashed line) for zooplankton (red) and fish (blue) samples. The continuous line indicates the 200 m isobath.

All samples were collected during PELACUS cruises in spring 2021 and 2022. Mesozooplankton was collected using vertical WP2 net tows. Fish samples were collected with a pelagic trawl (Bode *et al*., 2007). Four species of planktivorous fish were collected: Atlantic mackerel *Scomber scombrus* ('mackerel'), Atlantic chub mackerel *Scomber colias* ('chub mackerel'),

European sardine *Sardina pilchardus* ('sardine') and European anchovy *Engraulis encrasicolus* ('anchovy').

2.2. Stable isotope analysis

White muscle tissue from the dorsal spine for fish or the 200–500 µm size-fraction for mesozooplankton, were ground, homogenized and subsequently analyzed for $\delta^{13}C$ and $\delta^{15}N$ using an elemental analyzer coupled to an isotope-ratio mass-spectrometer (EA-IRMS). Values of $\delta^{13}C$ were corrected for the lipid-effect (Sweeting *et al.,* 2006, Smyntek *et al*., 2007). Additionally, amino acid $\delta^{15}N$ were determined using a gas-chromatograph coupled to an isotope-ratio mass-spectrometer (GC-IRMS). Methodological details can be found in Bode *et al.* (2021). Values of $\delta^{15}N$ for trophic and source amino acids were averaged following Bradley *et al*. (2015).

Trophic amino acids include alanine (Ala), isoleucine (Ile), leucine (Leu), proline (Pro), valine (Val) and the mixtures of glutamine (Gln) and glutamic acids (Glu), and aspartic acid (Asp) and aspartamine (Asn). Source amino acids include glycine (Gly), lysine (Lys), phenylalanine (Phe), serine (Ser), methionine (Met) and threonine (Thr) (Chikaraishi *et al*., 2009; McMahon and McMarthy, 2016).

2.3. Statistical analysis

To study species' trophic niche width, we calculated the 40% of the niche region sizes using bulk $\delta^{13}C$ and $\delta^{15}N$ values or $\delta^{15}N$ values from averaged trophic and source amino acids. Bayesian statistics were computed using the SIBER package (Jackson *et al.*, 2011) in R-4.4.0 (R Core Team, 2024).

3. RESULTS

Niches estimated with bulk stable isotopes showed a clear spatial segregation for zooplankton, with a wider niche, higher $\delta^{15}N$ values, and lower $\delta^{13}C$ values in Galicia compared to mar Cantábrico (Figure 2a). In turn, fishes' niches showed large overlap and similar width between zones (Figure 2a). Using amino acid $\delta^{15}N$, the ellipses for zooplankton showed greater overlap between zones but the separation between fish species was more evident, particularly in the case of *Scomber colias* and *Sardina pilchardus* (Figure 2b).

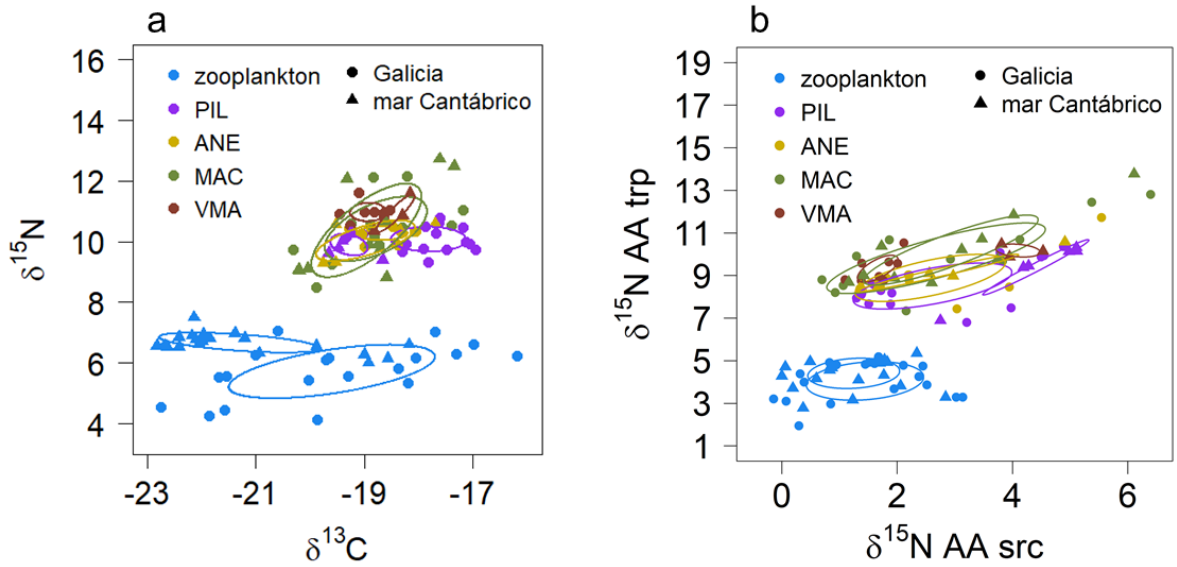

Figure 2. Standard ellipses for zooplankton and fish species determined by (a) bulk $\delta^{15}N$ and $\delta^{13}C$ values or (b) $\delta^{15}N$ values in trophic ($\delta^{15}Ntrp$) and source ($\delta^{15}Nsrc$) amino acids (AA) in Galicia and mar Cantábrico study areas. PIL: Sardina pilchardus, ANE: Engraulis encrasicolus, MAC: Scomber scombrus, and VMA: Scomber colias.

4. DISCUSSION

Bulk and amino acid isotope analyses differ in sensitivity depending on the organism: bulk analysis is useful for detecting trophic level differences and changes in the carbon sources, whereas amino acid $\delta^{15}N$ provide greater precision when nitrogen sources vary between food webs (Xing *et al*., 2020). These methods offer complementary metrics that enhance the detection of trophic segregation and potential interspecific competitions within complex food webs.

Across the study area, zooplankton, sardine and chub mackerel showed a wider niche in Galicia. This may be attributed to the high variability of the species composition of zooplankton in the productive upwelling area, as noted for the core region of the Canary Current upwelling system (Masski *et al.*, 2024), where the productivity is generally high. In contrast, mackerel and anchovy had wider niches in mar

Cantábrico, possibly related to their migratory behavior. Migration allows for feeding on food webs based on different nutrient sources, and thus migratory populations are expected to have broader niches than sedentary ones and greater niche overlap between niche fish species. These findings highlight the importance of considering the time spent by each species in different areas with distinct food web structures when interpreting potential trophic overlap and competition for food resources.

Zooplankton, with rapid isotopic turnover (Tiselius and Franssen, 2016), reflects short-term carbon variability, suggesting heterogeneous carbon sources (i.e., highly variable $\delta^{13}C$) but a dominant input of upwelling nitrogen (i.e., low variability of $\delta^{15}N$) in Galicia. Fishes, with slower turnover rates than zooplankton (Bode *et al.*, 2007), integrate long-term isotopic signals, where spatial patterns are smoothed by migrations between nearby areas. The relatively low variability in the source amino acid $\delta^{15}N$ values suggests that all the studied fish migrate between feeding areas in Galicia and mar Cantábrico, obtaining prey from different food webs. Only chub mackerel and sardine showed a clear separation between zones, suggesting the existence of local populations in the mar Cantábrico and Galicia. These populations must have been feeding in each area for enough time (several months) to equilibrate their isotopic composition with local $\delta^{15}N$ sources (Bode *et al*., 2007).

The detection of both locally and migratory feeding fish populations suggest that behavioral diversity within species contributes to structuring marine food webs, influencing predator-prey interactions and energy flow, which has a direct relevance for fisheries management and ecosystem-bases approach and conservation.

High overlap in $\delta^{15}N$ trophic axis among mid trophic level fish species suggests omnivory and potential interspecific competition (Bachiller and Irigoien, 2015), while regional differences in isotopic signatures may arise from species-specific behavioral patterns, as observed in the Mediterranean Sea (Bachiller *et al.,* 2020).

Overall, the findings reveal differences in the trophic niche width among zooplankton, with segregation between the two zones compared, probably as a consequence of the higher productivity in Galicia. In contrast, fish exhibit more homogeneous isotopic values between regions and greater overlap among species because of migrations. However, local feeding populations of sardine and chub mackerel were identified. In this last case, amino acid $\delta^{15}N$ analysis improves trophic niche resolution, highlighting food web segregation by nutrient sources. Regardless, continued investigation is required with more extensive data collection and throughout the year.

Acknowledgements

We are indebted to all the participants in PELACUS cruises for their assistance during sampling. PELACUS cruises were co-funded in part by the IEO-CSIC and the European Union through the Data Collection Framework. This research was supported by MCIN/AEI/10.13039/501100011033 (Spain) through projects QLOCKS (PID2020-115620RB-100) and MTL-FISH (PDI2023-147149NB-100), and postdoctoral Juan de la Cierva Grants to R.G.S. (FJC2019-040921-I) and I.G.V. (IJC2019-040554-I). R.G.S. also received funds from the EU NextGeneration/PRTR and the European Union's Horizon Europe research and innovation Marie Skłodowska-Curie Postdoctoral Fellowship (101150001-PelCon).

REFERENCES

Bachiller, E., Albo-Puigserver, M., Giménez, J., Pennino, M. G., Marí-Mena, N., Esteban, A., Lloret-Lloret, E., Jadaud, A., Carro, B., Bellido, J. and Coll, M. (2020). A trophic latitudinal gradient revealed in anchovy and sardine from the Western Mediterranean Sea using a multi-proxy approach. *Scientific Reports*, 10:17598. doi: 10.1038/s41598-020-74602-y

Bachiller, E. and Irigoien, X. (2015). Trophodynamics and diet overlap of small pelagic fish species in the Bay of Biscay. *Marine Ecology Progress Series*, 534:179-178. doi: 10.3354/meps11375

Bode, A., Alvarez-Ossorio, M.T., Cunha, M.E., Garrido, S., Peleteiro, J.B., Porteiro, C., Valdés, L. and Varela, M. (2007). Stable nitrogen isotope studies of the pelagic food web on the Atlantic shelf of the Iberian Peninsula. *Progress in Oceanography*, 74:115-131. doi: 10.1016/j.pocean.2007.04.005

Bode, A., Olivar, M.P. and Hernández-León, S. (2021). Trophic indices for micronektonic fishes reveal their dependence on the microbial system in the North Atlantic. *Scientific Reports*, 11:8488. doi:10.1038/s41598-021-87767-x

Bradley, C.J., Wallsgrove, N.J., Choy, C.A., Drazen, J.C., Hetherington, E.D., Hoen, D.K. and Popp, B.N. (2015). Trophic position estimates of marine teleosts using amino acid compound specific isotopic analysis. *Limnology and Oceanography: Methods,* 13:476-493.

Chikaraishi, Y., Ogawa, N.O., Kashiyama, Y., Takano, Y., Suga, H., Tomatine, A., Miyahita, H., Kitazato, H. and Ohkouchi, N. (2009). Determination of aquatic food-web structure based on compound-specific nitrogen isotopic composition of amino acids. *Limnology and Oceanography: Methods*, 7:740-750. doi: 10.4319/lom.2009.7.740

Jackson, A.L., Inger, R., Parnell, A.C. and Bearhop, S. (2011). Comparing isotopic niche widths among and within communities: SIBER – stable isotope bayesian ellipses in R. *Journal of Animal Ecology*, 80:595–602. doi:10.1111/j.1365-2656.2011.01806

Layman, C.A., Araujo, M.S., Boucek, R., Hammerschlag-Peyer, C.M., Harrison, E., Jud, Z.R., Matich, P., Rosenblatt, A., Vaudo, J., Yeager, L., Post, D. and Bearhop, S. (2012). Applying stable isotopes to examine food-web structure: An overview of analytical tools. *Biological Reviews*, 87:545–562. doi:10.1111/j.1469-185X.2011.00208.x

Newsome, S.D., Martínez del Río, C., Bearhop, S. and Philips, D. (2007). A niche for isotopic ecology. *Frontiers in Ecology and the Environment*, 5:429-436. doi: 10.1890/060150.1

Masski, H., Giménez, J., De Stephanis, R., Coll, M., Ragmane, S., Abdellaoui, S. and Tai, I. (2024). Trophic level, niche width, and site fidelity of Moroccan forage fish in two contrasting upwelling systems. *Estuarine, Coastal and Shelf Science*, 300:108703. doi: 10.1016/j.ecss.2024.108703

McMahon, K.W. and McCarthy, M.D. (2016). Embracing variability in amino acid $\delta^{15}N$ fractionation: Mechanisms, implications, and applications for trophic ecology. *Ecosphere*, 7:e01511. doi: 10.1002/ecs2.1511

Peterson, B.J. and Fry, B. (1987). Stable isotopes in ecosystem studies. *Annual Review of Ecology, Evolutions and Systematics*, 18:293–320. doi:10.1146/annurev.es.18.110187.001453

R Core Team (2024). *R: A language and environment for statistical computing*. http://www.R-project.org/. R Foundation for Statistical Computing, Vienna, Austria.

Smyntek, P.M., Teece, M.A., Schulz, K.L. and Thackeray, S.J. (2007). A standard protocol for stable isotope analysis of zooplankton in aquatic food web research using mass balance correction models. *Limnology and. Oceanography,* 52:2135-2146. doi:10.4319/lo.2007.52.5.2135

Sweeting, C.J., Polunin, N.V.C. and Jennings, S. (2006). Effects of chemical lipid extraction and arithmetic lipid correction on stable isotope ratios of fish tissues. *Rapid Communications in Mass Spectrometry,* 20:595-601. doi:10.1002/rcm.2347

Tiselius, P. and Fransson, K. (2016). Daily changes in $\delta^{15}N$ and $\delta^{13}C$ stable isotopes in copepods: Equilibrium dynamics and variations of trophic level in the field. *Journal of Plankton Research,* 38:751-761. doi: 10.1093/plankt/fbv048

Xing, D., Choi, B., Takizawa, Y., Fan, R., Sugaya, S., Tuchiya, M., Ohkouchi, N. and Chikaraishi, Y. (2020). Trophic hierarchy of coastal marine fish communities viewed via compound-specific isotopic analysis of amino acids. *Marine Ecology Progress Series,* 652:137-144. doi:10.3354/meps13475

Spatio-temporal variability of mixoplankton along the Portuguese coast

L. Gonçalves (1,2), A. Amorim (1), M. Pimentel (1), V. Veloso (1), J. Cruz (1) and A. Brito (1)

(1) MARE – Faculdade de Ciências da Universidade de Lisboa, Lisboa, Portugal.
layane.andrade.goncalves@marinha.pt
(2) Marinha Portuguesa, Lisboa, Portugal

Abstract: Mixoplankton are marine organisms that combine phototrophy and phagotrophy to acquire energy and nutrients, allowing them ecological flexibility under shifting environmental conditions. This study investigates the diversity, abundance, and spatial-temporal distribution of mixoplankton communities along the Portuguese continental shelf, using data from four oceanographic campaigns carried out between 2018 and 2020 as part of AQUIMAR project. Taxa were classified into trophic groups based on functional traits, and multivariate analyses were applied to assess community patterns and their environmental drivers. Results revealed high mixoplankton diversity, with marked different seasonal abundances. Higher relative abundance was observed during autumn campaigns, associated with temperature, turbidity and nutrient gradients. These findings underscore the role of mixoplankton in coastal systems and reinforce the importance of including this functional group in marine ecology studies.

Keywords: *mixoplankton, phytoplankton, Portuguese coast, marine ecology*

1. INTRODUCTION

Phytoplankton are at the base of most marine food webs, traditionally described as phototrophic, drifting within the euphotic layers of marine ecosystems, where they play a fundamental role. Phytoplankton communities are particularly important due to their diversity and the primary productivity they support (Vallina *et al.*, 2014). Over the past decade, many long-standing concepts have been revised considering new scientific evidence. It has become increasingly evident that the simplistic definition of these communities is no longer enough. The concept of phytoplankton is being re-evaluated, owing to growing awareness of the frequent coexistence of different trophic strategies in organisms traditionally considered to be photoautotrophic (Mitra *et al.*, 2016; Wilken and McManus, 2025).

It is even under consideration that true photoautotrophs may not exist since osmotrophy, the uptake of dissolved organic compounds, seems to be ubiquitous. Under this assumption, the underlying trophic traits defining phytoplankton are the combination of phototrophy and the absence of phagotrophy capacity. This reduces true phytoplankton in present day oceans to cyanobacteria and diatoms (Flynn *et al*. 2019).

On the other hand, mixoplankton are planktonic protists that combine photoautotrophy (photosynthesis) and phagocytosis to acquire energy and nutrients (Mitra *et al.*, 2016; Faure *et al.*, 2019; Flynn *et al.*, 2019). Within this group, there are several possible strategies by which mixoplankton acquire and use plastids. Constitutive Mixoplankton (CM) has permanent hereditary chloroplasts. Non-Constitutive Mixoplankton (NCM) acquire plastids from their prey and include species that use multiple prey sources, Generalists Non-Constitutive Mixoplankton (GNCM), plastidic Specialists (pSNCM) that depend on specific prey, and endosymbiotic Specialist (eSNCM) that host live photosynthetic symbionts (Flynn *et al.*, 2019).

Mixoplankton can play a fundamental role in the dynamics of marine ecosystems. Their metabolic flexibility may provide a competitive advantage, as plankton relying on a single strategy for energy and nutrient acquisition may be at a disadvantage under rising temperatures, hypoxic events, ocean acidification, and anthropogenic pollution. These environmental changes can affect vital rates, promote thermal stratification that limits vertical nutrient exchange, and alter the quantity, form, and stoichiometric balance of available nutrients (Glibert *et al.*, 2022). In such contexts, organisms that can adjust their trophic strategy are more likely to thrive than those with a fixed mode of survival (Mitra *et al.*, 2016).

Several mixoplankton species are associated with harmful algal blooms (HABs), increasingly observed in marine ecosystems worldwide (Hallegraeff *et al.*, 2021). These events illustrate the ecological prominence of mixoplankton and point to the need for a deeper understanding of the mechanisms driving

their success under varying environmental scenarios (Mitra *et al*., 2016).

Thus, studying phytoplankton communities along the western Iberian coast using a mixoplankton-based approach is of critical importance. The main objective of the present work is to categorize species into different trophic levels, taking mixotrophy into account, to understand their spatio-temporal variability. This work contributes to the assessment of the ecological role of mixoplankton in Iberian coastal systems and highlights the need for their inclusion in ecological models and coastal management policies. Future research should aim to deepen the understanding of the trophic functionality of this group.

2. MATERIAL AND METHODS

The present work is based on the analysis of data obtained during four oceanographic campaigns along the Portuguese continental coast: i) two during Autumn (October 2018 and 2019); and ii) two in Spring (April 2019 and late February 2020). They covered five distinct regions along the Portuguese coast from north to south (A, B, C, D, and E) (Figure 1).

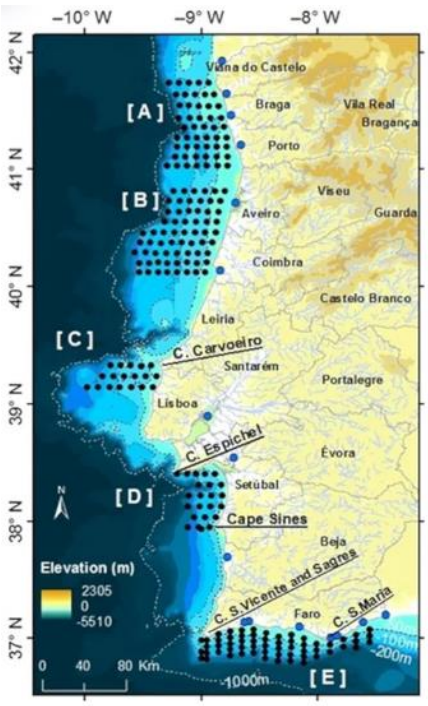

Figure 1. Location of sampling stations across the five study areas. Obtained from Favareto et al. (2023).

Data includes phytoplankton diversity and quantification (cells L^{-1}), based on identification to the lowest possible taxonomical rank under the light microscope, and in situ measurements of temperature, salinity, dissolved oxygen, nutrients, and chlorophyll *a*. The different taxa were categorized into distinct trophic strategies following Flynn *et al*. (2019): Mixoplankton (CM, pSNCM and eSNCM), Phytoplankton and Heterotrophs. A group named "Unknown" included all taxa that were not possible to classify.

3. RESULTS

The analysis from the four oceanographic campaigns revealed a variable planktonic protist community composition. Constitutive mixoplankton was present in all campaigns, with peaks observed during the autumn campaigns (1 and 3). In autumn 2018 (Campaign 1), this group was more abundant than the others and represented at least 40% of the total identified species.

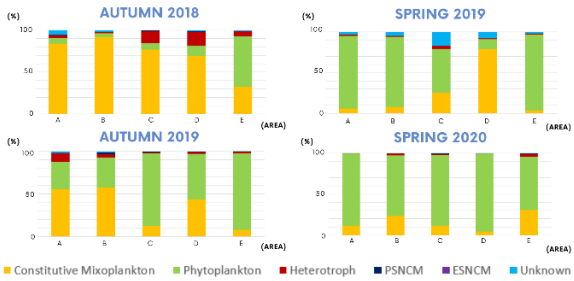

Figure 2. Percentage of abundance of the different trophic groups in the studied areas (A to E) for each campaign.

Campaign 4, conducted in early spring in 2020, between February and March, exhibited communities dominated by phytoplankton in all studied areas, reflecting an environment rich in nutrients. In contrast, Campaign 2, which occurred later in spring (April 2019), revealed an ecological transition along the west coast, with a progressive increase in the proportion of mixoplankton from N to S, and a phytoplankton dominated community along the S coast.

The first two axes of the PCO explained 75,3% of the variability (Figure 3). The analysis revealed a good separation between spring and autumn seasons, supported by variations in temperature, turbidity and nutrient gradients such as NOx and NH_3 (Figure 4). A statistically significant difference was also observed in the abundance of mixoplankton and heterotrophs in the autumn campaigns, and phytoplankton in the spring.

PCO1 is more closely related to Heterotroph with a correlation of 0.7 and PCO2 to Phytoplankton with a correlation of 0.75.

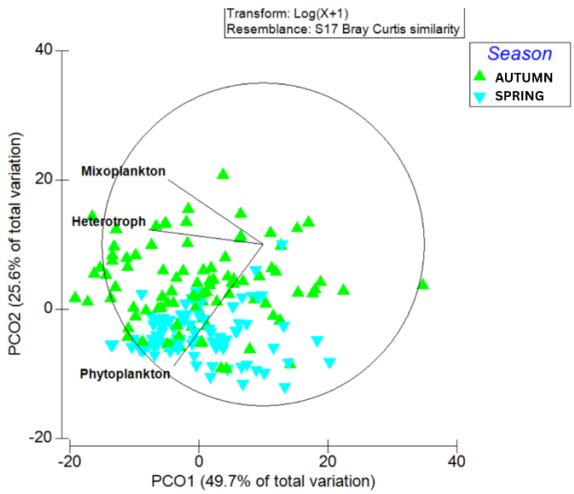

Figure 3. PCO considering the data collected by season. This analysis includes the following variables: Mixoplankton (cel/L), Heterotroph (cel/L) and Phytoplankton (cel/L).

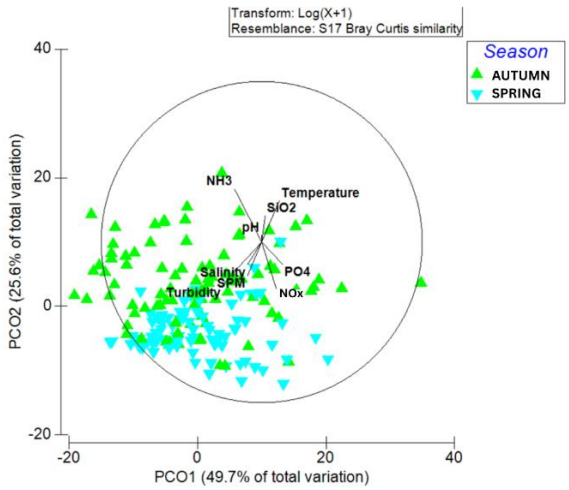

Figure 4. PCO considering the data collected by season. This analysis includes the following variables: temperature (ºC), salinity, PO4 (µmol/L), NOx (µmol/L), NH3 (µmol/L), pH, Suspended Particulate Matter (SPM) (mg/L), SiO_2 (µmol/L) and turbidity (FTU).

Some PERMANOVA analyses were carried out to better understand the relationship between the biological factors. Significant differences were observed between campaigns (*p*-value< 0.001) and between regions (A to E; *p*-value <0.001).

Although campaigns 2 and 3 were performed in different seasons, those were the campaigns that showed the least significant differences, with *p*-value> 0.05. Spring was characterized by lower temperatures, higher concentrations of NOx, Suspended Particulate Matter (SPM), turbidity, and salinity, along with reduced levels of NH_3 and silicate (SiO_2). In contrast, the autumn was associated with higher NH_3 and SiO_2, lower values of salinity, turbidity, SPM, NOx, but higher temperatures. These environmental patterns appear to structure the functional composition of the plankton community.

In addition to the observed functional diversity, some harmful species were identified throughout the campaigns. The potentially harmful *Prorocentrum cordatum* (Ostenfeld) J.D.Dodge, 1976, a constitutive mixoplankton dinoflagellate known for producing Diarrhetic Shellfish Toxins (DST), was found in significant concentrations in all campaigns, where alert levels indicated by the national authorities (100-200 cel/L and >500 cel/L for interdiction level, according to National Monitoring System for Bivalve Mollusks, IPMA, 2017) were reached in all areas, and at least in 4 of the 5 areas, levels reached concentrations sufficient for interdiction.

The species *Gymnodinium catenatum* H.W.Graham, 1943, also a constitutive mixotrophic dinoflagellate, one of the main causative HAB species in Iberia, known to produce Paralytic shellfish poisoning (PSP) toxins, was found in concentrations already considered alert level in all areas in autumn 2018 and in concentrations exceeding the level for prohibition at 16 stations covering most of the areas (alert level 500-1000 cel/L and >1500 cel/L for interdiction level, according to National Monitoring System for Bivalve Mollusks). In good agreement with these results, in October 2018, Lage *et al*. (2022) document high concentrations of PSP toxins in mussels collected from the entrance of the Tagus Estuary, South of Lisbon. Several other toxin-producing species were found during the campaigns, e.g. *Dinophysis spp.*, but none reached alert level concentrations.

4. DISCUSSION

The results obtained during the four oceanographic campaigns revealed the importance of mixoplankton as a functional component of the phytoplankton communities off the Portuguese coast. Their consistent presence, regardless of the time of year or region, reinforces the idea that mixotrophy is a widely successful adaptive strategy. The ability to combine photosynthesis with particle ingestion gives mixotrophic organisms a competitive advantage in stratified environments with low levels of NOx and PO_4, a condition observed above all in the fall campaigns (1 and 3), in which this group was more abundant.

The differences observed between campaigns suggest a strong influence of seasonality on the functional composition of the communities. The relative abundance of mixotrophs increased during periods of lower macro nutrient concentration, suggesting a competitive advantage of organisms with flexible trophic strategies, as can be seen in campaign 1. On the other hand, the spring campaigns (2 and 4) showed more functionally diverse communities, reflecting transitional conditions with greater vertical renewal and nutrient availability (Favareto *et al*., 2023).

These seasonal patterns indicate a classic ecological succession, beginning with a phase of high primary production driven by autotrophic phytoplankton, followed by a gradual transition to communities increasingly dominated by mixotrophic and heterotrophic protists. This interpretation agrees with the results of Favareto *et al*. (2023), who studied the spatio-temporal variability of chlorophyll *a* and its relation to physical and biogeochemical properties in the same oceanographic campaigns and documented coastal upwelling events responsible for bringing nutrient-rich subsurface waters to the surface, particularly during spring. These events were associated with notable increases in chlorophyll a. Taking together, these results suggest that seasonal changes in plankton functional groups are determined by nutrient availability, which in West Iberia is directly linked to processes such a seasonal coastal upwelling.

The presence of potentially toxic mixoplankton species such as *P. cordatum and G. catenatum* in different campaigns warns of the ecological risk associated with the growing dominance of mixotrophic organisms in coastal zones. Significant bloom events were recorded during all campaigns, and the repeated detection of these species in regions close to aquaculture zones highlights the importance of monitoring to anticipate and mitigate impacts on ecosystems and the blue economy. The data presented here reinforces the relevance of integrating mixoplankton into ecological models. Ignoring their multitrophic strategy when studying the flow of energy and matter in the ocean could compromise our ability to understand and predict the responses of marine ecosystems to global change.

Acknowledgements

L. Gonçalves would like to thank the Portuguese Navy for funding her doctoral research, and MARE - FCUL for being the host institution. The authors would like to thank all the collaborators of AQUIMAR project (MAR-02.01.01-FEAMP-0107) This study received further support from the FCT (htpps://doi.org/10.54499/UIDB/04292/2020).

REFERENCES

Favareto, L., Brotas, V., Rudorff, N., Zacarias, N., Tracana, A., Lamas, L., Nascimento, A., Ferreira, A., Gomes, M., Borges, C., Palma, C. and Brito, A.C. (2023). Response of phytoplankton to coastal upwelling: The importance of temporal and spatial scales. *Limnology and Oceanography*, 68(6), 1376-1387.

Faure, E., Not, F., Benoiston, A.-S., Labadie, K., Bittner, L. and Ayata, S.D. (2019). Mixotrophic protists display contrasted biogeographies in the global ocean. *The ISME Journal,* 13, 1072–1083.

Flynn, K.J., Mitra, A., Anestis, K., Anschütz, A.A., Calbet, A., Ferreira, G.D., Gypens, N., Hansen, P.J., John, U., Martin, J.L., Mansour, J.S., Maselli, M., Medić, N., Norlin, A., Not, F., Pitta, P., Romano, F., Saiz, E., Schneider, L.K., Stolte, W. and Traboni, C. (2019). Mixotrophic protists and a new paradigm for marine ecology: Where does plankton research go now? *Journal of Plankton Research,* 41(4), 375–391.

Guiry, M.D. and Guiry, G.M. (2024). *AlgaeBase*. World-wide electronic publication, National University of Ireland, Galway. Retrieved July 17, 2025, from https://www.algaebase.org

Hallegraeff, G., Enevoldsen, H. and Zingone, A. (2021). Global harmful algal bloom status reporting. *Harmful Algae,* 102, 101992.

Instituto Português do Mar e da Atmosfera (2017). *Tabela de classes de abundância para fitoplâncton em águas costeiras e de transição*. https://www.ipma.pt/export/sites/ipma/bin/docs/publicacoes/pescas.mar/tabela-062017-fitoplancton_zdp.pdf

Lage, S., Costa, P.R., Canário, A.V. and Da Silva, J.P. (2022). LC–HRMS profiling of paralytic shellfish toxins in *Mytilus galloprovincialis* after a *Gymnodinium catenatum* bloom. *Marine Drugs,* 20(11), 680.

Mitra, A., Flynn, K.J., Tillmann, U., Raven, J.A., Caron, D., Stoecker, D.K., Not, F., Hansen, P.J., Hallegraeff, G., Sanders, R., Wilken, S., McManus, G., Johnson, M., Pitta, P., Våge, S., Berge, T., Calbet, A., Thingstad, F., Jeong, H.J., Burkholder, J., Glibert, P.M., Granéli, E. and Lundgren, V. (2016). Defining Planktonic Protist Functional Groups on Mechanisms for Energy and Nutrient Acquisition: Incorporation of Diverse Mixotrophic Strategies. *Protist*, 167(2), 106–20. doi: 10.1016/j.protis.2016.01.003

Vallina, S.M., Follows, M.J., Dutkiewicz, S., Montoya, J M., Cermeño, P. and Loreau, M. (2014). Global relationship between phytoplankton diversity and productivity in the ocean. *Nature Communications, 5*, 4299.

Wilken, S. and McManus, G. (2025). Introduction to the themed section "Mixotrophs and mixoplankton: Conceptual integration into aquatic research". *Journal of Plankton Research,* 47(1), fbae056.

Translocation and monitoring of the endangered mollusc *Patella ferruginea* associated with the emergency works to repair the damage caused by the storms of March and April 2022 on the coast of Ceuta: specific study of adaptability and survival rates

E. Ostalé-Valriberas (1,2), A. Martín-Zorrilla (1), A. Sabino-Lorenzo (1), A. Pavón-Paneque (1,3) and J. C. García-Gómez (1)

(1) Laboratorio de Biología Marina de la Universidad de Sevilla (LBMUS)/Área de Investigación I+D+i del Acuario de Sevilla/Estación de Biología Marina del Estrecho (Ceuta), Universidad de Sevilla, Seville, Spain
(2) Instituto de Estudios Ceutíes, Paseo del Revellín 30, 51001 Ceuta, Spain.
(3) Centro Oceanográfico de Cádiz. Instituto Español de Oceanografía. Consejo Superior de Investigaciones Científicas (COCAD-IEO-CSIC). Muelle de Levante s/n, Cádiz, Spain.

Abstract: The natural settlement of the endangered limpet *Patella ferruginea* on artificial coastal defences in Ceuta (Alboran Sea) presents a management challenge during infrastructure repairs. Following storm damage in March–April 2022, emergency repairs prompted the development of a translocation protocol for this protected species. A total of 74 individuals (1.5–7.6 cm) were relocated across three zones using two extraction methods: spatula and drill. Mortality during translocation was 10 individuals, with causes detailed in supplementary material. Survival rates during the translocation phase were 73.33% (spatula) and 79.41% (drill), increasing to 83.33% and 89.41% respectively after correcting for natural mortality over 2.5 years. No significant difference was found between control and translocated populations. These findings demonstrate the viability of translocation as a conservation tool. Until *P. ferruginea* recovers its natural distribution, translocation should be implemented during coastal defence interventions to prevent biodiversity loss and socioeconomic conflicts.

Keywords: *endangered Patellogastropoda, translocation of individuals, coastal defence structures repair, management implications, socioeconomic problem*

1. INTRODUCTION

Patella ferruginea, one of the most endangered marine invertebrates in Europe, is an intertidal gastropod that plays a crucial ecological role in maintaining the structure of rocky intertidal communities (MTERD, 2023). This species currently faces critical threats due to habitat fragmentation and increasing anthropogenic pressures, especially along the coasts of the southern Iberian Peninsula and North Africa (Espinosa *et al.* 2014). Paradoxically, many of its surviving populations are found on artificial substrates such as breakwaters and port infrastructures (García-Gómez *et al.* 2023). However, these locations are frequently subject to works and modifications, which can result in the removal or destruction of entire populations.

2. OBJECTIVES

The present study aims to develop a methodology for the translocation of individuals with *P. ferruginea*, establish a protocol for future translocations, and enhance the conservation of this endangered species. Specifically, we compared two extraction techniques to determine which method offers better survival rates and evaluated the long-term viability of translocated individuals over a 2.5-year period.

3. METHODS

A total of 74 individuals were translocated from artificial structures damaged by storms in Ceuta, North Africa (Figure 1), to natural intertidal zones within a Special Area of Conservation (Natura 2000 Network).

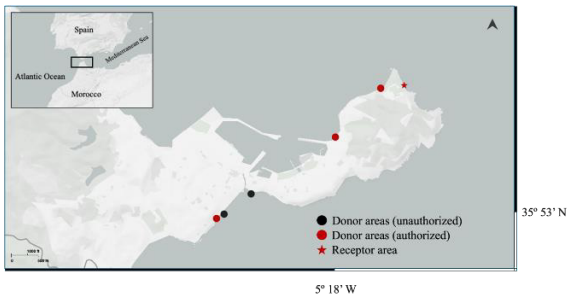

Figure 1. Location of the Strait of Gibraltar and the Spanish city of Ceuta (southern Strait) with the indication of the study stations.

Two extraction methods were tested:

1) Spatula extraction (n = 36)
2) Drill extraction (n = 38), using a hammer to preserve the limpet's surrounding substrate.

Survival was compared between the two translocated groups and a control group of 40 resident individuals. Survival was monitored over 2.5 years, with particular attention to the initial weeks following translocation.

4. RESULTS

Adjusted survival rates after 2.5 years were (Table I):

Spatula group: 83.33%

Core group: 89.41%

No statistically significant differences were found between the two treatments or between the translocated and control groups ($\chi^2 = 3.41$; $p = 0.181$).

Table I. (A) Number of individuals dead and alive throughout the study from August 2022 to February 2025; (B) Percentage of survival.

A	Dead	Alive in February 2025
Dead prior the translocation	2	-
Dead during the translocation (extraction, transfer and relocation)	10	-
Successfully resettled individuals	15	49
Total number of individuals control (natural mortality)	4	36
B	**Survival (%)**	**Mortality (%)**
Spatula treatment	73,33	26,67
Drill treatment	79,41	20,59
Spatula and drill treatment	76,56	23,44
Control treatment (natural mortality)	90,00	10,00
Spatula treatment (excluding natural mortality)	83,33	16,67
Drill treatment (excluding natural mortality)	89,41	10,59
Spatula and drill treatment (excluding natural mortality)	86,56	13,44

5. DISCUSSION

These results demonstrate that translocation of *P. ferruginea* is a viable conservation strategy when populations on artificial substrates are at risk (Ostalé-Valriberas *et al.* 2023; Pavón-Paneque *et al.* 2024). Both extraction methods were effective, although the drill method showed slightly higher survival rates. Short-term mortality (particularly within the first month) was the main limiting factor, suggesting that stabilization protocols during the critical post-translocation period could further improve success rates. The comparable survival of translocated and resident individuals indicates successful integration into the recipient habitat.

6. CONCLUSIONS

- Translocation is a feasible strategy to preserve *P. ferruginea* when artificial substrates cannot be maintained.
- Spatula and drill techniques are effective, but the drill method may offer slight advantages.
- Translocated individuals showed long-term survival comparable to that of native individuals in the receptor area.
- Continued refinement of translocation protocols is recommended, particularly for future long-distance interventions.
- The natural receptor area must have limited public access and be sheltered from prevailing winds and swell.
- Artificial micro-reserve networks could complement in situ conservation measures for this endangered species.

Acknowledgments

The authors express their gratitude to their families for their patience and understanding during the chaotic work hours on sampling days. It has been founded by Demarcación de Costas de Andalucía Atlántico (Cádiz) de la Dirección General de la Costa y el Mar and Sociedad, Obras, Infraestructuras y Medio Ambiente de Ceuta S.A.U. (OBIMASA).

REFERENCES

Espinosa, F., Rivera-Ingraham, G.A., Maestre, M., González, A.R., Bazairi, H. and García-Gómez, J.C. (2014). Updated global distribution of the threatened marine limpet Patella ferruginea (Gastropoda: Patellidae): an example of biodiversity loss in the Mediterranean. *Oryx*, 48(2), 266-275.

García-Gómez, J.C., Guerra-García, J.M., Espinosa, F., Maestre, M.J., Rivera-Ingraham, G., Fa, D., González, R., Ruiz-Tabares and López-Fé, C.M. (2015). Artificial Marine Micro-Reserves Networks (AMMRN s): an innovative approach to conserve marine littoral biodiversity and protect endangered species. *Marine Ecology*, 36(3), 259-277.

MTERD (2023). Estrategia para la conservación de la lapa ferrugínea (*Patella ferruginea*) en España. Ministerio para la Transición Ecológica y el Reto Demográfico (MTERD), Madrid, 35-36.

Ostalé-Valriberas, E., Sabino-Lorenzo, A., Ali-Ahmed, A., Pavón-Paneque, A., Sempere-Valverde, J., Espinosa, F., and García-Gómez, J.C. (2023). When the population of an endangered marine mollusc (*Patella ferruginea*) increases almost three-fold in ten years. Reality or fiction? *Frontiers in Marine Science*, 10, 1127630.

Pavón-Paneque, A., Ostalé-Valriberas, E., Sempere-Valverde, J., Sedano, F., Espinosa, F., and García-Gómez, J.C. (2024). Artificial portable plates: A brand new method for assisted colonization of an endangered marine invertebrate, *Patella ferruginea. Aquatic Conservation: Marine and Freshwater Ecosystems*, 34(1). https://doi.org/10.1002/aqc.4042

Functional Response Analysis of the Polyclad Flatworm *Postenterogonia orbicularis*: Implications for Predator-Prey Dynamics

E. Shorter-Rodríguez (1), R. López-Alonso (1), E. Pascual-Parra (1), M. Díez-Muñoz (1), V. Soto-López (2), D. Menéndez-Teleña (2), P. Rico-Fernández (1), P. Pereda-Bezanilla (1) and J. M. Rico (1)

(1) Department of Organisms and Systems Biology, University of Oviedo, Oviedo, Spain. UO282970@uniovi.es
(2) Department of Marine Science and Technology, University of Oviedo, Gijón, Spain

Abstract: The spread of invasive species, often driven by human activities and maritime transport, poses significant threats to biodiversity, ecosystems, and economies. In 2023, the invasive flatworm *Postenterogonia orbicularis* was identified for the first time in European waters near Avilés and Gijón, Spain. Morphological and genetic analyses confirmed an established population. As a known predator of bivalves, *P. orbicularis* presents a serious risk to local aquaculture, especially in the economically vital Asturias region. Laboratory experiments revealed a clear feeding preference for mussels (*Mytilus galloprovincialis*), with average consumption rates of 0.35 g/day per individual. Larger flatworms consumed less relative to body size. These findings highlight the importance of assessing the functional responses of invasive species to evaluate ecological impact and inform mitigation strategies. Given the difficulty of eradicating established populations, early detection and targeted management are essential to safeguard aquaculture and marine biodiversity.

***Key words**: Invasive species, Predation rate, Feeding behaviour, Bivalve predators*

1. INTRODUCTION

Invasive species are organisms that, as a result of direct or indirect human actions, establish populations beyond their natural geographic range and inflict significant ecological or economic damage (Courchamp *et al*., 2017; Ogden *et al*., 2019). However, assessing their impacts is often challenging, complicating their classification and delaying timely management responses (*Courchamp et al*., 2017). Ecosystems experiencing high levels of anthropogenic stress, such as pollution, fragmentation, or other disturbances, are especially prone to invasions, largely due to diminished biotic resistance and increased availability of unoccupied ecological niches (Fernández-Rodríguez *et al*., 2022).

Against this backdrop, the recent detection of the Pacific flatworm *Postenterogonia orbicularis* (Schmarda, 1859) along the Spanish coasts of Avilés and Gijón in 2023 is of particular concern. Verified through both morphological and molecular analyses (López-Alonso *et al.,* 2024), the presence of mature individuals indicates a likely self-sustaining population. This species belongs to the order Polycladida (phylum Platyhelminthes), a group comprising 800–1,000 globally distributed, free-living marine flatworms. Polyclads are generally large, carnivorous organisms with a folded pharynx and extensively branched digestive system. They are divided into two suborders: Cotylea, which possess a ventral sucker near the female genital opening, and Acotylea, which do not. Many polyclads feed on marine invertebrates, including arthropods, cnidarians, and molluscs (Ramos-Sánchez and Bastida-Zavala, 2022).

Of particular concern is their predation on commercially valuable bivalves such as mussels, oysters, and clams, which can result in substantial losses for aquaculture operations (López-Alonso *et al*., 2024). The genus *Postenterogonia* (Faubel, 1983), within the family Ilyplanidae Faubel, 1983, is monospecific and was first described from New Zealand and Australian waters, with additional sightings in Japan (Vieira *et al*., 2020). The sole species, *P. orbicularis*, is recognized as a major aquaculture pest in New Zealand, where it negatively impacts bivalve farming (Georgidaes *et al*., 2016).

Aquaculture, the farming of aquatic organisms such as fish, shellfish and seaweed, has become essential for global food security as wild fish stocks decline due to overfishing, habitat loss, pollution and climate change (Garlock *et al*., 2024). Unlike wild fisheries, aquaculture offers controlled production systems that ensure a stable and reliable supply of nutritious protein. It also supports millions of livelihoods, particularly in coastal and rural areas, contributing to local economies through both farming and related industries (Garlock *et al*., 2024). When managed responsibly, aquaculture provides environmental benefits, such as improved water quality and reduced pressure on wild fish populations, especially through integrated systems like shellfish and seaweed farming (Thomas *et al*., 2021). As global food systems face mounting pressure, aquaculture is increasingly vital

for sustainable development and long-term food resilience. A way of maintaining this type of industry is by studying the factors that can damage it, like, in this example, invasive species such as *P. orbicularis*.

2. METHODOLOGY

In this study, individuals of *P. orbicularis* were collected and used for experimental trials. A total of 54 isolated specimens were maintained individually in separate aquaria. Additionally, six control tanks were included to assess the amount of food lost due to immersion in water without the presence of the flatworms. The feeding preferences of *P. orbicularis* were evaluated using three types of prey: mussels (*Mytilus* galloprovincialis), oysters (*Crassostrea gigas*) and barnacles (*Pollicipes pollicipes*).

3. RESULTS

Observations showed that *P. orbicularis* did not feed on barnacles (*P. pollicipes*), possibly because they were either not recognized as prey or were too difficult to access or consume. In contrast, the flatworms fed readily on both mussels (*M. galloprovincialis*) and oysters (*C. gigas*), showing a strong preference for mussels when both were offered. This preference may be due to mussels being easier to open or more attractive in terms of scent or texture. On average, each flatworm consumed about 0.35 grams of mussel tissue per day. Interestingly, smaller flatworms ate more food relative to their size compared to larger ones, which may be due to differences in metabolism or energy needs. These results suggest that *P. orbicularis* could pose a greater threat to mussel populations, particularly in aquaculture settings where mussels are a key commercial species.

4. CONCLUSION

Understanding the functional response of animals, particularly invasive species, is critical for predicting their ecological impacts and managing their populations effectively. In the context of aquaculture, such knowledge enables the identification of potential threats to farmed species by revealing feeding behaviours, prey preferences and consumption rates of invasive organisms. This information is essential for developing targeted mitigation strategies

REFERENCES

Courchamp, F., Fournier, A., Bellard, C., Bertelsmeier, C., Bonnaud, E., Jeschke, J.M. and Russell, J.C. (2017). Invasion Biology: Specific Problems and Possible Solutions. *Trends in Ecology & Evolution*, 32(1), 13-22. https://doi.org/10.1016/j.tree.2016.11.001

Faubel, A. (1983). The Polycladida, Turbellaria - Proposal and estalishment of a new system Part I. The Acotylea. Mitteilungen aus dem Hamburgischen Zoologischen Museum und Institut. 80: 17-121.

Fernández-Rodríguez, I., López-Alonso, R., Sánchez, O., Suárez-Turienzo, I., Gutiérrez-Martínez, R. and Arias, A. (2022). Detection and prevention of biological invasions in marinas and ports: Epibionts and associated fauna of Mytilus galloprovincialis revisited. *Estuarine, Coastal and Shelf Science*, 274, 107943. https://doi.org/10.1016/j.ecss.2022.107943

Garlock, T.M., Asche, F., Anderson, J.L., Eggert, H., Anderson, T.M., Che, B. and Tveteras, R. (2024). Environmental, economic, and social sustainability in aquaculture: the aquaculture performance indicators. *Nature Communications*, *15*(1), 5274. https://doi.org/10.1038/s41467-024-49556-8

Georgiades, E., Fraser, R. and Jones, B. (2016). Options to strengthen on-farm biosecurity management for commercial and non-commercial aquaculture. Aquaculture Unit. Technical Paper No: *2016/47*.

López-Alonso, R., Pascual-Parra, E., González-Toral, C., del Cerro, A., Muñoz, M., Soto-López, V. and Arias, A. (2024). A new threat to the European marine environment: The exotic polyclad flatworm Postenterogonia orbicularis (Schmarda, 1859). *Regional Studies in Marine Science*, *78*, 103758. https://doi.org/10.1016/J.RSMA.2024.103758

Ogden, N.H., Wilson, J.R., Richardson, D.M., Hui, C., Davies, S.J., Kumschick, S. and Pulliam, J.R. (2019). Emerging infectious diseases and biological invasions: a call for a One Health collaboration in science and management. *Royal Society Open Science*, *6*(3), 181577. http://doi.org/10.1098/rsos.181577

Ramos-Sánchez, M. and Bastida-Zavala, J.R. (2022). Policládidos (Platyhelminthes: Rhabditophora) y nemertinos (Nemertea). *Invertebrados marinos y costeros del Pacífico sur de México*, 53-66.

Schmarda, L.K. (1859). Neue Turbellarien, Rotatorien und Anneliden, Beobachtet und Gesammelt auf einer Reise um die erde 1853 bis 1857. Erster hälfte. [Book]. 66 pp, W. Engelmann, Leipzig.

Thomas, M., Pasquet, A., Aubin, J., Nahon, S. and Lecocq, T. (2021). When more is more: taking advantage of species diversity to move towards sustainable aquaculture. *Biological reviews*, *96*(2), 767-784. http://doi.org/10.1111/brv.12677

Vieira, J., Bechade, M. and Benetiere, F. (2020). Observatoire ostréicole du Bassin d'Arcachon. *Rapport annuel*. http://doi.org/10.13140/RG.2.2.34923.52008

Preliminary characterization of the macrofauna associated to *Gelidium corneum* habitats in the infralittoral rocky coasts of Cantabria (Northern Spain)

B. Rincón (1), M. Huerta (1), A. Aja (1), N. L. Arroyo (2), I. Bolado (1), A. Serrano (1) and D. Díaz (3)

(1) Centro Oceanográfico Santander (COST), Spain. beatriz.rincon@ieo.csic.es
(2) Centro Oceanográfico Canarias (COC), Spain
(3) Centro Oceanográfico Baleares (COB), Spain

Abstract: This study provides the first description of macrofaunal assemblages associated with *Gelidium corneum* habitats along the Cantabrian coast (north Spain). This Rhodophyta forms dense aggregations on infralittoral rocky bottoms, representing the dominant habitat in the area. Despite its ecological importance, associated macrofauna remains poorly documented. Data were collected as part of the Spanish Marine Strategies Monitoring Program (2022–2023) using SCUBA visual transects at depths of 5–18 meters. Quadrats were sampled and analyzed in the laboratory to identify macrofauna, comparing sites with different levels of anthropogenic impact. Preliminary results show a dominance of crustaceans—mainly amphipods—followed by molluscs and annelids, consistent with findings from similar habitats. Faunal differences between high- and low-impact areas suggest that environmental and human-related factors shape community structure. This study lays the groundwork for the ecological characterization of *Gelidium corneum* habitats in Cantabria and contributes to assess biodiversity and the health of infralittoral ecosystems.

Keywords: *infralittoral ecosystems, benthic habitats, northern Spain*

Fish communities of infralittoral rocky bottoms in North Spain (Northeast Atlantic)

M. Huerta (1), B. Rincón (1), A. Aja (1), N. L. Arroyo (2), I. Bolado (1), A. Martín (3), S. Díez (4), D. Díaz (4) and A. Serrano (1)

(1) Centro Oceanográfico Santander (COST), Spain. maria.huerta@ieo.csic.es
(2) Centro Oceanográfico Canarias (COC), Spain
(3) Centro Oceanográfico Málaga (COMA), Spain
(4) Centro Oceanográfico Baleares (COB), Spain

Abstract: Fish communities are key indicators of marine environmental health. This study assesses the status of infralittoral rocky fish communities in the North Atlantic subdivision (southern Bay of Biscay and Galician waters), within the framework of the Infralittoral Benthic Habitats Monitoring Programme (MP) of the Marine Strategy Framework Directive (MSFD). Ecological indicators analyzed include taxonomic diversity, abundance, biomass, size distribution, and classical diversity indices. Non-destructive underwater visual censuses (SCUBA) were conducted between 2022 and 2025, totaling 55 dives across 270 transects. A total of 66 fish species from 23 families were recorded, with 19 identified as characteristic of the study area. Results show higher species richness and abundance in areas with lower anthropogenic pressure. Differences in size distribution of some species were also observed, likely linked to abiotic variability among sites. This study provides essential insights into the structure and condition of infralittoral fish communities, supporting effective marine environmental assessment.

Keywords: *fish, marine environmental health, infralittoral rocky, North Atlantic subdivision, ecological indicators, habitats, fish communities*

Morphological and Developmental Stages of Embryogenesis and Larval Growth in *Postenterogonia orbicularis*

E. Shorter-Rodríguez (1), R. López-Alonso (1), E. Pascual-Parra (1), M. Díez-Muñoz (1), V. Soto-López (2), D. Menéndez-Teleña (2), P. Rico-Fernández (1), P. Pereda-Bezanilla (1), J. M. Rico (1)

(1) Department of Organisms and Systems Biology, University of Oviedo, Oviedo, Spain. UO282970@uniovi.es
(2) Department of Marine Science and Technology, University of Oviedo, Gijón, Spain

Abstract: Global biodiversity loss is intensified by habitat degradation and the spread of invasive species, driven by climate change and human activities. Ports and marinas, due to disturbance and maritime transport, are major entry points for marine invasive species. In 2023, the invasive flatworm *Postenterogonia orbicularis* was recorded for the first time in European waters (Avilés and Gijón, Spain). Morphological and genetic analyses confirmed an established, reproducing population. As a predator of bivalves, *P. orbicularis* poses a threat to aquaculture. Its embryonic development was studied in the laboratory, revealing spiral cleavage and mosaic development, culminating in the formation of Müller's larvae. Developmental insights are essential for understanding the species' invasive potential, guiding early detection, and informing control strategies.

***Key words**: Invasive species, Polyclads, Postenterogonia orbicularis, Embryology*

1. INTRODUCTION

Invasive species are defined as organisms that establish outside their native range due to human activity and cause measurable ecological or economic harm (Courchamp *et al*., 2017; Ogden *et al.,* 2019). Determining invasiveness is complex due to difficulties in impact assessment, often delaying intervention (Courchamp *et al*., 2017). Degraded ecosystems, such as polluted or fragmented habitats, are particularly susceptible to invasions due to reduced biotic resistance and available ecological niches (Fernández-Rodríguez *et al.*, 2022).

In this context, the identification of the Pacific flatworm *Postenterogonia orbicularis* in European waters, specifically along the coasts of Avilés and Gijón (Spain) in 2023, is particularly noteworthy. The species was confirmed through both morphological and genetic analyses (López-Alonso *et al.,* 2023). The discovery of sexually mature individuals suggests the establishment of a reproducing population in the region. *P. orbicularis* belongs to the order Polycladida (phylum Platyhelminthes), which includes 800–1,000 species of free-living marine flatworms distributed worldwide. Polyclad flatworms are predominantly large, marine, carnivorous organisms, characterized by a folded pharynx and a complex branched intestine, and are classified into two suborders: Cotylea, which possess a ventral sucker near the female genital opening, and Acotylea, which lack this structure, with many species preying on invertebrates such as arthropods, cnidarians, and molluscs (Ramos-Sánchez and Bastida-Zavala, 2022). Bivalves, especially those of commercial interest like mussels, oysters, and clams, are particularly susceptible to predation by polyclads, leading to significant mortality and economic losses in aquaculture operations (López-Alonso *et al.,* 2023). The genus *Postenterogonia* (Faubel, 1893), within the family Ilyplanidae, is monospecific and was originally described from New Zealand and Australian waters, with subsequent reports from Japan (Vieira *et al*., 2020). The only known species, *P. orbicularis*, has been identified as a serious pest in New Zealand aquaculture, where it adversely affects bivalve production (Georgidaes *et al*., 2016).

The embryological processes of polyclad flatworms have long attracted scientific interest due to their conserved developmental patterns. Like other spiralians, they exhibit spiral cleavage during early development, producing both macromeres and micromeres. The 4d blastomere, or mesentoblast, is crucial for forming both mesodermal and endodermal tissues. However, there is ongoing debate regarding the precise lineage and division pattern of this cell. Research indicates that polyclad development is mosaic and determinate, meaning each cell has a fixed fate from early stages. Body axes are specified after the 8-cell stage, likely through cell–cell interactions. Gastrulation occurs via epiboly, where ectodermal cells spread over the embryo. The pharynx and brain originate from specific micromere lineages, with the brain forming near the animal pole before migrating anteriorly, and the gut extending posteriorly. The developmental process culminates in either a juvenile worm or a Müller's larva, a free-swimming, spherical larval stage with eight lobes and

three eyes, typical of many cotylean and some acotylean species (Martin-Durán and Egger, 2012).

2. METHODOLOGY

Larval development of *Postenterogonia orbicularis* was investigated under controlled laboratory conditions to better understand its reproductive biology and developmental timeline. Adult specimens were maintained in aquaria, where they deposited egg masses on submerged surfaces. These egg masses, notable for their distinctive zigzag patterning, served as a reliable morphological feature for species identification. Daily monitoring allowed for timely collection of freshly laid egg masses, which were individually labelled and tracked throughout development. Selected samples were fixed in EUKITT mounting medium to preserve embryonic structures for histological and microscopic analysis, enabling detailed observation of cleavage patterns, gastrulation, and larval formation. The samples were later analysed using an electronic microscope.

3. RESULTS

Embryogenesis spanned approximately 12 days under stable laboratory conditions, during which embryos progressed through a series of well-defined developmental stages characteristic of polyclad flatworms. Early cleavage followed a spiral pattern, producing both macromeres and micromeres, and was consistent with the mosaic, determinate mode of development typical of spiralian taxa**.** Gastrulation occurred via epiboly, as ectodermal cells migrated to enclose the yolky interior. Organogenesis proceeded with the differentiation of key structures, including the pharynx and central nervous system. Development culminated in the emergence of Müller's larvae (as seen in Figure 1), free-swimming, ciliated larvae with a spherical body, eight lobes, and three pigmented eyes, reflecting the typical morphology observed in many cotylean polyclads. These larvae represent a dispersive stage in the life cycle, enhancing the species' potential for colonization and contributing to its invasive success.

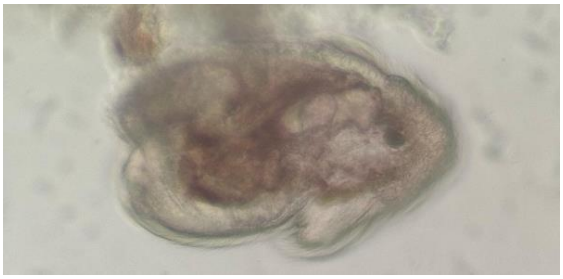

Figure 1. Image of Müller's larvae obtained trhough the experiment.

4. CONCLUSION

Understanding the developmental biology of invasive species like *P. orbicularis* is vital for predicting invasion potential and identifying life stages susceptible to control. Such insights are critical for developing effective early detection and management strategies, particularly in high-risk areas like ports and aquaculture facilities.

REFERENCES

Courchamp, F., Fournier, A., Bellard, C., Bertelsmeier, C., Bonnaud, E., Jeschke, J.M. and Russell, J.C. (2017). Invasion Biology: Specific Problems and Possible Solutions. *Trends in Ecology & Evolu*tion, 32(1), 13-22. https://doi.org/10.1016/j.tree.2016.11.001

Fernández-Rodríguez, I., López-Alonso, R., Sánchez, O., Suárez-Turienzo, I., Gutiérrez-Martínez, R. and Arias, A. (2022). Detection and prevention of biological invasions in marinas and ports: Epibionts and associated fauna of Mytilus galloprovincialis revisited. *Estuarine, Coastal and Shelf Science*, 274, 107943. https://doi.org/10.1016/j.ecss.2022.107943

Georgiades, E., Fraser, R. and Jones, B. (2016). Options to strengthen on-farm biosecurity management for commercial and non-commercial aquaculture. Aquaculture Unit. Technical Paper No: 2016/47.

López-Alonso, R., Pascual-Parra, E., González-Toral, C., del Cerro, A., Muñoz, M., Soto-López, V. and Arias, A. (2024). A new threat to the European marine environment: The exotic polyclad flatworm Postenterogonia orbicularis (Schmarda, 1859). *Regional Studies in Marine Science*, 78, 103758. https://doi.org/10.1016/J.RSMA.2024.103758

Martín-Durán, J.M. and Egger, B. (2012). Developmental diversity in free-living flatworms. *EvoDevo*, 3, 1-23. https://doi.org/10.1186/2041-9139-3-7

Ogden, N.H., Wilson, J.R., Richardson, D.M., Hui, C., Davies, S.J., Kumschick, S. and Pulliam, J.R. (2019). Emerging infectious diseases and biological invasions: a call for a One Health collaboration in science and management. *Royal Society Open Science*, 6(3), 181577. http://doi.org/10.1098/rsos.181577

Ramos-Sánchez, M. and Bastida-Zavala, J.R. (2022). Policládidos (Platyhelminthes: Rhabditophora) y nemertinos (Nemertea). Invertebrados marinos y costeros del Pacífico sur de México, 53-66.

Vieira, J., Bechade, M. and Benetiere, F. (2020). Observatoire ostréicole du Bassin d'Arcachon. Rapport annuel. http://doi.org/10.13140/RG.2.2.34923.52008

Impact of epibionts on Habitat Forming Species: The case of the octocoral *Paramuricea tingitana* (Cnidaria, Octocorallia, Malacalcyonacea) in the Gulf of Cádiz

S. Román (1), A. Rodríguez-Rúa (1), C. Caro de la Barrera (1), C. Farias (1), M. Sayago (1), R. Jiménez-Romero (1), J. Gil (1), M. Delgado (1) and M. M. González-Duarte (1)

(1) Centro Oceanográfico de Cádiz, Instituto Español de Oceanografía (IEO-CSIC). sara.roman@ieo.csic.es

Abstract: An ecosystem represented by mixed octocoral gardens in rocky circalitoral bottoms affected by high sedimentation levels was studied in the Gulf of Cadiz (SW Spain) by means of Remotely Operated Vehicle (ROV) photo imaging. This habitat was mainly composed by arborescent colonies of *Eunicella spp, Leptogorgia sarmentosa* and *Paramuricea tingitana,* the latter being by far the most important species in terms of abundance and biomass. These colonies of *P. tingitana* showed different extent of damage expressed by the colonization of the dead areas of the colonies by hydroids and bryozoans. The aim of this research was to evaluate these impacts in *P. tingitana* by image analysis, using VIER software. A total of 859 colonies were recorded, with 27% showed severe damages. These observations highlight the need for further research in order to inform and support effective managements strategies to protect these habitats.

Keywords: *gorgonian, Paramuricea tingitana, disturbance, Gulf of Cádiz, epibiosis*

1. INTRODUCTION

The Gulf of Cádiz (GoC) hosts areas of high biodiversity and a large number of protected and/or threatened species. However, there is a lack of studies on benthic communities associated with circalitoral rocky habitats, as well, as on their potential impacts.

Habitat- Forming Species (HFS) play a crucial role in marine ecosystems by creating stable conditions and providing refuge and food for many benthic species (Dayton, 1972; Buhl-Mortensen *et al*., 2010). Among them, octocorals show complex branching morphology and sufficient size to provide substrate and/or refuge for other species (Bo *et al*., 2012).

During the CIRCASUR 2023 oceanographic cruise, submarine images of shallow bottoms of the GoC were taken with a Remotely Operated Vehicle (ROV). One of the habitats observed might be called: "Mixed octocoral gardens in circalittoral rocky bottoms affected by high sedimentation". These coral gardens consist in species belonging to the families Eunicellidae (*Eunicella gazella* Studer, 1901; *Eunicella labiata* Thomson, 1927 and in a lesser extent *Eunicella verrucosa* (Pallas, 1766)), Gorgoniidae (*Leptogorgia sarmentosa* (Esper, 1791) and Acanthogorgiidae (*Paramuricea tingitana* Ocaña and Correa, 2022). Among all them we can highlight the abundance of the colonies of *Paramuricea tingitana.* These colonies showed different extent of epibiosis by hydroids and bryozoans. Octocorals, like other suspension-feeders, can be affected by intense sedimentation, which may provoque burial or asphyxiation, as these processes can obstruct their feeding and respiratory surfaces (Hendrick *et al*. 2016). Such conditions may cause partial necrosis of the colonies facilitating the colonization by epibionts (Erftemeijer *et al*., 2012). *Paramunicea tingitana,* considered as an HFS, is also an indicator of Vulnerable Marine Ecosystems and a key contributor to habitat type 1170 under the EU Habitat Directive. For these reasons, it is essential to evaluate the extent of the impacts and determine whether these species are experiencing negative effects, particularly if they are affected by severe epibiosis.

The main objective of the present study was evaluate these impacts in *P.tingitana* by using image analysis. This study will serve as an initial analysis of for the application of the Marine Strategy Framework Directive in circalittoral rocky bottoms in the Gulf of Cádiz (Spanish waters).

2. MATERIAL AND METHODS

In this preliminary study, one of the ROV transects carried out during the CIRCASUR 2023 oceanographic cruise for the monitoring of benthic habitats within the Marine Strategy Framework Directive was selected. The transect covers a distance of about 500 meters at 55-60 meters depth (Figure 1).

The bathymetry used in this study -5 m resolution grid- forms part of the database of the Marine Geology Group of IEO (ESMARES3 Project). The study area is located on a rocky outcrop on the continental shelf of the GoC.

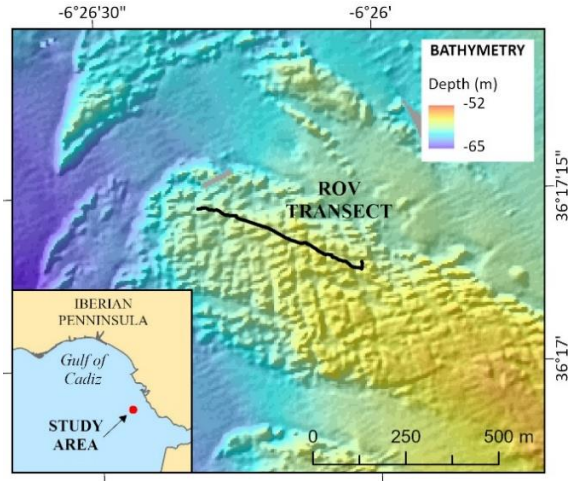

Figure 1. Map of the study area with the location of the ROV transect.

Submarine images were analyzed using VIER software (De la Torriente *et al*., 2024), to quantify the number of *P. tingitana* colonies affected by epibionts. Total number of colonies and the number of those affected by epibiosis were recorded.

A visual survey method was used to assess the condition of the colonies (Figuerola-Ferrando *et al*., 2023). To quantify the degree of impact, four categories were defined: 1) non–impacted/low impacted colonies (<10% of colony affected); 2) medium impact (≥10 y <30% of colony affected); 3) moderately impacted (≥30 y <60%) and 4) severely/high impacted) (≥60% of colony affected) (Figure 2). In addition, sampled were collected and preserved in 70% ethanol for subsequent identification in the laboratory. Identifications were carried out to the highest possible taxonomic resolution, in most of cases to the species level.

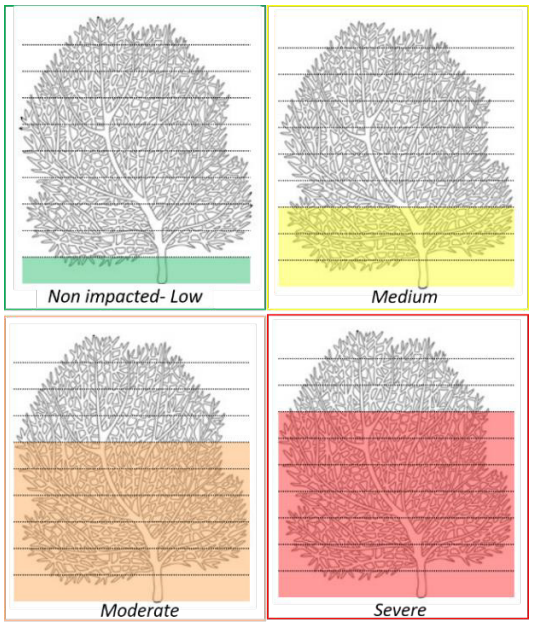

Figure 2. Scheme of impact categories used for visual analyses.

3. RESULTS

Most of the epibionts growing on *P. tingitana* were hydroids and bryozoans. A total of twelve species of hydroids were recorded, including both stolonal forms (e.g., *Campalunaria hincksii* Alder, 1856) and larger colonial forms (e.g., *Eudendrium* sp.). The most abundant species was *Antennella secundaria* (Gmelin, 1791). Likewise, a total of four species of bryozoans were found growing over *P. tingitana,* although damages by bryozoans were not quantify in this work.

A total of 859 *P. tingitana* colonies were recorded. Based on the analysis of submarine images, 27% of the colonies (233), showed severe damages, while 60% appeared unaffected (Figure 3). The two other impact categories (medium and moderate) accounted for less than 13% of the colonies.

These preliminary observations highlight the need for long-term monitoring of these species and habitats, as well as a thorough investigation into the underlying causes of the observed high sedimentation rates (whether they are driven by episodic events, sustained processes over time, or both) in order to inform and support effective management strategies aimed at protecting these habitats.

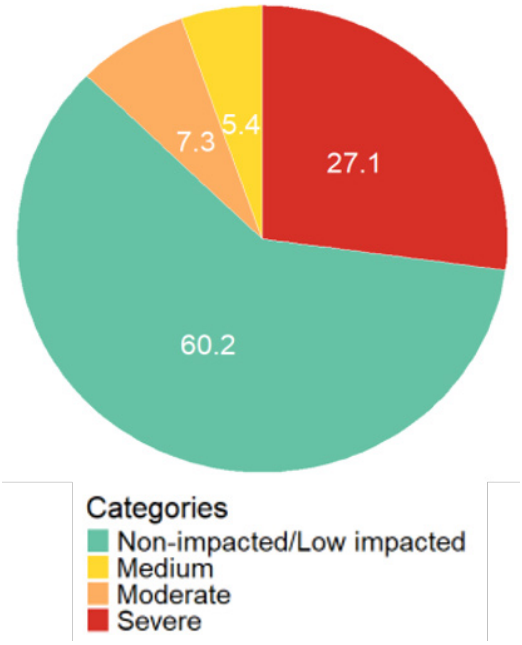

Figure 3. Percentage of the different categories of impact in Paramuricea tingitana found along the study transect.

Acknowledgments

This research was developed within the 18-ESMARES2-CIRCA and 6-ESMARES3-CIRCA projects, included in the scientific program "Asesoramiento científico-técnico para la protección del medio marino: Evaluación y seguimiento de las Estrategias

Marinas, Seguimiento de los espacios marinos protegidos de competencia estatal", funded by the General Di-rectorate of Sea Protection of the Ministry for the Eco-logical Transition and the Demographic Challenge. The authors thank the participants of the CIRCASUR 2023 survey, and the crew of the research vessels on which it was performed (R/V Ramón Margalef).

REFERENCES

Bo, M., Canese, S., Spaggiari, C., Pusceddu, A., Bertolino, M., *et al.* (2012). Deep Coral Oases in the South Tyrrhenian Sea. *PLoS One,* 7(11): e49870.

Buhl-Mortensen, L., Vanreusel, A., Gooday, A.J., Levin, L.A., Priede, I.G., Buhl-Mortensen, P., ... and Raes, M. (2010). Biological structures as a source of habitat heterogeneity and biodiversity on the deep ocean margins. *Marine Ecology*, 31(1), 21-50.

Dayton, P.K. (1972). Toward an understanding of community resilience and the potential effects of enrichments to the benthos at McMurdo Sound, Antarctica. In *Proceedings of the colloquium on conservation problems in Antarctica* (Vol. 96).

De la Torriente, A., Villazón, P., Antolínez, A. and Serrano, A. (2024). VIER – Viewing Images for Ecosystem Research.

Erftemeijer, P.L.A., Riegl, B., Hoeksema, B.W. and Todd, P.A. (2012). Environmental impacts of dredging and other sediment disturbances on corals: a review. *Marine pollution Bulletin,* 50, 125-146.

Figuerola-Ferrando, L., Garrabou, J. and Linares, C. (2024). A rapid assessment method to monitor the health status of habitat-forming species in coastal benthic ecosystems. *Aquatic Conservation: Marine and Freshwater Ecosystems,* 34(3), e4120.

Hendrick, V.J., Hutchison, Z.L. and Last, K.S. (2016). Sediment burial intolerance of marine macroinvertebrates. *PloS One*, *11*(2), e0149114.

Protocolo para una base de datos fiable usando equinodermos en aguas españolas: depuración, validación y visualización

L. M. García-Guillén (1), M. E. Manjón-Cabeza (2), J. Cristobo (1), P. Baragaño (1) y P. Ríos (1)

(1) Instituto Español de Oceanografía (IEO-CSIC) Gijón, España. laura.gagui@ieo.csic.es
(2) Universidad de Málaga (UMA) Málaga, España.

Abstract: Major open-access databases (DB), such as the Ocean Biodiversity Information System (OBIS) and the Global Biodiversity Information Facility (GBIF), provide extensive information across different areas. However, they present recurring issues, including duplicate records, taxonomic errors, and the absence of expert validation, which can lead to misinterpretations if used without prior filtering. This proposal aims to design a replicable protocol for building a refined and reliable DB, using echinoderms from Spanish Waters, specifically the South Atlantic Marine Subdivision as a case study, and taking the Official Spanish List of Marine Species (LPEM) as a reliable reference. Through critical review of records in public databases and the development of comparative distribution maps, current limitations will be identified. The protocol will incorporate quality criteria, expert validation, and visual representations of filtered and unfiltered data to highlight existing differences.

Keywords: *Data base, validation, marine biodiversity, Official Spanish List of Marine Species (LPEM), Echinoderms*

1. INTRODUCCIÓN

Las bases de datos abiertas como la Ocean Biodiversity Information System (OBIS) (2025) y la Global Biodiversity Information Facility (GBIF) (2025) son herramientas clave para el estudio de la biodiversidad marina, pero presentan limitaciones que pueden comprometer su uso directo. Estas plataformas recogen miles de registros biológicos, aunque a menudo incluyen errores taxonómicos, coordenadas imprecisas o falta de validación experta, incluso a veces ambas bases de datos contienen registros distintos para una misma área lo que hace necesario revisar y comparar ambas fuentes para una obtención de datos completa.

Los equinodermos, por su valor ecológico y su uso como bioindicadores, requieren datos fiables y depurados para su uso en estudios científicos rigurosos. Este trabajo desarrolla un protocolo metodológico para obtener una base de datos robusta centrada en el entorno marino español.

En concreto, las aguas marinas españolas están organizadas en demarcaciones marinas, en total son cinco (Figura 1). El presente trabajo se centra la demarcación marina Sudatlántica (Figura 1, S), esta presenta una menor cantidad de información sobre equinodermos en comparación con otras zonas como la Demarcación Noratlántica (Figura 1, N) Manjón-Cabeza *et al.* (2021) (2022); Ríos *et al.* (2022); García-Guillén *et al.* (2022a,b); García-Guillén *et al*. (2023); Macías *et al*. (2024); García-Guillén *et al.* (2025). Por ello, resulta adecuada para aplicar un protocolo piloto de depuración y validación, ya que permite mostrar de forma clara y operativa el análisis de las bases de datos. Además, profundizar en su estudio contribuiría a mejorar el conocimiento sobre la distribución real de los equinodermos en esta área, actualmente poco estudiada y por lo tanto infrarepresentada en las bases de datos abiertas.

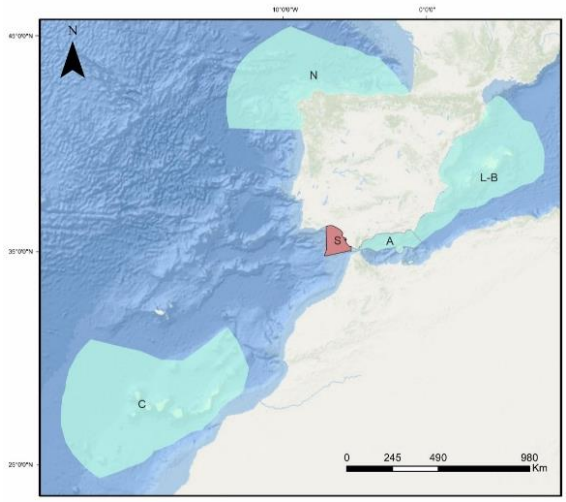

Figura 1. Demarcaciones marinas. N: Noratlántica. L-B: Levantina-balear. A: Alborán. S: Sudatlántica. C: Canaria.

2. MATERIAL Y MÉTODOS

2.1. Descarga y filtrado espacial

Se descargaron tablas en formato *csv* de OBIS y GBIF con registros de equinodermos correspondientes a la demarcación marina Sudatlántica. Las tablas suelen

presentar errores de formato, especialmente en las columnas de coordenadas, que aparecen normalmente con separadores incorrectos. Para corregir estos problemas, se utilizan scripts en Python que automatizan la limpieza y preparación de los datos para su uso en ArcGIS. Además, es imprescindible estandarizar las tablas de OBIS y GBIF, ya que cada una contiene campos distintos. Cada investigador debe seleccionar las columnas relevantes según los objetivos del estudio.

2.2. Análisis de registros y limpieza

Se compararon los registros obtenidos de OBIS y GBIF, evaluando tanto el número total como su procedencia (instituciones, autores, fuente). Se eliminaron los registros de baja fiabilidad, especialmente aquellos etiquetados como "observación humana" no respaldada. Muchas de estas observaciones se realizan *in situ* mediante fotografías generales en las que apenas pueden observarse caracteres diagnósticos claros. En el caso de los equinodermos, como la mayoría de especies bentónicas, es habitual que la correcta identificación exija el uso de guías especializadas, observación bajo lupa o microscopio, e incluso preparaciones con osículos u otras estructuras internas. Existen especies morfológicamente muy similares entre sí, imposibles de distinguir con una sola imagen superficial. Por tanto, para evitar errores de identificación, se descartan estas observaciones o se asignan únicamente a niveles taxonómicos superiores cuando sea necesario (género, familia). Se conservaron solo aquellos registros procedentes de publicaciones científicas revisadas, museos con ejemplares preservados y especialistas reconocidos en el campo.

2.3. Validación taxonómica

La lista resultante de especies se contrastó con la Lista Patrón Española de Especies Marinas (LPEM), usada como referencia oficial. La LPEM permite conocer en qué demarcaciones está presente cada especie, aunque no incluya coordenadas exactas. También se utilizaron herramientas como World Register of Marine Species (WoRMS) (2025) para confirmar la nomenclatura actual aceptada y detectar sinonimias.

2.4. Visualización comparativa

Se generaron visualizaciones para comparar el volumen y la distribución de los datos antes y después del filtrado. Se contrastaron los registros "en bruto" (originales de OBIS y GBIF) con la base depurada y validada. Asimismo, se realizó una comparativa entre el número total de especies en OBIS, GBIF y la LPEM, evaluando las coincidencias y divergencias. Este análisis permite valorar la aportación de cada base y la mejora alcanzada tras la aplicación del protocolo.

3. RESULTADOS ESPERADOS Y PERSPECTIVAS

Aunque el protocolo aún está en desarrollo, ya se han generado los primeros resultados preliminares. Se ha elaborado un mapa comparativo con los registros de equinodermos obtenidos de OBIS y GBIF sin depurar ni validar (Figura 2). Este primer análisis pone de manifiesto diferencias claras entre ambas bases de datos: OBIS contiene un número muy reducido de puntos para la demarcación Sudatlántica, mientras que GBIF presenta un número de registros mayor, que además no coinciden entre ellos.

El siguiente paso será revisar y analizar en detalle las tablas asociadas a cada punto para identificar los registros fiables, es decir, aquellos respaldados por instituciones reconocidas, publicaciones científicas o ejemplares de museo. Se espera que, tras la depuración, la base de datos final contenga información más precisa, consistente y útil para futuros estudios.

Este protocolo, además de mejorar la calidad de los datos disponibles para la demarcación marina Sudatlántica, puede replicarse en otras regiones o a otros grupos taxonómicos. También ofrece una base sólida para futuras colaboraciones científicas que permitan profundizar en el conocimiento de la biodiversidad bentónica en zonas actualmente subrepresentadas como la expuesta en este trabajo.

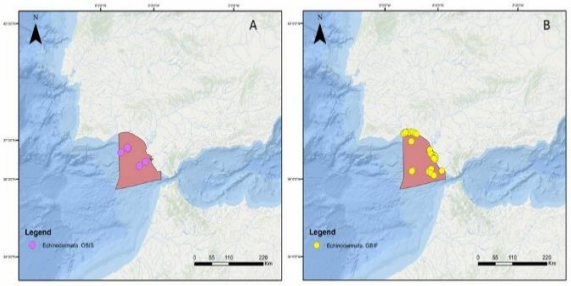

Figura 2. Comparación de los registros de equinodermos de OBIS y GBIF (brutos) en la demarcación Sudatlántica A. Registros de equinodermos de OBIS. A. Registros de equinodermos de GBIF.

Agradecimientos

Agradecemos al Ministerio para la Transición Ecológica y el Reto Demográfico la financiación del proyecto BIODIV: "Asesoramiento científico-técnico para el seguimiento de la biodiversidad marina: espacios y especies marinos protegidos de competencia estatal (2022-2025)". Proyecto financiado por la Unión Europea – NextGenerationEU a través del Plan de Recuperación, Transformación y Resiliencia; e impulsado por la Dirección General de Biodiversidad, Bosques y Desertificación del Ministerio para la Transición Ecológica y el Reto Demográfico y CSIC, a través del Instituto Español de Oceanografía (IEO). Cuyos resultados forman parte de esta comunicación,

en concreto en las Actividades A6: Apoyo científico en la actualización de las listas patrón de hábitats y especies marinas. Agradecemos también el apoyo del equipo del Centro Oceanográfico de Gijón, así como las aportaciones técnicas y científicas de los compañeros implicados.

REFERENCIAS

García-Guillén, L.M., Macías-Ramírez, A., Ríos, P. and Manjón-Cabeza, M.E. (2022a). Deep seastar fishes (Echinodermata: Asteroidea) from the Avilés Canyon System (Bay of Biscay), including two new records. *Estuarine, Coastal and Shelf Science*, 277(107993):1-14. DOI: 10.1016/j.ecss.2022.107993

Garcia-Guillen, L.M., Saucède, T., Ríos, P. and Manjón-Cabeza, M.E. (2022b). Deep-sea echinoids from the Avilés Canyons System (Cantabrian Sea: North Atlantic Ocean) *Estuarine, Coastal and Shelf Science*, 275(107967): 1-12. DOI: 10.1016/j.ecss.2022.107967

García-Guillén, L.M., Macías-Ramírez, A., Ríos, P. and Manjón-Cabeza, M.E. (2023). Deep-Sea asteroids (Echinodermata; Asteroidea) from the Galician Bank (North Atlantic Ocean). *Zootaxa*, 5297(2): 228–238. DOI: 10.11646/zootaxa.5297.2.3

García-Guillén, L.M., Saucède, T., Ríos, P. and Manjón-Cabeza, M.E. (2025). Deep-Sea Echinoids from the Galician Bank (North Atlantic Ocean). *Zootaxa*, 18 pp.

GBIF.org (2025). GBIF Home page. Available from: https://www.gbif.org

Macías-Ramírez, A., García-Guillén, L.M. and Manjón-Cabeza, M.E. (2024). Deep-Sea Ophiuroids (Echinodermata; Ophiuroidea) from the Avilés Canyon System: Seven New Records for the Spanish North Atlantic Marine Subdivision. *Diversity*, 16(7):407.

Manjón-Cabeza, M.E. (2022). Deep sea star shes (Echinodermata: Asteroidea) from the Avilés Canyon System (Bay of Biscay), including two new records. *Estuarine, Coastal and Shelf Science*, 277(107993):1-14. DOI: 10.1016/j.ecss.2022.107993

Manjón-Cabeza, M.E., Ríos, P., García-Guillén, L.M., Macías-Ramírez, A., Sánchez, F., Rodríguez-Básalo, A., Ibarrola, T.P. and Cristobo, J. (2021). Asteroids and Ophiuroids Associated with Sponge Aggregations as a Key to Marine Habitats. A Comparative Analysis Between Avilés Canyons System and El Cachucho, Marine Protected Area. *Frontiers in Marine Science*, 7:1-17. DOI: 10.3389/fmars.2020.606749

OBIS, 2025. Ocean biodiversity information system. Intergov. Oceanograph. Comm. UNESCO. www.obis.org.

Ríos, P., Altuna, A., Frutos, I., Manjón-Cabeza, M. E., García-Guillén, L.M., Macías-Ramírez, A., Ibarrola, T.P., Gofas, S., Taboada, S., Souto, J., Álvarez, F., Saiz-Salinas, J.I., Cárdenas, P., Rodríguez- Cabello, C., Lourido, A., Boza, C., Rodríguez-Basalo, A., Prado, E., Abad-Uribarren, A., Parra, S., Sánchez, F. and Cristobo, J. (2022). Avilés Canyon System: Increasing the benthic biodiversity knowledge. *Estuarine, Coastal and Shelf Science,* 274 (107924): 1-23. DOI: 10.1016/j.ecss.2022.107924

World Register of marine Species, WoRMS. (2025). Accessed at: https://www.marinespecies.org

Impactos de artes de pesca abandonados sobre organismos vulnerables en el Área Marina Protegida El Cachucho

L. M. García-Guillén (1), M. González-Martínez (2), J. Cristobo (1), F. González (1), P. Baragaño (1) y P. Ríos (1)

(1) Instituto Español de Oceanografía (IEO-CSIC) Gijón. España. laura.gagui@ieo.csic.es
(2) Universidad de Vigo (Uvigo) Vigo, España.

Abstract: This study analyzes the impact of lost or abandoned fishing gear (ALDFG) on vulnerable organisms in the El Cachucho Marine Protected Area (MPA), a site of high biodiversity and vulnerable species. The research is based on the analysis of underwater images collected with ROTV Politolana, ROV Liropus 2000, and a Lander system. These images were examined to assess the spatial distribution of ALDFG and local biodiversity over several years, allowing comparisons of the evolution of their impacts on the area and its vulnerable organisms. Exploratory surveys carried out in the Lastres Canyon and the Avilés Canyon System were also included for comparisons. The results confirm the presence of ALDFG in all surveyed areas. Overall, this study enhances the understanding of the threats posed by fishing debris and supports future conservation efforts for MPAs and their ecosystems.

Keywords: *lost or abandoned fishing gear, Marine Protected Area, El Cachucho, vulnerable marine species, underwater images.*

1. INTRODUCCIÓN

El impacto de las actividades humanas sobre los ecosistemas marinos ha adquirido una relevancia creciente en las últimas décadas, especialmente en áreas de alto valor ecológico como las Áreas Marinas Protegidas (AMP). Entre las amenazas más persistentes se encuentran las artes de pesca perdidas o abandonadas (APPA), también conocidas como "redes fantasmas", que continúan atrapando organismos marinos durante largos periodos de tiempo, alterando el equilibrio ecológico, degradando hábitats bentónicos y representando un riesgo tanto para la biodiversidad como para la integridad de los ecosistemas. El Cachucho, primera AMP designada en España en 2011 y ampliado en 2021 Ministerio de Medio Ambiente, y Medio Rural y Marino (2011); Ministerio para la Transición Ecológica y el Reto Demográfico (2021). Se trata de un monte submarino situado en la región nororiental del margen continental del mar Cantábrico (Figura 1), se localiza a unas 35 millas náuticas al norte de la costa asturiana, frente a Ribadesella y presenta una topografía que alcanza los 425 metros de profundidad en su punto más somero (cumbre de la montaña), extendiéndose hasta los más de 4000 m de profundidad en la base de la llanura abisal del golfo de Vizcaya. Alberga una biodiversidad de más de 700 especies, entre ellas se han identificado varios organismos vulnerables (Tabla I) como corales de aguas frías y poríferos (Figura 2). Muchas de estas especies son consideradas bioconstructoras, es decir, forman agregaciones tridimensionales que actúan como hábitats esenciales para peces demersales e invertebrados Ríos *et al.* (2020).

Desde finales de los años 70 ya hasta su protección esta zona fue explotada por las flotas pesqueras que operaban en el caladero, los principales artes utilizados eran: arrastre de fondo, palangre, enmalle y nasas. Este estudio analiza, de forma gráfica y cuantitativa, la distribución de APPA y su interacción con fauna vulnerable dentro del AMP y en zonas adyacentes aún en explotación.

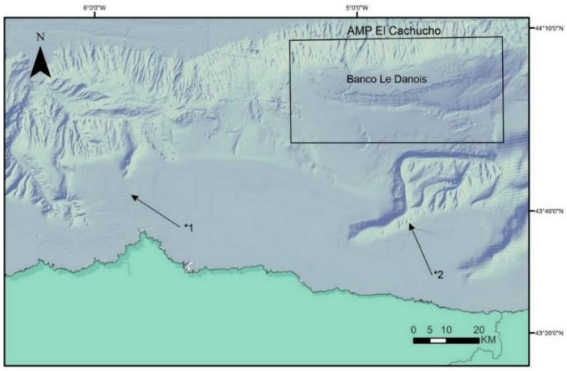

*Figura 1. Representación del área de estudio, recuadrando el AMP de El Cachucho, donde en su interior se encuentra el Banco Le Danois (montaña submarina). *1 señala el Sistema de cañones de Avilés. *2 señala los cañones de Lastres. Realizado con el software ArcGIS.*

Tabla I. Especies vulnerables de la zona de El Cachucho. Tabla verificada con Match taxa de World Register of Marine Species (Worms).

Especie	Autor	Filo
Dendrophyllia cornigera	(Lamarck, 1816)	Cnidaria
Desmophyllum pertusum	(Linnaeus, 1758)	Cnidaria
Madrepora oculata	Linnaeus, 1758	Cnidaria
Callogorgia verticillata	(Pallas, 1766)	Cnidaria
Pheronema carpenteri	(Thomson, 1869)	Porifera
Geodia spp.	Lamarck, 1815	Porifera
Phakellia spp.	Bowerbank, 1862	Porifera
Regadrella phoenix	Schmidt, 1880	Porifera
Asconema setubalense	Kent, 1870	Porifera

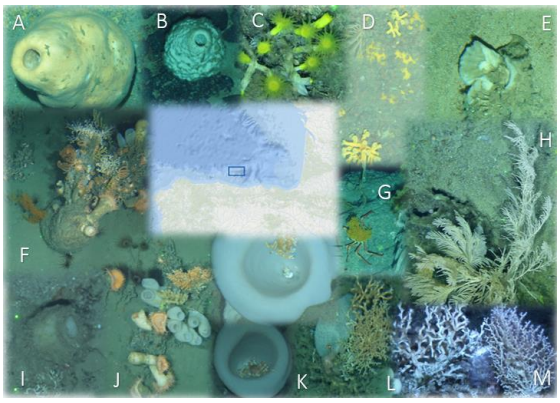

Figura 2. Localización geográfica del área de estudio con imágenes asociadas de las especies vulnerables presentes en la zona. A: Geodia megastrella, B: Geodia barretti., C-D: Dendrophyllia cornigera. E: Phakellia sp. *F: Antipatharios, Regadrella, etc. G: Paramola cuvieri con Placogorgia* sp. *H: Callogorgia verticillata. I: Pheronema carpenteri. J: Regadrella phoenix y Phelliactis hertwigii. K: Asconema setubalense. L: Madrepora oculata y Hexactinellida indet. M: Desmophyllum pertusum y Madrerpora oculata.*

2. MATERIAL Y MÉTODOS

Se analizaron 32.857 imágenes pertenecientes a 141 transectos realizados entre 2003 y 2021 por vehículos no tripulados como el ROV *Liropus 2000* o el ROTV *Politolana* y la plataforma fija Lander, en el marco de 9 campañas oceanográficas del IEO-CSIC. El análisis visual se centró en la presencia de APPA, basuras y la biodiversidad presente, prestando especial atención a las especies vulnerables como corales de aguas frías y esponjas estructurantes, registrando también posibles interacciones (enredo, abrasión, contacto).

A partir de la georreferenciación de cada transecto e imagen se utilizó el programa ArcGIS para la representación espacial del esfuerzo de muestreo, así como la presencia de las APPA, basuras y la distribución de especies vulnerables. Asimismo, se realizó una matriz de datos con ausencia y presencia de todas las especies, APPA y basuras a nivel de imagen, los datos obtenidos se analizaron con los programas: RStudio y Julia para el análisis cuantitativo, representando espacialmente los datos por año, zona y especie. Por otra parte, se transformaron las diferentes georreferencias de cada transecto analizado (cogiendo los puntos iniciales y finales de la latitud y la longitud correspondiente a cada transecto) en longitud total del transecto (km), con el fin de obtener una unidad de medida común que permitiera la comparación entre las diferentes zonas y años.

3. RESULTADOS

Todos los transectos analizados totalizan un esfuerzo de muestreo de 63,86 km. Dentro de la zona del AMP, donde se visualizaron 116 transectos, se detectaron APPA en un 1,49 % de las imágenes (375 de 25.233). Las más comunes fueron cabos, palangres y redes. Las especies vulnerables más frecuentemente encontradas junto a APPA fueron *Geodia* spp. (11,3 %), *Madrepora oculata* (6,8 %) y *Phakellia* spp. (4,1 %) (Figura 3A). Las interacciones fueron escasas pero documentadas: se observaron casos de enredo y contacto directo sobre organismos bentónicos (Figura 3B).

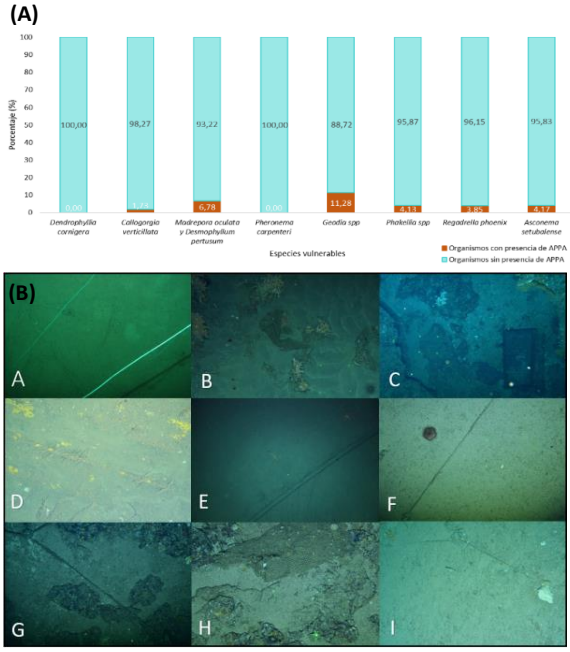

Figura 3. (A) Porcentaje de imágenes con presencia de individuos vulnerables con presencia y ausencia de APPA. (B) Imágenes de APPA junto con organismos vulnerables.

La presencia de APPA fuera del AMP, particularmente en el Sistema de Cañones de Avilés, fue significativamente mayor: 73 % de los registros en solo 11 transectos (2017). Las basuras marinas (botellas, plásticos) también aparecieron, con una frecuencia menor.

4. DISCUSIÓN

Los resultados confirman la eficacia relativa del AMP El Cachucho frente a zonas no protegidas, aunque también muestran que la designación como AMP no garantiza la eliminación del impacto si no va acompañado de un plan de gestión y regulación de zonas limítrofes. De las 32.857 imágenes analizadas, 25.233 pertenecen al AMP El Cachucho. En esta zona, se detectaron 375 imágenes con presencia de artes de pesca perdidas o abandonadas (APPA), lo que representa un 1,49 % del total de imágenes analizadas en el área protegida, por lo que lejos de su eliminación, se registró que la presencia d APPA se mantiene presente, actuando de manera acumulativa con el paso del tiempo. En 2017, se registró una mayor concentración de APPA en los transectos fuera del AMP, concretamente en el Sistema de Cañones de Avilés, donde la presión pesquera actual se encuentra presente. A pesar de ello, se documentó una rica diversidad de especies bentónicas en Avilés, incluyendo varias catalogadas como vulnerables. Por ello se sugiere una gestión integral del entorno. El hecho de que especies como *Geodia* spp. presenten alta coincidencia con APPA indica un riesgo potencial a largo plazo, especialmente en hábitats frágiles.

5. CONCLUSIONES

La mayoría de las imágenes no muestran impactos directos de las APPA sobre los organismos, pero se han detectado signos claros de daños físicos, especialmente sobre hábitats bentónicos sensibles. Asimismo, se demuestra que las artes de pesca perdidas o abandonadas se mantienen en la zona si no se retiran formando parte del propio ecosistema y cuya eliminación es muy dificultosa e incluso contraproducente al formarse, a veces, comunidades alrededor de ellas. El impacto indirecto y acumulativo de las APPA puede comprometer la integridad ecológica de los ecosistemas marinos a medio y largo plazo, sobre todo en zonas aún explotadas. Por ello se debe crear la necesidad de minimizar la pérdida de artes de pesca y fomentar la existencia de mayor número de AMP.

Este trabajo aporta una línea base valiosa para la gestión de las AMP ya existentes, resaltando la importancia de mantener programas de monitoreo y estrategias de mitigación enfocadas en la protección de zonas de interés ecológico y en la regulación de actividades en zonas limítrofes. El estudio de esta área es muy amplio, por lo que hacen falta otros estudios para depurar más al detalle en futuros proyectos.

Agradecimientos

Agradecemos al Ministerio para la Transición Ecológica y el Reto Demográfico la financiación del proyecto BIODIV: “Asesoramiento científico-técnico para el seguimiento de la biodiversidad marina: espacios y especies marinos protegidos de competencia estatal (2022-2025)”. Proyecto financiado por la Unión Europea – NextGenerationEU a través del Plan de Recuperación, Transformación y Resiliencia; e impulsado por la Dirección General de Biodiversidad, Bosques y Desertificación del Ministerio para la Transición Ecológica y el Reto Demográfico y CSIC, a través del Instituto Español de Oceanografía (IEO). Cuyos resultados forman parte de esta comunicación, en concreto en las Actividades A3: Seguimiento y evaluación del hábitat 1170 en la ZEC “El Cachucho” y A6: Apoyo científico en la actualización de las listas patrón de hábitats y especies marinas. Agradecemos también el apoyo del equipo del Centro Oceanográfico de Gijón, así como las aportaciones técnicas y científicas de los compañeros implicados.

REFERENCIAS

Ministerio de Agricultura Alimentación y Medio Ambiente. (2011). Real decreto 1620/2011, de 14 de noviembre, por la que se declara como Área Marina Protegida y como Zona Especial de Conservación el espacio marino de El Cachucho, y se aprueban las correspondientes medidas de conservación. BOE-A-2011-19246.

Ministerio para la Transición Ecológica y el Reto Demográfico (2021). Real Decreto 686/2021, de 3 de agosto, por el que se amplía el Área Marina Protegida "El Cachucho" y se aprueba su segundo plan de gestión (BOE-A-2021-13264). Boletín Oficial del Estado. https://www.boe.es/buscar/pdf/2021/BOE-A-2021-13264-consolidado.pdf

Ríos, P., Prado, E., Carvalho, F.C., Sánchez, F., Rodríguez Basalo, A., Xavier, J.R., Ibarrola, T.P. and Cristobo, J. (2020). Community composition and habitat characterization of a rocksponge aggregation (Porifera, Corallistidae) in the Cantabrian Sea. *Frontiers in Marine Science*, 7, 578. https://doi.org/10.3389/fmars.2020.00578

First insight of hydroxypyrene bile metabolite in *Merluccius merluccius* in the Iberian Atlantic coast

A. V. Filgueiras (1), J. Bargiela (1), B. Pérez-Fernández (1) and L. Viñas (1)

(1) Instituto Español de Oceanografía (IEO), Subida a Radio Faro, 50-52, 36390-Vigo, Spain. ana.filgueiras@ieo.csic.es

Abstract: Polycyclic aromatic hydrocarbons (PAHs) are ubiquitous in the natural environment and generated primarily during the incomplete combustion of organic materials. PAHs are able to form covalent bonds with the genetic material, a process associated with mutagenic, teratogenic, and carcinogenic effects. They metabolize quickly, so their metabolites have been used as biomarkers and an exposure control of their occurrence in the media. 1-hydroxypyrene (1-OHPyr) was chosen as a main breakdown product of pyrene, because it's easy to detect, shows up clearly in fish exposed to PAHs, and is the most common metabolite in bile. High-Performance Liquid Chromatography coupled to Fluorescence (HPLC-F) detection was selected to measure 1-OHPyr to monitor and evaluate PAH exposure in hake (*Merluccius merluccius)* on the Iberian Atlantic coast: Galicia, the Gulf of Biscay and Gulf of Cádiz**.** The quantification of 1-hydroxypyrene (1-OHPyr) in hake bile allowed to differentiation between sampling sites in the marine environment.

Keywords: *metabolite, PAH, hydroxypyrene, bile*

Polycyclic aromatic hydrocarbons (PAHs) are a group of chemical compounds with two or more condensed aromatic rings. PAHs are ubiquitous in the natural environment and are primarily generated during the incomplete combustion of organic materials

PAHs are among the most concerning organic pollutants because they can form covalent bonds with genetic material, a process associated with mutagenic, teratogenic, and carcinogenic effects (e.g., Reynaud and Deschaux, 2006). However, their direct determination in vertebrates is challenging due to rapid metabolization, especially in fish at higher trophic-levels (Zhang *et al*. 2015). These metabolites accumulate in the gallbladder and are excreted through the gastrointestinal tract (e.g., Honda and Suzuki, 2020).

Among these metabolites, 1-hydroxypyrene (a major metabolite of pyrene) has been selected as a biomarker of PAH exposure due to its relatively high toxicity, at least in fish (Honda and Suzuki, 2020). High-Performance Liquid Chromatography with Fluorescence detection (HPLC-F) was selected for its simplicity in sample preparation and short analysis time.

To assess PAH exposure in hake (*Merluccius merluccius)*, 1-hydroxypyrene (1-OHPyr) was used as a biomarker in specimens collected from Galicia, the Gulf of Biscay, and the Gulf of Cádiz along the Iberian Atlantic coast (Figure 1), during the autumn season each year from 2014 to 2019.

Figure 1. Sampling locations for hake (Merluccius merluccius) in three Atlantic coastal regions of the Iberian Peninsula: the Galician coast, the Gulf of Biscay, and the Gulf of Cádiz.

This fish species was selected due to its ability to bioaccumulate chemical pollutants, the broad geographic coverage represented by the sampling locations, and its importance as a commonly consumed species in the region. Female gall bladders were collected using disposable syringes and stored in cryogenic vials at -20ºC until analysis. Enzymatic hydrolysis was performed following the method described Kamman *et al.* (2014) based on Krahn *et al*. (1987).

The PAH metabolite 1-OH-Pyr was detected in 86% of the bile samples analysed. Measured concentrations in individual fish ranged from values below the limit of quantification (<1.5 µg kg^{-1}) up to a maximum of 57.5 µg kg^{-1}, with an overall mean of 8.48 ± 11.20 µg kg^{-1}. Mean and standard deviation values of 1-

hydroxypyrene (1-OHPyr) concentrations were calculated for each sampling area by pooling data from all years. The resulting values for each zone are as follows:

- Galician coast: <1.5 to 16.2 µg kg^{-1} (mean: 4.77 ± 4.03 µg kg^{-1})
- Gulf of Biscay: <1.5 to 57.5 µg kg^{-1} (mean: 18.1 ± 15.0 µg kg^{-1})
- Gulf of Cádiz <1.5 to 14.0 µg kg^{-1} (mean: 2.88 ± 2.90 µg kg^{-1})

Individuals from the Gulf of Biscay exhibited the highest mean concentration of 1-OH-Pyr, suggesting increased exposure to PAHs in this area. This may be attributed to anthropogenic inputs such as maritime traffic, industrial discharges, or urban runoff.

Table I summarizes the concentrations of the 1-OH-Pyr metabolite across all years and sampling locations. Although an increase in 1-hydroxypyrene (1-OHPyr) concentrations appears to be observed in the last sampling year in both Galicia and the Gulf of Cádiz, the Mann-Kendall test p-value were greater than 0.05 (p=0.4524 and p=0.8065, respectively) does not indicate a statistically significant upward trend in the results.

Table I. Results obtained for the 1-OH-Pyr metabolite and the number of hake specimens sampled in the three study areas each year between 2014 and 2019 are presented. Results are expressed as average value ± standard deviation ($\bar{x}$ ± sd) in µg kg^{-1}.

	Galicia		***Gulf of Biscay***		***Gulf of Cádiz***	
Year	***1-OH-Pyr***	***N***	***1-OH-Pyr***	***N***	***1-OH-Pyr***	***N***
2014	4.96±4.29	10	10.2±13.8	4	2.07±1.46	9
2015	4.68±5.16	10	8.93±7.56	13	3.28±3.54	15
2016	2.17±2.03	10	14.7±18.7	11	1.51±2.03	14
2017	2.67±2.76	11	21.7±14.9	15	2.04±1.27	13
2018	5.22±3.67	12	30.2±10.6	10	2.12±1.93	2
2019	7.29±3.76	17	19.6±14.7	9	7.57±2.19	7

Acknowledgments

The study was conducted at the Spanish Institute of Oceanography (IEO) and was funded by the ESMARES' projects. Thanks to the ARSA and PELACUS campaigns for sample provision and our sincere gratitude to the vessel crews for their assistance during fieldwork. The authors wish to thank the technical staff of the Marine Pollution Group at IEO-Vigo.

REFERENCES

Honda, M. and Suzuki, N. (2020). Toxicities of polycyclic aromatic hydrocarbons for aquatic animals. *International Journal of Environmental Research and Public Health*, 17(4):1363. DOI: 10.3390/ijerph17041363

Kammann, U., Brinkmann, M., Freese, M., Pohlmann, J.-D., Stoffels, S., Hollert, H. and Hanel, R. (2014). PAHs metabolites, GST and EROD in European eel (Anguilla anguilla) as possible indicators for eel habitat quality in German rivers. *Environmental Science and Pollution Research*, 21:2519–30. DOI: 10.1007/s11356-013-2121-z

Krahn, M.M., Burrows, D.G., MacLeod, W.D. and Malins, D.C. (1987). Determination of individual metabolites of aromatic compounds in hydrolysed bile of English sole from polluted sites in Puget Sound, Washington. *Archives of Environmental Contamination and Toxicology*, 16:511-522. DOI: 10.1007/BF01055807

Reynaud, S. and Deschaux, P. (2006). The effects of polycyclic aromatic hydrocarbons on the immune system of fish: a review. *Aquatic Toxicology*, 77:229-238. DOI: 10.1016/j.aquatox.2005.10.018

Zhang, G., Pan, Z., Wang, X., Mo, X. and Li, X. (2015). Distribution and accumulation of polycyclic aromatic hydrocarbons (PAHs) in the food web of Nansi Lake, China. *Environmental Monitoring and Assessment*, 187:173. DOI: 10.1007/s10661-015-4362-4

From Sargasso to Southern Portugal: Maritime Traffic and Noise as Barriers to European Eel Migration in the Arade and Guadiana Rivers

D. Menéndez-Teleña (1), V. Soto-López (1), K. Erzini (2), P. Guerreiro (2) and E. Garcia-Vazquez (3)

(1) Department of Marine Science and Technology, University of Oviedo. C/Blasco de Garay s/n 33394, Gijón, Asturias, Spain. menendezdeva@uniovi.es
(2) Centre of Marine Sciences (CCMAR), University of Algarve. Campus de Gambelas, 8005-139 Faro, Portugal
(3) Department of Functional Biology, University of Oviedo. C/Julián Clavería s/n 33006, Oviedo, Asturias, Spain

Abstract: The European eel (*Anguilla anguilla*) is a critically endangered catadromous species whose complex biology makes it particularly vulnerable to environmental stressors. This study aims to analyse the environmental suitability of the Arade and Guadiana rivers as habitats for this species, with a focus on maritime traffic and the noise pollution it generated. Anthropogenic noise, primarily from maritime transport and recreational boats, has been recognised as a significant environmental pollutant affecting the physiology and behaviour of fish.

Keywords: *Anguilla anguilla, estuaries, ports, marine traffic, underwater noise*

1. INTRODUCTION

The European eel (*Anguilla anguilla*) is a critically important catadromous species that has experienced a marked population decline in recent decades. Its complex life cycle begins in the Sargasso Sea, with the juvenile eels, known as elvers, migrating to European continental waters via estuaries. They then inhabit inland rivers and wetlands, passing through multiple barriers along the way (Daverat *et al*., 2012; Durif *et al*., 2005; Pike *et al*., 2020; Podda *et al*., 2021). Throughout this migratory journey, elvers are exposed to a variety of environmental man-made stressors, including accidental oil spills (Neuparth *et al*., 2012), microplastics (Li *et al*., 2016), antifouling paint compounds (Soon *et al*., 2019), marine litter (Corcoran, PL, 2015) and anthropogenic underwater noise (Popper and Hastings, 2009; Slabbekoorn *et al*., 2010), among others.

Over the past three decades, both the scientific community and environmental organizations have increasingly warned about the escalating impact of anthropogenic noise in aquatic environments (Williams *et al*., 2015). Although natural sources of noise, such as seismic activity, do exist, maritime transport remains the primary contributor to global underwater noise pollution (Hildebrand, 2009). At the regional scale, fishing activities, as well as commercial and recreational vessel traffic, substantially elevate ambient noise levels, particularly in estuaries and river systems (Harding *et al*., 2019; Slabbekoorn *et al*., 2010).

Approximately 11 billion tonnes of cargo are transported annually via international maritime shipping, a figure projected to more than triple by 2050 (Sardain *et al*., 2019). This anticipated growth in port activity places increasing pressure on aquatic ecosystems, particularly in regions such as southwestern Iberia, where the rivers under study are located.

This type of pollution has multiple consequences for fish, including activation of the stress axis leading to elevated cortisol levels (Barcellos *et al*., 2007); behavioural alterations (Simpson *et al*., 2016); temporary or permanent hearing loss (Smith *et al*., 2004); and reduced ability to detect prey or predators.

In species such as *Anguilla anguilla*, which are already exposed to various environmental stressors, noise can serve as an additional risk factor, further compromising recruitment rates. Moreover, noise pollution may act synergistically with other contaminants, such as heavy metals or microplastics, amplifying their detrimental effects (Slabbekoorn *et al*., 2010).

In this context, assessing the Arade and Guadiana rivers will help determine whether the levels of boat traffic and noise pollution are compatible with the conservation of this critically endangered species.

2. STUDY AREA

The study is conducted in the estuaries of the two main rivers in southern Portugal, the Arade River and the Guadiana River (Correia *et al*., 2020) (Figure 1). Data on these rivers can be accessed via the website of the National Information System on Water Resources, managed by the Portuguese Environment Agency (APA), https://snirh.apambiente.pt/.

Figure 1. Estuaries in which the study was carried out: A) Arade River and B) Guadiana River. Adapted images, source of the maps: https://earthexplorer.usgs.gov/.

2.1. Arade River Estuary

The Arade River estuary is located in southern Portugal, within the central-western region of the Algarve (37°07'11.8"N 008°31'27.8"W). The Arade River, approximately 75 km in length, originates in the Caldeirão mountain range and flows southward, merging with the Odelouca river before emptying into the Atlantic Ocean near the city of Portimão (Agência Portuguesa do Ambiente (APA), 2014). At its mouth, the Arade estuary holds both ecological and economic significance, hosting several ports and docking areas (Fernandes *et al*., 2014). Maritime traffic, alongside tourism and urban development along its banks, represents the primary anthropogenic pressures in the region. Vessel access is constrained by the estuary's draft limitations. Nonetheless, there is a small commercial port, a fishing area, and multiple marinas for recreational boats.

2.2. Guadiana River Estuary

The estuary of the Guadiana River is located in the southern Iberian Peninsula, forming the border between Spain and Portugal (37°11'28.4"N 007°24'31.8"W). This river, one of the most significant in the region, has a watershed covering approximately 67,000 square kilometres, making it the fourth largest in the area (Loureiro *et al*., 1986). It originates in Spanish territory at an altitude of 868 meters above sea level, flowing over 800 kilometres before emptying into the Atlantic Ocean between the towns of Vila Real de Santo António and Ayamonte. In Portugal, the Guadiana spans 260 kilometres, while its final 110 kilometres serve as a natural border between the two countries (Agência Portuguesa do Ambiente (APA), 2015). At its mouth, the river hosts port infrastructures on both banks, including a small commercial port area, berths for fishing boats and three marinas.

3. RESEARCH CONDUCTED

3.1. Marine Traffic

To analyze maritime traffic data, the website Marine Traffic (https://www.marinetraffic.com) is utilized. This platform provides global ship position information through the Automatic Identification System (AIS). It is important to note that AIS relies on radio frequency signals to enable the exchange of positions between vessels and between vessels and land-based stations. However, its use is mandatory only for ships exceeding 15 meters in length (International Maritime Organization, 2004). To supplement the data for smaller vessels, dock records from the Portimão Marina, Ayamonte Marina, and Porto de Recreio do Guadiana are reviewed.

Maritime traffic data is collected over two three-month periods: from December 2023 to February 2024, and from October 2024 to December 2024. These periods coincide with the migration of eels into European rivers. A citizen science initiative was organized to gather this data, providing volunteers with guidelines and instructions for data collection. A total of 21 participants, aged between 23 and 66 years, were recruited from the Faculty of Biology and the Higher School of Civil Marine at the University of Oviedo using the snowball methodology (Valerio *et al*., 2016).

3.2. Noise from maritime traffic

Submarine noise measurements are carried out using the high-precision digital hydrophone *"digitalHyd SR-1,"* developed by *Marsensing Lda* (https://www.marsensing.com/en/) a company specializing in advanced technologies for acoustic and underwater monitoring. The hydrophone allows for the detection of underwater sounds and environmental noise within a frequency range of 1 Hz to 400 kHz and a nominal sensitivity of -170 dB re 1V/µPa (Soares *et al*., 2020).

To facilitate accurate measurements, a custom-designed apparatus (Figure 2) is used. The setup includes a weighted base and a system of buoys that keep the cable holding the hydrophone vertical, ensuring optimal data collection (Te Velde *et al*., 2024). Measurements are taken at three locations in each analyzed river. At each site, four 1.5-hour recordings are made (morning and afternoon, weekdays and weekends), totalling six hours per site and 18 hours per river.

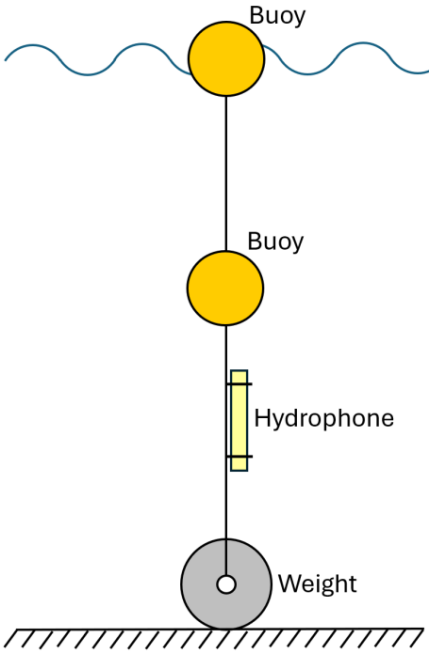

Figure 2. Diagram of the equipment used for hydrophone measurements.

This research is a necessary step towards understanding the impact of noise generated by marine traffic on aquatic environments and the survival of important species, such as the European eel.

Acknowledgements

The authors would like to express their gratitude to Marsensing Lda for providing the hydrophone used for the audiometric measurements. This study has been supported from the Ministry of Science of Innovation of Spain, Grant PID2022-138523OB-100. CCMAR receives Portuguese funds from FCT - Foundation for Science and Technology (grants UIDB/04326/2020 and LA/P/0101/2020).

REFERENCES

Agência Portuguesa do Ambiente (APA) (2015). Plano de Gestão de Região Hidrográfica - Região Hidrográfica: Guadiana (RH7).

Agência Portuguesa do Ambiente (APA) (2014). Plano de Gestão de Região Hidrográfica - Região Hidrográfica das Ribeiras do Algarve (RH8).

Corcoran, P.L. (2015) Benthic plastic debris in marine and fresh water environments. *Environmental Science: Processes & Impacts*, 17, 1363–1369. http://dx.doi.org/10.1039/C5EM00188A

Barcellos, L.J., Ritter, F., Kreutz, L.C., Mezzalira, R., Quevedo, Bolognesi da Silva, L., Calliari Bedin, A., Finco, J., and Cericato, L. (2007). Whole-body cortisol increases after direct and visual contact with a predator in zebrafish, Danio rerio.

Correia, C., Torres, A.F., Rosa, A., Cravo, A., Jacob, J., de Oliveira Júnior, L. and Garel, E., (2020). Export of dissolved and suspended matter from the main estuaries in South Portugal during winter conditions. *Marine Chemistry*, 224, 103827. https://doi.org/10.1016/j.marchem.2020.103827

Daverat, F., Lanceleur, L., Pécheyran, C., Eon, M., Dublon, J., Pierre, M., Schäfer, J., Baudrimont, M. and Renault, S. (2012). Accumulation of Mn, Co, Zn, Rb, Cd, Sn, Ba, Sr, and Pb in the otoliths and tissues of eel (Anguilla anguilla) following long-term exposure in an estuarine environment. *Sci. Total Environ.*, 437, 323-330. http://dx.doi.org/10.1016/j.scitotenv.2012.06.110

Durif, C., Dufour, S. and Elie, P. (2005). The silvering process of Anguilla anguilla: a new classification from the yellow resident to the silver migrating stage. *J. Fish Biol.*, 66(4), 1025-1043. http://dx.doi.org/10.1111/j.0022-1112.2005.00662.x

Fernandes, D., Pujol, S., Pérez-Albaladejo, E., Tauler, R., Bebianno, M.J. and Porte, C., (2014). Characterization of the environmental quality of sediments from two estuarine systems based on different in-vitro bioassays. *Marine Environmental Research, Pollutant Responses* in Marine Organisms" (PRIMO17) 96, 127–135. https://doi.org/10.1016/j.marenvres.2013.09.019

Harding, H.R., Gordon, T.A.C., Eastcott, E., Simpson, S.D. and Radford, A.N. (2019). Causes and consequences of intraspecific variation in animal responses toanthropogenic noise. *Behav. Ecol.*, 1501–11. https://doi.org/10.1093/beheco/arz114.

Hildebrand, J.A. (2009). Anthropogenic and natural sources of ambient noise in the ocean. *Marine Ecology Progress Series,* 395:5-20. http://dx.doi.org/10.3354/meps08353

International Maritime Organization (2004). Regulation V/19 – Carriage requirements for Automatic Identification Systems (AIS) of International Convention for the Safety of Life at Sea (SOLAS) [WWW Document]. URL https://www.imo.org/en/OurWork/Safety/Pages/AIS.aspx (accessed 12.12.24).

Li, W.C., Tse, H.F. and Fok, L. (2016). Plastic waste in the marine environment: A review of sources, occurrence and effects. *Science of The Total Environment*, 566–567, 333-349. https://doi.org/10.1016/j.scitotenv.2016.05.084.

Loureiro, J., Machado, M., Macedo, M., Nunes, M., Botelho, O., Sousa, M., Almeida, M. and Martins, J. (1986). Monografias hidrológicas dos principais cursos de água de Portugal continental. Direcção-Geral dos Recursos e Aproveitamentos Hidráulicos, Lisboa. 569 pp.

Neuparth, T., Moreira, S.M., Santos, M.M. and Reis-Henriques, M.A. (2012). Review of oil and HNS accidental spills in Europe: Identifying major environmental monitoring gaps and drawing priorities. *Marine Pollution Bulletin*, 64, 1085-1095. https://doi.org/10.1016/j.marpolbul.2012.03.016

Pike, C., Crook, V. and Gollock, M. (2020). Anguilla anguilla. The IUCN Red List of Threatened Species 2020: e.T60344A152845178

Podda, C., Palmas, F., Pusceddu, A. and Sabatini, A. (2021). Hard times for catadromous fish: the case of the European eel Anguilla anguilla (L. 1758). *Adv. Oceanog.*

Limnol., 12(2), 9997. https://doi.org/10.4081/aiol.2021.9997

Popper, A.N. and Hastings, M.C. (2009). The effects of anthropogenic sources of sound on fishes. *Journal of Fish Biology*, 75, 455–489. http://doi.org/10.1111/j.1095-8649.2009.02319.x

Sardain, A., Sardain, E. and Leung, B. (2019). Global forecasts of shipping traffic and biological invasions to 2050. *Nature Sustainability*, 2, 1-9. Doi: 10.1038/s41893-019-0245-y

Schoeman, R.P., Patterson-Abrolat, C. and Plön, S., (2020). A global review of vessel collisions with marine animals. *Front. Mar. Sci*., 7. https://doi.org/10.3389/fmars.2020.00292

Simpson, S., Radford, A., Nedelec, S. *et al*. (2016) Anthropogenic noise increases fish mortality by predation. *Nat. Commun*., 7, 10544. https://doi.org/10.1038/ncomms10544

Slabbekoorn, H., Bouton, N., van Opzeeland, I., Coers, A., ten Cate, C. and Popper, A.N. (2010). A noisy spring: the impact of globally rising underwater sound levels on fish. *Trends in Ecology and Evolution*, 25, 419–427. https://doi.org/10.1016/j.tree.2010.04.005

Smith, M.E., Kane, A.S. and Popper, A.N. (2004). Acoustical stress and hearing sensitivity in fishes: Does the linear threshold shift hypothesis hold water? *Journal of Experimental Biology*, 207(20): 3591-602. https://doi.org/10.1242/jeb.01188

Soares, C., Pacheco, A., Zabel, F., González-Goberña, E. and Sequeira, C. (2020). Baseline assessment of underwater noise in the Ria Formosa. *Marine Pollution Bulletin*, 150, 110731. https://doi.org/10.1016/j.marpolbul.2019.110731

Soon, Z.Y., Jung, J.-H., Jang, M., Kang, J.-H., Jang, M.-C., Lee, J.-S., Kim, M. Zinc. (2019). Pyrithione (ZnPT) as an antifouling biocide in the marine environment—A literature review of its toxicity, environmental fates, and analytical methods. *Water Air Soil Pollut*., 230, 310. http://doi.org/10.1007/s11270-019-4361-0

Te Velde, K., Mairo, A., Peeters, E.THM., Winter, H.V., Tudorache, C. and Slabbekoorn, H. (2024). Natural soundscapes of lowland river habitats and the potential threat of urban noise pollution to migratory fish. *Environmental Pollution*, 359, 124517. https://doi.org/10.1016/j.envpol.2024.124517

Valerio, M.A., Rodriguez, N., Winkler, P., Lopez, J., Dennison, M., Liang, Y. and Turner, B.J. (2016). Comparing two sampling methods to engage hard-to-reach communities in research priority setting. *BMC Medical Research Methodology*, 16, 146. https://doi.org/10.1186/s12874-016-0242-z

Williams, R., Wright, A.J., Ashe, E., Blight, L.K., Bruintjes, R., Canessa, R., Clark, C.W., Cullis-Suzuki, S., Dakin, D.T., Erbe, C., Hammond, P.S., Merchant, N.D., O'Hara, P.D., Purser, J., Radford, A.N., Simpson, S.D., Thomas, L. and Wale, M.A. (2015). Impacts of anthropogenic noise on marine life: Publication patterns, new discoveries, and future directions in research and management. *Ocean & Coastal Management*, 115, 17-24. https://doi.org/10.1016/j.ocecoaman.2015.05.021

Património histórico subaquático e geoarqueologia

Patrimonio cultural subacuático y geoarqueología

Underwater cultural heritage and geoarchaeology

MUCH Lagos – Maritime and Underwater Cultural Heritage and the evolution of the seascape of Lagos

G. C. Lopes (1) e J. Baço (2)

(1) CEAACP / UAlg, Portugal. gnlopes@ualg.pt
(2) CHAM – Centro de Humanidades NOVA FCSH-UAc. joanabaco@fcsh.unl.pt

Abstract: The MUCH Lagos project advances scientific research in Lagos, Portugal, focusing on underwater archaeology, maritime history, and seascape studies. Through rigorous investigation and effective science communication, we aim to enhance public access to this shared heritage. This research is conducted under a CEEC contract, funded by the FCT. Our work is based on archaeological evidence – anchors, ceramics, glass, metal, organic materials, and shipwrecks. Using data systematization and GIS analysis, we have mapped anchorage areas, examined harbour dynamics, characterized two *almadravas*, and explored human interaction with the aquatic environment. We also tried to implement ways in which Underwater Cultural Heritage (UCH) can drive social, economic, and cultural development, integrating local communities of divers and fishers while promoting dissemination and valorisation in schools. This project is fully aligned with the principles of the UNESCO 2001 Convention for the Protection of UCH and the UNESCO Sustainable Development Goals (2030 Agenda).

Keywords: *Maritime archaeology, Underwater archaeology, Maritime Cultural Landscape, Blue Humanities, Ocean Literacy*

1. INTRODUÇÃO

A ocupação humana em Lagos está atestada arqueologicamente desde a Pré-História, através de vestígios de superfície, de vários arqueossítios conhecidos no concelho, de menires Neolíticos, de vestígios de ocupação Calcolítica, ou de povoados e necrópoles das Idades do Bronze e do Ferro. Sobre este último período, destaca-se o Monte Molião, onde está documentada a presença pré-romana, desde meados do século IV a.C., mas sobretudo a ocupação romana (Arruda *et al*., 2008).

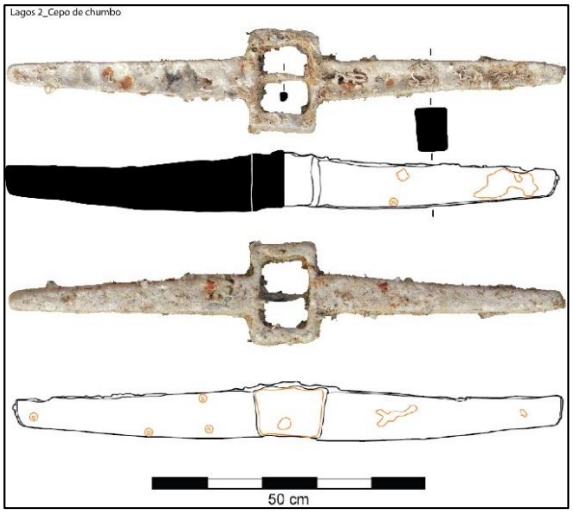

Figura 1. Lagos 2 – Cepo de chumbo de âncora romana (CNS 37377) recuperado em Março de 2024, pelo CNANS/PCIP.

No que concerne à arqueologia subaquática do concelho de Lagos, os mais antigos vestígios identificados são âncoras de pedra, cepos de chumbo pertencentes a âncoras de madeira e ânforas, que se enquadram, grosso modo, no Período Romano, e que no seu conjunto atestam a existência de uma ou mais zonas de fundeadouro na baía (Lopes *et al*., 2024) (Figura 1).

De Época Medieval existem alguns povoados, fortificações e, no que concerne à Idade Média, as evidências são escassas, contando-se quatro âncoras de ferro, um prumo de sonda náutica em chumbo, todas possivelmente de cronologia bizantina (Oleson, 2008) e alguns achados isolados de cerâmica (Lopes *et al*., 2024). Após a conquista muçulmana, a cidade passou a designar-se *Zawiya*, e daí exportavam-se vários produtos agrícolas (figos e azeite), mas também outros artesanais, como por exemplo âncoras de navios (Piccard, 1999), pormenor assaz interessante para estudos de arqueologia marítima da região.

Nesta altura, já os motores da economia eram a pesca e o comércio marítimo (Loureiro, 1991), datando também deste período a criação das duas *almadravas* conhecidas para a zona – Torralta (CNS 40909) e da Torraltinha (CNS 41080) (Baço, 2015). Nos anos seguintes assistiu-se à construção de edifícios políticos e religiosos, mas também ao aumento e reforço das muralhas e outras pequenas fortificações que auxiliaram na sua defesa (Lopes *et al*., 2024).

A partir do início do século XV, sobretudo com a expansão portuguesa, e o carácter marítimo do

Império Português, a importância estratégica de Lagos, na confluência da maioria das rotas transatlânticas, mas também com o Mediterrâneo, Norte da Europa e Norte de África, Lagos registou um crescimento socioeconómico e demográfico exponencial, tendo-se convertido numa plataforma de apoio crucial. Um dos resultados óbvios foi a constante presença de navios de várias nacionalidades, que aqui comerciavam ou apenas passavam e faziam escala (Loureiro, 1991).

Com efeito, as condições naturais da grande baía de Lagos, permitiam que um grande número de embarcações ali ancorasse, sendo conhecidos vários casos de expedições que fizeram escala antes de avançar para o continente africano. De facto, esta enorme baía, que apresenta condições naturais propícias à ancoragem e fundeio de embarcações, assumiu-se desde cedo como um importante ponto de abrigo e segurança, tanto para a navegação por cabotagem, como para as ligações entre o Atlântico e o Mediterrâneo e, mais tarde, como ponto de escala e apoio para as navegações oceânicas.

A este propósito importa mencionar, que o litoral Sul do Algarve está abrigado da ondulação altamente enérgica do Atlântico Norte e a baía de Lagos confere protecção dos ventos do quadrante norte, os mais recorrentes. Contudo, é uma zona que se encontra muito exposta a tempestades do quadrante sul, sendo permeável aos episódios cíclicos do levante e do sueste (Lopes *et al*., 2024). Estas dificuldades, referidas nas fontes históricas, ajudam a explicar a recorrente ocorrência de naufrágios e outros acidentes marítimos dentro da baía.

A arqueologia terrestre é rica em evidências deste período destacando-se edifícios de habitação, conventos, igrejas, capelas, cais, pontes e fortificações (Corrêa, 1998; Cardoso, 2004; Magalhães, 2004; Marado, 2006; Coutinho, 2008; Morán e Parreira, 2010). Paralelamente, mas em menor quantidade, também a arqueologia subaquática possui no seu registo vestígios que comprovam e ilustram a Época Moderna lacobrigense. Assim, as evidências mais recorrentes são as âncoras, de diferentes tipologias e cronologias, que na sua maioria constituem achados isolados e, em menor número, naufrágios (Baço, 2015), que na sua maioria conhecem-se, apenas, através de fontes documentais; numerosos achados isolados de cerâmicas, vidros, metais e alguns materiais orgânicos, que comprovam as rotas comerciais que passavam pela cidade (Lopes *et al*., 2024).

No seu conjunto, estes vestígios arqueológicos são evidências da navegação que passou por Lagos, ao longo do tempo, mas também das actividades marítimas praticadas nesse mesmo território.

O Período Contemporâneo é o que possui maior quantidade de vestígios, destacando-se de forma clara os relatos de naufrágios e encalhes de diferentes tipos de embarcações de pesca, nas costas do concelho, mas também o número de âncoras de tipologias enquadráveis neste período, podendo constituir parte integrante das almadravas já aludidas, ou a evidências de naufrágios. Surgem, igualmente, um par de casos relacionados com embarcações e aeronaves da Primeira e a Segunda Guerras Mundiais.

A arqueologia subaquática em Lagos tem demonstrado o seu potencial arqueológico. Primeiro ocorreram várias recuperações ilegais por parte de mergulhadores, que foram depois devidamente enquadradas, o que permitiu que a comunidade local de mergulhadores e pescadores iniciasse, anos mais tarde, uma fase de declarações de achados fortuitos. Neste contexto, existiram duas organizações que se dedicaram ao património cultural marítimo, nomeadamente o CEMAL e o GEO (Lopes *et al*., 2024).

Entre 2006 e 2016, desenvolveram-se projetos de investigação de arqueologia subaquática, coordenadas por Tiago Fraga, que permitiram a compilação de um importante manancial de informação (Fraga, 2008; Fraga *et al*., 2014; Fraga, 2013). Com efeito foram identificados cinco naufrágios – *Feira-Mar* (CNS 25508), "Lagos B" (CNS 40850), "Propelers Paradise" (CNS 40765), canhoneira *Faro* (CNS 31432) (Fraga e Martins, 2011; Fraga e Salgado, 2012) e "Lagos F" (CNS 40848) (Fraga, 2013) que se enquadram cronologicamente entre o final do século XVIII e meados do século XX, bem como mais de 150 âncoras de pedra e ferro, de diversas tipologias e cronologias. Por fim, foram identificados e, em alguns casos também recuperados, vários achados isolados fortuitos de espólio diverso, que podem ou não integrar naufrágios. Em 2023 e 2024, o CNANS realizou verificação de achados fortuitos e consequente recuperação de dois conjuntos de roldanas em liga de cobre e um cepo de chumbo (Lopes *et al*., 2024).

Em suma, a realidade marítima de Lagos encontra-se bem documentada pelas fontes escritas e, também, por evidências arqueológicas das últimas décadas.

2. MUCH LAGOS

Os dados disponíveis são o ponto de partida do MUCH Lagos, uma iniciativa dedicada ao avanço da investigação científica em Lagos, com foco na arqueologia subaquática, nos estudos marítimos, na história e nas paisagens marinhas. Este projeto decorre no âmbito de um Contrato individual de Estímulo ao Emprego Científico (CEEC), financiado pela Fundação para a Ciência e a Tecnologia (FCT).

Por um lado, procura-se aprofundar o conhecimento sobre Património Cultural Subaquático (PCS) existente

no fundo marinho de Lagos, bem como nas zonas intertidais, já identificado e conhecido de trabalhos anteriores, através da sua sistematização. Por outro, pretende-se compreender a evolução da paisagem cultural marítima precisamente através dessas evidências arqueológicas.

Ou seja, por agora, optámos por uma metodologia não intrusiva, baseada em prospecão visual com mergulhador e, pontualmente, auxiliados por detector de metais. Os artefactos e sítios arqueológicos, foram alvo de uma limpeza superficial, para facilitar o melhor registo possível. A limpeza manual envolveu o uso de escovas de cerdas, sobretudo na remoção de algas, mas também na ocasional remoção de sedimentos superficiais. A este respeito importa mencionar que a costa portuguesa, e em especial o Algarve, enfrenta uma grave invasão de algas alóctones, nomeadamente *Rugulopteryx okamurae*, dificultando consideravelmente a prospeção e o registo dos locais. Com efeito, temos constatado que nos sítios arqueológicos até uma profundidade de cerca de 20m, esta alga encontra-se bastante presente. Por oposição, a profundidades maiores a sua presença é praticamente nula.

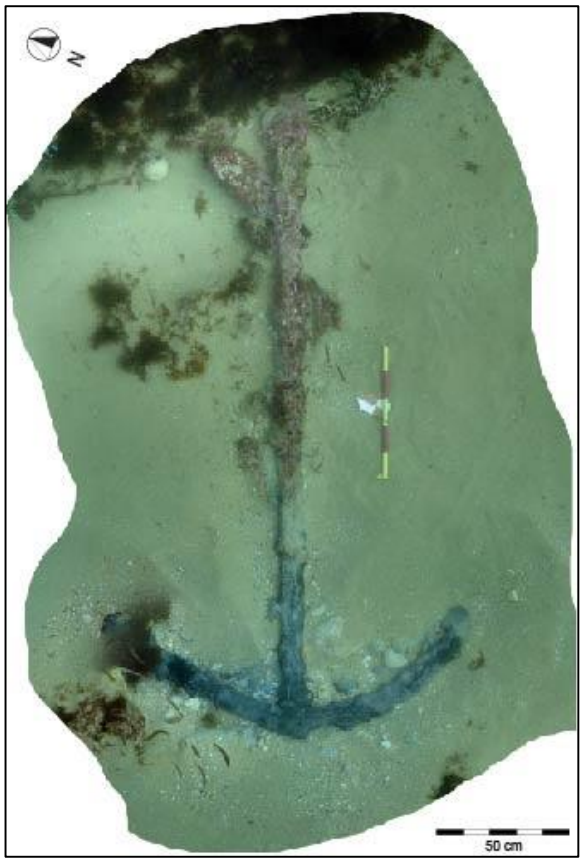

Figura 2. Âncora de ferro que integra o sítio arqueológico Porto de Mós 17 (CNS 40970), que se encontra em fundo de areia a 12m de profundidade, em frente à Praia do Canavial, em Lagos.

O registo arqueológico adoptado baseia-se na fotogrametria, um método rápido, eficaz e economicamente acessível, proporcionando resultados extremamente precisos e informativos. Esta técnica permitiu uma melhor compreensão dos sítios arqueológicos e, em certos casos, dos próprios artefactos, face às condições de visibilidade (Figura 2).

O sistema de posicionamento utilizado recorreu a coordenadas obtidas via GPS, através da boia de marcação de superfície utilizada pelos mergulhadores. Até ao momento, a margem de erro tem-se mantido abaixo dos 3 metros, permitindo localizar com sucesso os sítios arqueológicos sempre que necessário.

Neste mesmo alinhamento, queremos demonstrar que o PCS pode funcionar como um motor de desenvolvimento social, económico e cultural. Para isso, procurar-se-á a integração das comunidades locais de mergulhadores e pescadores no projecto e, paralelamente, pugnar-se-á pela transferência do conhecimento adquirido à sociedade em geral, numa lógica de usufruto do PCS. Para concretizar esta visão, procuramos estabelecer parcerias e obter financiamentos, que permitam a adopção de abordagens alternativas.

Este projecto é desenvolvido numa colaboração entre o Centro de Estudos em Arqueologia, Artes e Ciências do Património (CEAACP) da Universidade do Algarve (UAlg), a Câmara Municipal e o Centro de Ciência Viva de Lagos, associações privadas locais e regionais e outras entidades que, entretanto, sejam aglutinadas, como outros centros de investigação.

O nosso objetivo é centrar-nos na investigação, conservação, proteção, promoção e valorização do PCS. Não queremos apenas trabalhar para a comunidade, queremos trabalhar com a comunidade, envolvendo-a na preservação do PCS e tornando-a a sua principal guardiã e promotora. Contudo, esta iniciativa não se destina exclusivamente a mergulhadores. Assim, pretendemos selecionar alguns dos sítios arqueológicos conhecidos mais interessantes e torná-los acessíveis a pessoas não mergulhadoras. Um dos nossos propósitos é compreender de que forma o PCS pode revelar a evolução de uma paisagem marítima e aplicá-lo às realidades locais e regionais. Para tal, seguimos as pistas mais relevantes do registo arqueológico: os artefactos em si.

Este projeto está alinhado com as diretrizes e princípios da Convenção da UNESCO de 2001 sobre a Proteção do Património Cultural Subaquático, promovendo a conservação *in situ* e o acesso público ao PCS, bem como com os Objetivos de Desenvolvimento Sustentável da UNESCO (Agenda 2030).

Não pretendemos negligenciar o trabalho arqueológico realizado em Lagos nas últimas décadas.

Temos uma excelente oportunidade para consolidar e expandir os estudos existentes, nomeadamente os desenvolvidos por Tiago Fraga entre 2006 e 2015 (Fraga, 2013; Baço, 2015), melhorando-os essencialmente através de um registo arqueológico e geoposicionamento mais rigorosos, através de novos equipamentos disponíveis.

3. CONSIDERAÇÕES FINAIS

O projeto iniciou-se em agosto de 2024 e, até ao momento, realizaram-se um total de 82 mergulhos em 23 sítios arqueológicos. Estas imersões revelaram, por um lado, a existência de discrepâncias na localização de alguns arqueossítios, que se encontram agora corrigidos, com um erro absoluto inferior a 3 m, bem como delimitar melhor certas áreas, através da identificação de vestígios de superfície. Por outro, foram identificadas ou relocalizadas várias âncoras de ferro e de pedra, com cronologias que abrangem desde o período romano até meados do século XX.

Os dados recolhidos e produzidos estão a ser, neste momento, implantados e organizados em SIG. As bases cartográficas que estamos a utilizar correspondem à batimetria/topografia, linha de costa, fotografia aérea, cartografia histórica, entre outros. Sobre esta base, queremos implantar as áreas de trabalho e os registos fotogramétricos efectuados, de modo a ter uma melhor percepção de cada um dos sítios arqueológicos e, sobretudo, ter uma visão do conjunto de realidades relacionadas com o PCS do fundo marinho do território de Lagos.

Para sensibilizar a população sobre o PCS, desenvolvemos diversas atividades, incluindo a parceria estabelecida com o Centro de Ciência Viva de Lagos, reconhecido pelo seu serviço educativo. Pretendemos continuar a investigação subaquática e criar dois circuitos subaquáticos, um físico e outro virtual, para o público não mergulhador. Os dados obtidos serão utilizados para produzir conteúdos destinados a cinco mesas expositivas, que serão instaladas em pontos estratégicos da costa de Lagos, disponibilizando informações sobre o PCS identificado no concelho. Este empreendimento conta com o apoio da autarquia.

Os trabalhos desenvolvidos até ao momento, possibilitam uma caracterização diacrónica da navegação e da utilização do espaço marítimo do território de Lagos, evidenciando os múltiplos percursos e contactos que a cidade tem testemunhado ao longo de milénios.

Agradecimentos

Os autores agradecem a disponibilidade, interesse, trabalho e, sobretudo, amizade, de Christianne Kelkel, sem a qual o presente projecto não seria possível.

REFERÊNCIAS

Arruda, A., Sousa, E., Bargão, P. e Lourenço, P. (2008). “Monte Molião (Lagos) resultados de um projecto em curso”. In *Xelb*, 8. Silves: Câmara Municipal de Silves, pp. 61-192.

Baço, J. (2015). *Âncoras ao largo: um contributo arqueológico para o estudo das actividades marítimas em Lagos na Idade Moderna*. Dissertação de mestrado apresentada à FCSH-UNL, versão policopiada, 141pp.

Cardoso, M. T. (2004). *Estudo do manuscrito anónimo do século XVIII – Descrição da cidade de Lagos*. Amadora: Livro Aberto.

Corrêa, F. (1998). *Elementos para a História da Misericórdia de Lagos*. Lagos: Santa Casa da Misericórdia de Lagos.

Coutinho, V. (2008). *Lagos e o Mar Através dos Tempos*. Lagos: Câmara Municipal de Lagos, 95pp.

Fraga, T. M. (2008). *Projecto de Carta Arqueológica do Concelho de Lagos 2007/8*. Lagos: Câmara Municipal de Lagos, 101pp.

Fraga, T. M. (2013). “Survey Results from Lagos Bay, Portugal”. In *International Journal of Nautical Archaeology*, 42.2, 257-269.

Fraga, T. M. e Martins, A. S. (2011). “Lagos D wreck”. In *Nautical Archaeological Society Newsletter*, p. 11.

Fraga, T. M. e Salgado; A. A. (2012). “A Canhoneira Faro”. In *Revista da Marinha*, nº965, janeiro/fevereiro. Lisboa: Academia de Marinha.

Fraga, T. M., Baço, J. e Kelkel, C. (2014). Relatório intercalar 2013 – Projecto de Investigação Carta Arqueológica Subaquática da Baía de Lagos. Relatório entregue à DGPC a 21 de abril de 2014, que integra o processo 2012/041.

Lopes, G. C., Caleja, P. e Fonseca, C. (2024). *Relatório da 4ª Field survey do Projeto Water World – Lagos (outubro 2023)*. Lisboa: PCIP/CNANS (versão policopiada).

Loureiro, R. M. (1991). *Lagos e os Descobrimentos (até 1460)*. Lagos: Câmara Municipal de Lagos, 178pp.

Magalhães, J. R. (2004). *Foral de Lagos, 1504*. Lagos: Câmara Municipal de Lagos, 206pp.

Marado, C. A. (2006). *Antigos Conventos do Algarve: Um percurso pelo património da região*. Lisboa: Edições Colibri.

Morán, E. e Parreira, R. (2010). “A arqueologia urbana em Lagos: Uma década deactividade”. In *Xelb* 10. Câmara Municipal de Silves, pp. 899-917.

Oleson, J. P. (2008). *Testing the Waters: The role of Sounding Weights in Ancient Mediterranean Navigation, In Memoirs of the American in Rome*. Supplementary Volumes: The Maritime World of Ancient Rome. University of Michigan Press, 6, pp. 119-176.

Piccard, C. (1999). "A perda do Algarve vista do lado muçulmano". In Marques, M. D. G. M. (ed.) – *O Algarve da Antiguidade aos nossos dias*. Lisboa: Edições Colibri, pp. 103-106.

Interdisciplinary research and innovation for improving Underwater Cultural Heritage management

J. L. Garzon (1), L. Mills (1), F. Martins (1), P. Michalis (2), S. Oliveria (3), C. Veiga-Pires (1,3), C. Mazzoli (4), L. P. Cesareo (4), L. Germinario (4) and V. Karathanassi (5)

(1) Centro de Investigação Marinha e Ambiental (CIMA), Aquatic Research Network (ARNET), Universidade do Algarve, Faro, Portugal. jlhervas@ualg.pt
(2) Institute of Communication and Computer Systems (ICCS), Athens, Greece
(3) Centro Ciência Viva do Algarve, Faro, Portugal
(4) Department of Geosciences, University of Padova, Padova, Italy
(5) School of Rural, Surveying and Geoinformatics Eng., National Technical University of Athens, Athens, Greece

Abstract: Underwater Cultural Heritage holds undeniable historical, social, and cultural significance, yet natural hazards, human activities, and the growing impacts of climate change increasingly threaten the preservation of these sites. This work presents a set of research, technological, and innovative activities developed under the Horizon project THETIDA, aiming at safeguarding these valuable assets. The Consolidated B-24 Liberator US bomber, sunk in 1943 and resting off the southern coast of Portugal at a depth of 20 meters, was selected as one of the case studies. The outcomes of these activities underscore the necessity of interdisciplinary strategies to effectively address these complex threats.

Keywords: *THETIDA, B-24, Climate change, Oceanic hazards, Portugal*

1. INTRODUCTION

Climate change and natural hazards pose significant threats to underwater heritage sites, with cascading consequences for community identity and economy. However, limited knowledge exists on risk assessment and protective actions to mitigate these multiple hazards. To bridge this gap, the THETIDA project (https://doi.org/10.3030/101095253) focuses on the development of a preventive conservation strategy that includes monitoring, risk preparedness and management, for underwater and coastal cultural heritage (U&C-CH) sites. This is achieved through an interdisciplinary team of researchers, experts and practitioners that will develop, test and validate an integrated multiple heritage risk assessment and protection system with evidence-based monitoring frameworks, innovative tools and instruments and through participatory and crowdsourcing processes. With an EU contribution of 4 million euros, this 42-month project gathers professionals from 17 institutions and 8 participating countries.

The project actions are being implemented at seven pilot sites across Europe, linking social innovations with state-of-the-art technologies to enhance the resilience of underwater and coastal heritage sites. The present work aims to present the integrated efforts of the THETIDA consortium at the B-24 Liberator wreck in Portugal, one of the pilot sites, highlighting the importance of interdisciplinary activities focused on research, technological innovation, and community-engaged science living lab approaches. The objective is to demonstrate how collaborative strategies are being applied to document, preserve, and valorize underwater cultural heritage, contributing to achieving the main goals of this project.

2. PILOT SITE: CONSOLIDATED B-24 LIBERATOR

A Consolidated B-24 Liberator type D, a heavy bomber of the US Army crashed in the Atlantic Ocean in November 1943, around 1.5 km offshore from Praia de Faro in the southern coast of Portugal, and since then, it rests at 20 m depth (Figure 1). During the accident, the structure of the aircraft broke into several parts and only the wings and a part of the fuselage have been found so far. Additionally, other components such as propellers and some engines are located nearby. The aircraft was built predominantly in aluminum 2024 alloy, a well-known Alclad aircraft aluminum that resists corrosion in marine water, while the engine mounts and landing gear are in steel. The rest of the components are a mixture of magnesium, brass, plastic, rubber and other materials. Presently, the wreck serves as a refuge for the region's fauna and is included in the Portuguese National Underwater Ecological Reserve due to its ecological sensitivity, exposure and susceptibility to natural influences (Rangel *et al*., 2014).

3. INTERDISCIPLINARY METHODOLOGICAL APPROACH

During the first 30 months of the project, several activities were planned and executed. The next subsections explain the different methodological approaches proposed to achieve the project goals.

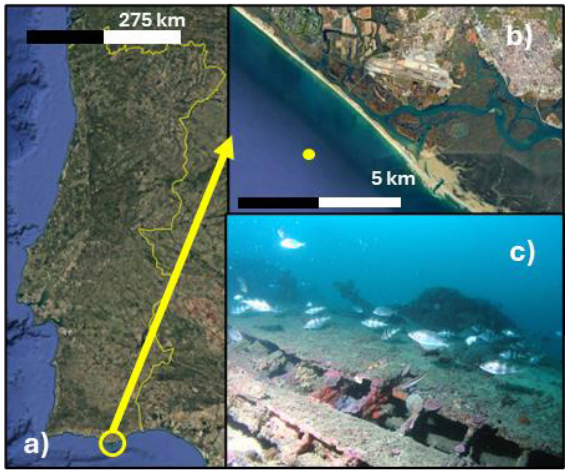

Figure 1.a) Limits of mainland Portugal with the yellow circle highlighting the region where the wreck is located. b) Location of the wreck in front of the Praia de Faro. c) Photography of the wreck (credit: Jose Vieira).

3.1. Citizens' science tools and Living labs

Citizen science (CS) is the practice of science that actively engages local communities in research. In this project, community members were involved in understanding changes and documenting their impacts. Living Labs (LLs) are another practice that involves social actors through interactive spaces to collaborate in co-creating new solutions to complex problems. The innovative goal of combining LLs' user-centered research and open innovation approaches with CS engagement is to enable local communities to place their participation within a personal, local, and cultural context. In this way, the two methodological approaches complement each other by directly engaging local stakeholders, end-users and community groups in collective data collection and decision-making, transforming management practices into more sustainable ones. As part of this activity, a training workshop on cultural heritage and climate change, LLs, and crowdsourcing tools for adaptation strategies was conducted with local stakeholders to facilitate the understanding of the THETIDA participatory approaches and the implementation of participatory methods and tools in this pilot site. A second activity consisted of an LL organized as a collaborative workshop with local stakeholders and civil society. A second LL is in preparation. Another type of activity, such as a Crowdsourcing and Citizens' Science app, will be developed for this site. This app will facilitate the visualization of content collected by divers, namely a 3D model of the wreck based on imagery. This application will use appropriate visualization techniques such as Augmented Reality technology and gamification mechanisms. This will create virtual environments for the presentation of the wreck without the necessity of diving at the site.

3.2. Analysis of heritage materials

Field campaigns have been designed to collect specimens of the main materials observed at the B-24, and their associated deterioration features. A total of 25 samples will be analyzed at the University of Padua. These include 15 samples distributed along the wreck structure and loose components of biological colonization. Sampling from the metal structure will be conducted using a chisel and hammer, collecting surfaces no larger than 20 × 20 mm, with fragments ranging from a few hundred milligrams to 3 grams in weight. The identification of algal and animal colonisers will begin with morphological analyses using optical and stereoscopic microscopy. Part of the biological material will be mechanically removed and subjected to DNA extraction for subsequent metabarcoding analysis, enhancing the reliability of the community assessment. Metal specimens will be analyzed using various analytical techniques – Optical Microscopy (OM), X-ray Powder Diffraction (XRPD), Scanning Electron Microscopy with Energy Dispersive Spectroscopy (SEM/EDS), and micro-Raman spectroscopy – to determine their composition, texture, and corrosion products. In parallel, coupons made from the same materials have been deployed in other carefully selected locations, which are exposed to different environmental conditions, to investigate the influence of these settings, including ocean acidification, on corrosion rates and biocolonization. Additional experiments are being conducted in the laboratory using a prototype MicroEnvironment Simulator (MES), which allows controlled variation of water pH, temperature, salinity, and pressure. In this case, the aim is to assess the influence of water parameters on corrosion in the absence of biological colonization. Electrochemical methods, such as Tafel analysis, will be used to measure corrosion potential. The overall objective of these complementary approaches is to quantify the effect of environmental parameters on corrosion rates, to be integrated into vulnerability assessment models.

3.3. Multi-hazard and risk modelling

A quantitative risk assessment was developed to account for the main hazards that impact the B-24. Thus, the risk is computed as a function of the hazard (with a given probability) and the vulnerability, following the UNISDR Terminology on Disaster Risk Reduction. UN, (2009):

$$R_i = \sqrt{SH_i \; x \; SV_i}$$

where R_i is the risk score for each hazard (i), SH_i is the score for a specific hazard, and SV_i is the score for the vulnerability to that hazard (i). The risk score ranges from 0 to 5. Four main degradation processes were included in the analysis: decontextualization, physical

degradation, biological degradation, and chemical degradation. The first three processes have been identified by previous studies as relevant for the long-term preservation of the UCH, being the wind-waves the main natural agent governing them (Fernández-Montblanc *et al.*, 2022). Furthermore, chemical degradation processes can also negatively impact metallic materials in long-term exposed conditions. After the computation of the hazard indicators, based on analytical models and statistical analyses, the values are ranked. The vulnerability of the UCH assets involves two factors: the properties of the materials of the sites and the environmental conditions affecting the susceptibility of elements to be impacted by a hazard. The total vulnerability is obtained as the geometric mean of all the vulnerability items, including both factors. This approach allows for individual assessments of different materials, such as aluminum and steel and comparison with other sites. Environmental data will be collected from Copernicus Services, consensus models and local partners.

3.4. Mathematical models for emergency response

An existing high-resolution coastal hydrodynamic model for the SW Iberian Coast (Janeiro *et al.*, 2017) was adapted to receive the new modules to be developed within THETIDA. Main adaptations are the operationalization of the modelling system and the automatization of the operational procedures. A new wave model was developed for the same area of the hydrodynamic model, based on the SWAN software (Figure 2). This model was calibrated and validated using available wave data from 4 different buoys covering the entire domain. The hydrodynamic model was coupled to the wave model, and the efficiency of different coupling methods was evaluated to find the best coupling mechanism. The results of this one-way coupling demonstrated that wave model runs forced with surface currents produced more accurate results than those simulations with no currents. The two-way reverse coupling of the wave model back to the hydrodynamic model is underway in order to include the influence of waves in the hydrodynamics. Next steps will involve the creation of a sediment transport model for the same region and the dynamic coupling of this model with the hydrodynamic and wave models (Figure 2). The final goal is to create a fully-integrated operational system able to perform in real time multi-hazard risk assessments similar to those described in the previous chapter.

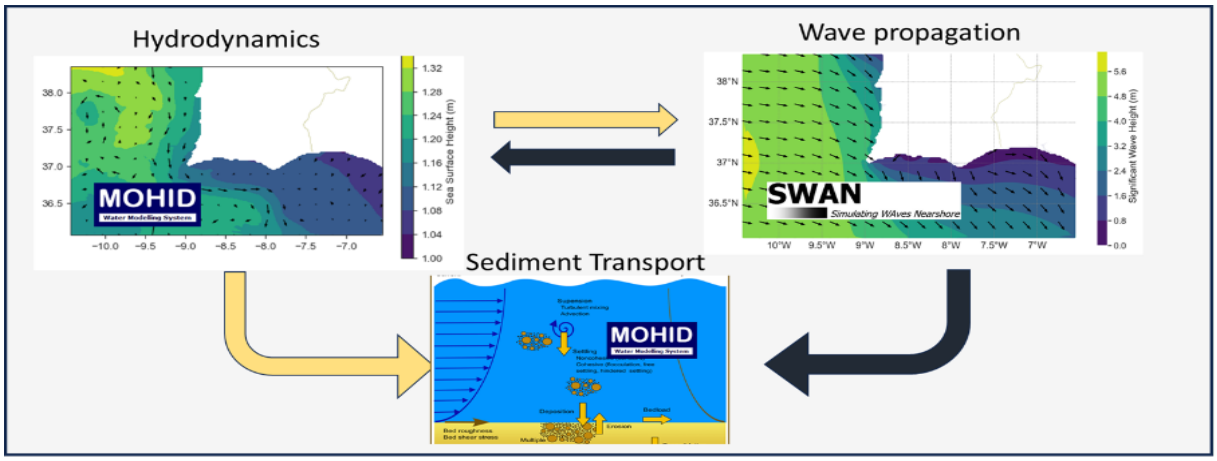

Figure 2. Numerical framework developed to assess oceanic risks on the wreck formed by three main components coupled: hydrodynamics, waves and non-cohesive sediment transport.

3.5. IoT devices In-situ monitoring tool

IoT (Internet of things) Conductivity-Depth-Temperature (CTD) sensors with dual functionality (Pavlopoulos *et al.*, 2024) will be deployed at the site (Figure 3). On one hand, they will be used as a wearable device for divers, offering immediate, real-time measurements during underwater expeditions. Alternatively, it can be fixed to the seabed or other submerged structures for long-term monitoring, continuously collecting data on environmental changes. The installation of the CTD sensor on the B-24 wreck or the adjacent seabed is planned to monitor these parameters over extended periods (6–12 months). Equipped with a cellular solution for dynamic data transmission, the CDT sensor can send collected data as soon as it resurfaces. Another underwater CTD sensor tested at this site was designed for real-time monitoring of the subaquatic heritage site from the surface by being attached to vessels.

3.6. Advanced imaging and sensing technologies for underwater exploration

The use of Autonomous Underwater Vehicle (AUV) platforms equipped with specific payloads, such as multibeam sonar and side scan sonar, combined with data fusion techniques from optical cameras and photogrammetric procedures, offers an advanced approach to exploring and documenting underwater environments. The AUVs will also be equipped with

hyperspectral cameras to identify and map biophysical changes in materials exposed to degradation processes. This pioneering technological development will be tested for the first time in the THETIDA sites. Here, this activity will focus on detecting degradation patterns in the materials of the plane caused by environmental factors (such as salinity, temperature, and pH) and biological factors (biofilm growth, microbial colonization). The AUV configuration allows the vehicle to work autonomously on pre-programmed missions or routes.

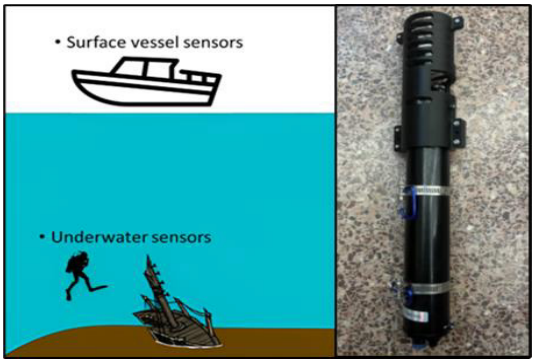

Figure 3. Two types of IoT approaches. Picture of the CTD sensor.

3.7 Decision Support System

The Decision Support System (DSS) within THETIDA Portal serves as a powerful tool for guiding decision-making processes in various domains related to marine and environmental sciences. It leverages advanced algorithms and models developed within THETIDA's platform to analyse complex datasets and generate actionable recommendations. Through interactive maps, charts, graphs, and 3D visualizations, users can dynamically explore spatial and temporal patterns, uncover insights, and gain a deeper understanding of complex environmental phenomena. The Middleware's DSS will allow to analyse complex datasets and provide actionable recommendations to stakeholders on this site. The output of our modelling and analysis will feed the DSS to provide appropriate adaptation and mitigation strategies, and support sustainable plans for protecting and preserving the B-24.

4. IMPACTS

The integration of citizen science tools and living labs fosters local stewardship, creating a shared responsibility for protecting the site. At the same time, laboratory analyses of the wreck's materials provide critical insights into degradation processes, supporting informed decisions on conservation strategies. Together, these approaches strengthen the connection between scientific knowledge and community action, ensuring that preservation efforts are evidence-based. Complementing these activities, advanced imaging and sensing technologies for underwater exploration including sonar, optical, and hyperspectral systems, will enable detailed mapping, documentation, and monitoring of the wreck at unprecedented scales. Multi-hazard risk models and mathematical models for emergency response provide a comprehensive understanding of dynamic threats, while real-time data from IoT devices and in-situ monitoring tools allow the detection of environmental changes. All this information is brought together within a Decision Support System, offering an integrated platform to guide managers and stakeholders in designing and implementing effective, adaptive, and sustainable preservation measures.

5. CONCLUSIONS

The preservation of the US bomber B-24 Liberator wreck will benefit significantly from the exploitation of advanced technologies, scientific research, and community engagement. This case study strengthens the project's impact by showcasing integrated solutions for preserving vulnerable maritime heritage under the threats of natural hazards, exacerbated by climate change and human pressure. The B-24 is the only underwater pilot site located in the Atlantic Ocean and will provide important insights to better understand the effects of these threats and the impacts of the local conditions concerning other regions (e.g., the Mediterranean Sea). Ultimately, these activities contribute to a strategy for safeguarding Europe's underwater cultural heritage.

Acknowledgements

This research has been funded by the European Union's Horizon Europe research and innovation programme under THETIDA project (Grant Agreement No. 101095253). The first author has been funded by the FCT through the project with reference CEECINST/00146/2018/CP1493/CT0012. The authors also acknowledge FCT funding to the Associate Laboratory ARNET under the project LA/P/0069/2020 and CIMA through the grant UIDP/00350/2020.

REFERENCES

Fernández-Montblanc, T., Bethencourt, M. and Izquierdo, A. (2022). Underwater Cultural heritage risk assessment methodology for wave-induced hazards: The showcase of the Bay of Cadiz. *Frontiers in Marine Science*, *9*, 1–18.

Janeiro, J., Neves, A., Martins, F. and Relvas, P. (2017). Integrating technologies for oil spill response in the SW Iberian coast. *Journal of Marine Systems*, *173*, 31–42.

Pavlopoulos, L., Michalis, P., Vlachos, M., Georgakopoulos, A., Tsiakos C. and Amditis, A. (2024). Integrated Sensing Solutions for Monitoring Heritage Risks, IEEE International Geoscience and Remote Sensing Symposium, Athens, Greece, 2024, pp. 3352-3355.

Rangel, M. O., Pita, C. B., Gonçalves, J. M. S., Oliveira, F., Costa, C. and Erzini, K. (2014). Developing self-guided scuba dive routes in the Algarve (Portugal) and analysing visitors' perceptions. *Marine Policy*, 45, 194–203.

UNISDR Terminology on Disaster Risk Reduction. UN, Geneva, 2009.

Geoarchaeological walks through the Cenomanian flint of the Western Iberian Margin

P. Jordão (1) and N. Pimentel (2)

(1) UNIARQ, Centre for Archaeology, FLUL, ULISBOA, Portugal. pjordao@letras.ulisboa.pt
(2) IDL, Instituto Dom Luiz, FCUL, ULISBOA, Portugal.

Abstract: Archaeological lithic raw material can be an important indicator of the local, regional, and even supra-regional geological framework. Provenance studies of flint from prehistoric sites located in Portuguese Estremadura have led to a more thorough petrographic, mineralogical, and geochemical characterisation of Cenomanian flint samples from the Lusitanian Basin. In both geological and archaeologically correlated samples, differences in siliceous microfacies were observed, with a north-to-south increase in micropalaeontological diversity and a decrease in continental terrigenous input, providing a more detailed palaeogeographical sketch of the Lusitanian Basin during the Upper Cenomanian.

Keywords: *Flint, Siliceous microfacies, Lusitanian Basin, Cenomanian, Raw materials*

1. INTRODUCTION AND OBJECTIVES

Lithic provenance studies from European prehistoric sites focused on siliceous rocks have led to a more exhaustive petrographic, mineralogical, and geochemical characterisation of flint and its host primary or secondary formation (e.g. Tarriño *et al.*, 2015; Delvigne *et al.*, 2020; Gurova *et al.*, 2022).

In recent years, similar studies from Copper Age sites located in the Portuguese Estremadura conclude that approximately 90% of the sampled material was formed in the Upper Cenomanian formations of the Lusitanian Basin (Jordão, 2023).

The identification of the main siliceous microfacies in flint samples from the Bica Formation, between Lisbon and Torres Vedras (Jordão and Pimentel, 2019a; b; Leitão *et al.*, 2019; Jordão *et al.*, 2022), enabled the production of a preliminary palaeogeographical sketch of the Lusitanian Basin in its Central and Southern Sectors.

Recent work (Jordão and Cardoso, 2024; Jordão *et al.*, accepted) and the ongoing exploratory project – "MOBlades 2023.13251.PEX – Provenance of blades' raw material as an indicator of human mobility during the Copper Age of the SW of the Iberian Peninsula" – has led to an increase in flint sampling, including different Mesozoic contexts of the Lusitanian Basin, as well as Cenozoic conglomerates containing inherited flint.

2. MATERIALS AND METHODS

The base for this work has been the *ARQUEOLit* litotheque hosted at the Centre for Archaeology of School of Arts and Humanities (University of Lisbon). The sampling includes 64 samples of previously studied Cenomanian flint (Jordão, 2023; Jordão and Pimentel, 2023; Jordão and Cardoso, 2024) and a new set of 12 samples collected from Santa Quitéria Formation (Pliocene), near Caxarias (Ourém), where the Neo-Chalcolithic flintknapping workshop of Casas de Baixo is located (Zilhão, 1994). Finally, 8 samples from Bica Formation (Cenomanian), near bifacial flaked stones workshop of Santana (Lisboa), were added to the set.

A Leica M205C stereo microscope was used, with 1008x maximum magnification. Thin sections were examined and characterized, using a Leica DM750P Pol microscope (×40 to ×100), focusing on general textures and particular allochems. Both compositional (Folk, 1959) and textural (Dunham, 1962) carbonate rocks terminology and classifications have been visually applied, regardless of its paleoenvironmental interpretation, taking into account that most flint nodules are a product of the silicification of previously carbonate rocks.

3. RESULTS

Microfacies present predominantly wackestone textures, containing small fragments of bioclasts, sometimes filled with mesocrystalline quartz, within a poorly preserved peloidal matrix. In the new samples of Caxarias flint, the presence of phytoclasts (e.g., fragments of vegetal tissues and carbonaceous material) reaching up to a centimetre, was also observed. In both microfacies, detrital elements are frequent, particularly fine grains of quartz and muscovite (Figure 1). In Torres Vedras, at the Central Sector of the Lusitanian Basin, in the upper member of the Bica Formation**,** four flint microfacies were recognised, mostly dominated by mudstone textures, and sometimes peloidal wackestones, with poor

micropalaeontological assemblages. Further South, in the Pero Pinheiro–Carenque area, wacke- to packstone textures, more common in Lisboa, with bivalve and gastropod fragments (Figure 1) were observed.

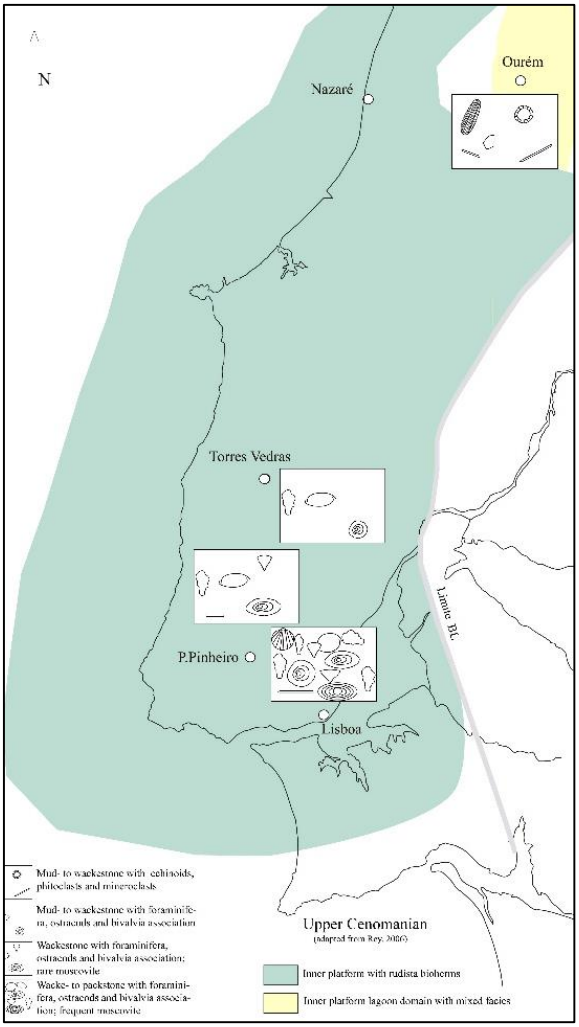

Figure 1. Main siliceous microfacies and synthesis of figurative elements from the Upper Cenomanian of the Lusitanian Basin, on a paleogeographic sketch of the Western Portuguese Margin (adapted from Rey et al. 2006).

4. DISCUSSION

The observed Nort to South differences in microfacies result from regional scale paleoenvironmental variations which controlled the compositional elements and textures of the primary carbonates and consequently the resulting silicified flints.

In the Northern Sector of the Lusitanian Basin, the Upper Cenomanian marks the beginning of a regressive period, whose lateral transition from marine to marginal-littoral domain may be observed in the Ourém-Olival area (Berthou and Lauverjat, 1979). This zone corresponds to a marginal lagoonal domain of marly facies with echinoids, exposed to terrigenous influences (Callapez, 2004; Hart *et al.*, 2005; Rey *et al.*, 2006). The Caxarias flint eroded from Cenomanian local formations exhibits microfacies with fragments of vegetal tissues and carbonaceous material that confirms the continental influence.

From north to south, there is a clear decrease in fine detrital elements and the bioclastic assemblages tend to become more diverse. However, a few differences were identified in the siliceous microfacies of the Central and Southern Sectors, which allowed a more detailed palaeogeographic sketch of the Western Portuguese Carbonate Platform during the Late Cenomanian (Rey *et al.*, 2006).

5. CONCLUSIONS

The preliminary results of the petrographic study of the siliceous microfacies of the Northern Sector of the Lusitanian Basin show a flint formed in shallow, confined and low-salinity waters, receiving fine continental terrigenous inputs during the Late Cenomanian.

In the Central Sector, around the Torres Vedras area, sedimentation seems to have occurred in a restricted lagoonal/marine environment, with low energy and shallow water depth.

Finally, in the Southern Sector, between Pero Pinheiro and Lisboa, the bioclastic assemblages become more diverse, with bivalve and gastropod fragments, suggesting sedimentation in a more open, exposed and agitated marginal zone.

Acknowledgements

This work was financed by Portuguese funds through FCT - Fundação para a Ciência e a Tecnologia in the framework of the project UID/00698: Centre for Archaeology. University of Lisbon.

REFERENCES

Andreeva, P., Stefanova, E. and Gurova, M. (2014). Chert raw materials and artefacts from NE Bulgaria: A combined petrographic and LA-ICP-MS study. *Journal of Lithic Studies*. doi: 10.2218/jls.v1i2.1129

Berthou, P.Y. and Lauverjat, J. (1979). Essai de synthèse paléogéographique et paléobiostratigraphique du bassin occidental portugais au cours du crétacé supérieur. *Ciências da Terra*, 5, 121–144.

Callapez, P. (2004). The Cenomanian-Turonian central West Portuguese carbonate platform. In: Cretaceous and Cenozoic Events in West Iberia Margins. 23rd IAS Meeting of Sedimentology – Coimbra 2004 Sedimentology and Society. Field Trip Guidebook (Ed. P. Dinis and P.P. Cunha), Coimbra, 2, 39–51.

Delvigne, V., Fernandes, P., Tuffery, C., Raynal, J.-P. and Klaric, L. (2020). Taphonomic methods and a database to establish the origin of sedimentary silicified rocks from the Middle-recent Gravettian open-air site of La Picardie

(Indre-et-Loire, France). *Journal of Archaeological Science: Reports*, 32, 102369.

Dunham, R. (1962). Classification of carbonate rocks according to depositional texture. In: *Classification of carbonate rocks* (Ed. W.E. Ham), 108–121.

Folk, R. (1959). Practical Petrographic Classification of Limestones. *AAPG Bulletin*. doi: 10.1306/0BDA5C36-16BD-11D7-8645000102C1865D

Gurova, M., Andreeva, P., Stefanova, E., Aladzhov, A. and Bonsall, C. (2022). Petrographic and geochemical analyses of flint raw materials from Bulgaria: A reliable combination for provenance studies of archaeological flint. *Quaternary International*, 615, 18–32.

Hart, M., Callapez, P., Fisher, J., Hannant, K., Monteiro, J., Price, G. and Watkinson, M. (2005). Micropalaeontology and Stratigraphy of the Cenomanian/Turonian boundary in the Lusitanian Basin, Portugal. *Journal of Iberian Geology*, 31, 311–326.

Jordão, P. (2023). A proveniência de sílex e a mobilidade no Calcolítico da Estremadura: Uma abordagem geológica e petroarqueológica.Tese de doutoramento em Geologia, Especialidade de Geodinâmica Externa. Lisboa: Faculdade de Ciências da Universidade de Lisboa. Doutoramento, Faculdade de Ciências da Universidade de Lisboa

Jordão, P. and Cardoso, J. L. (2024). Estudo petroarqueológico de proveniência de materiais siliciosos de Leceia, Barotas e Monte do Castelo (Oeiras, Portugal). *Estudos Arqueológicos de Oeiras*, 33, 181–232.

Jordão, P., Guedes, A. and Pimentel, N. (2022). Raman Microspectroscopy applied to flint provenance at the Chalcolithic settlement of Zambujal (Torres Vedras, Portugal). *Archaeometry*, 1–18.

Jordão, P., Neves, C., Soares, S., Diniz, M. and Arnaud, J.M. (accepted) Follow that blade! - petroarchaeological proxies as indicators of human mobility in Vila Nova de São Pedro (Portugal).

Jordão, P. and Pimentel, N. (2019a). O potencial dos terraços do rio Sizandro para o provisionamento em sílex na Pré-história da Estremadura. In: *III FRAGMENTOS DE ARQUEOLOGIA DE LISBOA 18- Extrair e Produzir… dos primeiros artefactos à industrialização (2018, November)*, Câmara Municipal de Lisboa (Ed. J.C. Senna-Martinez, A.C. Martins, A. Caessa, A. Marques, and I. Cameira), Lisboa, 45–55.

Jordão, P. and Pimentel, N. (2019b). Os terraços quaternários do rio Sizandro (Torres Vedras): caracterização de uma área-fonte de sílex. *Geonovas*, 32, 93–106.

Jordão, P. and Pimentel, N. (2023). Sobre a presença de sílex na Praia das Maçãs. In: *Arqueologia em Portugal/2023 - Estado da Questão*, 333–344.

Leitão, E., Pimentel, N., Didelet, C., Mourão, C., Luz, N. and Cardoso, G. (2019). Identificação e análise preliminar dos sílex da área oeste do município de lisboa. In: *III FRAGMENTOS DE ARQUEOLOGIA DE LISBOA 18- Extrair e Produzir… dos primeiros artefactos à industrialização (2018, November)*, Câmara Municipal de Lisboa (Ed. J.C. Senna-Martinez, A.C. Martins, A. Caessa, A. Marques, and I. Cameira), Lisboa, 35–44.

Rey, J., Dinis, J., Callapez, P. and Cunha, P.P. (2006). Da rotura continental à margem passiva: composição e evolução do Cretácico de Portugal. *INETI*, Lisboa.

Tarriño, A., Elorrieta, I. and García-Rojas, M. (2015). Flint as raw material in prehistoric times: Cantabrian Mountain and Western Pyrenees data. *Quaternary International*, 364, 94–108.

Zilhão, J. (1994). A oficina de talhe neo-calcolítica de Casas de Baixo (Caxarias, Vila Nova de Ourém). *Trabalhos de Arqueologia da EAM*, 2, 35–45.

Characterization of ancient Lisbon Estuarine Beaches

A. M. Costa (1), M. Silva (2), A. L. Rodrigues (3) and M. C. Freitas (4)

(1) Laboratório de Arqueociências (LARC) – PCIP | BIOPOLIS – CIBIO | IDL – Instituto Dom Luiz | UNIARQ – Centro de Arqueologia da Universidade de Lisboa, Calçada do Mirante à Ajuda, 10A, 1300-418 Lisboa, Portugal. acosta@patrimoniocultural.gov.pt

(2) Laboratório de Arqueociências (LARC) – Património Cultural, IP | IDL – Instituto Dom Luiz | IEM – Instituto de Estudos Medievais, Calçada do Mirante à Ajuda, nº 10A, 1300-418 Lisboa, Portugal

(3) C²TN/DECN – Instituto Superior Técnico, University of Lisbon, Campus Tecnológico e Nuclear, Estrada Nacional 10, 2695-066 Bobadela, Portugal

(4) IDL – Instituto Dom Luiz | Departamento de Geologia - Faculdade de Ciências da Universidade de Lisboa, Campo Grande Edifício C1, Piso 1, 1749-016 Lisboa, Portugal

Abstract: At the end of the 19th century, Ramalho Ortigão, Portuguese writer and journalist, described the Pedrouços beach "…like all those in the great Bay of the Tagus, smooth, flat, and with fine sand...". Soon after, an embankment was constructed to gain utilitarian land along the shore and to build the Pedrouços dock, causing the beach to disappear. The same occurred in several other beaches along the Lisbon estuarine margin. At present, due to the intricate morphology of the Tagus estuary and the significant human alteration of its northern margin, estuarine beaches predominantly develop along its left bank in the inner estuary and on both margins of the inlet. Beaches located in the inlet are essentially composed by very well calibrated to well calibrated fine to medium sand, while beaches occurring in the inner estuary are primarily constituted by moderately well calibrated medium to coarse sands. In this work we characterize the ancient Lisbon beaches. Present and former beaches are similar in terms of grain-size.

Keywords: *Tagus Estuary, Geoarchaeology, Lisbon Stories, Estuarine margins, Environmental evolution*

1. INTRODUCTION

Nowadays, the connection between the city of Lisbon and the Tagus estuary is defined by a protective two-meter-high wall, the result of successive constructions works and landfills carried out over time along the estuarine margins that displaced the coastline to the south. Due to the intricate morphology of the Tagus estuary and the significant human alteration of its northern margin, estuarine beaches predominantly develop along the left bank of the inner estuary and on both margins of the inlet (Freire *et al*., 2007, Freire *et al*., 2009, Taborda *et al*., 2009). In response to different factors, beaches located in the inlet are essentially composed by very well calibrated to well calibrated fine to medium sand, while beaches occurring in the inner estuary are primarily constituted by moderately well calibrated medium to coarse sands (Freire *et al*., 2007). Small urban beaches have developed in the Lisbon estuarine margin in four distinct areas, mostly nestled against its protective wall. These include the beaches at Parque Tejo (just south of the Trancão river mouth), Prainha do Braço de Prata, Praia do Cais das Colunas (in Cais do Sodré), and Praia de Algés (Figure 1). These beaches contain significant amounts of dumped materials and are not appropriate for bathing. In the past, however, several beaches such as other intertidal environments (e.g., salt marshes) lined the edge of the estuary, particularly in the bays formed at the mouth of northern Tagus tributaries that today flow channelized beneath the city.

Most of these ancient estuarine beaches, especially those located near the city centre, served as port areas since at least the Roman times, as evidenced by the abundant archaeological structures and artifacts related to maritime activities (e.g., Sarrazola, 2014a; Sarrazola, 2014b; Macedo *et al*., 2017; Bettencourt *et al*., 2021a; Bettencourt *et al*., 2021b). Nevertheless, some of the beaches, particularly the ones located further west, were also used for recreational purposes, at least until the middle of the 20th century, and are mentioned in national beach guides such as the one published by Ramalho Ortigão (1976) as well as depicted in photographs preserved in Arquivo Municipal de Lisboa (Figure 2).

The Lisbon estuarine front is considered a prime location nowadays, and consequently several buildings have been remodelled and constructed to accommodate a wide variety of activities. The (re)construction works along with associated salvage archaeological excavations, have provided access to the ancient estuarine marginal environments, including Lisbon´s historic beaches.

The aim of this study is to characterize the ancient estuarine beaches of Lisbon and to compare the findings with published data on present-day Tagus

estuarine beaches. The results will contribute to a better understanding of the Tagus estuarine dynamics over time and will allow to reconstruct the environmental conditions along the Lisbon estuarine margin during key chronological periods important for the history of development of the city.

Figure 1. Location and photography of the present-day estuarine beaches located in the northern margin of the Tagus estuary, in Lisbon Municipality. Photos © José Vicente | Agência Calipo | 2024.

Figure 2. Pedrouços beach in 1937. Photo © Eduardo Portugal, Arquivo Fotográfico de Lisboa, CML, Referência PT/AMLSB/POR/058935.

2. MATERIALS AND METHODS

2.1. Materials

Figure 3 presents the location of all the sediments collected in the Lisbon estuarine margin in salvage archaeological works and framed by the Lisbon Stories project. In this study, data from sediments collected at Pedrouços, Alcântara and Esteiro da Baixa (EB) will be presented (Figure 3). In Pedrouços and Alcântara, sediments were collected in profiles present below anthropogenic structures (see results for chronology). In EB sediments were collected below roman constructions. In this work we analyse the sediments considered as the beach deposited before the human interventions.

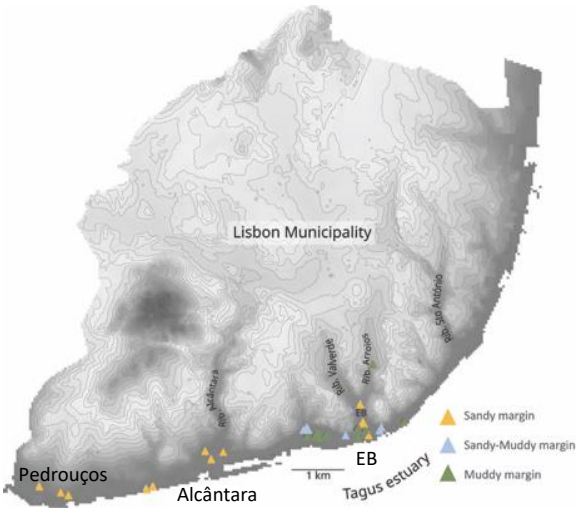

Figure 3. Location of sediments collected in the Lisbon estuarine margin in salvage archaeological works.

2.2. Methods

Sandy samples (>63 µm) were subjected to mechanical sieving for 15 minutes using a standardized series of ASTM sieves spaced at 0.5 ϕ intervals, ranging from -2 ϕ (4 mm) to 4 ϕ (63 µm), according to the Udden-Wentworth classification (Wentworth 1922). The results allowed for the calculation of statistical parameters of the grain size distribution (mean and standard deviation) using the graphical method (Folk and Ward, 1957) through the GRADISTAT software (Blott and Pye, 2001). Chronology of the sediments was achieved by their archaeological context. In some of the studied areas lacking archaeological information, samples are being absolute dated by optical stimulated luminescence (OSL).

3. RESULTS AND DISCUSSION

According to our results, the estuarine Roman beaches from the mouth of EB were composed by moderately to moderately well sorted, fine to medium sand (sand below the roman levels of NARC – Núcleo Arqueológico da Rua dos Correeiros) and medium to coarse sand (sand below the Roman cryptoporticus) (Costa *et al.*, 2018). The beaches at Alcântara (Alcântara Lisbon Offices) during the Contemporary period (below a dock wall built in the middle of 19th century) were constituted by moderately well sorted medium sand (Costa *et al.*, 2024). The pre-18th century landfill Pedrouços beach (Vila Garcia archaeological site) is composed by moderate well sorted to well sorted medium sand. All beach profiles present intercalations of coarser sands, probably reflecting higher energetic events related with winter storms.

4. FINAL REMARKS

To the writer Ramalho Ortigão, the Pedrouços beach was "…like all those in the great Bay of the Tagus, smooth, flat, and with fine sand. The sea is calm, serene like a lake, the best for bathing, at high tide...". In terms of grain-size former Lisbon beaches, including the Pedrouços beach, were mostly composed by moderately well sorted medium to coarse sands, and similar to the existent in the inner Tagus estuary (Figure 4).

New data concerning the composition of the sediments will improve the knowledge on the former Lisbon beaches and contribute to understand the source of sediments feeding northern margin of the Tagus estuary, in Lisbon.

Beaches, as other intertidal environments, are coastal features that protect inland areas as they contribute to reduce their vulnerability to future mean sea-level rise and coastal hazards. In Lisbon, only small urban beaches develop today, nested against the city protective wall. How will they evolve in the future and respond to climate change?

Acknowledgments

This work was done within the frame of the *Lisbon Stories* project and was supported by Património Cultural IP and FCT, I.P./MCTES through the national funds (PIDDAC): UID/50019/2025, LA/P/0068/2020 (https://doi.org/10.54499/LA/P/0068/2020), UIDB/00698/2020 (https://doi.org/10.54499/UIDB/00698/2020) and UIDP/00698/2020 (https://doi.org/10.54499/UIDP/00698/2020). Margarida Silva is supported by the PhD FCT grant PRT/BD/155050/2023 (https://doi.org/10.54499/PRT/BD/155050/2023), Ana Luísa Rodrigues is supported by the project CEECINST/00043/2021/CP2797/CT0011 and C2TN by UID/Multi/04349/2020.

The authors would like to thank to João Poiares (archaeology master student volunteer in the Lisbon Stories project) for the laboratorial analyses.

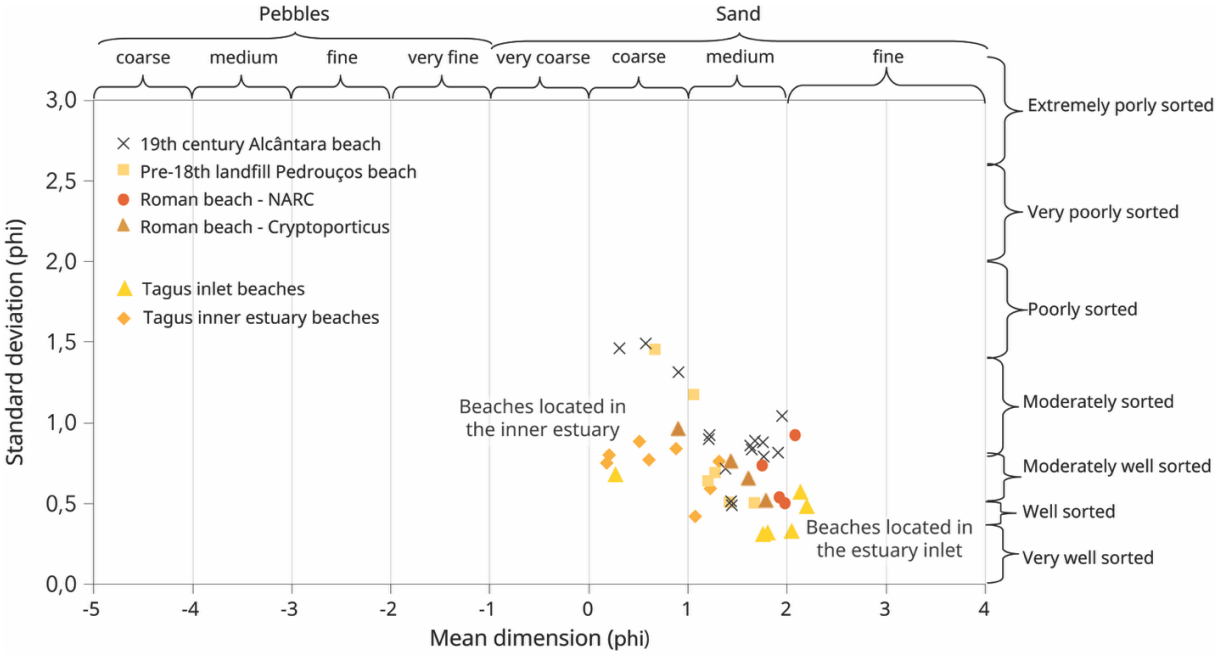

Figure 4. Characterization of present-day and former Tagus/Lisbon estuarine beaches.

REFERENCES

Bettencourt, J., Fonseca, C., Carvalho, P., Silva, T., Coelho, I. P. and Lopes, G. (2021a). Early Modern Age ships and ship finds in Lisbon riverfront: research perspectives. *Journal of Maritime Archaeology*, 16, 413-443.

Bettencourt, J., Lopes, G., Fonseca, C., Silva, T. Carvalho, P. and Coelho, I.P. (2021b). Boa Vista 1: context and construction details of an early modern ship discovered in Lisbon, Portugal. *Archaeonautica*, 21, 101-106.

Blott, S.J. and Pye, K. (2001). GRADISTAT: a grain size distribution and statistics package for the analysis of unconsolidated sediments. *Earth Surface Processes and Landforms*, 26, 1237-1248.

Costa, A.M., Freitas, M.C., Lopes, V., Bugalhão, J., Cascalho, J., Andrade, C. and Rocha, A. (2018). As praias fluvio - estuarinas da Idade do Ferro e do Período Romano da Baixa de Lisboa, Portugal. In Bernardes, J.P., Etchvarne, C., Lopes, M.C, Costa, C. (eds.) Arqueologia Urbana em Centros Históricos. Algarve, pp. 256 -273.

Costa, A.M., Freitas, M.C., Bugalhão, J., Rodrigues, E., Silva, C.M., Neto, N., Martinez, S. and Brito, S. (2024). Evolução natural holocénica e perturbação antrópica na foz da Ribeira de Alcântara, Estuário do Tejo (Lisboa). OPHIUSSA, Revista do Centro de Arqueologia da Universidade de Lisboa, 8, 5-27.

Folk, R.L. and Ward, W.C. (1957). Brazos River bar, a study in the significance of grain size parameters. *Journal of Sedimentary Petrology*, 27, 3.

Freire, P., Taborda, R. and Silva, A.M. (2007). Sedimentary characterization of Tagus estuarine beaches (Portugal): A contribution to the sediment budget assessment. *Journal of Soils and Sediments*, 7, 296-302.

Freire, P., Taborda, R. and Andrade, C. (2009). Caracterização das praias estuarinas do Tejo. Associação Portuguesa dos Recursos Hídricos. *VIII Congresso da Água*, Figueira da Foz (Portugal), 13 – 17 Fev., pp. 12.

Macedo, M.L., Silva, I.M., Lopes, G. and Bettencourt, J. (2017). A dimensão marítima do Boqueirão do Duro (Santos, Lisboa) nos séculos XVIII e XIX: primeiros resultados arqueológicos. In Arnaud, J.M, Martins, A. (Eds.) Arqueologia em Portugal – 2017 Estado da Questão 2017, 1915-1924.

Ortigão, R. (1876). As praias de Portugal. Guia do banhista e do viajante. Porto Magalhães & Moniz, Porto, p. 144.

Sarrazola, A. (2014a). O fundeadouro romano da actual Praça D. Luís I (Séculos I a.C. / VI d.C.)", Rossio: Estudos de Lisboa 3, pp. 34-46.

Sarrazola, A. (2014b). "A Grade de Maré da Praça D. Luís I: subsídios para o conhecimento histórico da Lisboa Ribeirinha em época *Moderna*", Rossio: Estudos de Lisboa 3, pp. 46-51.

Taborda, R., Freire, F., Silva, A., Andrade, C. and Freitas, M.C. (2009). Origin and Evolution of Tagus Estuarine Beaches. *Journal of Coastal Research*, SI56, 213-217.

Wentworth, C. K. (1922). A Scale of Grade and Class Terms for Clastic Sediments. *The Journal of Geology*, 30, 377-392.

Did aeolian sand invasion impact human settlement patterns during the Mesolithic of SW Iberia?

S. Costas (1), A. Costa (2), A. L. Rodrigues (3), R. Marques (3), D. Russo (3) and A. C. Araujo (4)

(1) CIMA / ARNET, Universidade do Algarve, Campus de Gambelas, 8005-139 Faro, Portugal. scotero@ualg.pt
(2) Laboratório de Arqueociências (LARC) – Património Cultural, IP | Associação BIOPOLIS – CIBIO | IDL – Instituto Dom Luiz | UNIARQ – Centro de Arqueologia da Universidade de Lisboa, Calçada do Mirante à Ajuda, nº 10A, 1300-418 Lisboa, Portugal
(3) C^2TN/DECN, Instituto Superior Técnico, Universidade de Lisboa, Campus Tecnológico e Nuclear, Estrada Nacional 10, 2695-066 Bobadela, Portugal
(4) Laboratório de Arqueociências (LARC) – Património Cultural, IP | Associação BIOPOLIS – CIBIO | UNIARQ – Centro de Arqueologia da Universidade de Lisboa, Calçada do Mirante à Ajuda, nº 10A, 1300-418 Lisboa, Portugal

Abstract: Episodes of aeolian activity, implying the formation of transgressive dunes, have proven to be highly valuable pieces of information for reconstructing the evolutionary trajectories of coastal segments and regional climate variability. Transgressive dune formation at the Portuguese coast has been linked to climate events of regional scale (North Atlantic Basin) during the late Pleistocene and Holocene, namely, to the enhancement of westerly winds related to the onset of cold climate events. However, the reduced number of dated deposits questions the temporal distribution of major episodes of aeolian activity across the Portuguese coast. Many of these landforms cover well-known Palaeolithic and Mesolithic coastal settlements. However, uncertainties regarding the age of the dunes preclude their use as an additional source of information for reconstructing the environmental conditions experienced by hunter-gatherer societies during the Pleistocene-Holocene transition. This work builds on research reconstructing the formation of transgressive dunes along the Portuguese coast to improve our understanding of their temporal occurrence, the mechanisms involved in their episodic formation and the possible cause-and-effect relationships between episodes of aeolian activity and human occupation. To this purpose, we analysed the spatial distribution, configuration and chronology of transgressive dunefields located in the Portuguese Estremadura (Magoito beach) and in SW Alentejo, in the vicinities of the Sardão Cape (Palheirões do Alegra and Medo Tojeiro), locations where archaeological sites dating to the Mesolithic are known. Results extend the temporal record of aeolian activity, documenting episodes during the Last Glacial Maximum, at the onset of the Northern Hemisphere deglaciation and Holocene, and during the Holocene, coinciding with well-documented cold climatic events. The results suggest that estudied Early Mesolithic occupations could have been rapidly buried by aeolian sands, immediately after, or in close succession to the human presence. This suggests the possible direct impact of environmental changes to human settlement strategies, encouraging the last hunter-gatherer communities to temporally abandon open coastal settings.

Keywords: *top-cliff dunes, transgressive dunes, OSL dating, human settlements*

1. INTRODUCTION

The Portuguese coast extends for more than 900 km, of which 60% are beaches and 36% exposes cliffs without beaches (Andrade *et al.*, 2002). Currently, 45% of the coast experiences severe problems of erosion. Despite the starved character of the present Portuguese littoral, large stabilized or fossil transgressive dunefields dominate the coast. These deposits document periods of significant sediment availability, contributing to the formation of the Portuguese littoral belt (Pereira and Angelucci, 2004). The Portuguese littoral belt is formed by consolidated and non-consolidated dunes. The consolidated dunes have been described and tentatively interpreted and dated (Pereira and Angelucci, 2004). References to the non-consolidated transgressive dunes are disperse, despite their larger spatial distribution. The oldest non-consolidated dunes of the Portuguese coast are located at São Pedro de Maceda beach (Ovar) and date back to 30 - 16 ka, combining radiocarbon and optically stimulated luminescence (OSL) dating (Granja et al., 2008). OSL dating of additional deposits along the coastal segment between Ovar and Nazaré documents successive episodes at 9.7, 8.2, 2.2, and 1.5 ka (Clarke and Rendell, 2006). The most recent episode of coastal dune building in Portugal was related to increased storminess during the Little Ice Age (LIA) and was coincident with a broader episode of dune

construction in western European coasts (Clarke and Rendell, 2009).

An exhaustive analysis of the record of aeolian activity from the central coast of Portugal, south of Lisbon, combining subsurface stratigraphy and OSL dating, traced favourable conditions for dune building episodes over the last 20.5 ka, with the main events centered at 17.5, 5.60, 1.10, and 0.35 ka (Costas *et al*., 2012, 2016). The identified episodes suggest the southward deflection of the North Atlantic storm track and the strengthening of the westerlies over southern Europe during well-known climatic extremes such as the Heinrich event 1 (HE1), the 5.6 ka event, the end of the Middle Ages, and the LIA.

Many of the transgressive dunes that invaded the Portuguese coast cover well-documented Palaeolithic and Mesolithic coastal settlements (e.g., Soares, 2003; Carvalho and Valente, 2005). However, the lack of documentation about the formation and age of these landforms, and the evidence of multiple episodes of aeolian activity along the coast, prevents our understanding of any possible link between the formation of transgressive dunes, human occupation, and the evolution of the surrounding landscape.

This work aims to reconstruct the formation of transgressive dunes adjacent to or covering archaeological sites dating to the Mesolithic period from the central and southern coast of Portugal. The selected sites are located in the Magoito beach (Estremadura, Central Portugal) and in the vicinities of Palheirões do Alegra and Medo Tojeiro sites, near Cabo Sardão (SW Alentejo) (Figure 1). Eleven sediment samples collected for OSL dating, combined with geomorphological analysis, were essential to reconstruct the formation and evolution of the dunes at the selected sites. OSL dating was carried out by the authors at Laboratório de Datação por Luminescência do Instituto Superior Técnico, Universidade de Lisboa.

2. STUDIED SITES

2.1. Magoito

This shell midden is covered by a consolidated sand dune at the top of the cliff backing Magoito beach (Figure 1), where a small stream flows to the Atlantic Ocean. The available information is scarce, but points to the presence of shell layers, organized combustion areas and occasional lithic artefacts (Daveau *et al*., 1982; Arnaud, 1994; Soares, 2003). The site is the result of successive short-term occupations over approximately 1000 years, between 11.2 and 10.2 ka cal BP (Sousa and Soares, 2016), i.e., during the Early Mesolithic.

The Magoito dune partially mantles the rocky promontory that defines the northern limit of the beach. It extends southward, covering the southern flank of the promontory. The internal structure of the consolidated dune is characterized by cross-stratification, with at least three vertically stacked

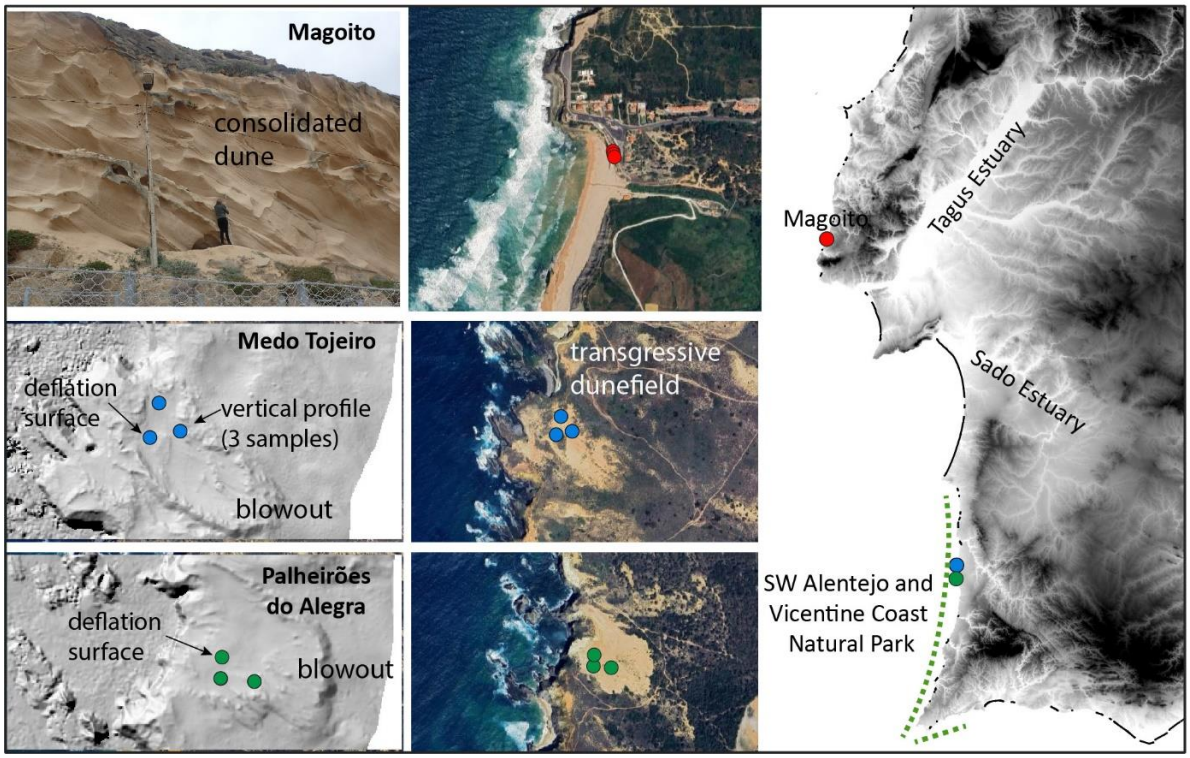

Figure 1. Location of the sediment samples collected within the transgressive dunes associated with archaeological sites.

sedimentary packages. These packages display south-dipping, truncated beds, thickening toward the south, which reflects the greater accommodation space created by the southward slope of the promontory. Samples for OSL dating were collected across the north to south gradient.

2.2. Palheirões do Alegra

Palheirões do Alegra is an open-air site located on the top of a rocky cliff. The site was most likely occupied during various Early Mesolithic stays around 10.0 - 9.5 ka cal BP. Apart from the thousands of lithic artefacts recovered mostly from the surface, 18 combustion structures have also been identified (Raposo, 1994).

The archaeological sites appear embedded or at the base of the transgressive dunes that extend inland from the edge of the cliff. Most of these transgressive dunes are easy to recognise in the available digital terrain models, especially in the LiDAR-derived one (Figure 1), mostly corresponding to fixed parabolic dunes and active ones related to local erosion and smaller scale re-activation. Samples were collected within an active aeolian blowout, including a sample from the aeolian unit below the deflation surface and two samples from the former dunes that are currently eroding through the migration of the blowout.

2.3. Medo Tojeiro

Medo Tojeiro is also located next to the cliff edge. This shell midden results from successive short-term seasonal occupations, mainly focused on the exploitation of marine molluscs. Dates from this site (Tavares da Silva *et al*., 1985), point to a more recent occupation, corresponding to the late Mesolithic. The archaeological site is buried by transgressive dunes. The dunes seem the lateral continuation of the transgressive system observed at Palheirões do Alegra. In Medo Tojeiro five samples were collected within a partially fixed blowout. This blowout is less open, allowing the partial preservation of the aeolian units. Samples were collected from the subsurface at the centre of the deflation surface and from the erosional walls, from which samples were collected from a vertical profile.

3. RESULTS AND DISCUSSION

The results document several episodes of transgressive dune formation in the studied sites (**Erro! A origem da referência não foi encontrada.**). The different packages visible in the dune of Magoito seem to have migrated and accumulated within a relatively short period of time, during the early Holocene (Figure 2). The dune appears to have migrated from the north, resembling the formation of a headland bypass dune associated with an episodic supply of sediment.

The formation of the transgressive dunes at the two sites in the SW Alentejo coast shows greater complexity with at least four episodes of major aeolian activity and dune inland migration, i.e., from the west to the east. The oldest age suggests that dunes were actively migrating inland during the Last Glacial Maximum (LGM). A subsequent phase of activity may have taken place around the onset of Northern Hemisphere deglaciation (c. 20 ka). However, the absence of additional samples from this time interval limits our ability to determine whether these dates represent a single continuous event or multiple distinct episodes. Previous works along the centre coast of Portugal document the occurrence of prolonged episodes of aeolian activity during the late Pleistocene, namely from 20 to 11.6 ka (Costas *et al*., 2016) and during the LGM (Granja *et al*., 2008), supporting the hypothesis of a single episode extending from the LGM.

After the deglaciation, evidence indicates a renewed episode of aeolian activity occurring shortly after the onset of the Holocene, roughly between 10 – 8.2 ka (Figure 2). This episode was recorded across the three examined sites. Our results also suggest a phase of dune stabilization during the Mid-Holocene, which was subsequently followed by a new episode of sand encroachment around 3.7 ka, and the reactivation of previously stabilised top-cliff transgressive dunes between 0.9 and 0.6 ka. These new episodes were only identified in Medo Tojeiro, where more samples were collected (Figure 2).

The occurrence of these large-scale events of aeolian activity has been linked to changes in the intensity of storms, coastal erosion and the strengthening of onshore winds driven by changes in atmospheric circulation patterns at regional scale (Costas *et al*., 2016; Jackson *et al*., 2019). In addition, the formation of identified transgressive dunes may have also been promoted by rapid sea-level rise and associated marine transgression along the coast.

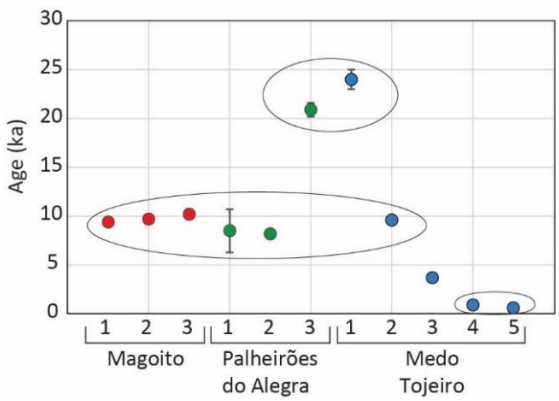

Figure 2. Age distribution of the dated transgressive dunes at the three selected sites. The circles highlight possible periods of intensified aeolian activity.

Combining these results with the available information about the distribution and age of Mesolithic settlements in the studied sites, we can tentatively infer that the large-scale event of aeolian activity, occurring during the early Holocene, may have significantly affected these Mesolithic coastal communities. The rapid landscape changes associated with the advance of transgressive dunes likely contributed to the abandonment of these sites, in particular along the coast of the Portuguese Estremadura. Conversely, the SW coast of Alentejo does not show such a decline in human settlements, with occupations from the Late Mesolithic (e.g., Medo Tojeiro), coinciding with the fixation of the dunes. The differences between the two coasts are not easily explained, but the evolution of the coastal landscape as a consequence of marine transgression could play a key role, maintaining or inhibiting favourable conditions for hunter-gatherer societies along the coast.

Encroachment of coastal communities by the advance of transgressive dunes has been repeatedly reported in the literature with examples from the Portuguese coast associated with Roman settlements (Costas *et al*., 2015) or from European coasts during the LIA (Jackson *et al*., 2019). The latter period extended for several centuries and coincided with a paradigm shift in the human-dune relationship, transitioning from a passive response, which implied the abandonment of the coast, to a more active approach based on the belief that humans can and should control nature.

Acknowledgments

This work is a contribution to CREST project (doi:10.54499/2022.05392.PTDC). S. Costas is supported by CEECINSTLA/00018/2022, A.L. Rodrigues by CEECINST/00043/2021/CP2797/CT0011 and R. Marques by CEECINST/00043/2021/CP2797/CT0010. Authors recognize the support of national funds LA/P/0069/2020 and UID/00350/2020 and UID/Multi/04349/2020.

REFERENCES

Andrade, C., Freitas, M.C., Cachado, C., Cardoso, A.C., Monteiro, J.H., Brito, P., Rebelo, L., Freitas, C., Cachado, C., Cardoso, A.C., Monteiro, J.H., Brito, P. and Rebelo, L. (2002). Coastal Zones, in: Santos, F.D., Forbes, K., Moita, R. (Eds.). Gradiva, pp. 173–219.

Arnaud, J.M. (1994). Mesolítico e Neolítico, in: Atlas de Arqueologia. Edições Zairol, Lisboa, pp. 292–309.

Carvalho, A.F. and Valente, M.J. (2005). Novos contextos conquíferos pré-históricos na Costa Vicentina, in: 2.° Encontro de Arqueologia Do Algarve (Xelb, Nº5). Câmara Municipal de Silves, Silves, pp. 9–26.

Clarke, M.L. and Rendell, H.M. (2009). The impact of North Atlantic storminess on western European coasts: A review. *Quaternary International*, 195, 31–41.

Clarke, M.L. and Rendell, H.M. (2006). Effects of storminess, sand supply and the North Atlantic Oscillation on sand invasion and coastal dune accretion in western Portugal. *The Holocene*, 16, 341–355.

Costas, S., Jerez, S., Trigo, R., Goble, R. and Rebêlo, L. (2012). Sand invasion along the Portuguese coast forced by westerly shifts during cold climate events. *Quaternary Science Reviews*, 42, 15–28.

Costas, S., Naughton, F., Goble, R. and Renssen, H. (2016). Windiness spells in SW Europe since the last glacial maximum. *Earth and Planetary Science Letters*, 436, 82–92.

Costas, S., Rebêlo, L., Brito, P., Burbidge, C., Prudêncio, M. and FitzGerald, D. (2015). The Joint History of Tróia Peninsula and Sado Ebb-Delta, in: Randazzo, G., Jackson, D.W.T., Cooper, J.A.G. (Eds.), Sand and Gravel Spits. Springer International Publishing, pp. 79–102.

Daveau, S., Pereira, A.R. and Zbyszewski, G. (1982). Datation au C14 du site archéologique de la plage de Magoito (Portugal), scellè par une dune consolidée. Clio 4, 133–135.

Granja, H.M., Groot, T.A.M.D. and Costa, A.L. (2008). Evidence for Pleistocene wet aeolian dune and interdune accumulation, S. Pedro da Maceda, north-west Portugal. *Sedimentology*, 55, 1203–1226.

Jackson, D.W.T., Costas, S. and Guisado-Pintado, E. (2019). Large-scale transgressive coastal dune behaviour in Europe during the Little Ice Age. *Global and Planetary Change*, 175, 82–91.

Pereira, A.R. and Angelucci, D.E. (2004). Formações dunares no litoral português, do final do Plistocénico e inícios do Holocénico, como indicadores paleoclimáticos e paleogeográficos. Evolução geohistórica do litoral português e fenómenos correlativos. Geologia, História, Arqueologia e Climatologia 221–256.

Raposo, L. (1994). O sítio de Palheirões do Alegra e a "questão do Mirense," in: Arqueología En El Entorno Del Bajo Guadiana: Actas Del Encuentro Internacional de Arqueología Del Suroeste. Huelva, pp. 55–69.

Soares, A.M.M. (2003). A duna de Magoito revisitada. Revista Portuguesa de Arqueologia 6, 83–100.

Sousa, A.C. and Soares, A.M. (2016). Continuity or discontinuity? Aquatic exploitation in the portuguese Estremadura during the Atlantic period: São Julião and Magoito shell middens as case studies. Archéologie des Chasseurs-Cueilleurs Maritimes. De la fonction des habitats à l'organisation de l'espace littoral. Actes de la Séance de la Societé Préhistorique Française. Rennes 10-11 Avril 2014 191–212.

Tavares da Silva, C., Soares, J. and Penalva, C. (1985). Para o estudo das comunidades neolíticas do Alentejo Litoral: o concheiro de Medo Tojeiro. *Arqueologia*, 11, 5–15.

Registo geológico de eventos marinhos extremos

Registro geológico de eventos marinos extremos

Geological record of extreme marine events

Submarine landslide on the shelf of Corvo Island triggered during the winter of 2018

R. Quartau (1,2), S. Innocentini (1,2), Z. Zhao (3) and A. Rodrigues (1,2)

(1) Divisão de Geologia Marinha, Instituto Hidrográfico, Portugal. rui.quartau@hidrografico.pt
(2) Instituto Dom Luiz, Faculdade de Ciências, Universidade de Lisboa, Portugal
(3) South China Sea Institute of Oceanology, Chinese Academy of Sciences, Guangzhou, China

Abstract: The southern shelf of Corvo Island, part of the Azores archipelago, shows compelling evidence of a recent mass-wasting event. This study identifies and characterizes a probable mass movement that occurred between two hydrographic surveys conducted in 2018 and 2019. The detected scar and measured landslide volume suggest a significant failure on a clinoform structure composed of unconsolidated medium sand. Analysis of historical wave climate data and seismic records indicates that intense wave loading, particularly from large southwest-directed storms, was the most probable trigger. These findings emphasize the need for further geological and geotechnical studies to assess the hazard potential near critical infrastructure, such as Corvo's harbour.

Keywords: *landslide, shelf, storm waves, Corvo Island, Azores*

1. INTRODUCTION

Corvo Island, part of the western group of the Azores archipelago, has a shelf frequently impacted by intense storms. Wave energy predominantly arrives from the northwest and west, although notable storm events from the north and southwest also occur. Despite their relative low frequency (approximately 8% of the time), southwest waves can reach substantial heights and rank among the most energetic after those from the northwest and west (Figure 1). Submarine landslides on island shelves pose significant geological hazards, with the potential to impact coastal infrastructure and nearby communities (Kelfoun *et al*., 2010).

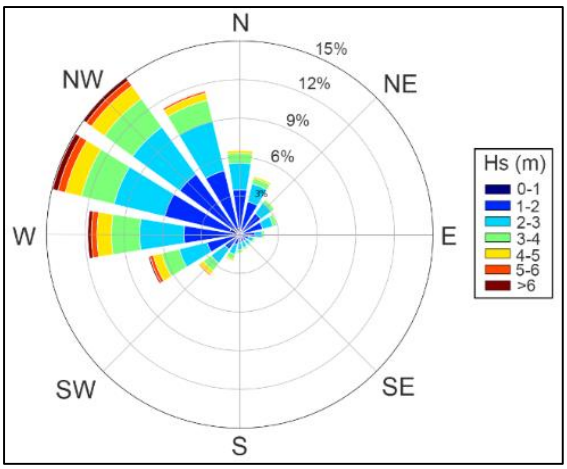

Figure 1. Wave rose generated from ERA5 reanalysis data (1940-2024) at coordinates 39.66°N, 31.11°W.

This study investigates a recently identified landslide scar on the southern shelf of Corvo Island, which affected part of the topset and the entirety of the foreset and bottomset of a clinoform body. Owing to its well-constrained timing, the event offers a unique opportunity to examine potential triggering mechanisms and assess broader implications for slope stability and coastal hazard management.

2. DATA AND METHODS

High-resolution bathymetric data were acquired during two hydrographic surveys (Figures 2A and 2B). The first survey, conducted aboard the NRP Almirante Gago Coutinho between May 17 and 23, 2018, used KONGSBERG EM120 and EM710 multibeam echosounders (MBES), operating at frequencies of 12 kHz and 70–100 kHz with an angular coverage of 120° (NRP Almirante Gago Coutinho, 2018). This survey collected data from depths of 2400 m up to 36 m. Positioning was provided by a FUGRO MARINESTAR Differential GNSS in OMNISTAR HP1 mode, ensuring high accuracy, while tidal corrections were applied using observations from a Thales tide gauge at Lajes das Flores harbour. The second survey was carried out between July 30 and August 13, 2019, by the Hydrographic Brigade of Instituto Hidrográfico aboard the platform Mergulhão (Brigada Hidrográfica, 2019). This survey utilized a KONGSBERG 2040C MBES operating at 300 kHz with an angular coverage of 100°, collecting bathymetric data from 110 m to 1 m depths. Near-harbour special-order surveys were conducted using RTK DGNSS positioning, while the surrounding 1a-order surveys relied on DGNSS combined with tidal observations. Both data surveys were processed using CARIS-HIPS software, producing high-resolution surfaces (2 m) using the CUBE algorithm.

The partial overlap between the two surveys allowed the detection of a prominent landslide scar (Figure 2B),

located approximately 400 meters south of Corvo's harbour. As this overlap did not fully cover the landslide area, earlier single-beam bathymetry data from 2000 (Figure 2A) were used to help reconstruct pre-event bathymetry in ArcGIS software. The 2000 survey was conducted by the Hydrographic Brigade of Instituto Hidrográfico between June 26 and 28 and utilized an ATLAS DESO 22 single-beam echosounder, with positioning provided by a TRIMBLE 4000DS operating in DGPS UHF mode (Brigada Hidrográfica, 2000). Landslide volume estimation was achieved by generating bathymetric grids for the pre- and post-event conditions and calculating the difference between them.

Two additional marine surveys were conducted in August/September 2022 and June 2023 around the Corvo Island shelf as part of the HAZARDOUS project. These surveys included the acquisition of Boomer seismic profiles and sediment sampling using a Smith MacIntyre grab. Two sediment samples collected approximately 600 meters northeast of the scar confirmed the presence of medium sand in the same clinoform structure where the landslide occurred. Hourly wave data (1940-2024) from the ERA5 reanalysis model at the 39.66N, 31.11W location (Hersbach *et al.*, 2019) and seismic event data (M > 4) from the USGS Earthquake Catalog (https://earthquake.usgs.gov/earthquakes/search/) were analysed to identify potential triggering mechanisms.

Wave orbital velocity near the seabed (U_m) at the clinoform rollover depth (~45 m) was calculated using the method of Soulsby (1997), based on the significant wave height (H_s) and period (T) of the most powerful storm identified between 2018 and 2019. This depth was selected because it marks the onset of the foreset, the portion of the clinoform most susceptible to failure due to its high gradient.

$$U_m = \frac{\pi H_s}{T sinh(kz)}$$

Where wave number k equals $2\pi/L$, z is the depth and L is the wavelength:

$$L = \frac{gT^2}{2\pi} \tanh\left(\frac{2\pi z}{L_0}\right)$$

where L_0 is deep water wavelength equal to $gT^2/2\pi$ and g is the gravitational acceleration (9.8 m s^{-2}).

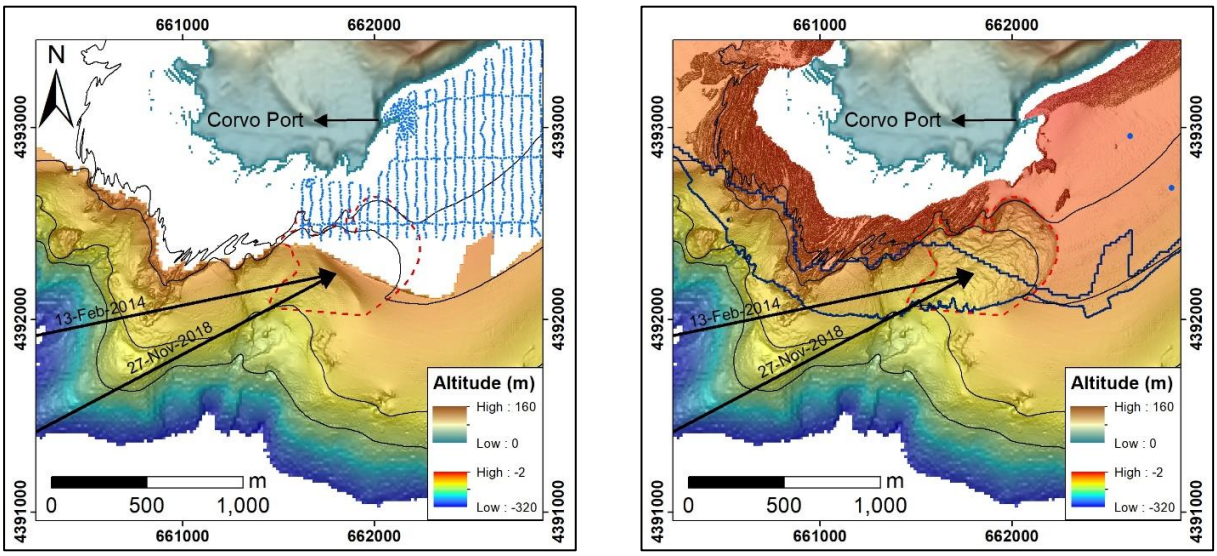

Figure 2. (A) Bathymetric data from 2000 (light-blue dots) and 2018 (colour ramp from blue to red), showing the landslide scar (dashed red line) and the approach directions of two storm waves (solid black arrows). Black contour lines indicate depths of 25, 50, 100, and 150 meters. (B) Merged bathymetric data from 2018 and 2019 (colour ramp from blue to red), with the overlapping survey area outlined in dark blue. Light blue dots represent the Smith MacIntyre grab samples.

3. RESULTS AND DISCUSSION

The submarine landslide scar mapped on the southern shelf of Corvo covers an area of approximately 0.291 km² and is associated with a displaced sediment volume of around 0.00463 km³ (Figure 3). The event occurred through a rotational mechanism, with the displaced volume directed toward the SSW. Analysis of the 2018 bathymetry revealed a clinoform body with a rollover depth between 42 and 45 meters and foreset slopes of 23–25° before the event. The steep slope and unconsolidated medium sand composition of the clinoform likely contributed to its susceptibility to failure. Additionally, a NW–SE-oriented seismic profile (Figure 4) crossing the landslide scar reveals a pre-existing depression in the basement, partially infilled with sediments. This feature suggests that a previous mass-wasting event likely occurred at this location (Innocentini, 2025). This structure, inclined toward the

SW, may have acted as a décollement surface, facilitating the recent landslide. Wave data analysis over the 2018-2019 period highlighted three storm events between the two surveys with waves higher than 6 meters (Table 1). The most intense occurred on 27-Nov-2018, at 12:00 UTC, with wave heights reaching 10.57 meters, a mean period of 12.49 seconds, and a wave direction of 242.24° - nearly perpendicular to the orientation of the clinoform rollover and headscar (Figure 2). The analysis of the broader period (1940-2024) confirmed this event as the sixteenth-largest storm impacting Corvo in the past 70 years, with only two events (13-Feb-2014 and 27-Nov-2018) showing wave directions arriving from the southwest (Table 3). Wave orbital velocity calculated at the rollover depth of 45 meters during the 27 November 2018 storm reached 1.42 m/s—an exceptionally high value. Such velocity is not only sufficient to mobilize medium sands but also to induce significant cyclic wave loading. This repeated loading can elevate pore water pressure within saturated, low-permeability sediments, thereby reducing effective stress and weakening shear strength. These conditions critically undermine slope stability, especially on such a steep gradient (23–25°) and may ultimately triggered failure. Regarding seismicity, no earthquakes with magnitudes >4 were recorded in the area during the study period, fact that excludes seismic activity as a trigger. While wave impact appears to be the most plausible trigger, offshore groundwater discharge is also known to increase pore pressure and capable of trigger slope failures (Micallef *et al.*, 2023). Such discharges have been reported on other islands in the Azores, including Terceira, where they are estimated to account for approximately 33% of total onshore precipitation (Rodrigues, 2002).

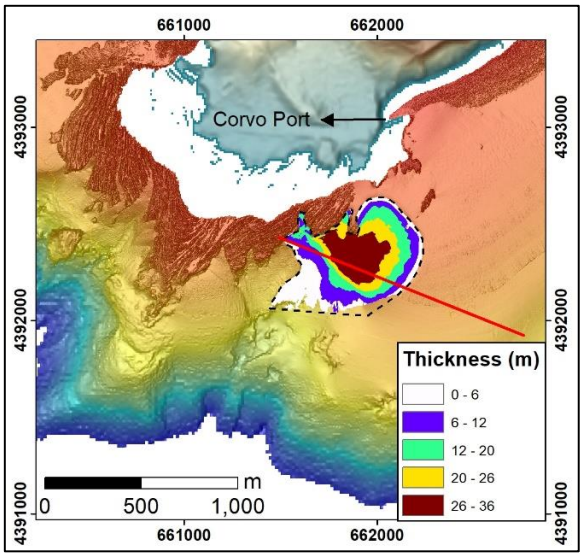

Figure 3. Thickness of displaced material from analysis of pre- and post-landslide bathymetry. Red line indicates the seismic profile location in Figure 4.

Table 1. Three highest wave events recorded between 23-May-2018 and 13-August-2019. The wave event most likely associated with the landslide trigger is highlighted in bold.

Date/time	Wave Height (m)	Wave Period (s)	Wave Direction (º)
15-Sep-2018 22:00	7.25	10.09	200 / SSW
27-Nov-2018 12:00	**10.57**	**12.49**	**242 / WSW**
23-Feb-2019 13:00	9.64	12.80	246 / WSW

Table 2. Fifteen highest wave events recorded between 1940 and 2024. The wave event most likely associated with the landslide trigger is highlighted in bold.

Date/time	Wave Height (m)	Wave Period (s)	Wave Direction (º)
16-Dec-1942 04:00	11.4	13.83	276 / WNW
28-Feb-1952 13:00	10.83	11.95	324 / NNW
11-Feb-1955 23:00	10.91	13.31	287 / WNW
14-Jan-1964 18:00	11.07	13.52	297 / WNW
17-Feb-1964 17:00	10.57	14.07	287 / WNW
19-Feb-1966 19:00	12.11	14.36	293 / WNW
08-Jan-1970 16:00	10.65	13.66	295 / WNW
15-Jan-1973 20:00	10.79	12.13	274 / WNW
22-Feb-1978 02:00	10.77	13.62	275 / WNW
06-Jan-1996 01:00	11.02	14.25	283 / WNW
17-Dec-1997 23:00	10.75	14.41	305 / WNW
28-Dec-1998 21:00	11.03	14.25	312 / WNW
12-Apr-2003 07:00	11.02	11.88	321 / NNW
13-Feb-2014 16:00	10.79	11.33	258 / WSW
27-Nov-2018 12:00	**10.57**	**12.49**	**242 / WSW**
02-Oct-2019 06:00	10.68	12.19	196 / SSW

However, observations of multiple older landslide scars on the eastern shelf of Corvo, located at depths between 40 and 55 meters, suggest a history of recurrent slope instability in the outer shelf region. This pattern may be more consistent with a wave-triggering mechanism, as groundwater seepage is typically limited to the inner shelf. The original rollovers of these failed clinoforms may have been situated as deep as 70 meters (Innocentini, 2025), indicating a progressive landward retreat of the failure structures over time.

The combination of steep foreset slopes, relatively shallow rollover depths, and loose sediment made the clinoform particularly vulnerable to wave loading induced by storm waves. Although this slope failure did not evolve into a retrogressive landslide that would

endanger the harbour, its proximity to key infrastructure highlights the associated potential risks. It is unlikely that such a small landslide volume could generate a significant tsunami, especially considering that numerical modelling of landslide-induced tsunamis in similar settings—with volumes approximately 20 times larger (~0.1 km³)—produced waves of only 2 meters upon reaching the nearby coast of La Réunion Island (Kelfoun *et al.*, 2010). Nevertheless, had this event involved a larger volume or extended back toward the harbour, it could have caused damage. This highlights the need for future geotechnical surveys to better understand the slope stability of shelf clinoforms and to assess the potential for future mass-wasting events capable of generating small tsunami waves such as those from La Réunion Island. Such waves could reach the coast within seconds to a few minutes, posing a serious threat to infrastructure and human life.

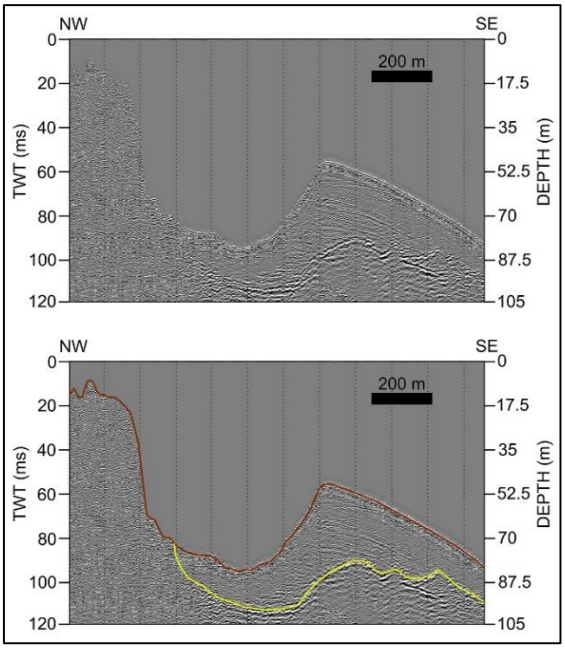

Figure 4. NW–SE-oriented Boomer seismic profile crossing the landslide scar. (A) Uninterpreted profile. (B) Interpreted profile, with the brown line indicating the seafloor and the yellow line outlining the basement.

These findings demonstrate the importance of understanding the stability of clinoform bodies on the marine environment, particularly near critical infrastructure such as Corvo's harbour. The presence of multiple scars at greater depths on the eastern shelf suggests recurring instability. In the absence of detailed geotechnical data, predicting future failures remains challenging; therefore, ongoing monitoring, hazard assessment, and targeted investigations are essential for ensuring coastal safety and effective planning.

4. CONCLUSIONS

A recent submarine landslide was identified on the southern shelf of Corvo Island, likely triggered by storm wave loading between May 2018 and August 2019. Steep foreset slopes, shallow rollover depths, a previous décollement surface and unconsolidated medium sand sediments contributed to the slope's instability. The most intense storm event during the study period — and one of the sixteen most powerful since 1940 — featured wave heights exceeding 12 meters and approached nearly perpendicular to the clinoform orientation, likely creating stress conditions conducive to failure.

Acknowledgements

This work was supported by the project HAZARDOUS (https://doi.org/10.54499/PTDC/CTA-GEO/0798/2020) funded by the Portuguese Fundação para a Ciência e a Tecnologia (FCT) I.P./MCTES.

REFERENCES

Brigada Hidrográfica (2000). Projecto HI 2103/00. Relatório final de trabalho (REL FT HI 15C/00). Levantamento hidrográfico no Porto da Casa na Vila Nova do Corvo. Ilha do Corvo-Açores.

Brigada Hidrográfica (2019). Elemento DT21MP01. Relatório técnico final (REL TF HI 13A/19 VOL.I). Levantamento topo-hidrográfico no Arquipélago dos Açores 18-07-2019 a 21-08-2019.

Hersbach, H., Bell, B., Berrisford, P., Biavati, G., Horányi, A., Muñoz Sabater, J., Nicolas, J., Peubey, C., Radu, R., Rozum, I., Schepers, D., Simmons, A., Soci, C., Dee, D., and Thépaut, J-N. (2019). ERA5 monthly averaged data on single levels from 1979 to present. *Copernicus Climate Change Service (C3S) Climate Data Store (CDS)*. Doi:10.24381/cds.f17050d7

Innocentini, S. (2025). *Gravitational, erosional, sedimentary and volcanic processes on the submarine environment of ocean volcanic islands: the case studies of Porto Santo Island (Madeira Archipelago) and Corvo Island (Azores Archipelago)*. PhD thesis. Faculdade de Ciências, Universidade de Lisboa. 158 p.

Micallef, A., Person, M., Gupta, S., Saadatkhah, N., Camille, A., and Gratacós, Ò. (2023). Can Offshore Meteoric Groundwater Generate Mechanical Instabilities in Passive Continental Margins? *Journal of Geophysical Research: Earth Surface*, 128, e2022JF006954.

NRP Almirante Gago Coutinho (2018). Elemento DT21MP01. Relatório técnico final (REL TF HI 10/18). Levantamento hidrográfico oceânico no Arquipélago dos Açores (04-05--2018 a 08-02-2018).

Rodrigues, F.C. (2002). Hidrogeologia da ilha Terceira (Açores – Portugal). Tese de doutoramento – Departamento de Ciências Agrárias. Faculdade de Ciências e Tecnologia. Universidade dos Açores.

Soulsby, R. (1997). *Dynamics of Marine Sands: A Manual for Practical Applications*. Thomas Telford, London.

Modelação Numérica de um Tsunami em Verde Lago, Algarve

R. Henriques (1), P. J. M. Costa (1,2), I. Bosnic (3) e F. Dourado (4)

(1) Departamento de Ciências da Terra, Faculdade de Ciências e Tecnologia, Universidade de Coimbra, Rua Sílvio Lima, Univ. Coimbra – Pólo II, 3030-790 Coimbra, Portugal. ricardofilipesimoes16@gmail.com
(2) Instituto Dom Luiz, Faculdade de Ciências, Universidade de Lisboa, Edifício C6, Campo Grande 1749-016, Lisboa, Portugal
(3) HAEDES Portugal, Rua Campos Júnior nº11, 1ª Lisboa, Portugal
(4) UERJ – Universidade do Estado do Rio de Janeiro, Avenida Marechal Rondon, 381, São Francisco Xavier, Rio de Janeiro – RJ – CEP: 20950-000

Abstract: This study uses numerical modelling to understand tsunami dynamics along Portugal's southern coast. Four tsunami-earthquake sources were simulated: the Gorringe Bank, Horseshoe Fault, Marquês de Pombal Fault, and a combined Gorringe and Horseshoe Fault scenario. To validate the tsunami inundation models, land lithostratigraphic surveys were conducted. Field data, including sediment samples from eight trenches and three cores, underwent textural analysis and radiocarbon age- estimation. A tsunami-related depositional unit was identified, this unit, dated to approximately 4000 BP, tentatively aligned with a 3600 cal yrs BP tsunami event previously found on the Algarve shelf. Results indicate the Horseshoe Fault seismic source as the best match between the observed deposits and predicted inundation patterns near Verde Lago. This research highlights the need for continued efforts in tsunami geosciences, both in recognizing past events through filed work and in using numerical models to define tsunami and seismic hazard.

Keywords: *extreme events, sediment transport, Delft3D*

1. INTRODUÇÃO

A modelação hidrodinâmica e morfodinâmica de paleotsunamis é crucial para uma melhor definição de risco costeiro. Este trabalho utiliza o modelo numérico Delft3D para simular a propagação e inundação de tsunamis, investigando as possíveis fontes sísmicas que afetam a costa sul portuguesa. A validação do modelo é feita através da caracterização (textural e composicional) de depósitos de tsunami em Verde Lago (Castro Marim). A combinação destas abordagens permite testar possíveis fontes sísmicas e quantificar o provável galgamento.

2. ÁREA DE ESTUDO

Verde Lago (concelho de Castro Marim) é uma depressão a leste de Altura, onde afloram sedimentos Plio-Pleistocénicos, pontuando uma planície aluvial e separada do mar por um sistema de praia-duna (Figura 1). Trata-se de uma zona costeira balnear, caracterizada por uma frente de praia de cerca de 550 metros e uma vasta extensão de dunas bem preservadas, onde a vegetação típica e espécies nativas/emblemáticas são abundantes.

Figura 1. Contexto geográfico da área de estudo. A – Localização em Portugal Continental; B – Concelho de Castro Marim.

3. METODOLOGIAS

3.1. Campanha de campo

O trabalho de campo decorreu com o objetivo de analisar a sequência estratigráfica e recolher amostras de potenciais depósitos de tsunami e sedimentos de duna e praia (Figura 2).

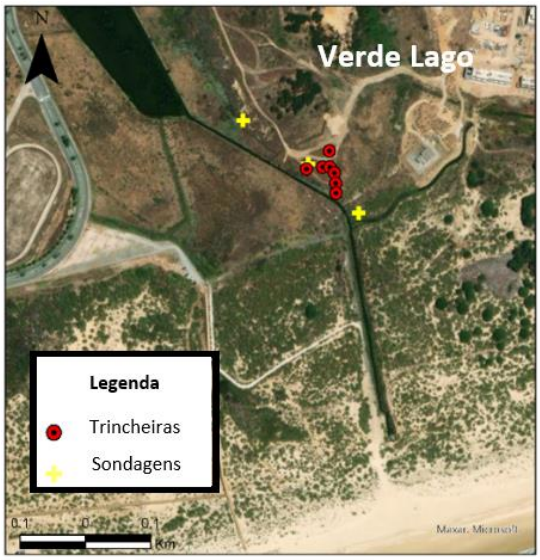

Figura 2. Localização das sondagens e trincheiras realizadas durante a campanha de campo em Verde Lago, Algarve.

Foram abertas oito trincheiras com recurso a uma retroescavadora. As restantes sondagens foram obtidas através de uma sonda manual Edelman, com uma profundidade máxima de 4,7 m para as sondagens e de 2 m para as trincheiras.

3.2. Modelação numérica

A modelação da geração e propagação de tsunamis, bem como do transporte de sedimentos, foi realizada utilizando o software Delft3D (Deltares, 2020). Este é um modelo numérico amplamente usado para simular tsunamis e eventos de tempestade, com validação extensiva através de experiências laboratoriais (e.g. Apotsos *et al.*, 2011). Especificamente, a propagação do tsunami foi calculada usando o módulo Delft3D *Flow*, que resolve as equações não lineares para águas rasas utilizando um esquema de diferenças finitas. Para cada caso de estudo, foram construídas 3 grelhas aninhadas (Figura 3) com resoluções espaciais de 232 m (Nível 0), 100 m (Nível 1), e 50, 25 e 5 m (Nível 2). Esta abordagem é semelhante à aplicada por Dourado *et al.* (2021).

Os dados topobatimétricos foram obtidos a partir do levantamento DGT 2008 (Digital Ground and Terrain), com 2 m de resolução, do Lidar DGT de 2 m de 2011 e de batimetria EMODNET com 115 m de resolução.

Consideraram-se 3 fontes como mecanismo gerador para este estudo: Falha da Ferradura (HSF), Banco de Gorringe (GB) e Falha do Marquês de Pombal (MPF). Adicionalmente, foi considerado um cenário hipotético, cenário SCN1, que consiste num rearranjo da fonte do sismo de 1969, combinando as fontes de GB e HSF. Estas fontes foram selecionadas com base em resultados recentes (Dourado, 2021) que indicam uma boa correlação entre os resultados da modelação numérica e os dados recolhidos no campo.

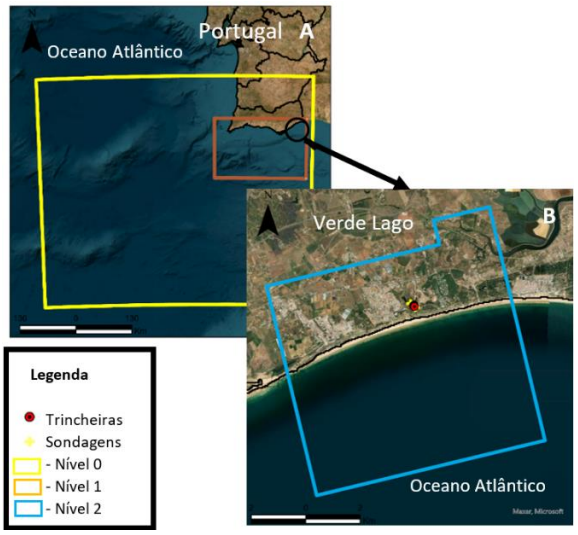

Figura 3. Contexto geográfico da área de estudo. A – Localização em Portugal Continental; B – Localização de Verde Lago; Grelha amarela – Nível 0 com resolução espacial de 232 m; Grelha laranja – Nível 1 com resolução espacial de 100 m; Grelha azul – Nível 2 com resolução espacial de 50, 25 e 5 m.

Para a geração das condições iniciais foi executado um modelo 2DH (bidimensional), utilizando condições de fronteira Riemann para calcular a hidrodinâmica, para o nível 0 e 1. Para o nível 2 foi utilizado um modelo 3D, com dez camadas sigma e um aumento da resolução em direção ao fundo. Esta abordagem visa resolver a dinâmica da camada limite do fundo.

O modelo morfodinâmico utiliza a formulação Van Rjin (2007) com dez camadas verticais, aplicada apenas no nível 2 (3D). Na simulação do Nível 2, o D50 do sedimento foi de 328.6 µm, com uma densidade de 2.650 kg/m^3 - este valor foi estabelecido com base nos resultados das amostras recolhidas. Os dados de sedimentos foram utilizados exclusivamente para o modelo morfodinâmico.

4. RESULTADOS

4.1. Estratigrafia e sedimentologia

A litoestratigrafia esquemática do Holocénico Superior observada em Verde Lago revela depósitos uma alternância entre ambientes deposicionais mais calmos de planície aluvial-estuarina (sedimentação lodosa) e episódios de maior energia, correspondendo a *washovers* e/ou transporte eólico (unidades arenosas). Foram identificadas e definidas cinco unidades litoestratigráficas, do topo para a base, solo eólico, areia com seixos, lodo castanho, areia média e lodo cinzento (Figura 4). Os sedimentos das unidades arenosas mostram uma assinatura marinha mais óbvia quando comparado com as unidades de lodo castanho e lodo cinzento, que correspondem a uma sedimentação de origem terrestre, dominada por silte. O padrão de sedimentação pertencente às unidades lodo castanho e lodo cinzento foi interrompido por um

evento responsável pela deposição da unidade arenosa, sugerindo condições de maior energia e sedimentação de origem marinha.

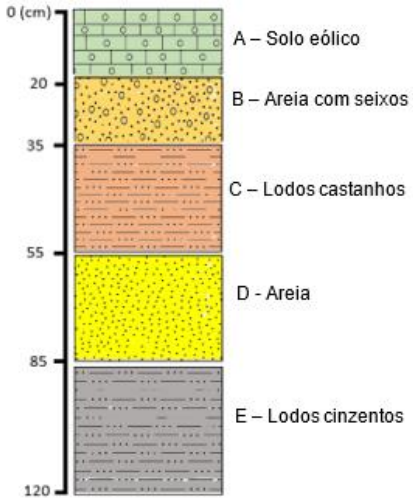

Figura 4. Registo esquemático da estratigrafia observada em Verde Lago (Algarve, Portugal), indicando as principais unidades litoestratigráficas.

4.2. Modelação hidrodinâmica

Foram analisados os resultados, Tabela I, da modelação das diferentes fontes sísmicas (Figura 5). Foi observado que para a fonte sísmica GB foi registada uma coluna de água de 2,4 m, com uma velocidade de 0,7 m/s. Neste caso, a extensão máxima de inundação foi de 32 m, não ocorrendo inundação no local onde foi realizada a campanha de campo e observados depósitos tsunamigénicos. Para a fonte HSF, foi modelada uma coluna de água de 5,5 m e uma velocidade de 2,8 m/s. A extensão máxima de inundação foi de 390 m na primeira onda e de 845 m na segunda onda, inundando diretamente a zona onde foi realizada a campanha de campo. Para a fonte MPF registou-se um nível de água máximo de 3,75 m e uma velocidade de 2,2 m/s. Verificou-se uma inundação máxima na primeira onda de 390 m. Por fim, para a fonte SCN1 registou-se um nível de água de 2,5 m e uma velocidade de 1,3 m/s. Com a segunda onda o máximo de inundação foi de 195 m.

Tabela I. Resultados da modelação hidrodinâmica das fontes GB, HSF, MPF e SCN1.

Fonte	Onda Ext. Maior	Extensão (m)	Vel. Máx. (m/s)	Nív. Água Máx. (m)
GB	Segunda	32	0.7	2.34
HSF	Segunda	846	2.8	5.34
MPF	Primeira	390	2.2	3.75
SCN1	Segunda	196	1.3	2.29

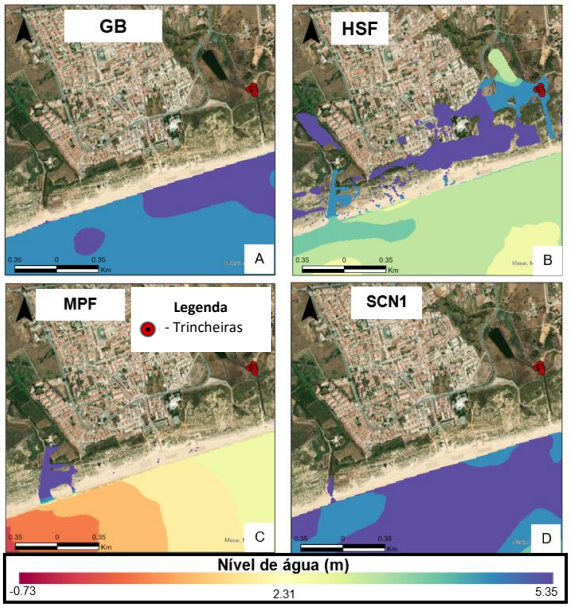

Figura 5. Resultados da modelação hidrodinâmica das fontes sísmicas: GB (A), HSF (B), MPF (C) e SCN1 (D).

4.3. Modelação morfodinâmica

Os resultados da modelação morfodinâmica estão representados na Figura 6.

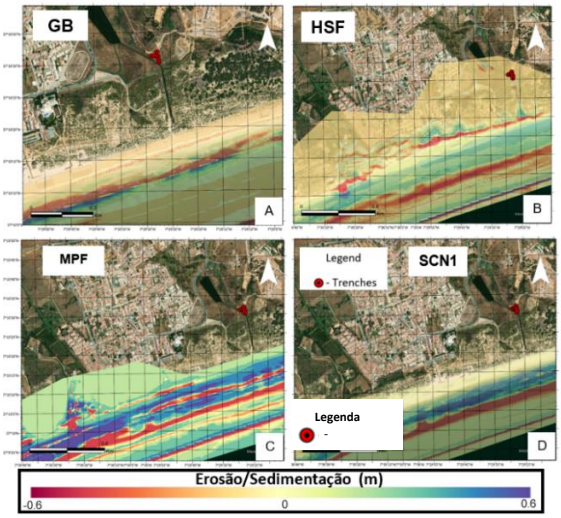

Figura 6. Resultados da modelação morfodinâmica das fontes sísmicas: GB (A), HSF (B), MPF (C) e SCN1 (D).

Embora não tenha causado inundações significativas em terra, a fonte GB gerou alterações morfológicas notórias perto da linha de costa. Esta fonte produziu mais erosão (a vermelho na Figura 5) do que deposição (a azul) ao longo da linha de costa. A fonte HSF provocou inundação na área de estudo, verificando-se alterações morfológicas mais significativas, em particular, na zona atualmente ocupada pelas dunas e praia submersa. Para a fonte MPF erosão e sedimentação consideráveis são observáveis na área inundada. Nesta fonte observou-se erosão em toda a área vegetada, com maior deposição nas zonas de

dunas, e menor, na praia submersa. Por fim, na fonte SCN1, os resultados revelam um extenso transporte de sedimentos, levando a uma erosão e acumulação na zona offshore, com deposição ao longo da praia submersa.

5. DISCUSSÃO

De todas as fontes testadas, apenas um evento gerado pela fonte HSF parece ser capaz de inundar a área onde os potenciais depósitos de tsunamis estão localizados. Estes resultados partilham semelhanças com o trabalho de Bosnic *et al.*, (2021), que se focou na zona dos Salgados, Algarve, a uma distância de aproximadamente 70 km a oeste de Verde Lago. Dourado *et al.* (2021) obteve resultados que apontavam para uma boa correlação entre a modelação e os dados de campo testando a fonte MPF. As diferenças entre o trabalho agora apresentado e os trabalhos referidos justifica-se pela diferença na distância e orientação da linha de costa dos locais estudados.

6. CONCLUSÃO

Este estudo sugere que a fonte sísmica HSF mostra melhor concordância com os padrões de alterações morfológicas obtidos no modelo morfodinâmico e os potenciais depósitos de tsunami observados em Verde Lago. É importante notar que este exercício não resolve a questão sobre a origem do sismo de 1755.

Agradecimentos

Um agradecimento aos responsáveis pela obra na urbanização Verde Lago bem como ao Professor César Andrade e Sebastião Teixeira.

REFERÊNCIAS

Apotsos, A., Buckley, M., Gelfenbaum, G., Jaffe, B., e Vatvani, D. (2011). Nearshore tsunami inundation model validation: toward sediment transport applications. *Pure and Applied Geophysics*, 168, 2097–2119.

Bosnic, I., Costa, P. J., Dourado, F., La Selle, S., e Gelfenbaum, G. (2021). Onshore flow characteristics of the 1755 CE Lisbon tsunami: Linking forward and inverse numerical modeling. *Marine Geology*, 434, 106432.

Buforn, E., Degaldeano, C.S., e Udias, A. (1995). Seismotectonics of the Ibero-Maghrebian region. *Tectonophysics*, 248(3–4), 247–261.

Deltares (2020). Delft3D-FLOW: Simulation of multi-dimensional hydrodynamic flows and transports phenomena, including sediments. User Manual, Version 3.15, Revision 66766 [Software]. Deltares. https://oss.deltares.nl/web/delft3d/get-started

Dourado, F., Costa, P.J., La Selle, S., Andrade, C., Silva, A.N., Bosnic, I., e Gelfenbaum, G. (2021). Can modeling the geologic record contribute to constraining the tectonic source of the 1755 CE Great Lisbon Earthquake? *Earth and Space Science*, 8(4), e2020EA001109.

van Rijn, L.C., Walstra, D.J.R., e van Ormondt, M. (2007). Unified view of sediment transport by currents and waves. IV: Application of morphodynamic model. *Journal of Hydraulic Engineering*, 133(7), 776-793.

Quartz grain microtexture analysis using Artificial Inteligence: applications on tsunami and storm deposits provenance studies

N. T. Marques (1, 2), P. J. M. Costa (1,2) and P. Pina (1,2)

(1) Departamento de Ciências da Terra, Faculdade de Ciências e Tecnologia, Universidade de Coimbra, Rua Sílvio Lima, Univ. Coimbra – Pólo II, 3030-790 Coimbra, Portugal. naterciatmarques@gmail.com

(2) Instituto Dom Luiz, Faculdade de Ciências, Universidade de Lisboa, Edifício C6, Campo Grande 1749-016, Lisboa, Portugal

Abstract: This study applies deep learning (DL) techniques to automate the classification of quartz grain microtextures under scanning electron microscopy (SEM), with the aim of supporting and standardising traditional microtextural analysis. Accurate microtextural analysis is crucial for sedimentary provenance and paleoenvironmental reconstructions, yet traditional methods are still prone to inter-operator variability. To overcome this, convolutional neural networks (CNNs) were trained on a diverse dataset of quartz grains from five depositional environments (dune, beach, fluvial, basal sands, nearshore) and two high-energy events (storm, tsunami). The models' performance was evaluated in parallel with model SandAI to test robustness across varied sedimentary contexts. CNNs demonstrated high accuracy in identifying grains from mechanically dominated environments. However, classification declined where microtextures were overprinted or poorly preserved. While unsupervised methods grouped grains by surface texture, they lacked consistency with depositional settings. Nonetheless, CNNs offer a promising, objective approach for sedimentary provenance and extreme event grain analysis, given robust datasets.

Keywords: *quartz grains, microtextures, SEM, deep learning, sedimentary provenance*

1. INTRODUCTION

Microtextural analysis of quartz grains under SEM is a well-established method in sedimentary provenance studies and paleoenvironmental reconstructions. Microtextures reflect mechanical, chemical, and biological processes that affect sediments from source to deposition, offering valuable clues about past environments.

The application of SEM to quartz microtextural analysis began in the 1960s (e.g. Krinsley and Takahashi, 1962), since then various atlases were created to standardising classification (e.g. Mahaney, 2002; Costa, 2012). Experimental studies (e.g. Krinsley and Takahashi, 1962) linked surface textures to sediment transport. The method has since been applied to paleoenvironmental reconstructions across fluvial, glacial, aeolian and coastal settings (e.g. Helland and Holmes, 1997). Quantitative and statistical approaches emerged in the late 1990s (e.g. Williams *et al.*, 1998), with applications in tsunami deposits (e.g. Costa *et al.*, 2012b; 2014b) and other extreme wave events deposits (Bruzzi and Prone, 2000).

Despite its extensive use, traditional microtextural analysis relies on expert visual interpretation, which is inherently subjective and affected by inter-operator variability (e.g. Costa *et al.*, 2012b). This limits reproducibility and the development of standardised classification criteria.

To overcome these challenges, recent developments have explored the integration of Artificial Intelligence (AI), particularly DL, into microtextural analysis workflows (e.g. Sikora *et al.*, 2024). DL, a subset of machine learning, employs artificial neural networks capable of learning complex patterns from large datasets (Alférez *et al.*, 2021). Within this framework, CNNs are especially suited for visual tasks, as they extract and hierarchise features related to texture and morphology (Minaee *et al.*, 2021). Recent studies have applied DL models for quartz grain classification based on microtexture analysis (Hasson *et al.*, 2024).

This study applies DL-based techniques to a large dataset of quartz grain SEM images, aiming to assess their potential for supporting and standardising microtextural classification. By integrating AI with geological expertise, this approach seeks to reduce subjectivity, enhance reproducibility.

3. DATASET

The study embraces a total of 18 distinct sampling areas, distributed across various geographical locations. Sediment samples were collected from extreme events (tsunamis and storms) and from potential sediment sources (beach, dune, subaqueous settings, among others). These sites correspond to low-energy depositional environments where

exogenous sediments are deposited by extreme wave events following coastal overwash. The selected areas include Scatsta Voe (Shetland), Stoneybridge (Hebrides), Sendai Plain (Japan), Lhok Nga (Sumatra), Bruny Island (Tasmania), Arauco (Chile), Moulay Bousselam (Morocco), and several Portuguese sites such as Nazaré, Santo André, Bordeira, Amado, Martinhal, Barranco, Zavial, Furnas, Boca do Rio, Alcantarilha and Salgados. These encompass lagoonal areas, alluvial plains, beaches, dunes and backshores, and are typically marked by medium to coarse sand layers within the upper Holocene, often with an erosional basal contact, indicative of high-energy, short duration overwash events.

Sediment samples were collected from modern depositional environments using trench excavation, dredging, scuba diving, and manual methods, with equipment including box-corers, Livingstone corers, Edelman and gauge augers, and Van der Staay suction corers (Costa, 2012). Grain size analysis followed standard dry sieving at 0.5Φ intervals, separating fractions into >63 µm and <63 µm (Costa, 2012).

Quartz grains within the 125–500 µm range (1–3Φ) were isolated under binocular microscopes, coated with gold or carbon (Costa, 2012; Costa *et al*., 2012b), and imaged using SEM at FCUL (Lisbon), the University of Clermont-Ferrand (France), and the Czech Geological Survey (Prague). Per sample, between 7 and 32 grains were analysed, with an average of 16 grains.

4. METHODOLOGY

4.1. Image classification

The classification of quartz grains was carried out following the methodology established by Costa (2012) and Costa *et al.* (2012b). Microtextural classification included angularity (Powers, 1953), fresh surfaces, percussion marks, adhering particles, and dissolution features, evaluated semi-quantitatively based on surface coverage (0 to 5 scale) and angularity (0 = very rounded; 5 = very angular) (Costa, 2012; Costa *et al.*, 2012b). Classification was conducted through direct visual inspection.

4.2. AI applied in microtexture analysis

All images were first standardised to PNG format and pre-processed using Python to remove backgrounds, eliminating visual noise from scales and grayscale backgrounds. The SandAI model (Hasson *et al.*, 2024), trained via unsupervised learning to classify quartz grains into Fluvial, Aeolian, Beach, and Glacial environments, was applied in seven sequential tests. These ranged from single-image trials to full-dataset classification and reproducibility assessments. One dataset version excluded images containing multiple grains to test for improved accuracy.

Separately, a CNN based on a modified ResNet-50 architecture was trained in five sessions using supervised learning, resulting in 5 Modelo_quartzo models. Images were resized, normalised, and augmented dynamically with transformations including rotations, flips, brightness/contrast shifts, and tonal inversion. The initial three sessions (Modelo_quartzo1 to Modelo_quartzo3) used seven classes (Basal Sands, Beach, Dune, Fluvial, Nearshore, Storm, Tsunami), with training durations of 30, 50, and 100 epochs respectively. Two subsequent sessions (Modelo_quartzo4 and 5) used a reduced four-class dataset (Fluvial, Beach, Dune, Nearshore) to improve balance and assess classification consistency, with training durations of 50 and 100 epochs.

Model performance was statistically evaluated using metrics such as percentage of grains classified per sample, overall accuracy (classified and total grains), with agreement with manual classification, enabling robust assessment of classification consistency and effectiveness across models.

5. RESULTS

The SandAI model displayed variable performance, with early tests (1–5) yielding classification rates below 45% and modest accuracy (Table I). Notably, performance improved significantly in Test 6, where untrained classes (basal sands, nearshore, tsunami, storm) were excluded, leading to 87.16% classification and 46.98% accuracy (Table I)—highlighting the model's limitations outside its trained domains (fluvial, beach, dune). In contrast, the custom-trained models (*Modelo_quartzo)* consistently classified 100% of grains and achieved higher accuracy (40.07–53.74%) (Table I), reflecting stronger adaptation to quartz microtextures.

Table I. Summary statistics of quartz grains for SandAI and all Modelo_quartzo models. BS- Basal sands; NS- Nearshore; TS- Tsunami; Strm – Storm.

AI Models	Tests	Mean classified grains (%)	Mean accuracy for classified grains(%)	Mean Accuracy total grains (%)	Overall accuracy (%)
SandAI model	Test 1	50.00	0	0	0
	Test 2	44.11	12.37	6.17	11.04
	Test 3	40.14	24.73	10.47	24.6
	Test 3 (without BS/ Ns/ Ts / Strm)	41.00	44.06	19.29	40.12
	Test 4	40.14	24.73	10.47	24.6
	Test 4 (without BS/ Ns/ Ts / Strm)	41.00	44.06	19.29	40.12
	Test 5	40.96	25.10	10.86	26.65
	Test 5 (without BS/ Ns/ Ts / Strm)	41.59	44.34	19.90	44.18
	Test 6	87.73	26.50	23.12	25.59
	Test 6 (without BS/ Ns/ Ts / Strm)	87.16	50.41	44.09	46.98
	Test 7	87.73	26.50	23.12	25.59
	Test 7 (without BS/ Ns/ Ts / Strm)	87.16	50.41	44.09	46.98
modelo_quartzo	MQ1	100.00	32.79	32.79	42.33
	MQ2	100.00	32.69	32.69	40.07
	MQ3	100.00	35.74	35.74	44.00
	MQ4	100.00	47.86	47.86	52.78
	MQ5	100.00	49.13	49.13	53.74

6. DISCUSSION

The SandAI model yielded variable results across tests, largely due to the confidence threshold of 75% applied

in the test code of the first five tests, which prevented the classification of many grains when the model's certainty was low. This conservative approach enhanced reliability but reduced coverage, particularly in earlier tests. When this threshold was removed in Tests 6 and 7, a clear increase in the number of classified grains was observed. Additionally, the model's performance improved markedly when restricted to the environments for which it had been trained—namely, fluvial, beach, and dune—highlighting the importance of training scope. In contrast, the *Modelo_quartzo* series, trained directly on the project's dataset, consistently classified 100% of the grains and achieved higher and more stable accuracies, suggesting greater adaptability to local microtextural variability. These results suggest that while the models captured some sedimentologically meaningful patterns, challenges remain in recognising complex or transitional microtextures.

The *Modelo_quartzo* models emphasise grain morphology and microtextures, distinguishing fluvial, basal sand, beach, dune, nearshore, and extreme event grains by characteristic shapes and surface features (Figure 1).

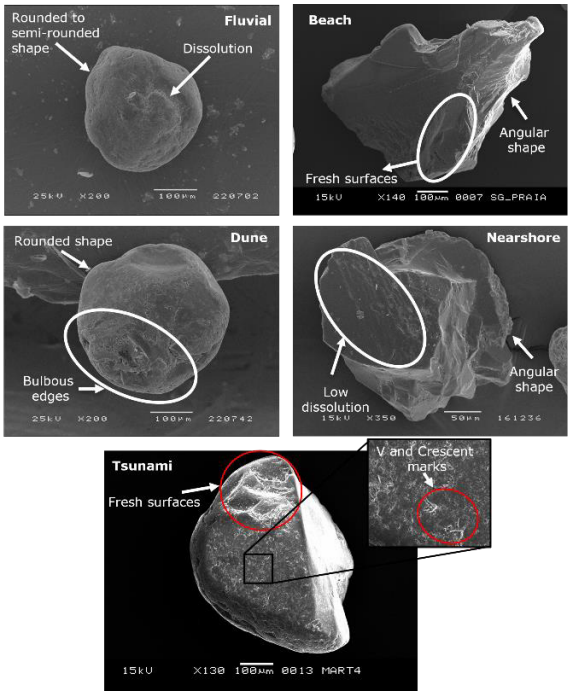

Figure 1. Feature maps used by the Modelo_quartzo models for classification. Mosaic illustrating the principal microtextural and morphological attributes identified by the Modelo_quartzo models during the automated classification of quartz grains from various sedimentary settings. Fluvial and basal sand grains are generally semi-rounded and exhibit dissolution features. In beach grains, the models rely on their angular shape and fresh surfaces. For dune grains, classification is based on their rounded shapes with bulbous edges. In nearshore sediments, the models focus on the pronounced angularity and slight dissolution of grains. Grains from extreme events (tsunamis and storms) are recognised by the presence of recent high-energy surface features.

In comparison, the SandAI model focuses on grain shape—rounding and angularity—and surface marks like fractures, effectively classifying grains in its original dataset (Figure 2).

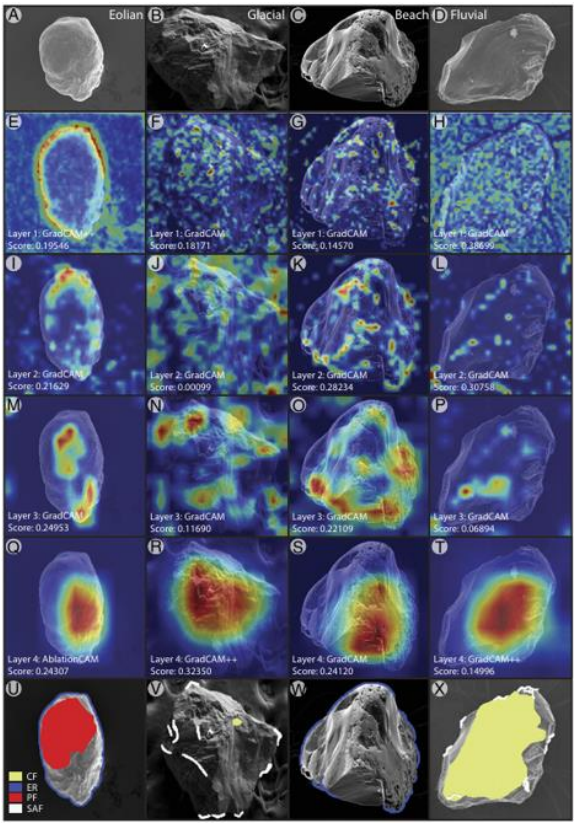

Figure 2. Feature maps used by the SandAI model for classification. Mosaic illustrating the key microtextural features extracted by the SandAI model when performing automatic classification of quartz grains across different sedimentary environments. CF = conchoidal fracture; ER = edge rounding; PF = precipitation features; SAF = sharp angular features. (Source: Hasson et al., 2024).

Model errors reflect real sedimentological patterns rather than randomness, indicating that models capture meaningful signals. However, limited accuracy arises from overlapping microtextures, as grains often exhibit mixed features from evolving depositional environments. Data augmentation aided training, but sedimentary complexity remains a challenge. Performance declines as the number of classes increases. Dataset size and image quality also limited model robustness, with natural microtexture overlap complicating classification further. Future work should prioritise supervised learning using expert-labelled microtexture sets to improve depositional environment classification. Expanding the microtexture library with specialised atlases and setting minimum microtexture presence criteria can enhance detail and accuracy. Additionally, dedicated models for extreme sedimentary events (tsunamis, storms) are recommended, as these grains' complex microtexture mixtures challenge current model performance.

7. CONCLUSION

This work addresses the inherent subjectivity of traditional microtextural analysis, which relies heavily on expert interpretation and is prone to observer bias, by exploring DL methodologies to automate the classification of quartz grain microtextures in sedimentary provenance studies. By comparing the SandAI model with newly developed CNN-based architectures (*Modelo_quartzo*), the capacity of these models to identify depositional environments solely from microtextural features was assessed. The results show that these models capture meaningful sedimentological patterns, although their accuracy decreases in more complex settings due to the natural overlapping of microtextures commonly found in sedimentary grains. In particular, the limited performance observed for grains from extreme events reflects the overprinting of microtextures produced by high-energy processes onto pre-existing features inherited from their source environments, resulting in complex surface signatures that challenge current classification approaches.

While the models demonstrate promising capabilities in recognising distinct microtextural characteristics, limitations remain.

This study demonstrates the value of AI-based microtextural analysis while underscoring the need for expanded datasets and tailored models to address the complex overprinted features characteristic of grains derived from high-energy depositional environments.

Acknowledgments

This work is supported by FCT project iCoast and IDL's funds from the Portuguese Fundação para a Ciência e Tecnologia, FCT, I.P./MCTES through national funds (PIDDAC): UID/50019/2025 and LA/P/0068/2020 https://doi.org/10.54499/LA/P/0068/2020).

REFERENCES

Alférez, G. H., Vázquez, E. L., Ardila, A. M. M., and Clausen, B. L. (2021). Automatic classification of plutonic rocks with deep learning. *Applied Computing and Geoscience*, 10, 100061. https://doi.org/10.1016/j.acags.2021.100061

Bruzzi, C., and Prone, A. (2000). A method of sedimentological identification of storm and tsunami deposits: Exoscopic analysis, preliminary results. *Quaternaire*, 11, 3-4., 167-177.

Costa, P. J. M. (2012). Sedimentological signatures of extreme marine inundations. PhD thesis. Universidade de Lisboa - Faculdade de Ciências Departamento de Geologia, 225pp.

Costa, P. J. M., Andrade, C., Dawson, A. G., Mahaney, W. C., Freitas, M. C., Paris, R., and Taborda, R. (2012b). Microtextural characteristics of quartz grains transported and deposited by tsunamis and storms. *Sedimentary Geology*, 275-276, 55-69. http://dx.doi.org/10.1016/j.sedgeo.2012.07.013

Costa, P. J. M., Andrade, C., and Freitas, M. C. (2014b). Assinaturas microtexturais de processos, ambientes e fontes sedimentares. O depósito de tsunami de 1755 na Boca do Rio - um caso de estudo. In Dinis, P., Gomes, A., Monteiro-Rodrigues, S., eds - Proveniência de materiais geológicos: abordagens sobre o Quaternário de Portugal. Associação Portuguesa para o estudo do Quaternário, 37-56.

Hasson, M., Marin, M. C., and Lapôtre, M. G. A. (2024). Automated determination of transport and depositional environments in sand and sandstones. *Proceedings of National Academy of Sciences, Earth, Atmospheric, and Planetary Sciences*, 121, 1-11. https://doi.org/10.1073/pnas.2407655121

Helland, P. E., and Holmes, M. A. (1997). Surface textural analysis of quartz sand grains from ODP Site 918 off the southeast coast of Greenland suggests glaciation of southern Greenland at 11 Ma. *Palaeogeography, Palaeoclimatology, Palaeoecology*, 135, 109-121.

Krinsley D., and Takahashi, T. (1962). The surface textures of sand grains - an application of electron microscopy: Glaciation. *Science*, 138, 1262-1264. DOI: 10.1126/science.138.3546.1262

Mahaney, W. C. (2002). Atlas of Sand Grain Surface Textures and Applications. Oxford University Press, New York, 237pp. ISBN 0-19-513812-0

Minaee, S., Boykov, Y., Porikli, F., Plaza, A., Kehtarnavaz, N., and Terzopoulos, D. (2002). Image Segmentation using deep learning: a survey. *IEEE Transactions on Pattern Analysis and Machine Intelligence*, 44(7), 3523-3542. DOI 10.1109/TPAMI.2021.3059968

Powers, M. C. (1953). A new roundness scale for sedimentary particles. *Journal of Sedimentary Research*, 23, 117–119.

Sikora, P., Kiac, M., Costa, P. J. M., Molinero-García., A., and Górska, M. E. (2024). Automatic image analysis applied to the recognition of quartz surface microtextures using neural. *Micron*, 182, 103638. https://doi.org/10.1016/j.micron.2024.103638

Williams, A. T., Wiltshire, R. J., and Thomas, M. C. (1998). Sand grain analysis--image processing, textural algorithms and neural nets. *Computers & Geosciences*, 24, 111-118.

Vulcanismo oceânico, mineralização e riscos submarinos

Vulcanismo oceánico, mineralización y riesgos submarinos

Oceanic volcanism, mineralisation and submarine hazards

MIA25 · LISBOA

Deep crustal structure and seismogenic potential of the SW Iberian Margin from new seismic and gravity constraints

R. Correia (1), M. Prada (2), V. Sallarés (2), A. L. Cameselle (2), L. M. Pinheiro (1), I. Grevemeyer (3) and C. R. Ranero (2,4)

(1) CESAM and Geosciences Department, University of Aveiro, Aveiro, Portugal. ricardocorreia@ua.pt
(2) Barcelona Center for Subsurface Imaging, ICM, CSIC, Barcelona, Spain
(3) Geomar and Christian-Albrechts University, Kiel, Germany
(4) ICREA, Barcelona, Spain

Abstract: This investigation aims to better understand the lithospheric structure of the Southwest Iberian Margin using an active seismic profile located southwest of Cape São Vicente. The profile extends from the Eastern Tagus Abyssal plain to the western edge of the Gulf of Cadiz accretionary wedge crossing the Tagus Abyssal Plain Fault, Marquês de Pombal Fault, and Horseshoe Fault. The crustal structure was determined from seismic data collected from both wide-angle seismics and multichannel seismic methods, further constrained and validated by gravity data. The inverted P-wave velocity structure, shows significant lateral velocity and structural changes marked by rough top of basement and sudden crustal thickness changes. Three main lithospheric domains consisting of continental, oceanic, and exhumed mantle affinity were identified. The inverted deep seismic phases revealed the existence of four southeast-dipping reflectors, providing new insights into the deep geometry of these regional thrust faults with seismogenic and tsunamigenic potential.

Keywords: *Southwest Iberian Margin, Lithospheric Structure, Wide-Angle Seismics, Multichannel Seismics, Seismic Tomography*

1. INTRODUCTION

The Southwest Iberian Margin (SWIM) has a complex tectonic setting and crustal structure derived from a succession of rift events related to the opening of North Atlantic and Neotethys, from the Mesozoic to the Lower Cretaceous (e.g. Schettino and Turco, 2009), and the subsequent convergence between Africa and Eurasia, from the Lower Oligocene to Present (e.g. Martínez-Loriente *et al*., 2014). This setting led to the reactivation of pre-existing strike-slip and extensional faults enhancing the seismogenic and tsunamigenic potential of the area (e.g. Zitellini *et al*., 2004).

In this geological framework, understanding of lithospheric structure along the SWIM is not only important for understanding the rift evolution but also for a better understanding of the distribution of the major lithospheric-scale boundaries, currently active and potentially capable of generating great seismic events of similar magnitude to the catastrophic 1755 Lisbon tsunamigenic earthquake, (e.g. Zitellini *et al*., 2001).

With the need to improve the current knowledge on SWIM lithospheric structure, in 2018, wide-angle seismic (WAS) and multichannel seismic (MCS) data were collected during the FRAME scientific cruises along a NW-SE trending, 320 km-long new geophysical transect, FRAME-1 (Figure 1).

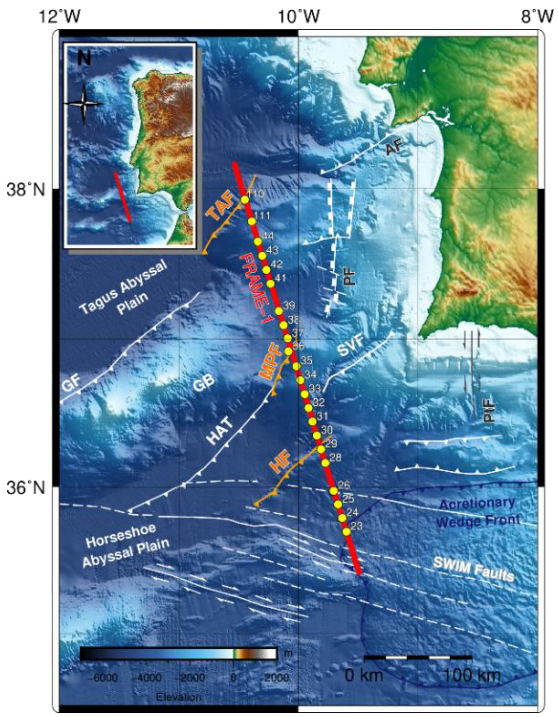

Figure 1. Bathymetric and topographic map of the Southwest Iberia Margin with the seismic transect FRAME-1 location (bold red line) and the respective station locations (yellow circles). Tectonic structures after Cunha et al. (2010), Duarte et al. (2013), Martinez-Loriente et al. (2014, 2018) and Serra et al. (2020). Abreviations: AF: Arrábida Fault; CPS: Coral-Patch Seamout; GB: Gorringe Bank; GF: Gorringe Fault; HF: Horseshoe Fault; HAT: Horseshoe Abyssal Plain Thrust; MPF: Marquês de Pombal Fault; PtF: Portimão Fault; PF: Pereira de Sousa Fault; SVF: São Vicente Fault; TAF: Tagus Abyssal Plain Fault.

2. METHODS

The WAS data were recorded with 22 ocean bottom seismometers and hydrophones (OBS/H), deployed each ~10km (Figure 1), while the MCS data was recorded with a 6 km-long streamer. Each OBS/H record was pre-processed on board for clock and position drift corrections. The signal contained in all records was later processed with an automatic gain compensation and a bandpass filter (5-18 Hz), to increase the signal-noise ratio and facilitate the seismic phase interpretation/picking.

A joint refraction and reflection travel-time tomography was applied to arrival times from both WAS and MCS datasets, using a modified version of the Tomo2D code (Korenaga *et al*., 2000; Meléndez *et al*., 2015). This allowed the inversion of a detailed 2D P-wave velocity model of the crust and uppermost mantle, along with the geometry of key seismic interfaces, including the top of the acoustic basement and the Moho.

To validate the imaged structure, the WAS-derived seismic velocity was submitted to an uncertainty analysis (Monte-Carlo approach) and converted into density using different empirical velocity-density correlations to calculate the gravity response and compare it to satellite observations.

3. RESULTS

The 2D tomographic model (Figure 2a) shows a P-wave velocity (Vp) structure with abrupt lateral velocity variations marked by a rough Top of Basement topography and strong crustal thickness variations.

The crust shows Vp values varying from 4-5 km s^{-1} at the top to 6-6.5 km s^{-1} at the bottom, and its thickness ranges from ~2.5 km thick to ~6.5 km. One segment of the profile (Seg. II, Figure 2a) does not display a distinct crust-mantle boundary. In this case the ~5 km-thick sedimentary cover appears to rest directly atop exhumed mantle rocks (under OBH 111; Figures 1 and 2). The Moho shallows beneath the north-eastward continuation of the Horseshoe Basin and the Gorringe Bank (Figures 1 and 2).

The mantle velocity below the Moho reflector is resolved by the deeper rays to 20-22 km depth. The velocity of the uppermost 3 km of the mantle exhibits noticeable lateral variations, with localized low velocity anomalies ranging 7.2-7.5±0.1 km s^{-1} along Segments II, III, V, and VII (Figure 2a).

The resolved velocity uncertainty in the tomographic model is less than ±0.2 km s^{-1} throughout most of the crustal section (Figure 2b). The higher velocity uncertainties are concentrated in the upper mantle, coincident with regions with limited ray coverage, reaching values of ±0.4 km s^{-1}. Concerning the Moho reflector, the depth uncertainty ranges from ± 0.3 km in regions well covered by Pg and PmP rays.

In this model, the density in the sedimentary layer ranges from 2.0 to 2.5 g cm^{-3}, while the crustal units exhibit densities around 2.6 g cm^{-3} in areas interpreted as having continental affinity (between 28 km and 215 km of the profile, encompassing segments I and III to VI). Beyond 215 km along the profile, interpreted as crust with oceanic affinity, higher density values around 2.7 g cm^{-3} are required to better explain the observed gravity anomaly, particularly along segment VII.

Reflected arrivals from the WAS data, with higher travel times and offsets, help constrain the deep geometry of four southeast-dipping reflectors (blue lines, Figure 2a) down to ~20 km depth, which may correspond to major regional faults.

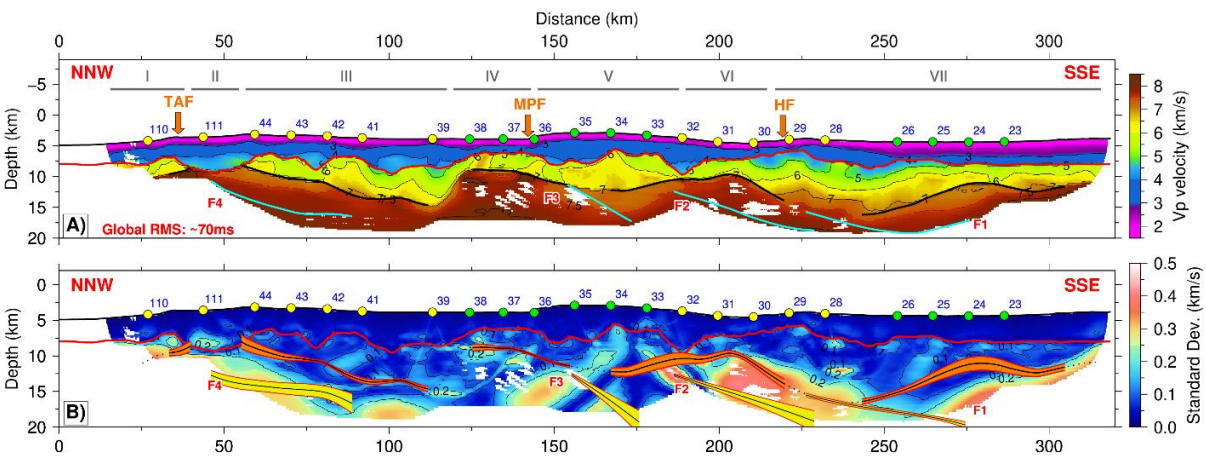

Figure. 2.(A) Final Vp Model for the profile P2AC1. The solid black and light-blue lines represent the Moho interface and the reflection planes of the potential faults respectively. (B) Standard deviation of Vp values of the average solution of the Monte-Carlo analysis for the profile P2AC1. The width of the red and yellow bands represents the standard deviation of the depth of the inverted horizons: Moho, F1, F2, F3 and F4. The circles on at the sea-bottom display the receiver locations: OBS (green) and OBH (yellow).

This interpretation is supported by the spatial coincidence between the prolongation of these deep reflectors towards the shallower crustal levels and the imaging of major fault structures on the MCS profile, namely the Tagus Abyssal Plain, Marquês de Pombal and Horseshoe faults (Figure 2a).

4. DISCUSSION

The results from the seismic tomographic inversion, combined with gravity modelling and MCS images support the interpretation that the various basement segments fall into three main lithological domains: continental crust (Segments I and III to VI, Figure 2a); exhumed and serpentinized mantle (Segment II, Figure 2a); and oceanic crust (Segment VII, Figure 2a). These domains exhibit a heterogeneous tectonic structure that reflects the geodynamic evolution of the SWIM.

The processed MCS profile reveal significant compressional and transpressional deformation along the SWIM, primarily resulting from Africa-Europe plate convergence since the Late Cretaceous, with major deformation phases occurring during the Eocene and Mid-Miocene. This deformation is strongly influenced by faulting, the nature of the basement lithology, and serpentinization processes in the mantle, which were likely triggered by fluid percolation along major fault systems, sometimes leading to local mantle exhumation.

The interpreted continental crust, particularly in segments I and III to VI (Figure 2a), shows a fault-bounded, rotated block structure. These blocks, controlled by NW-dipping normal faults, originated during earlier rifting phases and were later reactivated by Cenozoic convergence. The faults appear to extend into the mantle, intersecting serpentinized zones, reflecting progressive lithospheric stretching and crustal thinning that facilitated mantle exhumation during the initial stages of North Atlantic opening.

During rifting, brittle fracturing and deep faulting enabled fluid-rock interactions that promoted serpentinization in the upper mantle. This process caused changes in the mechanical properties of the lithosphere, observable as lower-than-normal seismic velocities beneath the main fault zones. The resulting rheological contrasts—caused by varying degrees of serpentinization—may have created weak zones that localized later compressional deformation. These weak zones correlate with key fault structures like the Tagus Abyssal Plain Fault and the Marquês de Pombal Fault, both of which overlie serpentinized mantle and display significant surface expression.

The Tagus Abyssal Plain Fault (F4) delineates the boundary between continental crust (Segment I) and exhumed mantle (Segment II), characterized by a pop-up structure, while the Marquês de Pombal Fault (F3) shows a vertical displacement exceeding 1 km, making it one of the most prominent features in the area. Another structure, Fault F2, does not correlate with known faults like the São Vicente Fault due to its dip and offset but may represent a lithospheric-scale detachment or a boundary of a distinct crustal block.

Towards the southeast end of the profile (Segment VII, Figure 2a), the crustal structure is less constrained due to a thick, complex sedimentary cover. The transition from continental to oceanic crust appears to be marked by the Horseshoe Fault (F1), whose deformation splays reach the seafloor and originate from the uppermost mantle. This indicates ongoing tectonic activity associated with the reactivation of the margin and supports the idea of active faulting around the Horseshoe fault system.

These new results provide a better-constrained basement affinity distribution for the SWIM, refining the boundaries between the main structural domains previously defined in earlier studies (e.g., Pinheiro *et al*., 1992; Martínez-Loriente *et al*., 2014). Additionally, they reveal a localized zone of exhumed mantle adjacent to the Tagus Abyssal Plain Fault.

The deep geometry of the major thrust faults modeled along this profile also provides new insights into the dimensions of potential rupture plane areas, and consequently, the maximum possible earthquake magnitude (Mw) for events along these structures. This reinforces the idea that the Marquês de Pombal Fault (MPF) is a lithospheric-scale fault that, either alone or in combination with the Horseshoe Abyssal Thrust (Martínez-Loriente *et al*. 2021), is a potential source of the region's largest earthquakes, were the 1755 Lisbon earthquake (estimated Mw 8.5+) is included.

5. CONCLUSIONS

The seismic data and gravity modeling from this research provide clear evidence of three distinct basement affinities along the SWIM, spanning from the southern Tagus Abyssal Plain to the westernmost extension of the Gulf of Cadiz. These affinities include continental crust, oceanic crust, and exhumed mantle. Continental crust predominates across most of the profile, extending from the eastern Tagus Abyssal Plain to the Horseshoe Abyssal Plain. However, this continuity is interrupted by a localized zone of exhumed mantle just south of the Tagus Abyssal Plain Fault. The oceanic domain is observed in the SE segment of the profile, starting around the Horseshoe Fault and continuing towards the Gulf of Cadiz accretionary wedge. These new results provide a

better-constrained basement affinity distribution for the study area, redefining the boundaries between the main domains and identifying a localized region of exhumed mantle adjacent to the Tagus Abyssal Plain Fault.

The deep geometry of major thrust, imaged for the first time down to down to approximately 20 km depth with both WAS and MCS data, allows the extraction of more descriptive and quantitative parameters for these structures and their correlation with regional seismicity. This has significant implications for their seismogenic potential and should be taken into account for accurate assessment of seismic hazards in the region.

Acknowledgements

We thank the teams involved in the two FRAME surveys. Special thanks to ship's officers and crew of the R/V Sarmiento de Gamboa, as well as the Spanish-UTM and GEOMAR technicians.

The Spanish Ministry of Science, Innovation and Universities funded the FRAME project (CTM2015-71766-R). ICM has also had funding support of the "Severo Ochoa Centre of Excellence" accreditation (CEX2019-000928-S), of the Spanish Research Agency (AEI).

R. Correia and L. M. Pinheiro thank the financial support to CESAM by national funds through FCT – Fundação para a Ciência e a Tecnologia I.P., under the project/grant UID/50006 + LA/P/0094/2020. They also thank FCT for the financial support from the research project PRORIFT (NSFC/0003/2016).

REFERENCES

Cunha, T. A., Watts, A. B., Pinheiro, L. M., and Myklebust, R. (2010). Seismic and gravity anomaly evidence of large-scale compressional deformation off SW Portugal. *Earth and Planetary Science Letters*, 293(1-2), 171–179.

Duarte, J. C., Rosas, F. M., Terrinha, P., Schellart, W. P., Boutelier, D., Gutscher, M.-A., and Ribeiro, A. (2013). Are subduction zones invading the Atlantic? Evidence from the southwest Iberia margin. *Geology*, 41(8), 839–842, Publisher: Geological Society of America.

Korenaga, J., Holbrook, W. S., Kent, G. M., Kelemen, P. B., Detrick, R. S., Larsen, H., Hopper, J. R., and Dahl-Jensen, T. (2000). Crustal structure of the southeast Greenland margin from joint refraction and reflection seismic tomography. *Journal of Geophysical Research: Solid Earth*, 105(B9), 21591–21614.

Martínez-Loriente, S., Gràcia, E., Bartolome, R., Perea, H., Klaeschen, D., Dañobeitia, J. J., Zitellini, N., Wynn, R. B., and Masson, D. G. (2018). Morphostructure, tectono-sedimentary evolution and seismic potential of the Horseshoe Fault, SW Iberian Margin. *Basin Research*, 30(S1), 382–400.

Martínez-Loriente, S., Sallarès, V., and Gràcia, E. (2021). The Horseshoe Abyssal plain Thrust could be the source of the 1755 Lisbon earthquake and tsunami. *Communications earth & environment*, 2, 145.

Martínez-Loriente, S., Sallarès, V., Gràcia, E., Bartolome, R., Dañobeitia, J. J., and Zitellini, N. (2014). Seismic and gravity constraints on the nature of the basement in the Africa-Eurasia plate boundary: New insights for the geodynamic evolution of the SW Iberian margin. *Journal of Geophysical Research: Solid Earth*, 119(1), 127–149.

Meléndez, A., Korenaga, J., Sallarès, V., Miniussi, A., and Ranero, C. R. (2015). TOMO3D: 3-D joint refraction and reflection traveltime tomography parallel code for active-source seismic data—synthetic test. *Geophysical Journal International*, 203(1), 158–174.

Pinheiro, L. M., Whitmarsh, R. B., and Miles, P. R. (1992). The ocean-continent boundary off the western continental margin of Iberia—II. Crustal structure in the Tagus Abyssal Plain. *Geophysical Journal International*, 109(1), 106–124.

Schettino, A., and Turco, E. (2009). Breakup of Pangaea and plate kinematics of the central Atlantic and Atlas regions. *Geophysical Journal International*, 178(2), 1078–1097.

Serra, C. S., Martínez-Loriente, S., Gràcia, E., Urgeles, R., Vizcaino, A., Perea, H., Bartolome, R., Pallàs, R., Iacono, C. L., and Diez, S. (2020). Tectonic evolution, geomorphology and influence of bottom currents along a large submarine canyon system: The São Vicente Canyon (SW Iberian margin). *Marine Geology*, 426, 106219.

Zitellini, N., Rovere, M., Terrinha, P., Chierici, F., and Matias, L. (2004). Neogene Through Quaternary Tectonic Reactivation of SW Iberian Passive Margin. *Pure and Applied Geophysics*, 161(3), 565–587.

Imaging the seismogenic sources of the 1941 and 1975 great strike-slip earthquakes (Central NE-Atlantic)

C. Roque (1,2), S. Manzoni (3) and J. Duarte (2,4)

(1) EMEPC, Estrutura de Missão para a Extensão da Plataforma Continental, Paço de Arcos, Portugal. croque@emepc-portugal.org
(2) IDL, Instituto Dom Luiz, Faculdade de Ciências da Universidade de Lisboa, Campo Grande, Lisboa, Portugal
(3) Agrupamento de Escolas de Alvalade, Lisboa, Portugal
(4) Departamento de Geologia, Faculdade de Ciências da Universidade de Lisboa, Campo Grande, Lisboa, Portugal

Abstract: The seafloor morphology of the areas of the great magnitude strike-slip 1941 and 1975 earthquakes was studied by multibeam bathymetry analysis and seismicity correlation. The morphostructural analysis allowed identifying a sigmoidal feature in the central segment of the dextral-strike slip Gloria Fault where is located the epicenter of the 1941 earthquake. This feature has been interpreted as a double restraining bend of the Gloria Fault. Seismicity analysis shows the presence of a cluster in this area with events reaching about 70 km depth and dipping southwards to the restraining bend. Unexpected microseismic activity is seen in the northern border of the Western Gap. The epicenter of the 1975 event seems to be located in a scarp in the eastwards prolongation of the Tydeman fracture zone. The seafloor morphology and seismicity distribution seems to suggest that this sector of the Africa (Nubia)-Eurasia plate boundary is under tectonic reorganization.

Keywords: *multibeam bathymetry, strike-slip earthquake, morphostructure, Gloria Fault*

1. INTRODUCTION

Great oceanic earthquakes with moment magnitude $M_w \geq 8.0$ are infrequent events and they concentrate mostly in subduction zones megathrusts'. The occurrence of great magnitude oceanic strike-slip earthquakes is comparatively rarer in the other plate boundaries, such as oceanic transform faults (OTF). OTF are commonly seismogenic at shallow depths (10-15 km below seafloor) (*e.g.* Abercrombie and Ekström, 2001). Usually, the OTF earthquakes have magnitude considered moderate ($M_w \leq 6$) even in long faults (up to 1000 km), indicating a small rupture area (Liu *et al.*, 2019; Hicks *et al.*, 2020). It is accepted that about 85% of slip on OTF occurs through aseismic creep (*e.g.* Kohli *et al.*, 2021). However, in the Atlantic Ocean a few events reached great magnitudes, such as the 1941 November 25 event (M_w8.4) (Baptista *et al.*, 2017) in the Gloria Fault, which is the central segment of the Africa (Nubia)-Eurasia plate boundary. Even rarer are strike-slip earthquakes in intraplate settings such as fracture zones, which are usually aseismic structures (Krebbenhoeft *et al.*, 2018; Lay, 2019). However, the 1975 May 26 earthquake located at ~200 km south of the Africa (Nubia)-Eurasia plate boundary reached a surface-wave magnitude of M_s7.9 (Lynnes and Ruff, 1985). This intraplate earthquake still remains a puzzling event (Lynnes and Ruff, 1985; Lay, 2019).

Morphological analysis has been recognized as a powerful tool to investigate the superficial expression of major earthquakes and how they shaped the recent seafloor (Aderhold and Abercrombie, 2016).

Therefore in this work we use unpublished multibeam bathymetry to perform a detailed morphostructural analysis of the Atlantic area affected by the 1941 and 1975 earthquakes (Figure 1) in order to characterize the surface rupture geometry associated with those events.

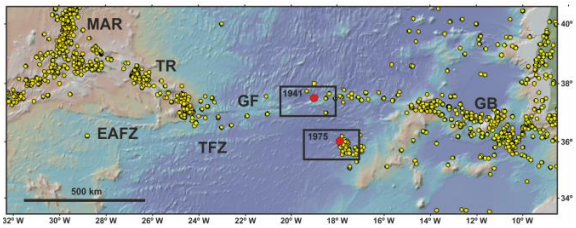

Figure 1. Study areas (black rectangles) and location of earthquakes. Yellow dots correspond to the location of earthquakes with $M_w \geq 4.5$ and red dots correspond to the epicenters of 1941 and 1975 events (catalogues USGS and SHARE). MAR: Mid-Atlantic Ridge; TR: Terceira Rift; EAFZ: East Azores Fracture Zone; GF: Gloria Fault; TFZ: Tydeman Fracture Zone; GB: Gorringe Bank.

2. THE 1941 AND 1975 EARTHQUAKES

The 1941 November 25 earthquake was felt in Madeira, Azores, western Portugal, Spain and Morocco (*e.g.* Baptista *et al.*, 2016). It was the largest strike-slip event ever recorded, being only surpassed in 2012 April 11 by the Mw 8.6 Sumatra earthquake (Meng *et al.*, 2012). The epicenter has been relocated by Baptista *et al.* (2016) in a position westwards of the one determined earlier. The first-motion focal

mechanism of this event has been reported as strike-slip with dextral slip on the E-W nodal plane (Udias *et al.*, 1976). According to Baptista *et al*. (2016), the earthquake ruptured approximately 160 km of the plate boundary.

The epicenter of the 1975 May 26 earthquake is located on the prolongation of the Tydeman Fracture Zone, which is approximately parallel to the Gloria Fault (Kaabouden *et al.*, 2008). The area is located within the Cretaceous Magnetic Quiet Zone and significant morphological features seem to be missing (Lay, 2019).

Another peculiarity of the 1941 and the 1975 events is that both triggered small tsunamis (0.5 to 2 m wave high, respectively) that reached south Portugal mainland, Azores Islands and Morocco (Kaabouden *et al*., 2008; Baptista *et al*., 2017).

3. DATA AND METHODS

We used multibeam bathymetry data (100 m cell-size) collected in the scope of the Project of Extension of Continental Shelf by the EMEPC (Estrutura de Missão para a Extensão da Plataforma Continental) in the areas of the 1941 and 1975 earthquakes (Figure 1). The morphological analysis and mapping made using ArcGis the was correlated with instrumental seismicity record available from public catalogues (SHARE, USGS, IPMA) and the microseismicity record published by (Krüger *et al.,* 2020). Vertical sections with the seismicity projection were made using Generic Mapping Tools (GMT5).

4. RESULTS

The analysis of the multibeam bathymetry allowed identifying an about 174 km long relief in the central segment of the Gloria Fault, in the area of the epicenter of the 1941 earthquake (Figure 2).

This feature presents a central sigmoidal/lozenge shape with complex morphology, being composed of four closely spaced ridges trending ~WSW-ENE. These ridges present an asymmetric shape characterized by an abrupt southern slope (indicate by "R2 in Figure 2). Its northern limit corresponds to an E-W elongated basin, the Western Gap. The southern limit of this set of blocks is sharp and marked by a steep slope with gradients between 5.4º and 6.6º. The top of these scarps is shallower at north (~3675 m) deepening toward south (~3980 m) (Figure 2).

Towards west an E-S rectangular basin is observed nearby a set of three closed E-W elongated blocks. Further west, another E-W narrow depression can be also observed (Figure 2).

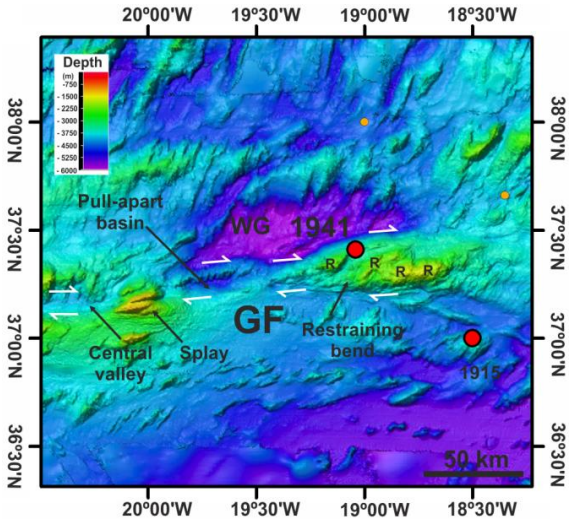

Figure 2. Multibeam bathymetry imaging the central segment of the Gloria Fault (GF) and showing the location of the 1941 earthquake epicenter (red dot) on top of a sigmoidal feature interpreted as a double restraining bend bounded by thrust-faults. WG: Western Gap; R: ridges.

The epicenter of the 1975 earthquake is located in a WSW-ENE scarp about 96 km long at ~4950 m water depth. This scarp corresponds to the eastwards prolongation of the Tydeman fracture zone (Figure 3).

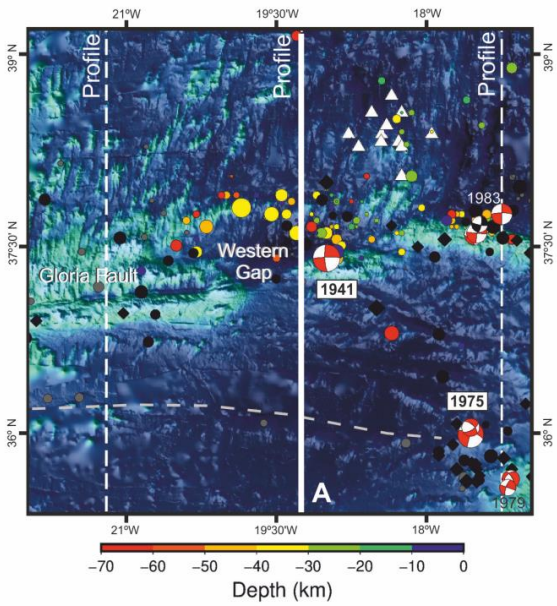

Figure 3. Map showing the location of epicenters and focal mechanisms of large earthquake in the study area, in particular of 1941 and 1979 events. White triangles correspond to the location of the DOCTAR experiment stations (Krüger et al., 2020). The different colors correspond to the depth of the respective hypocenter. The gray dashed line represents the location of the Tydeman fracture zone. Straight vertical white dashed lines mark the location of bathymetric and depth across seismicity clusters. Profile A across the sigmoidal feature is shown in Figure 4.

A seismicity and microseismicity cluster was recognized between 18º30'W and 20ºW (Figure 3). This seismicity increases toward east coinciding with

the central segment of the Gloria Fault, the Western Gap and the surrounding seafloor.

The 1941 earthquake epicenter is located within this cluster on the sigmoidal feature described previously (Figure 2). The focal mechanisms solution for this event, indicate a pure strike-slip motion and one of the nodal planes striking W-E and the other N-S. A roughly W-E trend of aligned events is observed to the north of the Gloria fault, following the northern border of the Western Gap and extending further east (Figure 3).

An N-S vertical section crossing this cluster and extending further north and south through the Tydeman fracture zone (*Figure 3*), shows the depth projection of the earthquakes and micro-earthquakes along this direction (Figure 4).

It is observed that the events are mostly concentrated between the DOCTAR stations network and the sigmoidal feature. They can reach 70 km depth dipping towards south in the direction of the sigmoidal feature, where occurred the 1941 earthquake (*Figure 4*).

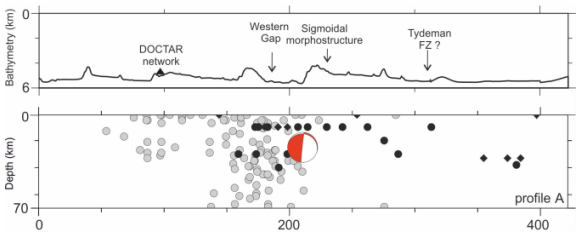

Figure 4. Profiles A across the seismicity cluster around the epicenter of the 1941 earthquake. Top: bathymetric profile. Bottom: depth projection of the earthquakes and micro-earthquakes. The focal mechanism of the 1941 events is also shown.

5. DISCUSSION

Taking in consideration the morphology display by the relief in the central segment of the Gloria Fault, we interpreted it as a double restraining bend. It is constituted by a succession of WSW-ENE elongated uplifted crustal-blocks bound by parallel thrust-faults, defining an asymmetric, NNW-verging positive flower structure. The rectangular basin located westwards from this feature has been interpreted as a pull-apart basin while other depression locate further west correspond to the central fault-valley, the set of closed E-W blocks has been interpreted as a fault splay.

The seismicity distribution (in space and depth) around the central segment of the Gloria Fault (sigmoidal feature) and in the northern border of the Western Gap, suggests that both features are accommodating the present-day deformation imposed by Africa (Nubia) and Eurasia movement.

Although, the Tydeman fracture zone has been considered an old and inactive fracture zone the occurrence of the 1975 event suggests that at least its easternmost part has been reactivated, while being located at about 200 km south of the present-day Africa (Nubia)-Eurasia plate boundary.

6. FINAL CONSIDERATIONS

The seafloor morphology and seismicity distribution seems to suggest that the central segment of the Africa (Nubia)-Eurasia plate boundary and the Tydeman fracture zone are presently accommodating deformation and probably under tectonic reorganization.

Acknowledgements

This work is supported by the Portuguese Fundação para a Ciência e Tecnologia, FCT, I.P./MCTES through national funds (PIDDAC): UID/50019/2025 and LA/P/0068/2020
https://doi.org/10.54499/LA/P/0068/2020).

REFERENCES

Abercrombie, R.E. and Ekström, G. (2001). Earthquake slip on oceanic transform faults. *Nature*, 410:74–77.

Aderhold, K. and Abercrombie, R.E. (2016). The 2015 M_w 7.1 earthquake on the Charlie-Gibbs transform fault: Repeating earthquakes and multimodal slip on a slow oceanic transform. *Geophysical Research Letters*, 43:6119–6128.

Baptista, M.A., Miranda, J.M., Batlló, J., Lisboa, F., Luis, J. and Maciá, R. (2016). New study on the 1941 Gloria Fault earthquakeand tsunami. *Natural Hazards and Earth Systems Sciences*, 16:1967–1977.

Baptista, M.A., Miranda, J.M., Matias, L. and Omira, R. (2017). Synthetic tsunami waveform catalogs with kinematic constraints. *Natural Hazards and Earth Systems Sciences*, 17:1253–1265.

Hicks, S.P., Okuwaki, R., Steinberg, A., Rychert, C.A., Harmon, N., Abercrombie, R.E., Bogiatzis, P., Schlaphorst, D., Zahradnik, J., Kendall, J-M., Yagi, Y., Shimizu, K. and Sudhaus, H. (2020). Back-propagating supershear rupture in the 2016 Mw 7.1 Romanche transform fault earthquake. *Nature Geoscience,* 13:647–653.

Kaabouben, F., Brahim, A.I., Toto, E., Baptista, M.A., Miranda, J.M., Soares, P. and Luis, J.F. (2008). On the focal mechanism of the 26.05.1975 North Atlantic event contribution from tsunami modeling. *Seismology*, 12:575–583.

Kohli, A., Wolfson-Schwehr, M., Prigent, C. and Warren, J.M. (2021). Oceanic transform fault seismicity and slip mode influenced by seawater infiltration. *Nature Geoscience*, 14:606–611.

Krabbenhoeft, A., von Huene, R., Miller, J.J., Lange, D. and Vera, F. (2018). Strike-slip 23 January 2018 MW7.9 Gulf of Alaska rare intraplate earthquake: Complex rupture of a fracture zone system. *Scientific Reports,* 8:13706.

Krüger, F., Dahm, T. and Hannemann, K. (2020). Mapping of Eastern North Atlantic Ocean seismicity from *Po/So* observations at a mid-aperture seismological broad-band deep sea array. *Geophysical Journal International,* 221:1055–1080.

Lay, T. (2019). Reactivation of oceanic fracture zones in large intraplate earthquakes? In: Duarte, J.C. (eds). *Transform Plate Boundaries and Fracture Zones*, Elsevier, pp. 89-104.

Liu, Y., McGuire, J.J. and Behn, M.D. (2020). Aseismic transient slip on the Gofar transform fault, East Pacific Rise. *Proceedings of the National Academy of Sciences*, 117:10188–10194.

Lynnes, C.S. and Ruff, L.J. (1985). Source process and tectonic implications of the great 1975 North Atlantic earthquake. *Geophyscal Journal of the Royal Astronomical Society,* 82:497-510.

Meng, L., Ampuero, J.P., Stock, J., Duputel, Z., Luo, Y. and Tsai, V.C. (2012). Earthquake in a maze: compressional rupture branching during the 2012 Mw 8.6 Sumatra earthquake. *Science*, 337:724-726.

Udias, A., Arroyo, A.L., Mezcua, J. (1976) Seismotectonic of the Azores-Alboran region. *Tectonophysics*, 31:259-289.

Sediment faulting and fluid migration in the Madeira Abyssal Plain (Central NE-Atlantic)

C. Roque (1,2), D. Gamboa (3,4) and V. Magalhães (5,2)

(1) EMEPC, Estrutura de Missão para a Extensão da Plataforma Continental, Paço de Arcos, Portugal. croque@emepc-portugal.org
(2) IDL, Instituto Dom Luiz, Faculdade de Ciências da Universidade de Lisboa, Campo Grande, Lisbon, Portugal
(3) Departamento de Geociências, Universidade de Aveiro, Aveiro, Portugal
(4) CESAM, Universidade de Aveiro, Aveiro, Portugal
(5) IPMA, Instituto Português do Mar e da Atmosfera, Lisboa, Portugal

Abstract: Evidence of pervasive sediment faulting and fluid migration was recognized in the Madeira Abyssal Plain based on the interpretation of multichannel seismic lines. Different types of fluid migration structures have been identified suggesting that they have distinct origins. We suggest that the fluid migration can be related to two different processes, i) dewatering and diagenetic processes within the sedimentary cover and ii) to serpentinization of the underlying oceanic crust.

Keywords: *abyssal plain, fluid migration, oceanic crust, Late Cretaceous*

1. INTRODUCTION

Abyssal plains are located between 4000 and 6000 m water depth and have been considered quiet and stable environments showing an almost flat, smooth and featureless shape only studded by a few abyssal hills and seamounts. This is due to a thick blanket of sediments overlying the structures of the oceanic crust, which results from the slow and continuous accumulation of pelagites only interrupted sporadically by the sudden deposition of turbidites. However, the acquisition of seismic reflection data over the last two decades changed this view. Abyssal plains are instead dynamic sittings, being swept by bottom currents forming contourite drifts, sediment waves and widespread erosional surfaces (Hernández-Molina *et al.,* 2008). Fluid flow processes are also prevalent on the oceanic domains, with the majority of subsurface fluid drainage and expulsion in sedimentary sequences being identified on continental margins (*e.g.* Hovland and Judd, 1988). Nevertheless, hydrothermalism and other processes related to the alteration of oceanic crust lithologies are prone to release fluids that, when overpressured, migrate within the sedimentary cover units. Since the majority of abyssal plains are located around passive continental margins and far-way from plate boundaries, they are regarded as tectonic quiescent places.

During the 1980's a few studies conducted in the Madeira Abyssal Plain (MAP) discovered that its sedimentary cover is unexpectedly cut by several sets of faults (Duin *et al.,* 1984). Early works tried to explain the formation of these faults by differential compaction or tectonic activity (Williams, 1987). Although these authors were unable to identify the mechanism(s) that caused the sediment-faulting in the MAP, they concluded that such deformation seem to be related to long-lived process(es). However, over the past forty years the question regarding the origin of this sediment faulting remained unanswered. In this work, we revisit these deep abyssal plain deformation features, although in a site located northwards from the one surveyed by Duin *et al.* (1984), to further improve their structural pattern and interpretations of their possible origin based on new and unpublished multichannel seismic lines.

2. GEOLOGICAL SETTING

The MAP is a nearly flat (<0.01°) sedimentary basin located at 5400 m water depth and within the Cretaceous Magnetic Quiet Zone (CMQZ), which extends from Chron M0 to Chron C34 (84.0 Ma) (Bird *et al.,* 2007). Although the precise age of the underlying oceanic crust is unknown, according to (Searle *et al.,* 1987), this basin developed over oceanic crust about 106-80 Myr old. The sedimentary cover of the MAP is composed of pelagites interbedded with turbidite layers mostly delivered by turbidity currents from the Moroccan Turbidite System and Madeira Distributary Channel Systems (Wynn *et al.,* 2002), in particular from the early Miocene to the Pleistocene. Calcareous turbidites from the Meteor Seamounts Chain have been also recognized (Lebreiro *et al.,* 1998).

3. DATA AND METHODS

This work is based on the seismic stratigraphy interpretation of long multichannel seismic lines of approximately 300 km length, running E-W and crossing the northern part of the MAP (Figure 1).

These lines were acquired in 2006 onboard the *R/V Akademik Shatskiy* using a 5720 in^3 bolt air-gun array, a streamer of 7950 m length with 636 channels and a shooting distance of 50 m.

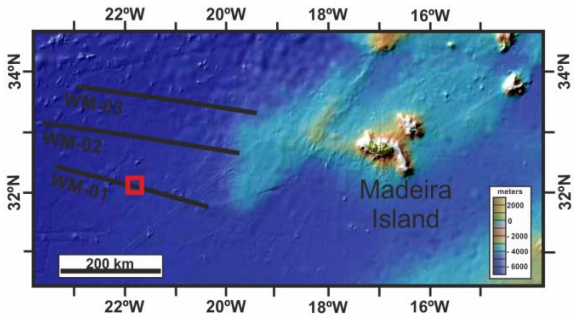

Figure 1. Location of multichannel seismic lines off Madeira Island. The red square indicates the location of seismic sections presented in Figure 2.

3. RESULTS

On the interpreted seismic data, the oceanic crust and the sedimentary cover units present very distinct facies. While the oceanic crust tends to show a chaotic facies, the sedimentary cover presents a well-organized stratified sequence, with long continuous reflectors extending significant distances (Figure 2).

Faulting of the sedimentary cover faulting is a pervasive phenomenon in the study area, affecting its entire vertical extent. Several sets of extensional faults cut through the sediments and several types of faults can be distinguished based on their geometry and stratigraphic position. The most abundant fault type corresponds to sets of near-vertical, closely spaced faults, rooted in the oceanic basement blocks and variable vertical extent. Some of these sets only propagate within the oldest sedimentary units, the ones that drape over the oceanic basement. The second set is characterized by faults cutting through younger sediments. A few faults affect the uppermost sediments and deform the seafloor. The other type of faults, in minor number and more localized, consists of a set of vertical, parallel, and equally spaced faults developed within a specific stratigraphic interval. Their tier-bound occurrence and geometry fit into the characteristics of polygon fault sets, prone to develop in fine-grained lithologies (Cartwright, 2011).

Fluid migration is indicated by i) localized acoustic turbidity, recognized as a good indication of gas and fluids presence; ii) vertical and narrow zones of acoustic wipe-out is observed associated with local amplitude anomalies, interpreted as pipes for fluid migration; and iii) pull-down narrow and vertical structures (buried pockmarks) (Figure 2). Acoustic turbidity is sometimes associated with the set of faults propagating in the sedimentary sequence.

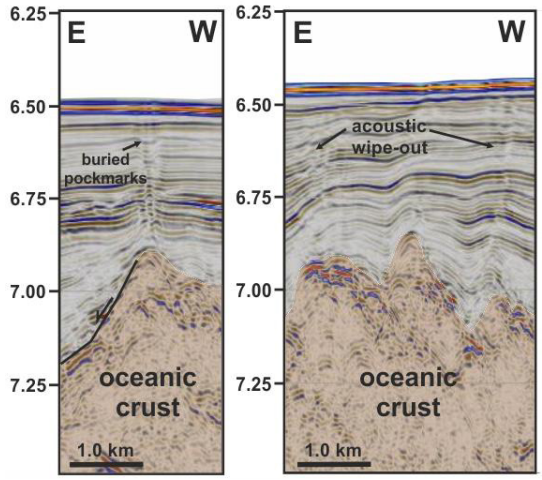

Figure 2. Sections of multichannel seismic line WM-01 showing evidence of fluid migration associated with basement highs. Vertical scale is in seconds TWTT. See Figure 1 for location.

4. DISCUSSION AND FINAL CONSIDERATIONS

The occurrence of fluid migration in the MAP sedimentary sequence seems to be a more prevalent process than previously though as supported by the analysis of the seismic data. Within the variety of fluid-originating processes in sedimentary basins, two can be fitting for the origin of the escape features in the MAP. Differential compaction, dewatering and diagenesis of sediments can be one of the mechanisms responsible for the fluid migration. As pressure builds up, fluids would migrate through the shallower faults. These processes are also tied to the origin of tier-bound faults, which are prone to from in tectonically quiescent areas. The fluid migration associated with faults deeply rooted in basement highs has probably a different origin, related to crustal processes. We propose that these fluids might result from oceanic crust serpentinization due to hydrothermal circulation through deep faults. The structural trends within the crustal blocks could aid the establishment of migration paths and their focus on the structures on which the deeper fault are rooted.

Acknowledgements

This work is supported by the Portuguese Fundação para a Ciência e Tecnologia, FCT, I.P./MCTES through national funds (PIDDAC): UID/50019/2025 and LA/P/0068/2020 https://doi.org/10.54499/LA/P/0068/2020).

REFERENCES

Bird, D.E., Hall, S.A., Burke, K., Casey, S.F. and Sawyer, D.S. (2007). Early Central Atlantic Ocean seafloor spreading history. *Geosphere,* 3: 282–298.

Cartwright, J. (2011). Diagenetically induced shear failure of fine-grained sediments and the development of

polygonal fault systems. *Marine and Petroleum Geology*, 28: 1593-1610.

Duin, E.J.Th., Mesdag, C.S. and Kok, P.T.J. (1984). Faulting in Madeira Abyssal Plain sediments. *Marine Geology*, 56: 299-308.

Hernández-Molina, F.J., Maldonado, A. and Stow, D.A.V., (2008). Abyssal plain contourites, In: M. Rebesco, A. Camerlenghi (eds.), *Contourites*. Developments in Sedimentology 60, Elsevier, pp. 345-378.

Hovland, M.J. and Judd, A.C. (1988). Seabed pockmarks and seepages-Impact on geology, biology and marine environment. Graham and Trotman, London. 293 pp.

Lebreiro, S.M., Weaver, P.P.E. and Howe, R.W. (1998). Sedimentation of the Madeira abyssal Plain Eocene-Pleistocene history of turbidite infill. In: Weaver, P.P.E., Schmincke, H-W., Firth, I.V. and Duffield W. (eds) *Proceedings of the Ocean Drilling Program, Scientific Report*, 157, 523-531.

Searle, R.C., Williams, S.R.J., Huggett, Q.J., Rothwell, R.G., Schultheiss, P.J. and Weaver, P.P.E. (1987). The geology of the Madeira Abyssal Plain further studies relevant to its suitability for radioactive waste disposal. *IOS*, Report 250, 87pp.

Williams, S.R.J. (1987). Faulting in abyssal-plain sediments, Great Meteor East, Madeira Abyssal Plain. In: Weaver P.P.E. and Thomson, J. (eds), *Geology and geochemistry of abyssal plains*. Geological Society Special Publication, 31: 87-104.

Wynn, R.B., Weaver, P.P.E., Masson, D.G. and Stow, D.A.V. (2002). Turbidite depositional architecture across three interconnected deep-water basins on the northwest African margin. *Sedimentology*, 49:669-695.

Crustal Thickness Modeling in the Azores Region Using Tesseroid-Based Gravity Methods

S. Gonçalves (1,2), C. Roque (1,3) and F. Artilheiro (1)

(1) Estrutura de Missão para a Extensão da Plataforma Continental, Paço D'Arcos, Portugal. g22.susana@gmail.com
(2) Instituto Português do Mar e da Atmosfera (IPMA), Lisboa, Portugal
(3) Instituto Dom Luiz, Faculdade de Ciências, Lisboa, Portugal

Abstract: Understanding crustal structure in oceanic island settings like the Azores Plateau is essential to unravel the complex geodynamic processes at play, including hotspot activity, ridge–ridge–ridge junctions, and lithospheric thinning. This study applies a tesseroid-based forward gravity modeling approach to estimate crustal thickness variations in the Northeast Atlantic, incorporating data from satellite gravity (ICGEM), sediment distribution (GLOBSED), and regional topography. The modeling workflow accounts for Earth curvature, crust–mantle density contrasts, sediment correction, and Airy isostatic compensation. By systematically removing the gravitational contributions of sediments, crust, and upper mantle, we isolate residual anomalies that provide insights into deep lithospheric structures. The results are validated through comparisons with Airy-based crustal thickness estimates, highlighting areas of significant deviation potentially linked to tectonic or magmatic processes. This gravity-based methodology demonstrates the value of integrated geophysical modeling in regions where seismic constraints are limited or spatially sparse.

Keywords: *Bouguer Anomaly, Crustal thickness, Azores Plateau, Forward modeling*

1. INTRODUCTION

Understanding the crustal structure and the processes involved in the formation of oceanic island settings — such as the Azores Plateau — is essential for advancing our knowledge of complex geodynamic systems. These regions often involve interactions between tectonic plates, magmatic activity, and mantle dynamics, making them ideal natural laboratories for studying lithospheric evolution.

The Northeast Atlantic, particularly around the Azores, is shaped by the interaction of the Mid-Atlantic Ridge (MAR), the Azores Triple Junction, and a presumed mantle plume or hotspot. This tectonically and volcanically active region presents both a challenge and an opportunity for gravity-based crustal modeling. In particular, gravity modeling constrained by topography, sediment load, and reasonable lithospheric density contrasts can offer valuable insights into crustal thickness and mass distribution. Such models may later be improved through the inversion of the gravity data with seismic data constrain.

In this study, we apply a tesseroid-based forward gravity modeling approach to estimate and evaluate the lateral variations in crustal thickness across the Azores region. The modeling workflow integrates detailed topography, sediment thickness (GlobSed), variable crustal and mantle densities, and an isostatic reference based on the Airy compensation model.

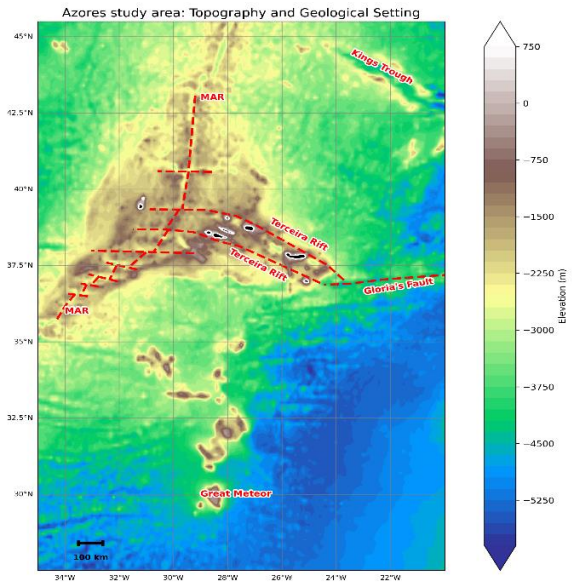

Figure 1. Topography and tectonic setting of the study area.

2. GRAVITY FORWARD PROBLEM

Forward gravity modeling at regional to lithospheric scales requires consideration of Earth's curvature to ensure accuracy, particularly when integrating long-wavelength gravity data from satellite missions such as GOCE (Gravity field and steady-state Ocean Circulation Explorer) and GRACE (Gravity Recovery and Climate Experiment). In this context, the Earth is more appropriately discretized using spherical mass elements known as tesseroids, rather than traditional

Cartesian rectangular prisms, as shown by Uieda *et al*. (2015). This approach allows for consistent treatment of gravitational effects over large spatial extents, making it particularly suitable for oceanic settings like the Northeast Atlantic and Azores region.

2.1. Data Sources

To construct the forward model, we integrate multiple geophysical datasets:

- Topography – 0,1ºx0,1º resolution grid from ICGEM, GFZ
- Full Gravity field – 0,1ºx0,1º resolution, SGG-UGM-2 model, reference to the ellipsoid, from ICGEM, GFZ
- Global sediment thickness grid (GlobSed) – 0,1ºx0,1º resolution from NOAA services
- Density values – standard values were considered taking into account literature like Christensen, N. I and Mooney, W. D. (1995) and Laske, G., (2013). Salt water density of 1030 kg/m³, sediment density of 2300 kg/m³, a variable crustal density between 2700-2900 kg/m³ and a mantle density of 3300 kg/m³

2.2. Modelling Workflow

The modeling follows a structured sequence:

1. **Preprocessing and gridding** of topography, gravity anomalies, and sediment thickness to a common resolution.
2. **Tesseroid discretization** of the **study** area in the spherical domain, incorporating topographic and sediment corrections.
3. **Computation of gravitational effect** of individual layers using tesseroid-based forward modeling.
4. **Airy isostasy modeling**: Crustal thickness variations are estimated assuming local compensation to evaluate deviations from isostatic equilibrium.

2.3. Goals

The forward modeling serves several goals:

- Quantify the gravitational contribution of known mass layers (topography, sediments, crust).
- Estimate crustal thickness variations under isostatic assumptions using density contrasts.
- Identify gravity anomalies not explained by isostasy alone, suggesting dynamic or thermal contributions (e.g., plume-related upwelling).
- Provide a foundation for future gravity inversion constrained by seismic or geodynamic data.

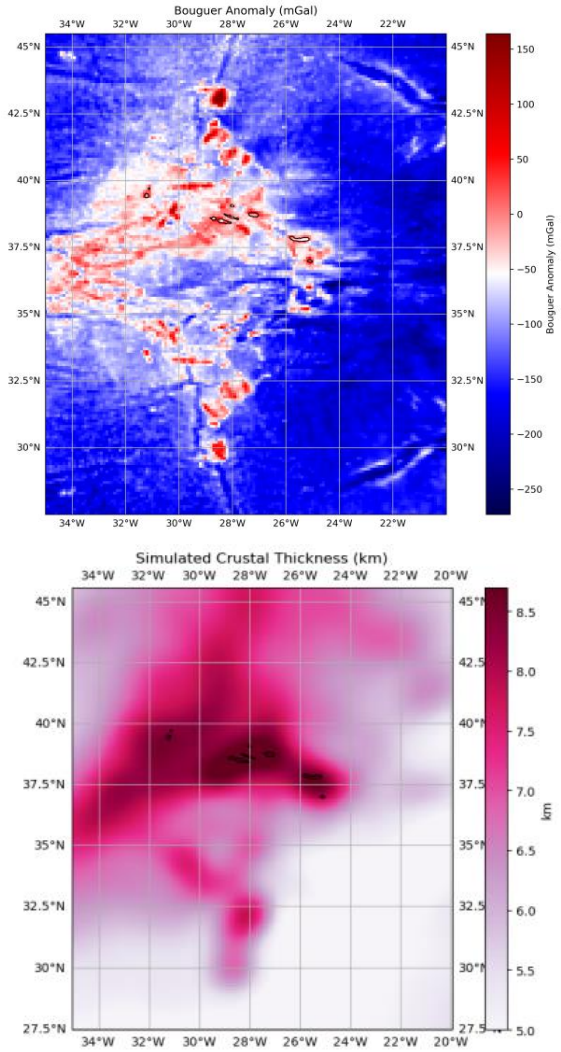

Figure 2. Bouguer anomaly obtained by removing normal gravity and topographic effect (Top); Simulated Crustal Thickness (km).

3. CONCLUSIONS

This study demonstrates the effectiveness of tesseroid-based forward gravity modeling in investigating crustal thickness variations in the tectonically complex Azores Plateau region. By incorporating realistic 3D Earth curvature, sediment corrections, and density stratification based on established geophysical constraints, the model provides valuable insights into the structure and isostatic state of the Northeast Atlantic lithosphere.

The integration of global gravity data (e.g., GOCE), topography, and sediment thickness yields a robust estimate of crustal architecture, highlighting thickened crustal regions associated with hotspot activity and ridge-triple junction interactions. The approach confirms that gravity modeling, when guided by geophysical principles and constrained by regional

data, is a powerful tool for understanding oceanic plateau formation and lithospheric processes.

Future work will incorporate seismic constraints and apply gravity inversion techniques to refine the model and better resolve lateral heterogeneities in crustal structure.

Acknowledgments

The authors gratefully acknowledges the use of several open-access datasets and software tools that made this work possible. Gravity field models were obtained from the International Centre for Global Earth Models (ICGEM), and sediment thickness data was sourced from the GLOBSED global sediment map. The Harmonica Python library, developed as part of the Fatiando a Terra project, provided key functionalities for gravity forward modeling using tesseroids. Additional utilities from the Verde and Boule packages were employed for spatial interpolation and geodetic calculations. The availability of these open-source resources significantly contributed to the reproducibility and transparency of this research.

REFERENCES

Christensen, N.I., and Mooney, W.D. (1995). Seismic velocity structure and composition of the continental crust: A global view. *Journal of Geophysical Research: Solid Earth*, 100(B6), 9761–9788.

Ince, E.S., Barthelmes, F., Reißland, S., Elger, K., Förste, C., Flechtner, F., and Schuh, H. (2019). ICGEM – 15 years of successful collection and distribution of global gravitational models, associated services and future plans. *Earth System Science Data*, 11, 647-674. http://doi.org/10.5194/essd-11-647-2019

Laske, G., Masters, G., Ma, Z., and Pasyanos, M. (2013). *Update on CRUST1.0 - A 1-degree global model of Earth's crust*. Abstract EGU2013-2658.

Soler, S. R., Pesce, A., Gimenez, M. E., and Uieda, L. (2019). Gravitational field calculation in spherical coordinates using variable densities in depth. *Geophysical Journal International*. Doi: 10.1093/gji/ggz277

Straume, E.O., Gaina, C., Medvedev, S., Hochmuth, K., Gohl, K., Whittaker, J.M., *et al*. (2019). GlobSed: Updated total sediment thickness in the world's oceans. *Geochemistry, Geophysics, Geosystems*, 20. Doi:10.1029/2018GC008115

Uieda, L. (2018). Verde: Processing and gridding spatial data using Green's functions. *Journal of Open Source Software*, 3(29), 957. Doi:10.21105/joss.00957

Uieda, L., Barbosa, V.C.F., and Braitenberg, C. (2015). Tesseroids: Forward-modeling gravitational fields in spherical coordinates. *Geophysics*, 81. Doi:10.1190/GEO2015-0204.1

Uieda, L., Oliveira Jr, V.C., and Barbosa, V.C.F. (2013), Modeling the Earth with Fatiando a Terra. *Proceedings of the 12th Python in Science Conference*, pp. 91-98. Doi:10.25080/Majora-8b375195-010

Modelação numérica e simulação de processos no ambiente marinho

Modelización numérica y simulación de procesos en el medio marino

Numerical modelling and simulation of processes in the marine environment

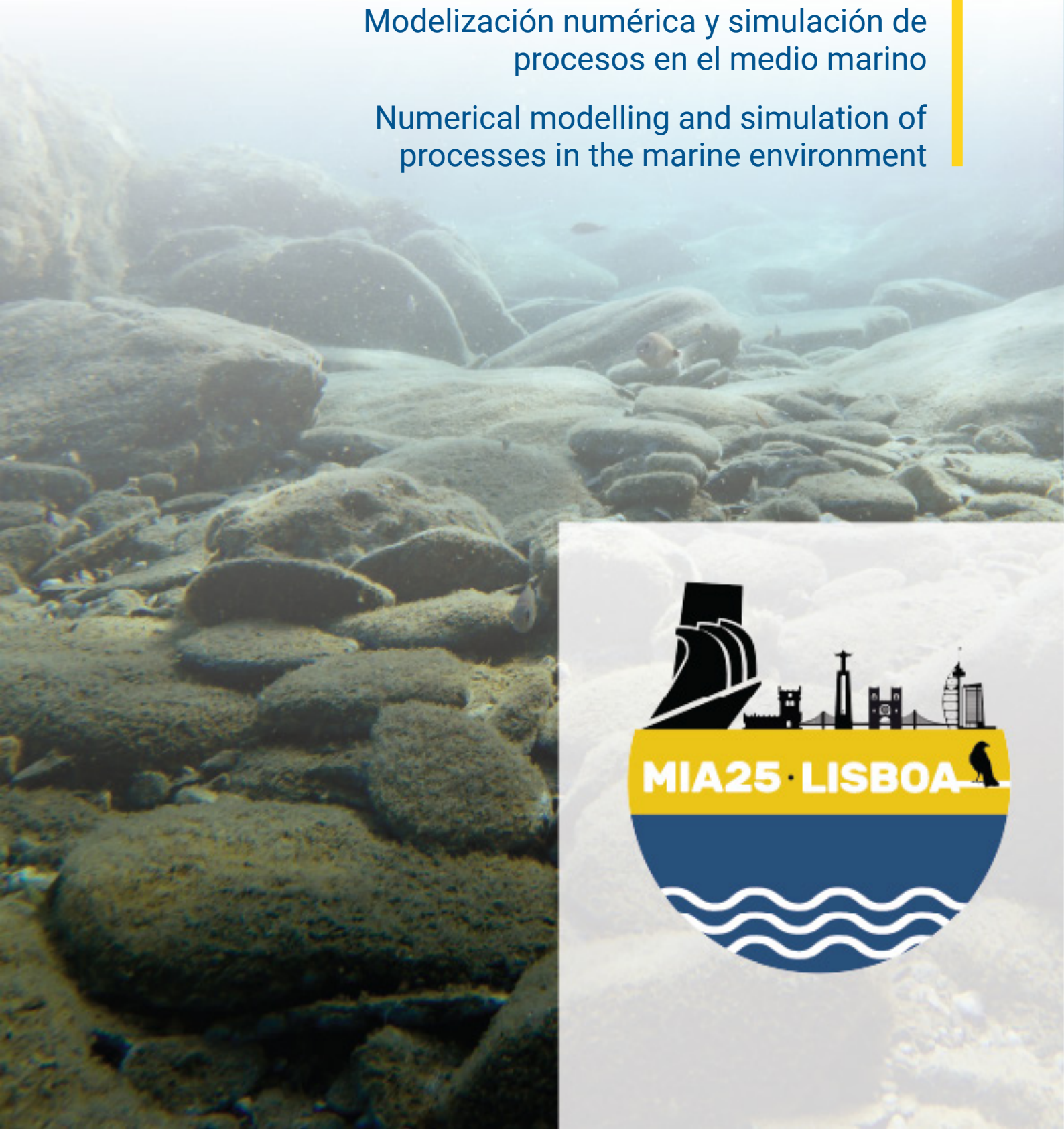

Caracterização da Agitação Marítima e Tempestades da Costa Ocidental Portuguesa, com Recurso a Bases de Dados Modelados

F. Romão (1), M. Lima (2), S. Costas (3) e C. Coelho (1)

(1) CERIS, Departamento de Engenharia Civil, Universidade de Aveiro, Campus Universitário de Santiago, Aveiro, 3810-193, Portugal. fredericoromao@ua.pt
(2) Centro Universitário do Porto (CUP), FCNET – Faculdade de Ciências Naturais, Engenharia e Tecnologias, Universidade Lusófona, Rua Augusto Rosa, No. 24, 4000-098, Porto, Portugal.
(3) CIMA/ARNET, Universidade do Algarve, Campus de Gambelas, Faro, 8005-139, Portugal

Abstract: The increasing frequency and intensity of storms are expected to place coastal communities at growing risk. Maintaining shoreline stability presents challenges, which are likely to intensify as climate change progresses. Effective coastal management relies on understanding and predicting shoreline evolution. Numerical models play a key role by simulating coastal processes. However, these models require calibration with site-specific data to ensure reliability. While various wave climate datasets are available, selecting the most suitable remains challenging. In this study, three wave climate datasets were used to characterize Costa Nova beach (Portugal). Statistical methods were applied to assess differences among them. A T-test revealed significant differences in mean values of the series. A similar pattern was observed when comparing the annual number of storms, with discrepancies between datasets. These findings emphasize the importance of appropriate dataset selection for modelling shoreline response to storms and average wave conditions.

Keywords: *Storms, Climate Change, Time Series, T-Test, ANOVA*

1. INTRODUÇÃO

As zonas costeiras têm sido áreas preferenciais para o estabelecimento e fixação de populações, devido à abundância de recursos naturais, alimento, vias de transporte e oportunidades económicas (Small e Nicholls, 2003). Metade das maiores cidades do mundo encontram-se localizadas nas zonas costeiras, onde vive cerca de 40% da população mundial (Kummu *et al.*, 2016). Este padrão de ocupação aumentou nas últimas décadas (Cunha *et al.,* 2025), impulsionado pelo crescimento populacional e urbanização contínua.

O aumento do nível médio das águas do mar e da frequência e intensidade de tempestades tornam as zonas costeiras mais vulneráveis à erosão, eventos de galgamento e danos em infraestruturas (Zhang *et al.*, 2025). Estes fatores aumentam o risco de galgamentos e inundações permanentes, os efeitos de erosão e a destruição de defesas costeiras, colocando vidas e infraestruturas em perigo (Magdalena *et al.*, 2025).

As tempestades, caracterizadas por valores elevados de altura de onda significativa, são resultado de perturbações na atmosfera, com consequências nas zonas costeiras, que incluem sobre-elevação do nível do mar, galgamentos e/ou inundações costeiras, danos em infraestruturas e construções, e perda de habitats. Em praias arenosas, estas condições têm impacto na morfologia, influenciando o transporte sedimentar, e promovendo a erosão e a vulnerabilidade à inundação.

Neste contexto, os modelos numéricos surgem como ferramentas importantes para simulação de eventos de tempestade e galgamento, permitindo apoiar a tomada de decisão e o planeamento de medidas de adaptação. Contudo, o uso de modelos numéricos depende de calibração e validação, para uma adequada representação da realidade (Roelvink *et al.*, 2009). A escolha dos parâmetros que representam os agentes forçadores possibilita a simulação dos eventos de agitação e tempestade e a adequada definição de cenários (Cheng e Wang, 2018).

A qualidade e características dos dados de entrada afeta o desempenho dos modelos numéricos. Desta forma, este trabalho visa comparar fontes de dados modelados, nomeadamente ERA5, Copernicus (COP) e *Puertos del Estado* (PE), com o objetivo de caracterizar a agitação marítima na área de estudo, situada ao largo da praia da Costa Nova, no distrito de Aveiro, Portugal. A análise das bases de dados permite também a avaliação da ocorrência de tempestades. Os resultados são relevantes para a caracterização dos agentes forçadores e condições de simulação a considerar na aplicação de modelos numéricos.

2. METODOLOGIA

A metodologia adotada neste trabalho foi estruturada em quatro fases principais: caracterização da área de estudo (secção 2.1); identificação e descrição das

bases de dados de agitação marítima (secção 2.2); descrição dos métodos estatísticos aplicados na análise das bases de dados (secção 2.3); e, análise do número anual de tempestades e duração/energia associada (secção 2.4). Esta abordagem permitiu compreender o impacto da escolha de bases de dados e de critérios de definição de tempestades para a caracterização da agitação marítima, fornecendo suporte à modelação numérica e à definição de estratégias de gestão costeira mais eficientes.

2.1. Área de estudo

A área de estudo situa-se ao largo da praia da Costa Nova, situada no distrito de Aveiro, Portugal (Figura 1).

Figura 1. Área de estudo: Praia da Costa Nova, Aveiro, Portugal; e pontos localizados a 98 km da costa (41º N, 9.5º W), para as bases de dados selecionadas: ERA5; Copernicus e Puertos del Estado.

Esta região apresenta uma elevada exposição à agitação marítima do Atlântico Norte, caracterizada por ondas provenientes de WNW e NW. A média da altura significativa da onda ronda os 2 m, com um período de pico de 11 s. No entanto, durante o inverno podem ocorrer episódios com alturas significativas de onda superiores a 4 m, associados a tempestades (Romão *et al.*, 2024). Para caracterização da agitação incidente na área de estudo foram selecionadas 3 bases de dados provenientes de modelos numéricos.

2.2. Bases de dados

As bases de dados selecionadas para este trabalho foram: ERA5 (reanálise global produzida pelo ECMWF); Copernicus (reanálise regional europeia); e dados do sistema de medição e previsão oceano-meteorológica de *Puertos del Estado* (regional). A base de dados do ERA5 disponibiliza dados desde 01/01/1940 até ao presente. A base Copernicus cobre o período de 02/01/1993 a 26/12/2021. Os dados de *Puertos del Estado* compreendem o período desde 03/03/1958 até à atualidade. Para cada base de dados foram extraídas três variáveis para caracterização do clima de agitação marítima: a altura significativa da onda (H_S), o período de pico (T_P) e a direção da onda (Dir). A média das alturas significativas da onda das bases de dados ronda os 2.20 m, com a média dos períodos de pico entre os 8.42 s e os 10.78 s (maior dispersão). As ondas provêm maioritariamente do quadrante NW, em todas as bases de dados. Para efeitos de comparação, foi selecionado um período de tempo comum às bases de dados, compreendido entre 01/10/1993 e 30/09/2021, com uma resolução temporal de 3 h.

2.3. Testes estatísticos

Para comparar as bases de dados foram realizados diferentes testes estatísticos. O teste de Kolmogorov-Smirnov (KS) é um teste estatístico não paramétrico, utilizado para comparar duas distribuições amostrais (Marsaglia *et al.,* 2003). Neste estudo, o teste KS foi aplicado para comparar as distribuições cumulativas de cada variável (H_S, T_P e Dir), considerando o tempo de registos comum às 3 bases de dados. O teste-T de Student é usado para comparar as médias das variáveis H_S, T_P e Dir, entre pares de bases de dados. Este teste permite avaliar se as diferenças nas médias entre as bases de dados são estatisticamente significativas (Brown e Forsythe, 1974). Por fim, o teste ANOVA (Análise de Variância), foi aplicado com o objetivo de comparar o número anual de tempestades identificadas em cada base de dados, considerando dois critérios distintos de definição de tempestade (ver seção 2.4). Este teste permite verificar se existem diferenças estatísticas entre três ou mais grupos amostrais, assumindo dados paramétricos (Seber e Lee, 2003).

A Hipótese nula (H_0) foi definida assumindo que as distribuições e as médias das séries são iguais. Para todos os testes realizados, assumiu-se um nível de confiança de 95% ($\alpha = 0.05$). O resultado dos testes é denominado de valor P, e representa a probabilidade de observar os dados, assumindo que H_0 é verdadeira. Se $P < \alpha$, rejeita-se H_0, o que resulta em séries com distribuições e médias significativamente diferentes. Se $P \geq \alpha$, não existem evidências suficientes para rejeitar H_0, logo os resultados podem ser iguais.

2.4. Análise de tempestades

Para a costa portuguesa, diferentes definições de tempestade podem ser encontradas na literatura, variando conforme o autor e a aplicação (Davies *et al.*, 2017; Marinho *et al.,* 2018; Lira-Loarca *et al.,* 2020). Neste trabalho, foram considerados dois critérios, diferindo na altura significativa da onda e duração mínimas necessárias para que um evento seja considerado tempestade. O Critério C1 segue a definição proposta por Boccotti (2000), em que uma tempestade ocorre quando $H_s > 1.5 \times \overline{H}_S$ ($\overline{H}_S$ representa a média da altura significativa das ondas), e cuja duração seja superior a 12 h. Neste caso, uma tempestade ocorre quando os valores são superiores a 3.32 m, 3.42 m e 3.44 m, dependendo da base de dados, respetivamente COP, PE e ERA5. O Critério C2 adota a definição de Oliveira *et al.* (2018), em que uma

tempestade ocorre quando Hs > 4.5 m, com duração mínima de 6 h. Para contabilizar o número anual de tempestades, considerou-se o ano hidrológico, compreendido entre 01/10 e 30/09 do ano seguinte. Esta escolha permite uma melhor representação da variabilidade sazonal, especialmente durante o inverno marítimo, onde ocorrem os eventos mais energéticos. Posteriormente, para cada base de dados e tempestade, quantificaram-se as médias de H_S, T_P, Dir, energia e potência, identificando-se também os valores representativos de cada ano.

3. RESULTADOS

Esta secção resume os resultados dos testes estatísticos efetuados. A Figura 2 apresenta as distribuições de H_S, T_P e Dir, considerando o período de tempo comum às três bases de dados.

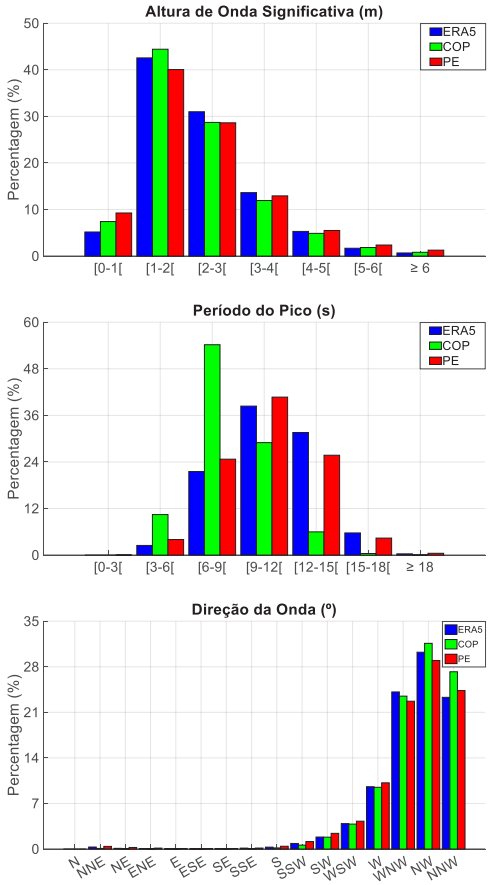

Figura 2. Distribuições da altura significativa das ondas, período de pico e direção média, para as diferentes bases de dados (1993 a 2021).

As bases de dados de H_S apresentam uma distribuição semelhante, com altura significativa das ondas predominantemente entre 1-2 m (Figura 2). No entanto, T_P mostra distribuições com comportamentos diferentes: ERA5 e PE com distribuição intermédia e deslocada para a direita, respetivamente (T_P dominante entre 9 e 12 s) e COP com distribuição deslocada para a esquerda (T_P dominante entre 6 e 9 s). O parâmetro Dir para as distintas bases de dados apresenta distribuição similar, com predomínio das ondas provenientes de NW (Figura 2).

O teste KS, efetuado para comparar as distribuições acumuladas, resultou em valores P > 0.05 para todas as variáveis, ou seja, não existem evidências suficientes para rejeitar H_0, sendo que as distribuições das séries são semelhantes. Apesar das distribuições de T_P serem mais diferentes, de acordo com o teste, essa diferença não é significativa.

O teste-T foi utilizado para avaliar os valores médios das séries das bases de dados, para cada variável (H_S, T_P e Dir). Ao comparar as séries de H_S de ERA5 e PE, o resultado indicou que não existem evidências estatísticas suficientes para rejeitar H_0, ou seja, as médias podem ser consideradas semelhantes (P > 0.05), sugerindo que estas séries representam condições marítimas equivalentes em termos de H_S. No entanto, este teste indicou P < 0.05 ao comparar as outras variáveis de diferentes bases de dados, o que sugere diferenças significativas entre as séries.

A Figura 3 apresenta a evolução anual do número de tempestades, considerando as 3 bases de dados e os 2 critérios definidos para a ocorrência de tempestades. O número anual de tempestades é maior no critério C1, devido ao menor limite de H_S adotado para definir os eventos. A escolha do critério influencia fortemente os resultados, sendo importante a escolha adequada do critério, de acordo com os objetivos do estudo.

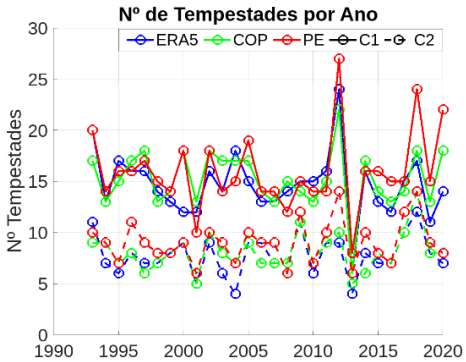

Figura 3. Número de tempestades por ano, considerando os critérios C1 e C2, para as diferentes bases de dados.

Em média, o critério C1 resulta em 15 tempestades por ano, enquanto o critério C2 resulta em 8, sendo que a base de dados PE foi a que registou o maior número de ocorrências. 2013-2014 corresponde ao ano com menor número de tempestades, quer no critério C1, quer no critério C2, nas 3 bases de dados. Contudo o ano de 2013-2014 teve tempestades mais longas, o que resulta também em registos elevados de energia, correspondendo ao ano com tempestades mais energéticas no período em análise. O maior número de tempestades ocorreu em 2012-2013, quando se

considera o critério C1, com valores entre 22 e 27 tempestades (ERA5, COP e PE). Para C2, os anos com mais tempestades são 2018-2019 (ERA5, COP e PE) e 2012-2013 (PE), com 12 a 14 registos de tempestade, dependendo da base de dados utilizada.

A análise ANOVA revelou diferenças estatisticamente significativas ($P < 0.05$), entre as diferentes bases de dados e critérios de definição de tempestade. As variações podem ser explicadas pelas diferentes fontes, resolução espacial e/ou dos métodos de cálculo, que afetam a frequência e intensidade com que os eventos de tempestade são registados.

4. CONCLUSÃO

Foi realizada uma comparação da altura significativa da onda (H_S), período de pico (T_P) e direção de proveniência da onda (Dir), com base em três fontes de dados modelados: ERA5, COP e PE. Estes dados foram também comparados com registos em boia.

A análise estatística às distribuições acumuladas (teste KS) mostrou que, para o nível de significância adotado, não foram encontradas diferenças estatisticamente significativas ($P > 0.05$) nas distribuições acumuladas das séries de dados, com os períodos de pico da COP a apresentarem as maiores diferenças. Ao comparar as distribuições acumuladas das diferentes bases de dados com registos da boia de Leixões costeira (valores medidos), verifica-se que as séries passam no teste KS ($P > 0.05$). As maiores diferenças para os valores observados registam-se também entre os períodos de pico da COP.

O teste-T revelou diferenças estatísticas entre as médias das variáveis nas bases de dados ($P < 0.05$), exceto para a altura significativa da onda, entre ERA5 e PE, consideradas semelhantes pelo teste. Ao comparar as séries das diferentes bases de dados com o observado na boia de Leixões, verifica-se que apenas as bases de dados de T_P e Dir, ambas do ERA5, podem ser consideradas semelhantes pelo teste.

Por fim, a análise ANOVA indicou que o número anual de tempestades varia consoante a base de dados e critério adotado ($P < 0.05$), indicando que a frequência de ocorrência de tempestades é sensível, tanto à origem dos dados, como ao critério utilizado. Apesar disso, a comparação entre as bases de dados usando o critério C1 mostrou semelhanças entre as séries.

De forma geral, todas as bases de dados podem ser utilizadas para caracterizar a área de estudo. No entanto, ao comparar as diferentes bases de dados com medições em boia, o ERA5 possui maior número de casos em que os resultados não são significativamente diferentes. Assim, a escolha da base de dados deve ser criteriosa e alinhada com os objetivos específicos de cada estudo, especialmente quando se pretende aplicar os dados como elementos forçadores de simulações em modelos numéricos.

REFERÊNCIAS

Boccotti, P. (2000). Wave Mechanics for Ocean Engineering. Elsevier Science B.V., Amesterdam, The Netherlands.

Brown, M.B. e Forsythe, A.B. (1974). 372: The Anova and Multiple Comparisons for Data with Heterogeneous Variances. *Biometrics*, 30(4), 719–724.

Cheng, W.C. e Wang, Y.H. (2018). Influences of sea level rise on tidal dynamics in the Taiwan Strait. *Journal of Coastal Research*, 34(3), 728-737.

Cunha, J., Elliott, M., Villasante, S., Balbi, S., Cabecinha, E. e Ramos, S. (2025). Assessing cumulative risks to coastal and marine habitats under management and climate change scenarios: The case of northern Portugal. *Ocean and Coastal Management*, 268, 107756.

Davies, G., Callaghan, D.P., Gravois, U., Jiang, W., Hanslow, D., Nichol, S. e Baldock, T. (2017). Improved treatment of non-stationary conditions and uncertainties in probabilistic models of storm wave climate. *Coastal Engineering*, 127, 1-19.

Kummu, M., De Moel, H., Salvucci, G., Viviroli, D., Ward, P.J. e Varis, O. (2016). Over the hills and further away from coast: global geospatial patterns of human and environment over the 20-21st centuries. *Environmental Research Letters* (2016).

Lira-Loarca, A., Cobos, M., Losada, M.Á. e Baquerizo, A. (2020). Storm characterization and simulation for damage evolution models of maritime structures. *Coastal Engineering*, 156.

Magdalena, I., Abidin, M.A., Azis, M.I., Widowati e Solekhudin, I. (2025). The effectiveness of the combination of breakwater and trench in reducing waves. *Results in Engineering*, 25, 103530.

Marsaglia, G., Tsang, W. e Wang, J. (2003). Evaluating Kolmogorov's Distribution. *Journal of Statistical Software*, 8(18), 1-4.

Oliveira, T.C.A., Neves, M.G., Fidalgo, R. e Esteves, R. (2018). Variability of wave parameters and Hmax/Hs relationship under storm conditions offshore the Portuguese continental coast. *Ocean Eng.*, 153, 10–22.

Roelvink, D., Reniers, A., Van Dongeren, A. P., De Vries, J.V.T., McCall, R. e Lescinski, J. (2009). Modelling storm impacts on beaches, dunes and barrier islands. *Coastal Engineering*, 56(11-12), 1133-1152.

Romão, S., Silva, P.A., Taborda, R., Cascalho, J., Silva, A.N. e Baptista, P. (2024) Assessing shoreface sediment transport at Costinha beach, Aveiro, Portuguese Northwest coast. Marine Geology, 467, 107200.

Seber, G.A. F. e Lee, A.J. (2003). *Linear Regression Analysis*. 2nd ed. Hoboken, NJ: Wiley-Interscience.

Small, C. e Nicholls, R.J. (2003) A global analysis of human settlement in coastal zones. *Journal of coastal research*, 19(3), 584-599.

Zhang, J., Tsai, B., Rafati, Y., Hsu, T.-J e Puleo, J.A. (2025). Cross-shore hydrodynamics and morphodynamics modeling of an erosive event in the inner surf zone. *Coastal Engineering*, 196, 104662.

Investigation of the suitability of machine learning for improving wave height forecasts in the Iberian Peninsula

C. Poullain (1) and J. L. Garzon (1)

(1) Centro de Investigação Marinha e Ambiental (CIMA), Rede de Infraestutura em Investigação Aquática (ARNET), Universidade do Algarve, Faro, Portugal. cazwinz@ualg.pt

Abstract: Reliable wave forecast systems are essential for many sectors of the blue economy. However, these systems can lack accuracy, especially during extreme events. The goal of this work is to develop a methodology to improve their accuracy by using the error prediction technique. Thus, the error will be predicted using machine learning models, and this error can be used to adjust the forecast system outputs at a given location. The Gijon buoy in the Cantabric sea was selected to correct the spectral significant wave height forecasted by the AIB system. The results show that this technique successfully managed to reduce the error of this system, especially during storm conditions, where the root-mean-square error was reduced between 46% and 55% for the forecast horizon assessed (6h, 12h and 24h).

Keywords: *Error prediction, XGBoost, Gijón, AIB system, spectral significant wave height*

1. INTRODUCTION

The blue economy includes activities such as tourism, marine energy, ship traffic that provide resources for economic growth and improved livelihoods. For the proper functioning and success of these activities, accurate predictions of wave height are essential. Also, skillful forecasts are critical for releasing timely alerts to protect coastal communities and save millions of euros and lives. Several agencies forecast wave conditions based on physics-based numerical models, artificial intelligence, and data assimilation. However, these systems are not faultless and they can lack accuracy, especially during extreme conditions. Thus, it is key to create methodologies that can contribute to developing more reliable forecast systems. In this regard, data assimilation from observations arises as a relevant tool. The so-called "Error prediction" method has proved to be a suitable approach to improve model predictions of different output variables at a specific location (Callens *et al*., 2020). This method requires 1) computing the errors between the modeled and observed values for past events, 2) developing techniques able to predict these errors and 3) incorporating the predictions of the error into the forecast systems, increasing their accuracy. A pivotal aspect of this procedure is the prediction of the errors. In that sense, machine learning algorithms are very suitable tools for this purpose owing to their excellent ability to simulate nonlinear mechanisms governing physical processes. Thus, the main goal of this work is to explore the suitability of data assimilation and machine learning techniques to improve the accuracy of the Peninsula and Balearic Islands (AIB) system to forecast wave conditions up to the next 24 hours.

2. METHODS

2.1 Study area and data

The suitability of the error-prediction method was investigated at the Gijón buoy. The required wave height observations were obtained from a buoy located in the Cantabric Sea, a few kilometers offshore from the northern coast of Spain (Lon = 5.66W and Lat = 43.62N) (Figure 1). The mooring depth is 54 m and the equipment is managed by the Spanish agency Puertos del Estado.

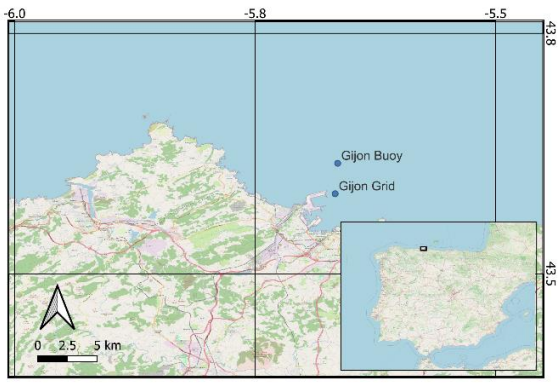

Figure 1. Location map showing the position of the Gijon buoy and the closest wave forecast grid node.

The wave forecast system assessed was the AIB system also managed by Puertos del Estado. This operational system provides hourly forecast information for the next 72 hours in advance. Updated predictions are released twice every day (midnight and noon). The predicted variables include: spectral significant wave height (VHM0), primary and secondary swell spectral significant wave height, wind sea spectral significant

wave height, wave direction relative to true north, primary and secondary swell direction relative to true north, wind sea direction relative to true north, spectral moments (0,2) wave period, primary and secondary swell spectral moments (0,2) wave period, wind sea spectral moments (0,2) wave period, and wave spectrum peak period. The model has a horizontal resolution of 0.027 degrees. The closest grid point to the buoy location was selected (Lon =5.66W, Lat =43.58N).

In addition, atmospheric information was obtained from the WRF-2D MeteoGaliza forecast system at the closest grid point to the Gijón buoy. The variables obtained were mean sea level pressure, wind module and direction at 10m, wind gust, and sea surface temperature. This system provides hourly forecasts for the next 84 hours.

The VHM0 forecast error (the target variable, calculated as wave height forecast minus observed wave height) along with the previously mentioned prediction variables (input variables) is integrated into the dataset to develop the machine learning models. This dataset spans from October 2018 to March 2025. We aim to improve the VHM0 predicted error for the forecast horizons of 6, 12 and 24 hours.

2.2 Machine learning for error prediction

In this work, the extreme gradient boosting (XGBoost) algorithm was selected to correct the AIB predictions. This algorithm has been successfully used for this task in previous studies (eg. Callens *et al*., 2020). Gradient boosting is a technique that builds an ensemble of shallow decision trees (weak learners – machine learning models that perform slightly better than chance), which sequentially minimize a loss function and hence reduce the overall prediction error by following the gradient of the loss (Callens *et al*., 2020). For regression tasks, the standard choice is the squared loss function, which is also applied in this study. XGBoost is a powerful and efficient version of gradient boosting decision trees, which is widely used due to its high performance and scalability (Chen, 2016).

To incorporate the temporal dynamics of the data, three lags were generated for each input variable. For instance, in the case of a 6-hour forecast horizon, Lag 1 corresponds to the 24-hour forecast from the previous day, Lag 2 to the 12-hour forecast, and Lag 3 to the 6-hour forecast — all from the same previous day. Additionally, cyclical features such as wind and wave direction were encoded using sine and cosine functions to account for the vicinity of higher and lower directions. The dataset was then temporally divided into a training/validation set (2018–2023) and a test set (2024–2025). Hyperparameters influence the quality of the predictions significantly. Different combinations of hyperparameters (see Table I) were tested and the combination that yielded the lowest error was chosen for the model. This work used a grid search algorithm to find the optimal combination.

Table I. Hyperparameter ranges for XGBoost

Paramter	Range
n_estimators	300, 600, 900
max_depth	3, 5, 7
learning_rate	0.01, 0.05, 0.1
subsample	0.7, 1
colsample_bytree	0.7, 1
gamma	0, 1, 5

2.3 Experiments

A set of experiments was designed to develop the error prediction model and to understand the importance of its components. The tested models with their main characteristics are shown in Table II.

Table II. Model characteristics

Id	Months	Lags	Station-dataset
0	May - Sept	0	Gijón
1	May-Sept	3	Gijón
2	Jan-Dec	3	Gijón

Models 0 and 1 were developed only with data from May to September, since during this period, the wave energy is lower, and consequently, the forecast error is lower as well. Moreover, they will allow to assess the importance of including lags in the model. Finally, model ID_2 considered data from every month in its development.

2.4 Model performance metrics

The model performance accuracy was assessed using five metrics such as:

$$Bias = \frac{\sum_{i=1}^{n}(\hat{y}_i - y_i)}{n}$$

$$\text{Mean absolute error (MAE)} = \frac{\sum_{i=1}^{n} |(\hat{y}_i - y_i)|}{n}$$

$$\text{R} - \text{squared } (\text{R}^2) = 1 - \frac{\sum_{i=1}^{n} (\hat{y}_i - y_i)^2}{\sum_{i=1}^{n} (\bar{y}_i - y_i)^2}$$

$$\text{Root mean squared error (RMSE)} = \sqrt{\frac{\sum_{i=1}^{n} (\hat{y}_i - y_i)^2}{n}}$$

$$\text{Scatter index (SI)} = \frac{RMSE}{\bar{y}_i}$$

where y_i is the observed wave heights, $\hat{y}_i$ is the predicted wave height, $\bar{y}_i$ is the mean of the observed wave height and *n* the total number of values. Lower values of the MAE, RMSE and SI along with a higher R^2 and a bias closer to zero, indicate better model performance. These metrics were computed for VHM0 predicted for both cases, AIB predictions and ML

corrected predictions. The former case will be considered as the base model.

3. RESULTS AND DISCUSSION

Models 0 and 1 aimed to correct the forecast error for the summer months (April – September). Their performance was assessed on the test dataset (2024 and 2025) across 6h, 12h, and 24h forecast horizons (Table III). Both Model 0 (no lags) and Model 1 (3 lags), outperformed the base model in nearly all skill metrics. At 12h, Model 1 achieved the lowest MAE (0.16) and highest R^2 (0.85), while also reducing SI from 0.18 (base) to 0.16. At 12h, Model 0 showed the strongest improvement in RMSE (from 0.23 to 0.21), SI (from 0.18 down to 0.16) and R^2 (from 0.81 to 0.85). For the 24h forecast, both models substantially reduced error metrics and improved R^2 from 0.77 (base) to 0.84 (Model 0) and 0.85 (Model 1), with SI decreasing from 0.19 to 0.16 for both models. Overall, the reduced scatter index across all horizons indicates improved accuracy in the corrected forecasts, with both lagged and non-lagged models delivering consistent forecast improvement. No significant differences were found between Model 0 and Model 1 in any of the three horizons assessed.

Table III. Model skills for the diferent forecast horizons.

Forecast	Metrics	Base Model	ID_0	ID_1
6h	MAE	0.19	0.16	0.16
	RMSE	0.26	0.21	0.26
	R2	0.76	0.84	0.84
	SI	0.20	0.16	0.16
	Bias	0.00	0.00	0.00
12h	MAE	0.18	0.15	0.16
	RMSE	0.23	0.21	0.21
	R2	0.81	0.85	0.85
	SI	0.18	0.16	0.16
	BIAS	0.05	0.00	0.01
24h	MAE	0.20	0.16	0.16
	RMSE	0.26	0.22	0.21
	R2	0.77	0.84	0.85
	SI	0.19	0.16	0.16
	BIAS	-0.07	0.00	0.00

The performance of Model 2, which is based on the entire year (January – December) and includes 3 lags, was also assessed across the 6h, 12h and 24h forecast horizons. The best overall skills were achieved for the 6h forecast, decreasing MAE from 0.25 (base) to 0.18, RMSE from 0.36 to 0.25 and improving R^2 from 0.83 to 0.91 (Figure 2). The SI was also decreased from 0.22 to 0.16 while keeping the bias constant. For the 12h and 24h forecast horizons, the model achieved an R^2 of 0.9 and an MAE of 0.19 (reduced from 0.25 and 0.27, respectively). The RMSE for the 12h forecast was also reduced from 0.36 to 0.26, and from 0.39 to 0.25 for the 24h forecast horizon.

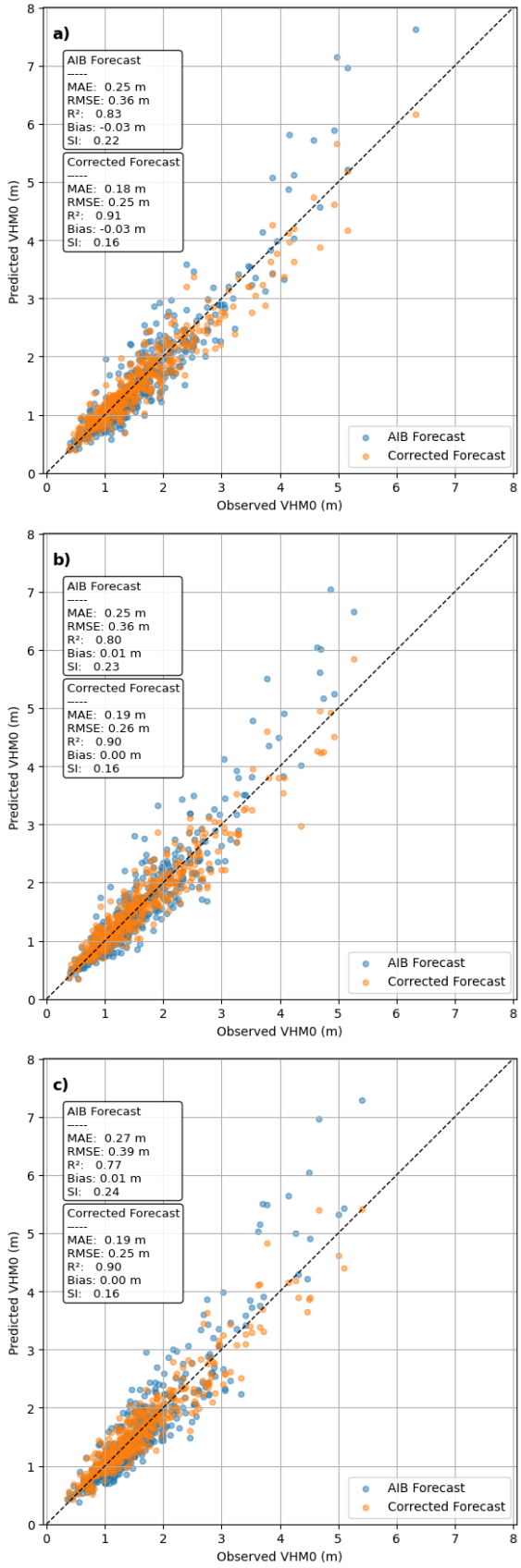

Figure 2. Model 2 skills (January - December): a) 6h forecast, b) 12h forecast, c) 24h forecast.

The SI was reduced from 0.23 and 0.24 (base for 12h and 24h, respectively) to 0.16 in both cases.

It is important to highlight that the model showed a strong performance especially for higher wave heights, where the base model struggled to maintain small errors, as can be seen in Figure 2. To further investigate the models performance for extreme cases, Table IV presents the skills evaluated by low-energy (low 95% of observed wave heights) and high-energy (high 5% of observed wave heights) events. The results show clearly that the AIB model faced severe problems to accurately predict high energy waves (even negative R^2 scores for all forecast horizons), while Model 2 improves these predictions reaching R^2 scores of 0.52, 0.34 and 0.29 for 6h, 12h and 24h forecast horizons, respectively. The MAE could be reduced from 0.66 to 0.4 (RMSE from 0.91 to 0.49) for 6h, from 0.78 to 0.4 (RMSE from 0.98 to 0.5) for 12h, and from 0.85 to 0.41 (RMSE from 1.12 to 0.51) for the 24h forecast of high-energy waves, indicating an improvement of more than 50% in some cases.

Table IV. Model skills for different forecast horizons and separated for low-energy and high-energy conditions.

Forecast	Metrics	Low Energy		High Energy	
		Base	ID_2	Base	ID_2
6h	MAE	0.22	0.17	0.66	0.4
	RMSE	0.30	0.23	0.91	0.49
	R2	0.75	0.84	-0.64	0.52
	SI	0.20	0.16	0.22	0.12
	Bias	-0.05	-0.01	0.44	-0.28
12h	MAE	0.22	0.18	0.78	0.40
	RMSE	0.31	0.24	0.98	0.50
	R2	0.75	0.85	-1.48	0.34
	SI	0.21	0.16	0.24	0.12
	BIAS	-0.02	0.01	0.68	-0.18
24h	MAE	0.24	0.18	0.85	0.41
	RMSE	0.31	0.23	1.12	0.51
	R2	0.73	0.85	-2.45	0.29
	SI	0.21	0.16	0.27	0.12
	BIAS	-0.03	0.01	0.72	-0.15

The results demonstrate that forecast error correction using both seasonal (Models 0 and 1) and all-year (Model 2) approaches can substantially improve wave height prediction accuracy. Model 0 and 1 performed similarly well across the board, while Model 2, trained on year-round data and enriched with lagged features, further emphasized the potential of the correction method using an expanded dataset and lagged variables to account for past values. The model performance was especially good with respect to high energy waves, improving significantly the AIB model in these extreme cases, which often have deeper impacts on real-world applications like marine safety, energy prediction or storm response. Even at longer horizons (24h), Model 2 maintained a similar level of skill to the shorter horizons, while the base model exhibited a reduction in accuracy with longer horizons.

4. FUTURE WORK

We aim to include more stations around the Iberian Peninsula, covering from the North Atlantic up to the Mediterranean Sea, to improve our approach with regard to different hydrographic and meteorological conditions. Also, we will compare the results achieved by the XGBoost algorithm with ML models based on Artificial Neural Networks (ANNs) and Convolutional Neural Networks (CNNs). Likewise, the effectiveness of these techniques to improve two more forecast horizons, 48h and 72h, will be investigated.

5. CONCLUSIONS

This study demonstrated that machine learning–based error prediction is an effective strategy to enhance the accuracy of wave forecasts from the AIB system (at given locations). By correcting forecast errors using XGBoost models, we achieved consistent improvements across all evaluated forecast horizons (6h, 12h, and 24h). Both seasonal (summer-only) and full-year models significantly reduced MAE, RMSE, and SI, while increasing the coefficient of determination (R^2), indicating more precise and reliable forecasts. This improvement was especially important for extreme cases. This highlights the potential of integrating data assimilation and machine learning into operational wave forecasting systems to contribute to the proper functioning of the blue economy sector.

Acknowledgements

This research has been funded by the FCT under the project DAMA (Ref: 2023.14738.PEX) https://doi.org/10.54499/2023.14738.PEX. The second author has been funded by the FCT through the project with reference CEECINST/00146/2018/CP1493/CT0012. The authors also acknowledge FCT funding to the Associate Laboratory ARNET under the project LA/P/0069/2020 and CIMA through the grant UIDP/00350/2020 (https://doi.org/10.54499/UIDP/00350/2020).

REFERENCES

Callens, A., Morichon, D., Abadie, S., Delpey, M. and Liquet, B. (2020). Using Random forest and Gradient boosting trees to improve wave forecast at a specific location. *Applied Ocean Research*, 104, 102339. https://doi.org/10.1016/j.apor.2020.102339

Chen, T. and Guestrin, C. (2016). Xgboost: a scalable tree boosting system. *Proceedings of the 22nd ACM SIGKDD International Conference on Knowledge Discovery and Data Mining*, San Francisco, 13-17 August 2016, 785-794. https://doi.org/10.1145/2939672.2939785

Artificial Intelligence for Short-Term Forecasting of Ocean Surface Currents in the South Coast of Iberia

L. Lamas (1), N. Zacarias (1), M. Narayan (1), P. Pinto (1), V. Lima (1), T. Dias (1), C. Videira (1) and T. Barroqueiro (1)

(1) Instituto Hidrográfico, Lisboa, Portugal. luisa.lamas@hidrografico.pt

Abstract: Within the AI-DORIS project, Instituto Hidrográfico (IH) is developing a short-term forecasting model based on artificial intelligence (AI), and data collected by MONIZEE's high-frequency radar (HFR) network on the south coast of the Iberian Peninsula—a region marked by complex and dynamic oceanographic conditions. The HFR-South network has been monitoring this area since 2016, offering a robust and extensive dataset for the development and testing of predictive models, with the aim of improving forecast accuracy at spatial and temporal scales relevant for coastal processes and maritime operations. This work focus on the results of AI-DORIS project, including the assessment of different machine learning algorithms, the performance of the model and the integration of the data and results into IH's marine spatial data infrastructure, Hidrográfico+, in compliance with FAIR principles and open data policies.

Keywords: *Coastal Monitoring, Ocean Currents, Machine Learning, Forecast, High Frequency Radars*

1. INTRODUCTION

Accurate knowledge of ocean surface currents is crucial for a wide range of applications, including environmental monitoring, climate and weather forecasting, marine navigation, search and rescue operations, offshore infrastructure planning, and marine resource management (Röhrs *et al.* 2021).

Surface current information is typically obtained through a combination of numerical models and observational techniques. Among observational methods, high-frequency radar (HFR) systems have emerged as a leading technology for providing the most effective measurements of surface currents over large coastal areas (Roarty *et al*., 2019). HFR systems operate by transmitting radio waves that scatter off ocean surface waves; the analysis of backscattered signals enables the estimation of surface current speed and direction (Barrick *et al*. 1977).

Despite their extensive spatial coverage, HFR systems do not provide forecasts, required for most operational applications. Hydrodynamic models are widely used for operational forecasts and decision support. While offering significant predictive capabilities, they are computationally intensive and often constrained by simplified parameterizations, which can limit their accuracy, especially at high spatial resolutions. In recent years, machine-learning approaches have gained relevance due to their favorable trade-off between computational demand and forecast precision. Several studies have demonstrated the potential of machine learning techniques for short-term HFR-based current prediction, offering a promising alternative to traditional methods (Frolov *et al*., 2012, Ren *et al.* 2018, Cavaiola *et al.* 2025).

2. PROJECT AI-DORIS

The AI-DORIS project (Figure 1) aims to develop an AI-driven short-term ocean surface current forecasting model using HFR data. The project will leverage emerging AI methods alongside IH's existing resources to collect high-quality ocean current data.

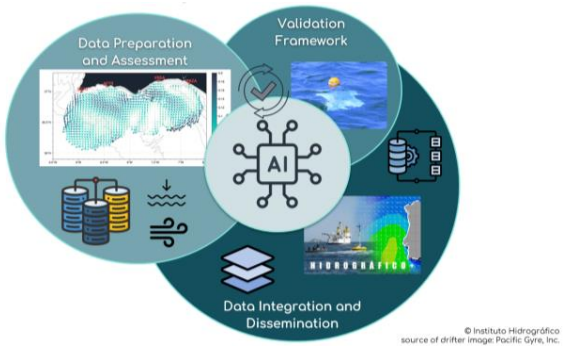

Figure 1. Graphical Abstract of AI-DORIS project.

The target area is situated on the south coast of the Iberian Peninsula, where the HFR network "HFR-South" has been in operation since 2016 (Figure 2). This network, part of the Portuguese Coastal Ocean Monitoring Network (MONIZEE) and integrated within the Joint European Research Infrastructure of Coastal Observatories (JERICO-RI), consists of four HFR antennas: three located along the Portuguese south coast (Sagres, Alfanzina, and Vila Real de Santo António) and one on the Spanish coast (Mazagón).

The region is located in the western part of the Gulf of Cadiz, characterized by complex ocean dynamics with different temporal and spatial scales. On the Atlantic side, the southwestern coast of Iberia is influenced by the larger-scale current system that comprises the Portugal, Canary and Azores Currents (Garcia Lafuente *et al*. 2006), and by a complex smaller scale system of currents and counter-currents that occur over the slope and shelf (Fanelli *et al.* 2024). On the eastern side, the dynamics are dominated by the interaction between the Atlantic and the Mediterranean waters entering the Gulf of Cadiz from the Strait of Gibraltar (Peliz *et al.* 2007). The south coast of Iberia is also known for its intense maritime traffic and marine activities, like fisheries, aquaculture, nautical sports and commercial shipping (EMODnet 2025).

The complexity of the ocean dynamics together with the availability of a long time series of HFR data, make this an ideal region to develop and deploy a short-term forecast service of ocean currents based on AI. Maritime actors, but in particular the ones that have responsibilities in the safeguard of life at sea, can benefit greatly from improved and accurate forecasts of surface currents, enhancing their operational efficiency and effectiveness.

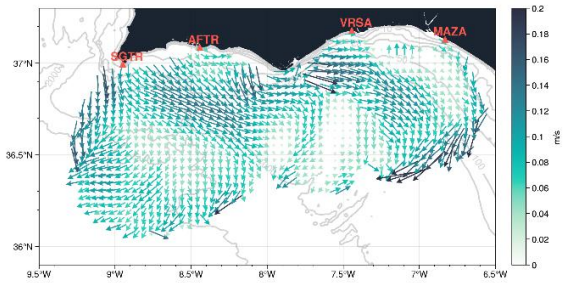

Figure 2. Surface current vectors (colored by magnitude) from the HFR-South network. Red markers indicate antennae locations: SGTR (Sagres), AFTR (Alfanzina), VRSA (Vila Real de Santo António), and MAZA (Mazagón).

3. EXPECTED OUTCOMES

All data products generated by the AI-DORIS project will be catalogued, integrated, and made available through the IH's marine spatial data infrastructure, Hidrográfico+, in accordance with the FAIR principles and relevant national and European open data policies. Data will be available for visualization through the H+ geoportal and for download through a THREDDS Data Server.

The project's primary beneficiaries include public agencies responsible for maritime safety and defense, such as the National Maritime Authority and the Portuguese Navy. However, the results are expected to support a wider user base, encompassing both public and private marine stakeholders. By applying advanced AI techniques to maximize the utility of existing HFR datasets, AI-DORIS contributes to national digital transformation goals and the development of high-value, data-driven services for scientific, operational, and societal applications.

Acknowledgements

The project AI-DORIS is funded by FCT https://doi.org/10.54499/2024.07521.IACDC.

HFR-South network is managed by Instituto Hidrográfico, Portugal and Puertos del Estado, Spain. https://doi.org/10.57762/RNCF-D423.

REFERENCES

Barrick, D. E., Evans, M. W., and Weber, B. L. (1977). Ocean surface currents mapped by radar. *Science*, 198(4313), 138-144.

Cavaiola, M., Marini, S., Magaldi, M. G., and Mazzino, A. (2025). AI-driven 6-hour ahead nowcasting of sea-surface currents using HF radar. *Applied Ocean Research, 158*, 104542.

European Marine Observation and Data Network (EMODnet) (2025). *Human Activities.*

Fanelli, C., Gomiz Pascual, J. J., Bruno-Mejías, M., and Navarro, G. (2024). Using a combination of high-frequency coastal radar dataset and satellite imagery to study the patterns involved in the coastal countercurrent events in the Gulf of Cadiz. *Remote Sensing*, 16(4), 687.

Frolov, S., Paduan, J., and Cook, M. (2012). Improved statistical prediction of surface currents based on historic HF-radar observations. *Ocean Dynamics*, 62, 1111-1122.

García Lafuente, J., Delgado, J., Criado-Aldeanueva, F., Bruno, M., del Río, J., and Vargas, J. M. (2006). Water mass circulation on the continental shelf of the Gulf of Cádiz. *Deep Sea Research Part II: Topical Studies in Oceanography*, 53, 1182–1197.

Peliz, A., Dubert, J., Marchesiello, P., and Teles-Machado, A. (2007). Surface circulation in the Gulf of Cádiz: Model and mean flow structure. *Journal of Geophysical Research: Oceans*, 112, C11015.

Ren, L., Hu, Z., and Hartnett, M. (2018). Short-term forecasting of coastal surface currents using high frequency radar data and artificial neural networks. *Remote Sensing*, 10(6), 850.

Roarty, H., Cook, T., Hazard, L., George, D., Harlan, J., Cosoli, S., Wyatt, L., Alvarez Fanjul, E., Terrill, E., Otero, M., Largier, J., Glenn, S., Ebuchi, N., Whitehouse, B., Bartlett, K., Mader, J., Rubio, A., Corgnati, L., Mantovani, C., Griffa, A., Reyes, E., Lorente, P., Flores-Vidal, X., Saavedra-Matta, K. J., Rogowski, P., Prukpitikul, S., Lee, S.-H., Lai, J.-W., Guerin, C.-A., Sanchez, J., Hansen, B., and Grilli, S. (2019). The global high frequency radar network. *Frontiers in Marine Science*, 6.

Röhrs, J., Sutherland, G., Jeans, G., Bedington, M., Sperrevik, A. K., Dagestad, K. F., and LaCasce, J. H. (2021). Surface currents in operational oceanography: Key applications, mechanisms, and methods. *Journal of Operational Oceanography*, 16(1), 60–88.

Evolução do vento e da profundidade da camada de mistura, nos sistemas de afloramento da corrente das Canárias e da Califórnia, de 1981 a 2020

J. M. R. Alves (1,2,3) e R. Caldeira (2,3)

(1) Universidade da Madeira, Faculdade Ciências da Vida. jose.alves@oom.arditi.pt
(2) Observatório Oceânico da Madeira, Agência Regional para o Desenvolvimento da Investigação Tecnologia e Inovação, Funchal, Madeira
(3) Instituto Dom Luiz, Faculdade de Ciências da Universidade de Lisboa

Abstract: Coastal upwelling systems are well-known for their productivity. Given their significant ecological and socio-economic importance, it is essential to assess the impact of global warming on these areas of wind stress and sea surface temperature intense cross-shore gradients. Here, we assessed the coastal wind stress, SST, and mixed layer depth evolution, analysing the ERA5 and the SODA reanalyses, in the Canaries and California upwelling systems. Warming of the upper ocean leads to increased vertical stratification and reduced upward transport, which sets intensified wind stress and upper ocean warming in a competitive role. Results show a preponderance of wind stress effects, which reduce upper ocean stratification, except in zones of intense surface warming, such as in the north of the California system, where a more stratified upper ocean is observed despite increasing wind stress.

Keywords: *coastal upwelling, global warming, wind, SST, mixed layer depth*

1. INTRODUÇÃO

As regiões de afloramento costeiro são importantes ecossistemas marinhos devido à sua elevada produtividade, o que as torna relevantes para atividades piscatórias. Estimativas indicam que 20% das pescas globais ocorrem em zonas de afloramento, que representam somente cerca de 2% da área dos oceanos (Pauly e Christensen, 1995). Devido à sua importância ecológica e socioeconómica é essencial analisar a sua evolução no passado e no futuro, em detalhe.

Para o final do século XXI um estudo recente mostrou que cenários do IPCC (Intergovernmental Panel on Climate Change) indicam um aumento significativo do vento na margem Ibérica Atlântica no Verão, associado a uma intensificação da depressão térmica da Ibérica (Alves *et al.*, 2025), o que deverá impor uma intensificação do afloramento costeiro. No presente estudo iremos averiguar se já existem indícios destas tendências, nos últimos 40 anos (1981-2020). Também será analisada a evolução da estratificação na camada superior do oceano, pois a sua intensificação tem um efeito contrário ao do vento no afloramento, por obstar ao transporte vertical.

1.1. Dados e métodos

Os sistemas de afloramento costeiro são caraterizados por intensos gradientes perpendiculares à costa de vento e de temperatura da superfície do mar, o que torna difícil quantificar com precisão a sua evolução multi-decadal recorrendo a simulações globais, que normalmente têm 1° a 2° de resolução espacial.

Neste estudo utilizamos dados das reanálises atmosférica ERA5 (Herbash *et al.*, 2020) e oceânica SODA 3.2.15 (Carton *et al.*, 2018), com ¼° (aproximadamente 31 km) de resolução espacial. A reanálise do oceano foi selecionada por ser forçada com dados ERA5 e compreender os 40 anos em estudo (1981-2020), com a mesma resolução. Estas reanálises combinam dados simulados numericamente com observações locais de estações meteorológicas, satélites, boias oceânicas e balões meteorológicos, o que as torna excelentes produtos para análises de processos climáticos de mesoescala no oceano e na atmosfera.

Utilizamos os dados ERA5 para analisar a evolução da temperatura de superfície do oceano, da tensão do vento e do correspondente rotacional e utilizamos os dados SODA para analisar e evolução da profundidade da camada de mistura (PCM), que mostra a profundidade onde a temperatura difere da camada de superfície (z=5m) por 0.2K.

As tendências foram estimadas pelo método de Theil-Sen (Theil, 1950 ; Sen, 1968), onde estas são calculadas pela mediana de todos os declives entre cada para pare de dados, o que torna o método robusto na análise de dados com valores extremos. Para calcular as tendências sazonais no Verão (Junho-Julho-Agosto) os dados foram previamente filtrados em cada célula

do domínio computacional removendo o ciclo anual médio.

2. RESULTADOS

O afloramento costeiro é essencialmente influenciado pela intensidade do transporte de Ekman, que pode ser dividido em contribuições da divergência costeira (ou seja, transporte perpendicular à costa) impulsionado pela componente do vento ao longo da costa e contribuições de correntes verticais impulsionadas pelo rotacional da tensão do vento. Por esta razão analisámos a evolução da tensão do vento e do seu rotacional.

2.1. Sistema de afloramento da corrente das Canárias

Os dados diários da reanálise ERA5 mostram que no Verão (JJA), entre 1981 e 2020, a tensão do vento intensificou-se numa estreita faixa junto à costa Oeste da Península Ibérica, aproximadamente entre 42N e 38N. A sul de 38N a intensificação é um pouco mais intensa junto à costa e estende-se para Oeste. O máximo absoluto da intensificação está localizado numa zona entre a ilha da Madeira, o cabo de São Vicente e a costa Africana (Figura 1a).

Junto à costa Oeste da Península Ibérica, em geral, a zonas de intensificação da tensão do vento correspondem zonas com um aquecimento da temperatura de superfície do mar (TSM) menor ou com arrefecimento (Figura 1c), como esperado, devido à intensificação do afloramento costeiro. Uma exceção ocorre no extremo noroeste da Península, junto ao cabo Finisterra, onde o menor aquecimento junto à costa é justificado por um aumento local do rotacional da tensão do vento responsável pelo transporte vertical (Figura 1b). O mesmo acontece na costa africana, aproximadamente entre as latitudes 30N e 32N.

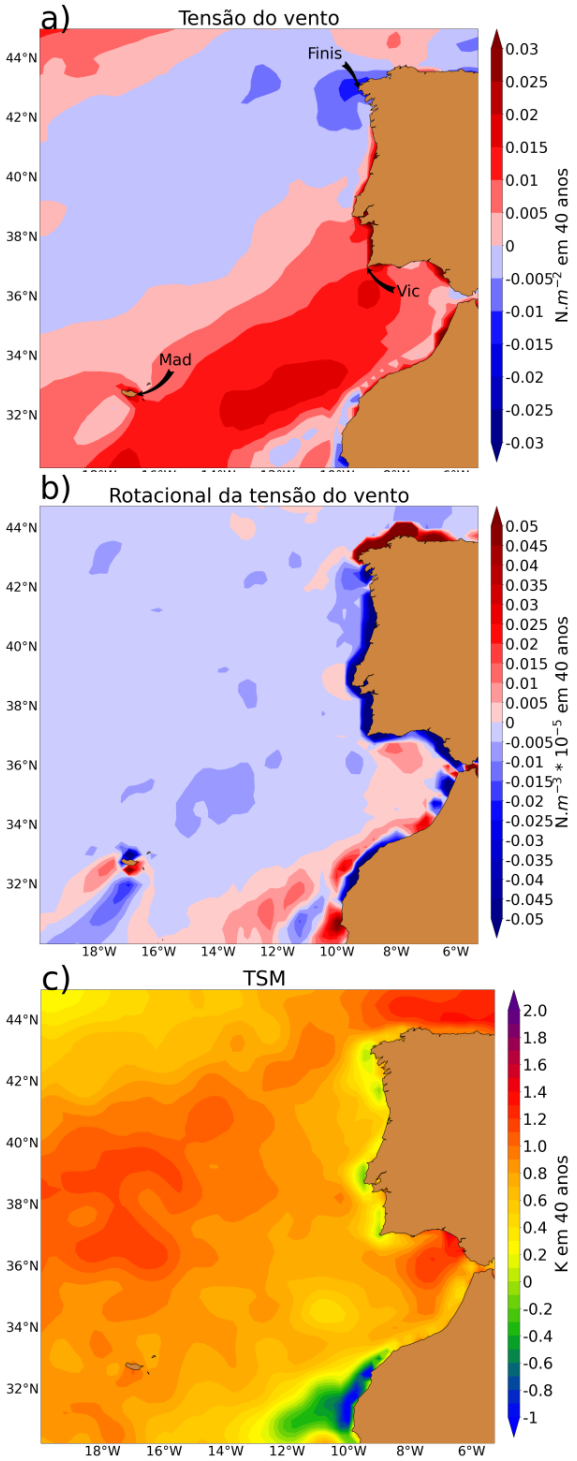

Figura 1. Tendências no Verão, junho-julho-agosto (JJA), de 1981 a 2020 calculadas pelo método de Theil-Sen com dados diários para a tensão do vento (a), rotacional da tensão do vento (b) e temperatura de superfície do mar (TSM) (c). Dados obtidos da reanálise ERA5. No painel a) as siglas Mad, Vic e Finis indicam a localização da ilha da Madeira e dos cabos São Vicente e Finisterra, respetivamente.

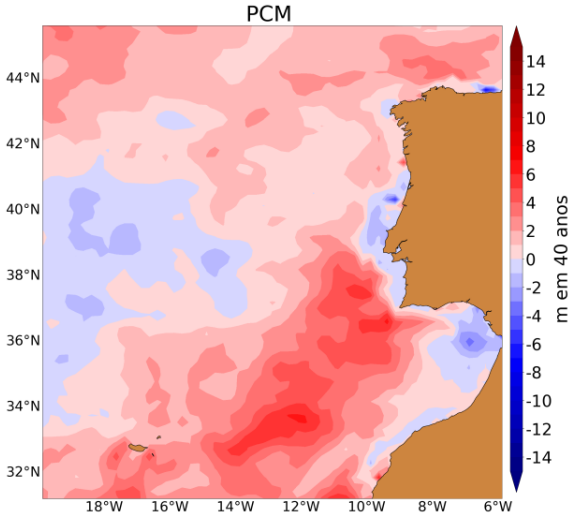

Figura 2. Tendências no Verão, junho-julho-agosto (JJA), de 1981 a 2020 calculadas pelo método de Theil-Sen da profundidade da camada de mistura (PCM) obtida da reanálise SODA3.2.15.

Analisando o efeito da evolução da tensão do vento e do aumento de temperatura à superfície na estratificação superficial do oceano, observa-se que coincidem as regiões onde a intensificação da tensão do vento e aumento da profundidade da camada de mistura são máximos (Figura 1a e Figura 2), o que mostra que nesta zona o efeito do aumento de mistura devido ao aumento da tensão do vento se sobrepõe ao efeito do aquecimento que deveria impor um oceano mais estratificado. Nas restantes zonas a PCM exibe tendências de sinal oposto, com valores reduzidos, maioritariamente entre ±1m.

2.2. Sistema de afloramento da corrente da Califórnia

No outro grande sistema de afloramento costeiro do Hemisfério Norte (localizado na corrente da Califórnia) observa-se uma intensificação da tensão do vento junto à costa, a norte do paralelo 36N (Figura 3a) o que impõe uma maior diferença na temperatura de superfície entre a costa e o largo (Figura 3b), devido à intensificação do afloramento costeiro, nestas latitudes.

Em relação à evolução da camada de mistura, a região a norte de 35N é caraterizada por uma diminuição da sua profundidade em quase todas as zonas (Figura 4), devido ao efeito do intenso aquecimento na superfície do oceano, entre 1 e 2 K, que se sobrepõe ao efeito do aumento da tensão do vento. Já a sul de 35N, onde o aquecimento não é tão intenso, observa-se uma PCM mais profunda devido à maior tensão do vento, exceto junto à costa onde o enfraquecimento da tensão do vento e as pequenas variações de temperatura à superfície impõem uma diminuição da PCM.

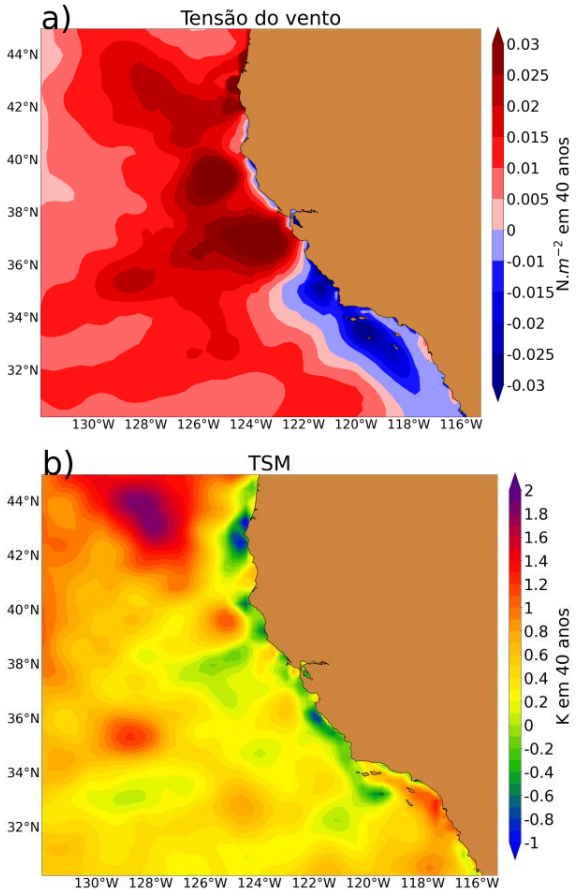

Figure 3. Tendências no Verão, junho-julho-agosto (JJA), de 1981 a 2020 calculadas pelo método de Theil-Sen com dados diários para a tensão do vento (a) e temperatura de superfície do mar (TSM) (b) com dados da reanálise ERA5.

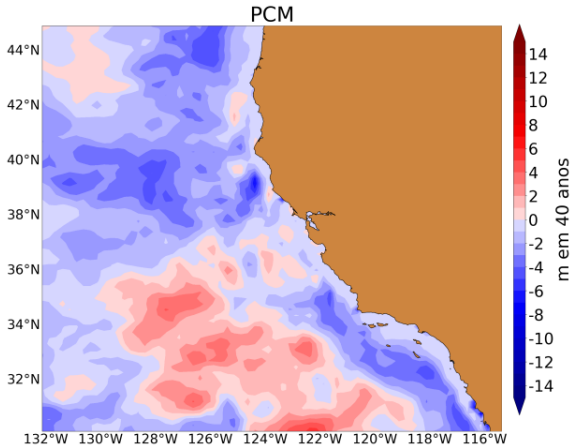

Figura 4 Tendências no Verão, junho-julho-agosto (JJA), de 1981 a 2020 calculadas pelo método de Theil-Sen da profundidade da camada de mistura (PCM) da reanálise SODA3.2.15.

3. DISCUSSÃO E CONCLUSÕES

A análise dos dois principais sistemas de afloramento costeiro do Hemisfério Norte (Canárias e Califórnia) mostra uma preponderância do efeito da tensão do vento sobre o efeito do aumento de temperatura à superfície na PCM, o que impõe um oceano menos estratificado (mais PCM) em zonas onde a tensão do vento mais se intensificou, como entre a ilha da Madeira, a costa africana e o cabo de São Vicente ou na parte sul do sistema da Califórnia. Mas em zonas onde o aquecimento na superfície do oceano é elevado observa-se uma preponderância do efeito do aquecimento à superfície que estabelece um oceano mais estratificado (menos PCM), mesmo em zonas onde a tensão do vento também se intensificou, como se verifica maioritariamente a norte no sistema da Califórnia.

O maior aquecimento e aumento da tensão do vento observado a norte na costa da Califórnia está de acordo com a expansão meridional para norte da cédula de Hadley referida em Fu *et al.* (2006), o que implica uma expansão na direção dos polos dos sistemas de afloramento costeiro. Mas o mesmo já não se observa no limite norte do sistema de afloramento da corrente das Canárias (costa oeste da Península Ibérica), possivelmente devido à orografia e orientação de linha de costa que fazem com que no Verão o anticiclone dos Açores se estenda frequentemente em crista para o Golfo da Biscaia (eg Alves *et al.* , 2025) o que faz com que a costa Oeste da Península Ibérica fique numa zona de vento pouco intenso devido ao efeito das regiões montanhosas no norte da Península no escoamento atmosférico para Sul. Sydeman *et al.* (2014) sintetizou resultados de 22 estudos sobre tendências de vento, publicados entre 1990 e 2012, e também notou que o sistema da corrente das Canárias não apresenta uma intensificação do vento no limite polar, em contraste com os outros 3 grandes sistemas de afloramento (Califórnia, Humboldt, Benguela).

Agradecimentos

Os autores agradecem ao ECMWF e à Universidade de Maryland por serem as instituições responsáveis pela elaboração das reanálises ERA5 e SODA, respetivamente.

REFERÊNCIAS

Alves, J.M.R., Miranda, P.M.A., Tomé, R. e Caldeira, R. (2025). Evolution of the subtropical surface wind in the north-east Atlantic under climate change. Climate Dynamics, 63, 3.

Carton, J.A., Chepurin. G.A. e Chen L. (2018). SODA3: a new ocean climate reanalysis. *J. Climate*, 31, 6967-6983.

Pauly, D. e Christensen, V. (1995). Primary production required to sustain global fisheries. *Nature*, 374, 255–57.

Hersbach, H., Bell, B., Berrisford, P., Hirahara, S., Horányi, A., *et al.* (2020). The ERA5 global reanalysis. *Quarterly Journal of the Royal Meteorological Society*, 146(730), 1999-2049.

Sen, P.K. (1968). Estimates of the regression coefficient based on Kendall's Tau. *J. Am. Stat. Assoc.*, 63, 1379–1389.

Theil, H. (1950). A rank-invariant method of linear and polynomial regression analysis. I, II, III, *Nederl. Akad. Wetensch., Proc.*, 53.

Sydeman, W.J., GarcíaReyes, M., Schoeman., D.S., Rykaczewski, R.R., Thompson, S.A., Black, B.A. e Bograd S.J. (2014) . Climate change and wind intensification in coastal upwelling ecosystems. *Science*, 345, 77-80.

Fu, Q., Johanson, C.M., Wallace, J.M., Reichler, T. (2006) Enhanced midlatitude tropospheric warming in satellite measurements. *Science*, 312:1179.

Theil, H. (1992). A rank-invariant method of linear and polynomial regression analysis in Henri Theil's Contributions to Economics and Econometrics. Advanced Studies in Theoretical and Applied Econometrics, Vol. 23, eds B. Raj and J. Koerts (Dordrecht: Springer).

Integrated wave-current modelling of the Arade estuary

A. Manz (1), J. L. Garzon (1), F. Martins (1) and L. Mills (1)

(1) CIMA, Centre of Marine and Environmental Research/ARNET - Infrastructure Network in Aquatic Research, University of Algarve, 8005-139 Faro, Portugal. amanz@ualg.pt

Abstract: To study wave-current interactions in coastal zones, it is necessary to establish a framework of several numerical models that are capable of not only simulating the hydrodynamic processes but also wave parameters. In this study, a high-resolution numerical framework was established to study hydrodynamics and wave parameters in the Arade estuary, South Portugal. The hydrodynamic MOHID model was validated against field data and coupled with a SWAN wave model. MOHID showed overall good agreement with water level measurements, with a maximum RMSE of 0.15 m. A comparison of the main harmonic constituents suggested a temporal delay of the tidal propagation by MOHID, potentially caused by bathymetric inaccuracies. The SWAN model results showed an increase of 0.4 m in significant wave height when currents and water levels are induced. Further assessment of the model results is needed in order to fully understand the interactions between wave propagation and surface currents.

Keywords: *numerical model, MOHID, SWAN, hydrodynamic modelling, wave-current interactions*

1. INTRODUCTION

Estuaries are highly complex and dynamic systems that are governed by tides, currents, river discharges, waves, as well as atmospheric drivers. These areas of exchange between fresh and saltwater are constantly changing in their morphology and vertical density structure. As most estuaries are densely populated areas with frequent port, fishing and recreational activities, it is particularly important to monitor and understand these systems.

To study the physical processes in estuaries like circulation, fresh and salt water mixing, stratification etc. the analysis of field observations and/or the application of numerical models have been the most common methods in recent years (Maljutenko and Raudsepp, 2019). However, to simplify and reduce the numerical effort in the assessment of hydrodynamic processes, the effect of waves is often neglected. Especially at the mouth of mesotidal estuaries, waves can have an impact on flow velocities, mixing and circulation patterns. On the other hand, it is crucial to consider the impact of surface currents when studying wave propagation in coastal regions. Previous studies have highlighted that water level variations caused by tidal oscillations strongly influences wave propagation and dissipation close to estuary mouths or inlets (Mengual *et al.*, 2022). Generally, ebb currents are considered to promote shoaling and wave steepening, as their flow is usually in the opposing direction, which can result in an increase in wave height of 20 – 80% (e.g. Dodet *et al.*, 2013; Rusu *et al.*, 2011). However, the contrary may occur when wave steepening exceeds a threshold and opposed currents can dissipate wave energy by white capping, particularly in shallow depths.

While several studies have shown the importance of investigating wave-current interactions in densely populated coastal areas, a deeper understanding of these interactions during storm wave conditions is needed. The objective of this study is to establish a high-resolution numerical framework to seamlessly simulate hydrodynamics and waves in the Arade estuary, Southern Portugal, by assimilating data from a regional system SOMA (Algarve Operational Modelling and Monitoring System). To achieve this goal, four objectives are proposed: i) Calibrate and validate the hydrodynamic MOHID-Arade model and its coupling with SOMA, ii) Develop a wave model SWAN and investigate the importance of the wave-current interaction iii) Assimilate wave information from the regional wave SOMA model and iv) Create a structure that manages input and output files automatically to run the numerical framework without human intervention. Objectives i) and ii) are addressed in this abstract and will be the foundation for the further development of objectives iii) and iv) in the short future.

Located on the South coast of Portugal, the Arade estuary is one of the main estuaries in the Algarve. It is approximately 15 km long and has a maximum width of 700 m at the river mouth (Figure 1). With a depth of 5 m on average it is relatively shallow. The two main rivers, Arade and Odelouca, are strongly regulated by upstream dams, storing water for agricultural and domestic use in the region (APS, 2017). In the lower estuary, the average freshwater discharge is approximately 10 m^3/s throughout the year and mainly governed by the tide. The area has a semi-

diurnal and mesotidal regime, with amplitudes ranging between 0.6 m and 1.3 m during neap and spring tides, while tidal currents range between 0.25 m/s on floods and 0.35 m/s on ebbs (Portela and Duarte, 2016).

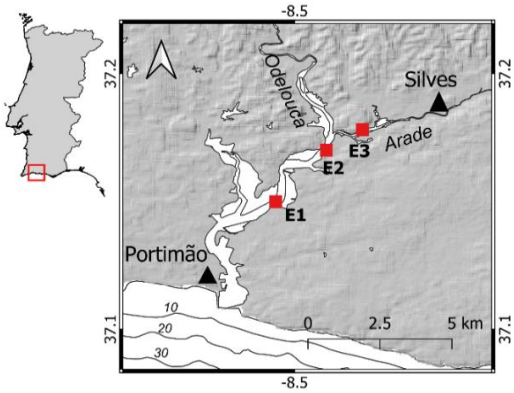

Figure 1. Map of the study area with red dots mark the locations of the deployed pressure sensors in the estuary (E1, E2, E3).

2. METHODS

2.1. MOHID model

For the simulation of hydrodynamic processes in the Arade estuary, the MOHID water modelling system was used (Martins *et al.*, 2001). MOHID solves the 3D Navier-stokes primitive equations in its incompressible form, assuming hydrostatic equilibrium as well as the Boussinesq and Reynolds approximations. Here, MOHID was used in 2D barotropic mode, with a computational constant mesh resolution of 20 m in the x-direction and a variable 20 – 45 m resolution in the y-direction, with the latter increasing towards the offshore boundary. The model domain was forced at the offshore boundary by water level, current, temperature and salinity retrieved from the SOMA (Janeiro *et al.*, 2017). To calibrate and validate the model, field observations of three pressure sensors deployed in the estuary were used (Figure 1). The model was calibrated with the model parameters bottom rugosity and viscosity, according to a previously conducted sensitivity analysis (Manz *et al.*, 2025). For further analysis, the tidal signals of both the model and the sensors were decomposed into their principal tide constituents which were then analysed for amplitude and phase errors.

2.2. SWAN model

The SWAN spectral wave model (Booij *et al.*, 1999), was used to simulate wave parameters in the entrance of the estuary. A nested approach was used, where the outer domain covered the larger Algarve region with a computational grid resolution of 165 x 140 m, passing the wave parameters at the boundary to the inner/nested domain, with a grid resolution of 20 m (Figure 2).

A synthetic storm equivalent to 50 return period of one week duration was simulated to analyse the model's wave propagation from the outer to the nested domain. In a second step, a one-way coupling of the nested SWAN model with the MOHID model was performed, in order to include sea surface height and current velocities. The importance of wave-current interactions was then investigated at a location close to the river mouth, by comparing both scenarios (SWAN and SWAN-MOHID).

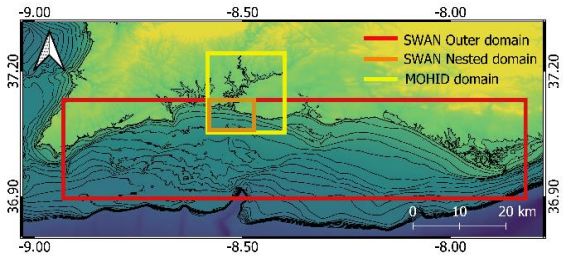

Figure 2. Map of numerical domains used for the wave simulations.

3. RESULTS AND DISCUSSION

3.1. MOHID model validation

The comparison between the observed and simulated water levels by the MOHID model at each station in the estuary are shown in Figure 3.

The results showed that generally the model estimated well the water levels at each location in the estuary, with the station closest to the river mouth (E1) having the best agreement with the field data.

The model performance deteriorated especially during spring tide conditions, where the difference between modelled and field data was larger. During those conditions, MOHID overestimated high water and underestimated low water. Overall, however, statistical measures showed a good agreement between field data and model results, with a Root-Mean-Square-Error (RMSE) of 0.14 m at E1, and 0.15 m at E2 and E3 and a Pearson correlation coefficient (r) of 0.98.

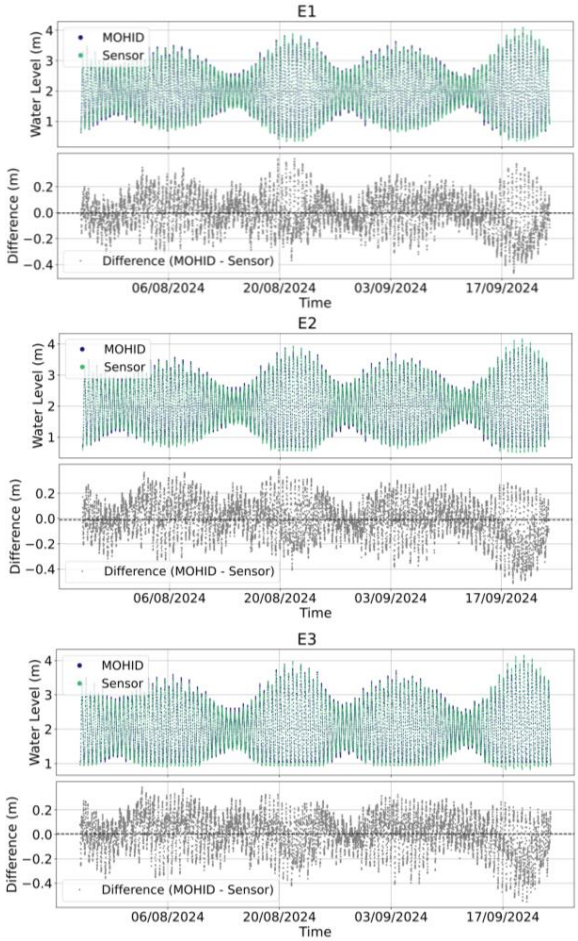

Figure 3. Comparison of observed (green dots) and simulated (blue dots) water levels in the top graph, difference between observed and simulated data in the bottom graph, for all stations E1, E2 and E3.

Table I. Results of statistics to assess level of agreement between modelled and observed water level data.

	n	RMSE	Bias	Pearson (r)	MAE
E1	8497	0.14	0	0.98	0.11
E2	8497	0.15	0.01	0.98	0.12
E3	8497	0.15	0	0.98	0.12

The analysis of the main harmonic constituents of the study area, which account for 85% of the total tidal energy, resulted in a good agreement between amplitudes and phase lags of the MOHID results in comparison with field data. Table II shows the errors of the main constituents between modelled and observed amplitudes and phase lags at each station.

The amplitudes of the five main constituents showed good agreement at all stations. While the amplitude of the main semi-diurnal constituent M2 was slightly overestimated by MOHID (0.01 m at E1 and E2), the model underestimated the amplitudes of the semi-diurnal constituents S2 and N2 and the diurnal constituent K1. In the analysis of the phase lags resulting from harmonic analyses, positive values in Table II indicated a delayed tidal signal simulated by MOHID, while negative values implied that the simulated tide propagated faster than reality. Phase differences indicating a temporal offset of the tidal signal could be observed for all constituents. The M2 constituent showed a 6° higher phase lag at all stations in MOHID simulations, which corresponds to a 12.4-minute delay of the M2 tidal peak. Similar findings were made for the S2 constituent. On the other hand, the N2 constituent propagated too fast in MOHID simulations.

Table II. Errors between modelled and observed amplitudes and phase lags of the main harmonic constituents (Mohid - Sensor).

	Error Amplitude (m)					Error Phase lag (°)				
Station	M_2	S_2	N_2	K_1	O_1	M_2	S_2	N_2	K_1	O_1
E1	0.01	-0.02	-0.02	-0.02	0.00	6	7	-3	14	3
E2	0.01	-0.01	-0.03	-0.02	0.00	6	6	-5	6	1
E3	0.00	-0.02	-0.02	-0.02	0.00	6	4	-6	7	-2

3.2. Wave-current interactions

When comparing the wave parameters estimated by the SWAN nested model with the wave parameters by the coupled SWAN nested – MOHID model, significant differences could be observed (Figure 4). The results showed that the water level and current velocities, implemented only in the coupled model, affect the significant wave height at the mouth of the estuary considerably, as well as the wave direction. The peak of simulated significant wave heights could be observed after 3 days, where the SWAN nested model resulted in 6 m significant wave height, while the coupled model reached 6.4 m. The latter occurred during flood, which showed a strong dependency of the tidal currents, with ebb tides resulting in smaller significant wave heights than floods. The wave direction changed by 2-4° depending on the tide.

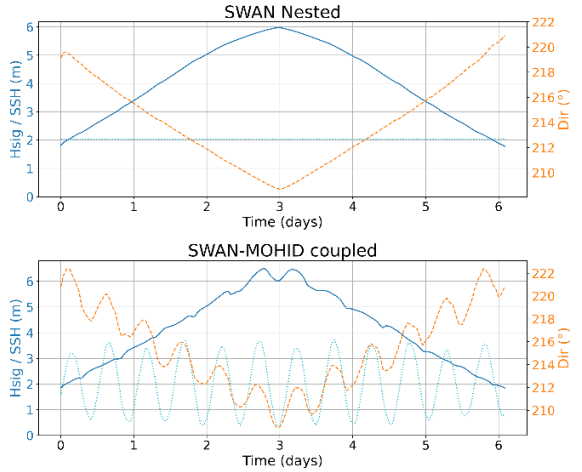

Figure 4. Comparison of simulated wave characteristics by the SWAN Nested model (top) and the coupled SWAN-MOHID model (bottom), showing significant wave height (Hsig), sea surface height (SSH) and wave direction (Dir), at the mouth of the estuary.

4. DISCUSSION AND FINAL REMARKS

The calibration and validation of numerical models with field observations is a fundamental step in order to obtain accurate results when simulating hydrodynamic processes in estuaries. The first part of this study showed that the MOHID model is capable of estimating water levels in the estuary with generally good precision. Errors in water level estimations can be caused by a coarse grid resolution of the computational domain, bathymetric errors or equipment errors. In the present case, all of those factors could have contributed to slight offsets in water level estimations. However, the validated MOHID model forms a valuable foundation for further studies (e.g. the coupling with SWAN).

The estimated phase differences in the harmonic analysis indicated a temporal offset of the tidal signal and could be observed for all constituents. Temporal offsets like these can be a result of bathymetric inaccuracies, but also problems with the implementation of boundary conditions or faulty use of frictional effects at the bottom. In order to identify, what caused the differences between field observations and model results, further investigation is needed.

The results of wave-current interactions confirmed the findings of previous studies, where water level oscillations and nearshore currents have been found responsible for considerable changes in wave characteristics close to estuary mouths. While the results suggested that the significant wave height increased when currents and water levels were imposed, particularly during flood, further insight is needed in order to fully understand wave-currents interactions during energetic conditions.

The comparison of both SWAN models of the study area, one without imposed currents and the other with imposed currents, revealed a strong dependency of simulated wave parameters on the tide and flow velocities in the coastal zone. While this study gave a first insight, further evaluation and modelling of the study area is needed to fully understand wave-current interactions during storm conditions outside the Arade estuary.

Acknowledgements

The authors acknowledge FCT funding to the Associate Laboratory ARNET under the project LA/P/0069/2020 and CIMA through the grant UIDP/00350/2020 (https://doi.org/10.54499/UIDP/00350/2020). Furthermore, the FCT Doctoral Fellowship 2023.02666.BDANA is acknowledged.

REFERENCES

APS - Administração dos Portos de Sines e do Algarve, S. (2017). *Projeto De Aprofundamento E Alargamento Do Canal De Navegação Do Porto De Portimão - Estudo de Impacte Ambiental*. Vol. II.

Booij, N., Ris, R.C., and Holthuijsen, L.H. (1999). A Third-Generation Wave Model for Coastal Regions: 1. Model Description and Validation. *Journal of Geophysical Research: Oceans* 104(C4), 7649–7666.

Dodet, G., Bertin, X., Bruneau, N., Fortunato, A.B., Nahon, A., and Roland, A. (2013). Wave-Current Interactions in a Wave-Dominated Tidal Inlet. *Journal of Geophysical Research: Oceans*, 118(3), 1587–1605.

Janeiro, J., Neves, A., Martins, F., and Relvas, P. (2017). Integrating Technologies for Oil Spill Response in the SW Iberian Coast. *Journal of Marine Systems*, 173, 31–42.

Maljutenko, I., and Raudsepp, U. (2019). Long-Term Mean, Interannual and Seasonal Circulation in the Gulf of Finland — The Wide Salt Wedge Estuary or Gulf Type ROFI. *Journal of Marine Systems*, 195, 1–19.

Manz, A., Garzon, J. L., and Martins, F. (2025). Hydrodynamic Processes in the Arade Estuary – A Field-Based and Modelling Analysis. *Increase Conference*, 1-4 July, Faro.

Martins, F., Leitão, P., Silva, A., And Neves, R. (2001). 3D Modelling in the Sado Estuary Using a New Generic Vertical Discretization Approach. *Oceanologica Acta*, 24, 51–62.

Mengual, B., Bertin, X., Place, F., Pezerat, M., Coulombier, T., Mendes, D., and Fortunato, A.B. (2022). Wave-Current Interactions at the Tagus Estuary Mouth (Portugal) under Storm Wave Conditions. *Ocean Modelling*, 175, 102035.

Portela, L.I., and Duarte, F. (2016). Evolução Morfológica Morfológica Sedimentar Do Porto de Portimão Entre 2000 e 2015. *Actas das 4as Jornadas de Engenharia Hidrográfica,* pp. 363–66.

Rusu, L., Bernardino, M., and Guedes Soares, C. (2011). Modelling the Influence of Currents on Wave Propagation at the Entrance of the Tagus Estuary. *Ocean Engineering*, 38(10), 1174–83.

ICCOE - A Virtual Laboratory to explore the coastal ocean

J. Vitorino (1) and V. Lima (1)

(1) Oceanography Division, Instituto Hidrográfico, Lisbon, Portugal. joao.vitorino@hidrografico.pt

Abstract: The Blue-Cloud 2026 is a European collaborative initiative, building on Blue-Cloud pilot, which aims towards a federated research ecosystem for marine environment. The project is a contribution to EOSC, based on a dedicated Virtual Research Environment, focusing on the development of several Virtual Laboratories and Workbenches, promoting Data Discovery & Access Service (DD&AS) offering FAIR and open data platforms. This work will focus on the development of the "Integration of Coastal Ocean Observation along European margins" (ICOOE) Virtual Laboratory, led by Instituto Hidrográfico, with the collaboration of the Balearic Islands Coastal Observing and Forecasting System (SOCIB- Spain) and the IEEE France Section (IEE-France).

Keywords: *Virtual Laboratories, Blue-Cloud 2026, coastal ocean, observations, data exploration and integration*

1. INTRODUCTION

The coastal ocean areas of the World concentrate the majority of human activities related to the marine environment. These are areas of high biological productivity, with rich and diversified ecosystems that are under a broad range of pressures. In direct contact both with open-ocean and continental influences, the coastal oceans are in the frontline of human impacts over the marine systems.

Given their extraordinary importance, it is key to understand the complex coastal ocean processes and their mutual interactions. This knowledge is the essential bedrock from which management decisions capable of assuring the biodiversity and sustainability of coastal oceans areas can be built.

During the last decades, an enormous effort was developed in installing observation capacities in coastal ocean regions. Nowadays, a large volume of observations of these areas is provided by permanent infrastructures, such as fixed platforms offshore (e.g. multiparametric buoys or benthic landers) and coastal stations (e.g. high-frequency HF radars, tide gauges), or by programs of observation conducted using robotic systems (e.g. gliders, autonomous underwater vehicles, unmanned surface vehicles, among others), research ships or ships of opportunity.

While coastal ocean observations are becoming increasingly available to researchers and other users, the use of these observations is frequently blocked by difficulties in the identification of the datasets that are available or on how these datasets can be manipulated, explored and integrated.

2. THE ICOOE VLAB AND BLUE-CLOUD 2026

The recognition of the difficulties reported in section 1 motivated the development and implementation of a Virtual Laboratory (VLab) specifically dedicated to support users in the identification, exploration, integration and visualization of coastal ocean observations and complementary information.

The "Integration of Coastal Ocean Observations along Europe" (ICOOE) Virtual Laboratory is being developed in the framework of the European project Blue-Cloud 2026, by a team integrating Instituto Hidrográfico (IH-Portugal), the Balearic Islands Coastal Observing and Forecasting System (SOCIB- Spain) and the IEEE France Section (IEE-France). The three institutions were partners in successive European projects that developed the Joint European Research Infrastructure for Coastal Observatories (JERICO), gathering a strong expertise in coastal ocean observation and coastal ocean processes.

Blue Cloud 2026 develops between 2022 and 2026 and is funded by the Horizon Europe program, gathering 40 partners. It follows from the pilot project Blue-Cloud (Horizon 2020) which implemented a Pilot Blue-Cloud ecosystem, federating services from Research Infrastructures and e-infrastructures, to provide researchers with open access to data, algorithms, and computing resources. Together, Blue-Cloud and Blue-Cloud 2026 are implementing the thematic node for the marine environment of the European Open Service Cloud (EOSC). EOSC was launched in 2016 by the European Commission with the aim of providing a virtual environment with open and seamless access to services for storage, management, analysis and re-use of research data, across borders and disciplines.

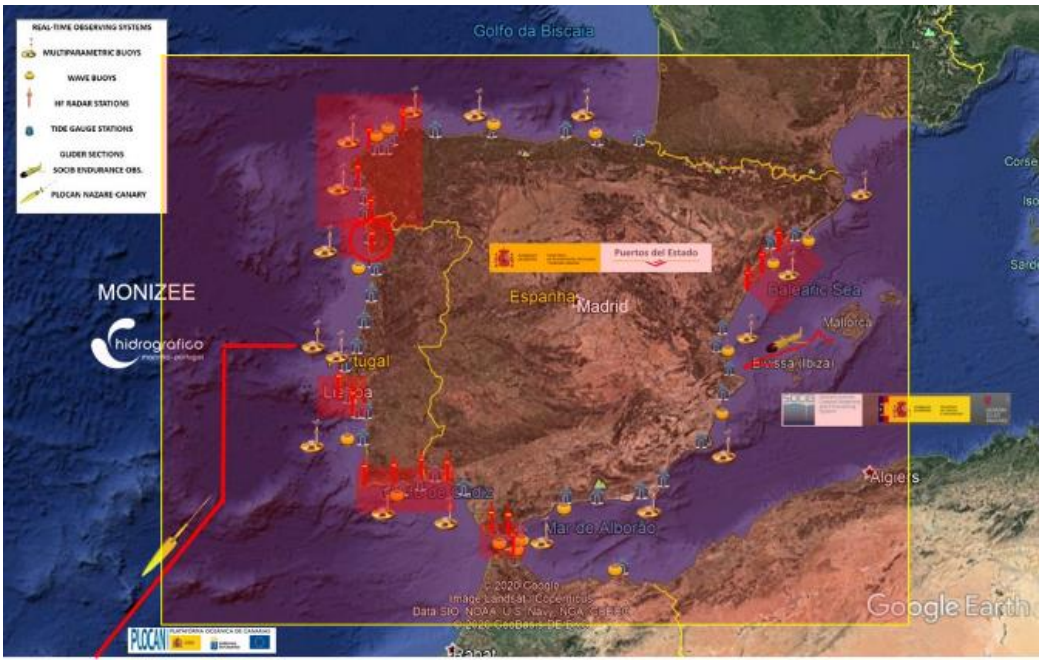

Figure 1. Iberian Atlantic Margin available observation networks, featuring MONIZEE system managed by the Hydrographic Institute, as well as Puertos del Estado monitoring network, PLOCAN glider section and SOCIB glider endurance sections.

3. ICOOE THEMATIC SERVICES

The ICOOE VLab takes full advantage of the Blue-Cloud Virtual Research Environment (VRE) (available through https://blue-cloud.d4science.org/group/icooe/) and integrates the expertise in coastal ocean processes gathered by the Joint European Research Infrastructure of Coastal Observatories (JERICO) community. ICOOE proposes three complementary thematic services, providing a number of FAIR oriented tools and services that take advantage of globally accepted Ocean Best Practices and standards, to explore key areas for the coastal ocean research and operational uses.

Thematic Service #1, "Transboundary Transport and Connectivity", is developed by IH in collaboration with IEEE-France and is aimed to support users interested in exploring transport mechanisms along the coastal ocean areas of Europe.

Thematic Service #2, "Extreme Events", is developed by IH in collaboration with IEEE-France and provides a number of tools to explore observations collected to the assessment of extreme events and their impacts in the coastal ocean areas.

Thematic Service #3, "Ocean Glider", is developed by SOCIB and aims to demonstrate the added value chain of glider missions from data acquisition to advanced products and visualizations for improved coastal information, integrating ocean state and variability derived from glider transects.

ICOOE is presently being open to the community, as one of the Blue-Cloud 2026 Virtual Labs. Interaction with the users will promote the fine-tuning of the available services as well as the rapid expansion of the installed capacities.

4. TWO EXAMPLES OF ICOOE VLAB SUPPORT

In the present contribution, examples are provided on how ICOOE Thematic Services #1 and #2 can be used to support coastal ocean research.

The Transboundary Transport and Connectivity Thematic Service (Thematic Service #1) is aimed to explore the intrinsic nature of coastal ocean areas as waveguides for the propagation of disturbances across long distances from their source. It uses a Dash Python user interface to allow users to select the geographical area of interest, the period of interest and the parameters of interest (surface and subsurface currents, temperature and salinity and sea surface height). Based on these choices, the service identifies the observations that are available for these options, from different data aggregators.

After selection of the datasets of interest, these are downloaded to the VLab user area. The thematic service then pre-processes the datasets to conform the specific requirements of the Thematic Service. This includes, for example, low-pass filtering the data in order to retain only the subinertial variability (here taken as variability with periods over 35 hours) or the filling of short gaps in the data by interpolation. The

VLab then presents a set of tools that can be used to support the users in the data exploration, integration and visualization.

Although not designed to confine a specific region, the Thematic Service is presently being demonstrated for the Iberian coastal ocean area (Figure 1) and for surface currents provided by the European HF Radar Node (HF radar observations) and by the Copernicus Marine Service (NEMO model results). The demonstration activities of the Thematic Service focus on the transport of contaminants and invasive species and their impacts on offshore aquacultures, marine protected areas and coastal environments.

The Extreme Events Thematic Service (Thematic Service #2) focuses on the assessment of extreme events and related impacts on the coastal ocean areas of Europe. Based on a user interface similar to the one described above, this Thematic Service provides users with a set of tools to support the characterization of the conditions associated with extreme storms, impacting the European coastal ocean and their effects on the bottom sedimentary cover. The presently available demonstrator for Thematic Service#2 uses a pre-defined set of data that corresponds to three specific extreme storms that affected the Iberian margin, Storm Ophelia (October 2017), Storm Emma (March 2018) and Hurricane Leslie (October 2018).

Acknowledgements

This contribution was supported by the European Union's Horizon Europe research and innovation programme Blue-Cloud 2026 project (grant number 101094227).

Data harmonization and availability as key elements in knowledge generation: A case study of small pelagic fish egg data for Individual-Based Early Life Stage Models

G. González-Nuevo (1), L. Sanz (2), D. Rodriguez-Abal (1), A. Sanjurjo (1), S. González (1), C. García (1), J. Otero (1), M. L. García (1), E. Tel (2) and M. Ruiz-Villareal (1)

(1) Instituto Español de Oceanografía (IEO-CSIC), Oceanography Center of A Coruña, Spain. gonzalo.gonzaleznuevo@ieo.csic.es

(2) Instituto Español de Oceanografía (IEO-CSIC), Oceanography Center of Madrid, Spain

Abstract: This work illustrates the importance of data harmonization and standardization in generating scientific knowledge, focusing on the development of Individual-Based Models (IBMs) for early life stages of small pelagic fish. The case study uses data from the PELACUS surveys, which monitor anchovy and sardine egg concentrations with CUFES, alongside acoustic assessments and comprehensive ecosystem observations. To ensure the datasets are FAIR (Findable, Accessible, Interoperable, Reusable), workflows include quality control, transformation into SeaDataNet CDI formats, storage in PostgreSQL/PostGIS, and dissemination through OGC-compliant services (WFS, WMS, CSW) via GeoServer and GeoNetwork. Applying standards consistently allows both human and machine access, enabling automated discovery and integration without custom developments. Harmonized datasets simplify defining climatic spawning areas, incorporating interannual variability in model forcing, and validating IBMs with empirical evidence. This approach demonstrates how accessible, standardized data improve predictive capacity and support the understanding of marine ecological processes.

Keywords: *Standards, FAIR principles, Individual-Based Models (IBMs)*

1. INTRODUCTION

The study of any process necessarily involves obtaining information about it. In oceanography, due to the inherent characteristics of the environment under investigation, it is especially challenging to characterize processes with sufficiently fine spatial, depth, and temporal resolutions. While this complexity is already significant in physical oceanography, it becomes even more pronounced when studying biological processes. The collection of biological data is often difficult to automate, and there is frequently no comprehensive characterization of the underlying processes—sampling efforts typically fall short in time, space, or depth resolution.

Despite these challenges, long-term sampling programs exist that have been collecting very high-quality data for years. However, an additional barrier in the process of generating scientific knowledge arises because this information is either not widely known to exist, not properly harmonized, or not made accessible for reuse.

Currently, efforts are underway at all levels of the data generation process to converge toward truly FAIR information systems—systems that ensure data are Findable, Accessible, Interoperable, and Reusable.

2. CASE STUDY

In the case study presented in this work, data on anchovy and sardine egg concentrations were collected at the surface using the CUFES system during the PELACUS surveys. These surveys are primarily designed for the acoustic assessment of small pelagic fish populations and are conducted annually in March and April since the year 2003. In addition to acoustic evaluation, they gather a broad range of complementary information describing the pelagic ecosystem, including physical and biogeochemical parameters, phytoplankton, picoplankton, zooplankton, the fish community, apex predators, and marine litter, among others.

The information generated on pelagic fish eggs through these surveys is highly valuable for its application in the development of Individual-Based Models (IBMs) focusing on the early life stages of small pelagic fish.

Once collected, these data are sent to the National Oceanographic Data Center (NODC), where they undergo basic quality control procedures, are securely stored, and are formally curated.

To make these data available according to FAIR principles, the NODC processes them into SeaDataNet

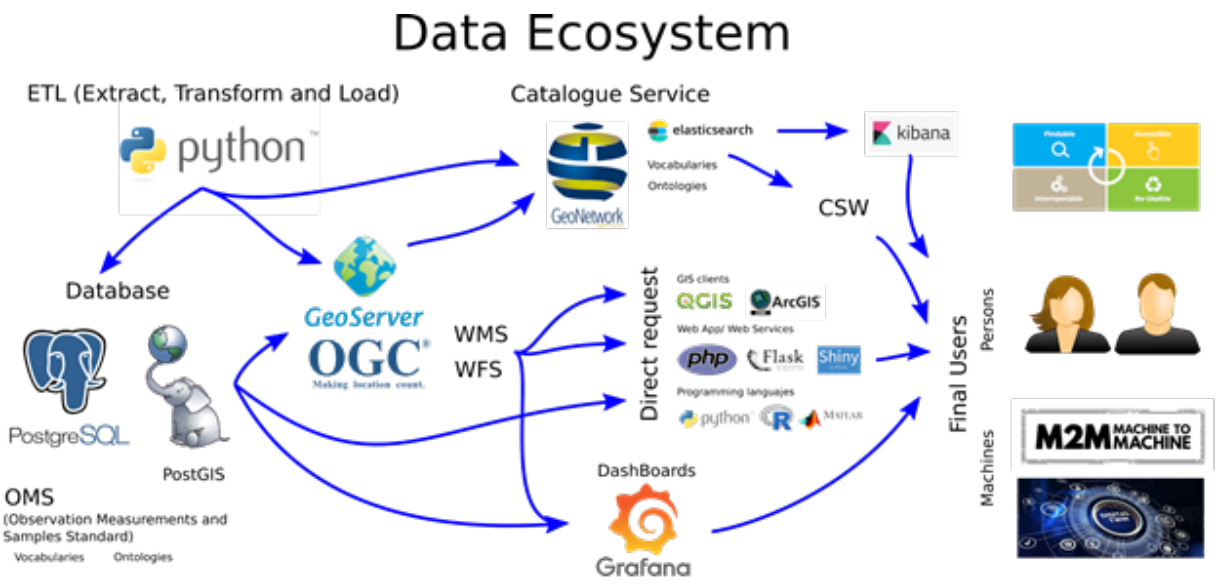

Figure 1. Data management and dissemination workflow supporting FAIR principles. Data are processed and stored in PostgreSQL/PostGIS, using data model standard and vocabularies, served through GeoServer and GeoNetwork, and accessed by users, applications, and machine-to-machine systems for analysis, visualization, and modelling.

CDI file formats and performs metadata curation using standardized vocabularies. In parallel, efforts are underway to incorporate this information into the standard Ocean Model Schema (OMSs) data model and to test dissemination through API Things interfaces.

With the data stored in a PostgreSQL database with PostGIS spatial support, efficient dissemination becomes possible by connecting a geographic information node such as GeoServer. This setup allows the information to be queried through standardized services like WFS (Web Feature Service) for vector data and WMS (Web Map Service) for visualization (Figure 1).

Furthermore, by registering the dataset in a catalog server like GeoNetwork, the dataset is comprehensively described with metadata, and all available access services are listed. Because WFS and WMS are used, users can even explore and visualize the data directly within the GeoNetwork interface as an initial step. These catalog servers also expose metadata through a CSW (Catalog Service for the Web) endpoint, which facilitates discovery, access, and exploitation of the data by both humans and machines (Figure 1).

So far, this workflow does not differ greatly from other well-established data pipelines that scientists are accustomed to using. A human user can easily locate the dataset and analyze it with the tools of their choice, supported by rich metadata that describes the content in detail.

However, the key difference in this case is the systematic effort to apply standards consistently at every level of the process. This ensures that machines can autonomously query the catalog, determine whether egg data are available, identify the dissemination services, and—because those services are based on shared standards—consume them directly for any required purpose. As a result, when developing automated systems, implementations can be generic rather than requiring custom programming for each specific dataset or source.

With pelagic egg data made available in this way, their integration into workflows for developing IBM simulations becomes much simpler. In the early conceptual phases of model development, it is relatively straightforward to define climatic spawning areas to support first approximations of model forcing.

In more advanced stages, the availability of annual data allows the inclusion of interannual variability of spawning processes in the model forcing, which makes the outputs more precise and reliable.

Finally, once models reach mature development phases, this information becomes essential for model validation processes.

Acknowledgements

This work is partially funded by the Galicia Marine Science programme, which is part of the Complementary Science Plans for Marine Sciences of the Ministry of Science, Innovation and Universities, included in the Recovery, Transformation and Resilience Plan (PRTR-C17.I1). Funded through the Xunta de Galicia with NextGenerationEU and the European Maritime, Fisheries and Aquaculture Fund.

Lagrangian simulations of Early Life Stages of Iberian sardine and European anchovy in the Atlantic Iberian margin

M. Ruiz-Villarreal (1), S. González-Pérez (1), A. Sanjurjo-García (1), G. González-Nuevo (1), L. M. García-García (1), D. Rodríguez-Abal (1), P. Sampedro (1), J. Martínez (2), J. Isern-Fontanet (2), M. Clavel (2), A. Sabatés (2), V. Raya (2) and E. García-Ladona (2)

(1) Centro Oceanográfico de A Coruña, Instituto Español de Oceanografía, IEO-CSIC, A Coruña, Spain. manuel.ruiz@ieo.csic.es

(2) Institut de Ciències del Mar (ICM-CSIC, Barcelona, Spain).

Abstract: A model of Early Life Stages of sardine and anchovy has been developed based on the review of the knowledge of the species as well as on the revision of existing models and parameterisations. The model allows us to study how the two species respond to the variability of environmental conditions and therefore to advance our knowledge of the ecology of the two species. In this contribution, we present an application of a biophysical model for sardine and anchovy eggs and larvae in the Atlantic Iberian Margin.

Keywords: *Biophysical ocean models, Individual Based Models, Fish Early Life Stages, Lagrangian particle dispersion*

1. INTRODUCTION

In recent years, the use of Early Life Stages (ELS) models of fish species, which simulate eggs and larvae as Lagrangian particles evolving in an environment described by an oceanographic model coupled to an ecological one, is becoming widespread in oceanography. Biophysical model account for horizontal and vertical advection and dispersion of particles, and also for biological behavior from a Individual Based Model (IBM) approach. Biological processes such as changes in buoyancy throughout the development of the egg stages, vertical larval migration, larval growth as a function of larval stage, with effects of temperature and food availability, larval migration for feeding, etc; are simulated (e.g. Garcia-Garcia *et al.*, 2016).

Particle models for larval population dispersal studies are highly dependent on the target species, although from a numerical point of view if a model is available for a species with a pelagic phase, the work required to get a model for other species is just to adapt the numerical code to the life history characteristics of the other species. During projects Phys2Fish and DEMON (in collaboration with ICM scientists), IEO A Coruña modelling team has produced a common code to simulate the ELS of four commercial species: sardine, anchovy and hake (fish) and common octopus (a cephalopod). This code is available as a module in the open source particle tracking model OpenDrift (Dagestad *et al.*, 2018) that can be forced by the output of available hydrodynamical simulations.

2. SIMULATIONS OF ANCHOVY AND SARDINE EARLY LIFE STAGES IN THE IBERIAN ATLANTIC MARGIN

In this contribution, we concentrate on the application of the biophysical model to study sardine and anchovy eggs and larvae development and dispersion in the Atlantic Iberian margin during spring time and especially near the time of Pelacus cruises, core surveys of the IEO carried out every spring since 1986.

Simulations of the transport of sardine and anchovy eggs and larvae in the Cantabrian Sea and Portugal have been performed for different years including 2006 and 2007, for which biochemical simulations are available (Garcia-Garcia *et al.*, 2023) and the ELS Lagrangian model has been forced with output from this simulations.

We have simulated the dispersion of ELS of sardine and anchovy during those years, see a preliminary result in Figure 1. Additionally, several metrics for the analysis of the transport (gravity center, particle density…) apart from codes for the analysis of parameters like age, length and depth of the particles have been developed.

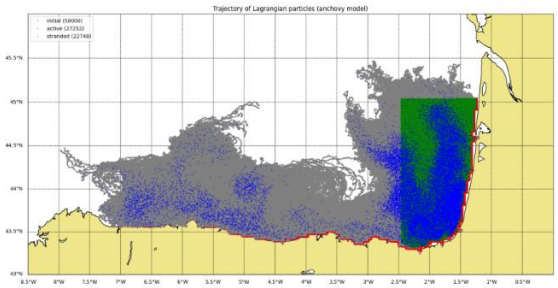

Figure 1. Dispersion of anchovy eggs and larvae in the Bay of Biscay in spring.

3. DISPERSION OF LAGRANGIAN DRIFTERS DURING PELACUS2025

Our studies of dispersion have highlighted the need for real drifting buoy measurements to calibrate the model. Consequently, in the framework of project DEMON, buoys have been launched in Galicia and in the Cantabrian Sea during the PELACUS2025 spring pelagic resource survey campaign. In Figure 2, the trajectories of Lagrangian drifters launched in PELACUS2025 are shown. The trajectories are available in the DEMON section at IEO GeoNetwork catalogue. Retention on the shelf and coastwards transport is observed in the Cantabrian Sea, while a southwards transport is evident for the drifters launched in the western Galician coast.

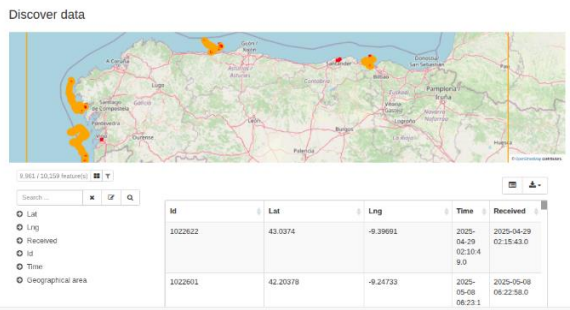

Figure 2. Lagrangian drifters launched in PELACUS 2025.

4. OUTLOOK

Modeling approaches that consider the interplay of physical conditions and biological behaviour of early life stages of pelagic species are becoming established tools and now the challenge is to use this information to understand marine population dynamics and to improve the management of fishery stocks. In Phys2Fish and DEMON projects, modelling teams are joining forces with fish scientists to compare estimations of recruitment obtained with the population dynamics models used in the stock assessments with those estimated from Lagrangian ELS models.

Acknowledgements

This contribution is part of projects DEMON (Dissipation of Energy in Ocean Models and Connectivity) funded by MCIN/AEI/10.13039/501100011033 and by ERDF; and Phys2Fish project of the Galicia Marine Science programme of the Complementary Science Plans for Marine Science of Ministerio de Ciencia, Innovaci´on y Universidades included in the Recovery, Transformation and Resilience Plan (PRTR-C17.I1). Funded through Xunta de Galicia with NextGenerationEU and the European Maritime Fisheries and Aquaculture Funds. Additional funding has been obtained from funds for consolidation of research groups of the Axencia Galega de Innovación to EPB group.

REFERENCES

Dagestad, K.-F., Röhrs, J., Breivik, Ø., and Adlandsvik, B. (2018). OpenDrift v1.0: a generic framework for trajectory modelling. *Geoscientific Model Development*, 11, 1405-1420. https://doi.org/10.5194/gmd-11-1405-2018

García-García, L. M., and Ruiz-Villarreal, M. (2023). Variability of plankton production during the spring bloom in NW Iberia. *Marine Ecology Progress Series*, 708, 45-78. https://doi.org/10.3354/meps14236

García-García, L. M., Ruiz-Villarreal, M. and Bernal, M. (2016). A biophysical model for simulating early life stages of sardine in the Iberian Atlantic stock. *Fisheries Research*, 173(3), 250-272. https://doi.org/10.1016/j.fishres.2015.10.002

Integración de observaciones y modelos para refinar la comprensión de la dinámica temprana de la merluza europea en el Atlántico noreste

A. Sanjurjo-García (1), C. García-Fernández (1), D. Rodriguez-Abal (1), P. Sampedro (1), J. Otero (1), M. Ruiz-Villarreal (1), S. González-Pérez (1), G. González-Nuevo (1) y L. M. García-García (1)

(1) Centro Oceanográfico de A Coruña, (IEO-CSIC), A Coruña, España. adrian.sanjurjo@ieo.csic.es

Abstract: European hake (*Merluccius merluccius*) is a demersal species in the Northeastern Atlantic with high commercially and ecologically importance. For the study of its Early Life Stages (ELS), an Individual Based Model (IBM) was developed, incorporating biological factors like egg buoyancy, mortality and larval growth, from hatching to settlement (two months). Implemented in OpenDrift and forced with ROMS hydrodynamic data from 2006 and 2007 for North Iberian waters, the model explored how oceanographic variability affects hake ELS dispersion, connectivity, and survival. Simulations were initialized in persistent spawning areas, using Total Egg Production to relate model particles (superindividuals) to real population sizes.

Keywords: *Hake, IBM, OpenDrift, connectivity, survival*

1. ELABORACIÓN DEL IBM

Dentro del marco de actuación del Programa de Ciencias Mariñas de Galicia se ha propuesto el estudio de tres especies de especial relevancia comercial en el noroeste peninsular: la sardina, el pulpo y la merluza europea. En este estudio se incluye además la elaboración de un Individual Based Model (IBM) para cada una de ellas. Si bien un IBM para la sardina atlántica ya fue desarrollado por García-García *et al.* (2016), dentro de este proyecto se ha conseguido desarrollar los IBMs restantes para el pulpo y la merluza.

Centrándonos en la merluza europea, este modelo IBM recoge partes de distintas publicaciones enfocadas en la elaboración e implementación de IBMs de otras especies tales como la sardina atlántica (García-García *et al.*, 2016; Sanjurjo-García, 2022) o la anchoa (Ospina-Álvarez, 2012; González-Pérez, 2024), así como estudios de laboratorio y de campo centrados en la merluza europea (Coombs y Mitchell, 1982; Palomera *et al*., 2005; Sánchez *et al*., 2011; Álvarez y Cotano, 2005) así como también en otras especies del mismo género tales como *merluccius capensis* (Sundby *et al*., 2001), *merluccius productus* (Bailey, 1982) y *merluccius australis* (Bustos *et al*., 2005), ya que no se encontró bibliografía suficiente respecto a la merluza europea.

- Toda esta recopilación bibliográfica nos da como resultado un modelo de crecimiento dividido en tres fases:
  Fase huevo: con efectos de flotabilidad debido a los cambios en la densidad de la partícula, así con una duración de la fase determinada por la temperatura.
- Fase larva endógena: marcado por un crecimiento lineal y una duración de dicha fase con dependencia respecto a la temperatura del medio.
- Fase larva exógena: continuación del crecimiento lineal anterior durante dos días (aproximadamente el tiempo que la larva de merluza desarrolla su parte posterior, siendo este crecimiento mayor al longitudinal). Transcurrido dicho tiempo, la pendiente de la recta de crecimiento deja de depender de la temperatura, con un rango válido hasta que llega al asentamiento tras dos meses desde la eclosión (Bjelland y Skiftesvik, 2006).

Se incluyen tres modelos sencillos de mortalidad: mortalidad por temperatura a 22 grados (Guevara-Fletcher *et al*., 2016), mortalidad en fase huevo al contacto con la superficie (0m) (Guevara-Fletcher *et al*., 2016) y eliminación de aquellas partículas que superen una profundidad de 330 m (Coombs y Mitchel, 1982).

2. IMPLEMENTACIÓN Y SIMULACIONES

Este IBM se ha implementado en OpenDrift (https://opendrift.github.io/, Degestad *et al*., 2018), y permite realizar simulaciones offline de partículas lagrangianas utilizando forzamientos de ROMS. Entre los distintos módulos que incluye OpenDrift, se ha tomado como base el modelo LarvalFish, que en su versión original incluye un modelo de crecimiento del bacalao del Atlántico norte.

El modelo hidrodinámico utilizado para este estudio es una configuración ROMS del IEO (Instituto Español de Oceanografía) con una resolución aproximada de 3.5km en la componente horizontal y 30 capas sigma en la componente vertical. El modelo cubre el área que se extiende por el norte y oeste de la península ibérica, entre las latitudes 37.25N hasta 46.0192 N, y las longitudes 0.7 W hasta 14.5 W. Incluye un forzamiento meteorológico obtenido de la configuración WRF que MeteoGalicia corre operacionalmente, condiciones de contorno provenientes de MyOcean (https://marine.copernicus.eu/es/datos-de-acceso/visor-myocean) y se incluyen los efectos de las mareas y de los ríos en el área de interés, utilizando datos de caudales diarios cuando están disponibles. Además, incluye un modelo biogeoquímico N2PZD2 con el nitrógeno como nutriente limitante, y con la relación temperatura/nitrato obtenida en las campañas oceanográficas Radprof comprendidas entre 2004 y 2008 (García-García *et al*., 2016; García-García y Ruíz-Villareal, 2022). El periodo de las simulaciones son los años 2006 y 2007 al completo. Los fenómenos físicos que se consideran en las simulaciones son la flotabilidad en fase huevo, la advección y dispersión horizontal y vertical, sin interacción con la costa (es decir, no hay deposición de partículas).

Puesto que en este estudio se quiere tener en cuenta la variabilidad interanual, se ha utilizado las zonas de puesta persistentes de esta especie como posiciones iniciales de lanzamiento de partículas (Figura 1). Estas zonas han sido estimadas con un modelo espacio-temporal teniendo en cuenta las notas de venta que registran huevas (en las flotas de volanta y palangre) y la posición geográfica asociada a estas (utilizando datos de VMS – vessel monitoring system) (García-Fernández *et al*., 2025).

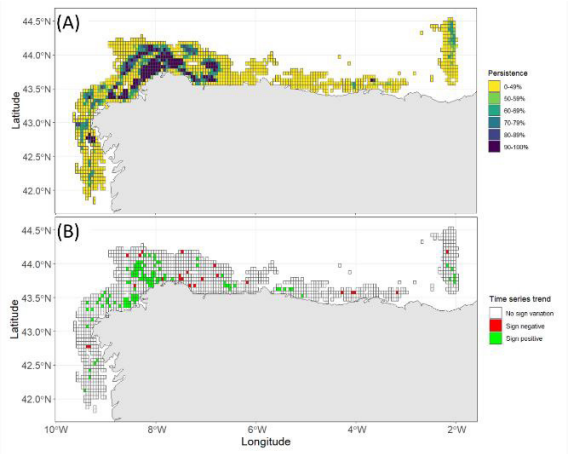

Figura 1. Áreas de persistencia anual de la merluza europea en la zona de estudio desde 2009 hasta 2022.

La estacionalidad de la puesta también se obtuvo de estos análisis. Esta aproximación permite obtener una relación del número de huevos/larvas que se corresponde a cada partícula en las simulaciones realizadas. De esta forma podemos completar este estudio no solo con la estimación a nivel superindividuo, sino también con los datos larvarios. El número inicial de partículas es constante en cada simulación (n = 24520), y para el estudio solo se consideran aquellas que han llegado activas al final de las simulaciones, es decir, al asentamiento. Estas simulaciones se han realizado cada 5 días (en base a la frecuencia de puesta de esta especie), obteniendo un total de 131 simulaciones durante 2006 y 2007.

Para el análisis de resultados se utilizaron las 5 áreas delimitadas en la campaña oceanográfica Sp-GFS-WIBTS-Q4 (Figura 2), las cuales vienen comprendidas entre Miño - Finisterre (MF), Finisterre - Estaca de Bares (FE), Estaca de Bares - Cabo Peñas (EP), Cabo Peñas – Ajo (PA) y Ajo-Bidasoa (AB), y nos permiten realizar un estudio en detalle sobre la conectividad de la merluza en distintos puntos del cantábrico, así como definir áreas de origen para el análisis de la dispersión de las larvas. También hemos dividido temporalmente de forma anual y trimestral los resultados para ver de forma más clara las posibles tendencias obtenidas.

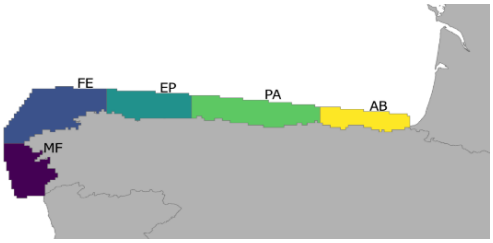

Figura 2. Zonas de Sp-GFS-WIBTS-Q4 utilizadas en este estudio.

3. SUPERVIVENCIA

Hemos observado que la supervivencia en los superindividuos bajo los efectos físicos del océano se correlaciona con los picos de puesta de esta especie, resultando un mayor asentamiento de larvas precisamente en los periodos en los que concluye el invierno y comienza la primavera.

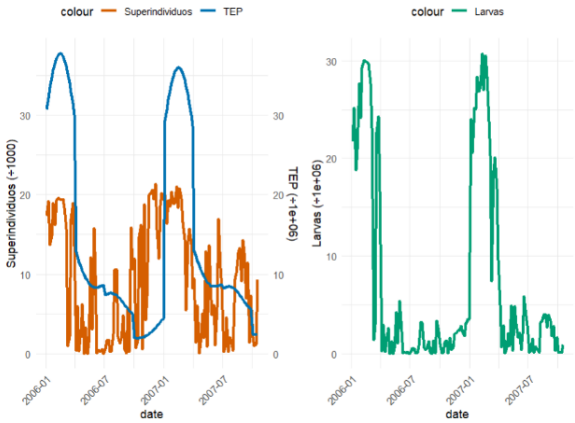

Figura 3. Izquierda) Producción total de huevos de merluza (TEP) en millones (línea azul) y supervivencia de superindividuos (/1000) (línea naranja) a lo largo de las simulaciones, Derecha) supervivencia total de larvas en millones a lo largo de las simulaciones.

4. DISPERSIÓN

Debido al efecto en las simulaciones de un fuerte empuje en la corriente desde el oeste hasta el este a comienzos del año se observa una mayor dispersión de partículas en dicho periodo, que influirá en los resultados del estudio de conectividad. Las distancias recorridas por las partículas en 2007 son mayores que la distancia en 2006, además de que se observa un cambio de desplazamiento en la trayectoria en los meses de verano de 2007 hacia las aguas portuguesas.

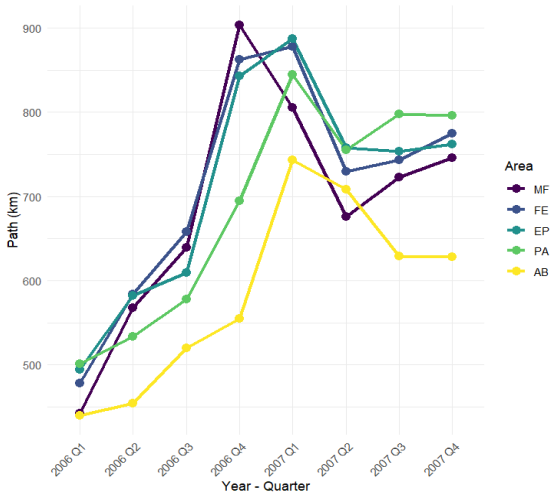

Figura 4. Promedio de las distancias recorridas (km) por las partículas desde las diferentes áreas de Sp-GFS-WIBTS-Q4 de origen a lo largo de las simulaciones.

También se analizan distintos índices de dispersión, tales como los centros de gravedad o el área positiva del dominio para encontrar correlación entre estos efectos.

5. CONECTIVIDAD

Se ha estudiado la conectividad entre las distintas áreas de las partículas lanzadas que alcanzan una de estas áreas en el asentamiento. En la Figura 5 se muestra este patrón de conectividad, mostrando abajo las áreas iniciales de procedencia y a la izquierda las áreas finales, calculando los porcentajes en base a su zona de origen (es decir, las columnas suman 100%) y mostrando los porcentajes de llegada en cada zona final. En el año 2006, la tendencia en el desplazamiento es de oeste a este, actuando las zonas MF y FE como fuente de partículas y EP, PA y AB como áreas de destino, si bien al no haber un gran efecto en la dispersión de las partículas, sus posiciones finales se concentran en esas tres áreas. Debido a esta tendencia en la corriente, ninguna partícula procedente de AB se desplazó hacia el oeste en el cuarto trimestre de 2006.

Sin embargo, la influencia de una corriente con mayor fuerza a comienzos de 2007 hace que las partículas cuyo origen es EP, PA y AB se desplacen lo suficiente como para que su posición final sea hacia el norte de la bahía de Vizcaya, fuera de la zona delimitada en la Figura 2. Con el cambio de corriente hacia verano comienza la influencia de las partículas procedentes de EP, PA y AB hacia FE y MF, incluso más allá, hacia la costa portuguesa, como veníamos adelantando en la sección anterior, donde el promedio de distancias que se obtiene es mayor que el del año previo (ver Figura 4).

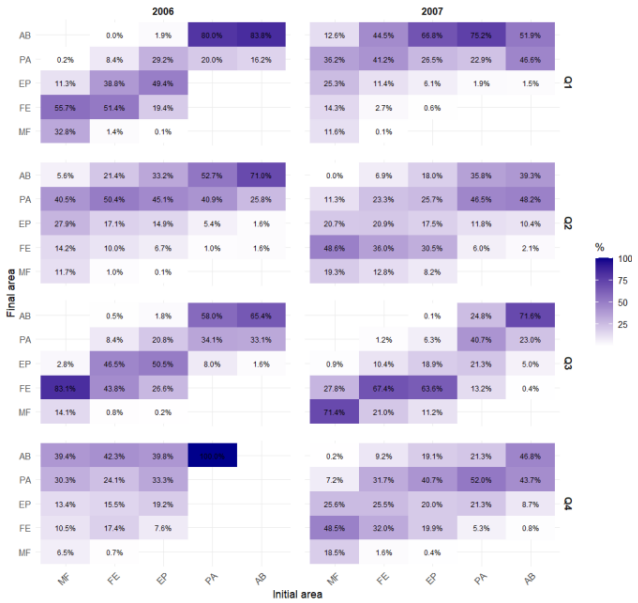

Figura 5. Matriz de conectividad entre zonas de origen y zonas destino de Sp-GFS-WIBTS-Q4 de las partículas en las simulaciones realizadas por trimestres (Q) en los dos años de estudio (2006-2007).

Agradecimientos

Agradecimientos a los compañeros del grupo de Ecología Planctónica y Biogeoquímica y el departamento Metmar, así como al Programa de Ciencias Mariñas de Galicia, proyecto en el cual se desarrolla este estudio.

REFERENCIAS

Álvarez, P. y Cotano, U. (2005). Growth, mortality and hatch-date distributions of European hake larvae, *Merluccius merluccius* (L.), in the Bay of Biscay. *Fisheries Research*, 76(3), 379–391.

Bailey, K.M. (1982). The early life of the Pacific hake, *Merluccius productus*. *Fishery Bulletin*, 80(3), 589–598.

Bustos, C. y Landaeta, M. (2005). Desarrollo de huevos y larvas tempranas de la merluza del sur, *Merluccius australis*, cultivados bajo condiciones de laboratorio. *Gayana*, 69, 402–408.

Coombs, S.H. y Mitchell, C.E. (1982). The development rate of eggs and larvae of the hake, *Merluccius merluccius* (L.) and their distribution to the west of the British Isles. *ICES Journal of Marine Science*, 40(2), 119–126.

García-Fernández, C., Domínguez-Petit, R., Aldanondo, N. y Saborido-Rey, F. (2020). Maternal effects and their seasonal variability in European hake *Merluccius merluccius*. *Marine Ecology Progress Series*, 650.

García-Fernández, C., Otero, J., Gomez-Suarez, F. y Sampedro, P. (2025). Revealing spatio-temporal Spawning Patterns of European Hake in Atlantic Iberian waters. Poster. III SIBECOL & XVII AEET Meeting.

García-Fernández, C. y Sanjurjo-García, A. (2025). Project Marine Science Programme of Galicia: Spatio-temporal spawning patterns of European hake; Individual Based Model (IBM) for early life stages of European hake. Working Document 3 in Report of ICES Working Group for the Bay of Biscay and Iberian Waters Ecoregion 2025.

García-García, L.M., Ruiz-Villarreal, M. y Bernal, M. (2016). A biophysical model for simulating early life stages of sardine in the Iberian Atlantic stock. *Fisheries Research*, 173, 250–272.

García-García, L.M. y Ruiz-Villarreal, M. (2023). Variability of plankton production during the spring bloom in NW Iberia. *Marine Ecology Progress Series*, 708, 45–78.

González-Pérez, S. (2024). Adaptación de modelo lagrangiano para simulación de Early Life Stages (ELS) de la anchoa. Trabajo de Fin de Máster, Máster en Matemática Industrial, UCM3-UDC-UPM-USC-UVigo-IEO.

Guevara-Fletcher, C.E. (2017). Characterization and influence of biotic and abiotic factors on the early life stages of European hake (*Merluccius merluccius* L. 1758) from the southern stock. Universidad del País Vasco.

Ospina-Álvarez, A. (2012). Early life history dynamics of European anchovy in the Western Mediterranean: an Individual-Based Modelling approach. Universitat de Barcelona.

Palomera, I., Olivar, M.P. y Morales-Nin, B. (2005). Larval development and growth of the European hake *Merluccius merluccius* in the northwestern Mediterranean.

Sundby, S., Boyd, A.J. y Huse, L. (2001). Interaction between Cape hake spawning and the circulation in the northern Benguela upwelling ecosystem. *South African Journal of Marine Science*, 23(1), 317–336.

Sanjurjo-García, A. (2022). Simulaciones lagrangianas de un modelo acoplado para simular dispersión de huevos y larvas y otros objetos a la deriva del océano. Trabajo de Fin de Máster, Máster en Matemática Industrial, UCM3-UDC-UPM-USC-UVigo-IEO.

Sánchez, F., Cal, R., Otero, J., Lago, M., Gómez, C. y Iglesias, J. (2011). The first spontaneous spawning of European hake *Merluccius merluccius* L.: Characteristic of eggs and early stages. *Aquaculture Research*, 42, 1–5.

Control batimétrico y estructuración interna de la MOW: evidencias preliminares a partir de la geomorfología derivada del BPI

L. M. Fernández-Salas (1), R. Sánchez-Leal (1), F. J. Hernández-Molina (2), I. Villar (3), D. Palomino (4), M. García-García (1) y INPULSE Team

(1) Instituto Español de Oceanografía (IEO-CSIC), Centro Oceanográfico de Cádiz, Cádiz, España. luismi.fernandez@ieo.csic.es
(2) Instituto Andaluz de Ciencias de la Tierra (IACT-CSIC), Granada, España
(3) Instituto Español de Oceanografía (IEO-CSIC), Centro Oceanográfico de Gijón, Gijón, España
(4) Instituto Español de Oceanografía (IEO-CSIC), Centro Oceanográfico de Málaga, Málaga, España

Abstract: This study aims to clarify the influence of seafloor morphology on the pathways and internal structuring of the Mediterranean Outflow Water (MOW) in a key sector of the Gulf of Cádiz, using high-resolution bathymetry (10 m). The study area, located between 35.67˚N–35.82˚N and 6.50˚W–6.82˚W at 329–818 m water depth, encompasses a well-defined along middle slope channel bordered to the south by a 50–70 m high sedimentary drift. Using Bathymetric Position Index (BPI) calculated at 250 m and 2000 m scales, we identify erosional depressions, transverse bedforms, and flow-aligned features suggesting complex internal structuring within the M1 branch of the MOW. Sub-branches and reorganization zones are interpreted from the BPI data. These geomorphological indicators are compared with existing oceanographic data, and a preliminary interpretation outlines detailed complex flow pathways and interactions that require further validation through high-resolution hydrographic measurements.

Keywords: *Mediterranean Outflow Water, high-resolution bathymetry, Bathymetric Position Index, bottom current*

1. INTRODUCCIÓN

La salida de la Masa de Agua Mediterránea (*Mediterranean Outflow Water*, MOW) a través del Estrecho de Gibraltar genera una vigorosa corriente densa (salina) que desempeña un papel fundamental en la circulación termohalina global. Al abandonar el Mediterráneo, esta masa de agua intermedia interacciona con el relieve del fondo marino, especialmente en el sector proximal al estrecho, donde los relieves batimétricos condicionan la división y evolución hidrodinámica de la MOW. Estudios previos (Sánchez-Leal *et al*., 2017) han identificado cinco ramas principales (M1 la más profunda, hasta M5, la más somera) asociadas a la MOW, las cuales se separan, curvan y reorganizan bajo el control de la topografía del margen continental ibérico, así como por su interacción con las masas de aguas circundantes.

El objetivo principal de este estudio es analizar cómo la morfología del fondo marino condiciona los patrones de circulación local y la estructura interna de la rama M1 de la MOW, en una zona clave del Golfo de Cádiz. Para ello, se utiliza batimetría de alta resolución (10 m), con el objetivo de descifrar patrones locales de circulación de la MOW en el fondo y su posible relación con procesos erosivos y deposicionales. Nuestra hipótesis se basa en el índice de posición batimétrica (*Bathymetric Position Index*, BPI), que permite interpretar morfologías asociadas a la acción de corrientes de fondo (Mena y Fernández-Salas, 2024). Esta información se complementa con datos oceanográficos *in situ* de alta resolución obtenidos recientemente en el marco del proyecto INPULSE, con vistas a una interpretación preliminar de la dinámica de flujos.

2. ÁREA DE ESTUDIO Y METODOLOGÍA

La zona de estudio se sitúa al oeste del Estrecho de Gibraltar, entre las coordenadas 35,67˚N, 6,50˚W y 35,82˚N, 6,82˚W, abarcando profundidades desde 329 hasta 818 m (Figura 1). Esta zona se corresponde con un tramo clave del talud medio del Golfo de Cádiz, donde la rama más profunda de la MOW (M1) describe una curva pronunciada en sentido horario hacia el noroeste.

En dicha zona, y de este a oeste, se identifica un alto morfológico en el extremo sureste (329–450 m de profundidad) que condiciona el encauzamiento de la MOW, y la formación de un canal que atraviesa la zona longitudinalmente. Este canal presenta un gradiente batimétrico de aproximadamente 260 m en 20 km, desde 465 m hasta 725 m de profundidad, limitado al sur por un depósito sedimentario de 50 a 70 m de altura relativa, que ha sido interpretado (Hernández-Molina *et al*., 2014) como un *drift* sedimentario adosado lateralmente al canal.

Para el análisis batimétrico se ha empleado la metodología propuesta por Mena y Fernández-Salas (2024), que utiliza BPI con un solo radio. Se calcularon dos rásteres de BPI: uno con 25 celdas (250 m) y otro con 200 celdas (2 km), aplicados sobre datos obtenidos con la ecosonda multihaz Kongsberg EM710 durante la campaña INPULSE_0719, procesados con una resolución de 10 m y corregido el efecto de las mareas referidas, por tanto, al nivel medio del mar.

3. INTERACCIÓN CON LA TOPOGRAFÍA Y MORFOLOGÍA DE FONDO

El análisis del BPI ha permitido identificar en la zona afectada por la rama M1 de la MOW al menos dos canales menores que podrían estar vinculados con la intensificación de un núcleo principal asociado a dicha rama (Figura 2C), lo que implica una asimetría Norte/Sur de la M1 que puede dar lugar a estructuras secundarias de menor escala. El BPI25 revela además rasgos del fondo erosivos y alineados que podrían ser interpretados como canales/incisiones de menores dimensiones (*furrows*) alineados con la dirección principal del flujo, probablemente asociadas a filamentos más estrechos y de mayor energía dentro de M1, reflejando una compleja estructuración del flujo (Figura 2D).

En la parte central del canal se observan depresiones interpretadas como áreas de intensa erosión producida por la corriente de fondo. Estas estructuras del fondo (Figura 2D) modifican el flujo generando un comportamiento más caótico de los filamentos anteriormente mencionados. Distalmente, y hacia el oeste, cuando terminan estas depresiones, se detecta una reorganización del flujo con alineamientos más regulares en el BPI, que permiten inferir una estabilización hidrodinámica en la M1. No obstante, la presencia de canales menores sugiere la continuación de núcleos secundarios bien definidos dentro de M1.

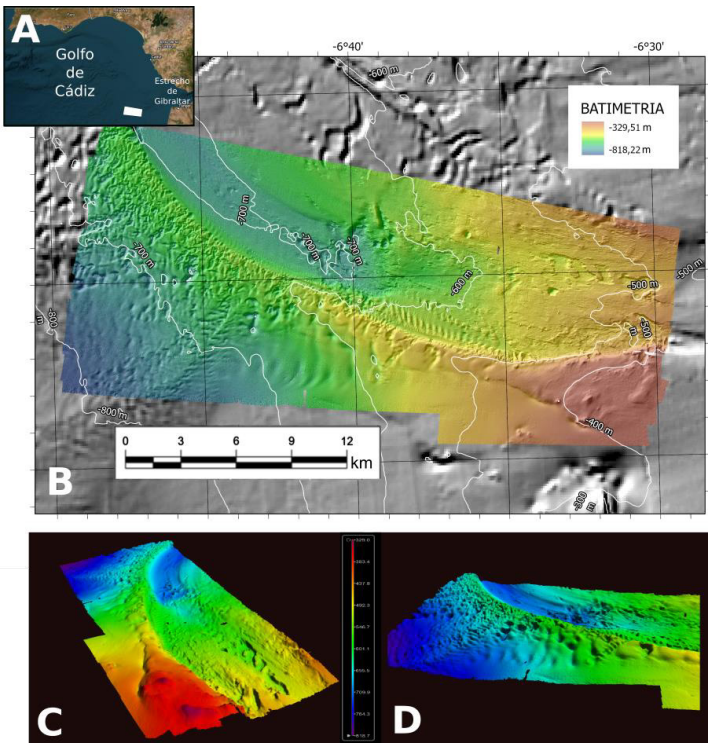

Figura 1. A) Localización general del Golfo de Cádiz con zona de estudio (recuadro blanco). B) Batimetría de alta resolución obtenida mediante ecosonda multihaz Kongsberg EM710 sobre un hillshade derivado de la batimetría de EMODnet (www.emodnet-bathymetry.eu). C) Vista tridimensional general desde el este mostrando la morfología del canal principal. D) Detalle del flanco sur del canal, donde se aprecian ondulaciones oblicuas al flujo de la MOW, asi como el drift sedimentario al sur de canal.

Finalmente, se destaca también la presencia de dos campos de dunas sedimentarias de dirección norte-sur en la mitad este del canal (Figura 1B), cuya orientación es perpendicular a ligeramente oblicua al eje principal del flujo. Estas dunas podrían haberse formado como resultado de procesos de circulación secundaria dentro del canal, los cuales generan patrones tridimensionales del flujo que favorecen la deposición de sedimentos en ciertas zonas laterales. Esto explicaría la presencia de sectores con dunas que desaparecen lateralmente y vuelven a aparecer más adelante, así como su orientación oblicua respecto al eje del flujo principal. Las áreas sin dunas corresponderían a sectores de mayor energía donde predominan procesos erosivos.

4. IMPLICACIONES OCEANOGRÁFICAS Y SEDIMENTARIAS

El núcleo de la masa de agua que transporta M1 presenta una salinidad superior a 37 (Figura 2A), con valores máximos concentrados en el centro del canal y un descenso hacia los laterales, especialmente hacia el borde sur. Estudios previos indican velocidades superiores a 1,0 m/s en el flanco sur, junto al drift sedimentario, y mínimos de 0,25 m/s hacia el norte (Sánchez-Leal *et al*., 2017), lo que sugiere que el núcleo de la MOW tiende a seguir el flanco del drift y su curvatura (Figura 2B). Sin embargo, en sectores más próximos al estrecho (6,75°W), se observa un desplazamiento puntual del núcleo hacia el flanco norte, donde se concentran salinidad y velocidad máximas. Esta inversión se atribuye a un resalte batimétrico que canaliza localmente el flujo, mostrando la alta sensibilidad de la MOW a la batimetría.

El análisis conjunto de batimetría, velocidad y salinidad revela un núcleo secundario de intensificación que se desplaza hacia la margen interna y alcanza el eje del canal. Hacia el sur, la masa de agua se ubica en la mitad meridional, con una sobreelevación de la interfase e inclinación del flujo hacia la margen externa. Esta distribución sugiere una circulación secundaria inducida por la batimetría, compatible con un flujo helicoidal forzado por la curvatura del canal.

En condiciones locales de mayor energía, el flujo principal puede superar el drift sedimentario, generando canales transversales hacia el talud inferior (Hernández-Molina *et al*., 2014). La presencia de rupturas en el drift, ondulaciones oblicuas respecto a la pendiente y depósitos sedimentarios en el flanco sur apoyan esta dinámica, que transporta sedimento desde el canal del talud medio al inferior. Los resultados obtenidos evidencian una transformación del flujo de la MOW, con asimetrías, filamentos menores y una estratificación más compleja de lo previamente descrito (Sánchez-Leal *et al.*, 2017). Su variabilidad y capacidad de transporte sedimentario dependen de la densidad, velocidad e interacción con la morfología del fondo. Esta región actúa como punto clave en la salida y distribución de las ramas principales de la MOW hacia el Atlántico Central, y en su mezcla con las aguas centrales atlánticas (ENACW) y la Masa de Agua Antártica Intermedia (AAIW).

5. CONCLUSIONES

Los resultados de este trabajo permiten proponer una hipótesis de circulación compleja de la MOW en el sector proximal del Golfo de Cádiz. La rama M1 se organiza en núcleos y filamentos que, al interactuar con el fondo, generan estructuras erosivas y deposicionales menores. Esta configuración, inferida a partir del relieve submarino, no había sido observada previamente y será próximamente contrastada con datos oceanográficos de alta resolución obtenidos en el marco del proyecto INPULSE.

Agradecimientos

Este trabajo ha sido financiado por el proyecto INPULSE (CTM2016-75129-C3-1-R), dentro del Programa Estatal de Investigación, Desarrollo e Innovación orientada a los Retos de la Sociedad (2016) del Ministerio de Economía y Competitividad (Gobierno de España). Se realiza en colaboración con el grupo de Investigación "*The Drifters*" (IACT-CSIC). Se agradece asimismo la asignación del B/O Ángeles Alvariño, cuya dotación contribuyó de manera esencial a la adquisición de los datos oceanográficos y batimétricos utilizados en este estudio.

REFERENCIAS

Hernández-Molina, F.J., Llave, E., Preu, B., Ercilla, G., Fontan, A., Bruno, M., Serra, N., Gomiz, J.J., Brackenridge, R.E., Sierro, F.J., Stow, D.A.V., García, M., Juan, C., Sandoval, N., y Arnaiz, A. (2014). Contourite processes associated to the Mediterranean Outflow Water after its exit from the Gibraltar Strait: global and conceptual implications. *Geology*, 42:227-230. https://doi.org/10.1130/G35083.1

Mena, A. y Fernández-Salas, L.M. (2024). Optimizing bathymetric position index (BPI) calculation: An analysis of parameters and recommendations for the selection of their optimal values. *Applied Computing and Geosciences*, 23:100168.

Sánchez-Leal, R.F., Bellanco, M.J., Fernández-Salas, L.M., García-Lafuente, J., Gasser-Rubinat, M., González-Pola, C., Hernández-Molina, F.J., Pelegrí, J.L., Peliz, A., Relvas, P., Roque, D., Ruiz-Villarreal, M., Sammartino, S. y Sánchez-Garrido, J.C. (2017). The Mediterranean Overflow in the Gulf of Cadiz: A rugged journey. *Science Advances*, 3(11):eaao0609.

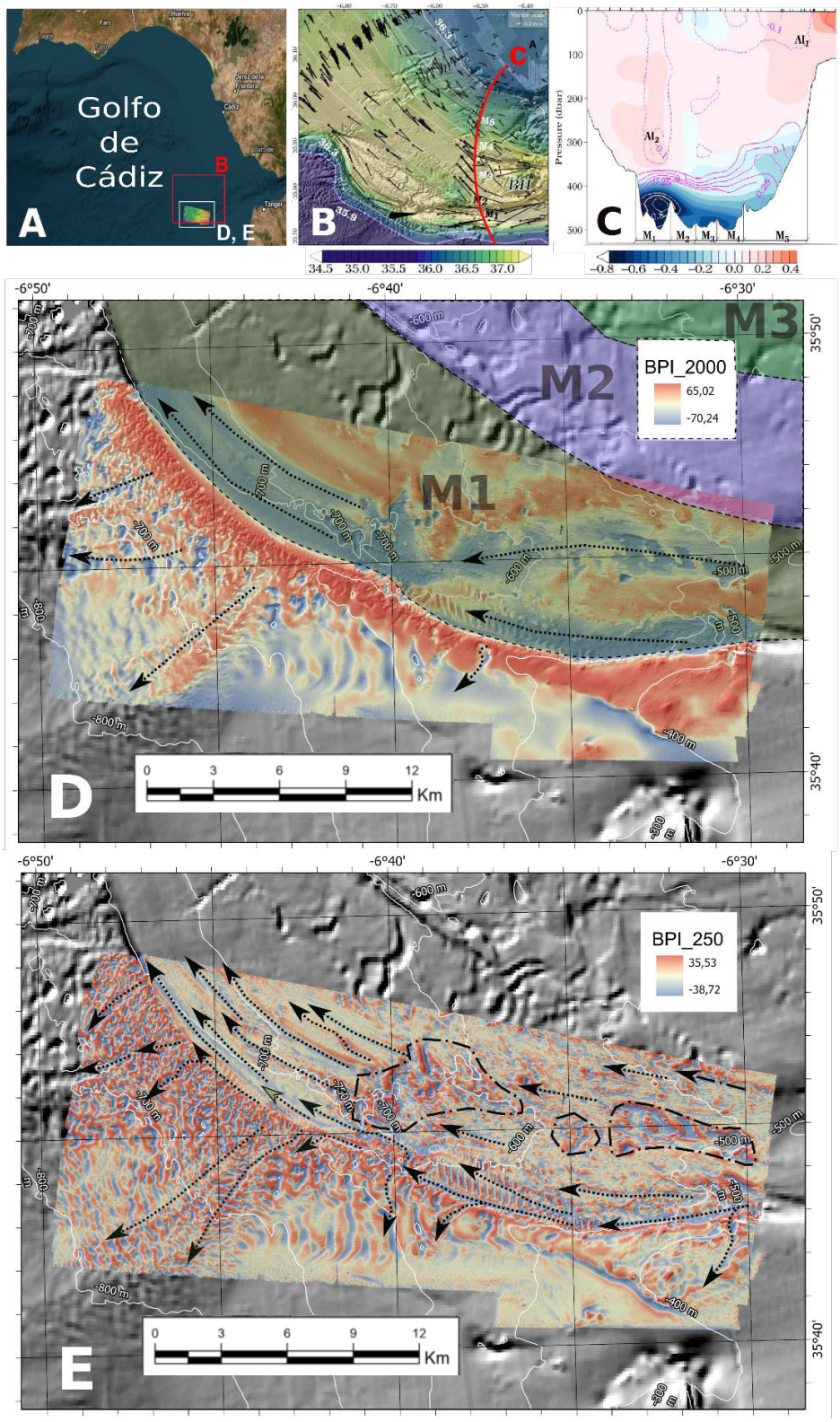

Figura 2. A) Localización general del Golfo de Cádiz, el recuadro blanco indica la localización de los paneles D y E, mientras que el área mostrada en el panel B se muestra con un recuadro rojo. B)Ramas (M1 a M5) de la Masa de Agua Mediterránea (MOW). La M1 describe un giro suave hacia el suroeste, mientras que M2 sigue una trayectoria recta hacia el noroeste. La línea curva roja indica la ubicación de la sección transversal mostrada en el panel C. Datos de A y B se han tomado de Sánchez-Leal et al. (2017). C) Sección transversal T4 mostrando la MOW bajo dos núcleos atlánticos (AI_1 & AI_2). Se observan núcleos divergentes a lo largo del talud, con velocidades máximas limitadas por la morfología del canal en su borde sur. D) Índice de posición batimétrica BPI2000 con las ramas M1–M3 (según Sánchez-Leal et al., 2017) y filamentos secundarios deducidos a partir del relieve. E) Propuesta de flujo de alta resolución sobre BPI250. Se indican flechas punteadas para las trayectorias del flujo y símbolos de líneas y puntos para depresiones erosivas.

Evaluación de métodos de bajo coste para el monitoreo de corrientes de resaca: Integración de GNSS-RTK y trazadores biodegradables

A. Marqués-Alonso (1), J. Á. García-Maza (1), M. Á. Reyes Merlo (2), D. Menéndez-Teleña (1)

(1) Department of Marine Science and Technology, University of Oviedo. C/Blasco de Garay s/n 33394, Gijón, Asturias. Spain. uo263295@uniovi.es

(2) State Coastal Authority of Asturias, Directorate-General for the Coast and the Sea, Ministry for the Ecological Transition and the Demographic Challenge, Asturias, Spain

Abstract: Rip currents are narrow water flows that return to the sea from the shore and pose a major risk to swimmers, being responsible for numerous rescues and drownings worldwide. Their formation depends on wave action and coastal topography, and although they can occur with relatively small waves, they have a significant impact on coastal dynamics. Despite extensive international research, no field experiments have been conducted on the Iberian Peninsula. Therefore, a low-cost experimental setup is proposed, using GNSS-RTK drifters attached to mannequins and fluorescent uranine tracers to simulate and analyze the behavior of these currents during the summer season. The collected data will help evaluate the effectiveness of these methods and develop a replicable model to enhance coastal safety. This study aims to promote the use of accessible tools for risk management in tourist beaches and strengthen prevention efforts against this hazardous coastal phenomenon.

Keywords: *Rip currents, drifters, beaches, dye-tracers, field experiment*

1. INTRODUCCIÓN

Las corrientes de resaca son flujos de agua estrechos y concentrados dirigidos hacia el mar que se extienden desde la costa a través de la zona rompiente y variando distancias en dirección a mar a dentro (Castelle, Scott, *et al.*, 2016; Scott *et al.*, 2016). Debido a su importancia, en el ámbito de la dinámica litoral, son uno de los fenómenos más estudiados a nivel mundial (Carpi *et al.*, 2021).

Además, su estudio y análisis se hace necesario a consecuencia del peligro que suponen para los bañistas de todo el mundo (Brighton *et al.*, 2013; Scott *et al.*, 2016). Estas corrientes son la principal causa de los rescates y ahogamientos en las playas a nivel mundial (Leatherman, 2013).

Su formación depende de las olas como fuerza generadora (Bowen, 1969). Estas, al avanzar hacia la costa, empujan las masas de agua que se acumulan progresivamente a medida que aumentan su velocidad y altura, hasta alcanzar el punto crítico de rotura. Dicha acumulación de agua en zonas de menor profundidad genera corrientes laterales denominadas *"feeders"* (Castelle, Scott, *et al*., 2016), que canalizan el exceso de agua hacia sectores específicos.

En esos puntos el flujo encuentra un camino de retorno hacia mar abierto, desplazándose a través de las ondas que continúan rompiendo en la playa (Kim y Shim, 2014).

En la Figura 1 se observa el esquema típico de intercambio de agua en la zona de rompiente, provocada debido a la formación de las corrientes de resaca.

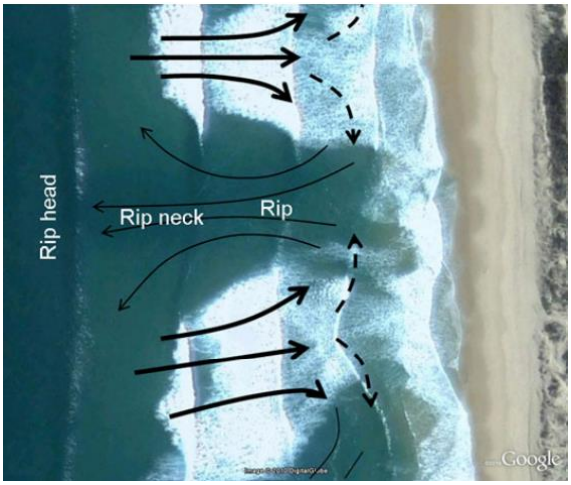

Figura 1.- Esquema tipo de la formación de las corrientes de resaca. Fuente: Mike Miloshis (2011).

Las corrientes de resaca pueden producirse en cualquier playa expuesta a diferentes tipos de oleaje (Wright y Short, 1984; Lippmann y Holman, 1989). Para su formación no son necesarias olas con una gran altura aparente, se encuentran con alturas de olas comprendidas entre 0,5 y 1,3 m (Bowman *et al*., 1988; Dusek y Seim, 2013; Benassai *et al.,* 2017).

Los primeros estudios sobre corrientes de resaca comenzaron en los años 40, siendo la primera organización que se dedicó a su estudio la *"Scripps Institution*

of Oceanography" en California. (Shepard *et al.*, 1941; Shepard y Inman, 1950; Inman y Quinn, 1951).

Desde entonces se han efectuado un gran número de investigaciones para comprender este fenómeno costero (Castelle, Scott, *et al.*, 2016; Scott *et al.*, 2016) y para analizar su peligrosidad (McCarroll *et al.*, 2013, 2015; Castelle, McCarroll *et al.*, 2016).

En concreto en los últimos años los estudios se han basado en intentar comprender y predecir los sistemas de corrientes de resaca en diferentes playas a nivel mundial, normalmente, playas con una gran afluencia de bañistas.

Los métodos empleados para su estudio son varios: cámaras fijas instaladas a lo largo de la playa (Surisetty *et al.*, 2023); modelos numéricos (Benassai *et al.*, 2017; Brambilla *et al.*, 2016; Dudkowska *et al.*, 2020; Hong *et al.,* 2021); tintes biodegradables (Arun Kumar *et al.*, 2021; Fatchurohman *et al.*, 2021; Kim y Kim, 2021); o drifters para la realización de análisis lagrangianos de los fluidos (Castelle *et al.*, 2014; Lee *et al.*, 2016; Scott *et al.*, 2016).

Sim embargo, y a pesar de la importancia de estas corrientes, en las costas de la península ibérica, no se ha realizado ningún experimento para el estudio de este fenómeno costero.

2. ÁREA DE ESTUDIO

La playa de estudio en la que se probará el experimento es *la de Salinas-El Espartal*. Se situada en la franja cantábrica de la península y es una de las principales playas del Principado de Asturias en cuanto a tamaño y afluencia de bañistas durante los meses de verano. En la Figura 2 se puede apreciar la localización de la playa, así como de una imagen aérea de la misma.

Figura 2. Situación playa de Salinas-El Espartal. Fuente: Fernández Pacheco et al. (2023).

3. METODOLOGÍA

Para preparar la investigación se ha diseñado un sistema de toma de datos low-cost basándose en las experiencias previas publicadas en diversas revistas de alto impacto.

Actualmente, el estudio de las corrientes de resaca está avanzando gracias al uso de sistemas baratos y flexibles. Se plantea emplear una serie de *drifters* con tecnología GNSS-RTK, acoplados a un maniquí que simula el movimiento de una persona atrapada por la corriente, para obtener datos de posición muy precisos, con errores de apenas un centímetro y frecuencias de muestreo muy bajas.

Para asegurar que este *"drifter"* describa fielmente la forma de la corriente de resaca, paralelamente a su lanzamiento, se dispersará una tinta en base de uranina que deja una mancha amarilla en el agua. Dicha tinta se distribuirá a lo largo de la corriente de resaca, tal como se puede apreciar en la Figura 3.

La tinta tendrá una presencia máxima de una hora antes de su completa degradación. El uso de tintas con base de uranina se ha empleado en la validación de distintas metodologías arrojando muy buenos resultados (Brander *et al.*, 2014; Fatchurohman *et al.*, 2021; Kim y Kim, 2021).

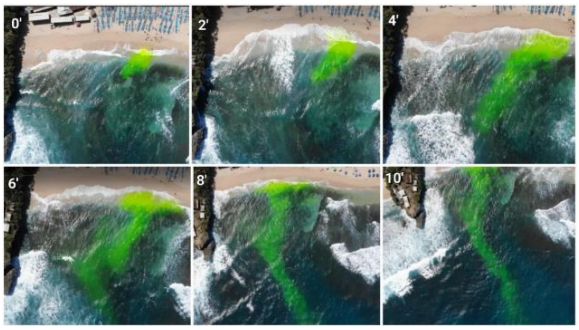

Figura 3. Ejemplo de la dispersión de una tinta en base de uranina empleada para el estudio de corrientes de resaca. Fuente: Fatchurohman et al. (2021).

El trabajo de campo se realiza durante los meses de verano del 2025, cuando la afluencia de bañistas e incidencias es máxima, los lanzamientos se realizarán bajo las diferentes condiciones meteorológicas a las que se ve sometida la playa. Además de comprobar la variabilidad de estas durante diferentes ciclos de marea.

4. RESULTADOS

Los resultados finales de la investigación constarán del análisis de las trayectorias obtenidas por los drifters GNSS-RTK como los de la Figura 4, que permiten la comparación con la dispersión superficial observada mediante los trazadores fluorescentes.

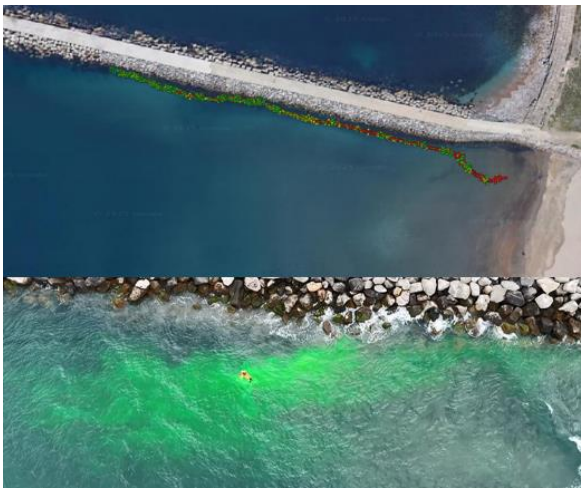

Figura 4. Ejemplo de toma de datos en la playa de Salinas-El Espartal (zona este de la playa, por la parte interior del espigón) empleando el drifter equipado con un equipo GNSS-RTK, la tinta con base de uranina y el maniquí. Fuente: elaboración propia.

A través de herramientas de análisis espacial y procesamiento de datos georreferenciados, se podrá caracterizar el comportamiento de las corrientes de resaca en las diferentes condiciones de marea y oleaje.

Asimismo, se evaluará la viabilidad del uso de sistemas low-cost para el monitoreo de estos fenómenos, destacando su posible integración en programas de prevención y rescate en playas de alta afluencia turística.

Se consiguió el propósito de generar un modelo replicable que permita mejorar la comprensión local de las corrientes de resaca, facilitando la toma de decisiones por parte de los servicios de salvamento, gestores costeros y autoridades competentes. Esto ayudará a conseguir una mayor conciencia de seguridad hacia este fatal fenómeno costero.

Esta investigación supone un primer paso hacia la implementación de tecnologías accesibles para la gestión del riesgo en zonas litorales, aportando datos valiosos tanto desde el punto de vista científico como operativo.

REFERENCIAS

Arun Kumar, S. V. V., Sivaiah, B., Venkateswarlu, C., Gireesh, B., Sridevi, T., Venkateswara Rao, K., Prasad, K. V. S. R., y Sharma, R. (2021). Investigation of rip current processes along Visakhapatnam beaches, east coast of India: A study based on GNSS drifters and dye experiments. *Journal of Earth System Science*, 130(2). https://doi.org/10.1007/s12040-021-01579-1

Benassai, G., Aucelli, P., Budillon, G., De Stefano, M., Di Luccio, D., Di Paola, G., Montella, R., Mucerino, L., Sica, M., y Pennetta, M. (2017). Rip current evidence by hydrodynamic simulations, bathymetric surveys and UAV observation. *Natural Hazards and Earth System Sciences*, 17(9), 1493-1503. https://doi.org/10.5194/nhess-17-1493-2017

Bowen, A. J. (1969). Rip currents: 1. Theoretical investigations. *Journal of Geophysical Research*, 74(23), 5467-5478. https://doi.org/10.1029/JC074i023p05467

Bowman, D., Arad, D., Rosen, D. S., Kit, E., Goldbery, R., y Slavicz, A. (1988). Flow characteristics along the rip current system under low-energy conditions. *Marine Geology*, 82(3), 149-167. https://doi.org/10.1016/0025-3227(88)90138-7

Brambilla, W., van Rooijen, A., Simeone, S., Ibba, A., y DeMuro, S. (2016). Field Observations, Video Monitoring and Numerical Modeling at Poetto Beach, Italy. *Journal of Coastal Research*, 825-U1368. https://doi.org/10.2112/SI75-166.1

Brander, R. W., Drozdzewski, D., y Dominey-Howes, D. (2014). "Dye in the Water": A Visual Approach to Communicating the Rip Current Hazard. *Science Communication*, 36(6), 802-810. https://doi.org/10.1177/1075547014543026

Brighton, B., Sherker, S., Brander, R., Thompson, M., y Bradstreet, A. (2013). Rip current related drowning deaths and rescues in Australia 2004–2011. *Natural Hazards and Earth System Sciences*, 13(4), 1069-1075. https://doi.org/10.5194/nhess-13-1069-2013

Carpi, L., Mucerino, L., Bonello, G., Besio, G., y Ferrari, M. (2021). Rip currents investigation on a Ligurian pocket beach, NW Mediterranean. *Estuarine, Coastal and Shelf Science*, 262, 107579. https://doi.org/10.1016/j.ecss.2021.107579

Castelle, B., Almar, R., Dorel, M., Lefebvre, J.-P., Senechal, N., Anthony, E. J., Laibi, R., Chuchla, R., y Penhoat, Y. du. (2014). Rip currents and circulation on a high-energy low-tide-terraced beach (Grand Popo, Benin, West Africa). *Journal of Coastal Research*, 70(sp1), 633-638. https://doi.org/10.2112/SI70-107.1

Castelle, B., McCarroll, R. J., Brander, R. W., Scott, T., y Dubarbier, B. (2016). Modelling the alongshore variability of optimum rip current escape strategies on a multiple rip-channelled beach. *Natural Hazards*, 81(1), 663-686. https://doi.org/10.1007/s11069-015-2101-3

Castelle, B., Scott, T., Brander, R. W., y McCarroll, R. J. (2016). Rip current types, circulation and hazard. *Earth-Science Reviews*, 163, 1-21. https://doi.org/10.1016/j.earscirev.2016.09.008

Dudkowska, A., Boruń, A., Malicki, J., Schönhofer, J., y Gic-Grusza, G. (2020). Rip currents in the non-tidal surf zone with sandbars: Numerical analysis versus field measurements. *Oceanologia*, 62(3), 291-308. https://doi.org/10.1016/j.oceano.2020.02.001

Dusek, G., y Seim, H. (2013). Rip Current Intensity Estimates from Lifeguard Observations. *Journal of Coastal Research,* 29, 505-518. https://doi.org/10.2307/23486335

Fatchurohman, H., Khasanah, A. N., y Cahyadi, A. (2021). Identification of Rip Current Hazards Using Fluorescent Dye And Unmanned Aerial Vehicle (A Case Study Of Drini Beach, Gunungkidul, Indonesia). https://doi.org/10.5194/nhess-2021-221

Fernández Pacheco, V. M., Amezqueta García, A., y Álvarez Álvarez, E. (2023). Análisis de la evolución del complejo

dunar Salinas-El Espartal mediante el empleo de ortofotografía, DSAS y LIDAR (1957-2021). Ingeniería del agua. https://doi.org/10.4995/Ia.2023.20021

Hong, X., Zhang, Y., Wang, B., Zhou, S., Yu, S., y Zhang, J. (2021). Numerical study of rip currents interlaced with multichannel sandbars. *Natural Hazards*, 108(1), 593-605. edssjs. https://doi.org/10.1007/s11069-021-04696-8

Inman, D. L., y Quinn, W. H. (1951). Currents in the surf zone. *Coastal Engineering Proceedings*, 2, Article 2. https://doi.org/10.9753/icce.v2.3

Kim, H. D., and Kim, K.-H. (2021). Analysis of Rip Current Characteristics Using Dye Tracking Method. *Atmosphere,* 12(6), 719. https://doi.org/10.3390/atmos12060719

Kim, K. H., y Shim, K. T. (2014). A Field Investigation of Waves and Wave-induced Currents at the Youngrang Coast of the Republic of Korea. *Journal of Coastal Research*, 72(sp1), 6-10. https://doi.org/10.2112/SI72-002.1

Leatherman, S. (2013). Rip Currents (pp. 811-831). https://doi.org/10.1007/978-94-007-5234-4_26

Lee, J., y Hong, S. (2023). Morphodynamics of Rip Current Systems at Haeundae Beach, Korea. *Journal of Coastal Research*, 39(1), 199-206. https://doi.org/10.2112/JCOASTRES-D-22TM-00008.1

Lee, J., Kim, D. H., Lee, S., y Lee, J. L. (2016). Lagrangian Observation of Rip Currents at Haeundae Beach Using an Optimal Buoy Type GPS Drifter. *Journal of Coastal Research*, 75(sp1), 1177-1181. https://doi.org/10.2112/SI75-236.1

Lippmann, T. C., y Holman, R. A. (1989). Quantification of sand bar morphology: A video technique based on wave dissipation. *Journal of Geophysical Research*, 94(C1), 995-1011. https://doi.org/10.1029/JC094iC01p00995

McCarroll, R. J., Brander, R. W., MacMahan, J. H., Turner, I. L., Reniers, A. J. H. M., Brown, J. A., y Bradstreet, A. (2013). Assessing the effectiveness of rip current swimmer escape strategies, Shelly Beach, NSW, Australia. *Journal of Coastal Research*, 784-789. https://doi.org/10.2112/SI65-133.1

McCarroll, R. J., Castelle, B., Brander, R. W., y Scott, T. (2015). Modelling rip current flow and bather escape strategies across a transverse bar and rip channel morphology. *Geomorphology*, 246, 502-518. https://doi.org/10.1016/j.geomorph.2015.06.041

Mike Miloshis (2011). Rip current escape strategies: Lessons for swimmers and coastal rescue authorities. https://doi.org/10.1007/s11069-011-9798-4

Scott, T., Austin, M., Masselink, G., y Russell, P. (2016). Dynamics of rip currents associated with groynes—Field measurements, modelling and implications for beach safety. *Coastal Engineering*, 107, 53-69. https://doi.org/10.1016/j.coastaleng.2015.09.013

Shepard, F. P., Emery, K. O., y La Fond, E. C. (1941). Rip Currents: A Process of Geological Importance. *The Journal of Geology*, 49(4), 337-369. https://doi.org/10.1086/624971

Shepard, F.P., y Inman, D.L. (1950). Nearshore water circulation related to bottom topography and wave refraction—Shepard—1950—Eos, Transactions American Geophysical Union—Wiley Online Library. https://agupubs-onlinelibrary-wiley-com.uniovi.idm.oclc.org/doi/10.1029/TR031i002p00196

Surisetty, V. v. a. k., Sharma, R., Venkateswarlu, C., Ramesh, M., Sheela Nair, L., Gireesh, B., y Naidu, C. v. (2023). Practical use of smartphone cameras in rip current monitoring studies. *Ocean and Coastal Management*, 243. https://doi.org/10.1016/j.ocecoaman.2023.106776

Wright, L. D., y Short, A. D. (1984). Morphodynamic variability of surf zones and beaches: A synthesis. *Marine Geology*, 56(1), 93-118. https://doi.org/10.1016/0025-3227(84)90008-2

Processos biogeoquímicos e interações atmosfera/ oceano/sedimento

Procesos biogeoquímicos e interacciones atmósfera/océano/sediment

Biogeochemical processes and atmosphere/ ocean/sediment interactions

Exploring 20 years of biogeochemical data on the Finisterre Section

E. Tel (1), R. Acerbi (2), M. Álvarez (2), R. Fernández-Graña (3), M. García-Ibáñez (4), G. Gonzalez-Nuevo (2), C. González-Pola (3), B. Marigomez Roldán (2), F. Redondo (1), M. Ruiz-Villareal (2), L. Sanz-Pinilla (1) and A. Viloria (5)

(1) Instituto Español de Oceanografía, IEO-CSIC, Madrid, 28002, Spain. elena.tel@ieo.csic.es
(2) Instituto Español de Oceanografía, IEO-CSIC, A Coruña, 15001, Spain
(3) Instituto Español de Oceanografía, IEO-CSIC, Gijón, 33212, Spain
(4) Instituto Español de Oceanografía, IEO-CSIC, Palma de Mallorca, 07015, Spain
(5) Instituto Español de Oceanografía, IEO-CSIC, Santander, 39004, Spain

Abstract: Oceanic long-time series, such as ship-based repeated measurements, are basic for marine science and coastal management. They enable the detection of long-term trends, and interannual variability, while also supporting anomaly and spike detection, systematic error control, and dataset quality enhancement. The Finisterre deep section (2003–2023) serves as a prime example, with dissolved oxygen and nutrient data rigorously quality-controlled and formatted to SeaDataNet standards by using controlled vocabularies, while metadata are harmonized and shared to meet FAIR standards. On the technological front, GeoNetwork provides a decentralized, standards-based platform for geospatial metadata management and harvesting across catalogues, boosting interoperability. Complementing this, Grafana offers powerful, open-source dashboards designed for time-series visualization, facilitating interactive exploration and monitoring of environmental variables such as nutrients and dissolved oxygen. Together, strategic observation systems as RADPROF and these IT infrastructures ensure high-quality, transparent, and interoperable oceanographic datasets—supporting science, climate studies, and predictive modeling.

Keywords: *ocean variability, monitoring, visualization tools, interoperability*

1. INTRODUCTION

Ocean time series programs, especially those based on repeated surveys, are critical for answering scientific questions and improving coastal management (Edwards *et al*., 2010). These observing systems provide the scientific community with the high-quality datasets needed to characterize ocean physics, climate, biogeochemistry and variability. In addition, they make it possible to examine and test current paradigms, as well as to generate new hypotheses about how the ocean works (Henson, 2014). Thanks to them, it is possible to differentiate changes due to the environmental natural variability, from those induced by human activity (Reid and Valdés, 2011).

In line with the need to generate historical timeseries, and within the framework of international programs, in the mid-1980s the Spanish Institute of Oceanography (IEO-CSIC) identified the need to carry out systematic and continuous observations of physical, chemical and biological variables in coastal waters. This materialized in the RADIALES program. In 2003, systematic deep-water sampling began in the framework of the VACLAN/RADPROF (Climate Variability in the North Atlantic) project, which since 2003 has been carrying out periodic sampling (see Figure 1), at least once a year, in the oceanic waters of the northwestern peninsular (Prieto *et al*., 2015). In following years, it consolidated its position as a fundamental part of the IEO observing system (IEOOS, Tel *et al*., 2016). At the regional level, in 2008 the Observatorio da Marxe Ibérica RAIA began operating as joint initiative of research centers, universities and administrations of Galicia and Portugal, for coastal monitoring and forecasting, positioning the Galicia-North Portugal Euroregion as one of the areas with the greatest coverage in operational oceanography in Europe. All together, these monitoring systems represent an integrated ocean observation infrastructure of high scientific-operational value, favoring knowledge that possibilities environmental management, the study of climate change and the development of predictive models in the region.

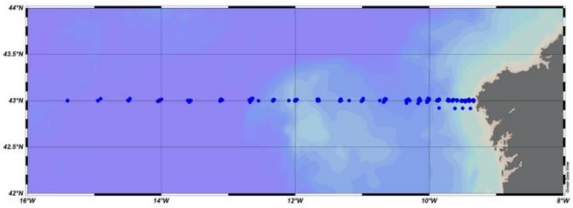

Figure 1. Stations map for Finisterre standard section during the period (2003-2023).

At the same time, in recent years the use of robust IT infrastructures that promote collaboration and interoperability between agencies has been consolidated. In order to facilitate data discovery and

access, geoportals, understood as web interfaces between humans and machines, have emerged as a key-solution for data management. Their implementation allows locating and accessing geographic information and associated services (visualization, editing and analysis) through the Internet, consolidating as an essential element of a Spatial Data Infrastructure (SDI). In this sense, the IEO is making an important effort for its institutional implementation linked to other important international initiatives in the framework of data management such as IODE/IOC/UNESCO (International Oceanographic Data Exchange), SeaDataNet (Pan-European infrastructure for ocean & marine data management) or EMODNET (European Marine Observation and Data Network). The time-series obtained through 20 years of oceanographic sampling are favored by this type of developments that offer a unique opportunity for the visualization and analysis of nutrient and dissolved oxygen.

2. METHODOLOGY AND RESULTS

Long-time series are essential to ensure data quality and reliability, especially in the marine environment. These continuously sampled records allow characterizing trends and patterns, identifying long-term trends and interannual variability, validating and detecting anomalies, establishing baselines and detecting outliers, as well as controlling systematic errors and spikes, improving the quality of the dataset. An exhaustive quality control of the dissolved oxygen and nutrient data obtained from the Finisterre Radial time series (2003-2023) has recently been performed. Table I, located at the end of this summary, shows the list of campaigns carried out in these years. The data obtained through bottle sampling have been systematically analyzed in the laboratory. After validation of the whole historical series, they have been conveniently formatted according to the European recommendations available at www.seadatanet.org. The metadata, created using standardized vocabularies, have been incorporated into existing networks allowing the IEO to respond to national and European demands.

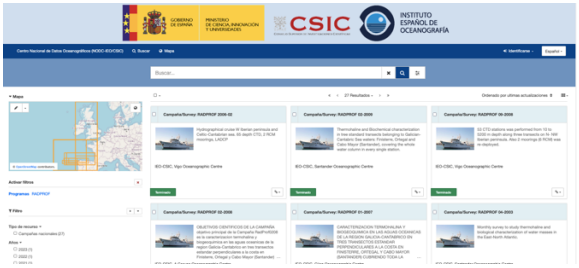

Figure 2. IEO Data catalogue with all the information related to RADPROF monitoring surveys program. (http://nodc.ieo.es/geonetwork → programas → RADPROF).

Although different solutions have been implemented over time and have changed as technology evolved, the most recent IEO web catalog (http://nodc.ieo.es/geonetwork) uses the open source tool GeoNetwork 4.2.1, which offers a standardized and decentralized geospatial information management system that it is based on international standards, providing a user-friendly interface for searching and accessing spatial data (Sanz-Pinilla *et al.*, 2025). Among other functionalities, this software allows managing metadata and operating without the need for a dedicated database, being fully customizable to meet IEO needs and ensuring compliance with FAIR principles (Wilkinson *et al.*, 2016). Thus, the information of all the performed surveys can be consulted in the institutional catalog where they have a dedicated tab (Figure 2). In addition, GeoNetwork technology facilitates the data harvesting from other IEO catalogs (e.g., https://centolo.co.ieo.es/geonetwork), centralizing the available information and automating its simultaneous integration in all metadata repositories. This ensures interoperability, visibility and efficient access to geo-referenced data generated in the different IEO centers and projects. Grafana (Grafana Labs, 2025) is an open-source platform for data exploration and visualization, especially designed to work with timeseries data (Figure 3), such as performance metrics, logs or distributed traces. In this sense it offers a unique opportunity for visualization and analysis of the nutrient and dissolved oxygen timeseries being collected at Finisterre section.

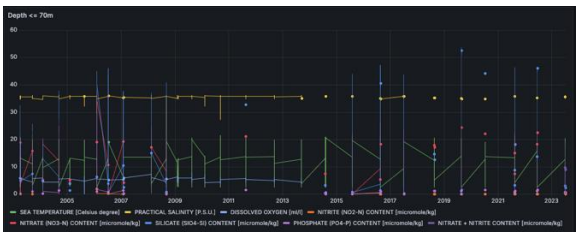

Figure 3. Example of the Finisterre section timeseries displayed with Grafana during the validation process.

3. CONCLUSIONS

The Finisterre Section data represent changes in the eastern boundary of the North Atlantic (Prieto *et al.*, 2015). They are a clear demonstration of the importance of systematic and repeated observations to capture relevant regional changes in the structure of the deep ocean and its water masses, with direct implications for understanding the dynamics of the North Atlantic and its response to climate forcings.

Having long-time records is key to defining robust reference patterns, detecting errors and anomalies, applying automated quality control, and adapting analyses to changing conditions. This not only

improves data integrity, but also facilitates reliable use of the information in climate change studies, environmental management, operational forecasting, and evidence-based decision making. The time series of the Finisterre Section, obtained over 20 years of annual sampling, have a great scientific value that can be highlighted with an adequate visualization, which favors decision making and synergies between different groups of activities.

Geoportals improve data integration, avoid duplication and promote collaborative work between public, private and academic entities. Their integrated use with data visualization and exploration tools such as Geonetwork and Grafana, constitute a strategic tool within a SDI. The implementation for the Finisterre Section, in this case, facilitates the access, use and integration of ocean data in an interoperable environment aligned with FAIR principles. Despite its growing relevance, its use in the marine domain is still limited, although the creation of examples such as the one presented here or SNIMar (Portugal) demonstrates its potential to support marine planning and governance.

Acknowledgements

The recent validation of the data timeseries used was carried out under JAEICU_24_01237 (CSIC). The projects that gave rise to the VACLAN (REN 2003-08193-C03-01/MAR) and COVACLAN (CTM2007-64600/MAR) series continued with IEO's own funding. The European Marine Observation and Data Network (EMODnet) Ingestion and Safe-keeping of Marine Data (CINEA/EMFAF/2021/3.4.10/02/SI2.868290 and EMODnet - Chemistry lot (EASME/EMFF/2020/ 3.1.11/Lot5/SI2.846161) have enabled the integration of data in accordance with currently accepted international standards.

The authors would like to express their deepest thanks to all the colleagues who made this time series possible, especially J. M. Cabanas, R. Carballo, N. González, A. Lavín and C. Rodríguez-Puente, who are now retired, as well as to the personnel of the research vessels involved.

REFERENCES

Edwards, M., Beaugrand, G., Hays, G.C., Koslow, J.A., and Richardson, A.J. (2010). Multidecadal oceanic ecological datasets and their application in marine policy and management. *Trends Ecol. Evol.*, 25, 602–610. https://doi.org/10.1016/j. tree.2010.07.007.

GeoNetwork OpenSource. (2022). GeoNetwork opensource Version 4.2.1 [Catálogo de información geoespacial; versión de software]. Open Source Geospatial Foundation. https://geonetwork-opensource.org

Grafana Labs. (2025). Grafana: analytics & monitoring platform [Software informal]. Recuperado de https://github.com/grafana/grafana

Henson, S.A. (2014). Slow science: the value of long ocean biogeochemistry records. Phil. Trans. R. Soc. A 372. https://doi.org/10.1098/rsta.2013.0334

Prieto, E., Gonzalez-Pola, C., Lavín, A., and Holliday, N. (2015). Interannual variability of the northwestern Iberia deep ocean: Response to large-scale North Atlantic forcing. *J. Geophys. Res. Oceans*, 120(2), 832–847. https://doi.org/10.1002/2014JC010436

Reid, P.C., and Valdes, L. (2011). ICES status report on climate change in the North Atlantic. ICES Coop. Res. Rep. 310, 262 pp.

Sanz-Pinilla, L., González-Nuevo, G., Tel, E., and Ruiz-Villarreal, M. (2025). Development of a new IEO Catalogue for the Visualization and Management of Marine Data. *Proceedings of the 12th International Workshop on Marine Technology – MARTECH 2025*, Pasaia (Gipuzkoa), España. ISBN 978-84-09-61714-2

Tel, E., Balbin, R., Cabanas, J. M., Garcia, M. J., Garcia-Martinez, M.C., Gonzalez-Pola, C., Lavin, A., Lopez-Jurado, J. L., Rodriguez, C., Ruiz-Villarreal, M., Sánchez-Leal, R. F., Vargas-Yáñez, M., and Vélez-Belchí,P. (2016). IEOOS: the Spanish Institute of Oceanography Observing Systems. *Ocean Science*, 12, 345-353. https://doi.org/10.5194%2Fos-12-345-2016

Wilkinson, M., Dumontier, M., Aalbersberg, I. *et al*. (2016) The FAIR Guiding Principles for scientific data management and stewardship. *Scientific Data*, 3, 160018. https://doi.org/10.1038/sdata.2016.18

Table I. List of RADPROF surveys carried out in the period 2003-2023 and stations sampled in them.

Survey	Dates	Research Vessel	Num. sampled stations
RADPROF 200303	24 MAR - 6 APRIL 2003	C. Saavedra	60
RADPROF 200304	08 - 18 APRIL 2003	C. Saavedra	37
RADPROF 200309	10 - 21 SEPT 2003	C. Saavedra	41
RADPROF 200402	04- 13 FEB 2004	C. Saavedra	8
RADPROF 200409	05 - 13 SEPT 2004	C. Saavedra	37
RADPROF 200501	26 JAN 04 FEB 2005	C. Saavedra	43
RADPROF 200508	20 AUG- 11 SEPT 2005	Thalassa	83
RADPROF 200602	05-12 FEB 2006	C. Saavedra	50
RADPROF 200607	07 - 29 JUL 2006	C. Saavedra	56
RADPROF 200701	31 JAN- 07 FEB 2007	C. Saavedra	40
RADPROF 200802	11 - 19 FEB 2008	C. Saavedra	53
RADPROF 200809	03 - 14 SEPT 2008	C. Saavedra	44
RADPROF 200902	28 JAN-14 FEB 2009	C. Saavedra	38
RADPROF 200908	10 - 23 AUG 2009	C. Saavedra	64
RADPROF 201002	03 - 15 FEB 2010	C. Saavedra	19
RADPROF 201009	01-14 SEPT 2010	C. Saavedra	41
RADPROF 201108	11 - 26 AUG 2011	C. Saavedra	56
RADPROF 201209	12 - 19 SEPT 2012	C. Saavedra	26
RADPROF 201309	12 - 20 SEPT 2013	A. Alvariño	26
RADPROF MODUPLAN 201408	04 - 24 AUG 2014	Sarmiento de Gamboa	58
RADPROF 201507	30 JUL - 10 AUG 2015	R Margalef	29
RADPROF 201608	15 - 26 AUG 2016	R Margalef	29
RADPROF 201701	01 - 14 JUL 2017	R Margalef	33
RADPROF 201808	18 - 27 AUG 2018	R Margalef	30
RADPROF 201908	18 - 29 AUG 2019	R Margalef	30
RADPROF iFADO 202007	08 - 22 JUL 2020	Sarmiento de Gamboa	55
RADPROF 202108	14 - 23 AUG 2021	R Margalef	44
RADPROF 202206	14 - 25 JUN 2022	R Margalef	25
RADPROF 202307	03 - 11 JUL 2023	R Margalef	20

Projeto CONNECT$^+$: Aplicação à Ria Formosa

A. Cravo (1), E. Garel (1), J. Jacob (1), E. Macieira (1) e M. Rodrigues (2)

(1) CIMA, Universidade do Algarve, Campus de Gambelas, 8005-139 Faro, Portugal. acravo@ualg.pt
(2) Laboratório Nacional de Engenharia Civil, I.P. Avenida do Brasil, 101, 1700-066 Lisboa, Portugal

Abstract: Coastal water quality monitoring is crucial for environmental and socioeconomic sustainability. The CONNECT$^+$ project implements an innovative coastal water quality monitoring system in Ria Formosa lagoon, Portugal. An instrumented buoy will continuously monitor (1 year), temperature, salinity, pH, and dissolved oxygen levels every 15 minutes, providing high-resolution data essential for understanding environmental patterns. This monitoring system supports crucial bivalve aquaculture activities that employ about 10,000 people. The project integrates observational data with sophisticated predictive models, simulation of lagrangean tracers on demand, 48-hour forecasts of various parameters including physical-chemical-biological parameters and satellite data from Copernicus Marine Service. A week data from June 2025 reveals substantial daily and tidal variations, particularly in dissolved oxygen and pH levels, demonstrating the significant impact of biological processes. Data will be made publicly available through a WebGIS portal, serving shellfish farmers, water managers, and researchers while supporting sustainable development aligned with EU environmental directives.

Keywords: *Monitoring Program, water quality, Ria Formosa*

1. INTRODUÇÃO

A monitorização da qualidade da água em sistemas costeiros assume uma relevância ímpar para a sustentabilidade ambiental e socioeconómica destes sistemas. Esta é uma atividade crítica que permite identificar padrões naturais e alterações antropogénicas nos ecossistemas marinhos, sendo essencial para a proteção da biodiversidade aquática e o funcionamento dos mesmos. A implementação efetiva de programas de monitorização também possibilita a deteção precoce de alterações adversas na qualidade da água, permitindo intervenções oportunas que minimizam impactos negativos sobre os ecossistemas marinhos e as populações humanas dependentes dos seus recursos naturais. Estes aspetos são de importância capital para atividades ligadas à qualidade da água, como a aquacultura e a pesca, contribuindo assim para o desenvolvimento sustentável.

A execução de programas de monitorização de qualidade de água, com alta resolução temporal, em ecossistemas marinhos, é fundamental para compreender adequadamente os complexos padrões dinâmicos que ocorrem nestes ambientes. A frequência de amostragem elevada permite capturar eventos críticos que podem ocorrer em escalas temporais muito curtas, como mudanças rápidas na química da água, quer por processos naturais quer por pressão antropogénica. Além disso, este tipo de monitorização, mantida por períodos de amostragem longos, permite identificar padrões de variação intra-anuais e interanuais, que são essenciais para entender como os ecossistemas marinhos respondem às mudanças ambientais globais. A resolução temporal elevada também permite melhorar a calibração e validação de modelos de previsão, tornando-se assim um instrumento crucial para o desenvolvimento de estratégias eficazes de conservação e gestão desses ecossistemas vitais.

No âmbito do projeto CONNECT$^+$, foi fundeada uma boia oceanográfica de superfície, na Ria Formosa, no Canal de Marim, junto da Praia dos Cavacos, numa zona pouco profunda, próxima de viveiros de bivalves (Figura 1), instrumentada com uma sonda multiparamétrica NKE, modelo WIMO, com aquisição de dados de temperatura, salinidade, pH e oxigénio dissolvido, com intervalo de amostragem de 15 minutos e transmissão em tempo quase-real, a cada 6 horas. Esta boia permanecerá fundeada por um período mínimo de 1 ano.

Os parâmetros chave de qualidade de água medidos são importantes para apoiar a aquacultura de bivalves, que depende intrinsecamente da qualidade da água e que pode contribuir para a proteção das águas costeiras e para o desenvolvimento da economia azul da Ria Formosa, na costa sul de Portugal.

Figura 1. Localização da Ria Formosa na costa sul de Portugal e localização do fundeamento da sonda na boia oceanográfica na Praia dos Cavocos, Canal de Marim, junto a Olhão.

O serviço de previsão e monitorização costeira CONNECT (Rodrigues *et al.*, 2025) implementa uma abordagem integrada, que combina dados observacionais, incluindo dados da rede de monitorização CoastNet (Castellanos *et al.*, 2021; França *et al.*, 2021), com modelos de previsão avançados, proporcionando resolução espacial elevada e resolução temporal adequada às necessidades específicas da gestão costeira. O serviço constitui uma infraestrutura avançada de suporte à gestão costeira, desenvolvida especificamente para responder às necessidades de monitorização sistemática das características físicas, químicas e biológicas das massas de água costeiras portuguesas.

O projeto CONNECT^{+} estende este serviço à região do Algarve, nomeadamente à Ria Formosa. Os novos dados observacionais, obtidos em tempo quase-real, serão integrados num portal WebSIG dedicado (https://connect-portal.lnec.pt/connect/), onde serão também disponibilizados dados adicionais sobre previsões diárias de variáveis físicas, químicas e biológicas (clorofila e bactérias indicadoras de contaminação fecal), utilizando o modelo SCHISM (Zhang *et al.*, 2016), operado pela ferramenta de previsão WIFF (Rogeiro *et al.*, 2018; Rodrigues *et al.*, 2021) e pelo serviço OPENCoastS (Oliveira *et al.*, 2020, 2021), e forçado por previsões dos modelos regionais do Copernicus Marine Service.

O portal WebSIG fornecerá assim previsões para 2-dias de várias variáveis físicas, químicas e biológicas, a simulação a pedido de traçadores passivos, e o acesso em tempo real aos dados da nova boia oceanográfica.

Este portal WebSIG proporcionará acesso público, disponibilizando múltiplos produtos operacionais, úteis para mariscadores, gestores de água e gestores ambientais, comunidade científica e público em geral. O sistema contribui diretamente para o cumprimento das diretrizes ambientais da União Europeia, nomeadamente da Diretiva Quadro da Água (DQA) e da Diretiva Quadro da Estratégia Marinha (DQEM).

2. MATERIAL E MÉTODOS

A sonda multiparamétrica NKE, modelo WIMO, instalada na boia oceanográfica de superfície apresenta-se na Figura 2.

As especificações técnicas, de gama de variação, exatidão e precisão dos sensores de temperatura, salinidade, pH e oxigénio dissolvido, instalados na sonda estão apresentadas na Tabela I.

Tabela I. Especificações técnicas, gama de variação, exatidão e precisão dos sensores de temperatura, salinidade, pH e oxigénio dissolvido, instalados na sonda NKE, modelo WIMO fundeada na Praia dos Cavacos, Ria Formosa.

Sensor	Gama de medição	Exatidão	Precisão
Temperatura	2 a +35 ^{0}C	± 0,1 ^{0}C	0,01 ^{0}C
Condutividade	0 – 100 mS/cm	± 0,5% da leitura	0,001 mS/cm
pH	0 – 14 pH	0,1 pH	0,01 pH
Oxigénio dissolvido	0 – 23 mg/L	± 0,1 mg/L	0,025 mg/L

A aquisição de dados fiáveis e robustos requer protocolos adequados de controlo e garantia de qualidade (Glasgow Jr. *et al.*, 2004), incluindo manutenção frequente, inspeção, limpeza e calibração (Garel e Ferreira, 2011), bem como a aplicação de métodos estatísticos adequados. Foram estabelecidos procedimentos de manutenção, para garantir a aquisição contínua, a qualidade dos dados e a segurança da sonda multiparamétrica. Estes procedimentos incluirão inspeção visual e limpeza manual da sonda, verificação e calibração de todos os sensores, exceto o de temperatura.

Figura 2. Sonda multiparamétrica NKE, modelo WIMO, instalada na boia oceanográfica de superfície, no Canal de Marim, junto à Praia dos Cavacos, na Ria Formosa.

O controlo de qualidade será assegurado seguindo rigorosamente os procedimentos de funcionamento e de calibração especificados pelo fabricante. A calibração será efetuada mensalmente. Será utilizada uma solução de calibração de condutividade de 50 mS/cm, três soluções de calibração de pH (pH 4, 7 e 10). Todas as soluções de calibração a ser utilizadas serão as recomendadas pelo fabricante.

O sensor de oxigénio irá ser calibrado utilizando o método recomendado pelo fabricante, colocando a sonda num copo de calibração húmido e arejado, obrigando a percentagem de saturação a ser 100%. O método de Winkler (Winkler, 1888) será também utilizado para verificar a exatidão do valor de concentração.

3. RESULTADOS E DISCUSSÃO

Serão analisados com detalhe dados de verão e outono, de junho a outubro de 2025, a diferentes escalas de resolução temporal, que permitirão avaliar eventos rápidos/extremos, diários/diurnos, semanais com influência de marés vivas e marés mortas, eventos de afloramento costeiro e/ou de contracorrente, bem como à escala sazonal. Em função dos resultados obtidos, rapidamente poderão ser dados alarmes a nível de oxigénio dissolvido, temperatura ou salinidade que podem afetar o recurso dos bivalves, apoiando assim a atividade de aquicultura e contribuindo para a proteção das águas costeiras e a economia azul da Ria Formosa, na costa sul de Portugal.

A título de exemplo, mostra-se na Figura 3 os dados recolhidos na primeira semana de fundeamento, no período semanal de 20 a 27 junho 2025, relativos a nível e temperatura da água, oxigénio dissolvido (expressa em percentagem de saturação), salinidade e pH.

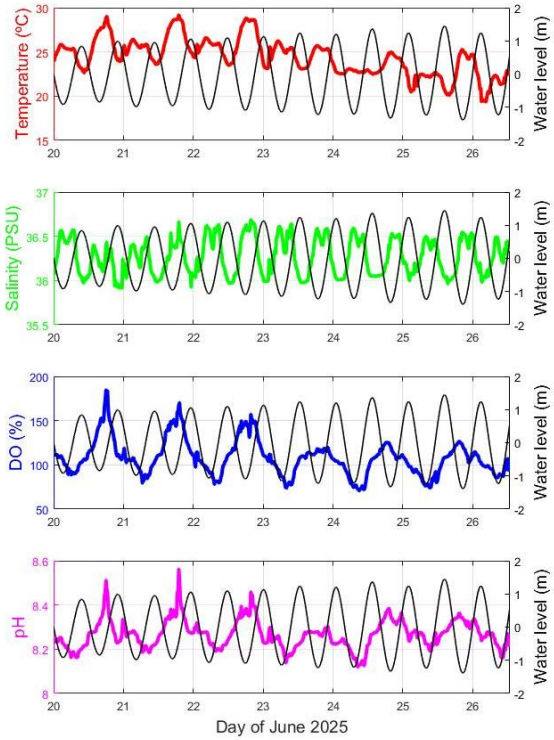

Figura 3. Variação da temperatura da água, salinidade, pH e percentagem de saturação de oxigénio dissolvido pela sonda multiparamétrica NKE, instalada na boia oceanográfica fundada na Praia dos Cavacos, Canal de Marim, na Ria Formosa, no âmbito do projeto CONNECT⁺, no período semanal de 20 a 27 de junho.

As variações de maré não são locais, mas correspondem a uma localização costeira próxima (Vila Real de Santo António). Representam aproximadamente a hora da preia-mar e baixa-mar, pois não incluem o atraso de 1 a 2 horas devido à propagação da maré dentro da Ria. Contudo, os dados

mostram claramente que para os parâmetros medidos pela sonda há variabilidade diária e também associada à fase da maré (vazante ou enchente).

Em geral, todos os parâmetros demonstram um padrão de variabilidade em anti-fase com a maré. Contudo, para o oxigénio dissolvido e para o pH o efeito diário (dia/noite) mostra claramente que o impacto dos processos biológicos (fotossíntese/respiração) é mais importante do que a própria altura da maré.

A variabilidade dos parâmetros foi mais acentuada para o oxigénio dissolvido (com concentrações entre 6 e 13,5 mg/L e percentagem de saturação entre 70% e 170%) e pH (8,0-8,5), que evidenciam a importância dos processos biológicos em termos de fotossíntese e respiração, nesta zona de baixa profundidade da Ria Formosa, com vegetação aquática e junto de viveiros de bivalves.

O aumento acentuado do oxigénio foi responsável pelos elevados valores de pH e neste período de 1 semana em junho, todos os valores de oxigénio estão acima do valor mínimo recomendado para águas conquícolas (VMR=70%, DL 236/98; Diário da Républica, 1998). Contudo, com o aumento da temperatura no período de verão é expectável que os valores durante a noite (por aumento de respiração) possam baixar para valores preocupantes para os bivalves, abaixo do valor mínimo admitido (VMA=60%).

Séries temporais mais longas permitirão avaliar as causas dos desvios nas medições em relação ao padrão típico e contribuir para a proteção da qualidade da água, tão importante para o setor de produção dos bivalves na Ria Formosa.

Agradecimentos

Os autores agradecem o financiamento do trabalho através da P/S 10PS00137 - MERCATOR OCEAN:24263L01-COP- INNO USER-9000.

Os autores agradecem ainda às entidades colaboradoras, nomeadamente AdA, APA, IPMA, Cooperativa Formosa, Capitania do Porto de Olhão

REFERÊNCIAS

Castellanos, P., Brito, A.C., Chainho, P., Quintella, B., da Costa, L., França, S., Cabral, H., e Costa, J.L. (2021). CoastNet Dataset from Mondego, Tejo and Mira Estuaries: Multiparametric measurements during 2020. *Frontiers in Marine Science*, 8:707089.

Diário da República (1998). Decreto-Lei 236/98. Estabelece normas, critérios e objectivos de qualidade com a finalidade de proteger o meio aquático e melhorar a qualidade das águas em função dos seus principais usos. Revoga o Decreto-Lei n.º 74/90, de 7 de Março, nº 176, Série I-A de 1998-08-01, pp. 3676 – 3722.

França, S., Fonseca, V.F., Tanner, S.E., Vasconcelos, R., Reis-Santos, P., Maia, A., Ruano, M., Cardoso, I., Henriques, S., Pais, M.P., Brandão, P., Brito, A.C., Castellanos, P., Chainho, P., Quintella, B., da Costa, L., Costa, M.J., Costa, J.L., e Cabral, H.N. (2021). Historical data in the CoastNet Geoportal: snapshot of estuarine fish communities. In: Portuguese estuaries. *Frontiers in Marine Science*, 8:685294.

Garel, E., e Ferreira, Ó. (2011). Monitoring estuaries using non-permanent stations: practical aspects and data examples. *Ocean Dynamics*, 61 (7):891–902.

Glasgow, Jr., Burkholder, J.M., Reed, R.E., Lewitus, A.J., e Kleinman, J.E. (2004). Realtime remote monitoring of water quality: a review of current applications, and advancements in sensor, telemetry, and computing technologies. *Journal of Experimental Marine Biology and Ecology*, 300:409–448.

Oliveira, A., Fortunato, A.B., Rodrigues, M., Azevedo, A., Rogeiro, J., Bernardo, S., Lavaud, L., Bertin, X., Nahon, A., Jesus, G., Rocha, M., e Lopes, P. (2021). Forecasting contrasting coastal and estuarine hydrodynamics with OPENCoastS. *Environmental Modelling & Software*, 143:105132.

Oliveira, A., Fortunato, A.B., Rogeiro, J., Teixeira, J., Azevedo, A., Lavaud, L., Bertin, A., Gomes, J., David, M., Pina, J., Rodrigues, M., e Lopes, P. (2020). OPENCoastS: An open-access service for the automatic generation of coastal forecast systems. *Environmental Modelling & Software*, 124:104585.

Rodrigues, M., Fortunato, A.B., Martins, R.J., Jesus, G., Brito, A.C., Oliveira, A., Nahon, A., Costa, J.L., Alves, E., Korani, M., e Azevedo, A. (2025). CONNECT – Local coastal monitoring service for Portugal. Book of papers, *IAHR 2024 – 8th IAHR Europe Congres*s, pp. 237-246.

Rodrigues, M., Martins, R., Rogeiro, J., Fortunato, A.B., Oliveira, A., Cravo, A., Jacob, J., Rosa, A., Azevedo, A., e Freire, P. (2021). A web-based observatory for biogeochemical assessment in coastal regions. *Journal of Environmental Informatics*, 38(1):1-15.

Rogeiro, J., Rodrigues, M., Azevedo, A., Oliveira, A., Martins, J.P., David, M., Pina, J., Dias, N., e Gomes, J. (2018). *Advances in Engineering Software*, 117:70-79.

Zhang, Y.I., Ye, F., Stanev, E.V., e Grashorn, S. (2016). Seamless cross-scale modeling with SCHISM. *Ocean Modelling,* 102:64-81.

Winkler, W.L. (1888). Di Bestimmund des in Wasser geloKsten Sauersto!en. *Berichte der Duetschen Chemischen Gesellschaft*, 21:2843–2855.

The RADPROF program (2003-2023): twenty years of hydrographic data in the North East Atlantic ocean

M. Álvarez (1), B. Marigomez Roldán (1), R. Fernández Graña (2), R. Acerbi (1) and C. González Pola (2)

(1) Instituto Español de Oceanografía, IEO-CSIC, A Coruña, 15001, Spain. marta.alvarez@ieo.csic.es
(2) Instituto Español de Oceanografía, IEO-CSIC, Gijón, 33212, Spain

Abstract: Ship-based time series of high quality hydrographic and oxygen data are precious to evaluate long term interannual changes driven by natural and climate change variability. Here we present a time series of 20 years in the Northeast Atlantic Ocean of CTD based data for temperature, salinity and dissolved oxygen. We perform strict first and secondary quality control procedures to show the reliability, internal and external coherence of the data set, which will be finally made publicly available following FAIR principles.

Keywords: *hydrography, time series, CTD, thermohaline, dissolved oxygen*

1. INTRODUCTION

The RADPROF (RADIALES PROFUNDOS) program (2003-2023) (Figure 1), established by the Spanish Institute of Oceanography Observing System (IEOOS), aims to monitor the hydrographic and biogeochemical properties of deep waters in the Galicia-Cantabrian region of northwest Iberia. This initiative focuses on understanding the long-term changes in water masses and ocean circulation, which are crucial for grasping the mechanisms that influence ocean variability in the context of climate change (Tel *et al*., 2016). The data collected by RADPROF are essential for international programs like ICES and MSFD contributing to global efforts to assess the health and dynamics of ocean systems.

This work focuses on presenting the Conductivity Temperature and Depth (CTD) continuous data gathered deploying sensors attached to the rosette frame, usually called CTD-data. This continuous and sensor-based data is contrasted against discrete measurements following best practices guides as the GO-SHIP Hydro Manual (Hood *et al*., 2010).

2. METHODOLOGY AND RESULTS

RADPROF cruises expand from 2003 to 2023 over the Iberian and North Iberian basins and the Bay of Biscay, although from 2010 they mostly concentrated in the Iberian Basin. Basic temperature, salinity and depth CTD data were gathered on every cruise. The other most measured sensor-based variable was dissolved oxygen using polarographic sensors attached to the CTD. Additional variables as fluorescence, transmittance were irregularly measured.

Unfortunately, no reversing thermometers were available to independently calibrate the CTD temperature sensors. Samples taken from the 24 or 12 Nikin bottle Rosette carrousel were taken on every cruise for discrete salinity and dissolved oxygen (Langdon, 2010) measurements to calibrate salinity and dissolved oxygen sensor data.

We present the data and quality control procedures for basic CTD data, temperature, salinity and dissolved oxygen, from the initial processing procedures to the final quality check with discrete data, especially for CTD oxygen data which is contrasted to discrete Winkler measurements. After a thorough check of all profiles in all stations and cruises, the first quality control check, we proceeded with an internal coherence control using as reference the bottom water mass in the three different areas or boxes delimited in Figure 1. Here we statistically explore the consistency of the data in this bottom layer, which is, within our period, temporally stable.

After the in between RADPROF cruises check we proceed with the secondary quality control procedure, where we check the RADPROF cruises against GLODAPv3 reference cruises. Studying the results from the crossover analysis between RADPROF stations and the high quality cruise data in GLODAPv3 we explore if any bias is detected in the RADPROF CTD data and if any correction factor is needed.

We prove that our data is high quality, ready to be used in climate studies, and be publicly used within FAIR principles, and submitted to open access and interoperable oceanographic data bases.

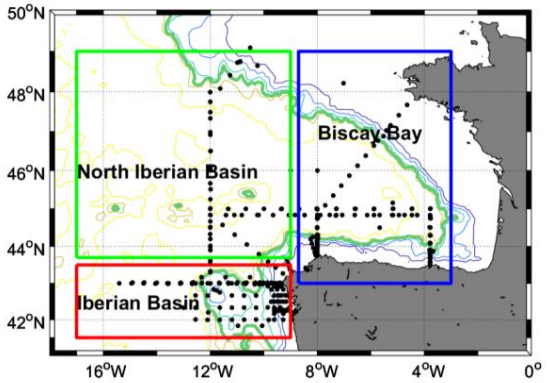

Figure 1. Distribution of RADPROF (2003-2023) CTD stations in three different areas in the Northeast Atlantic.

Acknowledgements

The RADPROF program was mostly sustained by IEO funds from FEMP and FEMPA programs. We are greatly greatful to the captains, crew and technitians on board RV Cornide Saavedra, RV Sarmiento de Gamboa, RV Ángeles Alvariño and RV Ramón Margalef.

REFERENCES

Hood E.M., Sabine, C.L. and Sloyan, B.M. (eds) (2010). The GO-SHIP Repeat Hydrography Manual: a collection of expert reports and guidelines, Version 1. (IOCCP Report 14), (ICPO Publication Series 134). Available: http://www.go-ship.org/HydroMan.html. DOI: https://doi.org/10.25607/OBP-1341

Langdon, C. (2010). Determination of Dissolved Oxygen in Seawater By Winkler Titration using Amperometric Technique. In, The GO-SHIP Repeat Hydrography Manual: A Collection of Expert Reports and Guidelines. Version 1, (eds Hood, E.M., C.L. Sabine, and B.M. Sloyan). 18pp. (IOCCP Report Number 14; ICPO Publication Series Number 134). DOI: https://doi.org/10.25607/OBP-1350

Tel, E., Balbin, R., Cabanas, J.M., García, M.J., García-Martinez, M.C., González-Pola, C., Lavin, A., López-Jurado, J.L., Rodríguez, C., Ruiz-Villareal, M., Sánchez-Leal, R.F., Vargas-Yanez, M. and Velez-Belchi, P. (2016) IEOOS: the Spanish Institute of Oceanography Observing System. *Ocean Science*, 12, 345-353. DOI: https://doi.org/10.5194/os-12-345-2016

Alkalinity enhancement field experiment in a saltmarsh as a carbon dioxide removal measure (CDR)

I. Mendes (1), J. Lübbers (1), J. Schönfeld (2), A. R. Carrasco (1), A. Gomes (3), P. Grasse (2, 4) and A. Cravo (1)

(1) Centro de Investigação Marinha e Ambiental (CIMA), Rede de infraestrutura em Recursos Aquáticos (ARNET), Universidade do Algarve, Faro, Portugal. imendes@ualg.pt
(2) GEOMAR Helmholtz Centre for Ocean Research Kiel, Kiel, Germany.
(3) Interdisciplinary Center for Archaeology and Evolution of Human Behaviour (ICArEHB), Universidade do Algarve, Faro, Portugal.
(4) German Centre for Integrative Biodiversity Research Halle-Jena-Leipzig (iDiv), Leipzig, Germany.

Abstract: Ocean alkalinity enhancement is a promising carbon dioxide removal strategy, which involves the addition of alkaline substrates. An in-situ experiment conducted in the Ria Formosa, in southern Portugal, evaluated the geochemical effects of applying olivine and basalt to salt marsh sediments. Monitored over six months, results showed an increase in total alkalinity (TA) and pH in both the surface and pore waters immediately after the substrates deployment, particularly in the finer-grained treatments. While the TA of the surface water returned to control levels the following month, the pore water maintained a high alkalinity, suggesting that the weathering of the substrates remained active for six months. Seasonal variations in salinity and pH were observed, with a persistent gradient of alkalinity from the pore water to the surface water, suggesting constant diffusion. These results emphasise the effectiveness of this approach in the short term. However, continuous monitoring is essential to assess its long-term impact and potential as a climate mitigation measure.

Keywords: *climate action, decarbonization, olivine, basalt, carbon uptake*

1. INTRODUCTION

Reducing atmospheric carbon dioxide (CO_2) concentrations to combat global warming and associated environmental changes is one of humanity's greatest challenges. To prevent temperature rise, technical measures such as carbon dioxide removal (CDR) are being developed to remove more CO_2 from the atmosphere and ensure its long-term storage (IPCC, 2023). One such measure is ocean alkalinity enhancement (OAE), which involves the addition of fine-grained mafic rocks or minerals to coastal and ocean areas. The increased alkalinity of the seawater, will bind more atmospheric CO_2 as bicarbonate and carbonate ions, and consequently increase the pH (e.g., Kheshgi, 1995; Moras *et al*., 2022). However, the rate of CO_2 consumption depends on the type of minerals used, grain sizes, temperature, pH, and other abiotic parameters (Feng *et al*., 2017). The minerals weathering will also release nutrients and other elements during dissolution (Bach *et al*., 2019), which may affect the environment and biodiversity (Meysman and Monserrat, 2017). Despite promising results obtained from modelling and laboratory studies (e.g. Montserrat *et al*., 2017; Bach *et al*., 2019), field experiments under natural conditions are urgently needed to evaluate the potential and the ecological impacts of ocean alkalinity enhancement (e.g., Cyronak *et al*., 2023).

Contributing to fulfil this gap of knowledge, an in-situ experiment was designed and installed at the Ria Formosa coastal lagoon (Figure 1), which offers the ideal conditions to perform an OAE experiment, running under natural conditions. Located on the southern coast of Portugal, this shallow mesotidal lagoon is characterized by a Mediterranean climate. The lagoon has a subtidal and intertidal surface area of 88 km^2, composed of tidal channels, tidal flats and saltmarsh with different types of vegetation, according to the level and duration of tidal submersion (e.g., Schönfeld and Mendes, 2021; Carrasco *et al*., 2021). This system has multiple inlets between barrier islands, with a mean, semi-diurnal tidal range of 1.3 m to 3.5 m, facilitating twice a day the exchange of water and nutrients with the ocean (e.g., Cravo *et al*., 2024). The availability of nutrients, the relative high-water residence time in the inner areas and the light penetration in this shallow lagoon sustain high primary productivity (Barbosa, 2010)

This work presents the results of monitoring the alkalinity enhancement experiment during the first six months. Data on variations in total alkalinity (TA), pH and salinity are included, obtained from both pore and surface water samples.

Figure 1. Location of the experimental site (red square) in the Ria Formosa coastal lagoon, in southern Portugal (Image from Google Earth 7.3).

2. MATERIAL AND METHODS

The experiment was installed in an undisturbed pioneer vegetation zone of the saltmarsh, colonized by *Spartina maritima,* in September 2022, and was monitored for two years. The experimental set-up is composed of three replicates, each with four deployments of fine and coarse-grained olivine and basalt, and an untreated control site, each one bordered by a pinewood frame (Figure 2). Surface water in contact with the substrates and pore water from inside the substrates, from each experimental field, were sampled monthly, starting the day after substrate deployment. Water samples were collected and stored in pre-cleaned, acid-decontaminated (10% HCl) vials. Porewater samples were extracted with rhizons (pore size: 0.1 µm), inserted horizontally into the 0.5–1 cm surface layer. Samples for analysis of alkalinity, nutrients and metals were immediately transported on ice to the Chemical Analysis Laboratory at the University of Algarve for further analysis. The salinity, oxygen content and pH of the surface and porewater were measured on site using a WTW Multi 3620 IDS multiparameter probe (see Mendes *et al*., 2025, for more details).

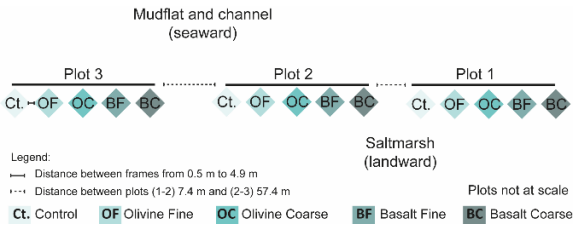

Figure 2. Schematic representation of the field experiment, composed by three plots, each one with the five experimental treatments installed in the salt marsh pioneer zone (adapted from Mendes et al., 2025).

3. RESULTS

As an arbitrary example, since no differences were found between plots, the data obtained from Plot 2 are presented.

3.1. Surface water

Surface water samples taken during the first six months of the experiment (September 2022 to February 2023) showed the greatest variation in total alkalinity (2.52–3.21 mM) in September 2022, the day after the olivine and basalt substrates were deployed. The lowest value was recorded in the olivine fine treatment, while the highest value was recorded in the basalt coarse treatment. During the remainder of the analysed period, total alkalinity (TA) varied with a maximum of 0.3 mM in November 2022 and a minimum of 0.08 mM in February 2023, with values in the treatments being similar to those in the control boxes (Figure 3). Immediately after the deployment of the substrates (September 2022), the pH value was higher in the control (8.14) than in the treatments (7.75–8.04). For the remainder of the period, the pH value ranged from 7.68 to 8.30. The lowest pH was obtained in December 2022 from basalt coarse, and the highest in February 2023, which was largely similar in the control and treatment boxes. Salinity showed similar values in the control and treatments, with the highest values obtained from September to November 2022 (36.5–36.7) and the lowest in December 2022 (33.9) (Figure 3).

3.2. Porewater

In the porewater, all the treatments showed a more pronounced alkalinity enhancement (from 4.2 to 6 mM), compared with the control (2.9 mM), on the day after deployment. The highest values were recorded by the fine treatments. Afterwards, a general decreasing trend in TA was observed in the treatments compared with the control, with the lowest variation recorded in February 2023 at 0.37 mM (Figure 4). Immediately after deployment of the substrates in September 2022, the pH value increased for all treatments (from 7.8 to 7.97) compared with the control (7.03). For the remainder of the period, pH showed lower variation between the control and treatments (0.40–0.10), except in January 2023 when higher values were obtained in the control (7.64) than in the treatments (7.07–7.30). Salinity also varied between the control and the treatments, being more pronounced in September 2022 (37.5–40.2). During the remaining months ranged from 35.8 to 38.7, except in December 2022, when lower salinity was recorded (32.7–34.0) (Figure 4).

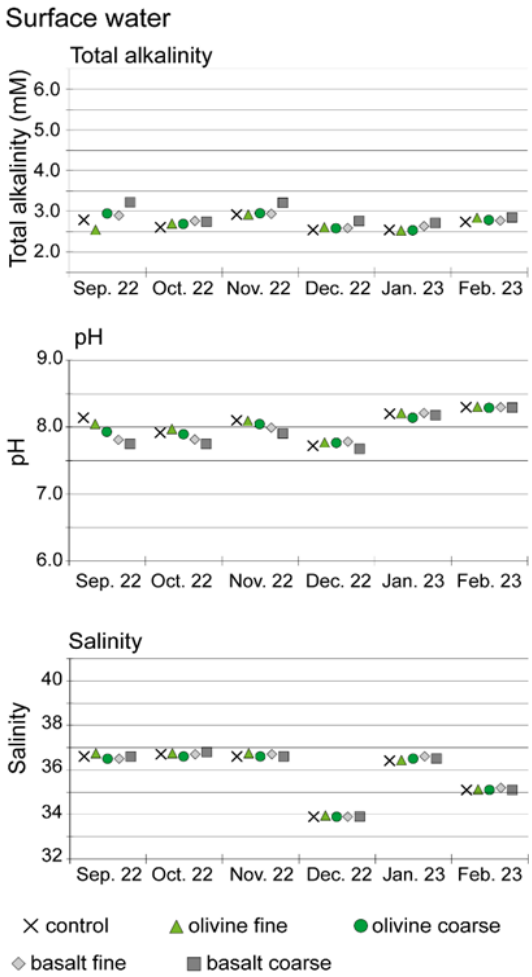

Figure 3. Records of total alkalinity, pH, and salinity measured in the surface water samples from plot 2, for the first 6 months of the experiment (adapted from Mendes et al., 2025).

3. DISCUSSION AND CONCLUSIONS

Total alkalinity increased in both the surface water and the pore water the day after the deployment of olivine and basalt in the pioneer vegetation zone of the Ria Formosa salt marsh. However, different effects were observed. In surface water, after an initial increase in TA, values returned to control levels within one month of the substrates being deployed. The other environmental parameters, such as salinity and pH, remained relatively similar as compared to control conditions, with recognition of seasonal variations (Figure 3).

In the porewater, a steep increase of TA was observed on the next day after the deployment, with higher values recorded in the finer treatments. This could be due to the high reactivity of the finest fraction of the supplied substrates in the different treatments. These fine particles are likely to weather faster, which would explain the strong increase in the porewater's alkalinity and pH. Once the fine particles were not reactive anymore, the coarser particles continue to weather at a slower rate and steadily increase the alkalinity of the porewater. The untreated control depicted no elevated alkalinity but showed a slight decrease from September to January 2022, probably reflecting a part of the seasonal cycle of natural alkalinity production (e.g., Reithmaier *et al*., 2023). The outlier of high pH and low alkalinity values in the control box in January 2023 can either be attributed to a transient coverage with mats of *Enteromorpha* algal filaments, which may change the pH due to photosynthesis/night respiration, or to an accidental influence of unseen crab or other animals' excretion products at the porewater sampling spot. The lower salinity values recorded in December 2022 in both surface and porewater were associated with a precipitation event that occurred a few days before water sampling.

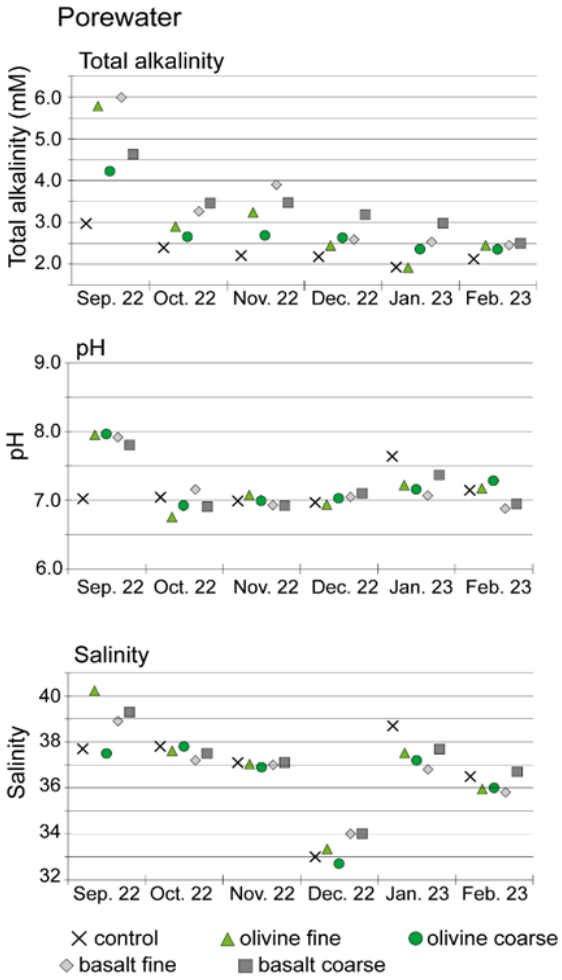

Figure 4. Records of total alkalinity, pH, and salinity measured in the porewater samples from plot 2, for the first 6 months of the experiment (adapted from Mendes et al., 2025).

The efficiency of the treatment with different substrates was displayed by the pervasive alkalinity gradient between the surface water and the porewater. As the alkalinity was always higher than in

the control box, the gradient depicts steady alkalinity production by the substrates and a slow diffusion to the overlying surface waters. The pervasive gradient indicates an alkalinity flux from the weathering substrate to the pore water, which was more intense after substrate deployment and effective during the first six months of the experiment.

Acknowledgements

Research conducted in the framework of the RECAP project, funded by the Fundação para a Ciência e a Tecnologia (FCT), Portugal, under grant number PTDC/CTA-CLI/1065/2021, which also supported J. Lübbers. I. Mendes was supported by the contract CEECINST/00052/2021/CP2792/CT0012, A.R. Carrasco by the contract CEECINST/00052/2021/CP2792/CT0007 and A. Gomes by the contract CEECINST/00146/2018/CP1493/CT0002, all funded by FCT. This study was also supported by FCT national funds under the project UIDB/00350/2020 granted to CIMA BASE and project LA/P/0069/2020 granted to the Associate Laboratory ARNET.

The authors acknowledge to the Instituto de Conservação da Natureza e das Florestas, DRCNF-Algarve (S-026426/2022) and Agência Portuguesa do Ambiente for authorization to carry out the RECAP experiment. The authors also acknowledge to Anke Dettner-Schönfeld and team members of the RECAP project Cátia Correia, and Óscar Ferreira for field work participation, Paulo Pedro for collaboration in alkalinity analyses in the Laboratory of Chemical Analysis (University of Algarve), and Margarida Ramires for all the collaboration in cleaning field work material. A special acknowledgment is extended to all volunteers participating in the RECAP field work campaigns.

REFERENCES

Bach, L. T., Gill, S. J., Rickaby, R. E. M., Gore, S. and Renforth, P. (2019). CO_2 Removal with Enhanced Weathering and Ocean Alkalinity Enhancement: Potential Risks and Co-benefits for Marine Pelagic Ecosystems. *Frontiers in Climate*, 1.

Barbosa, A. (2010). Seasonal and Interannual Variability of Planktonic Microbes in a Mesotidal Coastal Lagoon (Ria Formosa, SE Portugal) Impact of Climatic Changes and Local Human Influences. In M. J. Kennish and H. W. Paerl (Eds.), *Coastal Lagoons: Critical Habitats of Environmental Change*. CRC Press.

Carrasco, A. R., Kombiadou, K., Amado, M. and Matias, A. (2021). Past and future marsh adaptation: Lessons learned from the Ria Formosa lagoon. *Science of The Total Environment*, 790, 148082.

Cyronak, T., Albright, R. and Bach, L. T. (2023). Field experiments in ocean alkalinity enhancement research. Guide to Best Practices in Ocean Alkalinity Enhancement Research, 2-oae2023, 7.

Cravo, A., Jacob, J., Rosa, A. and Correia, C. (2024). Integrating physical and biogeochemical processes and oceanic exchanges at a coastal lagoon in Southern West Europe. *Estuarine, Coastal and Shelf Science*, 310, 108987.

Feng, E. Y., Koeve, W., Keller, D. P. and Oschlies, A. (2017). Model-Based Assessment of the CO_2 Sequestration Potential of Coastal Ocean Alkalinization. *Earth's Future*, 5(12), 1252-1266.

Kheshgi, H. S. (1995). Sequestering atmospheric carbon dioxide by increasing ocean alkalinity. *Energy*, 20(9), 915-922.

IPCC (2023). Climate Change 2023: Synthesis Report. Contribution of Working Groups I, II and III to the Sixth Assessment Report of the Intergovernmental Panel on Climate Change [Core Writing Team, H. Lee e J. Romero (eds.)]. IPCC, Geneva, Switzerland, pp. 35-115.

Mendes, I., Lübbers, J., Schönfeld, J., Baldermann, A., Carrasco, A.R., Cravo, A., Gomes, A., Grasse, P. and Stamm, F. (2025). Novel field experiment on alkalinity enhancement in intertidal environments - a trailblazer for natural climate solutions. *Journal of Geophysical Research: Biogeosciences*, 130, e2024JG008591.

Meysman, F. J. R. and Montserrat, F. (2017). Negative CO_2 emissions via enhanced silicate weathering in coastal environments. *Biology Letters*, 13(4), 20160905.

Montserrat, F., Renforth, P., Hartmann, J., Leermakers, M., Knops, P. and Meysman, F. J. R. (2017). Olivine Dissolution in Seawater: Implications for CO2 Sequestration through Enhanced Weathering in Coastal Environments. *Environmental Science & Technology*, 51(7), 3960-3972.

Moras, C. A., Bach, L. T., Cyronak, T., Joannes-Boyau, R. and Schulz, K. G. (2022). Ocean alkalinity enhancement – avoiding runaway CaCO3 precipitation during quick and hydrated lime dissolution. *Biogeosciences*, 19(15), 3537-3557.

Reithmaier, G. M. S., Cabral, A., Akhand, A., Bogard, M. J., Borges, A. V., Bouillon, S., Burdige, D. J., Call, M., Chen, N., Chen, X., Cotovicz, L. C., Eagle, M. J., Kristensen, E., Kroeger, K. D., Lu, Z., Maher, D. T., Pérez-Lloréns, J. L., Ray, R., Taillardat, P., Tamborski, J. J., Upstill-Goddard, R. C., Wang, F., Wang, Z. A., Xiao, K., Yau, Y. Y. and Santos, I. R. (2023). Carbonate chemistry and carbon sequestration driven by inorganic carbon outwelling from mangroves and saltmarshes. *Nature Communications*, 14(1), 8196.

Schönfeld, J. and Mendes, I. (2021). Environmental triggers of faunal changes revealed by benthic foraminiferal monitoring. *Estuarine, Coastal and Shelf Science*, 253, 107313.

An in-depth look at the dynamics of a long and narrow submarine canyon (Nazaré Canyon – W Portugal)

J. Vitorino (1), N. Zacarias (1), I. Martins (1), A. Mateus (1) and R. Guerreiro (1)

(1) Oceanography Division, Instituto Hidrográfico, Lisbon, Portugal. joao.vitorino@hidrografico.pt

Abstract: A comprehensive set of observations of the water column conditions in the area of influence of Nazaré Canyon was collected by Instituto Hidrográfico, in October 2024, in the framework of project FRESNEL. The data set comprises observations conducted onboard NRP D.Carlos I during a 5 days survey (CTD/LADCP profiles, glider section) and measurements collected by the systems that integrate the Nazaré Canyon Observatory MONICAN (multiparametric buoy, tide gauges). This set of observations is used to characterise the physical processes that prevailed in the Nazaré Canyon area of influence, during the period covered of the FRESNEL survey. The work is ongoing and the results to be presented at the Symposium will integrate the observations with a numerical model with data assimilation, providing a quasi-synoptic 3D picture of the oceanographic conditions and their evolution.

Keywords: *Nazaré Canyon, canyon dynamics, multisystem observations, FRESNEL project, MONICAN Observatory*

1. INTRODUCTION

The Nazaré Canyon is the largest submarine canyon of the Portuguese margin and one of the largest in the World. It extends for more than 200 km, from abyssal areas with depths in excess to 5000m to a few hundreds of meters from the beach of Nazaré (Vanney and Mougenot, 1990). The upper section of the canyon (the part of the section that cuts the continental shelf) shows impressive characteristics. At the canyon mouth, in the transition between the upper and middle sections, the canyon axis is about 1800m-1700m depth while the adjacent outer shelf is no more than 170m depth. The depth ratio of 10:1 is maintained all the way up to near the coast, with the canyon head (the terminal part of the canyon closest to the shore) presenting a depth of about 150m while the adjacent shelf waters are shallower than 20m.

Such an impressive structure, cutting the complete western Portuguese margin, impacts the conditions on the coastal ocean area, modifying the circulation partners, potentiating important vertical motions and intersecting the along shelf transit of particles. All these aspects, combined with the occurrence of persistent coastal upwelling conditions during the summer months (Sousa and Bricaud, 1992), render the area of influence of Nazaré Canyon a highly productive area marked by high biodiversity . This is particularly true in the UNESCO Berlengas Biosfere Reserve (Simões *et al.* 2025), in the southern part of this area of influence, which comprises the Berlengas Archipelago and a maritime corridor that extends from Berlengas to Cape Carvoeiro (Peniche).

The area of influence of Nazaré Canyon has been a central area of activity for Instituto Hidrográfico (IH) since the early days of this institute. First focusing on the detailed bathymetric mapping of this complex area, the activities of IH gradually expanded to include the research towards the understanding of the physical, chemical and geological processes that characterize the Nazaré Canyon and its area of influence. This work was developed in close collaboration with colleagues from other Portuguese or international institutions, particularly with partners of the marine biology domain, working in this same geographical area.

In October 2024, new insight on these processes was acquired from a program of observations of the Nazaré Canyon, conducted by Instituto Hidrográfico, University of Porto, University of Aveiro and Columbia University (USA).

2. THE FRESNEL EXPERIMENT

The program of observations was developed in the framework of the Field expeRiments for modElling, aSsimilation and adaptivE sampLing (FRESNEL) project, coordinated by University of Porto and funded by the US Office of Naval Research. FRESNEL had two key objectives: (1) to test observational strategies and evaluate the capacity to characterize and forecast the evolution of the prevailing coastal ocean conditions using a high resolution limited area model with assimilation, (2) to close the observation-prediction loop by adaptively driving the sampling of robotic vehicles, to enhance model skill.

The program of observations of the Nazaré Canyon area of influence that was conducted in October 2024 (FRESNEL experiment), comprised two components. Observations with autonomous systems and conducted from small rib boats was coordinated by University of Porto and conducted by a team operating from Nazaré. Observations in the global area were conducted by Instituto Hidrográfico, together with University of Aveiro, onboard one of the hydrographic vessels of the Portuguese Navy, the NRP D. Carlos I.

3. BUILDING THE PHYSICAL PICTURE

The present contribution focus on the characterization of the physical processes that prevailed in the Nazaré Canyon area of influence in October 2024, during the period of the FRESNEL experiment. This physical oceanography picture is drawn from the comprehensive data set collected by Instituto Hidrográfico using the systems operated onboard NRP D. Carlos I or that were part of a permanent monitoring systems installed in the area.

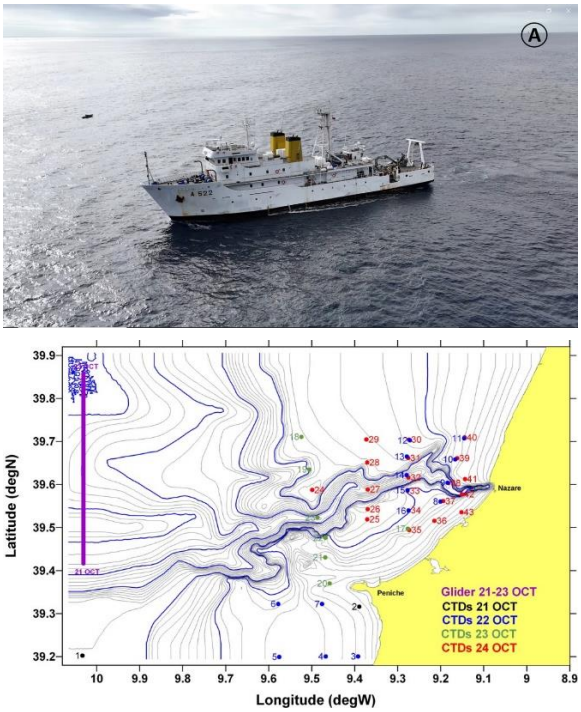

Figure 1. (Top) The NRP D. Carlos I offshore Nazaré, during the FRESNEL sea experiment. (Bottom) The program of observations conducted by the team onboard NRP D. Carlos I in October 2024.

Water column observations, complemented with water samples at selected depths, were collected at 43 stations, covered by NRP D. Carlos I, from 20 to 25 October 2024. The profiles of the main parameters of interest were collected using IH CTD system which is equipped with a 12 bottles Rosette sampler. One Idronaut 320 CTD probe equipped with pressure (P), temperature (T), conductivity (C), turbidity and dissolved oxygen sensors, was used in each station. In addition, in the CTD stations occupied, from 22 to 23 October, an additional YSI EXO probe was use. This probe was equipped with sensors P,T,C, Chlorophyll, Dissolved Oxygen, Total Algae chlorophyll and phycoerythrin (TAL PE), Total Dissolved Solids (TDS), pH. This probe was replaced from the 23 October by a RBR Concerto probe, equipped with sensors P, T, C, Chlorophyl-a, fDOM and turbidity.

In all CTD stations, a downward looking RDI Workhorse 300 kHz Acoustical Doppler Profiler (ADCP) was used in Lowered ADCP mode, attached to the CTD frame. This system provided current profiles from surface to the maximum depth reached by the CTD probe in each station.

The bad weather conditions that occurred during the period of the survey impacted considerable the operation. In particular, they force to concentrate the CTD/LADCP observations in the continental shelf and, more specifically, in the area of the upper section of Nazaré Canyon. In order to characterize the oceanographic forcing conditions acting offshore, an underwater glider from IH was used to provide observations along a meridional section offshore the slope. The glider used (Figure 2) was an Alseamar Glider Sea098 (named "Leonor") equipped with and *RBRlegato³* C.T.D, WETLABS ECO Puck FLNTU with turbidty e clorophill-a and *RBRcoda³* dissolved oxigen and temperature sensors. The glider operated from the 21st to the 23rd October 2024, until a technical problem forced its recover. Despite the short period of operation it was, nonetheless, able to cover the complete planned section, providing observations from the surface a maximum depth of 1000 m.

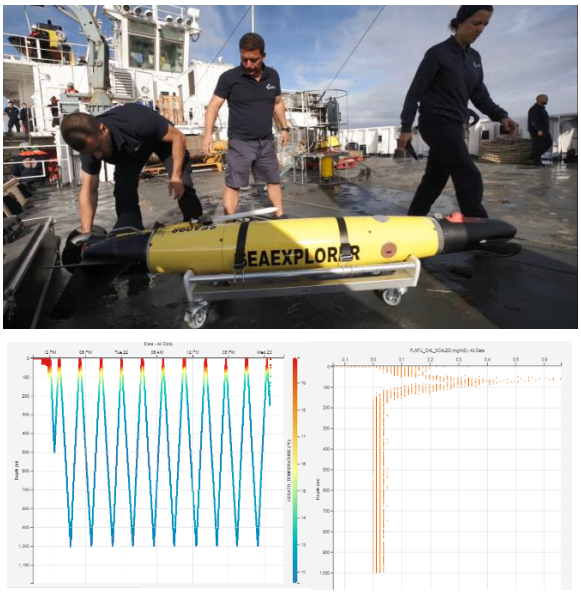

Figure 2. (Top) The IH glider onboard NRP D.Carlos I, being prepared for deployment. (Bottom left) Measurements of temperature along the track of the glider. (Bottom right) Ensemble of chlorophyll-a profiles for the overall section covered (bottom).

Complementary observations of the oceanographic conditions in the area of influence of Nazaré Canyon were provided by a number of permanent monitoring systems that IH operates in this area and that, together, form the Nazaré Canyon Observatory MONICAN. The MONICAN Observatory integrates two multiparametric buoys (WAVESCAN buoys from Fugro-Oceanor), one installed near the canyon mouth, in water depths of 1800m (MONICAN oceanic buoy), and the second one installed at the mid-shelf, in water depths of about 90m, about 10km from the port of Nazaré (MONICAN coastal buoy). The observatory also integrates two coastal tidal stations, one installed in the Nazaré port and the second one installed in the Peniche port.

During the time period covered by the observations collected onboard NRP D.Carlos I, the MONICAN coastal buoys was not in operation, due to damages caused by a storm a few months before. The MONICAN oceanic buoy, however, collected meteorological measurements (sensors installed at 3m height), wave measurements, surface temperature measurements and current and temperature measurements below the surface. The current measurements were collected using an downward looking 300 kHz RDI Workhorse ADCP, installed 7m below the buoy hull and providing hourly current measurements from about 12m depth to about 90m depth, with a vertical resolution of 3 m. The ADCP was also equipped with a thermistor, providing temperature measurements at 7m depth. The two coastal tidal stations were equipped with radar tide gauges and provided measurements of the evolution of sea surface height at the coast, in response to diverse forcing agents (e.g. tides, wind forcing conditions).

The in-situ data collected during the FRESNEL mission and by the MONICAN systems is also complemented with satellite images. Despite the unfavorable conditions, with frequent periods of cloud coverage, the available images can, however, provide important information regarding the evolution of the oceanographic conditions in the overall area.

4. ADVANCING IN THE UNDERSTANDING OF NAZARÉ CANYON IMPACTS

The program of observations conducted by Instituto Hidrográfico onboard NRP D.Carlos I, in October 2024, was held during a period of high variability in the weather conditions, associated with the impact of successive storm periods, with associated strong winds, important swells and seas and some precipitation. While these conditions greatly affected the operations at sea, they also provided an opportunity to advance in the understanding on how the Nazaré Canyon responds to these forcing conditions and how this response impacts the conditions in the canyon area of influence.

The mission at sea developed during a period of transition between wind forcing regimes. Previous observations of the Nazaré Canyon area of influence showed that these periods are particularly interesting since they potentiate the establishment of strong closed circulations cells over the canyon head area, a result of the dynamics directly promoted by the canyon (J. Vitorino, in prep.). The data collected during the FRESNEL sea experiment can provide insight on how these processes can significantly impact the biological development in the area.

The physical characterization of the processes is based on the physical data described in section 3. Given the essential non-synoptic character of the data collected by NRP D. Carlos I, a numerical model with data assimilation is used to build a consistent 3D synoptic view of the conditions in the area covered. The model is forced by the atmospheric forcing conditions and assimilates the CTD profiles collected during the cruise.

The physical characterization described here can then be used to infer the potential impacts on biological development, linking with other observations that were conducted during the FRESNEL survey to complete the overall picture. Water samples at selected depths were collected in each CTD station with the Rosette sampler system. These samples were analyzed at Instituto Hidrográfico for evaluation of nutrients, biogeochemical parameters, heavy metals, chlorophyll and microplastics. The nutrients distributions, presented to the Symposium in the communication "Nutrient and heavy metal distribution in the water column at the Nazaré Canyon" (Palma *et al*.), will highlight how the physical processes described here are contributing to boost biological development in the canyon area.

An Underwater Vision Profiler (UVP) system was connected to the CTD frame and operated by University of Aveiro. At each CTD station, this system provided images of the plankton communities present in the water column. These profiles, complemented with water samples collected at selected depth for plankton analysis, is presently being analyzed at University of Aveiro. Once completed, these results can provide insight on how the physical processes acting on the Nazaré Canyon in October 2024, are impacts the biological communities.

Acknowledgements

FRESNEL project was funded by the US Office for Naval Research through grant BBA Number: N00014-21-S-B001.

REFERENCES

Simões, M., Costa, C., da LuzCalado, M., Vasco-Rodrigues, N., Campos, M. J., Leandro, S. M., and Antunes, A. (2025) Unveiling the UNESCO Biosphere Reserve of the Berlengas Archipelago in Portugal as a Hotspot of Fish Species Using eDNA Metabarcoding and the Collaboration of Fishing Crews. *J. Mar. Sci. Eng.*, 13, 60. https://doi.org/10.3390/ jmse13010060

Sousa, F. M. and Bricaud, A. (1992). Satellite-Derived Phytoplankton Pigment Structures in the Portuguese Upwelling Area. *J. Geophys. Res.-Ocean.*, 97, 11343–11356.

Vanney, J. R. and Mougenot, D. (1990). A gouf-type canyon, the Canhao da Nazare, Portugal. *Oceanologica Acta*, 13(1), 1-14.

Vitorino, J. (in prep). “A long submarine canyon under variable forcing conditions (Nazaré Canyon, W Portugal)”.

Nutrient and heavy metal distribution in the water column at the Nazaré Canyon

C. Palma (1), J. M. Almeida (1), L. Duarte (1), C. Borges (1) and A. C. Rocha (1)

(1) Instituto Hidrográfico, Rua das Trinas 49, 1249-093 Lisboa (Portugal). carla.palma@hidrografico.pt

Abstract: This study aims to assess how hydro-oceanographic processes in the Nazaré Canyon influence the chemical structure of water masses and their potential to enhance biological productivity. As part of the FRESNEL project, water samples were collected at 43 CTD stations (25m – 1325 m) and analysed for nutrients, chlorophyll, and trace metals. The spatial distribution of these parameters will be used to interpret physical-biogeochemical interactions within the canyon. Results will be compared with data from the HERMES and HERMIONE projects to evaluate temporal trends and identify nutrient pathways. This work contributes to understanding ecosystem functioning in the Nazaré Canyon area of influence.

Keywords: *Trace metals, nutrients, Nazaré Canyon, FRESNEL project*

1. MOTIVATION

The Nazaré Canyon is a major geomorphological structure on the Portuguese continental shelf, strongly influencing the hydro-oceanographic dynamics of the surrounding region.

As part of the FRESNEL project (Field expeRiments for modElling, aSsimilation and adaptivE sampLing), coordinated by the University of Porto and funded by the U.S. Office of Naval Research, an oceanographic survey was carried out in October 2024 aboard the hydrographic vessel NRP D. Carlos I. One of the key objectives of the sampling campaign, as outlined in Vitorino *et al.*, (2025), was to characterise the chemical structure of the water masses by analysing nutrient and trace metal distributions throughout the water column. The nutrients and metals distribution will help illustrate how the physical processes described by Vitorino *et al.*, (2025) contribute to enhancing biological activity in the canyon area

Samples were collected at depths ranging from 25 m and 1325 m at 43 station (Figure 1), across various *in situ* data collection points (conductivity, turbidity and depth, CTD), and were analysed for nutrient (nitrate, nitrite, ammonia, phosphate, and silicate), chlorophyll and metal (As, Cd, Ni, Pb, Fe, Cu and Zn) concentrations, in order to describe the distribution pattern of chemical parameters.

The data obtained from this campaign will be integrated with previous results from the HERMES (Hotspot Ecosystem Research on the Margins of European Seas – FP6) and HERMIONE (Hotspot Ecosystem Research and Man's Impact On European Seas – FP7) projects (Beja *et al.*, 2007; Borges *et al.*, 2009), to provide a broader understanding of long-term trends in the region and to understand the chemical processes that characterize the Nazaré Canyon and its area of influence.

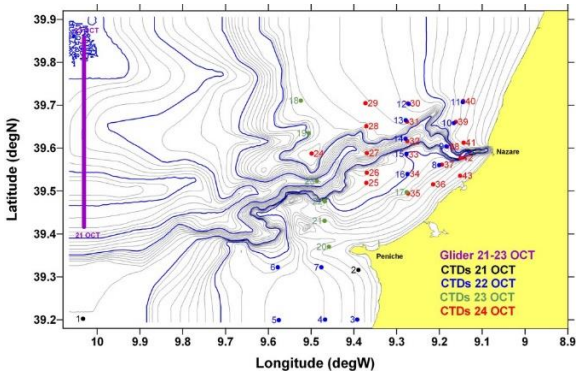

Figure 1. The program of observations conducted by the team onboard NRP D. Carlos I in October 2024.

Nutrient concentrations were determined using a Skalar SANplus Segmented Flow AutoAnalyser, specially for the analysis of saline water. For trace metal determination, samples were subjected to a simultaneous extraction and preconcentration. Final extracts were analysed by atomic absorption spectrometry (both flame and electrothermal), with Zeeman background correction for enhanced accuracy.

2. EXPECTED RESULTS

Previous results from the HERMES and HERMIONE projects indicate that during upwelling events, the Nazaré Canyon acts as a conduit for nutrient-rich waters from the open ocean to the coastal zone, displacing nutrient-depleted surface waters near the canyon head. These findings support the hypothesis that such nutrient inputs may originate from intermediate water layers rather than from the deep ocean. Despite generally low nutrient concentrations

when compared to the Western Atlantic or standard water mass reference values, this margin remains highly productive and supports important fisheries. Regarding metal concentrations, the Nazaré Canyon area appears to be uncontaminated, with no elevated levels of toxic elements detected, suggesting no apparent threat to local marine biological communities. The results obtained from the FRESNEL project are currently under analysis and will be compared with the previously collected data to assess temporal and spatial patterns.

Acknowledgements

FRESNEL project was funded by the US Office for naval Research through grant BBA Number: N00014-21-S-B001.

REFERENCES

Beja, J., Borges, C., Palma, C., and Vitorino, J. (2007). Nutrient and heavy metal distribution of the Portuguese Western margin - Nazaré Canyon case study. *2ª reunião anual do projeto Hermes*.

Borges, C., Palma, C., Valença, M., Oliveira, A., and Vitorino, J. (2009). Nutrient and heavy metal distribution of Nazaré Canyon and adjacent shelf. *3ª reunião anual do projeto Hermes*.

Vitorino, J., Zacarias, N., Martins, I., Mateus, A., and Guerreiro, R. (2025). An in-depth look at the dynamics of a long and narrow submarine canyon (Nazaré Canyon – W Portugal). *Proceedings of XI Symposium on the Atlantic Iberian Margin* (in this issue).

Metais em águas da costa do Algarve: avaliação de padrões de distribuição com incerteza associada

J. M. Almeida (1), L. Duarte (1), C. Macedo (2), C. Borges (1) e C. Palma (1)

(1) Instituto Hidrográfico, Rua das Trinas 49, 1249-093 Lisboa (Portugal). vaz.almeida@hidrografico.pt
(2) Serviços Municipalizados de Água e Saneamento de Almada, Praceta Ricardo Jorge 2, 2804-543 Almada (Portugal).

Abstract: Continuous monitoring of coastal regions is essential for detailed assessment of its environmental status. This includes contaminant detection concentration trends, and assessment of potential contamination sources (whether continuous or episodic) contributing to a more effective and sustainable coastal resource management. As part of the AQUIMAR project, water samples from the Algarve coast were collected between 2018 and 2020 to analyse trace metals. Results indicated that arsenic, iron, and nickel concentrations, despite exhibiting some spatial variability, remained relatively stable over the study period. Distribution patterns were analysed using the Megasampler model, which allows not only a metrological and robust evaluation of contaminant concentrations, but also, through the simulated results obtained, the identification of spatial distribution trends that may indicate contaminant sources.

Keywords: *trace metals, water, pollution, monitoring, distribution*

1. INTRODUÇÃO

A aquacultura tem vindo a ganhar preponderância na produção de pescado para consumo, como alternativa sustentável à pesca intensiva (Mosqueira *et al*., 2022). No entanto, porque as aquaculturas se encontram fixadas em locais específicos, estão permanentemente sujeitas às condições físico-químicas locais, assim como a diversas fontes de poluição e pressões antropogénicas.

A exposição de organismos marinhos a contaminantes como metais pesados pode resultar numa bioacumulação desses contaminantes nos organismos, atingindo níveis tóxicos, em caso de exposição prolongada (Souza Machado *et al*., 2016). Estes contaminantes podem ser transferidos para os seres humanos através do consumo de organismos que tenham estado diretamente expostos a ambientes poluídos ou que façam parte de cadeias alimentares contaminadas.

O projeto AQUIMAR desenvolvido entre 2018 e 2023, teve como objetivo identificar áreas adequadas para o estabelecimento de aquaculturas, através da caraterização das condições oceanográficas, físico-químicas, geoquímicas e biológicas da zona costeira portuguesa. Foram realizadas quatro campanhas oceanográficas em cinco áreas costeiras distribuídas de Norte a Sul de Portugal Continental, com recolha de amostras de água e sedimentos para análise de parâmetros clássicos, nutrientes, metais e compostos orgânicos. Dentro dos metais foram analisados o ferro (Fe), níquel (Ni), cobre (Cu), cádmio (Cd), chumbo (Pb), zinco (Zn) e o semi-metal arsénio (As), em amostras de água recolhidas na costa Algarvia. No presente estudo serão avaliados os padrões de distribuição de As e Ni. Relativamente ao mercúrio (Hg) não são apresentados os resultados uma vez que os seus valores deram sempre inferiores ao limite de quantificação do método (LQ).

2. METODOLOGIA

Nas quatro campanhas oceanográficas as amostras de água foram recolhidas a uma profundidade de aproximadamente 5 m. Os períodos amostrados na região da costa Algarvia foram de 5 a 6 e de 9 a 13 de outubro de 2018 (Campanha 1), de 18 a 22 de abril de 2019 (Campanha 2), de 10 a 13 de outubro de 2019 (Campanha 3), e de 28 de fevereiro a 2 de março de 2020 (Campanha 4). Os pontos de amostragem abrangeram toda a costa Algarvia entre Tavira e Sagres (Figura 1 (a)). A amostragem foi realizada com recurso a garrafas *Niskin* acopladas a um sistema CTD/Rosette. As amostras foram filtradas com filtros de policarbonato de 0,45 μm de poro e conservadas com adição de ácido nítrico, ajustando o pH para valores inferiores a 2. O controlo de qualidade efetuado incluiu brancos de campo, brancos de laboratório, ensaios em duplicado, padrões de controlo e ensaios de recuperação.

Para a análise dos metais Fe e Ni, as amostras foram ajustadas a pH = 6,5 e submetidas a uma pré-concentração através de extração em fase sólida. A análise do As foi realizada após extração com água régia em refluxo utilizando uma manta de aquecimento. A quantificação foi efetuada por espectrometria de absorção atómica (EAA), utilizando

queimador (Fe), câmara de grafite (Ni) e gerador de hidretos (As).

Os padrões de distribuição dos metais estudados foram obtidos por aplicação do modelo Megasampler (Borges, 2024), que permite a obtenção de resultados simulados de concentração de metais, dentro da área espacial estudada, considerando todas as componentes de incerteza associadas (i.e., incertezas analítica, de amostragem e de posicionamento). Este modelo permite não apenas uma avaliação metrológica e robusta das concentrações dos metais estudados, mas pode também possibilitar a identificação de padrões de distribuição dos metais que possam auxiliar na identificação da sua origem.

3. RESULTADOS E DISCUSSÃO

Na Tabela I apresentam-se como exemplo os valores médios, mínimos e máximos para o semi-metal As e os metais Fe e Ni nas quatro campanhas efetuadas, assim como os valores considerados nas Normas de Qualidade da Água (NQA), definidas no Decreto-Lei n. 218/2015. As NQA definem valores de referência para as substâncias prioritárias e "outros poluentes" no domínio da política da água. São ainda definidas, para "outras águas superficiais" (águas de transição, costeiras e territoriais), valores máximos médios anuais (NQA-MA) para proteção contra a exposição a longo prazo, e concentrações máximas admissíveis (NQA-CMA) para proteção contra a exposição a curto prazo.

Observa-se nas quatro campanhas efetuadas, que os valores médios de As variaram entre 1,28 μg L^{-1} e 1,43 μg L^{-1}, com o valor máximo de 1, 92 μg L^{-1}; o Fe apresentou valores médios a variarem entre 1,0 μg L^{-1} e 9,21 μg L^{-1}, e o valor máximo de 9,51 μg L^{-1}; os valores médios de Ni variaram entre 0,363 μg L^{-1} e 0,742 μg L^{-1}, e o valor máximo de 1,88 μg L^{-1}. Conclui-se que de uma forma geral, os dois metais e o semi-metal estudados apresentaram relativa estabilidade ao longo do ciclo de campanhas. Verifica-se ainda que nenhum dos metais e semi-metal avaliados, em nenhuma das campanhas, ultrapassou as NQA definidas (tanto os valores médios como os máximos). Assim, pode-se concluir que não se identificam quaisquer efeitos adversos para o meio ambiente ou organismos marinhos nas zonas amostradas.

Como exemplo apresenta-se o estudo dos padrões de distribuição no modelo Megasampler para as campanhas 3 e 4 e para o As e Ni (Figura 1 (a) e (b)).

Tabela I: Resultados de metais e valores de referência para águas de superfície.

	Campanha	x̄ (m – M) (μg L^{-1})	NQA-MA (μg L^{-1})	NQA-CMA (μg L^{-1})
As	1	1,43 (1,15 – 1,67)	20[(a)]	–
	2	1,42 (1,16 – 1,56)		
	3	1,28 (0,963 – 1,59)		
	4	1,42 (0,842 – 1,92)		
Fe	1	2,10 (0,211 – 6,92)	–	–
	2	1,78 (0,289 – 6,19)		
	3	1,0 (0,026 – 2,19)		
	4	9,21 (1,716 – 9,51)		
Ni	1	0,363 (0,11 – 0,709)	8,6	34
	2	0,495 (0,314 – 1,41)		
	3	0,401 (0,279 – 0,63)		
	4	0,742 (0,253 – 1,88)		

(a) Dureza da água classe 5;

x̄: média; m: mínimo; M: máximo.

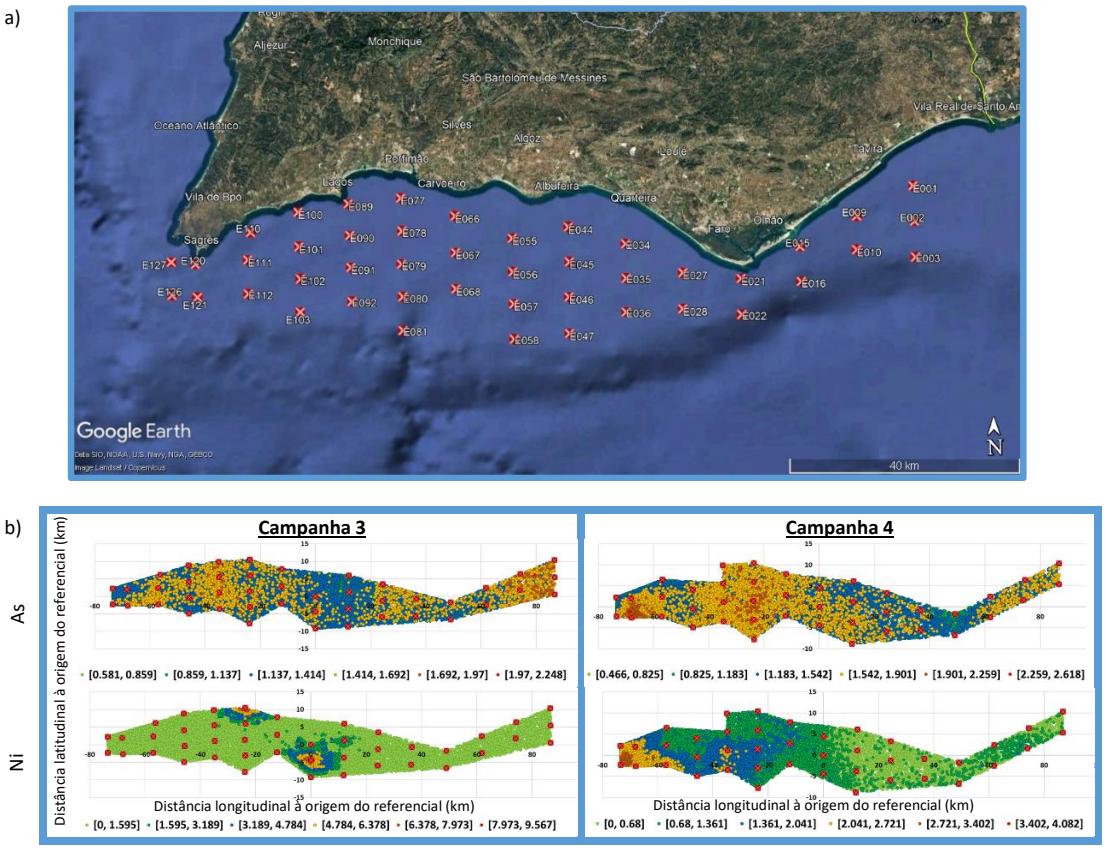

Figura 1 a) Posicionamento dos pontos de amostragem na costa sul algarvia, implantados sobre uma imagem do Google Earth. A origem geográfica do referencial de dados é referida às coordenadas de planeamento do ponto E056, aproximadamente coincidente com o centro da área de amostragem; b) Distribuição espacial simulada da concentração superficial (5 m) de As e Ni nas Campanhas 3 e 4. Os pontos de amostragem estão representados por ☒.

A Figura 1 (b) apresenta as distribuições espaciais simuladas obtidas para os dois períodos em estudo. No que respeita aos padrões de distribuição simulada, observam-se comportamentos distintos para o As e o Ni entre as duas campanhas analisadas.

O As evidenciou uma distribuição relativamente homogénea ao longo da costa, com exceção de concentrações mais elevadas junto à zona de Vila Real de Santo António na campanha 3, e na região próxima de Sagres na campanha 4.

Relativamente ao Ni, na campanha 3 verificou-se uma distribuição maioritariamente homogénea, com exceção de dois pontos de amostragem com concentrações superiores: um em frente a Portimão e outro entre Armação de Pera e Albufeira, este ultimo mais afastado da linha de costa. Já na campanha 4, observa-se um gradiente de concentração no sentido Este-Oeste, com valores mais elevados registados na zona de Sagres.

Os padrões de distribuição apresentados para o As e para o Ni não são semelhantes; contudo, destaca-se que, na campanha 4, ambos os metais apresentaram concentrações mais elevadas na região de Sagres.

Importa ainda referir que as campanhas decorreram em períodos distintos do ano, a campanha 3 no outono e a campanha 4 no final do inverno, fator que poderá influenciar os padrões de distribuição observados.

4. CONCLUSÕES

O estudo realizado no âmbito do projeto AQUIMAR permitiu caracterizar a presença e a distribuição dos metais Cd, Cu, Fe, Ni, Pb, Zn e do semi-metal As ao longo da costa Algarvia no período compreendido entre 2018 e 2020. Os resultados apresentados indicaram que as concentrações destes elementos permaneceram relativamente estáveis ao longo do período de monitorização. A aplicação do modelo Megasampler possibilitou uma avaliação robusta e metrológica das concentrações, ao considerar não apenas as concentrações determinadas, mas também a incerteza associada aos resultados analíticos e à amostragem.

A comparação desses resultados com estudos anteriores, nomeadamente Santos-Echeandía *et al.* (2012), mostra, por exemplo no caso do Ni, que os valores obtidos são da mesma ordem de grandeza — com concentrações até 30 nM na costa sul (Santos-Echeandía *et al.*, 2012) e até 32 nM no presente

trabalho. Estes dados, em conjunto com os anteriormente publicados, contribuem para o reforço da definição de valores de referência para as águas costeiras.

Os dados obtidos são fundamentais para o reforço da monitorização ambiental e para uma gestão sustentável das zonas aquícolas e costeiras, contribuindo para reduzir os riscos associados à contaminação por metais e semi-metais e para a preservação da qualidade ambiental na região.

Agradecimentos

Este trabalho foi financiado pelo programa Operacional Mar2020 através do Projeto "AQUIMAR-Caracterização geral de áreas aquícolas para estabelecimento de culturas marinhas" (MAR2020 n° MAR-02.01.01-FEAMP-0107).

REFERÊNCIAS

Borges, C. (2024). Optimized metrological and geochemical assessment of trends in estuarine and oceanic systems. Dissertação de Doutoramento, Universidade de Lisboa, Portugal, 174 + xxxiii pp. Disponível em http://hdl.handle.net/10400.5/99445

Decreto-Lei nº 218/2015 (2015). Diário da República, 1.ª série, 196, 8667-8685.

Diretiva 2008/105/CE (2008). Jornal Oficial da União Europeia, 348, 84-97.

Diretiva 2013/39/UE (2013). Jornal Oficial da União Europeia, 226, 1-17.

Mosqueira, M., Pombo, A., Borges, C., Brito, A. C., Zacarias, N., Esteves, R., e Palma, C. (2022). Potential for coastal and offshore aquaculture in Portugal: Insights from physico-chemical and oceanographic conditions. *Applied Sciences*, 12(5):2742.

Souza Machado, A. A., Spencer, K., Kloas, W., Toffolon, M., e Zarfl, C. (2016). Metal fate and effects in estuaries: a review and conceptual model for better understanding of toxicity. *Science of the Total Environment*, 541, 268-281.

Santos-Echeandía, J., Caetano, M., Brito, P., Canario, J., e Vale, C. (2012). The relevance of defining trace metal baselines in coastal waters at a regional scale: The case of the Portuguese coast (SW Europe). *Marine Environmental Research*, 79, 86–99.

Avaliação espácio-temporal e identificação de fonte de hidrocarbonetos aromáticos policíclicos em sedimentos costeiros de Portugal Continental

A. C. Rocha (1), L. Brás Gomes (1), C. Neto (1) e C. Palma (1)

(1) Instituto Hidrográfico, Lisboa, Portugal. catarina.rocha@hidrografico.pt

Abstract: Polycyclic aromatic hydrocarbons (PAH) are organic contaminants widely distributed in the marine environment. They may originate from petrogenic sources, derived from petroleum; pyrogenic sources, resulting from combustion processes; or biogenic sources, of natural origins. Environmental monitoring of sediments, which are the largest reservoir of organic contaminants in the marine ecosystems, allows the assessment of PAH contamination levels and their sources, which is essential for effective environmental management. The use of diagnostic ratios among PAH congeners helps to identify their origins, allowing for targeted action to mitigate potential emission sources. This study characterised PAH in coastal sediments from continental Portugal, revealing trace levels of contamination and predominantly PAH from pyrogenic origin. No significant temporal variations in PAH concentrations were observed, except in a few isolated cases. This monitoring is crucial to support informed environmental management and the implementation of effective contamination mitigation strategies.

Keywords: *Polycyclic Aromatic Hydrocarbons, Sediments, GC-MS, Source Apportionment, Spatio-Temporal Assessment*

1. INTRODUÇÃO

Os hidrocarbonetos aromáticos policíclicos (PAH) representam uma classe de contaminantes orgânicos persistentes amplamente dispersos no ambiente marinho. São conhecidos pela sua toxicidade, mutagenicidade e potencial carcinogénico e, como tal, prejudiciais aos ecossistemas marinhos. Estas substâncias tanto podem ter origem antropogénica, entrando no meio marinho em consequência da atividade do Homem (*e.g.*, atividade industrial, tráfego e queima de combustíveis fósseis e biomassa), como origem natural, cuja entrada no ambiente é efetuada pela própria Natureza (*e.g.*, atividade vulcânica e exsudações de jazidas de petróleo). Em ambas as origens, os PAH podem ser classificados de acordo com o seu processo de formação, o que está relacionado com a temperatura em que esse processo ocorre: petrogénicos, *i.e.*, provenientes do petróleo (*e.g.*, derrames de combustíveis fósseis e exsudações de jazidas), pirolíticos, *i.e.*, formados durante os processos de combustão a altas temperaturas (*e.g.*, tráfego e atividade vulcânica e industrial) e ainda biogénicos ou diagenéticos (origem biológica) (Yunker *et al.*, 2002; Bakhtiari *et al.*, 2009). As principais vias de entrada dos PAH são as descargas industriais, lixiviação de solo urbano, deposição atmosférica e derrames acidentais ou deliberados (Lubecki e Kowalewska, 2010). Considerando a sua alta hidrofobicidade, os PAH tendem a se fixar nos tecidos e nos sedimentos (Latimer e Zheng, 2003). Estes últimos revelam ser reservatórios destes poluentes, sendo bons indicadores de níveis de contaminação e de pressões antropogénicas nos sistemas estuarinos e costeiros.

A classificação da origem dos PAH encontrados em sedimentos de determinado ambiente marinho e a avaliação do nível de contaminação é essencial para a monitorização ambiental, pois permite a identificação de locais contaminados, além de estimar os riscos ecológicos associados. Uma adequada amostragem, intervalada no espaço e no tempo, possibilita a elaboração de distribuições espácio-temporais da concentração de poluentes, auxiliando a compreensão da evolução da contaminação dos sistemas marinhos.

Adicionalmente, o recurso a razões de diagnóstico entre PAH congéneres específicos permite inferir a natureza predominante dessas substâncias (pirolítica *vs*. petrogénica), contribuindo para a identificação de fontes pontuais ou disseminadas (Tobiszewski e Namieśnik, 2012; Stogiannidis e Laane, 2015; Rocha e Palma, 2019).

Este tipo de avaliações fornece conhecimentos relevantes sobre a evolução de fontes de poluição e da acumulação/remobilização de contaminantes presentes nos sedimentos, possibilitando atuar com medidas de mitigação da contaminação com maior eficácia. Mais ainda, esta abordagem revela ser crucial para alicerçar políticas de gestão ambiental, assim como para cumprir com normativos legislativos como a Diretiva-Quadro Estratégia Marinha (DQEM), que

estabelece objetivos para o alcance do bom estado ambiental dos sistemas marinhos.

Neste contexto, o estudo aqui apresentado intenta efetuar uma caracterização da ocorrência, distribuição e origem dos PAH em sedimentos de cinco áreas costeiras de Portugal continental (Figura 1), recorrendo a uma abordagem espácio-temporal e de identificação de pressões antropogénicas. As amostras de sedimento analisadas enquadram-se no projeto "Caraterização geral de áreas aquícolas para estabelecimento de culturas Marinhas" (AQUIMAR).

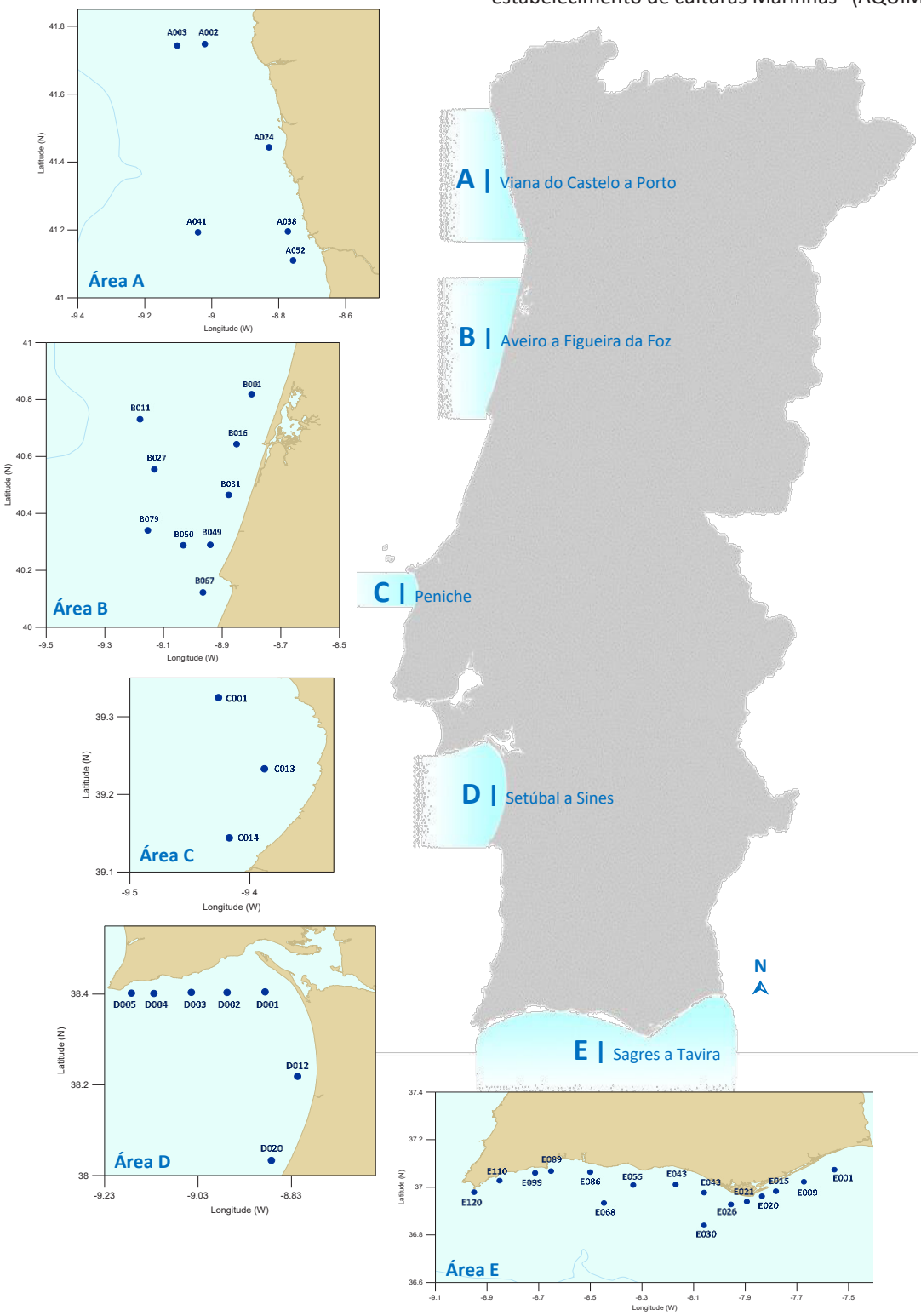

Figura 1. Estações de amostragem nas cinco áreas costeiras de Portugal continental.

2. AMOSTRAGEM E MÉTODOS

A amostragem de um total de 84 sedimentos superficiais foi realizada nos pontos de amostragem de cada uma das áreas A a E representadas na Figura 1, em duas épocas distintas entre 2018 e 2020, com o intuito de avaliar não só o grau de contaminação dos sedimentos consequentes de pressões antrópicas, como também a sua evolução espácio-temporal. Para a recolha das amostras recorreu-se a uma draga *Smith McIntyre*, operada a bordo de navios hidrográficos da Marinha Portuguesa em missões de amostragem no âmbito do projeto AQUIMAR acima mencionado.

Todas as amostras de sedimento foram processadas segundo os procedimentos laboratoriais internos do IH. As amostras de sedimento foram inicialmente crivadas tendo sido recolhida a fração <2 mm, liofilizadas e posteriormente moídas para homogeneização. A amostra seca e homogeneizada foi submetida a um processo de extração com recurso à técnica de Extração Pressurizada com Solvente, de modo a remover da matriz os compostos com interesse analítico, seguido de uma purificação de extrato para remoção de interferentes e finalizando com a análise instrumental para determinação dos teores de PAH. A análise instrumental foi efetuada por Cromatografia Gasosa acoplada a Espectrometria de Massa (GC-MS), tendo sido determinados os 16 PAH reconhecidos como substâncias prioritárias pela *United States Environmental Protection Agency* (US EPA), bem como o benzo(e)pireno (BeP), o perileno (Per) e alguns homólogos alquilados dos compostos naftaleno e fenantreno.

3. RESULTADOS E CONCLUSÕES

Considerando as duas épocas de amostragem realizadas em cada área, os teores totais de PAH parentais determinados, *i.e.*, 16 PAH US EPA, BeP e Per, (ΣPAH) variam entre <27,0 µg/kg (limite de quantificação) e 292 µg/kg na área A, <27,0 µg/kg e 1016 µg/kg na área D e <27,0 µg/kg e 1197 µg/kg na área E, sendo as áreas onde se observaram concentrações maiores de PAH. Nas áreas B e C, em todas as estações de amostragem e nas duas épocas foram observados ΣPAH <27,0 µg/kg.

Na Figura 2 são apresentados os resultados da ΣPAH observados nos sedimentos recolhidos nas duas épocas na área D e área E. Os sedimentos recolhidos nas estações D004, D005, E015, E020, E089, E099 e E110 revelam ΣPAH dispares nas duas épocas, designadamente outubro de 2018 e outubro de 2019.

O grau de contaminação dos sedimentos recolhidos pode ser avaliado segundo a classificação recomendada pela Portaria n.º 1450/2007 de 12 de novembro, que classifica o grau de contaminação de sedimento para posterior dragagem considerando intervalos de concentração para ΣPAH. Salvo algumas amostras recolhidas na área D e E (Figura 2) classificados como "Classe 2 – material com contaminação vestigiária" (300 µg/kg ≤ ΣPAH < 2000 µg/kg), todos os restantes sedimentos recolhidos foram classificados como "Classe 1 – material limpo" em ambas as épocas de amostragem (ΣPAH < 300 µg/kg).

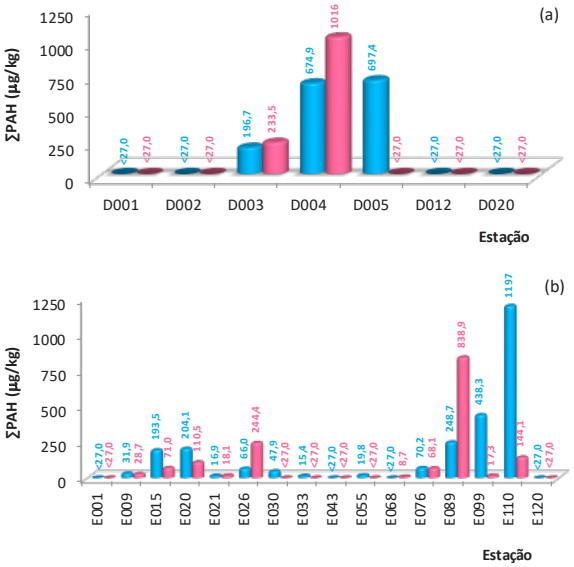

Figura 2. Teores totais de PAH parentais determinados (ΣPAH; <27,0 µg/kg – limite de quantificação) nos sedimentos recolhidos nas duas épocas de amostragem nas áreas (a) D e (b) E. ● Out2018; ● Out2019.

Os PAH mais abundantes nas amostras ensaiadas são o Fluoranteno e os isómeros Benzo(b+j+k)fluoranteno, ambos PAHs com 4 e 5 anéis, respetivamente, predomínio este que já aponta para uma prevalência de origem pirogénica.

Na Figura 3 estão apresentadas representações gráficas de três razões de diagnóstico, assim como os teores dos PAH de baixo e elevado peso molecular que possibilitam uma classificação da origem dos PAH. Os PAH encontrados nos sedimentos recolhidos são, de um modo geral, de origem pirolítica, provenientes da queima de biomassa ainda que com uma ligeira contribuição da queima de combustíveis fósseis.

Concluindo, apenas em determinados zonas da área D e E são notórias variações temporais da ΣPAH ainda que os sedimentos das zonas estudadas sejam, em geral, considerados sem contaminação por PAH. A caracterização aqui realizada vem demonstrar as vantagens de uma monitorização ambiental, visando o apoio à gestão ambiental sustentada em evidências e uma eventual necessidade de intervenção com vista à mitigação da poluição.

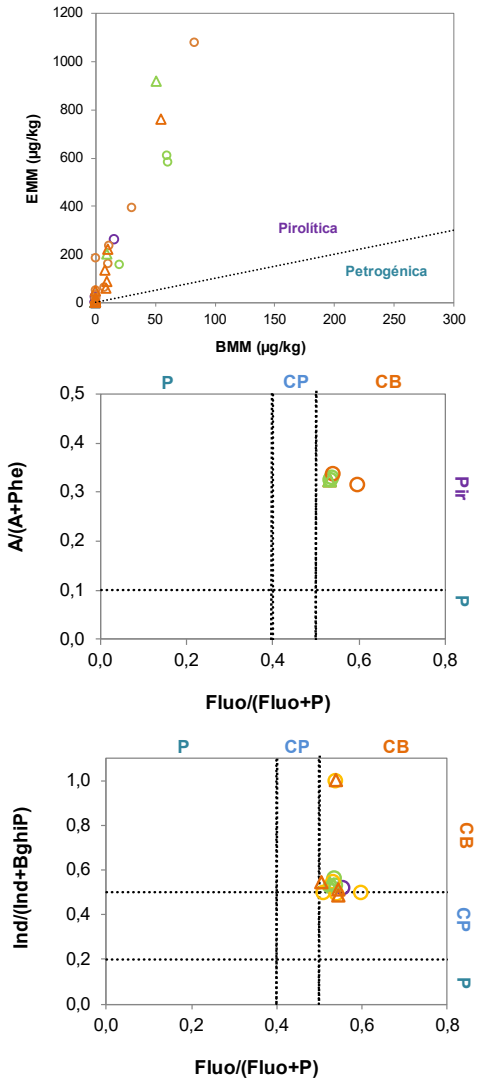

Figura 3. Teores de PAH, razões de diagnóstico e faixas limítrofes (Tobiszewski e Namieśnik, 2012) para classificação da origem de PAH (EMM – PAH de elevada massa molecular, BMM – PAH de baixa massa molecular, A – Antraceno, Phe – Fenantreno, Ind – Indeno(1,2,3-cd)pireno, BghiP – Benzo(g,h,i)perileno, P – Petrogénica, CP – Combustão de combustíveis fósseis, CB – Combustão de biomassa, Pir - Pirolítica): Área A (Out2018), Área A (Maio2020), Área B (Mar2019), Área B (Maio2020), Área C (Mar2019), Área C (Out2019), Área D (Out2018), Área D (Out2019), Área E (Out2018)e Área E (Out2019). Ausência de dados nos gráficos aponta para o facto de pelo menos uma das razões de diagnóstico ou teor de PAH não ter sido determinada em consequência de existir teores inferiores ao limite de quantificação do método.

Agradecimentos

Este trabalho foi financiado pelo programa Operacional Mar2020 através do Projeto "AQUIMAR-Caracterização geral de áreas aquícolas para estabelecimento de culturas marinhas" (MAR2020 n.° MAR-02.01.01-FEAMP-0107).

REFERÊNCIAS

Bakhtiari, A.R., Zakaria, M.P., Yaziz, M.N.H.L., Bi, X., e Rahim, M.C.A. (2009). Vertical distribution and source of polycyclic hydrocarbons in anoxic sediment cores of Chini Lake, Malaysia: perylene as indicator of land plant-derived hydrocarbons. *Applied Geochemistry*, 24:1777–1787.

Latimer, J.S. e Zheng, J. (2003). PAHs: the sources, transport, and fate of PAHs in the Marine Environment. In: Douben, P.E.T. (ed.), *An Ecotoxicological Perspective*. John Wiley & Sons Ltd., England, pp. 9–33.

Lubecki, L. e Kowalewska, G. (2010). Distribution and fate of polycyclic aromatic hydrocarbons (PAHs) in recent sediments from the Gulf of Gdańsk (SE Baltic). *Oceanologia*, 52:669–703

Rocha, A.C. e Palma, C. (2019). Source identification of polycyclic aromatic hydrocarbons in soil sediments: Application of different methods. *Science of the Total Environmental*, 652:1077–1089.

Stogiannidis, E. e Laane, R. (2015). Source characterization of polycyclic aromatic hydrocarbons by using their molecular índices: an overview of possibilities. In: Whitacre, D.M. (ed.), *Reviews of Environmental Contamination and Toxicology*. Springer, Switzerland, pp. 49–133.

Tobiszewski, M. e Namieśnik, J. (2012). PAH diagnostic ratios for the identification of pollution emission sources. *Environmental Pollution*, 162:110-119.

Yunker, M.B., Macdonald, R.W., Vingarzan, R., Mitchell, R.H., Goyette, D. e Sylvestre, S. (2002). PAHs in the Fraser River basin: a critical appraisal of PAH ratios as indicators of PAH source and composition. *Organic Geochemistry*, 33: 489–515.

Poluição por microplásticos: metodologias de análise e impactos nos ecossistemas

Contaminación por microplásticos: metodologías analíticas e impactos en los ecossistemas

Microplastic pollution: analytical methodologies and impacts on ecosystems

Using Singularity Exponents and Lagrangian Coherent Structures to assess the impact of freshwater fronts in the Toconao pellet spill

S. González-Pérez (1), M. Ruiz-Villarreal (1), A. Sanjurjo-García (1), G. González-Nuevo (1), L. M. García-García (1), J. Martínez (2), J. Isern-Fontanet (2) and E. García-Ladona (2)

(1) Centro Oceanográfico de A Coruña (IEO-CSIC, A Coruña, Spain). sofia.gonzalez@ieo.csic.es
(2) Institut de Ciències del Mar (ICM-CSIC, Barcelona, Spain)

Abstract: Lagrangian simulations were performed to study the Toconao pellet spill that occurred in the north coast of Portugal in December 2023. To study the influence of freshwater fronts on the Lagrangian dynamics, a relationship between Lagrangian Coherent Structures (LCS) and Singularity Exponents (SE) was explored. This contribution presents how these two techniques are related and demonstrates their usefulness for assessing the impact of freshwater fronts in this spill.

Keywords: *Lagrangian simulation, Singularity Exponents, Lagrangian Coherent Structures, Plastic drift*

1. THE TOCONAO PELLET SPILL

On December 8th 2023, 1050 sacks containing 25 kg of plastic pellets were spilled from the Toconao container ship about 80km offshore from Viana do Castelo, Portugal. These sacks began drifting in the ocean and were first sighted on the Galician coast on the 13th and 14th. From their first appearance on the Galician coastline (see Figure 1), sacks and pellets were collected by citizens in order to clean up the coast.

However, Coccoza *et al*. (2025) suggest that most of the recovered pellets did not originate from this spill, rather they were already drifting. For that reason, it's important to differentiate between sacks and pellets: the sacks most certainly come from this spill.

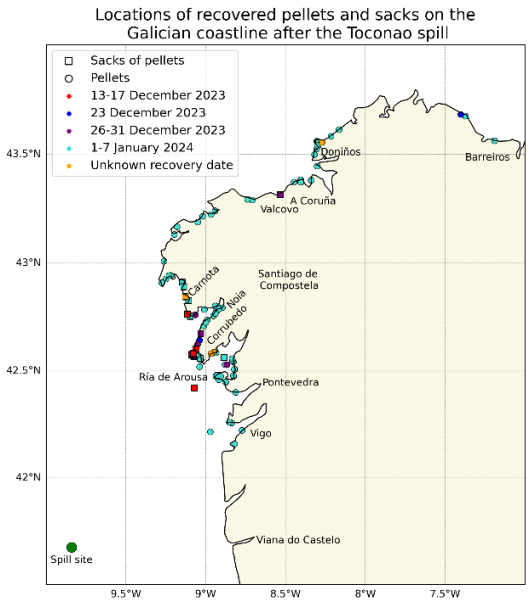

Figure 1. Compilation of available data on sacks and pellet recovery efforts provided by Unha Vez Máis and Noia Limpa associations, as well as El Pais, elDiario.es and El Español news media.

2. LAGRANGIAN SIMULATIONS

A set of Lagrangian simulations was performed to simulate the spill (see Figure 2). The open-source state-of-the-art code OpenDrift was used to carry out this study. OpenDrift (https://opendrift.github.io/, Degestad *et al*., 2018) is a Lagrangian trajectory model that operates offline, which allows the user to perform sensitivity analysis and save computational time.

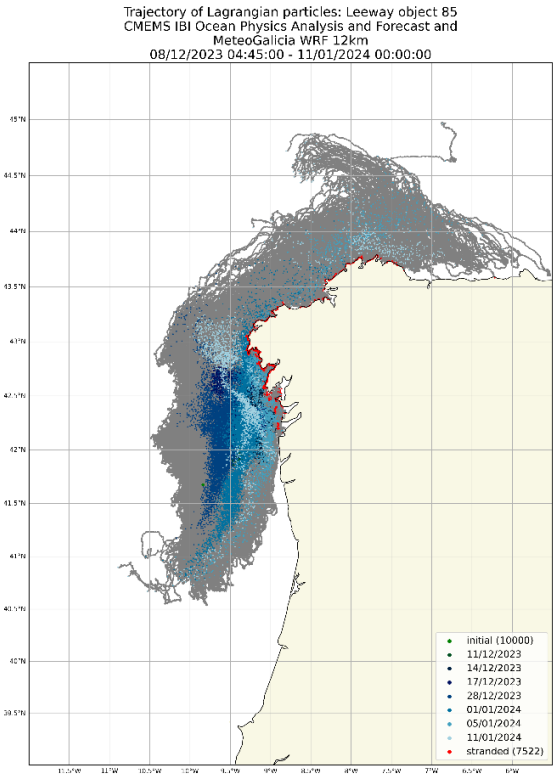

Figure 2. Trajectories of Lagrangian particles simulated as Leeway object 85 (syringes, small medical waste) forced by CMEMS IBI model and MeteoGalicia WRF 12 km model.

There was significant uncertainty when conducting our experiments due to the lack of available information: were they sacks or were they pellets drifting on their own? When did the sacks break, if they did? Given this uncertainty, Lagrangian simulations using different particle types were run, showing that the trajectory model is sensitive to this choice.

We also concluded that it is important to force particles by both a hydrodynamic model and an atmospheric one. Experiments only explain the spill data when both are used. We studied the sensitivity of the Lagrangian model to the configuration of hydrodynamic and atmospheric forcing.

3. EVALUATING THE IMPACT OF FRESHWATER FRONTS

It has already been established in several studies (Otero *et al.,* 2008) that freshwater fronts greatly influence the dynamics of the Galician Rías, as well as drift of different objects (Marta-Almeida *et al*., 2013; Ruiz-Villarreal *et al*., 2006). Even though winter is a typical downwelling season, studies have shown that the system presents variability on shorter time scales (days), in the form of downwelling and upwelling pulses that lead to the confinement and expansion of river plumes.

3.1. Lagrangian Coherent Structures

Lagrangian Coherent Structures (LCS, Haller, 2015; Martínez *et al.,* 2015) are material lines that shape transport. They allow us to identify attracting pathlines into which nearby fluid particles are attracted. These structures may act as Lagrangian barriers, preventing particles from reaching the coast when present in the flow.

Given that freshwater fronts act as Lagrangian barriers, we computed the LCSs to investigate whether some of them originated at the freshwater fronts (see Figure 3).

3.2. Singularity Exponents

Singularity Exponents (SE, Hoareau *et al*., 2018) allow us to measure the intensity of the fronts and were found to be a great tool for characterizing upwelling systems.

One of the main advantages of the SE analysis is that it can be performed on any given signal (ocean current speed, SST, SSS, etc.) from any type of product (ocean models, satellite remote sensing, ...).

Since we have already studied whether the presence of LCS is related to the formation of freshwater fronts, we have investigated the LCS relationship to current velocity SE.

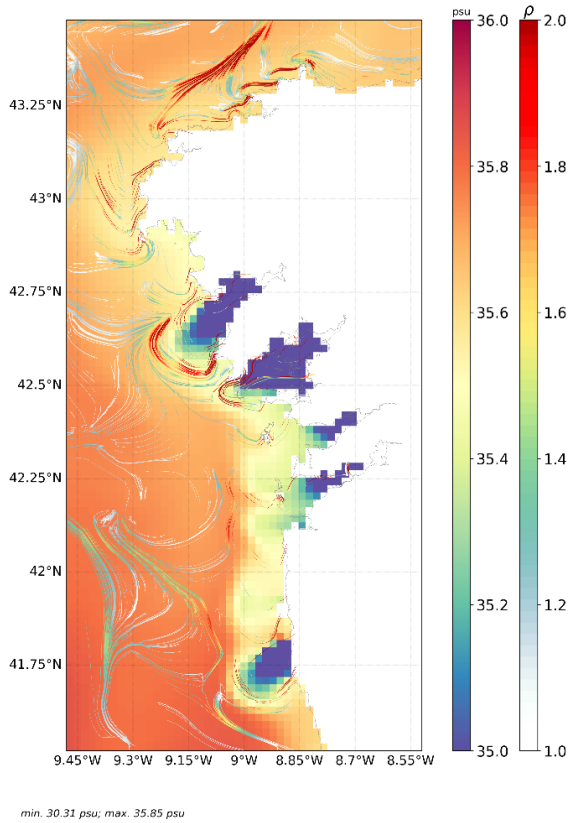

Figure 3. LCSs computed in ROMS model on 13/12/2023 between 16h and 21h and its salinity field on 13/12/2023 at 18h.

3.3. High resolution model: MeteoGalicia MOHID

Since SE analysis does not allow us to get close to the coast, we performed the same analysis on a higher resolution model: MeteoGalicia MOHID Arousa (300 m). In this contribution, it will be shown that LCSs were found at the freshwater fronts (see Figure 4), showing a fast response to the expansion and confinement of river plumes subjected to wind events. In addition, the SE analysis of this model will be also presented.

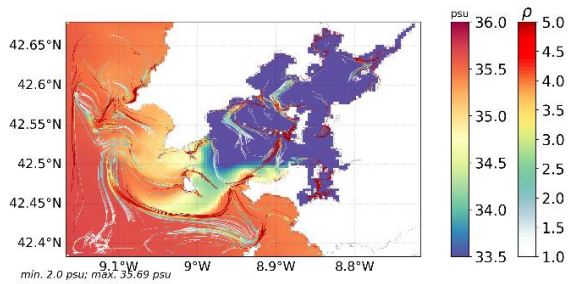

Figure 4. LCSs computed in MOHID Arousa model on 11/12/2023 between 10h and 16h and its salinity field on 11/12/2023 at 10h.

Acknowledgements

This contribution is part of the DEMON project (Dissipation of Energy in Ocean Models and Connectivity) funded by MCIN/AEI/10.13039/501100011033 and by ERDF.

Additional funding has been obtained from Phys2Fish project of the Galicia Marine Science program of the MICIN Complementary Science Plans for Marine Science, co-funded by Xunta de Galicia with NextGenerationEU and the EMFAF. We thank MeteoGalicia (https://www.meteogalicia.gal) for making available the output of their operational ROMS, WRF and MOHID models.

REFERENCES

Cocozza, P., Scarrica, V.M., Rizzo, A., Serranti, S., Staiano, A., Bonifazi, G., and Anfuso, G. (2025). Microplastic pollution from pellet spillage: Analysis of the Toconao ship accident along the Spanish and Portuguese coasts. *Marine Pollution Bulletin,* 211, 117430. doi: https://doi.org/10.1016/j.marpolbul.2024.117430

Dagestad, K.F., Röhrs, J., Breivik, Ø., and Ådlandsvik, B. (2018). Opendrift v1.0: A generic framework for trajectory modelling. *Geoscientific Model Development*, 11, 1405–1420. doi: https://doi.org/10.5194/gmd-11-1405-2018

Haller, G. (2015). Lagrangian Coherent Structures. *Annual review of fluid mechanics*, 47, 137–162. doi: 10.1146/annurev-fluid-010313-141322

Hoareau, N., Turiel, A., Portabella, M., Ballabrera-Poy, J., and Vogelzang, J. (2018). Singularity power spectra: A method to assess geophysical consistency of gridded products—Application to sea-surface salinity remote sensing maps. *IEEE Transactions on Geoscience and Remote Sensing*, 56(9), 5525-5536. doi: 10.1109/TGRS.2018.2819240

Marta-Almeida, M., Ruiz-Villarreal, M., Pereira, J., Otero, P., Cirano, M., Zhang, X., and Hetland, R.D. (2013). Efficient tools for marine operational forecast and oil spill tracking. *Marine pollution bulletin*, 71, 139–151. doi: https://doi.org/10.1016/j.marpolbul.2013.03.022

Martínez, J., García-Ladona, E., Ballabrera-Poy, J., Durán, R., and Isern-Fontanet, J. (2021). Quasy-steady Lagrangian Coherent Structures in the Mediterranean Basin and Iberian Atlantic Waters. *VI Expanding Ocean Frontiers conference* (EOF 2021). doi: 10.13140/RG.2.2.31618.61127

Otero, P., Ruiz-Villarreal, M. and Peliz, A. (2008). Variability of river plumes off Northwest Iberia in response to wind events. *Journal of Marine Systems*, 72(1-4): 238–255. doi: 10.1016/j.jmarsys.2007.05.016

Ruiz-Villarreal, M., González-Pola, C., del Río, G.D., Lavín, A., Otero, P., Piedracoba, S., and Cabanas, J. (2006). Oceanographic conditions in North and Northwest Iberia and their influence on the Prestige oil spill. *Marine Pollution Bulletin*, 53, 220–238. doi: https://doi.org/10.1016/j.marpolbul.2006.03.011

Inter-instrument definition of valid criteria for the automatic identification of microplastics by micro-Raman spectroscopy

R. Fernandes (1), P. Miclea (2), M. Fadda (3), M. Putzu (3), A. Sacco (3), A. M. Rossi (3), A. M. Giovannozzi (3), M. Barbaresi (4), M. Masino (4), M. Mattarozzi (4), M. Careri (4), C. Palma (5), J. Almeida (5), C. Drago (6), O. Pellegrino (7), R. Quendera (7), U. Barun (6) and R. B. Silva (1)

(1) Faculdade de Ciências da Universidade de Lisboa, Portugal. rafa_fernandes@outlook.pt
(2) Fraunhofer Center for Silicon Photovoltaics (CSP), Germany
(3) Istituto Nazionale di Ricerca Metrologica (INRiM), Italy
(4) Department of Chemistry, Life Sciences and Environmental Sustainability, University of Parma, Italy
(5) Instituto Hidrográfico, Portugal
(6) Umweltbundesamt, German Environment Agency, Germany
(7) Instituto Português da Qualidade, Portugal

Abstract: Assessing the environmental and human health risks of microplastic contamination requires a reliable identification of polymer types. µ-Raman spectroscopy is widely used for this purpose by comparing sample spectra with reference databases. However, automatic identification demands well-defined match algorithms and thresholds for this parameter to ensure high true positive rates (*TP*) with minimal false positives (*FP*), regardless of spectrometer or acquisition conditions. This study proposes a robust methodology to optimise microplastic identification by µ-Raman spectroscopy using data from different instruments and laboratories. A bootstrap approach was applied to determine the optimal match threshold without assumptions about match distribution. For polyethylene terephthalate (PET) microparticles, the best performance was achieved using Pearson's correlation coefficient (P5»P = 0.6244), yielding a *TP* of 95 % and an *FP* of only 4.9×10^{-7} %. Spectra with signal-to-noise ratios below 10 were flagged for manual verification. The proposed method proved effective, providing reliable, reproducible microplastic identification across varying experimental conditions.

Keywords: *Microplastics, Automatic identification, µ-Raman spectroscopy, Match threshold, Method Validation, True results rate.*

1. INTRODUCTION

The assessment of the impact of microplastic contamination on the environment and human health requires a reliable identification of the polymer type of these particles (Redko *et al*., 2024; Yang *et al*., 2024). Micro-Raman (µ–Raman) spectroscopy is a popular technique for identifying microplastics by comparing the reference spectra with those of the particles being analysed (Xu, J.L., 2019).

Automatic identification of microplastics requires defining an algorithm for the match between these spectra and setting a minimum match above which identification is performed with an adequately high true and low false result rate. Ideally, the algorithm and match threshold should apply to different spectrometers and spectra collection parameters (Morgado *et al*., 2021).

In this study, polyethylene terephthalate (PET) was chosen for microplastic identification as a representative polymer to assess the viability of the approach to determine match thresholds and evaluate match methods. Reference materials were in the form of soluble tablets containing PET microparticles, with a size distribution ranging from 10 µm to 100 µm. Spectra collected from three different laboratories and in various matrices, including ultrapure water and milk, were studied to assess the robustness of the methodology to these factors.

2. EXPERIMENTAL

This research presents a methodology to determine the best match algorithm for polymer identification using µ-Raman spectroscopy data collected on different instruments and laboratories, associated with a true positive rate (*TP*) of 95 % and a false positive rate (*FP*) lower than 5 %.

Determining the match threshold (*P*5»*P*) by the bootstrap method does not require assumptions regarding match distribution. The normal distribution of the match between the reference and a particle's spectra from a different material allows *FP* determination.

3. RESULTS AND DISCUSSION

Identifying PET microparticles was optimal using Pearson's correlation coefficient (*P*5»*P* = 0.6244, *TP* = 95 %, *FP* = 4.9×10^{-7} %). Identification quality was tested

based on three unweighted and three weighted correlation coefficients. Spectra with signal-to-noise ratios lower than 10 were forwarded to manual identifications. The MS Excel files used in the research are available as supporting information.

4. CONCLUSIONS

The developed methodology for setting up identification criteria of microplastics by spectroscopy proved to be adequate for μ-Raman assessments and robust to different spectrometers and spectra collection conditions.

Acknowledgments

PlasticTrace project - The project has received funding from the European Partnership on Metrology, co-financed from the European Union's Horizon Europe Research and Innovation Programme and by the Participating States.

REFERENCES

Morgado, V., Palma, C., and Bettencourt da Silva, R. J. N. (2021). Microplastics Identification by Infrared Spectroscopy – Evaluation of Identification Criteria and Uncertainty by the Bootstrap Method. *Talanta*, 224, 121814.

Redko, V., Wolska, L., Potrykus, M., Olkowska, E., Cieszyńska-Semenowicz, M., and Tankiewicz, M. (2024). Environmental Impacts of 5-Year Plastic Waste Deposition on Municipal Waste Landfills: A Follow-up Study. *Science of The Total Environment*, 906, 167710.

Yang, Y., Jalalah, M., Alsareii, S. A., Harraz, F. A., Thakur, N., Zheng, Y., Koutb, M., Yoon, Y., and Salama, E. S. (2024). Plastic Wastes (PWs) and Microplastics (MPs) Formation: Management, Migration, and Environmental Impact. *Journal of Environmental Chemical Engineering*, 12 112926.

Xu, J. L., Thomas, K. V., Luo, Z., and Gowen, A. A. (2019). FTIR and Raman Imaging for Microplastics Analysis: State of the Art, Challenges and Prospects. *TrAC - Trends in Analytical Chemistry*, 119, 115629.

Avaliação da contaminação por microplásticos com incerteza no oceano Atlântico ao largo de Cabo Verde

C. Palma (1), J. Almeida (1), V. Morgado (2), M. São Pedro (1) e R. Silva (3)

(1) Instituto Hidrográfico, Lisboa, Portugal. carla.palma@hidrografico.pt
(2) Laboratório Nacional de Energia e Geologia, Lisboa, Portugal
(3) Faculdade de Ciências da Universidade de Lisboa, Portugal

Abstract: Microplastic pollution in the ocean poses an increasing threat to marine ecosystem health. This study assesses the presence and distribution of microplastics in the Eastern Tropical Atlantic, near the Cabo Verde archipelago, with a focus on the uncertainty associated. Water samples were collected from multiple geographic locations and analysed using filtration, optical microscopy, and micro infrared spectroscopic technique (micro-FTIR). The measurement uncertainty, evaluated through replicates and detection limits, is highlighted as a critical factor in environmental data interpretation. The results reveal the best estimated contamination value associated with uncertainty for a 99% confidence level. The number of microplastics (MP) per volume of water filtrated (m^3) per the travelled distance of the ship (km) are between 0 MP m^{-3} km^{-3} and 6 MP m^{-3} km^{-3}.

Keywords: *microplastics, environmental contamination, Atlantic Ocean, seawater, uncertainty*

1. INTRODUÇÃO

Os microplásticos constituem uma ameaça relevante para o meio marinho, devido à sua abundância, persistência, e potencial de bioacumulação e toxicidade em organismos aquáticos. Estas partículas de plástico, com dimensões inferiores a 5 mm (Frias & Nash, 2019), podem ser transportadas a grandes distâncias, acumulando-se tanto em zonas costeiras como em regiões oceânicas remotas, incluindo o Oceano Atlântico Tropical. A crescente presença de microplásticos compromete não só a biodiversidade marinha, como também a segurança alimentar e a saúde humana, através das cadeias tróficas (Jiang *et al.,* 2022; Abelouah *et al*., 2022).

A monitorização da contaminação por microplásticos inclui a caraterização físico-química das partículas e deve integrar a incerteza da medição associada às análises de laboratório e à amostragem. Morgado el al, 2023, apresentou uma metodologia que identifica de uma forma objetiva a variação da contaminação por microplásticos numa área oceânica considerando todas as componentes da incerteza relevantes.

Neste contexto, o presente estudo tem como objetivo avaliar a distribuição de microplásticos em águas superficiais do Atlântico Tropical, nas proximidades de Cabo Verde, aplicando a metodologia desenvolvida por Morgado *et al*., 2023.

2. PARTE EXPERIMENTAL

2.1. Amostragem

A amostragem foi efetuada em 3 campanhas com a designação de MAR ABERTO 2020.2, MAR ABERTO 2021 e MAR ABERTO 2022. A campanha MAR ABERTO 2020.2 decorreu a bordo do NRP Almirante Gago Coutinho com as amostragens de microplásticos no período entre 01/12/2020 e 11/02/2021. A campanha MAR ABERTO 2021 decorreu a bordo do NRP D. Carlos I com as amostragens de microplásticos no período entre 30/10/2021 e 15/11/2021. A 3ª campanha MAR ABERTO 2022 decorreu a bordo do NRP D. Carlos I com as amostragens de microplásticos a decorrerem no período entre 20/11/2022 e 24/12/2022.

As amostras de água foram colhidas através do sistema de água do navio e crivadas num peneiro metálico com uma malha de 50 µm. A água foi recolhida ao nível do calado do navio, a aproximadamente 5,6 m de profundidade. O material retido no peneiro foi filtrado através de um filtro de fibra de vidro VWR de 1,2 µm de poro (Ø 47 mm, GF/C). Os filtros foram armazenados em caixas de Petri de vidro até serem analisadas em laboratório. Para controlar a possibilidade de contaminação aérea durante o processo de filtração, foram colocados filtros de controlo dentro de caixas de Petri abertas durante todo o processo de filtração da amostra.

2.2. Análise de microplásticos

O conteúdo dos filtros foi analisado num estereomicroscópio Leica MZ16F (ampliação de 10×), com as partículas suspeitas de serem plástico isoladas e posteriormente analisadas por um espectrómetro de infravermelho com transformada de Fourier (FTIR) acoplado a um microscópio (PerkinElmer Spotlight 200i), em modo de reflectância total atenuada (micro-ATR) com resolução espectral de 4 cm^{-1} para a faixa de 4000 cm^{-1} a 550 cm^{-1}. Para cada partícula foram registadas fotografias, dimensão, forma, cor e identificação do tipo de polímero. O número de microplásticos encontrado nos trajetos de amostragem percorridos é apresentado com a incerteza associada, de forma a permitir a comparação objetiva dos níveis de contaminação observados nos diferentes trajetos. Os intervalos de confiança para um nível de confiança de 99% foram calculados através de uma abordagem "bottom-up" ou subanalítica para a avaliação da incerteza, recorrendo à simulação dos fatores de incerteza relevantes pelo Método de Monte Carlo. Os efeitos aleatórios associados à contagem de partículas e à variabilidade na contagem foi simulada com base no desvio padrão das diferenças de contagem, usando o modelo de distribuição Poisson-lognormal descrito por Morgado *et al*. (2022). A partir das distribuições geradas, foram extraídos os parâmetros estatísticos, nomeadamente os percentis 0,5 e 99,5 ($P_{0.5}$ e $P_{99.5}$) para definir o intervalo de incerteza. O melhor valor estimado correspondeu ao valor mais frequente da distribuição de probabilidade. Com base no volume de água recolhido e o registo das coordenadas geográficas do ponto inicial e final da colheita — o nível de poluição foi expresso em "MP m^{-3} km^{-1}". Para as amostras que foram colhidas numa posição estática, foi assumido que seriam representativas de um percurso linear de 1 km. Esta unidade representa o número de microplásticos por metro cúbico de água filtrada (m^3) e por quilómetro percorrido (km) pela embarcação durante a amostragem.

3. RESULTADOS E DISCUSSÃO

Apresentam-se os resultados relativos às campanhas MAR ABERTO 2020.2 e MAR ABERTO 2021 (primeiro percurso efetuado). Na Campanha MAR Aberto 2020.2 foram isoladas 999 partículas, sendo identificadas 327 partículas como sendo polímeros plásticos (32,7%). As 327 partículas identificadas como plásticos foram comparadas com as amostras de controlo de forma a serem verificadas as possíveis contaminações externas à sua origem. No final resultaram 38 partículas identificadas como microplásticos. Na Campanha MAR ABERTO 2021 (primeiro percurso efetuado)foram identificados 29 microplásticos.

3.1. Propriedades Físico-Químicas

Na Figura 1 (a) e (b) apresentam-se as caraterísticas físicas dos microplásticos encontrados quanto à forma, dimensão e cor na campanha MAR ABERTO 2020.2 e MAR ABERTO 2021, respetivamente.

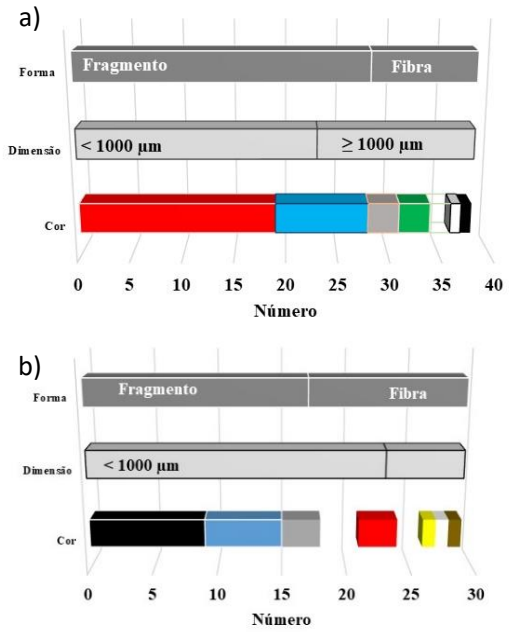

Figura 1. Forma, dimensão e cor registada dos microplásticos encontrados na campanha (a) MAR ABERTO 2020.2 e (b) MAR ABERTO 2021.

Relativamente à idêntidade química dos microplásticos encontrados, *i.e.*, tipo de polímero, foram identificados 26 poliesteres (68,4%), cinco poliuteranos (PU; 13.2%), duas poliamidas (PA; 5,3%), dois fluoreto de polivinildeno (PVDF; 5,3%), um polietileno (PE) (2,0%), um PMMA (2,0%) e um policloropreno (2.0%) (Figura 2).

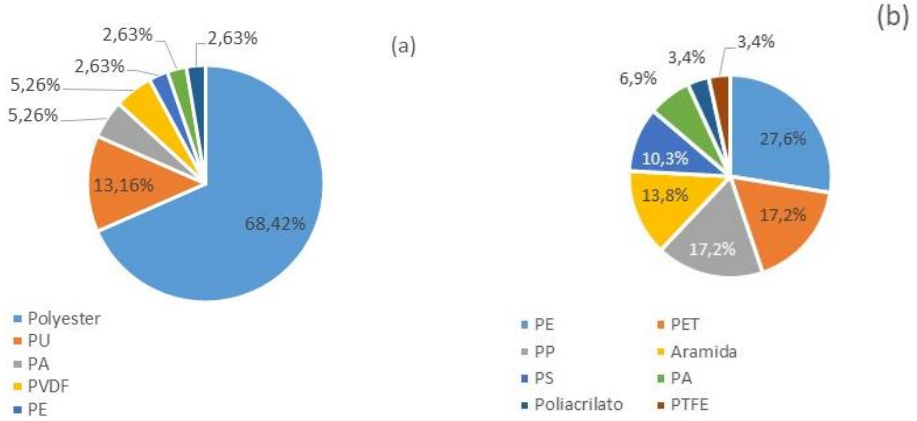

Figura 2. Tipos de polímero encontrados na campanha (a) MAR ABERTO 2020.2 e (b) MAR ABERTO 2021.

3.3. Concentração de microplásticos

Na Figura 3 apresentam-se as abundâncias de microplásticos encontrados na campanha MAR ABERTO 2020.2

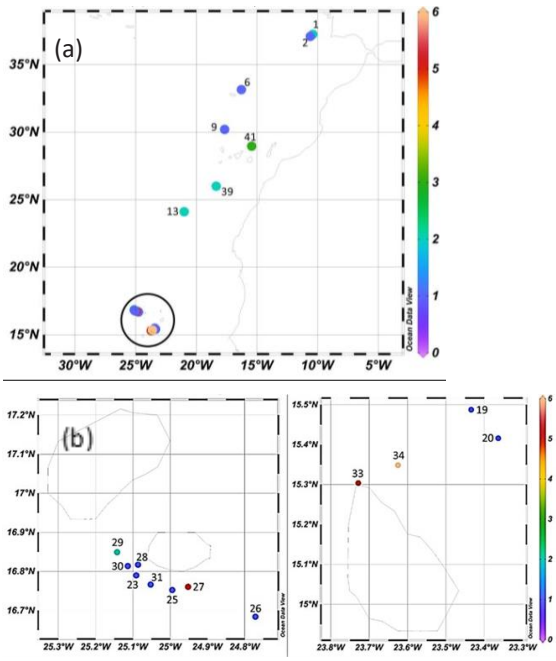

Figura 3. (a) Número de partículas de microplásticos encontradas na campanha MAR ABERTO 2020.2. (b) Zoom para as ilhas de Cabo Verde.

Além das ilhas de Cabo Verde, foram detetados microplásticos também nos percursos de trânsito entre Lisboa e o arquipélago. Nas duas primeiras estações, registaram-se duas fibras de poliéster na estação 1 (vermelha e transparente) e um fragmento azul de policloropreno na estação 2. Na estação 6, perto do Porto Santo (arquipélago da Madeira), foi identificada uma fibra transparente de poliéster. Nas estações 13 e 39, foram registados dois microplásticos em cada estação: na estação 13, dois poliésteres (um fragmento vermelho e uma fibra verde); na estação 39, um fragmento vermelho de polietileno (PE) e uma fibra cinzenta de poliéster. Em duas estações próximas das Ilhas Canárias, registou-se uma fibra cinzenta de poliéster na estação 9 e na estação 41 foram identificadas duas fibras de poliéster (cinzenta e verde) e um fragmento azul de PU.

A Figura 4 apresenta três exemplos da melhor estimativa do número de microplásticos por volume amostrado (m^3) e distância percorrida (km), para a primeira (MAR ABERTO 2020.2) e segunda (MAR ABERTO 2021) campanhas de amostragem. Os resultados são expressos para um nível de confiança de 99%, em "MP km^{-1} m^{-3}".

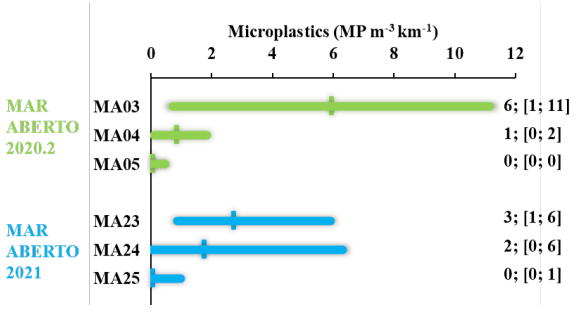

Figura 4. Exemplos da melhor estimativa do número de microplásticos por volume amostrado (m^3) e distância percorrida (km), para a primeira e segunda campanhas de amostragem.

Após uma avaliação metrológica dos níveis de contaminação entre amostras, verificou-se que a amostra MA04 apresenta um nível de contaminação metrologicamente equivalente às amostras MA03 e MA05, contudo a amostra MA03 apresenta um nível de contaminação superior à amostra MA05, para a primeira campanha de amostragem. Analogamente para a segunda campanha, MA24 apresenta um nível de contaminação metrologicamente equivalente às amostras MA23 e MA25, contudo a amostra MA23 apresenta um nível de contaminação superior à amostra MA25.

4. CONCLUSÕES

Verificou-se que a maioria das amostras apresentou concentrações de microplásticos reduzidas ou nulas, particularmente em zonas de mar aberto. As caraterísticas físicas dos microplásticos encontrados quanto à forma variam entre fragmentos e fibras; quanto à dimensão foram encontradas partículas com dimensões inferiores a 500 μm e superiores a 1000 μm; quanto ao tipo de polímero desta-se a presença de poliésteres. Relativamente à estimativa do número de microplásticos por volume amostrado e distância percorrida "MP km^{-1} m^{-3}", para um nível de confiança de 99% verifica-se que a maior parte das amostras apresentam níveis de contaminação metrologicamente equivalentes. A metodologia de avaliação da incerteza da contaminação usada demostrou, mais uma vez, a sua capacidade de se adaptar a qualquer nível de contaminação do oceano.

Agradecimentos

Agradecimento à tripulação dos navios NRP D. Carlos I e NRP Almirante Gago Coutinho que efetuaram a colheita das amostras e a filtração a bordo dos navios.

REFERÊNCIAS

Abelouah, M.R., Ben-Haddad, M., Hajji, S., De-La-Torre, G.E., Aziz, T., Qualid, J.A., Banni, M., e Alla, A.A. (2022). Floating microplastics Pollution in the Central Atlantic Oceano f Morocco: insights into the ocuurrence, characterization, and fate. *Marine Pollution Bulletin*, 182, 113969.

Frias, J. e Nash, R. (2019). Microplastics: finding a consensus on the definition. *Marine Pollution Bulletin*, 138, 145-147.

Jiang, Y., Yang, F., Kazmi, S.S.U.H., Zhao, Y., e Wang, J. (2022). A review of microplastic Pollution in seawater, sediments and organisms of the Chinese coastal and marginal deas. *Chemosphere*, 286, 131677.

Morgado, V., Palma, C., e Silva, R.J.N.B. (2022). Bottom-up evaluation of the uncertainty of the quantification of microplastics contamination in sediment samples. *Environmental Science & Technology*, 56(15), 11080-11090. DOI: 10.1021/acs.est.2c01828

Morgado, V., Palma, C., e Silva, R.J.N.B. (2023). Determination of microplastic contamination levels and trends in vast oceanic sediment areas with uncertainty: Objective contamination assessment. *Science of the Total Environment*, 884, 163612.

High microplastic concentration in limpets points at a plastic hotspot in the north Iberian cantabric shelf

L. Rivas-Iglesias (1), E. Casement (1), D. Menéndez-Teleña (2), E. García-Vázquez (1) and V. Soto-López (2)

(1) Department of Functional Biology, University of Oviedo, Oviedo, Spain. lucia.rivas.iglesias@gmail.com
(2) Department of Nautical Science and Technology, University of Oviedo, Gijón, Spain.

Abstract: Microplastics are an emerging pollutant of increasing concern for marine ecosystems. In this study, we quantified microfibers and microfragments in *Patella cf. vulgata* limpets collected from estuaries along the North Cantabrian and South Atlantic Iberian coasts, using standardized protocols. Results revealed microplastic concentrations in Cantabrian limpets were four to ten times higher than in those from the South. Comparable concentrations observed in previous years at different Cantabrian sites reinforce the hypothesis that this region is a persistent microplastic hotspot. These findings raise concern not only for local coastal ecosystems but also for human health, as limpets are still harvested for consumption in some areas. Statistical analysis confirmed significant spatial differences. This work contributes to the growing body of evidence on uneven microplastic distribution and its potential impacts on marine life and human consumers.

Keywords: *microplastics, limpets, estuarine ecosystems, Cantabrian coast, marine pollution*

1. INTRODUCTION

Plastic pollution is a growing concern for marine ecosystems worldwide. Among the various forms of plastic debris, microplastics (MPs; <5mm) have gained attention due to their persistence bioavailability, and potential to bioaccumulate in marine food webs (Hale *et al*., 2020; Cverenkárová *et al*., 2021). These particles originate from diverse sources such as textile fibres, degraded packaging, and fishing gear (Acharya *et al*., 2021; Kadac-Czapska *et al*., 2023; Sharma *et al*., 2024). Benthic invertebrates such as limpets (*Patella cf. vulgata*), which live attached to the rocks, are suitable bioindicators of microplastic contamination (Reguera *et al*., 2018; Riveiro *et al*., 2024).

Rocky intertidal habitats and estuarine zones, such as those found along the Cantabrian coast, host abundant limpet populations but are also exposed to increasing anthropogenic pressures, being areas specially threatened by MPs considering their oceanographic features and irregular topography (Doyle *et al*., 2020). Hence, the North Iberian coast has been proposed as a potential hotspot for microplastic pollution. This study aims to quantify and compare microplastic concentrations in limpets from estuarine and open coastal areas of the Iberian Peninsula, including sites on both the Cantabrian and southern Atlantic coasts, to assess spatial patterns and identify potential pollution hotspots.

2. MATERIAL AND METHODS

Specimens of *Patella cf. vulgata* (Figure 1) were collected in 2024 from three coastal locations on the Iberian Peninsula: The Nalón and Sella estuaries in the Cantabrian coast, northern Spain, and the Arade estuary, in Portimão, southern Portugal (Figure 2). At each site, 12 limpets were manually collected during low tide from the same intertidal point and transported to the laboratory where they remained at -20 ºC until their analysis. Individuals were of similar size, with long axis ranging from 28 to 52 mm and short axis from 23 to 46 mm.

Figure 1. Patella vulgate individuals on a rocky shore. Photo by Tango22, licensed under CC BY-SA 3.0.

In the lab, soft tissues were digested following the protocol described by Menéndez *et al*. (2022), by using Hydrogen Peroxide 30% AGR at 65 ºC for 7 days to eliminate organic matter. The resulting solutions were filtered through PES (poly-ethersulphone) membranes (PALL corporation) of 0.45 µ m pore. Filters were dried in petri dishes for 48 h at room temperature in closed chambers before MPs count. Filters were then examined under a

stereomicroscope (40x magnification) to visually identify MPs, following Masiá *et al*. (2022). Particles were counted and categorized by type (e.g., fibres, fragments) and colour (e.g., black, blue, white/transparent, red, green). To ensure accuracy, procedural controls were included in all steps to monitor contamination.

Figure 2. Geographic location of the three estuaries analyzed in this study: Nalón and Sella estuaries in northern Spain, and Arade (Portimão) in southern Portugal.

Microplastic concentration was expressed as MP/g. Statistical analysis were conducted to assess differences among sites. Normality and homoscedasticity assumptions were tested using Shapiro-Wilk and Levene's tests, respectively. Due to the data distribution, a Kruskal-Wallis test was performed to compare microplastics concentrations between estuaries. When significant differences were detected, post hoc pairwise comparisons were applied.

3. RESULTS

MPs concentrations varied significantly among the three estuaries (Figure 3). The average concentration was higher in the Sella estuary, suggesting increased exposure to plastic pollution in this area.

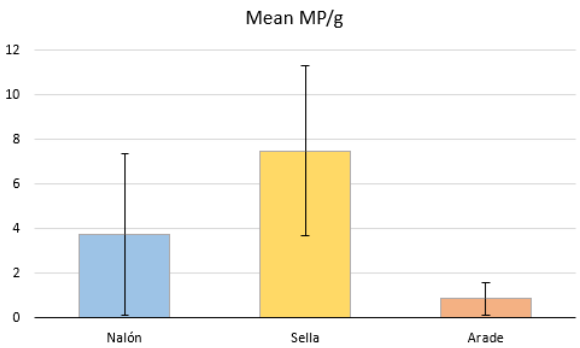

Figure 3. Comparison of the means (± standard deviation) of MP concentration in limpets in the three studied estuaries: Nalón, Sella and Arade. Bars represent the mean values, and error bars indicate data variability.

MPs concentrations showed significant differences among estuaries (Kruskal-Wallis, H = 20.59, $p < 0.0001$). Post-hoc pairwise comparisons using Dunn's test with Bonferroni correction revealed that limpets from both Nalón and Sella had significantly higher MP contents than those from Portimão ($p < 0.001$ in both cases). No significant differences were observed between the two Cantabric estuaries ($p = 0.918$). The results indicate that MP pollution is more severe in the northern estuaries compared to the southern estuary.

4. DISCUSSION

The presence of microplastics in the 97% of all sampled individuals confirms the widespread nature of plastic pollution in coastal ecosystems of the Iberian Peninsula. The higher concentrations observed in limpets from Cantabric estuary sites suggest that local environmental and anthropogenic factors may be contributing to differential contamination levels in that area.

Limpets have proven to be reliable bioindicators, as their sedentary behaviour and grazing feeding strategy increase their exposure to microplastics (Ojeda *et al*., 2021; Yücel and Kiliç, 2023). The observed spatial differences support their use in long-term monitoring programs for coastal pollution.

Further research should aim to clarify the influence of environmental drivers and to standardize methods for cross-regional comparisons. Incorporating environmental sampling and increasing temporal coverage would help better characterize the sources and distribution of microplastics along the Iberian coast.

Acknowledgements

This study received funding from the Ministry of Science and Innovation (Spain), Grant PID2022-138523OB-I00, and the Principality of Asturias (Spain) Grant GRU-GIC-24-051.

REFERENCES

Acharya, S., Rumi, S.S., Hu, Y. and Abidi, N. (2021). Microfibers from synthetic textiles as a major source of microplastics in the environment: A review. *Textile Research Journal*, 91(17-18).

Cverenkárová, K., Valachovicová, M., Machul'ak, T., Zemlicka, L. and Birosová, L. (2021). Microplastics in the Food Chain. *Life*, *11*(12), 1349.

Doyle, D., Frias, J., Nash, R. and Gammell, M. (2020). Current environmental microplastic levels do not alter emergence behaviour in the intertidal gastropod *Littorina littorea*. *Marine Pollution Bulletin*, 151:110859.

Hale, R.C., Seeley, M.E., La Guardia, M.J., Mai, L. and Zeng, Y. (2020). A Global Perspective on Microplastics.

Journal of Geophysical Research: Oceans, 125, e218JC014719.

Kadac-Czapska, K., Knez, E., Gierszewska, M., Olewnik-Kruszkowska, E. and Grembecka, M. (2023). Microplastics Derived from Food Packaging Waste-Their Origin and Health Risks. *Materials*, *16*(2), 674.

Masiá, P., Ardura, A. and Garcia-Vazquez, E. (2022). Microplastics in seafood: relative input of *Mytillus galloprovincialis* and table salt in mussel dishes. *Food Research International*, 153, 110973.

Menéndez, D., Álvarez, A., Acle, S., Peón, P., Ardura, A. and García-Vazquez, E. (2022). Microplastics across biomes in diadromous species. Insights from the critically endangered *Anguilla anguilla. Environmental Pollution*, 305, 119277.

Ojeda, M., Cossi, P.F., Rimondino, G.N., Chiesa, I.L., Boy, C.C. and Pérez, A.F. (2021). Microplastics pollution in the intertidal limpet, *Nacella magellanica*, from Beagle Channel (Argentina). *Science of The Total Environment*, 795, 148866.

Reguera, P., Couceiro, L. and Fernández, N. (2018). A review of the empirical literature on the use of limpets *Patella* spp. (Mollusca: Gastropoda) as bioindicators of environmental quality. *Ecotoxicology and Environmental Safety*, 148, 593-600.

Sharma, D., Dhanker, R., Bhawna, Tomar, A., Raza, S. and Sharma, A. (2024). Fishing Gears and Nets as a Source of Microplastic. In: Shahnawaz, M., Adetunji, C.O., Dar, M.A. and Zhu, D. (eds) *Microplastic Pollution*. Springer, Singapore, pp. 127-140.

Vasques Ribeiro, V., Avelino Soares, T.M., De-la-torre, G.E., Casado-Coy, N., Sanz-Lazaro, C. and Braga Castro, I. (2024). Microplastics in rocky shore mollusks of different feeding habits: An assessment of sentinel performance. *Environmental Pollution*, 346:123571.

Yücel, N. and Kiliç, E. (2023). Presence of microplastic in the *Patella caerulea* from the northeastern Mediterranean Sea. *Marine Pollution Bulletin*, 188, 114684.

Blue crab (*Callinectes sapidus*) as a microplastic pollution indicator in coastal environments

S. Villoria (1,2), G. Blanco-Heras (2), J. Gago (2), A. V. Filgueiras (2), C. Martínez-Gómez (3) and L. Viñas (2)

(1) Universidad de Alicante, Carr. De San Vicente del Raspeig, s/n, 03690-San Vicente del Raspeig, Spain. svc57@alu.ua.es
(2) Instituto Español de Oceanografía (IEO), Centro Oceanográfico de Vigo, Subida a Radio Faro, 50-52, 36390-Vigo, Spain.
(3) Instituto Español de Oceanografía (IEO), Centro Oceanográfico de Murcia c/ el Varadero, 1, 30740-San Pedro del Pinatar, Spain.

Abstract: Plastic pollution is widespread in marine environments. When particles are smaller than 5 mm, they are classified as microplastics. Microplastics can be categorized according to different criteria such as morphology, colour, size, polymeric composition, etc. Coastal areas are critical zones for microplastic accumulation due to their hydrodynamics, increasing the likelihood of ingestion by marine organisms. In this study, the Atlantic blue crab (*Callinectes sapidus*) was selected as the target species for the estimation of microplastic ingestion by organisms. Gill, hepatopancreas, and muscle tissues were dissected and subjected to chemical digestion using potassium hydroxide (KOH) and hydrogen peroxide (H_2O_2), followed by microplastic content analysis. No microplastics were detected in the gills, whereas fragments were the predominant type found in both the hepatopancreas and muscle. White was the most usual colour observed. Regarding to polymer composition, polypropylene was the most prevalent polymer in all tissues, followed by polyethylene in hepatopancreas and polyethylene terephthalate in the muscle.

Keywords: *blue crab, microplastics, hepatopancreas, muscle, bioindicator*

Plastic pollution is widespread in marine environments (UNEP, 2021). Due to photo-oxidation, biodegradation and mechanical degradation (Rashid *et al*., 2024) plastic litter becomes more likely to fragment. When plastic fragments are smaller than 5 mm in size, they are known as microplastics (Thompson *et a*l., 2004). Microplastics (MP) can be classified according to different criteria such as morphology, colour, size, polymeric composition, etc. All these characteristics of microplastics may make marine organisms susceptible to ingesting them.

Coastal areas are key microplastics accumulation zones due to local hydrodynamics, proximity to urban areas, and the intensity of surrounding tourism-related activities. The Mediterranean Sea is among the regions most impacted by plastic pollution (García-Rivera *et al*., 2017), with direct effects observed in marine fauna. The Mar Menor is the largest coastal lagoon on the Spanish Mediterranean coast (Region of Murcia) and one of the largest in the entire Mediterranean basin. This lagoon is heavily impacted by anthropogenic activities which have contributed to various forms of environmental degradation, including significant microplastic pollution within the lagoon. The exotic Atlantic blue crab (*Callinectes sapidus*, Rathbun, 1896) has well-established populations throughout the Mediterranean coastal areas, such as the Mar Menor lagoon (SE Spain), altering biodiversity, food webs and ecosystem services provided by local ecosystems (Ortega-Jimenez *et al*., 2025). This highly invasive species has a wide food spectrum, as well as a great capacity to adapt to diverse ranges of salinity and temperature making it a very versatile species (Castriota *et al*., 2024).

The main objective of this study is to assess the presence, abundance and diversity of microplastics in *Callinectes sapidus* from the Mar Menor lagoon, as well as to evaluate its suitability as a target species for monitoring microplastic pollution in invaded Mediterranean coastal ecosystems. For this preliminary assessment, a single sampling point was selected in Santiago de la Ribera (Encañizadas, Murcia) (Figure 1).

Blue crabs were sampled in March 2025 within the framework of the CRABMEDPOL project. Fifteen adult individuals were captured. Biometric data on length (cm), width (cm), length (cm) of the chela, wet weight (g) and sex were recorded in the laboratory. Maximum width was recorded as a function of distance from the cephalothorax - including lateral spines - using an ichthyometer. Sex was determined

based on the sexual characteristics of the species, particularly the shape of the abdomen.

Figure 1. Callinectes sapidus were collected in Santiago de la Ribera (Encañizadas, Murcia) location in Mar Menor lagoon in the South-east coast of Spain.

Gill, the hepatopancreas and muscle were dissected and weighted for each individual. Digestion was performed following the protocol described by Bessa *et al*. (2019). Briefly, 10% KOH was added at a ratio of 1:6 (tissue weight: solution volume) and samples were incubated at 40ºC for 72 hours. Subsequently, an equal volume of 30% H_2O_2 was added while stirring for 72 hours.

After the digestion procedure, the samples were filtered through steel filters with 20 µm mesh size. The filters were stored in a clean Petri dish. Red Nile (10 µg/mL in EtOH) was then poured over the filter and the plates were placed in the oven at 40°C for half an hour. The filters were then washed with ethanol to remove the excess of Red Nile.

Particles were visually identified using fluorescence microscopy with an MZ10F fluorescence magnifier equipped with a LED source and GFP LP filters. Then, particles larger than 500 µm were chemically characterised with FTIR-ATR (Fourier Transform Infrared Spectroscopy - Attenuated Total Reflectance), and particles smaller than 500 µm with LDIR (Laser Direct InfraRed) (lower size 20 µm).

All dissected crabs presented MP. They were usually found in the muscle and hepatopancreas, but not in the gills. Only two MP shapes were recorded, fragments (above 95%) and fibres. The most prevalent colour was white, followed by transparent. The vast majority of particles observed were smaller than 500 µm; therefore, LDIR was almost exclusively used for their analysis. Polypropylene (PP) was the most frequently identified polymer in both muscle and hepatopancreas, followed by polyethylene terephthalate (PET) in muscle and polyethylene (PE) in hepatopancreas. The presence of microplastics in the stomach of blue crabs have been reported (Renzi *et al*., 2020; Compa *et al*., 2023). Our results enhance the idea that, after MPs ingestion, crustaceans promote fragmentation of MPs, causing its translocation to other organs and tissues. Composition of main polymers found in pour study are consistent with previous findings in this species from other Mediterranean coastal lagoons following similar methodology (Simantiris *et al*., 2024). Although further studies are needed to validate and standardize methodologies, the blue crab emerges as a suitable target species for assessing microplastic contamination in the Mediterranean.

Acknowledgments

The study was conducted at the Spanish Institute of Oceanography (IEO, CSIC). The study was conducted at the Spanish Institute of Oceanography (IEO, CSIC) and funded by the Spanish Ministry of Science, Innovation and Universities, the State Research Agency (CRABMEDPOL Project, PID2022-138720OA-I00), and the ThinkinAzul programme, supported by MCIN with EU NextGenerationEU (PRTR-C17.I1) and Fundación Séneca (Region of Murcia, Spain).

REFERENCES

Bessa, F., Frias, J., Kögel, T., Lusher, A., Andrade, J.M., Antunes, J., Sobral, P., Pagter, E., Nash, R., O'Connor, I., Pedrotti, M.L., Kerros, M.E., León, V., Tirellli, V., Suaria, G., Lopez, C., Raimundo, J., Caetano, M., Gago, J., Viñas, L., Carretero, O., Magnusson, K., Granberg, M., Dris, R., Fischer, M., Scholz-Böttcher, B., Muniategui, S., Grueiro, G., Fernández, V., Palazzo, L., de Lucia, A., Camedda, A., Avio, C.G., Gorbi, S.. Pittura, L., Regoli, F., and Gerdts, G. (2019). Harmonized protocol for monitoring microplastics in biota. JPI-Oceans BASEMAN project. p. 30

Castriota, L., Falautano, M., and Perzia, P. (2024). When Nature Requires a Resource to Be Used—The Case of Callinectes sapidus: Distribution, Aggregation Patterns, and Spatial Structure in Northwest Europe, the Mediterranean Sea, and Adjacent Waters. *Biology*, 13(4), 279.

Compa, M., Perelló, E., Box, A., Colomar, V., Pinya, S., and Sureda, A. (2023). Ingestion of microplastics and microfibers by the invasive blue crab Callinectes sapidus (Rathbun 1896) in the Balearic Islands, Spain. *Environmental Science and Pollution Research*, 30(56), 119329-119342.

García-Rivera, S., Lizaso, J.L.S., and Millán, J.M.B. (2017). Composition, spatial distribution and sources of macro-marine litter on the Gulf of Alicante seafloor (Spanish Mediterranean). *Marine Pollution Bulletin*, 121(1-2), 249-259. DOI: 10.1016/j.marpolbul.2017.06.022

Ortega-Jiménez, E., Vilas, C., de Carvalho-Souza, G.F., Martinez-Lage, A., and González-Ortegón, E. (2025). Isotopic variability of the invasive blue crab Callinectes sapidus in the Gulf of Cadiz: Impacts and implications for coastal ecosystem management. *Journal of Environmental Management*, 374, 124015.

Rashid, E., Hussain, S.M., Ali, S., Munir, M., Ghafoor, A., Yilmaz, E., Alshehri, M.A., Riaz, D., Naeem, A., and Naeem, E. (2024). Impacts of microplastic accumulation in aquatic environment: physiological, eco-toxicological, immunological, and neurotoxic effects. *Aquatic Toxicology*, 107232.

Renzi, M., Cilenti, L., Scirocco, T., Grazioli, E., Anselmi, S., Broccoli, A., ... and Specchiulli, A. (2020). Litter in alien species of possible commercial interest: The blue crab (Callinectes sapidus Rathbun, 1896) as case study. *Marine Pollution Bulletin*, 157, 111300.

Simantiris, N., Cladas, Y., Chochos, C.L., Gregoriou, V.G., Koutsikopoulos, C., Karapanagioti, H.K., ... and Vardaki, M.Z. (2024). First evaluation of microplastics in juveniles of the invasive blue crab Callinectes sapidus from a Mediterranean coastal lagoon. *Estuarine, Coastal and Shelf Science*, 302, 108775.

Thompson, R.C., Olsen, Y., Mitchell, R.P., Davis, A., Rowland, S. J., John, A.W., McGonigle, D., and Russell, A.E. (2004). Lost at sea: where is all the plastic? *Science*, 304(5672), 838-838.

United Nations Environment Programme (2021). From Pollution to Solution: A global assessment of marine litter and plastic pollution. Nairobi.

Sampling microplastic in surface waters: what method to choose?

E. Cacabelos (1), J. Gago (1) and P. Otero (1)

(1) Centro Oceanografico de Vigo, Instituto Español de Oceanografía (IEO), CSIC, Vigo, Spain.
eva.cacabelos@ieo.csic.es

Abstract: Microplastic (MP) pollution in aquatic environments is a growing global concern, demanding harmonisation and standardisation of sampling methods to enable accurate monitoring and assessment. This report presents a comprehensive review of microplastic sampling techniques in natural water bodies, with a specific focus on low-cost methodologies and the performance of the widely used Manta trawl. The review covers a diverse set of sampling strategies, including nets, grab samplers, and pump-based systems, analysing their advantages, limitations, and applicability in various aquatic contexts. It emphasizes the critical impact of mesh size, net design, and environmental conditions on sampling effectiveness and data comparability. Despite being the most frequently used method, the Manta trawl presents significant limitations in estimating filtered water volumes and sampling smaller MP fractions, raising concerns over data accuracy. The need for harmonized protocols and standardized reporting to enhance comparability across studies and support the development of reliable monitoring frameworks is underlined.

Keywords: *microplastics, sampling methods, manta trawl, harmonization, aquatic pollution*

1. BACKGROUND

Marine litter is a global challenge for modern society due to the continuous rise in plastic production, disposal, and accumulation in aquatic environments (Horton and Barnes, 2020). Microplastics (MPs, defined as plastic particles <5 mm), are widely distributed due to their persistence and buoyancy. Accurate quantification and mapping of their distribution are crucial for understanding environmental impacts and for implementing mitigation measures.

Estimating the abundance and/or distribution of MPs in water bodies has become internationally important demanding effective and harmonized sampling methods to enable accurate monitoring and assessment (Michida *et al*., 2019, Horton and Barnes, 2020) are urgently needed across institutions and countries, particularly in line with efforts by MSFD, OSPAR, and UNEP to harmonize monitoring frameworks. Despite extensive research, significant variability exists in MP concentration reports, largely due to inconsistencies in applied methodologies (Lv *et al*., 2021). Key issues include the lack of standardized sampling equipment (e.g., net type and mesh size), procedural inconsistencies, and varying detection limits. Moreover, the lower size threshold of MPs often remains operationally defined by the smallest mesh or pore size used, limiting comparability across studies (Defontaine and Jalón-Rojas, 2023). It is crucial to harmonize and standardize analytical methods for microplastics as soon as possible, as the lack of common optimized and validated methodologies continues to limit the comparability of data despite extensive research on environmental microplastics (Lv *et al*., 2021; Sharma *et al*., 2024). Additionally, the development of novel methods for nanoplastic analysis remains a pressing necessity.

An extensive, up-to-date review of current microplastic sampling techniques in natural aquatic environments was carried out, addressing the methodological challenges and technical limitations of microplastic sampling in aquatic environments, providing an in-depth overview of the techniques employed globally and their implications for data comparability, monitoring reliability, and environmental assessment. The literature review was carried out from up to 2024 using databases (such as Scopus, Science Direct and Google Scholar) and selecting only research studies on MPs in aquatic systems. It covers a wide array of sampling strategies, with a specific focus on low-cost methodologies and the performance of the widely used Manta trawl, analyzing their advantages, limitations, and applicability in various aquatic contexts. It also examines recent advancements and regional initiatives aimed at harmonizing protocols and guideline to improve the detection, quantification, and understanding of microplastic pollution.

2. METHODS OF SAMPLING MICROPLASTICS FROM AQUATIC ENVIRONMENT

The study of microplastics in aquatic environment can be done through various sampling methods to collect particles, and its abundance is contingent upon the specific sampling methodology employed (Poli *et al*.,

2024). MP sampling in aquatic systems encompasses a range of methodologies tailored to different study objectives, water column depths, and available resources. When comparing methodologies for MP field collection, simplicity and accessibility, accuracy, and comparability are all important elements to consider (Mogensen, 2024).

The most frequently methods for sampling of MPs in surface waters are sampling nets (e.g. Neuston, Manta or other nets; Ermolin, 2024; Michida *et al*., 2019; Pasquier *et al*., 2022), that allow for sampling of this large volumes of water, from the surface to the bottom layer (Kang et al., 2015; Lima *et al.*, 2014; Cutroneo *et al*., 2020; Defontaine and Jalón-Rojas, 2023). These nets are typically towed behind vessels at slow speeds (1–5 knots), capturing floating particles retained by mesh sizes often between 300–333 µm. However, their effectiveness is limited by the lower particle-size threshold dictated by the mesh size, excluding smaller MPs and nanoplastics from analysis (Lindeque *et al*., 2020; Barrows *et al*., 2017).

Pumps and in-situ filtration devices or bottles allow for the collection of water at different depths. They are used to study the vertical distribution of MP and allow for high-resolution particle size separation, down to 1 µm, through the use of interchangeable filters (Setälä *et al*., 2016; Defontaine and Jalón-Rojas, 2023), whereas neuston nets are limited to sampling the surface layer of water (up to 0.5 m) (Nayebi *et al*., 2023). These methods offer greater precision and control, particularly in calm conditions or fixed sampling stations. Nonetheless, their applicability can be limited by logistical complexity, risk of filter clogging, and potential sample contamination from the pump mechanisms themselves.

Using precleaned metal or glass bottles is the most straightforward method for sampling MPs and allows one to collect small microplastics fractions, but one limitation of this method is the small sample volume. Therefore, though ideal for capturing fine MPs and microfibers, this kind of grab sampling requires multiple replicates to ensure representativeness (Barrows *et al*., 2017). Despite these limitations, it is particularly valuable in citizen science projects and when minimal infrastructure is available.

When combined, these tools provide a comprehensive view of the presence and concentration of microplastics in the aquatic environment.

Advantages and limitations of MP field sampling methodologies based on simplicity, accuracy and comparability are detailed in Table I.

The most commonly used mesh sizes between 300 and 390 µm (e.g. Hidalgo-Ruz *et al*., 2012; Li *et al*., 2020; Schönlau *et al*., 2020), an approach similar to plankton sampling, i.e., using nets of various mesh sizes to filter out particles of a certain size category. The representativeness of sampled water volume depends on the targeted MP size and concentration. For MPs larger than 300 µm, typically collected using net-based methods, a large water volume than that collected by grab samples is necessary for representativeness when occur at low concentrations (e.g., <1 particle/m³) (Poli *et al*., 2024).

Table I. Comparison of the advantajes and disadvantajes of microplastic field sampling methodologies (nets, grabs and pumps) based on simplicity, accuracy and comparability (adapted from Mogensen, 2024).

Field sampling	Nets	Grab	Pumps
Simplicity and Accessibility			
Flexible sampling collection	-	+	-
Low cost equipment	-	+	-
Widely available materials	-	+	-
Conductive for citizen science	-	+	-
Accuracy			
Standard sample volume	-	+	+
Comprehensive particle size range	-	+	+
Comprehensive particle morphology	+	-	+
Less susceptible to environmental variation	+	-	+
Less susceptible to secondary contamination	+	-	+
Comparability			
Broad comparatability across studies	+	-	+

Recently, new technologies have been developed to investigate microplastic pollution in a more automatic way. Automatic rosette water samplers or even ROV have been used for MP sampling in ocean waters as well as Continuous Plankton Recorder and continuous-flow centrifuges (Defontaine and Jalón-Rojas, 2023).

Studies consistently emphasize that each method presents trade-offs in terms of resolution, volume, representativeness, and contamination risk (Mogensen, 2024). As such, the choice of technique should be aligned with study goals, environmental conditions, and the targeted MP size fraction.

3. CRITICAL ISSUES IN NET-BASED SAMPLING

Different kinds of nets can be used for sampling MP, including neuston net, plankton net, manta net, continuous net, and manual net (Bergmann, 2015; Gago *et al*., 2016; Gerber, 2017; Hidalgo-Ruz *et al*., 2012; Löder and Gerdts, 2015; Cutroneo *et al*., 2020). Choice of net is usually determined by the intended size of the microplastic and vertical height of the water column. While Manta nets have become the standard tool for surface water MP sampling due to their ease of use and capacity to sample large areas, several technical limitations undermine their effectiveness and data reliability.

One of the most significant challenges is the accurate estimation of filtered water volume. The semi-submerged nature of the Manta net during towing, combined with wave motion and wind conditions, complicates precise volume calculations. Commonly, volume is estimated using flowmeters or by multiplying the trawl mouth area by towing distance, yet both methods are subject to substantial variability (Montoto-Martínez *et al*., 2022; GESAMP, 2019). Misestimations in filtered volume can skew concentration metrics and reduce data comparability across studies.

The lack of standardization in net frame size and mesh configuration introduces another level of inconsistency. Variations in the dimensions of net mouths—from 30 cm to 120 cm in width and 10 to 75 cm in height—can significantly affect the sample volume and the type of MPs collected (Pasquier *et al*., 2022; Figure 1).

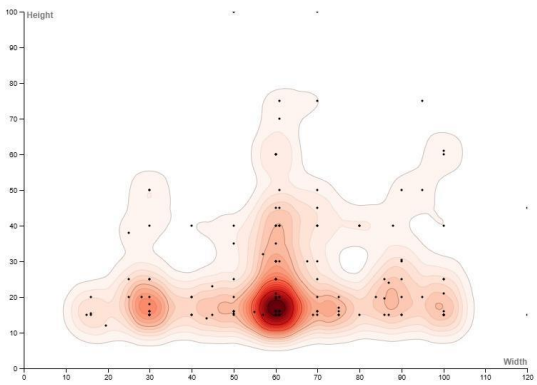

Figure 1. Distribution of manta height and width in the reviewed literature, including studies of both saltwater and freshwater environments.

Similarly, although mesh sizes of >330 µm are commonly used (De-la-Torre *et al*., 2022; GESAMP, 2019; Mogensen, 2024), this cutoff excludes a large proportion of microplastics, particularly microfibers and small particles, which dominate environmental samples (Lindeque *et al*., 2020).

Beyond the primary considerations in microplastic sampling, other aspects related to trawling can influence the results. Environmental conditions such as wave height, wind speed, and water turbidity further influence sampling efficiency. These factors affect net submersion depth and may cause net hopping or skipping, thereby impacting the actual volume sampled and the vertical distribution of collected particles (Kovač Viršek *et al*., 2016; Michida *et al*., 2019). Sampling during high plankton abundance can also cause net clogging, further skewing data and requiring the adjustment of trawling time or distance (Pasquier *et al*., 2022).

Additionally, contamination from the sampling equipment and external sources poses a significant risk. Components of the Manta net and external contamination from vessel paint chips or sampling ropes must be minimized through rigorous decontamination procedures and the use of blank samples (Defontaine and Jalón-Rojas, 2023; GESAMP, 2019).

Given these challenges, there is an urgent need for harmonized guidelines, including both sampling protocols and environmental metadata collection to ensure reliable and comparable data.

4. INNOVATIONS AND FUTURE PERSPECTIVES

This review highlights the substantial influence of mesh size, net configuration, and environmental factors on the effectiveness and comparability of microplastic sampling.

Although Manta nets are practical and widely used for surface sampling, they lack sensitivity and precision, particularly in accurately estimating filtered water volumes and detecting smaller microplastic particles—limitations that can significantly affect the reliability of the resulting data. In contrast, pump-based and grab sampling methods achieve better resolution for smaller particles but face limitations in representativeness at broader spatial scales.

To address these discrepancies, the harmonization of sampling protocols, standardized methodologies and collaborative efforts are key to advancing reliable and comparable monitoring across aquatic environments. Furthermore, the development of shared databases following FAIR principles would enhance data integration and policy relevance.

Acknowledgments

This study has been supported by FreeLitterAt Project: “Advancing towards litter-free Atlantic coastal communities by preventing and reducing macro and micro litter” (EAPA_0009/2022) funded by the INTERREG Atlantic Area Programme (2021–2027).

REFERENCES

Barrows, A. P. W., Neumann, C. A., Berger, M. L., and Shaw, S. D. (2017). Grab vs. neuston tow net: A microplastic sampling performance comparison and possible advances in the field. *Analytical Methods*, 9(9), 1446-1453.

Bergmann, M. (with Gutow, L., and Klages, M.) (2015). Marine Anthropogenic Litter. Springer International Publishing AG.

Cutroneo, L., *et al.* (2020). Microplastics in seawater: Sampling strategies, laboratory methodologies, and identification techniques applied to port environment. *Environmental Science and Pollution Research*, 27(9), 8938-8952.

Defontaine, S., and Jalón-Rojas, I. (2023). Physical processes matters! Recommendations for sampling microplastics in estuarine waters based on hydrodynamics. *Marine Pollution Bulletin*, 191, 114932.

De-la-Torre, G. E., Pizarro-Ortega, C. I., Dioses-Salinas, D. C., Castro Loayza, J., Smith Sanchez, J., Meza-Chuquizuta, C., Espinoza-Morriberón, D., Rakib, M. R. J., Ben-Haddad, M., and Dobaradaran, S. (2022). Are we underestimating floating microplastic pollution? A quantitative analysis of two sampling methodologies. *Marine Pollution Bulletin*, 178, 113592.

Ermolin, M. S. (2024). Assessment of the Microplastics Content in Natural Waters and Sediments: Sampling and Sample Preparation. *Journal of Analytical Chemistry*, 79(5), 500-519.

Gago, J., Galgani, F., Maes, T., and Thompson, R. C. (2016). Microplastics in Seawater: Recommendations from the Marine Strategy Framework Directive Implementation Process. *Frontiers in Marine Science*, 3.

Gerber, G. (2017). More than just food: Mussels as biomonitors of microplastic pollution in the KwaZulu-Natal coastal environment.

GESAMP (2019). Guidelines or the monitoring and assessment of plastic litter and microplastics in the ocean (Kershaw P.J., Turra A. and Galgani F. editors No. 99; IMO/FAO/UNESCO-IOC/UNIDO/WMO/IAEA/UN/UNEP/UNDP/ISA Joint Group of Experts on the Scientific Aspects of Marine Environmental Protection), p. 130).

Hidalgo-Ruz, V., Gutow, L., Thompson, R. C., and Thiel, M. (2012). Microplastics in the marine environment: A review of the methods used for identification and quantification. *Environmental Science & Technology*, 46(6), 3060-3075.

Kang, J.-H., Kwon, O. Y., Lee, K.-W., Song, Y. K., and Shim, W. J. (2015). Marine neustonic microplastics around the southeastern coast of Korea. *Marine Pollution Bulletin*, 96(1-2), 304-312.

Kovač Viršek, M., Palatinus, A., Koren, Š., Peterlin, M., Horvat, P., and Kržan, A. (2016). Protocol for Microplastics Sampling on the Sea Surface and Sample Analysis. *Journal of Visualized Experiments*, 118, 55161.

Li, W., Luo, Y., and Pan, X. (2020). Identification and Characterization Methods for Microplastics Basing on Spatial Imaging in Micro-/Nanoscales. En D. He and Y. Luo (Eds.), *Microplastics in Terrestrial Environments* (Vol. 95, pp. 25-37). Springer International Publishing.

Lima, A. R. A., Costa, M. F., and Barletta, M. (2014). Distribution patterns of microplastics within the plankton of a tropical estuary. *Environmental Research*, 132, 146-155.

Lindeque, P. K., Cole, M., Coppock, R. L., Lewis, C. N., Miller, R. Z., Watts, A. J. R., Wilson-McNeal, A., Wright, S. L., and Galloway, T. S. (2020). Are we underestimating microplastic abundance in the marine environment? A comparison of microplastic capture with nets of different mesh-size. *Environmental Pollution*, 265, 114721.

Löder, M. G. J., and Gerdts, G. (2015b). Methodology Used for the Detection and Identification of Microplastics—A Critical Appraisal. En M. Bergmann, L. Gutow, and M. Klages (Eds.), Marine Anthropogenic Litter (pp. 201-227). Springer International Publishing.

Lv, L., Yan, X., Feng, L., Jiang, S., Lu, Z., Xie, H., Sun, S., Chen, J., and Li, C. (2021). Challenge for the detection of microplastics in the environment. *Water Environment Research*, 93(1), 5-15.

Michida, Y. et al. (2019). Guidelines for Harmonizing Ocean Surface Microplastic Monitoring Methods.

Mogensen, H. (2024). Microplastic Trends in Estuarine Surface Waters.

Montoto-Martínez, T., Meléndez-Díez, C., Melián-Ramírez, A., Hernández-Brito, J. J., and Gelado-Caballero, M. D. (2022). Comparison between the traditional Manta net and an innovative device for microplastic sampling in surface marine waters. *Marine Pollution Bulletin*, 185, 114237.

Nayebi, B., Khurana, P., Pulicharla, R., Karimpour, S., and Brar, S. K. (2023). Preservation, storage, and sample preparation methods for freshwater microplastics – a comprehensive review. *Environmental Science: Advances*, 2(8), 1060-1081.

Pasquier, G., Doyen, P., Kazour, M., Dehaut, A., Diop, M., Duflos, G., and Amara, R. (2022). Manta Net: The Golden Method for Sampling Surface Water Microplastics in Aquatic Environments. *Frontiers in Environmental Science*, 10, 811112.

Poli, V., Litti, L., and Lavagnolo, M. C. (2024). Microplastic pollution in the North-east Atlantic Ocean surface water: How the sampling approach influences the extent of the issue. *Science of The Total Environment*, 947, 174561.

Schönlau, C., Karlsson, T. M., Rotander, A., Nilsson, H., Engwall, M., Van Bavel, B., and Kärrman, A. (2020). Microplastics in sea-surface waters surrounding Sweden sampled by manta trawl and in-situ pump. *Marine Pollution Bulletin*, 153, 111019.

Setälä, O., Magnusson, K., Lehtiniemi, M., and Norén, F. (2016). Distribution and abundance of surface water microlitter in the Baltic Sea: A comparison of two sampling methods. *Marine Pollution Bulletin*, 110(1), 177-183.

Sharma, P., Sharma, P., and Abhishek, K. (2024). Sampling, separation, and characterization methodology for quantification of microplastic from the environment. *Journal of Hazardous Materials Advances*, 14, 100416.

VI.

ÍNDICE DE AUTORES

Índice de autores
Authors list

N

O

P

Q

R

Organização

Marinha

hidrográfico
marinha · portugal

Patrocinadores

Casco Antiguo

exail

KONGSBERG

vórtice
Equipamentos Científicos, Lda.

qualitas instruments